ZAŠTITA MATERIJALA

G o d i n a LXVI **B e o g r a d, 2025.** **B r o j 1**

Izdavač- Publisher:

INŽENJERSKO DRUŠTVO ZA KOROZIJU, Beograd, Kneza Miloša 9/I,
Tel/fax (011) 3860 - 867 i (011) 3230–028,
E-mail:editor@idk.org.rs; idk@idk.org.rs, www.idk.org.rs, E-mail:caslav.lacnjevac@gmail.com

EVROPSKA FEDERACIJA ZA KOROZIJU (EFC) SMATRA OVAJ ČASOPIS ZVANIČNOM PUBLIKACIJOM ZA OBJAVLJIVANJE IZVEŠTAJA I INFORMACIJA

EUROPEAN FEDERATION OF CORROSION (EFC) CONSIDERES THIS JOURNAL TO BE THE OFFICIAL PUBLICATION FOR PUBLISHING THE REPORTS AND INFORMATION

SADRŽAJ – CONTENT

SUIZDAVAČI

INSTITUT ZA TEHNOLOGJU NUKLEARNIH I DRIGIH MINERALNIH SIROVINA, BEOGRAD

UDRUŽENJE INŽENJERA SRBIJE ZA KOROZIJU I ZAŠTITU MATERIJALA

CRNOGORSKO DRUŠTVO ZA ZAŠTITU MATERIJALA

DONATORI

JP ELEKTROMREŽA SRBIJE, BEOGRAD
JKP DRUGI-OKTOBAR, VRŠAC
"NIS - FAM", KRUŠEVAC
GALFOS, BEOGRAD
PD DRINSKO LIMSKE ELEKTRANE, BAJINA BAŠTA
INSTITUT ZA PREVENTIVU, NOVI SAD
MAŠINSKI FAKULTET, BEOGRAD
TEHNOLOŠKO-METALURŠKI FAKULTET, BEOGRAD
TEHNIČKI FAKULTET, BOR
TEHNOLOŠKI FAKULTET, LESKOVAC
ALFA PLAM ad, VRANJE
„HELIOS“, DOMŽALE
ŠUMARSKI FAKULTET, BEOGRAD
AGRONOMSKI FAKULTET, ČAČAK
GRAĐEVINSKO-ARHITEKTONSKI FAKULTET, NIŠ
TEHNOSAM, SUBOTICA
"PITURA", NOVI BEOGRAD
UNIPROMET, ČAČAK
FAKULTET ZAŠTITE NA RADU, NIŠ
INSTITUT ZA VODOPRIVREDU „JAROSLAV ČERNI“, BEOGRAD
„GALVA“, KRAGUJEVAC
PERIĆ & PERIĆ, POŽAREVAC
HORIZONT PRES, BEOGRAD
VISOKA TEHNOLOŠKA ŠKOLA STRUKOVNIH STUDIJA, NOVI BEOGRAD
VISOKA STRUKOVNA ŠKOLA, NIŠ
VISOKA TEH. SKOLA STRUK. STUDIJA, NOVI SAD
INSTITUT ZA PUTEVE, BEOGRAD
IMPOL SEVAL, UŽICE
ALFATERM, ČAČAK
METALAC A.D., GORNJI MILANOVAC
SINVOZ DOO, ZRENJANIN

U finansiranju izdavanja časopisa "ZAŠTITA MATERIJALA" učestvuju:

MINISTARSTVO NAUKE, TEHNOLOŠKOG RAZVOJA I INOVACIJA REPUBLIKE SRBIJE

INŽENJERSKA KOMORA SRBIJE

CIP - Katalogizacija u publikaciji
Narodna biblioteka Srbije, Beograd

620.1
ZAŠTITA MATERIJALA = Materials Protection / Glavni urednik .Časlav Lačnjevac), [Štampano izd.]. - God. 1, br. 1 (1953)-god. 22, br. 3/4 (1974) ; god. 23, br. 1 (1982)-. - Beograd: Inženjersko društvo za koroziju, 1953-1974; 1982- (Zemun : Akademska izdanja). - 29 cm

Dostupno i na: https://www.zastita-materijala.org - Tromesečno. - Drugo izdanje na drugom medijumu: Zaštita materijala (Online) = ISSN 2466-2585

ISSN 0351-9465 = Zaštita materijala

COBISS.SR-ID 4506626

Redakcija: Beograd, Kneza Miloša 9/I, Tel/fax (011) 3860 - 867, i (011) 3230 - 028,E-mail: idk@idk.org.rs;
E-mail:editor@idk.org.rs, www.idk.org.rs; www.zastita-materijala.org/index.php/home/issuse

Tekući račun: 205 - 24967 – 71, Komercijalna banka, Beograd; Časopis izlazi četiri puta godišnje
Rukopisi se ne vraćaju; Štampa: Akademska izdanja, Zemun

ISTORIJAT INŽENJERSKOG DRUŠTVA ZA KOROZIJU

Inženjersko društvo za koroziju, koji je pravni naslednik Saveza inženjera i tehničara za zaštitu materijala Srbije i Crne Gore, je društveno stručna organizacija koja je član Saveza inženjera i tehničara Srbije. Savez inženjera i tehničara za zaštitu materijala Jugoslavije, kako se prvobitno zvalo Inženjersko društvo za koroziju, početke svog delovanja je imao još 1952. godine preko Komisije za zaštitu od korozije. Ova komisija je postojala u okviru Društva hemičara i tehnologa DIT-a , mada se neki koreni iz zaštite od korozije pominju i pre drugog svetskog rata. Inicijatori za oformljenje ove Komisije bili su dr.inž Frano Podbrežnik, prof.dr Blažon, prof.dr Milan Pajević i Sveta Živanović. Komisija je imala 15 aktivnih članova i radila je u tri potkomisije.

Januara 1953. godine ova Komisija prerasta u Centar za zaštitu od korozije sa osnovnim zadatkom da radi na antikorozionoj zaštiti svih materijala, uređaja, opreme i instalacija. Već u prvoj godini postojanja ovaj Centar je obrazovao svoju servisnu radionicu za fosfatiranje i pristupio izdavanju svojih stručnih publikacija.

Dalji rad Centra, do svog prerastanja u Društvo a kasnije u Savez, odvijao se u komisijama i servisnim radionicama preko kojih se intenzivno radilo na održavanju raznih kurseva i predavanja iz oblasti korozije materijala i zaštite od nje a, takođe, i na izradi projekata za korozionu zaštitu raznih objekata i opreme za mnoga preduzeća.

PREDSEDNIŠTVO IDK: Predsednik IDK prof.dr Časlav Lačnjevac Potpredsednik IDK Zoran Ivljanin, dipl.inž.tehn. Članovi Upravnog odbora – Srećko Stefanović, dipl. inž. tehn. – Dragan Petrović, dipl. elek. inž. – Momir Đurović, dipl. inž. tehn. Članovi Nadzornog odbora – Ljupče Milosavljević, dipl.inž.tehn. – Miodrag Jovanović, dipl.građ.inž. – Mirko Bačilović, dipl.ecc. Tehnički sekretar IDK – Srbislav Nešić, dipl.maš.inž.

Delatnost strukovnih udruženja (udruživanje u okviru profesije i tehničkih oblasti, uključujući i udruženja specijalista angažovanih u naučnoj delatnosti); – Obrazovanje odraslih (obrazovanje na seminarima, naučno-stručnim skupovima, specijalističkim kursevima i sl.); – Istraživanje procesa korozije i zaštite od korozije; – Izrada tehničke dokumentacije, ekspertiza i vršenje nadzora iz oblasti hidroizolacije, antikorozione zaštite i protivpožarne zaštite.

Inženjersko društvo za koroziju Republike Srbije je izdavač časopisa Zaštita materijala, počlo je sa radom daleke 1953. godine, kao deo Centra za zaštitu od korozije u okviru Saveza inženjera i tehničara za zaštitu materijala Jugoslavije. Iste godine, Društvo je pokrenulo časopis Zaštita materijala, koji i danas aktivno izlazi. Pridružite se bezbrojnim čitaocima koji su imali koristi od njegovog zanimljivog naučnog sadržaja.

Otvaranje naučnog skupa

Zaštita materijala je recenzirani časopis koji sadrži radove o originalnom eksperimentalnom ili teorijskom istraživanju i značajno unapređuju razumevanje u oblastima korozije i zaštite materijala, zaštite životne sredine, ekološkog inženjerstva i tehnologija, inženjerstva materijala (keramika, polimeri, kompoziti; biomaterijali, materijali za skladištenje i konverziju energije, itd.); nanomaterijala i nanotehnologija; hemijskog i biohemijskog inženjerstva, primenjene hemije, upravljanja tehnologijom, i obrazovanja o održivom razvoju. Časopis prihvata radove koji prikazuju eksperimentalne i teorijske naučne i inženjerske rezultate na osnovu dostavljenih podataka.

Naučni radovi za ZM moraju biti dostavljeni na **engleskom jeziku** i treba da sadrže rezime na engleskom i srpskom jeziku. Za autore van srpskog govornog područja, izdavač će obezbediti rezimee i naslove tabela i slika na srpskom jeziku. Časopis izlazi 4 puta godišnje.

Časopis je indeksiran u Scopus, DOAJ, International Scientific Indexing (ISI), Journalspedia (JPSA), Sherpa Romeo itd.

Digitalne kopije časopisa su arhivirane u repozitorijumu.

Subrata Das[1], Kaliappan Prathasana[1], Pathipalayam Arumugam Nitin[1], Krishnan Ramamoorthi Lakshimi Jaya Priya[1], Vemban Mathivanan[2]

[1]Department of Fashion Technology, Bannari Amman Institute of Technology, Sathyamangalam, Erode District, Tamil Nadu, India; [2]Ordnance Clothing Factory, Ministry of Defence, Govt. of India, Avadi, Chennai, India

Review paper
ISSN 0351-9465, E-ISSN 2466-2585
https://doi.org/10.62638/ZasMat1202

Zastita Materijala 66 (1)
5–14 (2025)

Protection from Ballistic Threats: An Exploration of Textile Materials for Bullet-Resistant Outerwear

ABSTRACT

Bullet-resistant jackets are one of the innovations that demonstrate how textile engineering and technology can work together to protect people from ballistic threats. To improve the protective qualities of bulletproof jackets, it is imperative to comprehend the wide variety of textile materials that are used in them. This study aims to clarify the complex interplay between protection, flexibility, and comfort that is inherent in these kinds of clothes by a thorough analysis of a variety of fibers, fabricsand composites, each offering unique characteristics that contribute to the overall effectiveness of these types of garments. Important factors were determined to take into account when choosing the best material based on particular needs like flexibility, comfort, weight, and degree of protection through careful analysis and comparison. This exploration shall provide valuable insights for researchers, manufacturers, and consumers alike, fostering advancements in protective garment design and promoting informed decision-making in the realm of personal safety.

Keywords: *Bullet-resistant jacket, protective garment, degree of protection, flexibility, comfort, safety*

1. INTRODUCTION

In a time when people place a greater value on personal safety, developing protective gear has become critical. Bullet-resistant jackets are one of these innovations that demonstrate how textile engineering and technology can work together to protect people from ballistic.The concept of threat levels encompasses a range of ballistic hazards, including handgun rounds, rifle ammunition, and specialized projectiles. These threats are typically classified based on their kinetic energy, velocity, and penetrating capabilities, with standardized testing protocols employed to evaluate the performance of bullet-resistant materials against them. The materials used in the construction of these jackets have a major impact on their efficacy. Therefore, to improve the protective qualities of bullet-resistant jackets, it is imperative to comprehend the wide variety of textiles that are used in them[1]. To analyze the characteristics, advantages, and disadvantages of the textile materials used in bullet-resistant jackets, this study has been undertaken. After a thorough analysis of a variety of textiles, from conventional choices to state-of-the-art inventions, we aim to clarify the complex interplay between protection, flexibility, and comfort that is inherent in these kinds of clothes.The evolution of bullet-resistant materials has seen a transition from rigid and cumbersome armour to lightweight, flexible solutions, thanks to advancements in textile technology[2]. Today, an array of fibers, fabrics, and composites are utilized, each offering unique characteristics that contribute to the overall effectiveness of bullet-resistant jackets. From traditional aramid fibers like Kevlar® to high-performance polyethylene fibers such as Dyneema®, the market presents a diverse spectrum of options for manufacturers and consumers alike[3].Moreover, the study examines the manufacturing processes involved in integrating these materials into wearable garments.

* Corresponding author: Subrata Das
E-mail: subratactl@gmail.com
Paper received: 28.04.2024.
Paper accepted: 9.06.2024.
Papir is available on the website: www.idk.org.rs/journal

Techniques such as weaving, knitting, laminating, and layering play pivotal roles in optimizing the protective capabilities of bullet-resistant jackets while ensuring wearer comfort and mobility.Not only that, but factors go beyond choosing the right materials and production methods. To give a comprehensive picture of the textile landscape in bulletproof clothing, factors like durability, cost-effectiveness, and environmental impact are also carefully considered. In the end, this research aims to clarify the complex interactions that occur between textile composition and the level of protection provided by jackets resistant to bullets[4]. Continuous effort is required to improve individual safety in an unpredictable world by combining current knowledge and investigating cutting-edge innovations.Through this exploration, we endeavour to provide valuable insights for researchers, manufacturers, and consumers alike, fostering advancements in protective garment design and promoting informed decision-making in the realm of personal safety.The specific textile materials commonly employed in bullet-resistant jackets were studied, analyzed their properties, applications, and potential avenues for future development.

2. PURPOSE OF BULLET RESISTANCE JACKET

A bullet-resistant jacket's main goal is to shield its wearer from ballistic threats that could cause harm or even death. The jacket lessens the severity of trauma to critical organs and aids in preventing penetration by absorbing and dispersing the kinetic energy of incoming bullets or projectiles.Bullet-resistant jackets are essential safety equipment for law enforcement officers, military personnel, and security professionals who may be exposed to firearms and other weapons in the line of duty[5]. These jackets help mitigate the risks associated with confrontational situations and provide a critical layer of protection for individuals serving in high-risk environments.In addition to professionals, civilians in a variety of settings and occupations where there is an increased chance of coming into contact with firearms—security guards, private investigators, journalists covering hostilities—also wear bulletproof jackets[6]. In addition, when they feel that their safety is in danger, civilians may decide to arm themselves with bulletproof jackets for personal defence.

3. THREAT LEVEL

Major threats faced by the Indian armedforces, paramilitary, state police forces, and other law and enforcement agencies shall be classified into 6 threatlevels. Bullet-resistant jackets, also known as ballistic vests or body armour, are designed to protect the wearer from various ballistic threats, including bullets and projectiles. These jackets are typically classified into different threat levels based on their ability to withstand different types of ammunition and the kinetic energy they carry. The threat levels are often standardized by organizations like the Bureau of Indian Standards (BIS) (Table 1) or international standards bodies like the National Institute of Justice (NIJ) in the United States[7].

Table 1: Threat levels standardized by Bureau of Indian Standards (BIS)[8]

Sl no.	Threat Level	Ammunition	bullet Weight (see note) g	Bullet type	Impact velocity m/s	Distance of impact m	Remarks
(1)	(2)	(3)	(4)	(5)	(6)	(7)	(8)
	1	9x19 mm	7.4-8.2	FMJ/Pb	430±15	5±0.5	For all flexible panels
	2	7.62x39 mm	7.45-8.05	FMJ/MSC	710±15	10±0.5	
	3	7.62x51 mm	9.4-9.6	FMJ/Pb	840±15	10±0.5	In addition, shall be in compliance with threat level 2
	4	5.56x45 mm	3.5-4.0	FMJ(SI+Pb)	890±15	10±0.5	In addition, shall be in compliance with threat level 3
	5	7.62x39 mm	7.45-8.05	HSC	700±15	10±0.5	In addition, shall be in compliance with threat level 3
	6	7.62x52 R	10.3-10.5	API	830±15	10±0.5	In addition, shall be in compliance with threat level 3
	special	Any other requirement by the user. Complete details of ammunition shall be stored for future up gradation of the standard.					
NOTE - Routine ballistic evaluation may use service ammunition where bullet weight is not considered. Bullet weight shall be considered for reloaded ammunition. FMJ: Full Metal Jacket Pb: Lead Core MSC: Mild Steel Core SI: Steel InsertHSC: Hard Steel Core API: Armour Piercing Incendiary							

3. COMPONENTS OF JACKET

The two primary components of a bullet-resistant jacket are:

Soft armour panel “SAP” and Hard armour panel “HAP” typically refer to different levels of protection against ballistic threats

3.1. Soft Armour Panel:

Soft armour panels are inserts that are flexible and usually composed of materials such as Aramid fibers and Ultra-high molecular weight polyethylene (UHMWPE). These panels lessen the chance of penetration and wearer injury by absorbing and dispersing the kinetic energy of incoming projectiles. Soft armour panels can withstand bullets from handguns and some rifle ammunition with a lower muzzle velocity. Wearers can move freely and the armour can be bent or flexed at will while still being protected from ballistic threats thanks to the balance of protection and flexibility they offer.Minimum coverage areas of components of Soft Armour Panel I shown in Table 2.

Table 2: Minimum Coverage Areas of Components of Soft Armour Panel[9].

Sl. no	Size	Total protection area for sap (including Torso, Neck, Shoulders, and groin) m²	Total protection area for shoulders only m²	Total protection area for groin only m²	Total protection area for neck and collar only m²
(1)	(2)	(3)	(4)	(5)	(6)
	XS	0.45	0.035	0.05	0.05
	S	0.50	0.035	0.05	0.05
	M	0.55	0.035	0.05	0.05
	L	0.60	0.04	0.06	0.06
	XL	0.65	0.04	0.06	0.06

3.2. Hard armour panel:

Hard armour plates are inflexible inserts composed of steel, ceramic, or composite materials that are designed to withstand the impact of heavy projectiles like rifle rounds fired at high speeds. To provide additional ballistic resistance against rifle fire, hard armour plates are usually inserted into specially made pockets or carriers within the bulletproof jacket. Hard armour plates are vital components for scenarios where there is a high risk of coming into contact with rifle fire, even though they are less flexible and heavier than soft armour panels. Minimum coverage areas of components of Hard Armour Panel / Hard armour plates also provide better protection against more powerful threats[10] as shown in Table 3.

Table 3: Minimum Coverage Areas of Components of Hard Armour Panel (m’)[11]

size / Panel	XS	S	M	L	XL
Front/back	0.0667	0.0700	0.0735	0.0772	0.0810
Side (optional)	0.0326	0.0342	0.0359	0.0377	0.0396
Groin (optional)	0.0370	0.0370	0.0370	0.0370	0.0370
Throat (optional)	0.0245	0.0257	0.0270	0.0284	0.0298
Total (considering front and back, two sides throat and groin)	0.260	0.271	0.283	0.295	0.308
Total (considering front and back)	0.133	0.140	0.147	0.154	0.162

Together, soft armour panels and hard armour plates form the dual protection system within a bullet-resistant jacket, providing wearers with comprehensive protection against a wide range of ballistic threats.Design example of front and side plate (medium size) is given in figure 1.

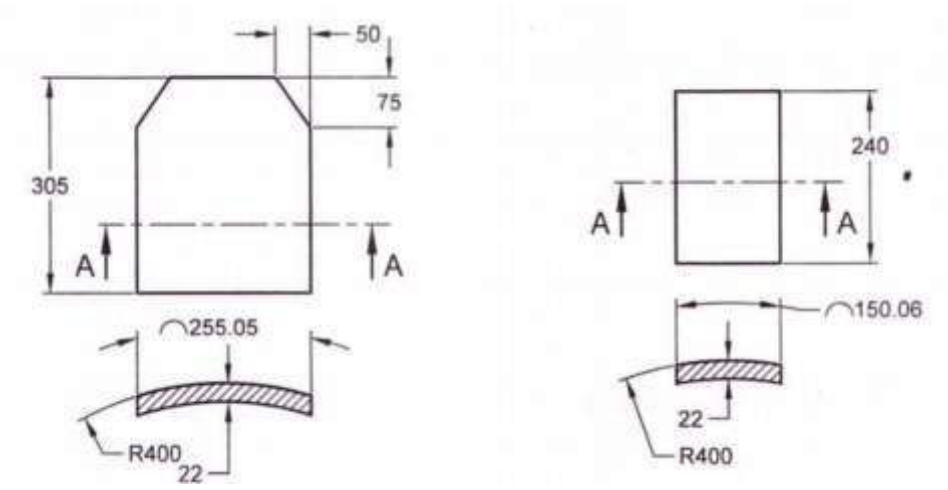

a) b)

Figure 1.Design example of front(a) and side plate(b) (medium size)

4. MATERIAL REQUIREMENTS

Differentiating their functions and performance characteristics, Hard Armor Plates (HAP) and Soft Armour Panels (SAP) in bulletproof jackets require different materials.

1. Materials in SAP:

1. Ultra high molecular weight polyethylene (UHMWPE):

The thermoplastic polyethylene subclass includes ultra-high-molecular-weight polyethylene (UHMWPE, UHMW). It is also referred to as high-modulus polyethylene (HMPE), and it is characterized by incredibly long chains that typically have a molecular mass of 3–7 million amu. Through the strengthening of intermolecular interactions, the longer chain helps to transfer the load to the polymer backbone more effectively [12] . As a result, this material is incredibly durable and has the highest impact strength of any thermoplastic currently in use.

It is highly resistant to corrosive chemicals, has extremely low moisture absorption and a very low coefficient of friction; is self-lubricating, and highly resistant to abrasion, in some forms being 15 times more resistant to abrasion than carbon steel.

UHMWPEfibers are commonly used in soft body armour and have contributed to vast improvements when compared with p-aramid fibers making them 40% stronger. For body armour, the fibers are aligned and bonded into sheets, which are then layered at various angles to give the resulting composite material strength in all directions[13]. Dyneema ® is the trade name of ultra-high molecular weight polyethylene (UHMWPE), manufactured exclusively by Netherland based DSM[14].Chemical formula of UHMWPE is given in Figure 2.

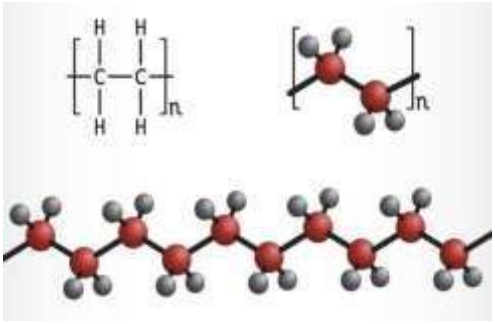

Figure 2.Chemical formula of UHMWPE

4.1.2. Kevlar:

Kevlar is a synthetic fiber known for its remarkable strength and heat resistance. It is a type of aramid fiber, which are long-chain synthetic polyamide molecules with strong bonds between individual molecules they are synthetic fibers like aramid. After spinning, it becomes very high-strength fibers. So it is considered one of the most popular fibers that are used in lead jackets. Kevlar fibers consist of long molecular chains made of PPTA [poly (p-phenyleneterephthalamide)] and the Strength property of Kevlar fibers lies in the multiple chemical bonds between their chains molecular as well as hydrogen bonds of

adjacent polymer chains[15]. Kevlar has strength, high stiffness, high tensile, and high modulus. They have low weight and density. It is unidirectionallywoven into textile materials and is extremely strong and lightweight, with resistance to corrosion and heat. It is used in vast applications such as aerospace engineering (such as the body of the aircraft), body armour, bulletproof vests, car brakes, and boats[16]. Chemical structure of Kevlar is given in Figure 3.

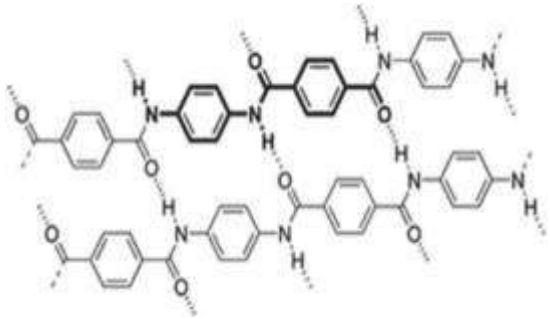

Figure 3.Chemical structure of Kevlar

4.1.3. Polycarbonate sheet:

In a bullet-resistant jacket, multiple layers of different materials are often used to create a composite structure. Polycarbonate sheets may be integrated into this layered structure to provide additional protection against certain types of ballistic threats. Polycarbonate material is used in bullet resistance jackets because of its good impact resistance. The use of polymers is increasing across many industries due to their low weight, low cost, and even straightforward manufacturing processes [17]. One of the main reasons polycarbonate might be used in bullet-resistant jackets is for its spall protection properties. Spall refers to the fragments or splinters that can break off from the back face of a material when it's struck by a projectile. Polycarbonate can help contain or minimize the spall created by the impact of a bullet, reducing the risk of secondary injuries to the wearer.Chemical structure of Polycarbonate sheet is given in Figure 4.

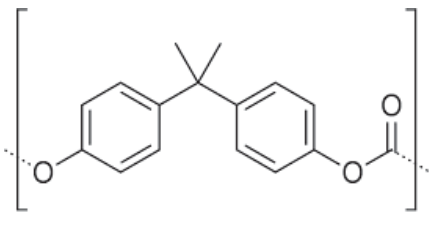

Figure 4.Repeating unit of Polycarbonate polymer

4.1.4. Polyurethane (pu) composite foam:

Polyurethane (PU) composite foam can be utilized in bullet-resistant jackets as part of the protective material system. However, it's important to note that while PU foam can provide cushioning and impact absorption, it's typically not used as the primary material for bullet resistance. Instead, PU foam is often incorporated into the design of bullet-resistant jackets for comfort, flexibility, and shock absorption[18]. Figure 5 representsPolyurethane (PU) composite foam.

Figure 5.Polyurethane (PU) composite foam

4.2. Materials in HAP:

Hard armour panels are made of steel, polyethylene, or ceramic materials. They are designed to survive impacts from projectiles with high velocity, such as rifle bullets. HAPs are also often referred to as Level III and Level IV panels to denote their degree of defence against ballistic threats.

4.2.1. Ceramic plates:

Many fields have been using ceramic materials for decades because of their high compressive strength, low density, and high hardness; even though they can be brittle. Silicon carbide is highly effective in stopping various types of ballistic threats, including rifle rounds and armour-piercing ammunition. When used in combination with other materials such as aramid fibers or UHMWPE, silicon carbide can provide multi-hit protection against high-velocity projectiles[18]. The projectile and the target configuration with dimensions in mm is given in figure 6.

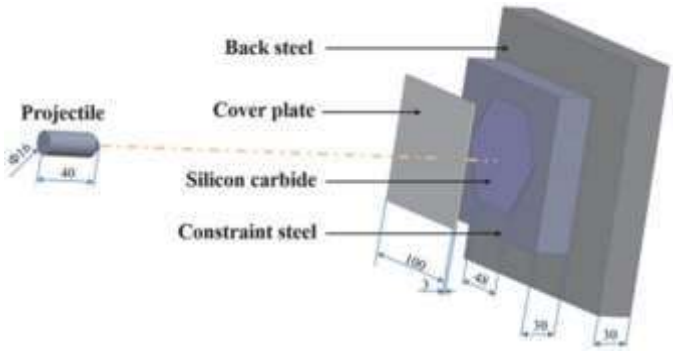

Figure 6. The projectile and the target configuration with dimensions in mm

4.2.2. Steel plates:

In order to save energy and improve mobility, it is crucial for defence systems against ballistic threats to use lightweight armour. Steels have a long history of use in armour applications due to their vast technological database and ability to be produced at a comparatively lower cost. They can also have a very broad range of mechanical properties[20]. However, due to its relatively high density, steel is not a good choice for use as lightweight armour. Because steel armour is heavier than other materials and does not provide the same level of protection in defence systems, researchers are looking into lighter alternatives- teel plates for hard armour panel is given in Figure 7.

Figure 7 Steel plates for hard armour panel

4.2.3. UHMWPE with ceramic plates:

UHMWPE has an exceptional strength-to-weight ratio, making it lightweight compared to traditional materials like steel. This property allows for the construction of lightweight hard armour panels that provide high levels of protection without significant added weight.UHMWPE has a low density, typically around 0.93 to 0.94 g/cm³, which contributes to the lightweight nature of hard armour panels[21] . This low density minimizes the overall weight burden on the wearer while maintaining high levels of protection. When combined with ceramic plates, UHMWPE is typically used as a backing material or as a composite layer to provide additional strength and support to the ceramic tiles. The combination of UHMWPE with ceramic plates offers a synergistic effect, with the ceramic providing high hardness and fracture resistance to defeat incoming projectiles, while the UHMWPE helps to absorb and disperse the impact energy[22]. UHMWPE with ceramic plates is shown in Figure 8.

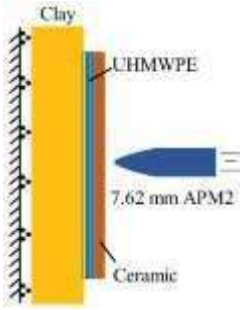

Figure 8. UHMWPE with ceramic plates

4.2.4. Backing face material clay:

The clay material used in bullet-resistant jackets is typically a type of ballistic clay, which is a specially formulated mixture designed to simulate human tissue for ballistic testing purposes. It usually consists of a combination of clay, water, and other additives to achieve the desired density and mechanical properties. It is used as backing material in ballistic tests. Backing material in ballistic tests is given in Figure 9.

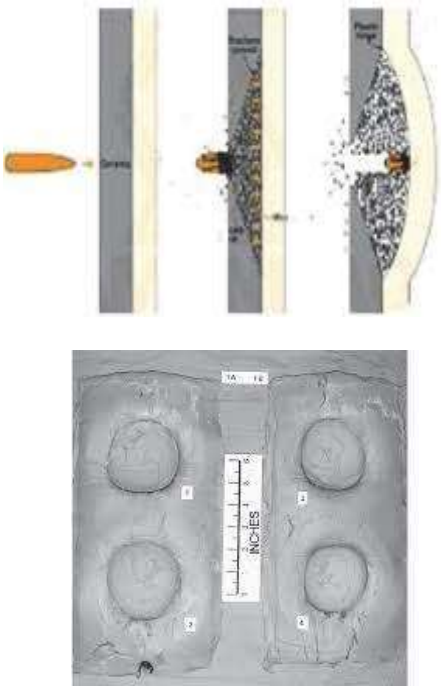

Figure 9. Backing material in ballistic tests

3. Physical requirements of non-ballistic components:

The outer-carrier fabric, hook and loop fasteners, belt loop, trauma pad, water-repellent SAP and HAP covers, webbings, buckles, and other items are examples of non-ballistic materials.

1. Outer carrier fabric:

The outer carrier fabric made of woven fabric, and the color/print can be customized according to the purchaser's needs.Nylon 66 is known for its high durability, which means it can withstand wear and tear over time, maintaining the integrity of the bullet-resistant jacket.It is relatively lightweight compared to other materials, which can make the bullet-resistant jacket more comfortable for the wearer. But the effectiveness of a bullet-resistant jacket depends not only on the outer carrier material but also on the ballistic panels and overall design of the jacket.This fabric is coated with a layer of polyurethane (PU)[23]. PU coating adds several beneficial properties to the fabric, including water resistance, abrasion resistance, flexibility, and improved durability. The fabric is designed to be heat sealable, meaning it can be bonded or sealed using heat. This feature allows manufacturers to create seams and join different pieces of fabric together without the need for stitching[24].PU coated nylon 66 fabric is shown in figure 10. Requirement of outer carrier fabric is shown in Table 4.

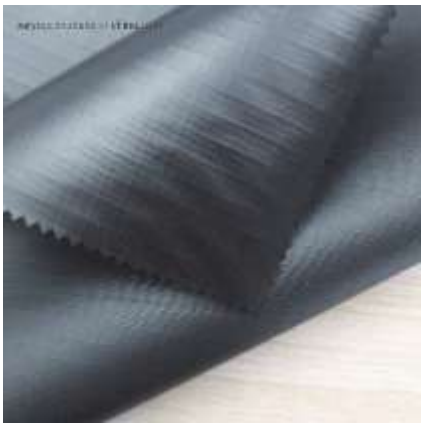

Figure 10.PU coated nylon 66 fabrics

Table 4.Requirement of Outer Carrier Fabric[25]

Sl. No	Test parameter	Requirements	Method of test, Refer to
(1)	(2)	(3)	(4)
i.	Mass, g/m', Max	160	IS 7016 (Part I)
ii.	Tensile strength, N, Min: a) Warp wise b) Weft wise	 1150 900	IS 7016 (Part II)
iii.	Tear strength, N, Min: a) Warp wise b) Weft wise	 160 140	IS 7016 (Part 3), Method A2, Trouser shaped test piece, Single tear method
iv.	Flame resistance test: a) Duration of flame (After flame time), s, Max b) Duration of afterglow, s, Max	 5 5	IS 11871, Method A
v.	Resistance to water penetration at hydrostatic pressure head of 30 cm water column height for 30 minutes	There shall be no water penetration	IS 7016 (Part 7)
vi.	Colour fastness rating to light (Change in colour on blue wool), Min	4	IS 2454

4.3.2. Hook and loop fastener:

All the clothing flaps of the jackets shall be provided with hook and loop fastener, so that it can be worn and taken off easily and quickly. Hook and loop is made to withstand the rigors of military use. It is frequently constructed from premium materials like nylon that are resistant to deterioration. Two parts make up the hook and loop system: hooks and loops. By holding onto the loops, the hooks form a dependable and safe fastening mechanism. Unintentional detachment during demanding activities is avoided by this design[26]. In certain military applications, the quiet operation and lack of noisy hook-and-loop separation sounds that could jeopardize operational security are critical requirements for hook-and-loop fasteners.

4.3.3. Pocket with flaps

The jacket shall be provided with minimum two externalpockets in outer carrier fabric tohouse two magazinesof self-carried assault rifle in each pocket. Two pocketsshall also be provided to accommodate one grenade ineach pocket.Pattern for pocket with flaps is given in figure 11.

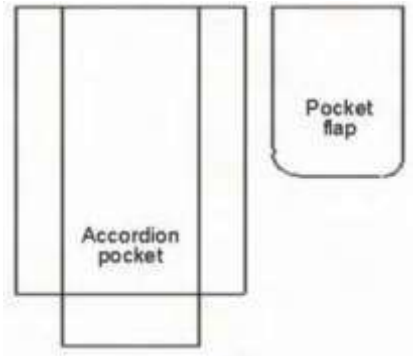

Figure 11. Pattern for pocket with flaps

4.3.4. Beltlkamarband

In order to properly secure the bulletproof jacket with the wearer's body around the waist and distribute the weight of the jacket across the waist and shoulders, an additional belt made of nylon material with a minimum width of 10 mm must be provided[27]. A hook and loop fastener for double jacket locking is included with the belt/kamarband.Strong and long-lasting nylon webbing is frequently used for belts and straps in outdoor and tactical equipment. It is appropriate for usage in harsh environments because of its strong tensile strength and abrasion resistance.

5. CONCLUDING REMARKS

Wide range of textile materials, each with special qualities and benefits that are used to make bulletproof jackets.Important factors to take into account when choosing the best material based on particular needs like flexibility, comfort, weight, and degree of protection through careful analysis and comparison. The variety of materials available in the field of ballistic protection is impressive, ranging from conventional materials like Kevlar® aramid fibers to advanced composites that incorporate ceramics and ultra-high-molecular-weight polyethylene (UHMWPE). It is crucial to strike a balance between material characteristics in order to maximize performance and satisfy the needs of practical applications by providing insights that can guide the development and selection of textile materials for bullet-resistant jackets in a variety of environments and scenarios of ballistic protection. Safer and more durable protective clothing for people in high-risk occupations and circumstances is continuing to push the boundaries of material science and ballistic engineering.

REFERENCES

1 I.G.Crouch, L.Arnold, A.Pierlot, H.Billon (2017) Fibres, textiles and protective apparel.In *The science of armour materials,* p. 269-330.Woodhead Publishing.

2 A.Kushwaha, P.Kushwaha, N.Nagayach (2018) Impact Analysis of bullet on different ballistic resistant material usingAnsys, *Int J Recent TechnolSci Manage, 12*(1), 33-42.

3 X.Chen, Y.Zhou (2016) Technical textiles for ballistic protection. In *Handbook of technical textiles,* p. 169-192. Woodhead Publishing.

4 Y.Regassa, G.Likeleh, UppalaR (2014) Modeling and simulation of bullet resistant composite body armor, *Inter. J. Res. Studies and Sci*, *1,* 39-44.

5 S.Kant, T.Joshi, R.Sharma (2020) In *Advances in Engineering Design: Select Proceedings of FLAME*, p. 375-386. Springer Singapore.

6 S.Mitra, L K Behera (2020) Enhancing the Effectiveness of Defence Indigenization: The Case of Bullet-Resistant Jackets. *Strategic Analysis*, *44*(6), 553-569.

7 R.F. A. Mahbub (2015) *Comfort and stab-resistant performance of body armour fabrics and female vests* (Doctoral dissertation, RMIT University).

8 T'extiles - Bullet Resisfant Jackets - Performanc.eRequirements IS 17051 : 2018 6-7.

9 Textiles - Bullet Resisfant Jackets - Performanc.eRequirements IS 17051 : 2018 3-5.

10 N. V. David, X L Gao, Zheng (2009) Ballistic Resistant Body Armor: Contemporary and Prospective Materials and Related Protection Mechanisms, *Applied Mechanics Reviews*, *62,* 050802.

11 T'extiles - Bullet Resisfant Jackets - Performanc.eRequirements IS 17051 : 2018 7

12 S.Cao, D.Zhou, Z.Wang, L.Chen (2024) An experimental study of the penetration resistance of UHMWPE laminates with limited thickness. *Thin-Walled Structures*, *196,* 111438.

13 M. K. Hazzard, S. Hallett, P. T. Curtis, L. Iannucci, R. S. Trask (2017) Effect of fibre orientation on the low velocity impact response of thin Dyneema® composite laminates. *International Journal of Impact Engineering*, *100,* 35-45.

15 S. Elsheikhi, K. Y. Benyounis (2022) Review of recent developments in polymer matrix composites with fiber reinforcements. Reference Module in Earth Systems and Environmental Sciences, Elsevier Ltd.

16 D. Kyriacos (2017) In *Brydson's Plastics Materials,* Butterworth-Heinemann, p.457-485.

17 T. Fan, S. S. Xue, Zhu, W. B.Zhang, Y. Y., Li, Y. Q., Z. K. Chen, and S. Y Fu (2022) Multifunctional polyurethane composite foam with outstanding anti-impact capacity for soft body armors, *ACS Applied Materials & Interfaces*, *14*(11), 13778-13789.

[18] D. Luo, Y. Wang, F. Wang, H. Cheng, B. Zhang, Y. Zhu (2020) The influence of metal cover plates on ballistic performance of silicon carbide subjected to large-scale tungsten projectile. *Materials & Design*, *191*, 108659.

19 M. Übeyli, R. O. Yıldırım, B. Ögel (2007) On the comparison of the ballistic performance of steel and laminated compositearmors. *Materials & design*, *28*(4),1257-1262.

20 T. Demir, M. Übeyli, R. O.Yıldırım (2009) Effect of hardness on the ballistic impact behavior of high-strength steels against 7.62-mm armor piercing projectiles. *Journal of Materials Engineering and Performance*, *18,* 145-153.

21 J. Lin, Y. Li, S. Liu, H. Fan (2023) Numerical investigation of the high-velocity impact performance of body armor panels. *Thin-Walled Structures*, *189,*110909.

22 Y. Yang, X. Chen (2017) Investigation of failure modes and influence on ballistic performance of Ultra-High Molecular Weight Polyethylene (UHMWPE) uni-directional laminate for hybrid design. *Composite Structures*, *174*, 233-243.

23 A. S Koohestani, A. Bashari (2020) Advanced bullet-proof and stab-and spike-resistant textiles. In *Advances in Functional and Protective Textiles,* p.261-289. Woodhead Publishing.

24 S. Kanesalingam, R. Nayak, L. Wang, R. Padhye, L. Arnold (2019) Stab and puncture resistance of silica-coated Kevlar–wool and Kevlar–wool–nylon fabrics in quasistatic conditions. *Textile research journal*, *89*(11), 2219-2235.

25 T'extiles - Bullet Resisfant Jackets - Performance Requirements IS 17051 : 2018 4

26 E. A.S.K. Fernando, S. M. N. Niles, A. N. Morrison, P. Pranavan, I. U. Godakanda, M. M. Mubarak (2015) Design of a bullet-proof vest using shear thickening fluid, *International journal of advanced scientific and technical research*, *1*(5), 434-444.

27 M.A.Kislov, M.Chauhan, S.V.Leonov, Y.I.Pigolkin (2022) Forensic medical characteristics of firearm exit wounds in cases with armour protection. *Legal Medicine*, *54*, 102002.

IZVOD

ZAŠTITA OD BALISTIČKIH PRETNJI: ISTRAŽIVANJE TEKSTILNIH MATERIJALA ZA GORNJU ODEĆU OTPORNU NA METKE

Jakne otporne na metke su jedna od inovacija koje pokazuju kako tekstilni inženjering i tehnologija mogu da rade zajedno da zaštite ljude od balističkih pretnji. Da bi se poboljšali zaštitni kvaliteti neprobojnih jakni, neophodno je razumeti širok spektar tekstilnih materijala koji se koriste u njima. Ova studija ima za cilj da razjasni složenu interakciju između zaštite, fleksibilnosti i udobnosti koja je svojstvena ovim vrstama odeće kroz detaljnu analizu različitih vlakana, tkanina i kompozita, od kojih svaki nudi jedinstvene karakteristike koje doprinose ukupnoj efikasnosti ovih vrsta odeće. odevnih predmeta. Određeni su važni faktori koje treba uzeti u obzir pri izboru najboljeg materijala na osnovu posebnih potreba kao što su fleksibilnost, udobnost, težina i stepen zaštite kroz pažljivu analizu i poređenje. Ovo istraživanje će pružiti vredne uvide istraživačima, proizvođačima i potrošačima, podstičući napredak u dizajnu zaštitne odeće i promovišući informisano donošenje odluka u oblasti lične bezbednosti.

Ključne reči: *jakna otporna na metke, zaštitna odeća, stepen zaštite, fleksibilnost, udobnost, bezbednost*

Naučni rad

Rad primljen: 28.04.2024.

Rad prihvaćen: 9.06.2024.

The ORCID Id of the author:

Subrata Das: https://orcid.org/0000-0002-7118-5490

Guadalupe Canosa[1], Carlos A. Giudice[2], Paula V. Alfieri[3]*

[1,2,3] Facultad Regional La Plata, Universidad Tecnológica Nacional 60 y 124, (1923) Berisso, Argentina, Tel: +542214124387

Scientific Paper
ISSN 0351-9465, E-ISSN 2466-2585
https://doi.org/10.62638/ZasMat1167

Zastita Materijala 66 (1)
15–21 (2025)

Antifungal Coating for Wood Protection

ABSTRACT

Antifungal hydro-repellent coatings were formulated for Pinus ponderosa panels' protection. The fomulated coatings were based on a hydroxylated acrylic resin chemically modified with n-octyltriethoxysilane (R8), n-octadecyltriethoxysilane (R18), and some mixtures of them as hybrid film-forming material. Diatomaceous silica was used as a pigment. The share of silane was 20% higher than the stoichiometric ratio to allow its interaction with cellulose hydroxyl groups (-OH).

Results indicated that the best antifungal efficiency was reached with coating formulated with 70R8/30R18 ratio due to the chemical reaction of cellulose hydroxyl groups (causing its blocking) and the physical barrier created by the degree of compaction of the film itself. Moreover, Biodeterioration of the film caused by the specific fungi was not observed, whit confirms the durability effect of the treatment. The protection mechanism is related to the water repellency and the blocking of the substrate.

Keywords: *Antifungal coating, Wood, Chemically modified acrylic resin, Silane, Water repellence, Decay resistance*

1. INTRODUCTION

The protective treatments of wood (impregnation and/or application of coatings) are applied, in many cases, to prevent its decay by water repellency of wood; however, solely the water repellency is not sufficient to prevent biodeterioration of wood.

An efficiency protective method that is being used against biodeterioration is wood chemical modification. This is based on the reaction between the cellulose hydroxyl groups with active protective products to improve dimensional stability, decay resistance, flame retardance and UV deterioration. The mentioned modification prevents biodeterioration because with only a random inclusion of a substituent in a hydroxyl group of any glycosidic ring prevents its enzymatic attack by the non-formation of the enzyme-substrate complex [1-6].

It is known that curing of the silanes involves hydrolysis and condensation reactions of the metal-organic precursors. When wood is treated with silanes, the chemical modification takes place which involves condensation reaction of the hydroxyl groups of cellulose (C-OH) with hydrolyzed silanes (≡Si-OH) forming ≡Si-O-C≡ bonds [7-16].

The aim of this paper was to formulate reactive hybrid coatings based on a hydroxylated acrylic resin and silanes mixture for the *Pinus ponderosa* panels protection, by proper combination of the main properties of wood in service: decay resistance, water repellency and water vapor permeability.

EXPERIMENTAL

Pigmented coatings were formulated with a hydroxylated acrylic resin chemically modified with n-octyltriethoxysilane, n-octadecyltriethoxysilane and some mixtures of them. The amount of silane was 20% upper to the stoichiometric ratio to allow its interaction with cellulose hydroxyl groups (-OH). As extender was used diatomaceous silica to improve the hardness and adhesion of the films and to give opacity to coatings.

Diatomaceous silica was dispersed in the film-forming material in form of the solution of hydroxylated acrylic resin to achieve a concentration

* Corresponding author: Guadalupe Canosa
E-mail: guadalupecanosa@yahoo.com.ar
Paper received: 20.05.2024.
Paper accepted: 9.06.2024.
Papir is available on the website: www.idk.org.rs/journal

of approximately 20% v/v of the dry film; the process was conducted in a high-speed disperser for 25-30 minutes (7-8 NS of Hegman Scale). Silanes and silanes mixtures were used in its original liquid state. The solvent mixture was formulated with ethanol / ethylene glycol acetate, 1/2 v/v and was used to adjust the solids content of all coatings to 70% v/v.

Solid wood panels made of *Pinus ponderosa*, kept in laboratory environment (25 ºC y 40%RH) were coated with brush; the dry film thickness (measured by ultrasound PosiTector 200B) ranged from 74-81µm. In all cases, and to ensure the total drying and curing of the films (hydrolysis and condensation reactions involved in the sol-gel process), the specimens were kept in the controlled laboratory conditions for ten days before start laboratory tests.

LABORATORY TESTS

The following tests were conducted after curing of the coatings:

- ***Contact angle*** *(Ø).* Ø was measured by the sessile drop technique, using a microscope and a suitable source of illumination, with a CCD camera coupled to ocular (in triplicate). Drop Shape Analysis was made using the ImageJ software (NIH). Contact angle measurements were conducted on uncoated and coated wood panel samples.

- **Water Repellency Effectiveness** (WRE)**.** The size of the panels was 50x100x300mm; efficiency was determined under guidelines of ASTM D5401-03 (2014). The WRE values were evaluated by eight immersion cycles (in triplicate).

- ***Capillary water absorption*** (w)**.** The specimen sizes were 80x80x40mm (radial x tangential x axial). The test was carried out according to guidelines of ISO15148:2002 (in triplicate).

- ***Water vapor permeability.*** This test was performed on free films of coatings, under the guidelines of DIN52615:1987-11 (until the constant weight of samples in 24 hour intervals). DIN18558:1985-01 considered coating as water vapor permeable when Sd value is lower than 2m; for higher quality level should be Sd lower than 0.10m. Firstly, it was calculated the flux density of water vapor diffusion (DDV) in $g.m^{-2}.day^{-1}$ and then, the air thickness equivalent to the diffusion of water vapor (Sd, air layer that has the same resistance to the water vapor diffusion that the paint film thickness considered). For this purpose, it was used the expression Sd = 20/DDV.

- ***Fungal resistance.*** The specimen sizes were 20x20x20mm. The coated specimens of *Pinus ponderosa* were exposed, under laboratory conditions, to the action of *Trametes versicolor* and *Chaetomium globosum*, following general guidelines of ASTM D2017-05 (2014) and to *Aspergillus niger,* following guidelines of ASTM D4300-01 (2021).

RESULTS AND DISCUSION

- Contact angle. All coated panels had higher contact angle than untreated wood (ø = 50°), Table 1. Furthermore, Ø increased proportionally to the increase of R18 in coating composition. This would be based on presence of long hydrocarbon chain in R18 linked to the –OH of cellulose and acrylic resin giving hydrophobicity to the system. These findings are consistent with those reported by Chae Eun Pyo and Jeong Ho Chang [17], who reported a fourfold increase in contact angles for surfaces modified with C18 compared to unmodified surfaces.

Table 1. Contact angle

Alkoxide		Contact angle	Hidrofobicity
n-octyltriethoxysilane (R8)		60 ± 3	Low
n-octadecyltriethoxysilane (R18)		142 ± 2	Excellent
R8/R18, ratio v/v	90/10	70 ± 3	Low
	80/20	81 ± 5	Low
	70/30	91 ± 4	Regular
	60/40	95 ± 4	Regular
	50/50	98 ± 2	Regular
	40/60	100 ± 6	Regular
	30/70	108 ± 3	Regular
	20/80	113 ± 3	Satisfactory
	10/90	130 ± 5	Excellent
Reference		50 ± 2	Low

- Water repellent efficiency. Water repellent efficiency of the coated panels was analyzed by the coefficient WRE, Figure 1. The WRE values for coated wood were similar for all immersion cycles; this could be on the consequence of the high stability that the coatings have when are exposed to moisture-drying cycles.

The results show that the coating modified only with R8, although would form a compact dense coating, would not prevent the ingress of liquid water because the lack of high water repellency; the improved performance in terms of water repellence, in comparison to the untreated wood, can be explained by the chemical modification of the wood cell walls.

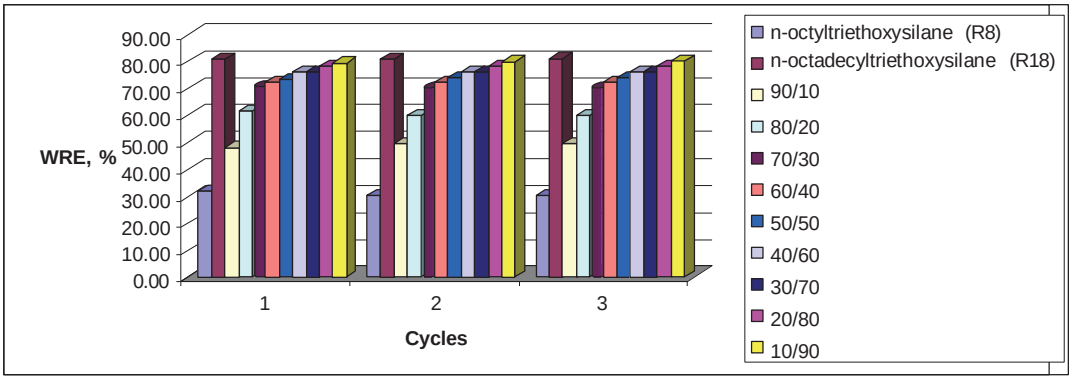

Figure 1. Water Repellence, WRE %

Meanwhile, the coating modified only with R18 also formed a reactive coating but hydrophobic and discontinuous because of the steric hindrance; this gives the best water repellency (WRE = 80.75 ± 0.16%) compared to the untreated wood and even to the treated only with R8 (WRE = 30.71 ± 0, 34%).

Regarding coatings formulated with mixtures of silanes, the results indicate that the increased level of R18 led to increased WRE, Figure 1; WRE values increase strongly with the increasing of R18 up to 60/40 R8/R18 ratio. This can be explained by the fact that while the packing density is lower (steric effect between R8 and R18 groups) the hydrophobicity of system is optimal. This aligns with the findings of Chen et al. [18], who emphasized the significance of alkyl chain length in establishing a hydrophobic network.

- Capillary water absorption. W coefficient decreased with increasing of R18 in binder, Figure 2; this probably the consequence of the film packing density and the chemical modification of wood. The coating that includes only R8 as cobinder forms a dense and compact film, but it was not sufficient to prevent the ingress of water; despite, the ingress of water was lower than for the untreated wood (2.30 ± 0.13 and 2.41 ± 0.12 respectively), due to the physical barrier which prevent capillary uptake.

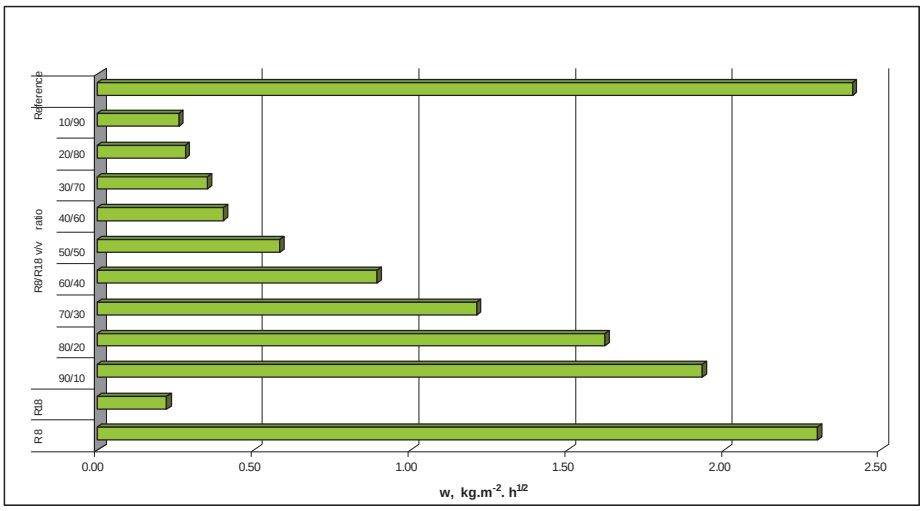

Figure 2. Water Repellence, w coefficient

Meanwhile, wood protected with coating that includes only R18 as cobinder also form physical barrier but with strongly hydrophobic characteristics; based on the best value of w (0.22 ± 0 01) [18].

For intermediate values of R8/R18, acceptable w values were obtained between 50/50 and 0/100 R8/R18 ratios (0.58 and 0.22 respectively). This is due to the achieved balance between water repellency and loss of fibers capillarity, resulting from the shutter of the -OH with the silanes employed.

- Water vapor permeability. The recorded Sd values were between 0.07 and 0.14 m; values that exceed 0.10 m correspond to R8 and to 90/10 R8/R18 ratio, Figure 3. What could have happened is that the long chains of R18, as their ratio increases, made the coating film more porous, decreasing the Sd up to the film with 60/40 ratio; after which water repellence begun to have more preponderance, and the Sd increased progressively. This agrees with Josip Mikulčić, Vlatka Jirouš-Rajković [19] who reported that for non-porous materials, there is no theoretical difference between the penetration of liquids and water vapor, but due to the porous structure of the coating, water can also move by capillary flow, which can affect the differences in water and water vapor permeability [20]. It is known that uptake of moisture in liquid form occurs both by capillary sorption and moisture diffusion and consequently is strongly dependent on the structure of the wood [21].

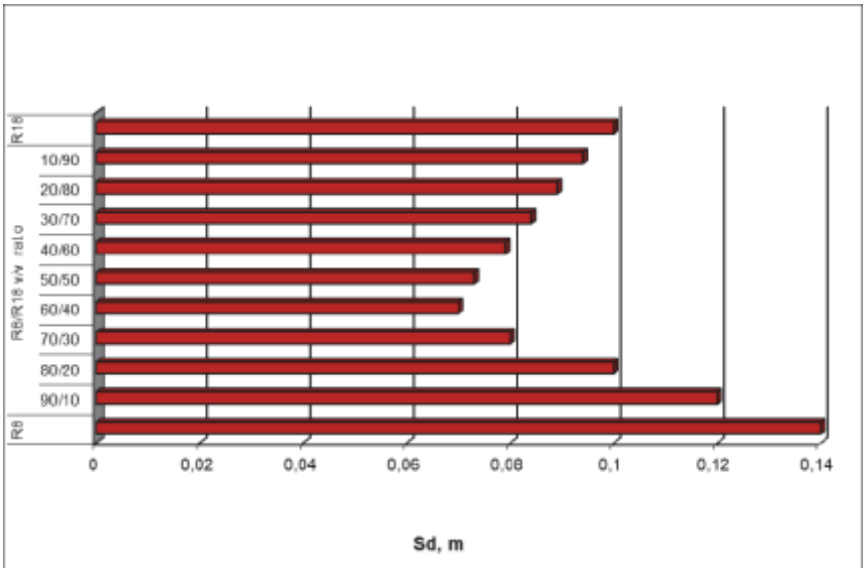

Figure 3. Water vapor permeability, Sd

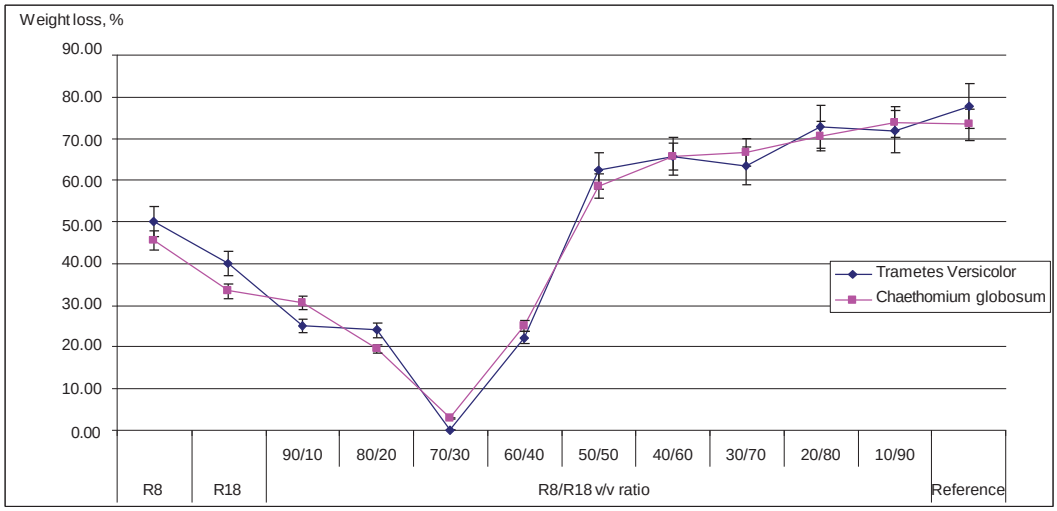

Figure 4. Decay resistance, Weight loss of specimens exposed to fungi

After analyzing the steric effect, it can be concluded that all films enabled water vapor permeability and natural wood movement, thus preventing loss of film adhesion [22].

- Fungal resistance. The analysis of results indicates that for the coating film with only R8 in its composition two effects occurred: high mass loss, but fungal vegetative body growth was not observed, Figure 4.

Moreover, in films with R8/R18 mixtures the following was observed: (i) reduced mass loss, with maximum for 70/30 R8/R18 ratio, where the mass loss becomes zero; (ii) no growth of fungal vegetative body; (iii) increased mass loss with the growth of the fungal vegetative body on the surface.

Finally, for the coating film wit only R18 it was observed: (i) high mass loss and (ii) growth of the fungal vegetative body.

The best antifungal efficiency was achieved with the coating formulated with 70/30 R8/R18 ratio, which can be explained by the achieved suitable degree of compatibility between the blocking of the cellulose (by chemical reaction with OH groups of coating), the physical barrier of film created by the compaction of the film (mainly conferred by R8 silane) and the hydrophobicity (primarily provided by the R18 silane). The protection mechanism based on the water repellency and the blocking of the substrate bonds was reported in previous works by many authors: In García et al. [23], the antifungal efficacy of acrylic varnishes on pine wood was studied, revealing that acrylic coatings form a protective film that prevents the entry of moisture and oxygen, both necessary for fungal growth. Miklečić and Jirouš-Rajković [19] also highlight the effectiveness of finishes in protecting wood against liquid water and water vapor. Finishes create an impermeable barrier that prevents moisture absorption, crucial for preventing fungal growth.

Regarding exposure to *Aspergillus niger*, there was no growth recorded on any film surface or in the surrounding encirclement, Figure 5. This result confirmes the durability of the treatment.

In summary, comparing findings in the literature, it could be observe that whether Hybrid (Cutz et al. [24]), Commercial (Jusic et al. [25]), Natural (Arminger et al. [26]), Acrylics (García et al. [23]), or Water-based Acrylics (Custódio et al. [27]) coatings, the aim is to achieve an Impermeable finish coat (Miklečić and Jirouš-Rajković [19]) and the excellent adhesion (Kúdela and Liptáková [28]), leading to an efficient physical and hydrophobic barrier that prevents the ingress and development of wood-degrading microorganisms. Each of these studies highlights different aspects and mechanisms contributing to the antifungal protection of coatings, from the incorporation of active agents like titanium dioxide, the use of chemical biocides, to the formation of physical barriers preventing moisture penetration.

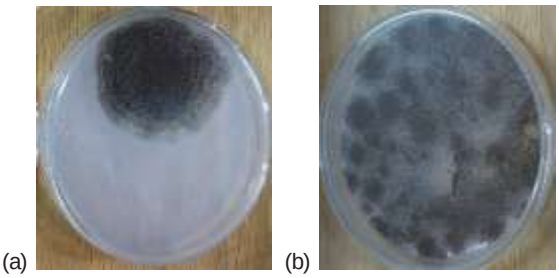

Figure 5. Decay resistance, Inhibition of Aspergillus níger growth (a) respect to control (b)

CONCLUSIONS

- The best antifungal efficiency was achieved with the coating formulated for the 70/30 R8/R18 ratio, which can be explained by achieved compatibility between the blocking of the cellulose (by chemical reaction of its -OH groups with coating components), the physical barrier created by the compaction of the film (mainly confirmed by R8 silane) and the hydrophobicity (primarily provided by R18 silane). This means that this treatment blocks all possible mechanisms of fungal attack.
- The values of Sd showed that the adhesion of the coating films to wood panels was very good in the range of 70/30 R8/R18 to 40/60 R8/R18 ratios. In this case the antifungal performance was ensured by physical blocking of the coating film.
- The water repellence, another important factor of biodeterioration prevention, increased with the level of R18 in binder. This shows that the water repellency of film is affected by the hydrophobicity of the co-binder employed, with positive impact of the long hydrocarbon chains in the composition to the water repellence.
- The results of eexposure of films to *Aspergillus niger,* allow us to conclude that formulated coatings resists to common environmental fungi action. This conclusion is important knowing that these fungi regulate the humidity of the colonized material.

REFERENCES

1 C.Brischke, G.Alfredsen (2020) Wood-water relationships and their role for wood susceptibility to fungal decay, Appl Microbiol Biotechnol., 104, 3781-3795. https://doi.org/10.1007/s00253-020-10479-1

2 B.Goodell, J.E.Winandy, J.J.Morrell (2020) Fungal Degradation of Wood: Emerging Data, New Insights and Changing Perceptions, Coatings, 10, 1210. https://doi.org/10.3390/coatings10121210

3 S.L.Zelinka, G.T.Kirker, A.B.Bishell, S.V.Glass (2020) Effects of Wood Moisture Content and the Level of Acetylation on Brown Rot, Decay. Forests., 11, 299. https://doi.org/10.3390/f11030299

4 H.Giacomelli Ribeiro, S.T. Van Der Sand (2024) Exploring the Trends in Actinobacteria as Biological Control Agents of Phytopathogenic Fungi: A (Mini)-Review, Indian J. Microbiol, 64, 70–81. https://doi.org/10.1007/s12088-023-01166-6

5 A.Chelaghema, N.Durand, A.Servent et al (2022) Antifungal and antimycotoxic activities of 3 essential oils against 3 mycotoxinogenic fungi, Arch Microbiol, 204, 1–16. https://doi.org/10.1007/s00203-022-03115-1

6 Z.Vidholdová, F.Kačík, L.Reinprecht, V.Kučerová, J.Luptáková (2022) Changes in Chemical Structure of Thermally Modified Spruce Wood Due to Decaying Fungi. J. Fungi., 8, 739. https://doi.org/10.3390/jof8070739

7 V.Kamperidou, I.Ratajczak, W.Perdoch, B.Mazela (2022) Impact of thermal modification combined with silicon compounds treatment on wood structure, Wood Res., 67(5), 773-784. https://doi.org/10.37763/wr.1336-4561/67.5.773784

8 M.Broda (2018) Biological effectiveness of archaeological oak wood treated with methyltrimethoxysilane and PEG against Brown-rot fungi and moulds, Int. Biodeterior. Biodegrad., 134, 110-116. https://doi.org/10.1016/j.ibiod.2018.09.001

9 M.Broda, N.Plaza (2023) Durability of model degraded wood treated with organosilicon compounds against fungal decay, Int. Biodeterior. Biodegrad., 178,105562. https://doi.org/10.1016/j.ibiod.2022.105562

10 S.Donath, H.Militz, C. Mai (2006) Creating water-repellent effects on wood by treatment with silanes, Holzforschung, 60 (1), 40-46. https://doi.org/10.1515/HF.2006.008

11 V.Kamperidou (2019) The Biological Durability of Thermally- and Chemically-Modified Black Pine and Poplar Wood Against Basidiomycetes and Mold Action, Forests., 10, 1111. https://doi.org/10.3390/f10121111

12 M.Odalanowska, G.Cofta, M.Woźniak, I.Ratajczak, T.Rydzkowski, S.Borysiak (2022) Bioactive Propolis-Silane System as Antifungal Agent in Lignocellulosic-Polymer Composites, Materials., 15, 3435. https://doi.org/10.3390/ma15103435

13 T.Kanokwijitsilp, P.Traiperm, T.Osotchan, T.Srikhirin (2016) Development of abrasion resistance SiO2 nanocomposite coating for teak wood. Prog. Org. Coating, 93, 118-126.https://doi.org/10.1016/j.porgcoat.2015.12.004

14 E.E.Soytürk, S.N.Kartal, M.S.Onses, et al. (2023) Preliminary evaluation of polydimethylsiloxane and hydrophobic silica nanoparticles to improve water repellency and boron leachability in wood. Eur. J. Wood Prod., 81, 89-98. https://doi.org/10.1007/s00107-022-01883-7

15 G.G.Goffredo, et al. (2017) Nanotechnology on wood: The effect of photocatalytic nanocoatings against Aspergillus niger. Journal of Cultural Heritage, 27, 125-136. https://doi.org/10.1016/j.culher.2017.04.006

16 F.Foadi, N.Celik, A.Esidir, M.S.Onses (2024) Roughness-dependent hydrophobicity of polydimethylsiloxane grafted titanium thin films, Surface and Coatings Technology, 483,130749, https://doi.org/10.1016/j.surfcoat.2024.130749

17 C.E.Pyo, J.H.Chang (2021) Hydrophobic Mesoporous Silica Particles Modified With Nonfluorinated Alkyl Silanes, ACS Omega, 6 (24), 16100-16109, https://doi.org/10.1021/acsomega.1c01981

18 W.Chen et al. (2021) Surface hydrophobicity: effect of alkyl chain length and network homogeneity, Front. Chem. Sci. Eng., 15(1), 90–98, https://doi.org/10.1007/s11705-020-2003-0

19 J.Miklečić, V.Jirouš-Rajković (2021) Effectiveness of finishes in protecting wood from liquid water and water vapor, Journal of Building Engineering, 43, 102621,ISSN 2352-7102, https://doi.org/10.1016/j.jobe.2021.102621

20 O.Gezici-Koç et al. (2019) Moisture content of the coating determines the water permeability as measured by 1D magnetic resonance imaging, Prog. Org. Coating, 130, 114-123, https://doi.org/10.1016/j.porgcoat.2019.01.043

21 M.de Meijer (2002) Comparison between laboratory water permeability tests and wood moisture content of full-scale window frames, Surf. Coating. Int. B Coating. Trans., 85, 131-137, https://doi.org/10.1007/BF02699753

22 J.Kúdela, E.Liptáková (2006) Adhesion of coating materials to wood. Journal of Adhesion Science and Technology, 20(8), 875-895. https://doi.org/10.1163/156856106777638725

23 M. García, A. Dominguez, A. Escobar, C. Valencia (2019). Estudio de la eficacia antifúngica de barnices acrílicos en madera de pino. Revista Chapingo Serie Ciencias Forestales y del Ambiente, 25(2), 175-184. https://doi.org/10.5154/r.rchscfa.2018.09.070

24 L.Cutz, U.Tiringer, W.de Jong, A.Mol (2023) Hybrid sol-gel coatings for reducing wettability and storage degradation of biomass pellets. Materials Chemistry and Physics, 304,127861, https://doi.org/10.1016/j.matchemphys.2023.127861

25 J.Jusic, S.Tamantini, M.Romagnoli, V.Vinciguerra, E.Di Mattia, F.Zikeli, M.Cavalera, G.Scarascia Mugnozza (2021) Improving sustainability in wood

coating: testing lignin and cellulose nanocrystals as additives to commercial acrylic wood coatings for bio-building. iForest 14, 499-507. http://doi.org/10.3832/ifor3782-014

[26] B.Arminger, J.Jaxel, M.Bacher, W.Gindl-Altmutter, C.Hansmann (2020) On the drying behavior of natural oils used for solid wood finishing. Progress in Organic Coatings, 148, 105831 https://doi.org/10.1016/j.porgcoat.2020.105831

[27] J.E.P.Custódio (2006) Waterborne acrylic varnishes durability on wood surfaces for exterior exposure. Progress in Organic Coatings, 56, 59–67. https://doi.org/10.1016/j.porgcoat.2006.02.008

IZVOD

ANTIFUGALNI LAK ZA ZAŠTITU DRVETA

Antifungalni hidro-repelentni premazi su formulisani za zaštitu panela Pinus ponderosa. Formulisani premazi su zasnovani na hidroksilovanoj akrilnoj smoli hemijski modifikovanoj sa n-oktiltrietoksisilanom (R8), n-oktadeciltrietoksisilanom (R18) i nekim njihovim smešama kao hibridnim materijalom za formiranje filma. Kao pigment je korišćen dijatomejski silicijum. Udeo silana je bio 20% veći od stehiometrijskog odnosa da bi se omogućila njegova interakcija sa hidroksilnim grupama celuloze (-OH).

Rezultati su pokazali da je najbolja antifungalna efikasnost postignuta sa premazom formulisanim u odnosu 70R8/30R18 usled hemijske reakcije celuloznih hidroksilnih grupa (koje izaziva njeno blokiranje) i fizičke barijere stvorene stepenom zbijenosti samog filma. Takođe, nije primećeno biopropadanje filma izazvano specifičnim gljivama, što potvrđuje efekat dugotrajnosti tretmana. Mehanizam zaštite je vezan za vodoodbojnost i blokiranje podloge.

Ključne reči: *premaz protiv gljivica, drvo, hemijski modifikovana akrilna smola, silan, vodoodbojnost, otpornost na propadanje*

Naučni rad

Rad primljen: 20.05.2024.

Rad prihvaćen: 09.06.2024

The ORCID Ids of all the authors are as follows:
Guadalupe Canosa: https://orcid.org/0000-0001-6399-0193,
Carlos A. Giudice: https://orcid.org/0000-0003-3604-3347,
Paula V. Alfieri: https://orcid.org/0000-0001-9640-3143

Mena Khaleel Tweek[1],
Shaymaa Abbas Abdulsada[2*]

[1, 2] *Department of Materials Engineering, Faculty of Engineering, University of Kufa, Iraq*

Scientific paper
ISSN 0351-9465, E-ISSN 2466-2585
https://doi.org/10.62638/ZasMat1105

Zastita Materijala 66 (1)
22–29 (2025)

Synergistic effect of inhibitors on Corrosion of Reinforced Concrete Structures According to ACI Standards

ABSTRACT

The application of low-cost, low-toxic corrosion inhibitors lowers the rate of corrosion of reinforced concrete in a salt-aqueous medium. The purpose of this work is to compare an innovative, supposedly environmentally benign inhibitor derived from fruit waste (pomegranate peels extract (PPE)) with sodium benzoate, an organic inhibitor. The inhibitors were introduced to the concrete mixture at quantities of two and four percent by weight of cement according to ACI standards. The maximum extraction yield in terms of entire phenolic content was obtained by using an aqueous solvent and the Soxlet technique. The efficiency of corrosion inhibitors in preventing corrosion was investigated using compressive strength and optical microscopy methods. PPE forms an organic layer made up of several components in a variety of salt environments, providing both a chemical antioxidant activity and a mixed-type corrosion inhibitor, most likely due to the polyphenol concentrations.

Keywords: *Green inhibitor, Sodium benzoate, Reinforced concrete, Compressive strength, Optical microscopy.*

1. INTRODUCTION

Reinforcement corrosion is the main cause of early collapse of reinforced concrete structures worldwide, and it attracted a lot of attention at the end of the 1980s and the start of the 1990s. [1]. Steel embedded in concrete is often in a passive state against corrosion due to a thin layer of iron oxide that forms on the steel's surface and remains stable in the extremely alkaline environment of the concrete. There are two primary methods for depassivation, which is the process of removing the protective layer that shields steel from corrosion: using chlorides (seawater, deicing salt, unwashed sea sand, admixtures, etc.) to attack the steel, or carbonating the cover concrete by reacting with carbon dioxide to reduce the alkalinity of the concrete. The reinforced concrete structure may fully degenerate electrochemically once corrosion has commenced. Here on the steel surface are the anodic and cathodic areas. [2–6]. During the carbonation process, carbon dioxide seeps into the concrete and reacts with hydroxides. This results in the production of carbonates and water, which lower pH and harm the passivation layer on the steel. [7–10]. CaO and SiO_2 make up the majority of the oxide combination that is dry Portland cement. Calcium oxide hydrates to produce portlandite [$Ca(OH)_2$] when combined with water. This compound can then react with carbon dioxide to form $CaCO_3$. Concrete that is porous is sealed by $CaCO_3$, which has a larger volume than $Ca(OH)_2$ [11]. This dangerous damage could be caused by a decrease in the reinforcing section, the formation of fractures in the cement covering, or a lack of adhesion between the metallic substance and the concrete. The significant impact of chloride ions in the environment is one significant element limiting the longevity of concrete constructions and complicating the work of civil engineers. As seen in Fig. 1, the chloride ions catalyse the dissolving reaction, causing fast disintegration, chipping, and cracking by removing the protective layer Fe_2O_3 [12].

The methods for preventing corrosion that have been developed include cathodic protection, coat-

* Corresponding author: Shaymaa Abbas Abdulsada
E-mail: shaymaa.radhi@uokufa.edu.iq
Paper received: 25. 05. 2024.
Paper accepted: 4. 06. 2024.
Papir is available on the website: www.idk.org.rs/journal

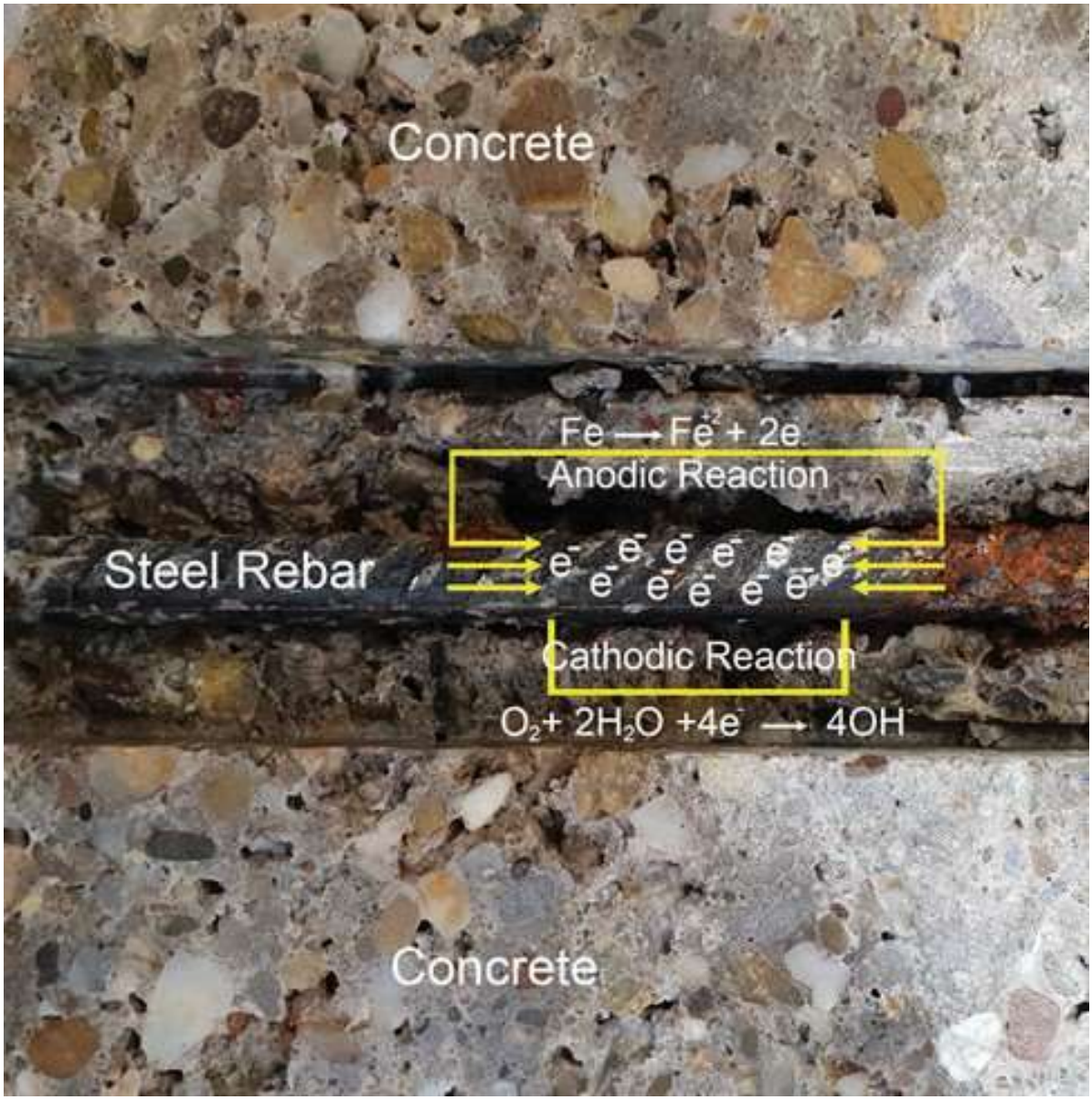

Figure 1 Mechanism of corrosion of reinforced concrete [3].

ings, and corrosion inhibitors. Among all of them, using inhibitors to reinforce steel became standard procedure [7]. Corrosion inhibitors are chemical substances that change the surface state of reinforced steel when added to the concrete mix in small amounts, which slows or stops the rate of corrosion [8]. Using inhibitors was the most effective way to deal with this harmful event. Corrosion inhibitors can be grouped according to the corrosion protection method, environment, layer of protection, type of structure and composition, and physicochemical properties. While total inhibition of corrosion is practically unachievable, inhibitors can be used to limit the rate and abrasiveness of the process. Environmental constraints frequently result in the substitution of less harmful compounds for inorganic inhibitors [9]. The most ecologically friendly method of corrosion inhibitor is green technology, which is based on the usage of plants and biodegradable in nature [10].

The main objective of this research is to report an experimental study that monitors and evaluates corrosion processes in the surface of steel rebar used in reinforced concrete using optical microscopy and compressive strength—a green inhibitor and an organic inhibitor for comparison.

2. EXPERIMENTAL PART

1. Materials used

The Portland cement sulphate-resistant cement utilised in this work was produced by the Karbala cement factory, and the cement's physical and chemical test results were in line with the Iraqi IQS No. 5- 2019 [13] for class 42.5 N cement. Coarse aggregate is defined as river gravel that meets the reapproved Iraqi criteria IQS 45–84 and has a grade of 5–19 mm [14]. Sand from a najaf quarry (grading area no. 2) that complies with Iraqi specifications IQS 45-84 [14] is considered fine aggregate and is utilised in all concrete mixtures. In this work, the specimens were made and cured using tap water. Pomegranate peels extract were employed as a green inhibitor in this study. The organic inhibitor utilised in this experiment was sodium benzoate, which has the formula C_6H_5COONa.

Since the research was limited to addressing external chloride attacks, all concrete materials were chosen based on their chloride concentration, staying within permissible limits. The concentration of chloride salt in the aqueous solution to which the specimens were exposed was represented by the exposure conditions, which were 2% or 4%.

All specimens utilised mild steel, whose chemical makeup is given in Table 1. Samples of steel rebar with a diameter of 10 mm in the transverse direction (shear reinforcement) and 16 mm in the longitudinal direction (primary reinforcement protruding 5 cm above specimen surface.

Table 1 Chemical composition of rebar

Element	**C**	**Si**	**Mn**	**P**	**S**	**N**
Weight [%]	0.24	0.65	1.66	0.058	0.058	0.014

2.2 Preparing of Concrete Mixtures

ACI standard technique was used for designing the concrete mix. In order to create concrete with a mean 28-day compressive strength of 35 MPa, ACI 211.1.91 was reapproved in 2002 [15]. This strength was selected to stand in for the typical concrete used in traditional building. The mix had the following proportions: 1:1.62:3.01 for cement, sand, and gravel; the w/c ratio was 0.55. In both combinations, 210 kg/m3 of water were used. The model symbols and additive proportions for concrete mixtures are displayed in Table 2.

Table 2 The preparation of the concrete mixtures (specimens) for the experiments

Symbol of Mix	**Type of Mix**	
	% of Adding Pomegranate Peels Extract Inhibitor	**% of Adding sodium benzoate Inhibitor**
A, A1, A2 Reference	without	without
B ,B1 ,B2	_	2% by weight of cement
C, C1, C2	_	4% by weight of cement
D ,D1 ,D2	2% by weight of cement	_
E, E1, E2	4% by weight of cement	_

2.3 Acceleration of Chloride ion permeation

The purpose of this method to bring chlorides into the concrete to the level of the rebar by diffusion. It A system comprising a glass water container that was constructed to fit the tested reinforced concrete specimens was utilised to expedite the penetration of the chloride ion carried by the soil into the reinforced concrete, utilising „The electrical migration technique" [16]. Concrete specimens were used to partition each container into two sections. As a representation of the salt-laden soil the concrete was exposed to while in use, the first section was partially filled with water containing chloride salt. The specimen was exposed on two sides, and it was raised using a tiny glass base that let saline water come into touch with

the targeted portion of the specimen. Distilled water was poured into the second section of the container. Silicone material was put at the points of contact between the glass and the specimens, between the touched glass pieces, or between the concrete pieces themselves to isolate these two sections from one another (see Fig. 2).

2.4 The Tests

2.4.1 Compressive Strength Test

The compressive strength was assessed using the LEL International machine, which is housed in the structural laboratory of the University of Kufa's civil engineering department, in accordance with

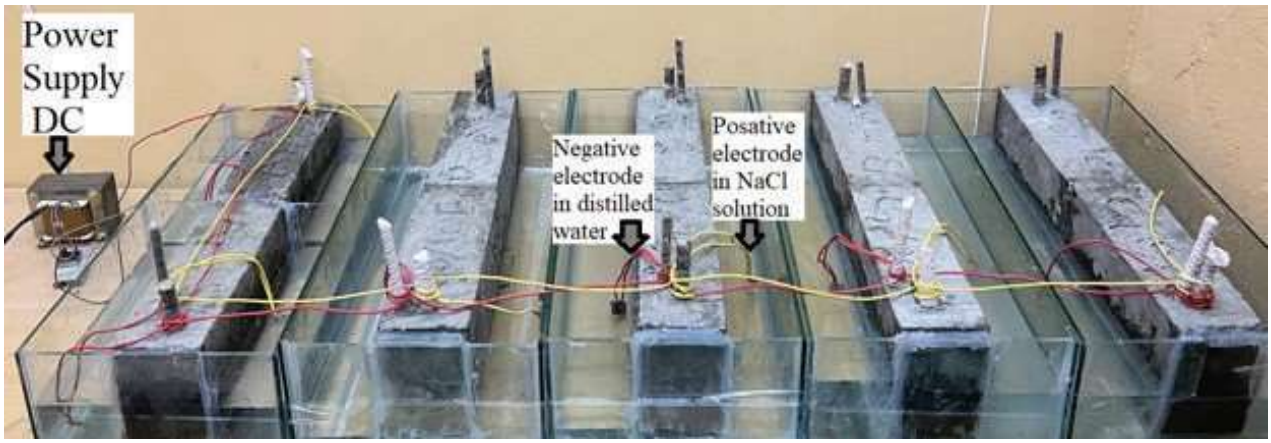

Figure 2 Cell accelerates the penetration of chloride ions

British Standard [B.S. 1881: part 116: 1989] [17]. The cubes were taken out of the curing water after 28 days and used to measure the compressive strength of the concrete. Three samples on average from each type of concrete mix were used to report the values.

2.4.2 Optical Microscopy

Optical microscopy (OM)was specifically used to detect areas of rust and its spatial distribution on surfaces of reinforcing steel samples. This test was performed at the Nanotechnology Unit at the University of Kufa using an optical microscope device (NMM-800RF, Xiamen Phio, China Origin) equipped with appropriate reflected illumination for observation. Non-transparent surfaces of objects. The camera is connected to computer programs and has the ability to display and show images of the surfaces of objects.

3. RESULTS AND DISCUSSION

3.1 Compressive Strength Test

The results of the compressive strength test at age 28 days for samples containing 2% and 4% by weight of cement of both organic (sodium benzoate) and green (pomegranate peel extract) inhibitors are shown in Fig. 3.

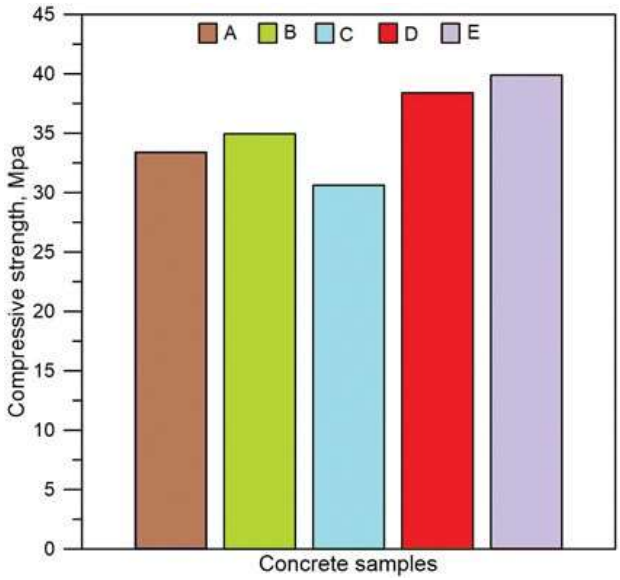

Figure 3 Compressive strength of concrete samples with green inhibitor and organic Inhibitor after immersion in tap water for 28 days.

The addition of sodium benzoate admixture (2% by weight of cement) to concrete does not result in a reduction in compressive strength after 28 days, but the addition of sodium benzoate inhibiter admixture (4% by weight of cement) to concrete does. This admixture may act as a retarder [18], delaying the action of tricalcium aluminate (C3A) and altering the concrete's compressive strength during its early ages.

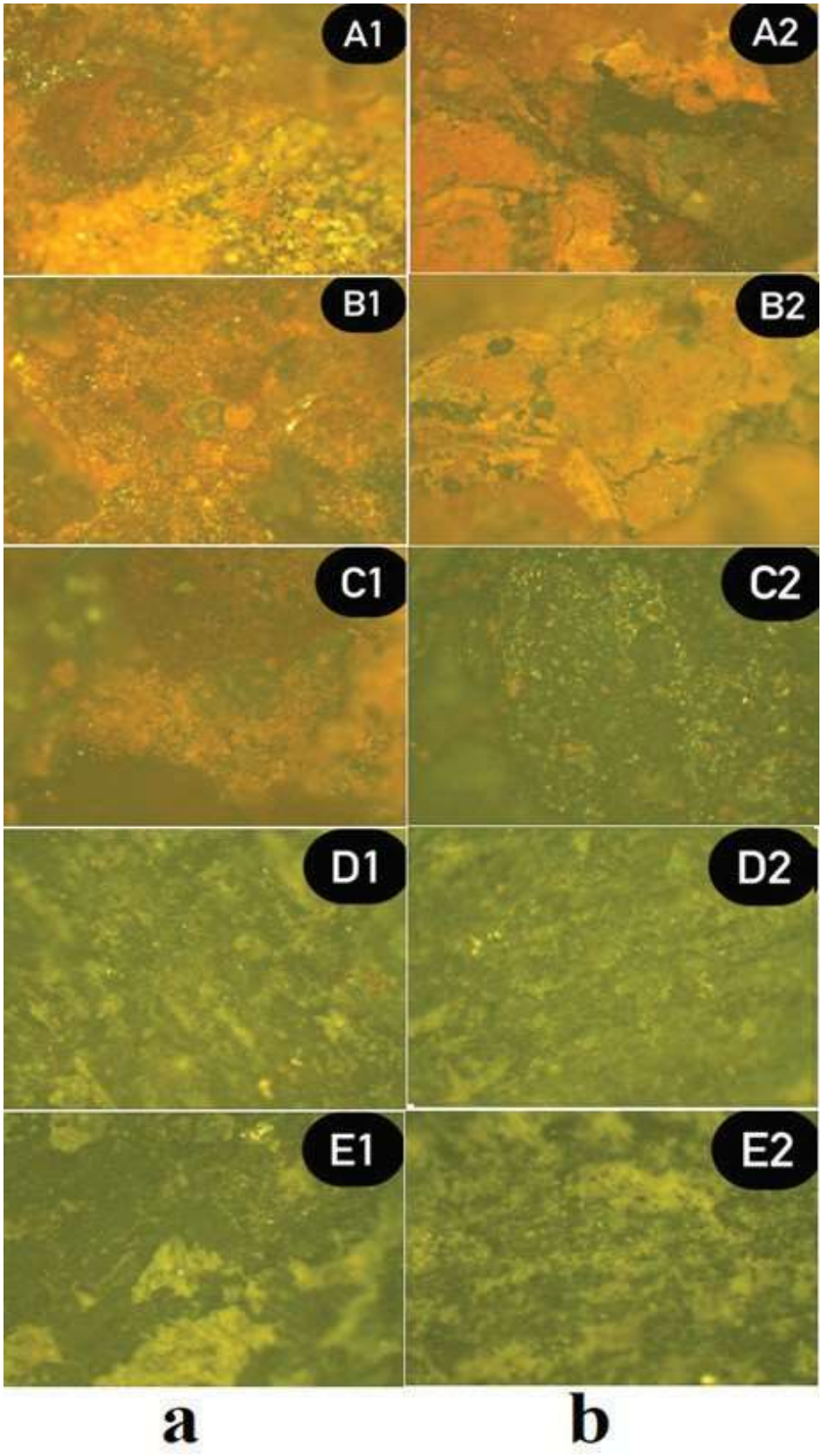

Figure 4 Light optical micrographs of the steel surface with magnification 20X of the concrete columns samples and with and without inhibitors showing the microstructure and the corrosion attack: a) immersed in 2% NaCl solution, b) immersed in 4% NaCl solution.

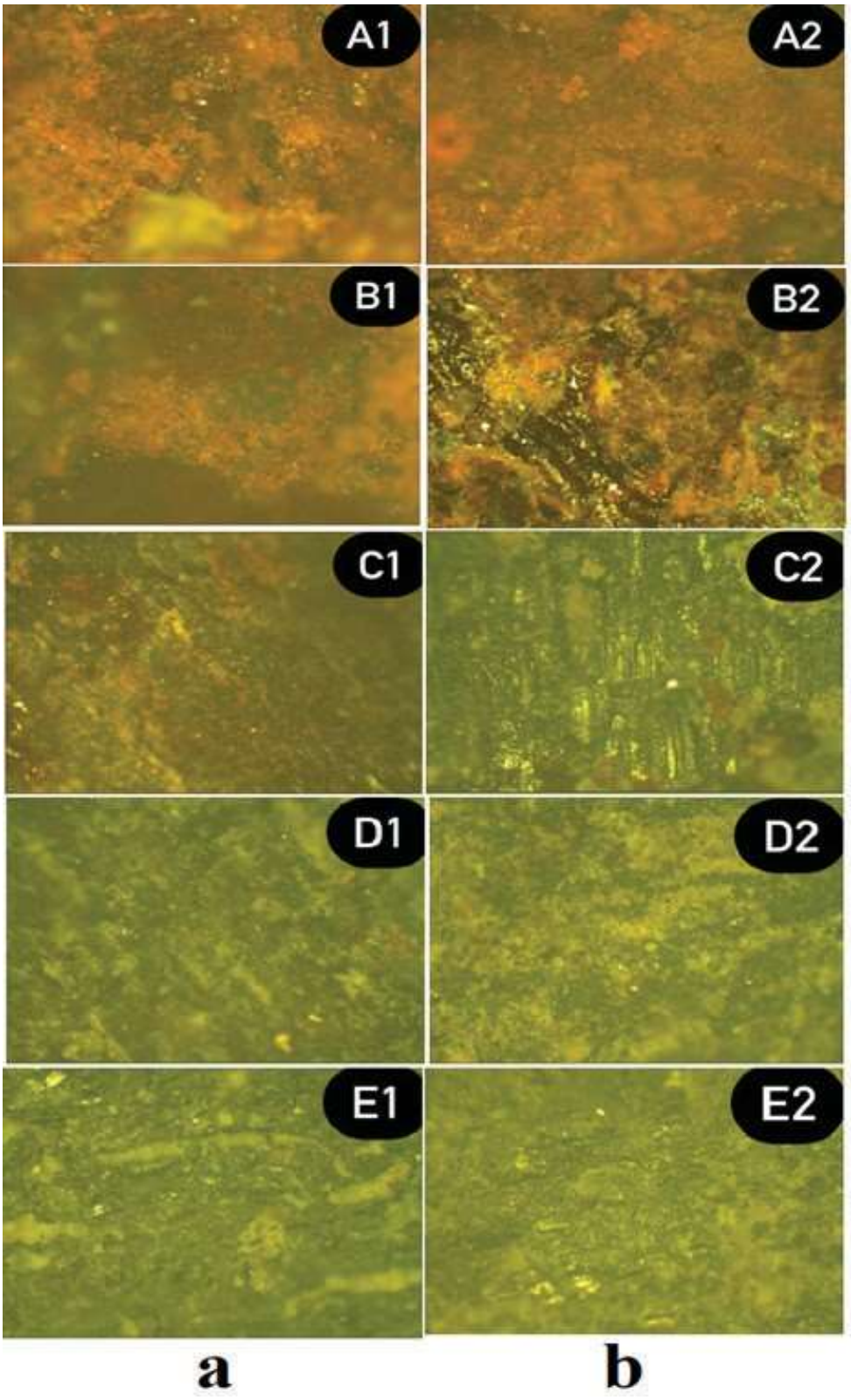

Figure 5 Light optical micrographs of the steel surface with magnification 20X of the concrete beams samples and with and without inhibitors showing the microstructure and the corrosion attack: a) immersed in 2% NaCl solution, b) immersed in 4% NaCl solution.

Following the application of a green inhibitor, pomegranate peel extract added at 2% and 4% by weight of cement increases compressive strength by 3.39% and 4.90%, respectively. Pomegranate peel extract increases the durability of concrete and is responsible for the noted increase in compressive strength. Pomegranate peels, which have a calcium content of 162.1 mg per 100 g, help to build additional calcium gel, which increases the strength of the concrete by producing C-S-H gel. The densification effect was brought about by this gel, which filled the spaces between the cement matrixes [19, 20].

3.2 Optical Microscopy

Optical micrographs of all reinforced concrete samples with or without the presence of inhibitors types are shown in the Figs. 4 and 5. Visual inspection revealed that in most cases of corrosion the corrosion began between the ribs of the reinforcement or directly at the edge of the rib as shown in Fig. 4 (some flash rust spots can also be seen on the surface of beams and columns steel samples).

In Fig. 5, there are also some minor rust areas on the steel surface of the samples.

Inspection of the steel concrete surface at the onset of corrosion typically revealed a single distinct corrosion point, which in some cases was surrounded by much smaller corrosion pits, as shown in Fig. 5. Small corrosion pits have been interpreted as sites where corrosion had begun but were unable to reach stable pit growth (as opposed to a dominant corrosion site), and these pits were typically covered by a crust of corrosion products.

3.3 Conclusion

1 This study investigated a green technique to maintain the environmental cleanliness of organic materials, limit the aggravation of chemical combinations applied to concrete, and promote sustainable engineering. This is accomplished by using pomegranate peel extract, a low-cost, readily available, and non-toxic corrosion inhibitor, in reinforced concrete exposed to chloride attack.

2 A concrete mix that contains 2% or 4% of pomegranate peel by weight will have a higher compressive strength; additionally, the addition of pomegranate peel promotes the creation of calcium gel, which further enhances the concrete's strength development by producing C-S-H gel. Densification is caused by this gel, which filled the spaces between the cement matrixes. The compressive strength of fresh concrete mix is affected when 2% and 4% of sodium benzoate by weight of cement is added. This is because sodium benzoate serves as a retarder after 28 days of immersion.

3- Optical microscopy revealed that the amount of oxides formed as a result of corrosion (iron oxide and chlorides) increased while the concentration of inhibitors (pomegranate peel extract and sodium benzoate) decreased on the surface of the reinforcing steel after it was removed from the concrete blocks. Corrosion products were also found on the surface of the reinforcing steel in samples C2, D1, D2, E1, and E2. Simply looking at the surface reveals that these samples have a less corroded surface or are practically corrosion-free.

Declaration of interests

The authors declare that they have no known competing financial interests or personal relationships that could have appeared to influence the work reported in this paper.

*** Data availability**

Data generated or analyzed during this study are available from the corresponding author upon reasonable request.

REFERENCES

1. M.K. Tweek, S.A. Abdulsada (2023) Improvement corrosion properties of reinforcement concrete by corrosion inhibitors: A brief review, *Koroze a Ochrana Materialu*, 67, 50-58, https://doi.org/10. 2478/kom-2023-0007.
2. S.A. Abdulsada, R. Bak, A. Heczel, I.T.Tamás (2020) Corrosion studies on XD3 reinforced concrete samples prepared by using calcium nitrate as inorganic corrosion inhibitor with different superplasticizers, KOM – Corrosion and Material Protection Journal, 64, 11-18, https://doi.org/10.2478/kom-2020-0002.
3. S.A. Abdulsada, A.I. Al-Mosawi (2023) Analysis of corrosion rate, inhibition efficiency, and economic cost of XD3 reinforced concrete related to inhibitor and plasticiser types, *Eng. Res. Express*, 5 035032, https://doi.org/10.1088/2631-8695/acee46.
4. S.A. Abdulsada, I.T.Tamás, F. Éva (2018) Preliminary corrosion testing of steel rebar samples in 3.5%NaCl solution with and without a green inhibitor, *Építőanyag-Journal of Silicate Based and Composite Materials*, 70, 48-53, https://doi.org/10.14382/epitoanyag-jsbcm.2018.109.
5. S.A.Abdulsada, F.Éva, I.T. Tamás (2019) Corrosion testing on steel reinforced XD3 concrete samples prepared with a green inhibitor and two different superplasticizers, *Materials and Corrosion*, 70, 1262-1272, https://doi.org/10.1002/maco.201810695.

6. S.A. Abdulsada, F.Éva, I.T.Tamás (2018) Corrosion studies of steel rebar samples in neutral sodium chloride solution also in presence of a bio-based (green) inhibitor, *International Journal of Corrosion and Scale Inhibition*, 7, 38-47, https://doi.org/10.17675/2305-6894-2018-7-1-4.
7. S.A. Abdulsada, I.T.Tamás (2020) Studying chloride ions and corrosion properties of reinforced concrete with a green inhibitor and plasticizers, *Structural Concrete*, 21, 1894-1904, https://doi.org/10.1002/suco.201900580.
8. S.A. Abdulsada, I.T.Tamás (2020) Investigations on the resistivity of XD3 reinforced concrete for chloride ions and corrosion with calcium nitrate inhibitor and superplasticizers, *Cement Wapno Beton*, 25, 330-343, https://doi.org/10.32047/cwb.2020.25.4.7
9. S.A. Abdulsada, K. Ferenc, I.T.Tamás (2020) Distribution of corrosion products at the steel-concrete interface of XD3 concrete samples, *Magazine of Civil Engineering*, 100, 10005, https://doi.org/10.18720/MCE.100.5.
10. S.A. Abdulsada, A.I. Al-Mosawi (2016) Using of nucleus dates waste with a nanoscale particles as a green inhibitor, *International Journal of Mechanical & Mechatronics Engineering*, 16, 27-32.
11. W.Kurdowski, W.Kurdowski (2014) Mineral additions for cement production. *Cement and Concrete Chemistry*, 533-83. https://doi.org/10.1007/978-94-007-7945-7_7
12. T.A. Söylev, M. Richardson (2008) Corrosion inhibitors for steel in concrete: State-of-the-art report. *Construction and Building Materials*, 22(4):609-22. https://doi.org/10.1016/j.conbuildmat.2006.10.013
13. COSQC, Iraqi standard specification No.5. 2019, IQS 5–19,"Portland Cement", Baghdad, Iraq.
14. COSQC, Iraqi standard specification No.45.1984, IQS 45– 84,"Aggregate from Natural Sources for Concrete and Construction", Baghdad, Iraq.
15. Standard A. Standard practice for selecting proportions for normal, heavyweight, and mass concrete. ACI Man Concr Pract. 1996:1-38.
16. K.Stanish, R.D. Hooton, M.D.Thomas (2001) Testing the chloride penetration resistance of concrete: a literature review. *University of Toronto*, FHWA Contract DTFH61-97-R-00022.
17. Standard B. Part-116 (1983) Method for Determination of Compressive Strength of Concrete Cubes, London. British Standard Institution. 1881.
18. L.D. Matlob, A.M. Amir, N.F.Hassan (2008) Effect of using corrosion inhibitors on concrete properties and their activity. *journal of kerbala university*, 6, 121-39. https://doi.org/10.1201/b11570-30
19. J.Baskaran, S.Paramasivam (2023) Performance of pomegranate peel extract coated rebars in concrete. *Građevinar*, 75, 883-92. https://doi.org/10.14256/JCE.3511.2022
20. W.S. Kareem (2017) Strength Behavior of Concrete Using Pomegranate Peel Admixture. *Journal of Engineering and Sustainable Development*, 21, 184-99.

IZVOD

SINERGISTIČKI EFEKAT INHIBITORA NA KOROZIJU ARMIRANOBETONSKIH KONSTRUKCIJA PREMA ACI STANDARDIMA

Primena jeftinih, niskotoksičnih inhibitora korozije smanjuje stopu korozije armiranog betona u medijumu sa slanom vodom. Svrha ovog rada je da se uporedi inovativni, navodno ekološki benigni inhibitor dobijen iz voćnog otpada (ekstrakt kore nara (PPE)) sa natrijum benzoatom, organskim inhibitorom. Inhibitori su uvedeni u betonsku mešavinu u količinama od dva i četiri procenta mase cementa prema ACI standardima. Maksimalni prinos ekstrakcije u pogledu celokupnog sadržaja fenola dobijen je korišćenjem vodenog rastvarača i Soklet tehnikom. Efikasnost inhibitora korozije u sprečavanju korozije je ispitivana primenom metoda čvrstoće na pritisak i optičke mikroskopije. LZO formira organski sloj sastavljen od nekoliko komponenti u različitim okruženjima soli, obezbeđujući i hemijsku antioksidativnu aktivnost i inhibitor korozije mešovitog tipa, najverovatnije zbog koncentracije polifenola.

Ključne reči: *zeleni inhibitor, natrijum benzoat, armirani beton, čvrstoća na pritisak, optička mikroskopija.*

Naučni rad
Rad primljen: 25.05.2024.
Rad prihvaćen: 4.06.2024.

The ORCID Ids of all the authors are as follows:
1. Mena Khaleel Tweek -- https://orcid.org/0009-0002-8616-2918
2. Shaymaa Abbas Abdulsada -- https://orcid.org/0000-0001-7006-2950

Rashmi Kakkar[1,2]; Dilraj Preet Kaur[*1], Seema Raj[1]*

[1]School of Basic and Applied Sciences, K.R. Mangalam University, Gurugram, India; [2] Department of Physics, Govt. College for Girls, Gurugram, India

Scientific Paper
ISSN 0351-9465, E-ISSN 2466-2585
https://doi.org/10.62638/ZasMat1077

Zastita Materijala 66 (1)
30–39 (2025)

Investigations of Nanomaterial-Based Membranes for Efficient Removal of Contaminants from Wastewater via Membrane Distillation: A Critical Review

ABSTRACT

The requirement for wastewater treatment is paramount in ensuring environmental sustainability and safeguarding public health. As industrialization and urbanization accelerate, the volume of wastewater generated continues to increase, containing a diverse range of pollutants and contaminants. Untreated wastewater poses serious threats to ecosystems, water bodies, and human communities, leading to pollution, waterborne diseases, and ecological imbalances. Effective wastewater treatment becomes essential to mitigate these adverse effects by removing or reducing pollutants before discharge into natural water sources. This process helps to preserve water quality, protect aquatic life, and maintain the overall health of ecosystems. Membrane distillation (MD) has emerged as a promising technology for wastewater treatment, offering an innovative approach to address the challenges associated with conventional treatment methods. In MD, a hydrophobic membrane serves as a selective barrier, allowing water vapor to pass through while preventing the passage of contaminants. This paper offers an extensive overview of the latest advancements in nanotechnology and membrane distillation applied in wastewater treatment. We will delve into different types of nanomaterials that have been used to enhance the properties of MD membranes, such as nanocomposites, nanoparticles, and nanofiber membranes. We also explore the mechanisms by which these nanomaterials improve the separation efficiency, anti-fouling properties, and durability of MD membranes. Additionally, we highlight the potential of hybrid membranes that combine different types of nanomaterials for further improving the performance of MD in wastewater treatment. We provide examples of recent studies that have investigated the use of hybrid membranes, including carbon nanotube-graphene oxide hybrid membranes, nanocomposite nanofiber membranes, and silver nanoparticle-embedded membranes. We also identify some areas for future research and development, such as the scale-up and commercialization of nanotechnology-based MD systems. In summary, this review paper highlights the potential of nanotechnology to enhance the performance of MD in wastewater treatment, leading to improved water quality and a cleaner environment.

Keywords: *Nanocomposite; Nanofibers; Wastewater treatment; Membrane Distillation*

* Corresponding author: Dilraj Preet Kaur
E-mail: dilraj.k@krmangalam.edu.in
Paper received: 23.04.2024.
Paper accepted: 9.06.2024.
Papir is available on the website: www.idk.org.rs/journal

Graphical Abstract:

INTRODUCTION

Indeed, chemical contamination of water has gained significant attention from the public sector, society, and, most significantly, the whole industrialized globe [1]. There are two main sources, point and non-point. The initial description pertains to pollutants originating from a singular origin, such as industrial emissions directly entering water bodies. On the other hand, the second refers to pollutants discharged from various sources. Water pollution stems from various contributors, including energy consumption, radioactive waste, urban expansion, sewage discharge and treatment, industrial effluents, mining operations, as well as the use of pesticides and chemical fertilizers. Every activity that uses water, whether it be residential, agricultural, or industrial, will cause pollution since the effluent will contain undesired contaminants, some of which may be dangerous [2]. Nanotechnology has great potential for improving the efficiency and effectiveness of wastewater treatment. It involves the use of nanoscale materials and processes to remove contaminants from wastewater [1,2]. By utilizing membranes with nanoscale pores, Nanofiltration and Reverse Osmosis processes offer efficient and effective treatment solutions, ensuring the production of clean and safe water for various applications. Nanofiltration membranes can remove particles down to 1 nm in size, while reverse osmosis membranes can remove particles down to 0.1 nm in size [3,4]. Nanoparticles can also be used to adsorb contaminants from wastewater. Overall, the use of carbon nanotubes, graphene oxide, and metal oxide nanoparticles in wastewater treatment holds great promise for addressing the global water pollution crisis. These advanced materials, with their unique properties and exceptional pollutant removal capabilities, offer a sustainable and efficient solution for the purification of wastewater [5-7]. Nanoparticles can also be used as photocatalysts to break down contaminants in wastewater. Titanium dioxide nanoparticles are commonly used for this purpose, as they can be activated by UV light to generate reactive oxygen species that can degrade organic compounds [8]. Another one is Nanobubble Technology, according to which nanobubbles are small bubbles (less than 100 nm in diameter) that can be used to enhance aeration and mixing in wastewater treatment. They can also help to remove contaminants by attaching to them and carrying them to the surface of the water [9]. Figure 1 presents some of the technologies employed in water treatment, where nanoparticle and nanotechnology are extensively used.

Figure 1: Innovations of Nanotechnology in water treatment

Nanotechnology and membrane distillation

By leveraging the unique properties of nanomaterials, researchers can develop advanced membranes with improved flux rates, higher selectivity, and reduced fouling. Furthermore, nanotechnology enables the integration of membrane distillation with other treatment technologies, opening up new possibilities for more efficient and sustainable wastewater treatment processes. Membrane distillation entails a separation technique employing a hydrophobic membrane to isolate impurities from water via vaporization and subsequent condensation. The simplest and mostly employed configuration of MD is Direct Contact Membrane Distillation (DCMD). Figure 2 presents the DCMD (simplest configuration). Top of FormThe process operates at low pressure and low temperature, making it energy-efficient and suitable for treating wastewater [10]. Recent Researches reported some ways that nanotechnology can be used to improve membrane distillation for wastewater treatment [11-14]:

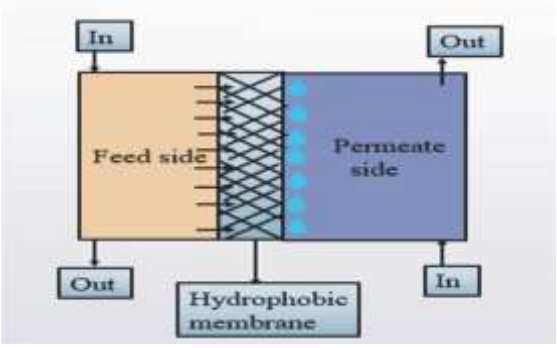

Figure 2: Schematic diagram of DCMD Configuration

- **Nanocomposite Membranes**: Membranes made of nanocomposites can have improved hydrophobicity and stability, leading to better separation efficiency and durability. For example, adding carbon nanotubes or graphene oxide to the membrane matrix can enhance its thermal conductivity and make it more resistant to fouling.
- **Nanofiber Membranes**:

Top of Form

The extensive surface area of electrospun nanofiber membranes offers benefits across different fields such as filtration, tissue engineering, and energy storage applications. In filtration applications, the large surface area allows for efficient capture of particles and contaminants, enabling improved separation efficiency. The narrow pore size distribution of these membranes further enhances their filtration capabilities, as it restricts the passage of larger particles while allowing smaller molecules to permeate through. These nanofiber membranes can be functionalized with nanoparticles or nanocomposites to enhance their hydrophobicity and anti-fouling properties. Here are some examples: Polyvinylidene fluoride (PVDF) nanofiber membrane, Polyacrylonitrile (PAN) nanofiber membrane, Polysulfone (PSf) nanofiber membrane etc.

- **Hybrid Membranes**: Hybrid membranes that incorporate different types of nanomaterials, such as carbon nanotubes and graphene oxide, offer numerous advantages over traditional single-component membranes. These membranes demonstrate superior separation efficiency, anti-fouling properties, thermal stability, and mechanical strength. With their potential for enhanced performance in various applications, hybrid membranes are poised to revolutionize the field of membrane-based separations [15]. Nuthenya et al. synthesized PVDF membrane embedded with SiO_2 nanoparticles for MD. They found that the embedded nanoparticles enhanced the hydrophobicity of the membrane surface, resulting in higher water vapor flux and reduced fouling [16]. Zhang et al. (2018) reported that a PVDF membrane embedded with TiO_2 nanoparticles exhibited excellent thermal stability and anti-fouling properties [17]. In addition, various studies have investigated the effect of different types of nanoparticles on MD performance. For instance, Alkhouzaam et al. investigated the use of graphene oxide (GO) nanoparticles embedded in a PVDF membrane for MD. They found that the embedded GO nanoparticles improved the

membrane's hydrophobicity and thermal stability, resulting in higher water vapor flux and reduced fouling [18].

Wastewater Treatment via Membrane Distillation

Sangeetha (2022) conducted a study investigating the effectiveness of dual-layered omni phobic electrospun nanofibrous membranes (ENFMs) within the realm of direct contact membrane distillation (DCMD). These dual-layered membranes were created using polyvinylidene fluoride (PVDF) and a fluoropolymer known as perfluorohexane (PFH) through the process of electrospinning. The study included testing the dual-layered ENFMs with simulated seawater, and the results showcased their exceptional vapor performance. Being tested with simulated seawater, the dual-layered ENFMs had outstanding vapor flux of 8.5 L/m^{2}h and salt rejection of greater than 99.99%. They also revealed a high porosity and water contact angle (WCA) of 143˚. When tested with synthetic wastewater containing pharmaceutical substances, the constructed ENFMs (Electrospun Nanofiber Membranes) exhibited excellent permeate quality. The permeate showed a low organic content of 1 ppm (parts per million) and had a conductivity of 30 S/cm (siemens per centimeter). These results indicate that the ENFMs are highly effective in removing pharmaceutical substances from wastewater [19]. Jingjee Ju's (2020) study investigated the fabrication and performance of hierarchically structured superhydrophobic polytetrafluoroethylene (PTFE)/polyhedral oligomeric silsesquioxane (POSS) nanofibrous membranes for MD. The membrane fabrication procedure included electrospinning, succeeded by surface modification employing a fluorinated silane agent. The main focus of the study was to optimize the PTFE/POSS nanofibrous membrane, specifically the membrane labeled as #POSS-2. This particular membrane exhibited a remarkable three-dimensional (3D) superhydrophobic property, with a WCA measured at 151 ± 4°. The vinyl-POSS concentration was varied to identify the optimal concentration that would result in the desired membrane performance. Similarly, different temperatures and salt concentrations were tested to understand their influence on the membrane's performance. The study conducted on #POSS-2 in the field of membrane distillation has yielded promising results. Specifically, it has shown a remarkably competitive water flux of 40 ± 2 L/m^{2}h during the DCMD process. This achievement was obtained when the feed temperature was maintained at 60 °C, while the permeate temperature was kept at 20 °C.

Alongside its notable water flux performance, #POSS-2 has showcased exceptional long-term stability throughout a continuous DCMD operation lasting for 200 hours.Top of Form This indicates that the material is capable of maintaining its effectiveness and efficiency over an extended period of operation [20]. In their study, Hadi Attia et al. (2017) documented the effectiveness of a superhydrophobic electrospun membrane for removing heavy metals through Air Gap Membrane Distillation (AGMD). The membrane was prepared by combination of electrospinning technique and surface modification with a fluorinated silane agent. The research conducted revealed important findings regarding the manufacturing of an immaculate beadless membrane mat. Through experimentation, it was determined that a polymer concentration of 15 wt.%, combined with a cationic surfactant concentration of 0.05 wt.%, produced the desired results. In terms of the solvent mixture, a ratio of 6:4 of dimethylformamide (DMF) to acetone was found to be optimal for the membrane mat production. Additionally, an electric field strength of 14 KV was applied during the manufacturing process. The performance of the membrane mat was evaluated based on various parameters. The lead rejection rate achieved was 72.77%, indicating the membrane's ability to effectively remove lead from the solution. The liquid entry pressure was measured to be 17 psi, suggesting the membrane's ability to withstand pressure differentials and prevent liquid penetration. Furthermore, the WCA was determined to be 132°, indicating the hydrophobic nature of the membrane. This property is significant as it allows for the efficient separation of water from other substances. Composite PVDF membranes containing 11 wt.% and 20 wt.% functionalized alumina (Al_2O_3) membranes performed better than composite PVDF membranes with 18° WCA and 27 psi liquid entry pressure, with 99.36% heavy metal rejection and 5.9% higher permeate flow [21]. Jiaxin Cui et al. (2020) focuses on the application of electrospun nanofiber membranes for wastewater treatment. Electrospun nanofiber membranes exhibited high porosity and specific surface area, providing an efficient platform for various filtration and separation processes. The nanofiber membranes showed excellent mechanical strength and stability, which can be further improved by optimizing the electrospinning parameters such as polymer concentration and solvent type. The performance of electrospun nanofiber mem-

branes can be enhanced by incorporating functional materials such as nanoparticles and biopolymers. Electrospun nanofiber membranes demonstrated superior adsorption and removal efficiency for various pollutants in wastewater, including heavy metals, dyes, and organic compounds. The application of electrospun nanofiber membranes in wastewater treatment can significantly improve the efficiency and reduce the cost compared to conventional technologies. Overall, the study provides quantitative evidence for the potential of electrospun nanofiber membranes as an efficient and cost-effective platform for wastewater treatment [22]. Mohamed Shaban (2015) aimed to investigate the effect of incorporating titanium dioxide (TiO_2) nanotubes into a mixed matrix polyethersulfone (PES) membrane on its performance in terms of water flux and rejection of various pollutants. The VMD mathematical model was used to calculate the best membrane performance under optimal conditions. The experimental findings showed that by employing 0.53% TiO_2NTs in the membrane preparation solution, it was able to generate a high-performance NF/RO mix membrane with a salt rejection percentage of 97% and a permeate flow of 18.2 L/m^{2}h [23]. Junghyun Kim et al. (2022) presented a novel membrane modification method using multi-layered single-wall carbon nanotubes (SWCNTs) and polyvinylidene fluoride (PVDF) to improve the performance of membrane distillation (MD). The research aimed to explore how electrical repulsion influences membrane performance and fouling prevention. Quantitative findings revealed that among the membranes tested, the SWCNT/PVDF membrane with the greatest number of SWCNT layers (10 layers) demonstrated the highest water flux (up to 43 L/m² h) and the lowest contact angle (29°).The fouling resistance of the modified membranes was evaluated by using humic acid as a model foulant, and the results demonstrated that the SWCNT/PVDF membrane with 10 layers exhibited the highest fouling resistance with a flux decline of only 6% after 6 hours of operation. The study concluded that the incorporation of SWCNTs in the PVDF membrane can improve the membrane performance in terms of water flux and fouling resistance by inducing electrical repulsion between the membrane surface and the foulants. Moreover, increasing the number of SWCNT layers can further enhance the membrane performance, making it a promising approach for the development of high-performance MD membranes [24]. Navya Thomas's (2021) study investigated the use of antiscaling 3D printed feed spacers coated with nanoparticles for membrane distillation (MD) applications. The 3D printed feed spacers were coated with silica nanoparticles using a facile dip-coating method. A scale-inducing aqueous solution of calcium sulphate was used as the feed of a direct contact MD process to evaluate the antiscaling effectiveness of uncoated and FS coated spacers. The FS coated spacer had a scalant (Ca^{2+}) attachment of 0.24 mg cm^2, which is 74% less than the uncoated 3D spacer's attachment of 0.95 mg cm^2. Additionally, 60% less scaling on the membrane surface was seen when the antiscaling FS coated spacer was used. Microscale roughness-induced hydrophobicity and decreased surface-free energy, which impaired the scalant's interaction with the spacer surface, were the main variables that lowered scaling with FS coating. The results showed that the coated spacers exhibited a higher water vapor flux and salt rejection rate compared to the uncoated spacers [25]. Teoh et al. (2022) aimed to investigate the effectiveness of using DCMD for the simultaneous recovery of water and nutrients from aquaculture wastewater. The final membrane has surpassed the standard for super hydrophobicity. It attained a high 153.3° WCA and a low 8.4° contact angle hysteresis. A slight and consistent decrease in flow rate by 1.4 L/m^{2}h was observed during the continuous separation and treatment of fish farm effluent, indicating reduced fouling of the surface-printed membrane. The water recovery in the batch feed concentration process reached 86.3%. The initial concentrations of ammonia (ranging from 16.4 to 82.2 mg/L), phosphate (from 18.0 to 99.8 mg/L), and potassium (between 68.0 to 384.8 mg/L) were all at least five times higher in the retentate concentration of fish farm water. This concentrated feed could potentially serve as the primary nutrient source in liquid fertilizer production. Except for ammonia (>86%), all chosen inorganic compounds in the feed concentration process are rejected at a rate higher than 99%. Overall, the results suggest that the DCMD system has great potential for the sustainable management of aquaculture wastewater [26]. Table 1 presents the recent research trends in DCMD incorporating nanoparticles: Insights from Literature. Figure 3 presents correlation between Feed Temperature and WCA and Flux in Nanoparticle-Embedded Polymer Membrane. The Michal Bodzek (2019) titled "Nanotechnology in water and wastewater treatment. Graphene – the nanomaterial for next generation of semipermeable membranes" reviews the potential of graphene-based

materials for water and wastewater treatment. The author concludes that graphene-based materials have the potential to revolutionize the field of membrane technology due to their unique properties, such as high mechanical strength, thermal stability, and exceptional water transport properties. Graphene-based membranes have shown promising results for desalination, water purification, and wastewater treatment applications. However, the paper also highlights that more research is needed to address the challenges related to the scalability and cost-effectiveness of these membranes [27].

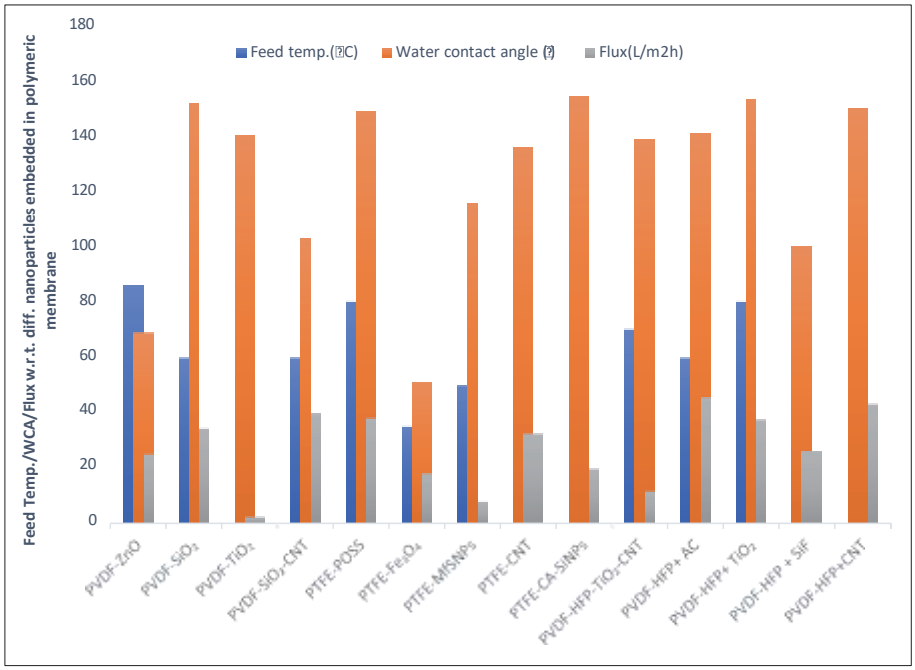

Figure 3: Variation in Water Contact Angle (WCA) and Flux with Changing Feed Temperature in Polymer-Embedded Nanoparticle Membrane

Table 1: Exploring Nanoparticle Integration in DCMD: Overview of Recent Investigations.

S. No.	MD Configuration	Polymer -Nanoparticle Membrane Material	Feed temp. (˚C)	Water contact angle (˚)	Liquid entry pressure (kPa)	Membrane Thickness (μ□)	Pore Size (μ□)	Porosity (%)	Flux (L/m²h)	Salt Rejection (%)	References
1	DCMD	PVDF-CNT	60	150.4	40.5	88	1.12	89.4	NA	NA	28
2	DCMD	PVDF-ZnO	86	69	900	NA	NA	14	25	99	29
3	DCMD	PVDF-SiO2	60	151.7	72.3	135	1.27	79.9	34.2	≥99.9	30
4	DCMD	PVDF-TiO2	40	140	NA	84.5	0.41	44.43	2.5	97	31
5	DCMD	PVDF-SiO2-CNT	60	103	590	NA	0.22	63.6	39.77	99	32
6	DCMD	PTFE-POSS	80	149	16	NA	0.5	70	38	99.99	33
7	DCMD	PTFE-Fe3O4	35	51	379	221	NA	60.7	18	NA	34
8	DCMD	PTFE-MfSNPS	50	115.5	NA	NA	NA	NA	8	99.1	35
9	DCMD	PTFE-CNT	65	136	483	NA	0.292	NA	32.49	99.9	36
10	DCMD	PTFE-CA-SiNPs	53	154.2	NA	303	0.47	50.6	19.92	NA	37
11	DCMD	PVDF-HFP-TiO2-CNT	70	139	81	73	0.46	86	11.85	NA	38
12	DCMD	PVDF-HFP+ AC	60	140.9	1.36	200	0.805	91.3	45.6	99.99	39
13	DCMD	PVDF-HFP+ TiO2	80	153.4	90.5	99	0.76	89.8	37.6	99.99	40
14	DCMD	PVDF-HFP + SiF	70	100	250	142	0.23	59	26	NA	41
15	DCMD	PVDF-HFP+CNT	55	150	136	NA	0.715	NA	43	99.8	42

CONCLUSION

- Silicon dioxide exhibits compatibility with PVDF, modifying the water contact angle to 151.7˚ with the inclusion of nanoparticles and enhancing flux to 34.2 L/m²h. Likewise, POSS shows good compatibility with PTFE.
- Additionally, the combination of silicon dioxide and carbon nanotubes with PVDF demonstrates a high flux of 39.7 L/m²h.
- Inclusion of CNT to the polymer results in major enhancement in measurement of WCA and Flux.
- Pore size, liquid entry pressure, water contact angle, temperature and salinity of feed water are the key parameters which affects the performance of membranes in terms of flux and wettability.
- Nanofibrous polymer membranes and nano particles embedded polymer membranes have shown high flux and stability for seawater desalination

Despite the remarkable progress in nanoparticle-enhanced polymeric membranes, several challenges remain to be addressed. These include scalability, cost-effectiveness, long-term stability, and environmental impacts associated with nanoparticle synthesis and disposal. Additionally, there is a need for further research to understand the interactions between nanoparticles and polymeric matrices, as well as their effects on membrane performance under real-world conditions. Overall, nanoparticle-modified polymeric membranes hold great promise for advancing the field of wastewater treatment by offering sustainable, cost-efficient, and high-performance solutions. Continued interdisciplinary research and collaboration will be essential in realizing the full potential of these innovative membrane materials for addressing global water challenges and ensuring access to clean water for all.

ACKNOWLEDGEMENTS

The authors acknowledge the support received from the leadership and management of K.R. Mangalam University in the form of seed grant (KRMU/ADMIN/SEED/2021-22/2845(A). Dr. Dilraj Preet Kaur thankfully acknowledges Dr. B.S. Lalia to be a guiding person in pursuit of achieving the research goals.

REFERENCES

1. K.Jain, A.S.Patel, V.P.Pardhi, S.J.Flora (2021) Nanotechnology in wastewater management: a new paradigm towards wastewater treatment. Molecules, 26(6), 1797. https://doi.org/10.3390/molecules26061797
2. S.Cheriyamundath, S.L.Vavilala (2021) Nanotechnology-based wastewater treatment. Water and Environment Journal, 35(1), 123-132.https://doi.org/10.1111/wej.12610
3. J.Radjenović, M.Petrović, F.Ventura, D.Barceló (2008) Rejection of pharmaceuticals in nanofiltration and reverse osmosis membrane drinking water treatment. Water research, 42(14), 3601-3610. https://doi.org/10.1016/j.watres.2008.05.020
4. S.K.Nataraj, K.M.Hosamani, T.M.Aminabhavi (2006) Distillery wastewater treatment by the membrane-based nanofiltration and reverse osmosis processes. Water Research, 40(12), 2349-2356. https://doi.org/10.1016/j.watres.2006.04.022
5. L.Madhura, S.Singh, S.Kanchi, M.Sabela, K.Bisetty, F.Inamuddin (2019) Nanotechnology-based water quality management for wastewater treatment. Environmental Chemistry Letters, 17, 65-121. https://doi.org/10.1007/s10311-018-0778-8
6. G.Z.Kyzas, E.A.Deliyanni, K.A.Matis (2014) Graphene oxide and its application as an adsorbent for wastewater treatment. Journal of Chemical Technology & Biotechnology, 89(2), 196-205. https://doi.org/10.1002/jctb.4220
7. S.Nizamuddin, M.T.H.Siddiqui, N.M..Mubarak, H.A.Baloch, E.C.Abdullah, S.A.Mazari, G.J. Griffin, M.P.Srinivasan, A.Tanksale (2019) Iron oxide nanomaterials for the removal of heavy metals and dyes from wastewater. Nanoscale materials in water purification, 447-472. https://doi.org/10.1016/B978-0-12-813926-4.00023-9
8. M.B.Tahir, M.Sohaib, M.Sagir, M.Rafique (2022) Role of nanotechnology in photocatalysis. Encyclopedia of smart materials, 578. https://doi.org/10.1016/B978-0-12-815732-9.00006-1
9. M.Sakr, M.M.Mohamed, M.A.Maraqa, M.A.Hamouda, A.A.Hassan, J.Ali, J.Jung (2022) A critical review of the recent developments in micro–nano bubbles applications for domestic and industrial wastewater treatment. Alexandria Engineering Journal, 61(8), 6591-6612. https://doi.org/10.1016/j.aej.2021.11.041
10. A.Deshmukh, C.Boo, V.Karanikola, S.Lin, A.P.Straub, T.Tong, D.M.Warsinger, M.Elimelech (2018) Membrane distillation at the water-energy nexus: limits, opportunities, and challenges. Energy & Environmental Science, 11(5), 1177-1196. https://doi.org/10.1039/C8EE00291F
11. A.H.Behroozi, M.Al-Shaeli, V.Vatanpour (2023) Fabrication and modification of nanofiltration membranes by solution electrospinning technique: A review of influential factors and applications in water treatment.

Desalination, 116638. https://doi.org/10.1016/j.desal.2023.116638

12. A.Ammar, A.M.Al-Enizi, M.A.A.AlMaadeed, A.Karim (2016) Influence of graphene oxide on mechanical, morphological, barrier, and electrical properties of polymer membranes. Arabian journal of chemistry,9(2):274-86. https://doi.org/10.1016/j.arabjc.2015.07.006
13. J.H.Jhaveri, Z.V.P.Murthy (2016) A comprehensive review on anti-fouling nanocomposite membranes for pressure driven membrane separation processes. Desalination, 379, 137-154. https://doi.org/10.1016/j.desal.2015.11.009
14. U.Chadha, S.K.Selvaraj, S.Thanu, V.Cholapadat, A.M.Abraham, M.Zaiyan, M.Manoharan, V. Paramsivam (2022) A review of the function of using carbon nanomaterials in membrane filtration for contaminant removal from wastewater. Materials Research Express, 9(1), 012003. DOI 10.1088/2053-1591/ac48b8
15. M.Khraisheh, S.Elhenawy, F.AlMomani, M.Al-Ghouti, M.K.Hassan, B.H.Hameed (2021) Recent progress on nanomaterial-based membranes for water treatment. Membranes, 11(12), 995. https://doi.org/10.3390/membranes11120995
16. L.N.Nthunya, L.Gutierrez, N.Khumalo,S.Derese, B.B.Mamba, A.R.Verliefde, S.D.Mhlanga (2019) Superhydrophobic PVDF nanofiber membranes coated with an organic fouling resistant hydrophilic active layer for direct-contact membrane distillation. Colloids and Surfaces A: Physicochemical and Engineering Aspects, 575, 363-372. https://doi.org/10.1016/j.colsurfa.2019.05.031
17. J.Zhang, Z.Wang, X.Zhang, X.Zheng, Z.Wu (2015) Enhanced antifouling behaviors of polyvinylidene fluoride membrane modified through blending with nano-TiO2/polyethylene glycol mixture. Applied Surface Science, 345, 418-427. https://doi.org/10.1016/j.apsusc.2015.03.193
18. A.Alkhouzaam, H.Qiblawey (2021) Functional GO-based membranes for water treatment and desalination: Fabrication methods, performance and advantages. A review. Chemosphere, 274:129853. https://doi.org/10.1016/j.chemosphere.2021.129853
19. V.Sangeetha, N.J.Kaleekkal (2022) Investigation of the performance of dual-layered omniphobic electrospun nanofibrous membranes for direct contact membrane distillation. Journal of Environmental Chemical Engineering, 10(6), 108661. https://doi.org/10.1016/j.jece.2022.108661S
20. J.Ju, K.Fejjari, Y.Cheng, M.Liu, Z.Li, W.Kang, Y.Liao (2020) Engineering hierarchically structured superhydrophobic PTFE/POSS nanofibrous membranes for membrane distillation. Desalination, 486, 114481. https://doi.org/10.1016/j.desal.2020.114481.
21. H.Attia, S.Alexander, C.J.Wright, N.Hilal (2017) Superhydrophobic electrospun membrane for heavy metals removal by air gap membrane distillation (AGMD). Desalination, 420, 318-329. https://doi.org/10.1016/j.desal.2017.07.022
22. J.Cui, F.Li, Y.Wang, Q.Zhang, W.Ma, C.Huang (2020) Electrospun nanofiber membranes for wastewater treatment applications. Separation and Purification Technology, 250, 117116. https://doi.org/10.1016/j.seppur.2020.117116
23. M.Shaban, H.AbdAllah, L.Said, H.S.Hamdy, A.A.Khalek (2015) Titanium dioxide nanotubes embedded mixed matrix PES membranes characterization and membrane performance. Chemical Engineering Research and Design, 95, 307-316. https://doi.org/10.1016/j.cherd.2014.11.008
24. J.Kim, E.T.Yun, L.Tijing, H.K.Shon, S.Hong (2022) Mitigation of fouling and wetting in membrane distillation by electrical repulsion using a multi-layered single-wall carbon nanotube/polyvinylidene fluoride membrane. Journal of Membrane Science, 653, 120519. https://doi.org/10.1016/j.memsci.2022.120519
25. N.Thomas, M.Kumar, G.Palmisano, R.K.Al-Rub, R.Y.Alnuaimi, E.Alhseinat, R.Rowshan, H.A.Arafat (2021) Antiscaling 3D printed feed spacers via facile nanoparticle coating for membrane distillation. Water Research, 189, 116649. https://doi.org/10.1016/j.watres.2020.116649
26. G.H.Teoh, Z.A.Jawad, B.S.Ooi, S.C.Low (2022) Simultaneous water reclamation and nutrient recovery of aquaculture wastewater using membrane distillation. Journal of Water Process Engineering, 46, 102573.https://doi.org/10.1016/j.jwpe.2022.102573
27. M.Bodzek, K .Konieczny, A.Kwiecińska-Mydlak (2020) Nanotechnology in water and wastewater treatment. Graphene–the nanomaterial for next generation of semipermeable membranes. Critical reviews in environmental science and technology, 50(15), 1515-1579.https://doi.org/10.1080/10643389.2019.1664258
28. Y.Kim, J.Suhr, H.W.Seo, H.Sun, S.Kim, I.K.Park, S.H.Kim, Y.Lee, K.J.Kim, J.D.Nam (2017) All biomass and UV protective composite composed of compatibilized lignin and poly (lactic-acid). Scientific Reports, 7(1), 43596. https://doi.org/10.1038/srep43596
29. F.Ardeshiri, S.Salehi, M.Peyravi, M.Jahanshahi, A.Amiri, A.S.Rad (2018) PVDF membrane assisted by modified hydrophobic ZnO nanoparticle for membrane distillation. Asia-Pacific Journal of Chemical Engineering, 13(3), e2196. https://doi.org/10.1002/apj.2196
30. L.N.Nthunya, L.Gutierrez, A.R.Verliefde, S.D.Mhlanga (2019) Enhanced flux in direct contact membrane distillation using superhydrophobic PVDF nanofibre membranes embedded with organically modified SiO2 nanoparticles. Journal of Chemical Technology & Biotechnology, 94(9), 2826-2837. https://doi.org/10.1002/jctb.6104
31. H.F.Tan, W.L.Tan, N.Hamzah, M.H.K.Ng, B.S.Ooi, C.P.Leo (2020) Membrane distillation crystallization using PVDF membrane incorporated with TiO_2 nanoparticles and nanocellulose. Water Supply, 20(5), 1629-1642. https://doi.org/10.2166/ws.2020.068

32. I.Chimanlal, L.N.Nthunya, O.T.Mahlangu, B.Kirkebæk, A.Ali, C.A.Quist-Jensen, H.Richards (2023) Nanoparticle-enhanced PVDF flat-sheet membranes for seawater desalination in direct contact membrane distillation. Membranes, 13(3), 317. https://doi.org/10.3390/membranes13030317
33. J.Ju, K.Fejjari, Y.Cheng, M.Liu, Z.Li, W.Kang, Y.Liao (2020) Engineering hierarchically structured superhydrophobic PTFE/POSS nanofibrous membranes for membrane distillation. Desalination, 486, 114481. https://doi.org/10.1016/j.desal.2020.114481
34. J.Ju, K.Fejjari, Y.Cheng, M.Liu, Z.Li, W.Kang, Y.Liao (2020) Engineering hierarchically structured superhydrophobic PTFE/POSS nanofibrous membranes for membrane distillation. Desalination, 486, 114481. https://doi.org/10.1016/j.desal.2020.114481
35. R.Huang, Z.Liu, Y.C.Woo, W.Luo, S.R.Gray, M.Xie (2020) Emerging investigator series: engineering membrane distillation with nanofabrication: design, performance and mechanisms. Environmental Science: Water Research & Technology, 6(7), 1786-1793. DOI: 10.1039/D0EW00100G
36. L.Francis, N.Hilal (2023) Electrohydrodynamic atomization of CNT on PTFE membrane for scaling resistant membranes in membrane distillation. NPJ Clean Water, 6(1), 15.https://doi.org/10.1038/s41545-023-00229
37. D.Hou, Z.Wang, K.Wang, J.Wang, S.Lin (2018) Composite membrane with electrospun multiscale-textured surface for robust oil-fouling resistance in membrane distillation. Journal of Membrane Science, 546, 179-187. https://doi.org/10.1016/j.memsci.2017.10.017
38. M.R.El-Marghany, A.H.El-Shazly, M.S.A.Salem, M.N.Sabry, N.Nady (2019) Novel membrane suitable for membrane distillation: Effect of mixed nanofillers on the membrane performance. Key Engineering Materials, 801, 325-330. https://doi.org/10.4028/www.scientific.net/KEM.801.325
39. L.Zhao, C.Wu, X.Lu, D.Ng, Y.B.Truong, Z.Xie (2018) Activated carbon enhanced hydrophobic/hydrophilic dual-layer nanofiber composite membranes for high-performance direct contact membrane distillation. Desalination, 446, 59-69. https://doi.org/10.1016/j.desal.2018.09.002
40. E.J.Lee, A.K.An, P.Hadi, S.Lee, Y.C.Woo, H.K.Shon (2017) Advanced multi-nozzle electrospun functionalized titanium dioxide/polyvinylidene fluoride-co-hexafluoropropylene (TiO_2/PVDF-HFP) composite membranes for direct contact membrane distillation. Journal of Membrane Science, 524, 712-720. https://doi.org/10.1016/j.memsci.2016.11.069
41. O.Makanjuola, S.F.Anis, R.Hashaikeh (2021) Enhancing DCMD vapor flux of PVDF-HFP membrane with hydrophilic silica fibers. Separation and Purification Technology, 263, 118361. https://doi.org/10.1016/j.seppur.2021.118361
42. L.Francis, N.Hilal (2022) Electro sprayed CNTs on electrospun PVDF-Co-HFP membrane for robust membrane distillation. Nanomaterials, 12(23), 4331. https://doi.org/10.3390/nano12234331

IZVOD

ISTRAŽIVANJA MEMBRANA NA BAZI NANOMATERIJALA ZA EFIKASNO UKLANJANJE ZAGAĐIVAČA IZ OTPADNIH VODA PREKO MEMBRANSKE DESTILACIJE: KRITIČKI PREGLED

Zahtevi za tretman otpadnih voda su najvažniji u obezbeđivanju održivosti životne sredine i očuvanju javnog zdravlja. Kako se industrijalizacija i urbanizacija ubrzavaju, količina proizvedene otpadne vode nastavlja da se povećava, koja sadrži raznolik spektar zagađivača. Neprečišćena otpadna voda predstavlja ozbiljnu pretnju ekosistemima, vodnim telima i ljudskim zajednicama, što dovodi do zagađenja, bolesti, koje se prenose vodom, i ekološke neravnoteže. Efikasno prečišćavanje otpadnih voda postaje neophodno za ublažavanje ovih štetnih efekata uklanjanjem ili smanjenjem zagađivača pre ispuštanja u prirodne izvore vode. Ovaj proces pomaže u očuvanju kvaliteta vode, zaštiti vodenog sveta i održavanju opšteg zdravlja ekosistema. Membranska destilacija (MD) se pojavila kao obećavajuća tehnologija za prečišćavanje otpadnih voda, nudeći inovativan pristup za rešavanje izazova povezanih sa konvencionalnim metodama prečišćavanja. U MD, hidrofobna membrana služi kao selektivna barijera, dozvoljavajući vodenoj pari da prođe, dok sprečava prolaz zagađivača. Ovaj rad nudi opširan pregled najnovijih dostignuća u nanotehnologiji i membranskoj destilaciji primenjenoj u tretmanu otpadnih voda. Udubićemo se u različite vrste nanomaterijala koji su korišćeni za poboljšanje svojstava MD membrana, kao što su nanokompoziti, nanočestice i membrane od nanovlakna. Takođe istražujemo mehanizme pomoću kojih ovi nanomaterijali poboljšavaju efikasnost odvajanja, svojstva protiv obraštanja i izdržljivost MD membrana. Pored toga, ističemo potencijal hibridnih membrana koje kombinuju različite vrste nanomaterijala za dalje poboljšanje performansi MD u tretmanu otpadnih voda. Dajemo primere nedavnih studija koje su istraživale upotrebu hibridnih membrana, uključujući hibridne membrane ugljenik nanocevi-grafen oksid, membrane od nanokompozitnih nanovlakna i membrane ugrađene u nanočestice srebra. Takođe identifikujemo neke oblasti za buduća istraživanja i razvoj, kao što je povećanje i komercijalizacija sistema MD zasnovanih na nanotehnologiji. Ukratko, ovaj pregledni rad naglašava potencijal nanotehnologije da poboljša performanse MD u tretmanu otpadnih voda, što dovodi do poboljšanog kvaliteta vode i čistije životne sredine.

Ključne reči: *nanokompozit; Nanofibers; Tretman otpadnih voda; Membranska destilacija*

Naučni rad

Rad primljen: 23.04.2024.

Rad prihvaćen: 9.06.2024.

The ORCID Ids of all the authors are as follows:

1. Rashmi Kakkar: https://orcid.org/0009-0001-9565-2946

2. Dr. Dilraj Preet Kaur: https://orcid.org/0000-0002-9032-0088

3. Dr. Seema Raj: https://orcid.org/0000-0001-7217-063X

Nishant Kumar[*1], *Ikhwan Syafiq Mohd Noor*[2], *Muhd Zu Azhan Yahya*[3], *Satya Prakash*[1]

[1]*Department of Civil Engineering, Sharda University, Greater Noida, India;* [2]*Physics Division, Centre of Foundation Studies for Agricultural Sciences, Universiti Putra Malaysia, UPM Serdang, Selangor Darul Ehsan, Malaysia;* [3]*Faculty of Defence Science and Technology, Universiti Pertahanan Nasional Malaysia (UPNM), Kuala Lumpur, Malaysia.*

Review Paper
ISSN 0351-9465, E-ISSN 2466-2585
https://doi.org/10.62638/ZasMat1092

Zastita Materijala 66 (1)
40–55 (2025)

Botanical Corrosion Inhibitors in Reinforced Concrete: Material Sustainability Assessment and Analysis - A Review

ABSTRACT

Various methodologies have emerged over the past few decades aimed at controlling and mitigating corrosion. A new field has emerged in controlling corrosion through the use of plant-based corrosion inhibitors. The exploration of botanical extracts' efficacy marks a significant shift in corrosion science, tapping into the potential and utility offered by green plants. This comprehensive study serves as a review encompassing the spectrum of botanical extracts and their applications in diverse contexts concerning reinforced structures. This research critically assesses the correlation between phytochemical compositions, the methodologies employed in solvent extraction, and the adsorption mechanisms pivotal for enhancing the efficacy of plant extracts in corrosion inhibition. The primary objective lies in uncovering the role of inhibitors in safeguarding embedded steel within concrete structures while aiming to curtail corrosion rates. A focal point of this investigation revolves around the transition from employing toxic inhibitors to environmentally friendly botanical extracts for corrosion mitigation. Furthermore, this study accentuates the range of botanical extracts used as corrosion inhibitors shedding light on the specific phytochemical components responsible for driving the corrosion inhibition process. Notably, it expounds upon the future prospects of corrosion inhibitors, outlining the inherent challenges that must be addressed to facilitate their scalability for widespread commercial utilization.

Keywords: *Corrosion Inhibitors, performance evaluation, corrosion protection, botanical inhibitors, concrete deterioration.*

1. INTRODUCTION

Corrosion is the process of a material eroding attributable to chemical or electrochemical interaction of the environments, leading to material mass loss over some time [1]. Concrete and reinforcing bars are constituents of Reinforced Cement Concrete (RCC) where concrete withstands the compressive strength and the reinforcing bars govern the tensile strength. Presence of corrosion affects the durability of the concrete structures leading to failure of structures in adverse situations. Most of the structures today are made of reinforced bars. The reinforcing bars used in RCC structures should be good enough to bear tensile strength. When the corrosion starts on one region of the bars the chances of getting corrosion on the other side of the bars gets increase [1]. Due to the rapid deterioration process involved, serviceability criteria design using reinforced bars gets compromised. The corrosion of steel bars induces the concrete to swell, and triggers scaling and fissures in the concrete, resulting in catastrophic events due to compromised performances through structural deterioration [1]. The tendency of a metal to corrode is governed by its microstructures, its composition as generated during alloying, or the temperature developed during manufacturing for the deformation of a single metal surface. It would be more pragmatic to prevent corrosion instead of endeavouring to eliminate it. Corrosion mechanisms can be as diversified as the environments to which

* Corresponding author: Nishant Kumar
E-mail: Nishant.kumar4@sharda.ac.in
Paper received: 15.05.2024.
Paper accepted: 14.06.2024.
Papir is available on the website: www.idk.org.rs/journal

a substance is exposed, which makes them harder to comprehend [1]. However, it can be controlled simply by understanding the mechanisms of a reaction involved in the process. As per the study conducted by CORCON Institute of Corrosion in 2023, the corrosion-related damage and deterioration of structures is responsible for an economic impact of around 4% of the world's GDP annually. In India, this figure can even surpass an estimated 5% of the GDP per year. This is a clear indication about the lack study on protection of concrete structures against corrosion related damages which ultimately leads to reduction in the design life of the structures. The study also revealed that the saving costs can be increased between 15% to 35% of total cost if different corrosion management and controlling practices are followed [2-4]. The cost of corrosion becomes a burden due to its impacts on the economy, the safety of human life, and material resources and energy. Furthermore, the direct and indirect corrosion costs are increased due to ignoring corrosion which adds up to the economic loss for any country. The cost of corrosion as shown in Figure 1 comprises the economic loss and safety of human life [5].

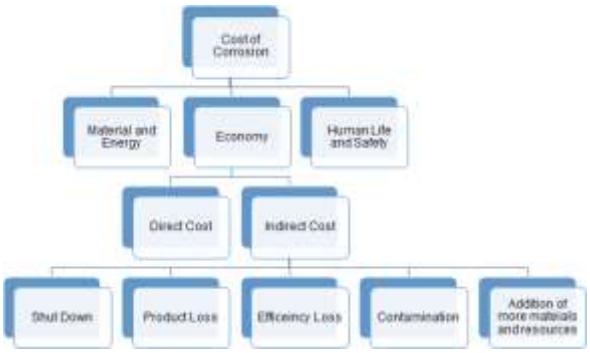

Figure 1. Cost incurred due to corrosion [5]

In Reinforced structures, trillions of dollars have been invested to control the corrosion. Research are going on in finding the best implementable corrosion protection methods [5]. The concept of green corrosion always has better scopes due to its multiple advantages. Furthermore, the efficiency of the green corrosion inhibitors is higher than the toxic organic and inorganic inhibitors. Thousands of green corrosion inhibitors are available that can be used in the form of solutions and paste in the reinforcing bars. The coating can be very effective in different environments ranging from acidic to basic to saline environments. The inhibition efficiency of those natural extracts and eco-friendly materials used in different concentrations is efficacious for use in RC structures [5].

Reinforced Concrete have flaws due to the possibility of corrosion seen in a reinforced bar, this process cannot be reversed rather it can be controlled. The phenomenon of the corrosion process is unpredictable and incalculable. Due to the influence of numerous factors including pH and temperatures, the exact calculation and prediction become difficult [6]. The corrosion behaviour shows contrast in every testing specimen too. So, the tasks become more challenging to find accurate results. The influence of the performances of the materials, and reaction on the environment show a direct impact on the corrosion process. Different preventive techniques have been introduced for a few decades. With the recent advancement in technology, numerous inorganic commercial corrosion inhibitors are available, affirming having the highest efficiency of protection of rebars. Some studies have proved that the use of arsenates, chromates, phosphates molybdates etc. inhibits corrosion in a different medium [7-9]. However, these inhibitors are expensive, non-eco-friendly, and sometimes toxic. Different standards have banned such inhibitors due to their impact on human lives. So, the need for natural inhibitors is seen in more demand due to their multiple advantages over conventional inhibitors. this review attempts to study corrosion and its mechanism in RC structures. In addition, it explains some of the major constituents of different plant-based extracts corrosion inhibitors, their mechanisms of inhibitions, and some plant-based extracts in different environments. Furthermore, this study outlook at using corrosion inhibitors for different applications, including RC structures. The phenomenon involved in corrosion initiation to corrosion inhibition process with different adsorption processes on metal surfaces.

2. LITERATURE OVERVIEW

For a better understanding of the use of corrosion inhibitors in reinforced concrete, an extensive literature review was done and the papers were analysed from 2004 to 2023. As per the database report from Google Scholar, the number of articles published on the use of corrosion inhibitors in reinforced concrete vis-à-vis year is as,

2004-2009: 9,380

2010-2014: 13,200

2015-2019: 16,500 and

2020-2023: 20,100

As evident through the increasing trend in the number of articles published on the use of corrosion inhibitors in concrete, it highlights the ongoing potential for further research in this field. The online database used to search the relevant literature on the use of corrosion inhibitors in reinforced concrete were, Scopus (www.scopus.com) and Web of Science (www.webofscience.com). The keywords that were used to search the literature were “Corrosion Inhibitors”, “corrosion”, “corrosion protection”, “botanical inhibitors”, “durability of concrete” resulted in 203 articles. After scrutinizing and removing the irrelevant and duplicate literature 84 articles were selected for the study. The selected papers were classified according to publication year and publication area.

The year-wise distribution of the articles (Figure 2) shows an increase in the number of papers published with each passing year since 2017. However, a decrease in the numbers of papers was observed in the years 2017 and 2015. Also the point to focus is from the year 2019, almost 61% of the total papers used in the study were published in the last 5 years which shows the tremendous potential of the research in this field.

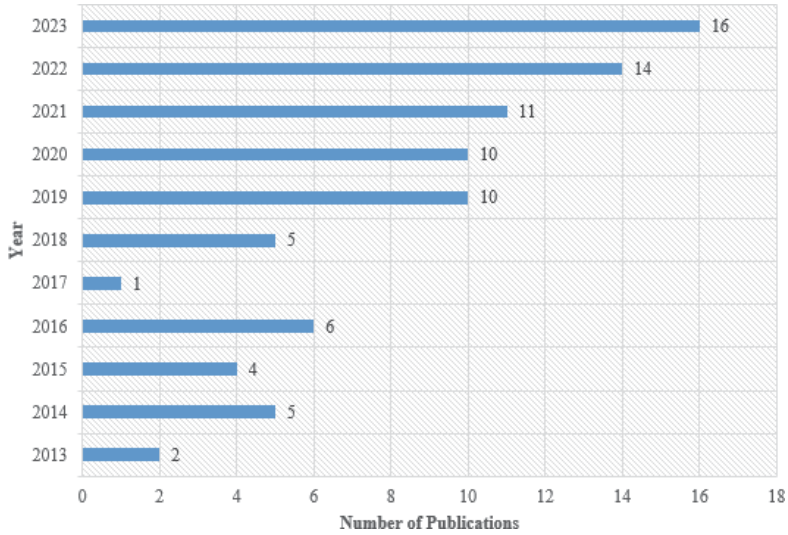

Figure 2. Papers published in last 10 years

The spatial spread of the publications revealed that almost 43% of the research was carried out by India and China, followed by Nigeria, Iran and Morocco as depicted in Figure 3. Latin America, North America, UK and South East Asia contributed very less to the research.

Figure 3. Spatial spread of the literature survey

3. CORROSION MECHANISM OF EMBEDDED REINFORCEMENT BAR

Corrosion is the inevitable degradation of steel influenced by numerous environmental parameters such as acid, moisture, etc. making it phenomenon more complex. The reactivity of the metal, the presence of inclusions, the availability of oxygen, humidity, gases such as Sulphur dioxide and carbon dioxide, and the availability of electrolytes are all factors that induce corrosion. While interlinked capillary porosity makes it very difficult for chloride ions, oxygen, and moisture to permeate concrete fractures and gives a more direct route to react with reinforced bar thus increasing the probability of corrosion [10-12]. Figure 4 explains the corrosion mechanism of reinforced concrete structures.

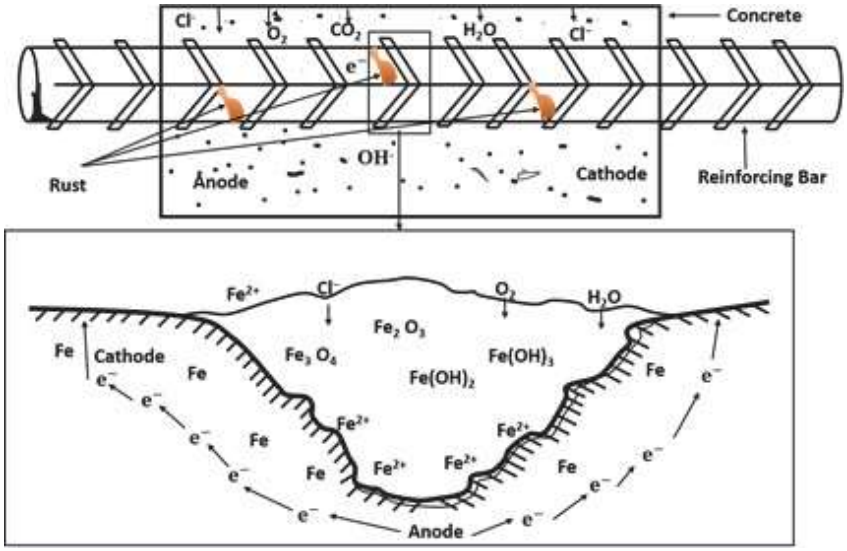

Figure 4. Corrosion mechanism in Reinforced concrete [12]

Figure 5 explains the various stages of deterioration in concrete due to corrosion of reinforcement. Initially concrete has a pH value of 11-13 which indicates high alkalinity due to the presence of $Ca(OH)_2$ which protects the reinforcement from corrosion. Carbonation is a process of chemical reaction of alkaline components in concrete (i.e. $Ca(OH)_2$) with atmospheric carbon dioxide which enters inside concrete through the surface cracks developed and causes a reduction of pH below 11 [12].

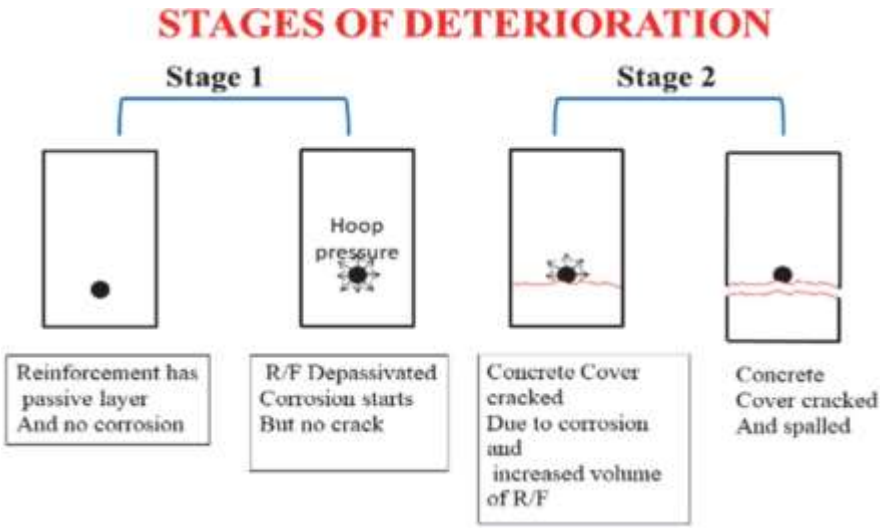

Figure 5. Stages of Deterioration due to corrosion in Reinforced concrete

During the Carbonation process, CO_2 reacts with water or moisture available near structures, since concrete is a permeable material, this gas penetrates concrete cover and reduces alkalinity to 10 or 9, and the passivating layer is damaged and once the passivating layer is damaged, corrosion starts. Once the corrosion starts, rust is formed on the surface of the steel bar which exerts hoop pressure on the surrounding concrete. Due to this continuous hoop pressure, the concrete cracks and eventually spalling of concrete occurs.

The performance of RC structures diminishes as concrete structures deteriorate due to adverse climatic conditions, and the untimely disintegration of structures before the periodic maintenance life is a primary issue for engineers and researchers. The rate at which structures degrade is influenced by the conditions of exposure and the intensity of maintenance. Corrosion, which is triggered by chemical or electrochemical responses, seems to be the most prevalent cause of RC structure deterioration. It is primarily governed by chloride ingress and RC structure carbonation depth. Carbonation and infiltration of chloride ions are the two most common causes of rebar corrosion in concrete constructions. Corrosion of RC structures begins when chloride ions pierce concrete beyond the predefined threshold or when carbonation depth surpasses concrete cover.

If corrosion commences in concrete structures, it proceeds and diminishes the structures' service life, and the pace of corrosion has an impact on the remaining serviceability of RC structures [13]. Nevertheless, these extreme environments promote reinforcement corrosion unless the requisite concentrations of oxidative degradation are accessible at the rebar level in concrete structures. Corrosion can significantly impair the strength and life of structures, and contaminants from the atmosphere can permeate through the concrete cover and induce corrosion of steel in humid situations. As explained in Figure 6 the cathode and anode are formed in various locations of the same reinforcing bar. Whenever the corrosive process is initiated, the section is degraded in the anodic region. The iron gets transformed into ferrous ionic species, which also are transferred from the anode to the cathode. These regions on the reinforcement bar exhibiting positive electrochemical potential serve as cathode material using moisture, reducing oxygen, and devouring electrons from the anode to form hydroxyl ions. Inside the electrochemical system, the steel bars act as conducting materials, whereas the concrete solution functions as the electrolytic medium whereby the ions migrate [14].

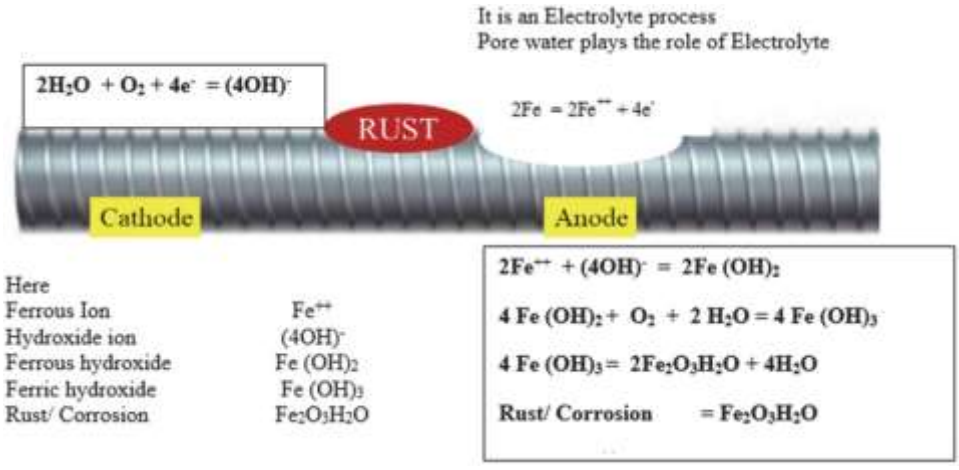

Figure 6. Anode-Cathode formation on steel reinforcement bar [14]

4. CORROSION INHIBITORS

Corrosion inhibitors are additives to concrete that are used to minimize or delay the start of corrosion in reinforced concrete structures. Corrosion inhibitors are substances that, when introduced in minute doses to corrosive environments, avoid or minimize the metal from interacting with it [15]. The majority of inhibitors stabilize steel by generating a protective layer on its surface; nevertheless, certain inhibitors react with concrete complexes to restrict the concrete's permeability. Corrosion inhibitors are typically incorporated into the normal concrete mixture in modern constructions, but they can also be sprayed on the concrete surface during repairs. Corrosion inhibitors help in reducing the ion's move-

ments within the surfaces which results in slowing down of corrosion process. Furthermore, inhibitors are known to increase the reinforcing bar's cathodic and anodic polarization behavior. The implementation of relevant and effective inhibitors is one of the most appropriate strategies for preserving metals against severe corrosion breakdown [16]. In recent decades, researchers have been looking into the inhibitory capabilities of bioactive antioxidants derived from plants, and they have revealed that they are potent inhibitors. Natural products have the advantage of becoming environmentally friendly and ecologically accepted. Different synthetic inhibitors have serious health consequences, consequently, natural products that seem to be affordable, non-toxic, and environmentally preferable must be used instead [16].

Organic and inorganic inhibitors have shown promising potential in inhibiting efficiency. Different green materials have been studied to understand the nature of the inhibiting action it can bestow for the corrosion-reducing process [17]. The inhibitors inhibit corrosion by increasing anodic or cathodic polarizing behavior, reducing ion mobility on the metallic surface, and raising the metallic surface's electrical resistance [17]. Corrosion inhibitors in concrete have become immensely popular in recent years due to their low cost and accessibility of use in today's scenario, concrete and reinforcing bars have been used worldwide [18].

4.1. Botanical Corrosion Inhibitors

Green Corrosion inhibitors are such inhibitors that serve the purpose of inhibiting corrosion mechanisms without harming human health and environment as they are non-toxic. Botanical corrosion inhibitors are called plant-based extract inhibitors. Due to their abundant availability and being environmentally friendly, the use of corrosion inhibitors has been used widely in different applications [19]. The use of such corrosion inhibitors can add to up structure's life from early deterioration. Using botanical extracts is pertinent for corrosion protection as potential botanical extracts have wide areas of applications. Leaf, roots, fruits, flowers, oil, whole plants, wooden parts including stem, branch, bark, waste, etc. all comprises the parts of plants. All parts of plants have different inhibiting compounds. Different studies on the materials and the methodology were carried out to understand the potential plant-based extract material.

It showed that the plant has an incredible corrosion inhibition potential. Similarly, the use of curcumin properties of turmeric powder had an inhibiting efficacy of 90% in 0.5M H_2SO_4 on the carbon steel [19]. A similar study was carried out on the use of Xanthan gum in a 15% HCl environment to see the insights of inhibiting efficiency. Experimental data from the lab on mild steel and Density functional theory (DFT) were used for correlation which resulted in better inhibition performances [20]. Furthermore, the use of Xanthan gum as a corrosion inhibitor in aluminium in 0.5 M HCl was also studied and it was observed that the inhibition efficiency was increased while increasing the concentration of gum extract and decreased with an increase in the temperatures [20]. Numeral studies were carried out on plant-based extracts which suggests that the corrosion mechanisms are inhibited when using corrosion inhibitors and are influenced by the substrates. These all-potential plant-based extracts have shown the influence of different adsorption mechanisms in inhibiting efficiency [21-24].

4.2. Phytochemicals in Botanical Extracts

The study of phytochemicals present in the plant-based extract is very important to understand the concentration required for corrosion inhibition for the intended applications [25-28]. Along with this, the study of different phytochemicals helps in understanding which extracts to be used from the plants. The reactivity and the adsorption types involved in the metal substrate help to identify the efficiency of botanical extract corrosion inhibitors. The phenolic acids compounds, terpenoids, carbohydrates, lipids, and alkaloids-based compounds have been proven to be effective in slowing down the corrosion process [26-28]. Figure 7 illustrates the composition of the phytochemicals present in plant-based extracts which are absorbed into the surface of metal following the process of physisorption and chemisorption. Alkaloids and phenolic acids are the most commonly seen phytochemicals in botanical extracts. The combination of different plants-based extracts and their compatibility the similar kinds of phytochemicals can be effective for increasing efficiency [29].

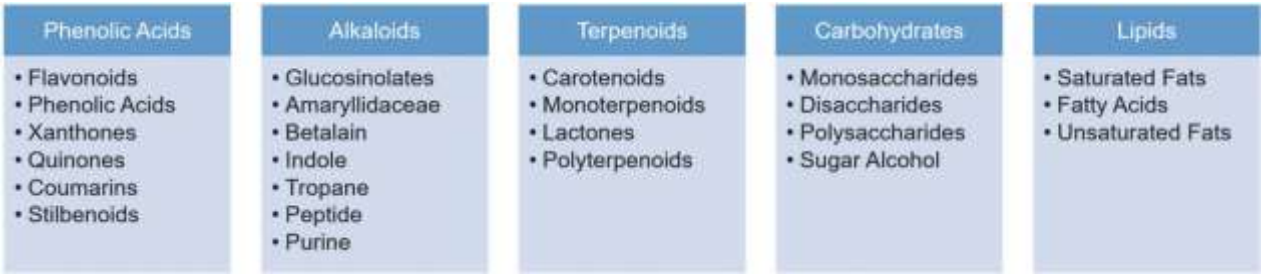

Figure 7. Phytochemicals present in botanical extract [25-29]

4.3. Solvent Extraction Methods of Botanical Extracts

The identification of phytochemicals with characterizations and quantification of plant-based extraction are done using different types of methodological approaches [30]. Figure 8 comprises both conventional and advanced solving extraction methods which are more commonly used for corrosion inhibitors solvent extractions. Maceration, percolation, decoction, etc. come under the conventional extraction methods. These methods require a higher volume of solvents with a considerably longer time for extraction. To overcome such problems, greener and advanced extraction methods were introduced like supercritical fluid (SFC), Pressurized Liquid Extraction (PLE), microwave-assisted extraction (MAE), etc. the advantages of using such methods can be as the consumption of organic solvents is lesser and has a very shorter extraction [31-32]. Such advanced methods are very effective in possessing and without losing any of those phytochemical compounds.

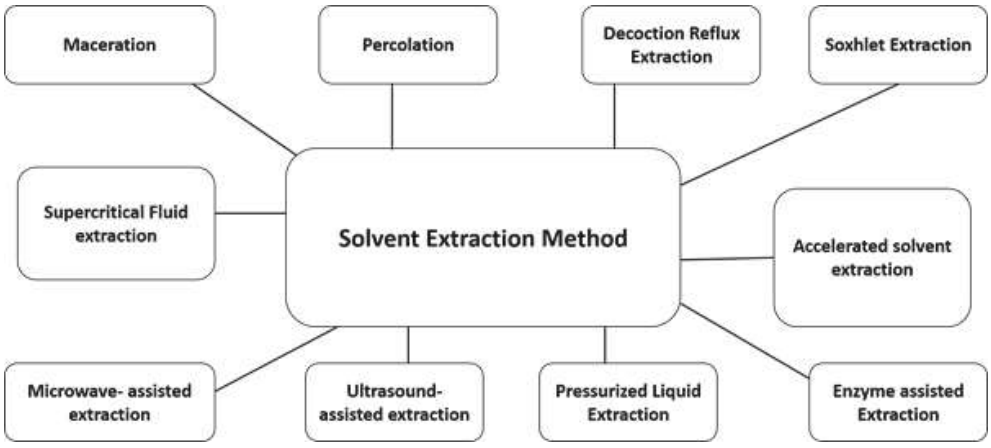

Figure 8. Solvent extraction methods of botanical extracts [33]

4.4. Performances of Botanical Extracts

Botanical extracts have been proven to be the best environmental friendly alternative due to their numerous benefits including higher efficiency in different acidic, alkaline, and saline environments [34-44]. Different advanced methods have been employed for corrosion measurement which makes it more efficient [45-61]. The role of inhibitors plays a vital role in the performance of botanical extracts. The parts of plants like leaves, fruit, peel, bark, seed, root, etc. all can have different performances with different efficiency. Studies revealed that leaf extracts are potential parts for corrosion protection [62-78]. These extracts can inhibit the corrosion process more than the other extracts. Table: 1 in acidic, Table: 2 in alkaline, and Table: 3 in saline environments show some of the potential botanical extracts capable of inhibiting the corrosion process with better efficiency.

Table: 1 Botanical extracts in acidic environment

S. No.	Plants	Parts used	Concentration	Substrate	Medium	Methodology	Efficiency (%)	References
1	Brassica oleracea	Leaves	300 mg/l	Q2355 steel	1 M HCl	XPS, FTIR, UVS, XRD Surface topography	93.8	[34]
2	Neem Leaf	Leaves	4g/200ml	Mild Steel	HCl	WL. Phytochemical test, FTIR, and GCMS	93.24	[35]
3	Solanum Lasiocarpum	Leaves	1g/L	A3 steel	HCl	WLM, PDP, EIS, FTIS, SEM	93.31	[36]
4	Triticum aestivum	straw	4g/L	Stainless Steel (SS-410)	15% HCl	PDP, AFM, XPS, SEM, XRD	92.6	[37]
5	Lilium Brownii	Leaves	200 mg/L	X70 Steel	1M HCl	EIS, FTIR, ECM	85	[38]
6	Green Eucalyptus	Leaves	800 mg/l	Mild Steel	1M HCl	EIS and polarization test	88	[39]
7	Citrullus lanatus	fruit	800 mg/l	Mild steel	1M HCl	PDP, EIS, SEM, AFM	91	[40]
8	Pomelo Peel	Fruit waste	8gm/l	Mild steel	0.1M HCL	PDP, EIS, SEM, FTIR, EDS	74.64	[41]
9	Natural Nutmeg oil	Oil	500 mg/l	L-52 carbon steel	1 M HCl	EIS, WL, ECM	94.73	[42]
10	Glycyrrhiza glabra	leaves	800g/l	Mild Steel	1 M HCl	ECM, surface Characterizations, MD simulations	88%	[43]
11	Cuscuta reflexa	Fruit	500 mg/L	Mild Steel	0.5 M H_2SO_4	UV, FTIR, AFM, SEM, DFT	95.47	[44]
12	Peganum Harmala	Leaves	283.4 g/l	C-Steel	0.25 M H_2SO_4	FTIR, EIS, SEM, UV-spectroscopy	98	[45]
13	Sunflower	Seed hull	400 g/l	Mild steel	1 M HCl	EIS, FTIR, GC analysis and dynamic polarization	98.5	[46]
14	Ginkgo	Leaves	200 mg/l	X 70 steel	1 M HCl	Electrochemical measurements, FE-SEM, AFM	90	[47]
15	Locust bean	Gum	5mM	Q 235 steel	0.5 M H_2SO_4	OCP, PDP, EIS, MDS, QCC	89.8	[48]
16	Tinospora crispa	leaves	8 g/l	Mild Steel	1 M HCl	WLM, PDP, EIS,	80	[49]
17	Punica granatum	leaves	1g/l	Mild steel	1 M HCl	FTIR, XRD, WLM, PDP	94	[50]
18	Gantiana olivieri	Fruit	800mg/l	Mild steel	0.5 M HCl	EIS, HPLC, SEM/EDX	93.7	[51]
19	Tender arecanut	Seed	4.5 g/l	Aluminum	0.5 M HCl	AIS, AFM, electrochemical measurements	94.4	[52]
20	Tagetes erecta	flower	1 g/l	Mild steel	0.5 M H_2SO_4	Gravimetric, PDP, EIS	96.1	[53]
21	Luffa Aegyptiaca	leaf	0.24 g/l	Mild steel	0.5 M H_2SO_4	PDP, FTIR, EIS	93.3	[54]
22	Borage flower	Flower	0.8 g/l	Mild Steel	1 M HCL	WLM, PDP, EIS	91	[55]

23	Red apple (malus domestica)	Fruit	5g/l	Mild steel	0.5M HCL	WLM, PDP, EIS, SEM	87.9	[56]
24	Ammi visnaga	seed	1 g/l	Mild steel	1 M HCl	PDP, EIS	84	[57]
25	Ircinia strobilina	Crude	2g/l	Mild steel	1 M HCl	WLM, PDP, LPR, EIS LC-MS	82	[58]
26	Kappaphycus alvarezii	Thallus	0.5g/l	Mild steel	1 M H_2SO_4	WLM, PDP, EIS, SEM, AFM	79.44	[59]
27	Myristica fragrans	Fruit	0.5g/l	Mild steel	0.5 M H_2SO_4	WLM, EIS, UV, SEM, AFM	87.81	[60]
28	Phyllanthus amarus	Leaves	4% (V/V)	Mild steel	1 M HCl	WLM, Gasometric technique	96.1	[61]
29	Coffea canephora	Seed	1g/l	Carbon steel	1 M HCl	EIS, SEM, WLM, PDP	94	[62]
30	Barley	Whole plant	0.1 g/l	Mild Steel	1 M HCl	WLM, EIS, SEM, PDP	92	[63]
31	Grewa Venusta	Root	8% (v/v)	Mild steel	1 M HCl	AAS, GC-MS, SEM,	97.9	[64]
32	Magnolia grandiflora	Leaves	500 mg/l	Carbon Steel	1 M HCl	WLM, PDP, EIS	88.2	[65]
33	Orange peel waste	Fruit	0.25%	Mild Steel	1 M HCl	WLM, PDP, EIS	95.36	[66]
34	Nigella sativa	seed	0.4 g/l	Mild steel	0.5 M HCL	PDP, EIS	74	[67]
35	Armoracia Rusticana	root	100 mg/l	Mild steel	0.5 M H_2SO_4	WLM, PDP, EIS, FTIR, SEM	95.74	[68]
36	Maesobatrya barteri	Leaves	0.5 g/l	Aluminum	2 M HCl	WLM, Thermometric analysis	45.15	[69]

LC-HRMS: -Liquid chromatography-high resolution mass spectrometry, EIS: Electrochemical impedance Spectroscopy, PDP: - Potentiodynamic polarization, WLM, weight Loss Method, AFM: - Atomic force Microscope , FTIR: - Fourier -Transform infrared spectroscopy, SEM: - Scanning Electron Microscope, MDS: - Molecular Dynamics Simulations , AAS: - Atomic Absorption Spectroscopy, ECM: - Electrochemical Measurement, GC-MS: - Gas Chromatography- Mass Spectrometry, OCP: - Open Circuit Potential, HPLC: - High performance liquid chromatography, UVS:- Ultraviolet Visible Spectroscopy, XRD: - X-ray Powder Diffraction Spectroscopy, LPR: - Linear Polarization Resistance, XPS: - X-ray Photoelectron spectroscopy

Table: 2 Botanical extracts on Alkaline medium

S. No.	Plants	Parts used	Concentration	Substrate	Medium	Methodology	Efficiency (%)	Referenc-es
1	Henna powder	leaves	50 mg/l	Tin	1 M NaOH	WLS, AIS, TS, SEM	95.97	[70]
2	Arecanut	husk	18 g/l	Mild Steel	0.5 M NaOH	PDP, AFM, SEM, EIS, XRD	91.66	[71]
3	Gossipium hirsutum	Leaves	52% v/v	Aluminum	2 M NaOH	Chemical Techniques, WL	97	[72]
4	(Pentaclethra macrophylla Bentham)	Root	0.3 g/l	Mild Steel	0.5 KOH	WLM, PDP, EIS	91	[73]

Table: 3 Botanical extracts in Saline environments

S. No.	Plants	Parts used	Concentration	Substrate	Medium	Methodology	Efficiency (%)	References
1	Catharanthus roseus	Stem	5mg/l	Mild steel	3.5% NaCl	WLM, PDP, EIS, SEM, XRD, DFT	96	[74]
2	Phyllanthus muellerianus	leaf	0.0833% - 0.416%	Mild steel	3.5% NaCl	WLM, PPS, AIS	97.6	[75]
3	Pomelo peel	Fruit waste	8g/l	Low carbon steel	3.5% NaCl	WLM, SEM, PDP, EDS, EIS,FTIR	71.15	[76]
4	Cascabela Thevetia	leaves	3 g/l	Carbon steel	3.5%NaCl	PDP, EFM, EIS, AFM, OCP	94.4	[77]
5	Echium amoenum fisch	Whole plant	8g/l	ST37 steel	3.5%NaCl	EIS, FTIR, SEM	99.32	[78]

5. CHALLENGES AND FUTURE SCOPE

The use of botanical extracts as corrosion inhibitors in RC structures will have a dominating demand due to their abundant availability, cost-effectiveness, eco-friendly nature, and high efficiency [34-78]. However, for larger commercial purposes, arduous efforts and innumerable challenges comes because of the different parameters involved for the adsorption mechanism facilitating corrosion inhibition [79-81]. The effectiveness of corrosion inhibition properties of various botanical extracts is distinctive [82-84]. Furthermore, the research to prove the inhibition mechanism of all potential plants is still inadequate. In addition to this, the efficient parts of each plant-based extracts exhibit different efficiency and the adsorption mechanisms of each extract are different. The solvent extraction process of extracting the samples becomes expensive when moving toward for commercial use of such inhibitors. The inhibitors inhibiting period, extraction period, storage, etc. makes a challenging task for the use of botanical extracts as corrosion inhibitors. Numeral plants-based extracts which are explored have shown problems of compatibility with other extracts, although some have showed an increase in the inhibiting efficiency but still there is inadequate research on aspects like concentration required for the highest inhibition possible, optimal concentration for compatibility etc. The study on the corrosion-inhibiting phenomena of potential ideal botanical extracts and their combination with other extracts will be beneficial to understand and apply the corrosion inhibitors for intended applications.

Also another area of research can be presence of corrosion inhibitors as coating on the reinforcement bars. As we know that the corrosion occurs on the surface of reinforcement, so there can be a possibility of providing a coating of botanical corrosion inhibitors on the surface of reinforcement to delay or prevent the corrosion. Furthermore, when coatings are provided on the surface of the reinforcement, the coating thickness plays a vital role in development of the bond strength between steel and surrounding concrete. This can be another study area to obtain the optimum coating thickness of the surface applied corrosion inhibitors. The study of corrosion inhibitors in concrete presents diverse and compelling research opportunities that can significantly contribute to the advancement of infrastructure sustainability and durability. One avenue for investigation lies in the comparative analysis of the effectiveness of various corrosion inhibitors employed in concrete. This research can delve into the differences between commonly used inhibitors, such as calcium nitrite, calcium nitrate, organic inhibitors, and silicate-based inhibitors, providing insights into their specific advantages and limitations.

Additionally, there is an opportunity to deepen our understanding of the mechanisms underlying corrosion inhibition in concrete structures. By exploring the molecular and chemical processes at play, researchers can uncover the intricate details of how inhibitors interact with the concrete matrix and prevent corrosion, paving the way for more informed and targeted approaches in inhibitor design and application. Long-term performance assessment is another crucial dimension that warrants exploration. Investigating the durability of corrosion inhibitors over extended periods of exposure to harsh environmental conditions will provide valuable data on the

sustainability of inhibitor treatments and inform maintenance strategies for aging infrastructure.

Furthermore, researchers can explore the compatibility of corrosion inhibitors with various types of concrete mixtures, including high-performance concrete, self-compacting concrete, and lightweight concrete. This line of inquiry can lead to optimized formulations that address the specific needs of different construction scenarios. A holistic approach involves considering the environmental impact of corrosion inhibitors. Assessing the eco-friendliness of inhibitors and their potential effects on the surrounding ecosystem is imperative for sustainable construction practices. Complementing this, a study of inhibitor applications in aggressive environments, such as marine or industrial settings, can provide insights into real-world challenges and opportunities for improvement.

6. CONCLUSION

Corrosion, an inevitable and relentless process, exhibits a complexity influenced by various factors. Countless protective measures have been devised to inhibit corrosion across diverse applications. Among these, the widespread use of efficient corrosion inhibitors stands out. While inorganic corrosion inhibitors demonstrate strong efficacy, their drawbacks, such as limited availability and non-eco-friendly characteristics, render them less than ideal for inhibition purposes. In contrast, botanical extracts as corrosion inhibitors present a promising prospect due to several advantages. These natural extracts are abundantly available and offer higher efficiency while employing environmentally friendly processes. This comprehensive review seeks to highlight the potential of environmentally sustainable corrosion inhibitors within different contexts. It investigates into the significance of phytochemicals present in botanical extracts, explores various solvent extraction methods, and elucidates the adsorption mechanisms utilized to enhance inhibiting efficiency. By focusing on botanical inhibitors and their comparison to toxic inorganic corrosion inhibitors, this study emphasizes the shift towards more eco-conscious solutions. Additionally, it provides an overview of the feasibility and advantages of employing botanical inhibitors across various applications, including their relevance in safeguarding reinforced concrete (RC) structures.

The exploration of botanical extracts as corrosion inhibitors unveils a promising pathway towards sustainable corrosion prevention strategies. The accessibility of these natural compounds coupled with their increased efficiency in mitigating corrosion showcases a potential alternative to conventional inhibitors. Furthermore, this review aims to draw attention to the pressing need for environmentally viable corrosion inhibition methods, advocating for a shift towards botanical inhibitors as a feasible and eco-friendly solution in combating the pervasive issue of corrosion in diverse settings.

ACKNOWLEDGEMENT

This work is supported by Department of Civil Engineering, School of Engineering and Technology, Sharda University, Greater Noida.

REFERENCES

1 O. Abakedi, I.Moses. (2016) Aluminium corrosion inhibition by Maesobatrya barteri root extract in hydrochloric acid solution. American Chemical Science Journal, 10(3), 1-10. https://doi.org/10.9734/acsj/2016/21812.

2 Y.Abboud, A.Chagraoui, O.Tanane, A.El Bouari, H.Hannache (2013) Punica granatum leave extract as green corrosion inhibitor for mild steel in Hydrochloric acid. In MATEC Web of Conferences, vol. 5, p. 04029. EDP Sciences. https://doi.org/10.1051/matecconf/20130504029.

3 A. Ahmad, R.Kumar, A.Kumar (2019) Effect of sodium molybdate and sodium tungstate in concrete rebar corrosion. Anti-Corrosion Methods and Materials, 66(3), 253-263. https://doi.org/10.1108/acmm-06-2018-1960.

4 S. Ahmad (2003) Reinforcement corrosion in concrete structures, its monitoring and service life prediction—a review. Cement and concrete composites, 25(4-5), 459-471. https://doi.org/10.1016/s0958-9465(02)00086-0.

5 N. Al Otaibi, H. H. Hammud (2021) Corrosion inhibition using Harmal leaf extract as an Eco-friendly corrosion inhibitor. Molecules (Basel, Switzerland), 26(22), 7024. https://doi.org/10.3390/molecules26227024.

6 E. Alibakhshi, M. Ramezanzadeh, G. Bahlakeh, B. Ramezanzadeh, M. Mahdavian, M. Motamedi (2018) Glycyrrhiza glabra leaves extract as a green corrosion inhibitor for mild steel in 1 M hydrochloric acid solution: Experimental, molecular dynamics, Monte Carlo and quantum mechanics study. Journal of Molecular Liquids, 255, 185–198. https://doi.org/10.1016/j.molliq.2018.01.144.

7 L. X. Alvarez, O. Troconis de Rincón, J. Escribano, B. C. Rincon Troconis (2023) Organic compounds as corrosion inhibitors for reinforced concrete: a review. Corrosion Reviews, 41(6), 617-634. https://doi.org/10.1515/corrrev-2023-0017.

8 K. K. Anupama, K. Ramya, A. Joseph (2016) Electrochemical and computational aspects of surface interaction and corrosion inhibition of mild steel in hydrochloric acid by Phyllanthus amarus leaf extract (PAE). Journal of Molecular Liquids, 216, 146–155. https://doi.org/10.1016/j.molliq.2016.01.019.

9 M. A. Asaad, G. F. Huseien, M. H. Baghban, P. B. Raja, R. Fediuk, I. Faridmehr, F. Alrshoudi (2021) Gum Arabic nanoparticles as green corrosion inhibitor for reinforced concrete exposed to carbon dioxide environment. Materials, 14(24), 7867. https://doi.org/10.3390/ma14247867.

[10] H. Ashassi-Sorkhabi, S. Mirzaee, T. Rostamikia, R. Bagheri (2015) Pomegranate (Punica granatum) peel extract as a green corrosion inhibitor for mild steel in hydrochloric acid solution. International Journal of Corrosion, 2015, 1–6. https://doi.org/10.1155/2015/197587.

[11] S. A. Asipita, M. Ismail, M. Z. Abd Majid, Z. A. Majid, C. Abdullah, J. Mirza, (2014) Green Bambusa Arundinacea leaves extract as a sustainable corrosion inhibitor in steel reinforced concrete. Journal of Cleaner Production, 67, 139-146. https://doi.org/10.1016/j.jclepro.2013.12.033.

[12] S. A. Austin, R. Lyons, M. J. Ing (2004) Electrochemical behavior of steel-reinforced concrete during accelerated corrosion testing. Corrosion, 60(2), 203-212. https://doi.org/10.5006/1.3287722.

13 E. Baran, A. Cakir, B. Yazici (2019) Inhibitory effect of Gentiana olivieri extracts on the corrosion of mild steel in 0.5 M HCl: Electrochemical and phytochemical evaluation. Arabian Journal of Chemistry, 12(8), 4303–4319. https://doi.org/10.1016/j.arabjc.2016.06.008.

14 M. Barbouchi, B. Benzidia, A. Aouidate, A. Ghaleb, M. El Idrissi (2020) Theoretical modeling and experimental studies of Terebinth extracts as green corrosion inhibitor for iron in 3% NaCl medium. Journal of King Saud University-Science, 32(7), 2995-3004. https://doi.org/10.1016/j.jksus.2020.08.004.

15 N. Bhardwaj, P. Sharma, V. Kumar (2021) Triticum aestivum extract as corrosion inhibitor for stainless steel (SS-410) in acidic media: Experimental and theoretical study. Current Research in Green and Sustainable Chemistry, 4(100189), 100189. https://doi.org/10.1016/j.crgsc.2021.100189.

16 T.K. Bhuvaneswari, P. Arulmathi (2020) Corrosion inhibition of mild steel in hydrochloric acid by leaves extract of Tephrosia purpurea. Journal of Adhesion Science and Technology, 34(22), 2424-2447. https://doi.org/10.1080/01694243.2020.1766395.

17 A. Biswas, P. Mourya, D. Mondal, S. Pal, G. Udayabhanu (2018) Grafting effect of gum acacia on mild steel corrosion in acidic medium: Gravimetric and electrochemical study. Journal of Molecular Liquids, 251, 470–479. https://doi.org/10.1016/j.molliq.2017.12.087.

18 A. Biswas, S. Pal, G. Udayabhanu (2016) Xanthan Gum and Gum Acacia as corrosion inhibitor for mild steel in 15% HCl medium. Proceedings of the International Conference on Nanotechnology for Better Living. https://doi.org/10.3850/978-981-09-7519-7nbl16-rps-70.

19 A. Biswas, S. Pal, G. Udayabhanu (2015) Experimental and theoretical studies of xanthan gum and its graft co-polymer as corrosion inhibitor for mild steel in 15% HCl. Applied surface science, 353, 173-183. https://doi.org/10.1016/j.apsusc.2015.06.128.

20 Y. Cao, C. Zou, C. Wang, W. Chen, H. Liang, S. Lin (2021) Green corrosion inhibitor of β-cyclodextrin modified xanthan gum for X80 steel in 1 M H_2SO_4 at different temperature. Journal of Molecular Liquids, 341, 117391. https://doi.org/10.1016/j.molliq.2021.117391.

21 S. Chen, S. Chen, B. Zhu, C. Huang, W. Li (2020) Magnolia grandiflora leaves extract as a novel environmentally friendly inhibitor for Q235 steel corrosion in 1 M HCl: Combining experimental and theoretical researches. Journal of Molecular Liquids, 311(113312), 113312. https://doi.org/10.1016/j.molliq.2020.113312.

22 L. J. Dacio, O. M. Troconis de Rincon, L. X. Alvarez, H. Castaneda, L. Quesada Román, B. C. Rincon Troconis (2023) Evaluating 1-Benzyl-4-Phenyl-1H-1, 2, 3-Triazole as a Green Corrosion Inhibitor in a Synthetic Pore Solution to Protect Steel Rebars. Corrosion, 79(4), 405-418. https://doi.org/10.5006/4207.

23 A. Dehghani, G. Bahlakeh, B. Ramezanzadeh, M. Ramezanzadeh (2019) A combined experimental and theoretical study of green corrosion inhibition of mild steel in HCl solution by aqueous Citrullus lanatus fruit (CLF) extract. Journal of Molecular Liquids, 279, 603–624. https://doi.org/10.1016/j.molliq.2019.02.010.

24 R. Dharmaraj, S. R. Samuyktha, K. Thansiya, S. S. Manzoor, B. N. Kumar, S. Maruvarasan (2021) Turkey berries leaves extract as corrosion inhibitor embedded steel in concrete. In IOP Conference Series: Materials Science and Engineering (Vol. 1145, No. 1, p. 012073). IOP Publishing. https://doi.org/10.1088/1757-899x/1145/1/012073.

25 P. Divya, S. Subhashini, A. Prithiba, R. Rajalakshmi (2019) Tithonia Diversifolia flower Extract as green Corrosion Inhibitor for Mild Steel in Acid Medium. Materials Today: Proceedings, 18, 1581–1591. https://doi.org/10.1016/j.matpr.2019.05.252.

26 G. Fekkar, F. Yousfi, H. Elmsellem, M. Aiboudi, M. Ramdani, I. Abdel-Rahman, L. Bouyazza (2020) Eco-friendly Chamaerops humilis L. fruit extract corrosion inhibitor for mild steel in 1 M HCl. International Journal of Corrosion and Scale Inhibition, 9(2), 446-459. https://doi.org/10.17675/2305-6894-2020-9-2-4.

27 C. M. Fernandes, T. Ferreira Fagundes, N. Escarpini dos Santos, T. Shewry de M. Rocha, R. Garrett, R. M. Borges, E. A. Ponzio (2019) Ircinia strobilina crude extract as corrosion inhibitor for mild steel in acid medium. Electrochimica Acta, 312, 137–148. https://doi.org/10.1016/j.electacta.2019.04.148.

28 G. A. Gaber, M. M. Ghobashy, M. Madani, D. M. Alshangiti, S. A. Alkhursani, S. A. Al-Gahtany, N. Nady (2021) Study of the corrosion-inhibiting activity of the green materials of the Posidonia oceanica leaves' ethanolic extract based on PVP in corrosive media (1 M of HCl). Green Processing and Synthesis, 10(1), 555–568. https://doi.org/10.1515/gps-2021-0055.

29 K. M. O. L. Goni, M. A. Mazumder (2019) Green corrosion inhibitors. Corrosion inhibitors, 30(4), 77-83. https://doi.org/10.5772/intechopen.81376.

30 L. Guo, R. Zhang, B. Tan, W. Li, H. Liu, S. Wu (2020) Locust Bean Gum as a green and novel corrosion inhibitor for Q235 steel in 0.5 M H_2SO_4 medium. Journal of Molecular Liquids, 310(113239), 113239. https://doi.org/10.1016/j.molliq.2020.113239.

31 Z. A. Hadi, A. S. Mahdi, S. S. Bahar (2020) Reed Leaves Extract as Corrosion Inhibitor for Reinforcing Steel in Concrete. In IOP Conference Series: Materials Science and Engineering (Vol. 871, No. 1, p. 012003). IOP Publishing. https://doi.org/10.1088/1757-899x/871/1/012003.

32 R. Haldhar, D. Prasad, A. Saxena (2018a) Armoracia rusticana as sustainable and eco-friendly corrosion inhibitor for mild steel in 0.5M sulphuric acid: Experimental and theoretical investigations. Journal of Environmental Chemical Engineering, 6(4), 5230–5238. https://doi.org/10.1016/j.jece.2018.08.025.

33 R. Haldhar, D. Prasad, A. Saxena (2018b) Myristica fragrans extract as an eco-friendly corrosion inhibitor for mild steel in 0.5 M H_2SO_4 solution. Journal of Environmental Chemical Engineering, 6(2), 2290–2301. https://doi.org/10.1016/j.jece.2018.03.023.

34 H. Hassannejad, A. Nouri (2018) Sunflower seed hull extract as a novel green corrosion inhibitor for mild steel in HCl solution. Journal of Molecular Liquids, 254, 377–382. https://doi.org/10.1016/j.molliq.2018.01.142.

35 B. Hou (2019) The Cost of Corrosion in China. Springer Singapore. https://doi.org/10.1007/978-981-32-9354-0.

36 M. H. Hussin, M. Jain Kassim, N. N. Razali, N. H. Dahon, D. Nasshorudin (2016) The effect of Tinospora crispa extracts as a natural mild steel corrosion inhibitor in 1M HCl solution. Arabian Journal of Chemistry, 9, S616–S624. https://doi.org/10.1016/j.arabjc.2011.07.002.

37 S. Jyothi, J. Ravichandran (2014) Luffa aegyptiaca leaves extract as corrosion inhibitor for mild steel in hydrochloric acid medium. Journal of Adhesion Science and Technology, 28(22-23), 2347-2363. https://doi.org/10.1080/01694243.2014.966886.

38 C. Kamal, M. G. Sethuraman (2014) Kappaphycus alvarezii–A marine red alga as a green inhibitor for acid corrosion of mild steel. Materials and Corrosion, 65(8), 846-854. https://doi.org/10.1002/maco.201307089.

39 A. Khadraoui, A. Khelifa, H. Hamitouche, R. Mehdaoui (2014) Inhibitive effect by extract of Mentha rotundifolia leaves on the corrosion of steel in 1 M HCl solution. Research on Chemical Intermediates, 40(3), 961–972. https://doi.org/10.1007/s11164-012-1014-y.

40 M. Khan, M. M. S. Abdullah, A. Mahmood, A. M. Al-Mayouf, H. Z. Alkhathlan (2019) Evaluation of Matricaria aurea extracts as effective anti-corrosive agent for mild steel in 1.0 M HCl and isolation of their active ingredients. Sustainability, 11(24), 7174. https://doi.org/10.3390/su11247174.

41 D. S. Kharitonov, M. Zimowska, J. Ryl, A. Zieliński, M. A. Osipenko, J. Adamiec, A. Wrzesińska, P. M. Claesson, I. I. Kurilo (2021) Aqueous molybdate provides effective corrosion inhibition of WE43 magnesium alloy in sodium chloride solutions. Corrosion Science, 190, 109664. https://doi.org/10.1016/j.corsci.2021.109664.

42 N. Kumar, S. Saharan (2022) Use of Lawsonia inermis and sodium nitrite as surface applied corrosion inhibitors. International Journal of Sustainable Construction Engineering and Technology, 13(1), 1-8. https://doi.org/10.30880/ijscet.2022.13.01.001.

43 N. Kumar, B. Chalisey, S. Saharan, M. Gupta (2019) Effect of Surface Applied Organic and Inorganic Corrosion Inhibitors on Reinforced Steel in Concrete. International Journal of Engineering and Advanced Technology, 9(2), 3023-3031. https://doi.org/10.35940/ijeat.b4092.129219.

44 N. Kumpawat, A. Chaturvedi, R. K. Upadhyay (2012) Comparative study of corrosion inhibition efficiency of naturally occurring ecofriendly varieties of holy basil (Tulsi) for tin in HNO_3 Solution. Open Journal of Metal, 02(03), 68–73. https://doi.org/10.4236/ojmetal.2012.23010.

45 H. Li, Y. Qiang, W. Zhao, S. Zhang (2021) A green Brassica oleracea L extract as a novel corrosion inhibitor for Q235 steel in two typical acid media. Colloids and Surfaces. A, Physicochemical and Engineering Aspects, 616(126077), 126077. https://doi.org/10.1016/j.colsurfa.2020.126077.

46 J. O. Madu, C. Ifeakachukwu, U. Okorodudu, F. V. Adams, I. V. Joseph (2019) Corrosion inhibition efficiency of Terminalia catappa leaves extracts on stainless steel in hydrochloric acid. Journal of Physics. Conference Series, 1378(2), 022092. https://doi.org/10.1088/1742-6596/1378/2/022092.

47 F. M. Mahgoub, A. M. Hefnawy, E. H. Abd Alrazzaq (2019) Corrosion inhibition of mild steel in acidic solution by leaves and stem extract of Acacia nilotica. Desalination and Water Treatment, 169, 49-58. https://doi.org/10.5004/dwt.2019.24681.

48 I. Manciulea, C. Bogatu, E. Comanita, A. Duta, L. Dumitrescu (2009) Mannich basis - corrosion inhibitors in saline water. Environmental Engineering and Management Journal, 8(4), 877–882. https://doi.org/10.30638/eemj.2009.125.

49 A. L. Matilla, M. I. P. Barrio, A. C. Escamilla, J. P. Ferrer, T. G. Prieto (2024) Analysis of the Effectiveness of the Application of Corrosion Inhibitors to Steel Re-Bars Embedded in Concrete. Applied Sciences, 14(8), 3364. https://doi.org/10.3390/app14083364.

50 Z. V. P. Murthy, K. Vijayaragavan (2014) Mild steel corrosion inhibition by acid extract of leaves of Hibiscus sabdariffa as a green corrosion inhibitor and sorption behavior. Green Chemistry Letters and Reviews, 7(3), 209-219. https://doi.org/10.1080/17518253.2014.924592.

51 N. A. Odewunmi, S. A. Umoren, Z. M. Gasem, S. A. Ganiyu, Q. Muhammad (2015) l-Citrulline: An active corrosion inhibitor component of watermelon rind extract for mild steel in HCl medium. Journal of the Taiwan Institute of Chemical Engineers, 51, 177–185. https://doi.org/10.1016/j.jtice.2015.01.012.

52 J. O. Okeniyi, A. P. I. Popoola, E. T. Okeniyi (2018) Cymbopogon citratus and $NaNO_2$ Behaviours in 3.5% NaCl-Immersed Steel-Reinforced Concrete: Implications for Eco-Friendly Corrosion Inhibitor Applications for Steel in Concrete. International Journal of Corrosion, 2018, 1–11. https://doi.org/10.1155/2018/5949042.

53 A. Okewale, F. Omoruwuo (2018) Neem leaf extract as a corrosion inhibitor on mild steel in acidic solution. International Journal of Engineering Research in Africa, 35, 208–220. https://doi.org/10.4028/www.scientific.net/jera.35.208.

54 M. A. Omran, M. Fawzy, A. E. D. Mahmoud, O. A. Abdullatef (2022) Optimization of mild steel corrosion inhibition by water hyacinth and common reed extracts in acid media using factorial experimental design. Green Chemistry Letters and Reviews, 15(1), 216–232. https://doi.org/10.1080/17518253.2022.2032844.

55 O. Oyewole, B. T. Ogunsemi, A. Akinmoladun, T. Oshin, J. Adeoye, P. Otowo, A. Tunbosun, T. Oreofe (2024) Performance Evaluation of Bryophyllum Leaves Extract as Corrosion Inhibitor for Mild Steel in 1M Phosphoric Acid. https://doi.org/10.21203/rs.3.rs-3996094/v1.

56 A. Pal, C. Das (2022) New eco-friendly anti-corrosion inhibitor of purple rice bran extract for boiler quality steel: Experimental and theoretical investigations. Journal of Molecular Structure, 1251, 131988. https://doi.org/10.1016/j.molstruc.2021.131988.

57 G. Palumbo, K. Berent, E. Proniewicz, J. Banaś (2019) Guar gum as an eco-friendly corrosion inhibitor for pure aluminium in 1-M HCl solution. Materials, 12(16), 2620. https://doi.org/10.3390/ma12162620.

58 D. A. Pineda Hernández, E. Restrepo Parra, P. J. Arango Arango, B. Segura Giraldo, C. D. Acosta Medina (2021) Innovative method for coating of natural corrosion inhibitor based on Artemisia vulgaris. Materials, 14(9), 2234. https://doi.org/10.3390/ma14092234.

59 Y. Qiang, S. Zhang, B. Tan, S. Chen (2018) Evaluation of Ginkgo leaf extract as an eco-friendly corrosion inhibitor of X70 steel in HCl solution. Corrosion Science, 133, 6–16. https://doi.org/10.1016/j.corsci.2018.01.008.

60 P. B. Raja, M. G. Sethuraman (2008) Natural products as corrosion inhibitor for metals in corrosive media—a review. Materials letters, 62(1), 113-116. https://doi.org/10.1016/j.matlet.2007.04.079.

[61] S. Z. Salleh, A. H. Yusoff, S. K. Zakaria, M. A. A. Taib, A. Abu Seman, M. N. Masri, M. Mohamad, S. Mamat, S. Ahmad Sobri, A. Ali, P. T. Teo (2021) Plant extracts as green corrosion inhibitor for ferrous metal alloys: A review. Journal of Cleaner Production, 304, 127030. https://doi.org/10.1016/j.jclepro.2021.127030.

62 É. Santos, R. Cordeiro, M. Santos, P. R. P. Rodrigues, A. Singh, E. D'Elia (2019) Barley Agro-industrial residues as corrosion inhibitor for mild steel in 1mol L-1HCl solution. Materials Research, 22(2). https://doi.org/10.1590/1980-5373-mr-2018-0511.

63 A. Saxena, D. Prasad, R. Haldhar (2018) Investigation of corrosion inhibition effect and adsorption activities of Cuscuta reflexa extract for mild steel in 0.5 M H_2SO_4. Bioelectrochemistry (Amsterdam, Netherlands), 124, 156–164. https://doi.org/10.1016/j.bioelechem.2018.07.006.

[64] A. Saxena, D. Prasad, R. Haldhar, G. Singh, A. Kumar (2018) Use of Saraca ashoka extract as green corrosion inhibitor for mild steel in 0.5 M H_2SO_4 Journal of Molecular Liquids, 258, 89-97. https://doi.org/10.1016/j.molliq.2018.02.104.

[65] K. Shanmuga priya, B. S. Prathibha, V. G. Vasudha, H. P. Nagaswarupa (2018) Spathodea campanulata as a corrosion inhibitor for mild steel in 1N H_2SO_4 media. Materials Today: Proceedings, 5(10), 22595–22604. https://doi.org/10.1016/j.matpr.2018.06.633.

[66] P. R. Shrestha, H. B. Oli, B. Thapa, Y. Chaudhary, D. K. Gupta, A. K. Das, A. P. Yadav (2019) Bark extract of Lantana camara in 1M HCl as green corrosion inhibitor for mild steel. Warasan Witsawakamsat. Chulalongkorn University, 23(4), 205–211. https://doi.org/10.4186/ej.2019.23.4.205.

67 E. C. Souza, B. Ripper, D. Perrone, E. D'Elia (2016) Roasted coffee extracts as corrosion inhibitors for mild steel in HCL solution. Materials Research, 19(6), 1276–1285. https://doi.org/10.1590/1980-5373-mr-2015-0740.

68 T. A. Söylev, M. G. Richardson (2008) Corrosion inhibitors for steel in concrete: State-of-the-art report. Construction and Building Materials, 22(4), 609-622. https://doi.org/10.1016/j.conbuildmat.2006.10.013.

69 M. Tariq Saeed, M. Saleem, A. H. Niyazi, F. A. Al-Shamrani, N. A. Jazzar, M. Ali (2020) Carrot (Daucus carota L.) peels extract as an herbal corrosion inhibitor for mild steel in 1M HCl solution. Modern Applied Science, 14(2), 97. https://doi.org/10.5539/mas.v14n2p97.

70 A. Thomas, M. Prajila, K. M. Shainy, A. Joseph (2020) A green approach to corrosion inhibition of mild steel in hydrochloric acid using fruit rind extract of Garcinia indica (Binda). Journal of Molecular Liquids, 312(113369), 113369. https://doi.org/10.1016/j.molliq.2020.113369.

71 Y. Tian, J. Bao, D. Xie, B. Wang, P. Zhang, T. Zhao, D. Lei (2023) The effects of organic corrosion inhibi-

tor on concrete properties and frost resistance. Journal of Building Engineering, 65, 105762. https://doi.org/10.1016/j.jobe.2022.105762.

72 İ B. Topçu, A. Uzunömeroğlu (2020) Properties of corrosion inhibitors on reinforced concrete. Journal of Structural Engineering and Applied Mechanics, 3(2), 93–109. https://doi.org/10.31462/jseam.2020.02093109.

73 S. Umoren, I. B. Obot, Z. Gasem, N. A. Odewunmi (2015) Experimental and theoretical studies of Red Apple fruit extract as green corrosion inhibitor for mild steel in HCl solution. Journal of Dispersion Science and Technology, 36(6), 789–802. https://doi.org/10.1080/01932691.2014.922887.

74 B. Valdez-Salas, R. Vazquez-Delgado, J. Salvador-Carlos, E. Beltran-Partida, R. Salinas-Martinez, N. Cheng, M. Curiel-Alvarez (2021) Azadirachta indica leaf extract as green corrosion inhibitor for reinforced concrete structures: corrosion effectiveness against commercial corrosion inhibitors and concrete integrity. Materials, 14(12), 3326. https://doi.org/10.3390/ma14123326.

75 K. K. Veedu, T. P. Kalarikkal, N. Jayakumar, N. K. Gopalan (2019) Anticorrosive performance of Mangifera indica L. Leaf extract-based hybrid coating on steel. ACS omega, 4(6), 10176. https://doi.org/10.1021/acsomega.9b00632.

76 X. Wang, H. Jiang, D. X. Zhang, L. Hou, W. J. Zhou (2019) Solanum lasiocarpum L. extract as green corrosion inhibitor for A3 steel in 1 M HCl solution. International Journal of Electrochemical Science, 14(2), 1178–1196. https://doi.org/10.20964/2019.02.06.

77 S. A. Xavier Stango, U. Vijayalakshmi (2018) Studies on corrosion inhibitory effect and adsorption behavior of waste materials on mild steel in acidic medium. Journal of Asian Ceramic Societies, 6(1), 20–29. https://doi.org/10.1080/21870764.2018.1439608.

78 B. Yang, W. Chen, D. H. Mu (2014) Study of garlic extract as a green corrosion inhibitor for mild steel in acidic media. Advanced Materials Research, 960, 118-125. https://doi.org/10.4028/www.scientific.net/amr.960-961.118.

79 Y. P. Yee, S. N. Saud, E. Hamzah (2020) Pomelo peel extract as corrosion inhibitor for steel in simulated seawater and acidic mediums. Journal of Materials Engineering and Performance, 29(4), 2202–2215. https://doi.org/10.1007/s11665-020-04774-1.

80 A. Zaher, R. Aslam, H. S. Lee, A. Khafouri, M. Boufellous, A. A. Alrashdi, M. Ouhssine (2022) A combined computational & electrochemical exploration of the Ammi visnaga L. extract as a green corrosion inhibitor for carbon steel in HCl solution. Arabian Journal of Chemistry, 15(2), 103573. https://doi.org/10.1016/j.arabjc.2021.103573.

81 H. Zhang, Z. Ni, H. Wu, P. Xu, Z. Li, W. Zhang, H. Huang, Q. Zhou, X. Yue, J. Bao, X. Li (2020) Corrosion Inhibition of Carbon Steel in Hydrochloric Acid by Chrysanthemum Indicum Extract. International Journal of Electrochemical Science, 15(6), 5487–5499. https://doi.org/10.20964/2020.06.22.

82 A. Zhao, H. Sun, L. Chen, Y. Huang, X. Lu, B. Mu, H. Gao, S. Wang, A. Singh (2019) Electrochemical Studies of Bitter Gourd (Momordica charantia) fruits as Ecofriendly Corrosion Inhibitor for Mild Steel in 1 M HCl Solution. International Journal of Electrochemical Science, 14(7), 6814–6825. https://doi.org/10.20964/2019.07.75.

83 X. Zheng, M. Gong, Q. Li, L. Guo (2018) Corrosion inhibition of mild steel in sulfuric acid solution by loquat (Eriobotrya japonica Lindl.) leaves extract. Scientific reports, 8(1), 9140. https://doi.org/10.1038/s41598-018-27257-9.

84 X. Zuo, W. Li, W. Luo, X. Zhang, Y. Qiang, J. Zhang, H. Li, B. Tan (2021) Research of Lilium brownii leaves extract as a commendable and green inhibitor for X70 steel corrosion in hydrochloric acid. Journal of Molecular Liquids, 321, 114914. https://doi.org/10.1016/j.molliq.2020.114914.

IZVOD

BILJNI INHIBITORI KOROZIJE U ARMIRANOM BETONU: PROCENA I ANALIZA ODRŽIVOSTI MATERIJALA - PREGLED

Tokom proteklih nekoliko decenija pojavile su se različite metodologije koje imaju za cilj kontrolu i ublažavanje korozije. Pojavilo se novo polje u kontroli korozije upotrebom inhibitora korozije na bazi biljaka. Istraživanje efikasnosti botaničkih ekstrakata označava značajan pomak u nauci o koroziji, koristeći potencijal i korisnost zelenih biljaka. Ova sveobuhvatna studija služi kao pregled koji obuhvata spektar botaničkih ekstrakata i njihovu primenu u različitim kontekstima u vezi sa ojačanim strukturama. Ovo istraživanje kritički procenjuje korelaciju između fitohemijskih sastava, metodologija korišćenih u ekstrakciji rastvaračem i mehanizama adsorpcije, koji su ključni za povećanje efikasnosti biljnih ekstrakata u inhibiciji korozije. Primarni cilj leži u otkrivanju uloge inhibitora u zaštiti ugrađenog čelika unutar betonskih konstrukcija sa ciljem smanjenja stope korozije. Fokus ovog istraživanja je oko prelaska sa upotrebe toksičnih inhibitora na ekološki prihvatljive botaničke ekstrakte za ublažavanje korozije. Štaviše, ova studija naglašava niz botaničkih ekstrakata koji se koriste kao inhibitori korozije, bacajući svetlo na specifične fitohemijske komponente odgovorne za pokretanje procesa inhibicije korozije. Naročito, objašnjava buduće izglede inhibitora korozije, naglašavajući inherentne izazove koji se moraju rešiti da bi se olakšala njihova skalabilnost za široku komercijalnu upotrebu.

Ključne reči: *Inhibitori korozije, ocena performansi, zaštita od korozije, biljni inhibitori, propadanje betona.*

Pregledni rad

Rad primljen: 15.05.2024.

Rad prihvaćen: 14.06.2024.

The ORCID Ids of all the authors are as follows:

Nishant Kumar: https://orcid.org/0000-0001-5477-3293

Ikhwan Syafiq Mohd Noor: https://orcid.org/0000-0003-0983-782X

Muhd Zu Azhan Yahya: https://orcid.org/0000-0003-1129-0552

Satya Prakash: https://orcid.org/0000-0001-6633-7480

Rashi Chaudhary[1], Nakshatra Bahadur Singh[2], Garima Nagpal[3], Fredrick K Saah[3], Amit Kumar Singh[4]*

[1]Department of Life Science, Sharda University, Greater Noida, India [2]Department of Chemistry and Biochemistry, Sharda University, Greater Noida, India, [3]Department of Environmental Science, Sharda University, Greater Noida, India, [4]Department of Pharmacy Practice, Galgotia University, Greater Noida

Scientific paper
ISSN 0351-9465, E-ISSN 2466-2585
https://doi.org/10.62638/ZasMat1256

Zastita Materijala 66 (1)
56 - 65 (2025)

Nanomaterials in bacterial detection: current trends and future outlook

ABSTRACT

Contamination by pathogenic bacteria represents a severe risk to public health and well-being. We outlined current approaches to detecting and sensing harmful bacteria by integrating recognition elements with nanomaterials (NMs) in this study. Nanomaterials have emerged as a transformative technology for bacterial detection due to their unique physicochemical properties, including high surface area, quantum effects, and enhanced reactivity. This review highlights the current trends in the application of various nanomaterials, such as gold nanoparticles, carbon nanotubes, and quantum dots, in the detection of bacterial pathogens. These materials enable the development of selective, and rapid detection methods through mechanisms like surface plasmon resonance, electrochemical sensing, and fluorescence. Furthermore, integrating nanomaterials with microfluidic devices and biosensors is discussed, showcasing advancements in point-of-care diagnostics. Challenges such as stability, reproducibility, and potential toxicity of nanomaterials are addressed, alongside regulatory considerations. The future outlook emphasizes the potential of emerging nanomaterials, such as graphene and metal-organic frameworks, to revolutionize bacterial detection. This review aims to enhance the scalability, cost-effectiveness, and environmental sustainability of these technologies, paving the way for widespread clinical and environmental applications.

Keywords: *Contamination, nanomaterial, nanoprobes, pathogenic bacteria, sensing*

1. INTRODUCTION

Rapid identification of pathogenic bacteria in hospital and clinical diagnostics, environmental and water quality controls, and resource-constrained situations may all help reduce food- and water-borne outbreaks [1]. Approximately one-third of all fatalities worldwide are attributed to bacterial food poisoning, which also causes 47.8 million ailments across many states annually and expensive product recalls [2]. Most cases of bacteria originate from infection or poisoning with *Listeria monocytogenes*, *Escherichia coli* O157:H7, tuberculosis, *Bacillus cereus*, *Salmonella typhimurium*, and *Clostridium perfringens*. Medicines may be used to treat the majority of bacterial illnesses; however, a significant issue arises because certain harmful bacteria have developed resistance to one or more medicines. The World Health Organisation predicts that throughout the next one to two decades, the ability of present antibiotics to combat diseases will decline [3]. The development of bacterial biofilms on production equipment surfaces in food and medical processing environments may lead to raised expenses and risk by promoting corrosion, increasing fouling, and contaminating products [4].

The PCR and ELISA have long been the gold standards for bacterial infection diagnosis [5]. Staining a urine sample is the non-culturing strategy used to identify bacterial infections; however, this method takes more time and has lower accuracy [6]. To lessen the danger of these new hazards in food, medicine, and the environment, it is urgently necessary to create reliable, early-stage screening techniques.

Magnetic NPs, gold NPs, silver NPs, and quantum dots (QDs) are examples of nanotechnology-based methods that demonstrate selective target-binding properties. They are the best options for the biosensing and detection of bacterial illnesses because of their qualities [7]. The NMs

*Corresponding author: Garima Nagpal
E- mail: gnagpal19fb@gmail.com
Paper received: 30. 01. 2024.
Paper corrected: 12. 05. 2024.
Paper accepted: 01. 07. 2024.
the website: https://www.zastita-materijala.org/

used in biosensors for the detection of bacteria were reviewed in this paper. Using nanomaterials, we highlighted the key biosensing recognition components and processes of bacterial sensing.

2. BACTERIAL SENSING AND ITS IMPORTANCE IN VARIOUS FIELDS

Bacteria can proliferate as single cells, a process known as planktonic growth, or as cellular clumps known as biofilms [8]. Increased resistance to antimicrobials and the host defence systems are among the unique physical and chemical characteristics that the biofilm community benefits from, due to a self-produced matrix of extracellular polymeric molecules [9]. At now, there are no techniques used for the identification of biofilm, despite its clinical significance [10]. Instead, most bacterial detection methods use culture-based procedures that enable the growth of bacteria to levels that can be recorded using optical density before being analyzed on a chromogenic or selective medium. These approaches have a lengthy turnaround time and need skilled users, which raises the total cost of therapy dramatically. Therefore, techniques for the accurate, quick, as well as reliable identification of harmful bacteria continue to be difficult to come across [11].

Complying with the need for lightweight, prompt diagnosis, easily navigable equipment is being designed. The development of biosensors for uses ranging from infection detection to metabolic illnesses has been fuelled by the need for point-of-care biosensor devices for healthcare purposes to have a straightforward appearance [12, 13].

3. NANO-MATERIALS FOR BACTERIAL SENSING: TYPES AND PROPERTIES

Compared to normal materials, NMs have distinct mechanical, optical, magnetic, electrical, and physical properties because of their very tiny size. This is the nano biosensor's extra benefit and the source of all its improved sensing capabilities. Various NMs have been used by researchers to improve biosensing findings' accuracy, sensitivity, and shelf life [14]. A wide range of potential uses exist for biosensors in agricultural production, and environmental monitoring, including online, in-field, and real-time detection of antibiotics, microbes, toxic materials, pathogens, pesticides, proteins, odor-causing bacteria, etc. in water, air, animals, food, soil, plants, and food processing. Biosensors are combined with cutting-edge techniques in NMs, microfluidics, and molecular biology.

Recently, there has been a lot of interest in biosensors. They are thought to be potent new instruments for identifying different biomarkers in healthcare and environmental monitoring [15]. A biosensor is a tiny apparatus that converts an identification of a biological molecule—complete cell, antibody, DNA or RNA, protein, etc. into an optical signal, nanomechanical signal, piezoelectric signal, electrical signal, mass-sensitive signal, etc [16]. When compared to traditional analytical procedures, biosensors may give a quick response in an ultrasensitive biomolecule detection, a short amount of time, and the ability to be miniaturized for portable usage with little sample processing. Fig. 1 represents a schematic image of a conventional biosensor.

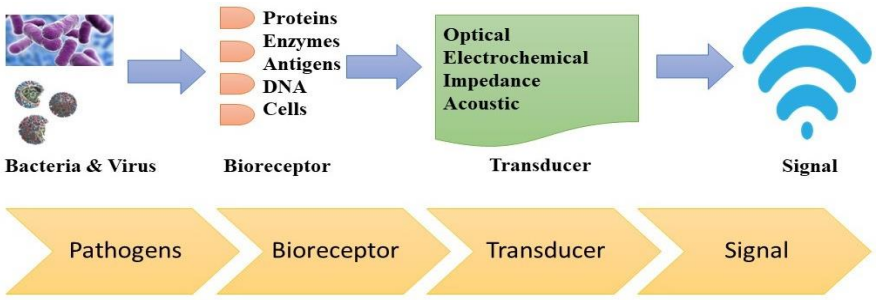

Figure 1.Guidelines for using biosensors [17]

Biosensors may find use in the following areas: bacterial sensing, water analysis, farming, healthcare,water treatment, and agriculture [15]. Numerous applications that operate in real-time have made use of biosensors. One possible method to address the aforementioned demands is to use biosensor-based detection techniques [19]. A transducer, which converts the binding event into a quantifiable signal, and a recognition element, which binds to target analytes, are the essential parts of a biosensor [20]. The surface plasmon resonance (SPR) that metal nanoparticles show is the basis for biosensor development being worked on by several research groups [21]. Various metal nanoparticle compositions and sizes may be engineered to scatter light at various wavelengths based on their unique surface plasmon resonance [22].

It is known that materials' magnetic, mechanical, optical, as well as electrical characteristics change as they are reduced to nanoscopic scales. Particles with diameters less than 100 nm that exist at the nanoscale level are referred to as nanoparticles. Because of their

distinctive physical characteristics, including homogeneity, special optical qualities, conductivity, and a high surface area to volume ratio that provides a greater area for sensing and identification, nano-materials are of interest to scientists and biologists [23]. Particles with diameters less than 100 nm that exist at the nanoscale level are referred to as nanoparticles. Various kinds of NPs and the sensing techniques employed for bacterial sensing are shown in Fig. 2.

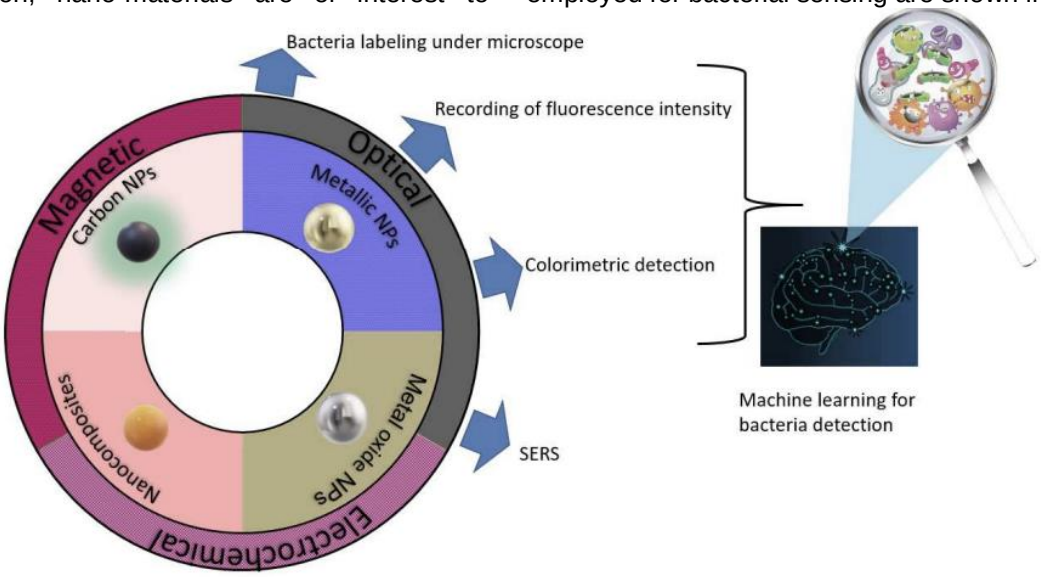

Figure 2.Figure illustrating the many types of nanoparticles, the methods of detecting bacteria, and the critical role that machine learning may play in creating a point-of-care system for infectious illness detection [24]

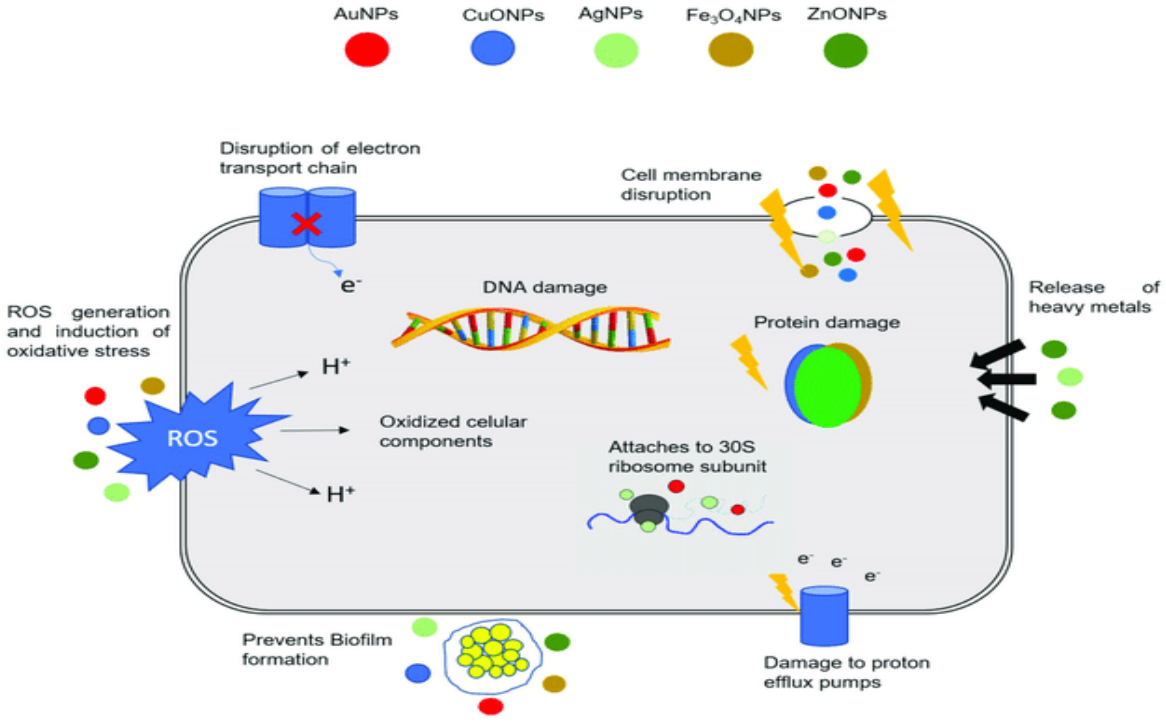

Figure 3.Several ways that NPs work in bacterial cells [26]

4. MECHANISMS OF BACTERIAL SENSING USING NANOMATERIALS

Many different mechanisms allow NMs to exert their antibacterial activity: (1) induction of intracellular effects, such as interactions with DNA and proteins; (2) reactive oxygen species (ROS) production; (3) triggering of both innate and adaptive host immune responses; and (4) direct contact with the cell wall of the bacteria; (5) reduction of the development of biofilms. They are very useful against MDR bacteria since they do not exhibit the same mechanisms of action as regular antibiotics (Figure3) [25].

Table 1. Biosensors based on nanoparticles for identifying harmful microorganisms

Trans-duction	NP	Pathogen	Function of NP	Advantages	LOD	Ref.
	Paramagnetic Nanoparticles	*E. coli*	Biosensing system	Greater sensitivity than biosensors using a self-assembling multilayer structure	10 CFU/mL	[31]
Magnetic	Magnetic Nanoparticles	*S. aureus*	Signal amplification	Assay time 15 min Turbid sample measurements made without any prior preparation Sample volumes (5–10 lL)	1 * 10^3 CFU/mL	[32]
Magnetic	Superparamagnetic Nanoparticles	*E.coli* nucleic acid *Salmonella* antibiotic-resistant genes	Biosensing system	Assay time 3 min	4–250 pM	[33]
	Superparamagnetic Nanoparticles	*E. coli*O157:H7	Biosensing system	Long-term stability Minimized noise and interferences	1 * 10^5CFU/mL	[34]
Magnetic	Gold Nanoparticles-modified screen-printed carbon electrodes	*E. coli*O157:H7	Signal amplification	–	6 CFU/ strip	[35]
	Polyaniline-coated magnetic NPs	*B. anthracis* endospores	Biosensing system	Assay time 16min	4.2 * 10^2 CFU/mL	[36]
Magnetic	SWCN (Single-walled carbon nanotubes)	*E. coli*	Biosensing system	Assay time < 20 min	–	[37]
Magnetic	Nanogold/chitosan-MWCN (multi-walled carbon nanotubes)	*S. aureus* enterotoxin B	Biosensing system	–	0.5 ng/mL	[38]
Electrochemical	Platinum Nanoparticles-coated gold nanoporous film	*E. coli*	Signal amplification	No sample pretreatment	10 CFU/mL	[39]
Electrochemical	Potassium ferrocyanide encapsulated liposomes	Cholera toxin	Biosensing system	–	1015 g/mL	[40]
Electrochemical	SWCN (Single-walled carbon nanotubes)	*S. infantis*	Biosensing system	Assay time 1 h Label-free system	100 CFU/mL	[41]
Electrochemical	Gold Nanoparticles-based graphite epoxy composite	*Salmonella sp*. ssDNA	Signal amplification	Novel material with improved properties	9 fmol	[42]
Electrochemical	Magnetic Nanoparticles-coated carbonnanotubenanocomposite	*E. coli*	Biosensing system	–	10 CFU/mL	[43]
Electrochemical	Gold Nanoparticles Magnetic Nanoparticles	*S. enteritidis* insertion element gene	Biosensing systems	–	1 ng/mL	[44]
Electrochemical	Gold Nanoparticles	*E. coli* *S. aureus*	Signal amplification	LOD was 5500 times lower than it was in the absence of Au NP	58.2 ± 1.37 pg/mL 7 * 10^5CFU/mL	[45]
Electrochemical	Gold -silver nanoparticles	*S. aureus* enterotoxin B	Biosensing system	-	0.1 ng/mL	[46]
Optical	Gold nanoparticles	*B. subtilis* genomic DNA	Biosensing system	–	2.5 fM	[47]
Optical	PAMAM-NH2dendrimer	*E. coli*	Signal amplification	–	1 * 10^4CFU/mL	[48]
Optical	CdSe/ZnS core/shell dendronnanocrystals	*E. coli*O157:H7	Biosensing system	Sensitivity greater than comparable published systems	2.3 CFU/mL	49]
	Dye-doped silica Nanoparticles	*E. coli*O157:H7	Biosensing system	High sensitivity Assay time 20 min	1 CFU/m	[52]
Optical	Liposome	RNA sequences from *B. anthracis*, *C. parvum, E. coli*	Signal amplification	Universal system	10–1000 fmoL	[51]
Optical	PAMAM-OH dendrimer	*P. aeruginosa*	Signal amplification	350% increase in sen-sitivity over the absen-ce of PAMAM-OH	–	[52]

5. TYPES OF NANOMATERIAL-BASED BACTERIAL SENSORS

The process of translating biological information into a digital signal by chemical or physical means underlies the idea of bacterial detection utilizing biosensors. This biological information is obtained by the interactions among recognition elements (bacteria, antibodies, enzymes, nucleic acids, and viruses) and their associated biological targets. Recognition components are usually immobilized through adsorption, cross-linking, covalent binding, trapping, or encapsulation onto a transducer surface [27].

Indirect (labeled) and direct (label-free) detection methods are the two categories into which biosensors fall. While the result of biological processes is identified through a labeled probe utilizing a sensor in indirect detection systems, physical changes caused by the interaction of the target analyte are measured directly and in real-time in direct detection systems, meaning no label is needed. Due to their simplicity of use, cheap cost, high sensitivity, quick response, high signal-to-noise ratio, adaptability in using recognition components, instrumental simplicity, and little interference with food matrices, electrochemical biosensors are among the numerous transducer types that show great promise [28]. Even at low concentrations in a turbid medium, bacterial cell may be detected with high sensitivity and selectivity thanks to electrochemical biosensors.

Zero-dimension (0D) and three-dimension (3D) carbon NMs have been modified for the creation of electrochemical biosensors [29]. When it comes to electrochemical sensing of bacterial infections, carbon NMs like graphene, carbon nanotubes (CNTs), and their derivatives provide a number of benefits, particularly with regard to their high field-effect sensitivity and mobility [30]. Table 1 provides an overview of the typical nanomaterial-based sensors and how well they work for quickly detecting water contaminants.

6. RECENT ADVANCES IN NANO-MATERIALS FOR BACTERIAL SENSING

NMsare being used in commercial goods at a very fast rate. By 2010, there were about four times as many commercial items on the market that claimed to have improved qualities because they used nanomaterials in 2006 [53]. The most often utilized nanomaterial in goods is silver, which is followed by materials based on carbon and metal oxides like TiO_2.

Recently, biosensors have been considered as appealing substitutes for the traditional pathogen detection platforms that are now in use. Biosensors are devices that are intended to identify and measure different biological substances such as certain DNA sequences, proteins, oligonucleotides, viruses, and bacteria [54]. A lot of the biosensors that have been created so far are affinity-based, which means that the target molecule is selectively bound by an immobilized capture probe. Detecting a change at a localised surface therefore becomes the difficulty of detecting a target in solution. A range of techniques, including surface plasmon resonance, evanescent wave, and amperometric measurements, may then be used to quantify this shift [55].

Surface water resources that are contaminated with water-borne pathogens pose a serious hazard to human health and life on a global scale [56]. Therefore, maintaining pathogen (bacteria and virus) control is essential. A unique, multifunctional magneto-plasmonic nanosensor (MPnS) with target antibodies (MPnS-Ab) was created by Panchal et al., [57] based on replaceable sandwich ELISA. In order to directly detect the bacterium *Escherichia coli* (*E. coli*), Nair et al., [58] created a unique silicon nanowire (SiNWs)-based sensing platform covered with reduced graphene oxide (RGO). *E. coli* showed preferential adherence to the SiNWs network throughout the study, which led to a drop in resistance and an increase in current. As a direct, quick, and accurate nanosensor for the detection of *E. coli* bacteria in aqueous solutions, the discovered technology shows great promise. Salaun et al., [59] described silicon nanowire-based biosensors for electrical detection of *Escherichia coli*. The sensors displayed great specificity, which was made possible by chemically modifying the nanowires to bind certain antibodies to the intended *E. coli* target. Silver nanoparticles (Ag-NPs) functionalized with fruit extracts from banana peel (*Musa paradisiaca*) and grape (*Vitis vinifera*) were green synthesized, as shown by Nqunqa et al., [60], and utilized as optical and electrochemical sensors for the detection of *E. coli*. The published limit of detection values for the optical and electrochemical sensors, respectively, are $1x10^2$ CFU/mL and $3.5x10^1$ CFU/mL, which are both within the range for *E. Coli* in saltwater.

7. CHALLENGES AND LIMITATIONS

Differentiating and identifying living from dead bacteria is a major problem when it comes to germs. Agar medium plating is capable of distinguishing between live bacteria. However, it does not include viable but uncultivable cells. Different types of optical sensors provide a number of obstacles. For example, label-based biosensors involve tagging samples with distinct fluorescent tags, which increases detection time and expense and may harm cell function. When creating biosensors to identify bacteria, the design should have high specificity, no label, viable distinguishability, affordability, small size, portability, ease of use, and minimal sample preparation processes.The biosensor designs that are now on the market can detect the sample at

various concentrations ranging from fM to aM [61]. Consequently, a highly sensitive biosensing platform that falls within the pM, zM, and yM range must be able to detect the target sample at a very low concentration. One major obstacle in the development of implanted biosensors is power consumption, which may be overcome with a self-powered gadget. Optical sensors are more expensive and difficult to use in environments with limited resources since they need filters, spectrometers, microscopes, light sources, and fluorometers. For the Patho BactD, only colorimetric and fluorescence-based sensors among many optical biosensing systems are commercially available [62]. The development of interferometric, SERS, and plasmonics-based sensors is ongoing. It's crucial to note that because of the electromagnetic field's shallow penetration depth into bacteria, plasmonic sensors' commercial uses are restricted to the detection of tiny compounds, cancer cells, and chemicals. One of the key issues is that calibration which labels may help with is necessary for the estimation of the amount of bacteria that the sensor detects [63].Other problems are more innate to the newly introduced innovative technology, like poor selectivity in microbial mixtures and intricate physiological settings [64].

8. ENVIRONMENTAL AND SOCIETAL IMPACT

Bacteria emit tiny membranous structures known as BEVs into the extracellular milieu. From a conceptual standpoint, BEVs are conceptually comparable to EVs seen in other animals, especially eukaryotes. Experimental evidence has demonstrated that different BEV phenotypes can arise from different bacterial origins and the unique mechanism of BEV production, leading to unique biological capabilities. The source of membrane vesicles (MV) is Gram-positive bacteria. In this review, all of these vesicle subtypes that originate from bacteria are referred to as BEVs, regardless of the biogenesis mechanism [65].Microbes, such as bacteria, fungi, as well as viruses, are often found in water systems. Many of these microbes are harmful to humans. A subspecies of the bacterium *Escherichia coli* (*E. coli* O157:H7) [66], which is extensively distributed in the environment and may be very harmful to humans, is one of the most hazardous diseases [67]. The “US Environmental Protection Agency (EPA)” has advised keeping an eye on *E. coli* in freshwater as an indicator organism for water danger. Thus, one of the most important requirements for maintaining such a vital natural resource is the ongoing monitoring of water quality for different pollutants in water distribution and treatment systems. To maintain continuous control over the quality of the water and to prevent tragedies that might endanger public safety, this calls for precise and easily accessible detecting systems. via enhancing water safety, the use of fast sensors to detect contaminates in the water might improve public health via early notification of biological and chemical contamination.

Few reviews have concentrated on the rapid detection of water contaminants, despite the fact that numerous reviews have summarised the current state-of-the-art achievements of nanomaterial-based sensors for water contaminant detection, such as 2-D graphene nanosheets, 1-D nanowires, and CNTs, and 0-D nanoparticles (NPs) [68]. Early recognition is one of the most promising approaches for future water sensors and smart systems since it eliminates negative impacts on the environment and human health by allowing early notifications of water pollution or ongoing water quality monitoring.

9. FUTURE PROSPECTS AND EMERGING TRENDS

The development of inexpensive, eco-friendly, user-friendly, and portable sensors that need a small amount of material for analysis has gained traction in recent years. Contemporary techniques for detecting water quality in real-time, such as MEMS, optical sensors, and biosensors, are fiercely competitive with more established ways. These sensors can analyze data in real-time and have excellent selectivity, sensitivity, and rapid reaction times. They can also identify pathogens (bacteria) and minute amounts of contaminants with high confidence and little sample preparation [69]. Combining contemporary sensing methods into one system may provide better sensitivity and selectivity as well as the potential for real-time data processing.

A transducer (optical, electrochemical, thermal, etc.) to produce a signal and a biological-indicator molecule interface make up a biosensor [70]. Antibodies, tissue slices, microbial organisms, enzymes, and cell membrane receptorsthat interact with a certain parameter might all be considered biological indicators [71]. Transducers describe a change in a physical or chemical process by generating a signal (potential or current) that is proportionate to the goal [72]. Biosensors use the selective target-immobilized target indicator interaction. There are some microfluids assays also which have been developed for the same purpose of work. They have outstanding sensing properties and advances in nanomaterials especially high surface area to volume ratio that facilitated the expansion of their application to various purposes [73].

10. CONCLUSION

Nanomaterials have undeniably revolutionized the field of bacterial detection, offering unprecedented sensitivity, selectivity, and speed. Selecting appropriate NMs provides sensitive signal transduction pathways for the sensing of

bacterial cells. The development of "next-generation" biosensors that can meet societal demands is made possible by carefully choosing the right blend of recognition components and nanomaterial transducers. The unique properties of nanomaterials, such as high surface area and enhanced reactivity, enable the development of innovative diagnostic tools that significantly improve the efficiency of pathogen detection. Current trends demonstrate the successful integration of nanomaterials with advanced technologies like microfluidic devices and biosensors, fostering the creation of portable and user-friendly point-of-care diagnostics. Despite the remarkable progress, several challenges remain. Issues related to the stability, reproducibility, and potential toxicity of nanomaterials must be thoroughly addressed to ensure safe and reliable applications.

Moreover, regulatory frameworks need to evolve in parallel with technological advancements to facilitate the commercialization and widespread adoption of nanomaterial-based detection systems. Looking ahead, emerging nanomaterials such as graphene and metal-organic frameworks hold great promise for further enhancing the capabilities of bacterial detection methods. Continued research and development efforts are essential to overcome existing limitations and to improve the scalability, cost-effectiveness, and environmental sustainability of these technologies. As these advancements come to fruition, nanomaterials are poised to play a pivotal role in safeguarding public health through more efficient and accessible bacterial detection methods, with significant implications for clinical diagnostics, environmental monitoring, and food safety.

11. REFERENCES

[1] P.D. Patel (2002) (Bio) sensors for measurement of analytes implicated in food safety: a review. Trends in Analytical Chemistry.; 21(2), 96-115. https://doi.org/10.1016/S0165-9936(01)00136-4

[2] K.E. Jones, N.G. Patel,, M.A. Levy, A. Storeygard, D. Balk, J. Gittleman, P. Daszak (2008) Global trends in emerging infectious diseases. Nature., 451(7181), 990-993. https://doi:10.1038/nature06536

[3] P.C. Ray, S.A. Khan, A.K. Singh, D. Senapati, Z. Fan (2012) Nanomaterials for targeted detection and photothermal killing of bacteria. Chemical Society Reviews.; 41(8), 3193-209. https://doi.org/10.1039/C2CS15340H

[4] L.V. Poulsen (1999) Microbial Biofilm in Food Processing. LWT - Food Science and Technology.; 32(6), 321–326. https://doi.org/10.1006/fstl.1999.0561

[5] M.S. Kumar, S. Ghosh, S. Nayak, A.P. Das (2016) Recent advances in biosensor-based diagnosis of urinary tract infection. Biosensors and Bioelectronics.; 80, 497-510. https://doi.org/10.1016/j.bios.2016.02.023

[6] J.D. Nostrand Van, A.D. Junkins, R.K. Bartholdi (2000) Poor predictive ability of urinalysis and microscopic examination to detect urinary tract infection. American journal of clinical pathology.; 113(5), 709-13. https://doi.org/10.1309/428N-60XK-UQ3Q-BXLC

[7] R. Naravaneni, K. Jamil (2005) Rapid detection of food-borne pathogens by using molecular techniques. Journal of medical microbiology.; 54(1), 51-54. https://doi.org/10.1099/jmm.0.45687-0

[8] G.O'. Toole, H.B. Kaplan, R. Kolter (2000) Biofilm formation as microbial development. Annual Reviews in Microbiology.; 54(1), 49-79. https://doi.org/10.1146/annurev.micro.54.1.49

[9] P. Stoodley, K. Sauer, D.G. Davies, J.W. Costerton (2002) Biofilms as complex differentiated communities. Annual Reviews in Microbiology.; 56(1), 187-209. https://doi.org/10.1146/annurev.micro.56.012302.160705

[10] M. Goudarzi, M. Navidinia, N. Khadembashi, R. Rasouli (2021) Biofilm Matrix Formation in Human: Clinical Significance, Diagnostic Techniques, and Therapeutic Drugs. Archives of Clinical Infectious Diseases.; 16(3), 12345, https://doi.org/10.5812/archcid.107919

[11] D. Ivnitski, I. Abdel-Hamid, P. Atanasov, E. Wilkins (1999) Biosensors for detection of pathogenic bacteria. Biosensors and Bioelectronics.; 14(7), 599-624. https://doi.org/10.1016/S0956-5663(99)00039-1

[12] A.M. Pappa, O. Parlak, G. Scheiblin, P. Mailley, A. Salleo, R.M. Owens (2018) Organic electronics for point-of-care metabolite monitoring. Trends in Biotechnology.; 36(1), 45-59. https://doi.org/10.1016/j.tibtech.2017.10.022

[13] A. Haleem, M. Javaid, R.P. Singh, R. Suman, S. Rab (2021) Biosensors applications in medical field: A brief review. Sensors International.; 2, 100100. https://doi.org/10.1016/j.sintl.2021.100100

[14] A. Munawar, Y. Ong, R. Schirhagl, M.A. Tahir, W.S. Khan, S.Z. Bajwa (2019) Nano sensors for diagnosis with optical, electric and mechanical transducers. RSC advances.; 9(12), 6793-803. https://doi.org/10.1039/C8RA10144B

[15] Z. Kotsiri, A. Vantarakis, F. Rizzotto, D. Kavanaugh, N. Ramarao, J. Vidic (2019) Sensitive detection of E. coli in artificial seawater by aptamer-coated magnetic beads and direct PCR. Applied Sciences.; 9(24),5392. https://doi.org/10.3390/app9245392

[16] C.A. Choi, Z.A. Mazrad, G. Lee, I. In, K.D. Lee, S.Y. Park (2018) Boronate-based fluorescent carbon dot for rapid and selectively bacterial sensing by luminescence off/on system. Journal of Pharmaceutical and Biomedical Analysis.; 159, 1-0. https://doi.org/10.1016/j.jpba.2018.06.043

[17] Z. Kotsiri, J. Vidic, A. Vantarakis (2022) Applications of biosensors for bacteria and virus detection in food and water–A systematic review. journal of environmental sciences.; 111, 367-79. https://doi.org/10.1016/j.jes.2021.04.009

[18] M. Kundu, P. Krishnan, R.K. Kotnala, G. Sumana (2019) Recent developments in biosensors to combat agricultural challenges and their future

prospects. Trends in food science & technology.; 88, 157-78.
https://doi.org/10.1016/j.tifs.2019.03.024

[19] M.A. Islam, A. Karim, B. Ethiraj, T. Raihan, A. Kadier (2022) Antimicrobial peptides: Promising alternatives over conventional capture ligands for biosensor-based detection of pathogenic bacteria. Biotechnology Advances.; 55, 107901. https://doi.org/10.1016/j.biotechadv.2021.107901

[20] K. Saha, S.S. Agasti, C. Kim, X. Li, V.M. Rotello (2012) Gold nanoparticles in chemical and biological sensing. Chemical reviews.; 112(5), 2739-79. https://doi.org/10.1021/cr2001178

[21] A.J. Haes, R.P. Van Duyne (2002) A nanoscale optical biosensor: sensitivity and selectivity of an approach based on the localized surface plasmon resonance spectroscopy of triangular silver nanoparticles. Journal of the American Chemical Society.; 124(35), 10596-604.
https://doi.org/10.1021/ja020393x

[22] T.A. Taton, G. Lu, C.A. Mirkin (2001) Two-color labeling of oligonucleotide arrays via size-selective scattering of nanoparticle probes. Journal of the American Chemical Society.; 123(21), 5164-5. https://doi.org/10.1021/ja0102639

[23] T. Adam, S.C. Gopinath (2022) Nanosensors: Recent perspectives on attainments and future promise of downstream applications. Process Biochemistry.; 117, 153-73.
https://doi.org/10.1016/j.procbio.2022.03.024

[24] M. Alafeef, P. Moitra, D. Pan (2020) Nano-enabled sensing approaches for pathogenic bacterial detection. Biosensors and Bioelectronics.; 165, 112276. https://doi.org/10.1016/j.bios.2020.112276

[25] R. Singh, M.S. Smitha, S.P. Singh (2014) The role of nanotechnology in combating multi-drug resistant bacteria. Journal of Nanoscience and Nanotechnology.; 14(7), 4745-56.
https://doi.org/10.1166/jnn.2014.9527

[26] P.V. Baptista, M.P. McCusker, A. Carvalho, D.A. Ferreira, N.M. Mohan, M. Martins, A.R. Fernandes (2018) Nano-strategies to fight multidrug resistant bacteria— "A Battle of the Titans". Frontiers in Microbiology.; 9, 1441.
https://doi.org/10.3389/fmicb.2018.01441

[27] R.A. Luz, R.M. Iost, F.N. Crespilho (2013) Nanomaterials for biosensors and implantable biodevices. Nanobioelectrochemistry: From Implantable Biosensors to Green Power Generation.; p.27-48. https://doi.org/10.1007/978-3-642-29250-7_2

[28] M. Berrettoni, D. Tonelli, P. Conti, R. Marassi, M. Trevisani (2004) Electrochemical sensor for indirect detection of bacterial population. Sensors and Actuators B: Chemical.; 102(2), 331-5. https://doi.org/10.1016/j.snb.2004.04.022

[29] P. Lakhera, V. Chaudhary, P. Kush, P. Kumar (2022) Nanomaterial-mediated biosensors: concept and biological applications. Multifunctional Nanocarriers.; p.523-553.
https://doi.org/10.1016/B978-0-323-85041-4.00020-2

[30] M.D. Angione, R. Pilolli, S. Cotrone, M. Magliulo, A. Mallardi, G. Palazzo, L. Sabbatini, D. Fine, A. Dodabalapur, N. Cioffi, L. Torsi (2011) Carbon based materials for electronic bio-sensing. Materials Today.; 14(9), 424-33.
https://doi.org/10.1016/S1369-7021(11)70187-0

[31] H.A. Joung, N.R. Lee, S.K. Lee, J. Ahn, Y.B. Shin, H.S. Choi, C.S. Lee, S. Kim, M.G. Kim (2008) High sensitivity detection of 16s rRNA using peptide nucleic acid probes and a surface plasmon resonance biosensor. Analytica Chimica Acta.; 630(2), 168-73.
https://doi.org/10.1016/j.aca.2008.10.001

[32] M. Koets, T. Van der Wijk, J.T. Van Eemeren, A. Van Amerongen, M.W. Prins (2009) Rapid DNA multi-analyte immunoassay on a magneto-resistance biosensor. Biosensors and Bioelectronics.; 24(7), 1893-8.
https://doi.org/10.1016/j.bios.2008.09.023

[33] H.Lee, E.Sun, D.Ham, R.Weissleder (2008) Chip–NMR biosensor for detection and molecular analysis of cells. Nature Medicine.; 14(8), 869-74.

[34] M.Mujika, S.Arana, E.Castano, M.Tijero, R.Vilares, J.M. Ruano-López, A. Cruz, L. Sainz, J. Berganza (2009) Magnetoresistive immunosensor for the detection of Escherichia coli O157: H7 including a microfluidic network. Biosensors and Bioelectronics.; 24(5), 1253-8.
https://doi.org/10.1016/j.bios.2008.07.024

[35] S. Zhu, C. Du, Y. Fu (2009) Localized surface plasmon resonance-based hybrid Au–Ag nanoparticles for detection of Staphylococcus aureus enterotoxin B. Optical Materials.; 31(11), 1608-13. https://doi.org/10.1016/j.optmat.2009.03.009

[36] H.A. Joung, N.R. Lee, S.K. Lee, J. Ahn, Y.B. Shin, H.S. Choi, C.S. Lee, S. Kim, M.G. Kim (2008) High sensitivity detection of 16s rRNA using peptide nucleic acid probes and a surface plasmon resonance biosensor. Analytica Chimica Acta.; 630(2), 168-73. https://doi.org/10.1016/j.aca.2008.10.001

[37] D. Zhang, D.J. Carr, E.C. Alocilja (2009) Fluorescent bio-barcode DNA assay for the detection of Salmonella enterica serovar Enteritidis. Biosensors and Bioelectronics.; 24(5), 1377-81. https://doi.org/10.1016/j.bios.2008.07.081

[38] H.D. Hill, R.A. Vega, C.A. Mirkin (2007) Nonenzymatic detection of bacterial genomic DNA using the bio bar code assay. Analytical Chemistry.; 79(23), 9218-23. https://doi.org/10.1021/ac701626y

[39] J. Ji, J.A. Schanzle, M.B. Tabacco (2004) Real-time detection of bacterial contamination in dynamic aqueous environments using optical sensors. Analytical Chemistry.; 76(5), 1411-8.
https://doi.org/10.1021/ac034914q

[40] Y. Liu, R. Brandon, M. Cate, X. Peng, R. Stony, M. Johnson (2007) Detection of pathogens using luminescent CdSe/ZnS dendron nanocrystals and a porous membrane immunofilter. Analytical chemistry.; 79(22), 8796-802.
https://doi.org/10.1021/ac0709605

[41] A.C. Chang, J.B. Gillespie, M.B. Tabacco (2001) Enhanced detection of live bacteria using a dendrimer thin film in an optical biosensor. Analytical Chemistry.; 73(3), 467-70.
https://doi.org/10.1021/ac000460a

[42] W. Shen, B.D. Schrag, M.J. Carter, G. Xiao (2008) Quantitative detection of DNA labeled with magnetic nanoparticles using arrays of MgO-based magnetic tunnel junction sensors. Applied Physics Letters.; 93(3), 34-42.. https://doi.org/10.1063/1.2963970

[43] S.J. Mechery, X.J. Zhao, L. Wang, L.R. Hilliard, A. Munteanu, W. Tan (2006) Using bioconjugated nanoparticles to monitor E. coli in a flow channel. Chemistry–An Asian Journal.; 1(3), 384-90. https://doi.org/10.1002/asia.200600009

[44] Q. Yang, Y. Liang, T. Zhou, G. Shi, L. Jin (2009) Electrochemical investigation of platinum-coated gold nanoporous film and its application for Escherichia coli rapid measurement. Electrochemistry Communications.; 11(4), 893-6.
https://doi.org/10.1016/j.elecom.2009.02.021

[45] S. Pal, E.C. Alocilja (2009) Electrically active polyaniline coated magnetic (EAPM) nanoparticle as novel transducer in biosensor for detection of Bacillus anthracis spores in food samples. Biosensors and Bioelectronics.; 24(5), 1437-44. https://doi.org/10.1016/j.bios.2008.08.020

[46] Y.H. Lin, S.H. Chen, Y.C. Chuang, Y.C. Lu, T.Y. Shen, C.A. Chang, C.S. Lin (2008) Disposable amperometric immunosensing strips fabricated by Au nanoparticles-modified screen-printed carbon electrodes for the detection of foodborne pathogen Escherichia coli O157: H7. Biosensors and Bioelectronics.; 23(12), 1832-7.
https://doi.org/10.1016/j.bios.2008.02.030

[47] Z.G. Chen (2008) Conductometric immunosensors for the detection of staphylococcal enterotoxin B based bio-electrocalytic reaction on micro-comb electrodes. Bioprocess and Biosystems Engineering.; 31, 345-50. DOI 10.1007/s00449-007-0168-2

[48] H.M. So, D.W. Park, E.K. Jeon, Y.H. Kim, B.S. Kim, C.K. Lee, S.Y. Choi, S.C. Kim, H. Chang, J.O. Lee (2008) Detection and titer estimation of Escherichia coli using aptamer-functionalized single-walled carbon-nanotube field-effect transistors. Small.; 4(2), 197-201. https://doi.org/10.1002/smll.200700664

[49] S. Viswanathan, L.C. Wu, M.R. Huang, J.A. Ho (2006) Electrochemical immunosensor for cholera toxin using liposomes and poly (3, 4-ethylenedioxythiophene)-coated carbon nanotubes. Analytical Chemistry.; 78(4), 1115-1121.
https://doi.org/10.1021/ac051435d

[50] P.R. Brasil de Oliveira Marques, A. Lermo, S. Campoy, H. Yamanaka, J. Barbe, S. Alegret, M.I. Pividori (2009) Double-tagging polymerase chain reaction with a thiolated primer and electrochemical genosensing based on gold nanocomposite sensor for food safety. Analytical Chemistry.; 81(4), 1332-9.
https://doi.org/10.1021/ac801736b

[51] R.A. Villamizar, A. Maroto, F.X. Rius, I. Inza, M.J. Figueras (2008) Fast detection of Salmonella Infantis with carbon nanotube field effect transistors. Biosensors and Bioelectronics.; 24(2), 279-83.
https://doi.org/10.1016/j.bios.2008.03.046

[52] Y. Cheng, Y. Liu, J. Huang, K. Li, Y. Xian, W. Zhang, L. Jin (2009) Amperometric tyrosinase biosensor based on Fe3O4 nanoparticles-coated carbon nanotubes nanocomposite for rapid detection of coliforms. Electrochimica Acta.; 54(9), 2588-94.
https://doi.org/10.1016/j.electacta.2008.10.072

[53] A.D. Maynard, R.J. Aitken, T. Butz, V. Colvin, K Donaldson, G Oberdörster, MA Philbert, J Ryan, A Seaton, V Stone, SS Tinkle. (2006) Safe handling of nanotechnology. Nature. Nov 16, 444(7117):267-9. 10.1038/444267a

[54] M. Matsishin, A. Rachkov, A. Errachid, S. Dzyadevych, A. Soldatkin (2016) Development of impedimetric DNA biosensor for selective detection and discrimination of oligonucleotide sequences of the rpoB gene of Mycobacterium tuberculosis. Sensors and Actuators B: Chemical.; 222, 1152-8. https://doi.org/10.1016/j.snb.2015.08.012

[55] H. Vaisocherová-Lísalová, I. Víšová, M.L. Ermini, T. Špringer, X.C. Song, J. Mrázek, J. Lamačová, N.S. Lynn Jr, P. Šedivák, J. Homola (2016) Low-fouling surface plasmon resonance biosensor for multi-step detection of foodborne bacterial pathogens in complex food samples. Biosensors and Bioelectronics.; 80, 84-90.
https://doi.org/10.1016/j.bios.2016.01.040

[56] P.K. Pandey, P.H. Kass, M.L. Soupir, S. Biswas, V.P Singh (2014) Contamination of water resources by pathogenic bacteria. Amb Express.; 4, 1-6. 10.1186/s13568-014-0051-x

[57] N. Panchal, V. Jain, R. Elliott, Z. Flint, P. Worsley, C. Duran, T. Banerjee, S. Santra (2022) Plasmon-Enhanced Bimodal Nanosensors: An Enzyme-Free Signal Amplification Strategy for Ultrasensitive Detection of Pathogens. Analytical Chemistry.; 94(40), 13968-77.
https://doi.org/10.1021/acs.analchem.2c03215

[58] S. Nair, V. Gautam, R. Kumar, A. Verma, V.K. Jain, S. Nagpal (2022) A novel sensing platform using silicon nanowires/reduced graphene oxide to detect pathogenic E. coli (MTCC4430) and its application in water samples. Toxicology and Environmental Health Sciences.; 14(3), 253-60.
https://doi.org/10.1007/s13530-022-00136-7

[59] Y. Benserhir, A.C. Salaün, F. Geneste, N. Oliviero, L. Pichon, A. Jolivet-Gougeon (2022) Silicon nanowires-based biosensors for the electrical detection of Escherichia coli. Biosensors and Bioelectronics.; 216, 114625.
https://doi.org/10.1016/j.bios.2022.114625

[60] S. Nqunqa, T. Muluadzi, N. Njomo, U. Feleni, R.F. Ajayi (2022) Musa Paradaisica and Vitis vinifera Functionalised Ag-NPs: Electrochemical and Optical Detection of Escherichia coli in Seawater. Journal of Surface Engineered Materials and Advanced Technology.; 12, 35-59.
https://doi.org/10.4236/jsemat.2022.123004

[61] M. Huang, X. Zhou, H. Wang, D. Xing (2018) Clustered regularly interspaced short palindromic repeats/Cas9 triggered isothermal amplification for site-specific nucleic acid detection. Analytical Chemistry.; 90(3), 2193-200.
https://doi.org/10.1021/acs.analchem.7b04542

[62] S. Riedel, K.C. Carroll (2010) Blood cultures: key elements for best practices and future directions. Journal of infection and chemotherapy.;16, 301-16. doi 10.1007/s10156-010-0069-1

[63] W. Villena Gonzales, A.T. Mobashsher, A. Abbosh (2019) The progress of glucose monitoring—A review of invasive to minimally and non-invasive techniques, devices and sensors. Sensors.; 19(4), 800. https://doi.org/10.3390/s19040800

[64] K.S. Jaiswal, N.N. Kadamannil, R. Jelinek (2023) Carbon nanomaterials in microbial sensing and bactericidal applications. Current Opinion in Colloid & Interface Science, 66, 101719. https://doi.org/10.3390/s19040800

[65] C. Liu, N. Yazdani, C.S. Moran, C. Salomon, C.J. Seneviratne, S. Ivanovski, P. Han (2024) Unveiling clinical applications of bacterial extracellular vesicles as natural nanomaterials in disease diagnosis and therapeutics. Acta Biomaterialia.; 180, 18-45. https://doi.org/10.1016/j.actbio.2024.04.022

[66] S. Ishii, M.J. Sadowsky (2008) Escherichia coli in the environment: implications for water quality and human health. Microbes and Environments.; 23(2), 101-108. https://doi.org/10.1264/jsme2.23.101

[67] S.D. Richardson (2012) Environmental mass spectrometry: emerging contaminants and current issues. Analytical Chemistry.; 84(2), 747-778. https://doi.org/10.1021/ac202903d

[68] G. Aragay, J. Pons, A. Merkoçi (2011) Recent trends in macro-, micro-, and nanomaterial-based tools and strategies for heavy-metal detection. Chemical Reviews.; 111(5), 3433-58. https://doi.org/10.1021/cr100383r

[69] V.B. Juska (2020) Design, development and characterization of nanostructured electrochemical sensors (Doctoral dissertation, University College Cork). https://hdl.handle.net/10468/10021

[70] S. Rodriguez-Mozaz, M.J. Lopez de Alda, D. Barceló (2006) Biosensors as useful tools for environmental analysis and monitoring. Analytical and Bioanalytical Chemistry.; 386, 1025-1041. DOI 10.1007/s00216-006-0574-3

[71] G. Griffiths, J. Gruenberg, M. Marsh, J. Wohlmann, A.T. Jones, R.G. Parton (2022) Nanoparticle entry into cells; the cell biology weak link. Advanced Drug Delivery Reviews.; 29, 114403. https://doi.org/10.1016/j.addr.2022.114403

[72] J.Y. Lai, Y.T. Chen, T.H. Wang, H.S. Chang, J.L. Lai (2007) Biosensor integrated with the transducer to detect the glucose. IEEE International Symposium on Circuits and Systems New Orleans, LA, USA.; 2015-2018. IEEE. https://doi.org/10.1109/ISCAS.2007.378433

[73] S.K. Bhardwaj, N. Bhardwaj, V. Kumar, D. Bhatt,A. Azzouz, J. Bhaumik, K.H. Kim, A. Deep (2021) Recent progress in nanomaterial-based sensing of airborne viral and bacterial pathogens. Environment International.; 146, 106183. https://doi.org/10.1016/j.envint.2020.106183

IZVOD

NANOMATERIJALI U DETEKCIJI BAKTERIJA: TRENUTNI TRENDOVI I BUDUĆI IZGLEDI

Kontaminacija patogenim bakterijama predstavlja ozbiljan rizik po javno zdravlje i dobrobit. U ovoj studiji izneli smo trenutne pristupe otkrivanju štetnih bakterija integracijom elemenata za prepoznavanje sa nanomaterijalima (NM). Nanomaterijali su se pojavili kao transformativna tehnologija za detekciju bakterija zbog svojih jedinstvenih fizičko-hemijskih svojstava, uključujući veliku površinu, kvantne efekte i poboljšanu reaktivnost. Ovaj pregled naglašava trenutne trendove u primeni različitih nanomaterijala, kao što su nanočestice zlata, ugljenične nanocevi i kvantne tačke, u detekciji bakterijskih patogena. Ovi materijali omogućavaju razvoj selektivnih i brzih metoda detekcije kroz mehanizme kao što su površinska plazmonska rezonanca, elektrohemijski sensing i fluorescencija. Štaviše, raspravlja se o integraciji nanomaterijala sa mikrofluidnim uređajima i biosenzorima, pokazujući napredak u dijagnostici na licu mesta. Izazovi kao što su stabilnost, ponovljivost i potencijalna toksičnost nanomaterijala su adresirani, zajedno sa regulatornim razmatranjima. Izgledi za budućnost naglašavaju potencijal nanomaterijala u nastajanju, kao što su grafen i metal-organski okviri, da revolucionišu otkrivanje bakterija. Ovaj pregled ima za cilj da poboljša skalabilnost, isplativost i ekološku održivost ovih tehnologija, utirući put širokoj kliničkoj i ekološkoj primeni.

Ključne reči: *Kontaminacija, nanomaterijal, nanosonde, patogene bakterije, sensing*

Naučni rad
Rad primljen: 30.01.2024.
Rad korigovan:12.06.2024.
Rad prihvaćen: 01.07.2024.

Dr. Garima Nagpal https://orcid.org/0000-0002-5182-8233.
Dr. Amit Singh https://orcid.org/0009-0006-4993-4201.

*Sribharathy Vijayagopal [1],Viswadhara Nagarajan[1], Jeyaprabha Chellappa[2]**

[1]Department of chemistry, Anna Adarsh College for Women, Anna Nagar, Chennai , India, [2]Department of Science and Humanities – Chemistry, Anna University – University College of Engineering Dindigul, Dindigul , India

Scientific paper
ISSN 0351-9465, E-ISSN 2466-2585
https://doi.org/10.62638/ZasMat1189

Zastita Materijala 66 (1)
66 - 74 (2025)

Bio-inspired synthesis of sulphur nanoparticles and its application

ABSTRACT

We employed an economical, swift, and environmentally friendly approach to synthesize sulphur nanoparticles, utilizing an extract from Ficus religiosa leaves. Comprehensive characterization of these nanoparticles was performed through UV-Visible Spectroscopy, FTIR, XRD, and FESEM techniques. The X-Ray diffraction method unequivocally confirmed the nanometre-scale dimensions of the synthesized sulphur nanoparticles. SEM analysis elucidated their spherical morphology, while XRD data indicated a crystalline size of 23.4 nm for these prepared nanoparticles. Besides, the antibacterial assessment of sulphur nanoparticles produced from Ficus religiosa leaves exhibited superior bioactivity against harmful bacteria species such as Escherichia Coli and Staphylococcus aureus.

Keywords: *Sulphur nanoparticles, Ficus religiosa, bioactivity, green synthesis*

1. INTRODUCTION

Sulphur ranks as the third most abundant mineral in the human body, found within essential amino acids like methionine and cysteine, crucial for protein synthesis in tissues such as skin, hair, and nails. Our body acquires necessary Sulphur from diverse sources, including animal and plant proteins, sulfinates, allicin, and sulphides. Additionally, Sulphur is a component of thiamine (vitamin B-1) & biotin (vitamin H) [1, 2].Sulphur plays vital roles in DNA construction, cell protection against diseases like cancer, metabolism, and the health of skin, tendons, and ligaments. Methionine, an essential amino acid, must be sourced from proteins, while cysteine, a non-essential amino acid, is synthesized within the body.

Furthermore, Sulphur is present in supplements like glucosamine sulfate, chondroitin sulfate, and methylsulfonylmethane (MSM), often used for alleviating joint pain and inflammation [3]. Some natural health practitioners speculate on their potential to enhance skin, fingernails, and other tissues, possibly due to the presence of serum sulphates.

However, these therapeutic claims lack comprehensive scientific validation.It's imperative to consult healthcare professionals and rely on evidence-based research before using any supplements for therapeutic purposes. While Sulphur is undeniably vital for bodily functions, its specific impact on skin, nails, and tissues may vary from person to person, necessitating further research for conclusive evidence.

Glucosamine sulphate, chondroitin sulphate, and methylsulfonylmethane (MSM) are commonly used supplements for joint health, and they do contain Sulphur in various forms. Some individuals believe these supplements can also benefit the skin and other tissues, but these claims are often anecdotal and not supported by rigorous scientific studies.It's crucial to consult with healthcare professionals and rely on evidence-based research before using any supplements for therapeutic purposes. While Sulphur is undoubtedly important for the body's functions, its specific effects on skin, nails, and other tissues may vary from person to person and require further research to establish definitive conclusions.

However, its application in agrochemical industries is currently limited due to the requirement of bulk quantities and the potential development of resistance in target species. Additionally, the high hydrophobicity of Sulphur has restricted its practical use. Nevertheless, the emergence of nanotechnology offers a new avenue

*Corresponding author: Jeyaprabha Chellappa
E-mail: drcjeyaprabha@gmail.com
Paper received: 12.10.2023.
Paper corrected: 20.06.2024.
Paper accepted: 05.07.2024.
The website: https://www.zastita-materijala.org/

for Sulphur utilization. Surface-modified nano-sized Sulphur nanoparticles (SNPs) have shown remarkable antimicrobial and antifungal activities, as reported in previous studies [4-6]. Polymeric sulphur nanoparticles are found to be effective against gram-positive methicillin resistantS.aureus and gram-negative P.aeruginosa [7,8]. These SNPs have also been utilized in the production of anticancer and antibacterial agents [9].

GREEN SYNTHESIS OF NANOMATERIALs

In the past decade, nanoscience and technology have seen intriguing developments in novel synthesis methods for various nanomaterials, including metal nanoparticles; quantum dots, carbon nanotubes, graphene materials and their related composites [10-15]. Researchers have explored two fundamental principles of synthesis, namely top-down and bottom-up methods, to achieve nanomaterials with desired sizes, shapes, and functionalities, as depicted in Fig.1[16]. Earlier techniques involved lithographic methods, ball milling, etching, and sputtering [17]. In the bottom-up approach, the nanoparticles are prepared from small molecules using techniques such as PVD (physical vapour deposition), CVD (chemical vapour deposition), sol-gel method, spray and laser pyrolysis methods, etc.The morphological characteristics of nanoparticles such as size, shape can be controlled by adjusting chemical concentrations and reaction conditions, such as temperature and pH.

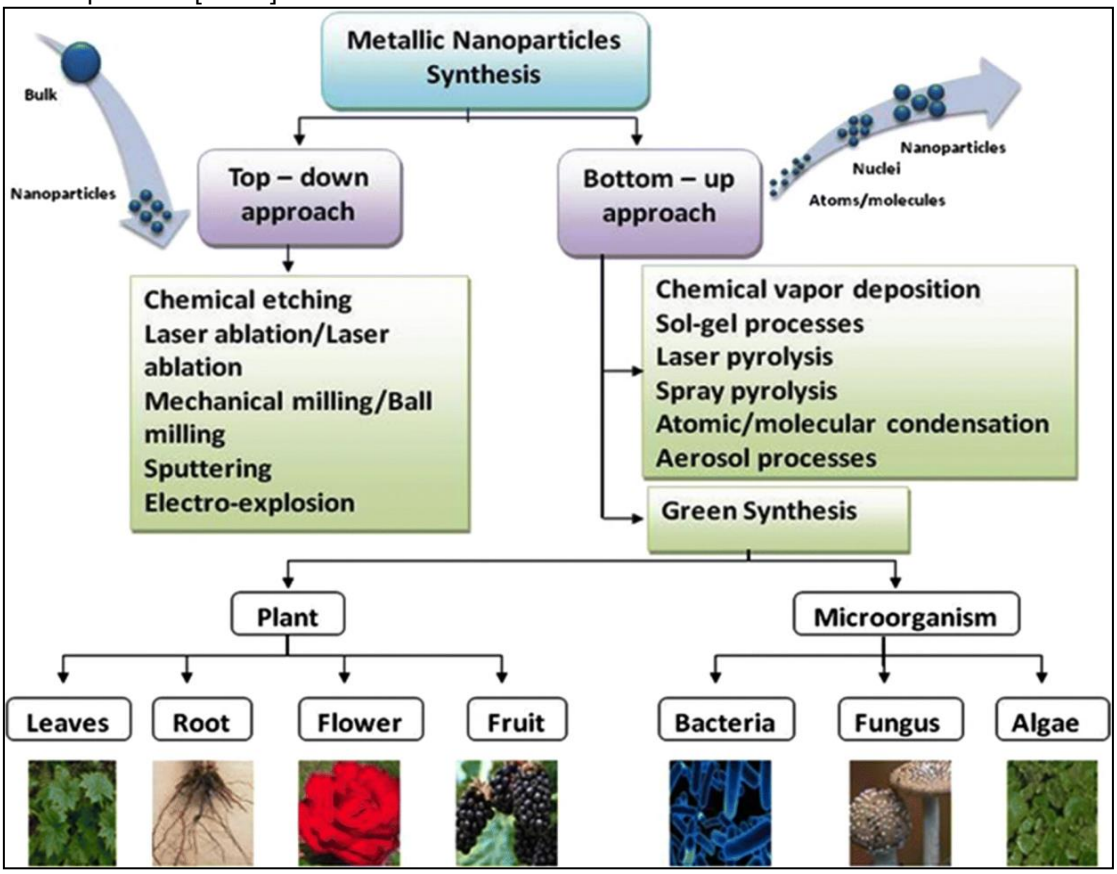

Figure 1. Top Down and Bottom-up approaches of synthesis of Nano particles [15]

However, these produced nanomaterials face challenges when applied practically including stability in aggressive environments, lack of understanding in fundamental mechanisms, modelling factors, bioaccumulation/toxicity concerns, extensive analysis requirements, need for skilful operators, challenges in device assembly and structures, and issues related to recycling/reuse/ regeneration. To address these limitations, there is a growing focus on green synthesis approaches in current materials science and technology research and development. Green synthesis methods, involving regulation, control, clean-up, and remediation processes, enhance the environmental friendliness of materials/ nanomaterials. Green synthesis principles include minimizing waste, reducing derivatives/pollution, and utilizing safer or non-toxic solvents/auxiliaries and renewable feedstock.

To prevent the formation of unwanted by-products and establish consistent, sustainable, eco-friendly synthesis procedures, the use of suitable solvent systems and natural resourcessuch as organic systems, is crucial. Green synthesis of metallic nanoparticles has gained momentum, especially utilizing biological materials viz., microorganisms – bacterial species, fungus species, algal extract and plant extracts. Among these methods, plant extract-mediated synthesis is a simple, easily adaptable and scalable process, making it easy to produce the nano scale materials on a large scale compared to microorganisms mediated synthesis. The resulting materials are collectively fall under the category of biogenic nanoparticles [18, 19].

'Green Synthesis' isvitaland mostly practiced method now-a-days, mainly to minimize the production of unwanted and harmful by-products formation during the build-up of reliable, sustainable and eco-friendly synthesis methods. The use of suitable solvent systems and naturally available resources are necessary to achieve the goal. Green synthesis of metallic nanoparticles has been accepted to have scope for various biological materials. Among the available eco-friendly methods of synthesis for nanoparticles, utilization of plant extracts is quite simple and easy process to prepare nanoparticles at large scale relative to other microorganisms mediated synthesis. These products are known collectively as biogenic nanoparticles [19, 20].

To synthesize sulphur nanoparticles, we utilized leaves from the *Ficus religiosa* tree, a significant and revered species in Indian culture due to its mythological, religious, and medicinal importance. Traditional Indian medicine has long utilized different parts of this tree for various ailments. The bark serves as an antibacterial, antiprotozoal, antiviral, astringent, and anti-diarrheal agent, treating conditions like gonorrhea and ulcers. Moreover, the leaves are used for skin diseases, exhibiting anti-venom properties and regulating menstrual cycles.

Both aqueous and ethanolic extracts from *F.religiosa*leaves demonstrated antibacterial effects against multiple strains, including Staphylococcus aureus, *Salmonella paratyphi, Shigella dysenteriae, Salmonella typhimurium, Pseudomonas aeruginosa, Bacillus subtillis, Escherichia coli,*etc. Notably, the methanolic extract of *F.religiosa*leaves inhibited the production of nitric oxide and proinflammatory cytokines in LPS-stimulated microglia via the mitogen-activated protein kinases (MAPK) pathway, as confirmed by cell viability, nitric oxide, and enzyme-linked immune-sorbent assays(ELISA)[21]. This extract showed robust anti-inflammatory properties in microglial activation, suggesting a potential neuroprotective effect against inflammation mediated by inflammatory mediators such as nitric oxide.

Synthesizing nanoparticles using plant extracts offers several advantages compared with other green synthesis methods because plants are eco-friendly and easy to handle [22]. Moreover, it offers energy efficiency, low toxicity, high yield, time-, cost-effectiveness, availability. Phytochemicals in plants, such as neo-clerodane flavanol glycosides, ergosterol, iridoid glycosides, phytoecdysones, other polyphenols, play an essential role in the green synthesis of nanoparticles as reducing, capping, and stabilizing agents [23].

In the present study, sulfur nanoparticles (SNPs) were prepared through an environmentally friendly process using *F.religiosa* leaf extract. *F.religiosa*leaves were selected due to their proven activity as an efficient biomaterial for the synthesis of nanoparticles and ease of availability.*F.religiosa* is tolerant to widely varying climatic conditions. *F.religiosa* is used in traditional medicine systems such as Ayurvedic, Siddha and Unani for disorders like asthma, diabetes, diarrhoea, gastric trouble, inflammatory disordersand infectiousdiseases.Moreover *F.religiosa* has a lifespan 900 and 1,500 years.

2. EXPERIMENTAL PROCEDURES

2.1. Materials required

*Ficus religiosa*leaves were collected from trees in Anna Nagar, Chennai. Sodium thiosulphate pentahydrate ($Na_2S_2O_3 \cdot 5H_2O$, 99.5%), citric acid ($C_6H_8O_7$) and deionized water were procured from lab chemicals (Chennai).

2.2. Preparation of leaf extract

Ficus religiosa leaves were washed thoroughly with tap water and then with deionized water until all the unwanted visible dirt particles were removed. Subsequently, the leaves were allowed to dry at room temperature to remove surface moisture. The dried leaves were chopped into fine pieces and 100gm of them were dispersed into 1000 ml of deionized water. The mixture was boiled at 100°C for 2 hours and filtered. The filtrate solution was used as a leaf extract. The supernatant liquid was found to exhibit fluorescence when kept under UV light and a laboratory test was performed to detect the presence of sulphur.

2.3.Preparation of sulphur nanoparticles (SNPS)

Before the synthesis of SNPs, all the glassware was cleaned using an *aqua regia* solution to remove the potential nucleation sites on the surface of the glassware. First, sodium thiosulpate pentahydrate (0.078 M) was dissolved in 250 ml deionised water and to this solution 100 ml *Ficus religiosa* leaf extract was added. After 5 min of continuous stirring, 125 ml of 20% citric acid ($C_6H_8O_7$) was added into the preceding reaction mixture. After the mixture was kept for 1 h at continues stirring, a precipitation was observed. The moisture was then centrifuged for 15 minutes at 5000 rpm and supernatant was removed. The precipitate was then washed and dried; the scheme diagram is shown **in Fig. 2.**

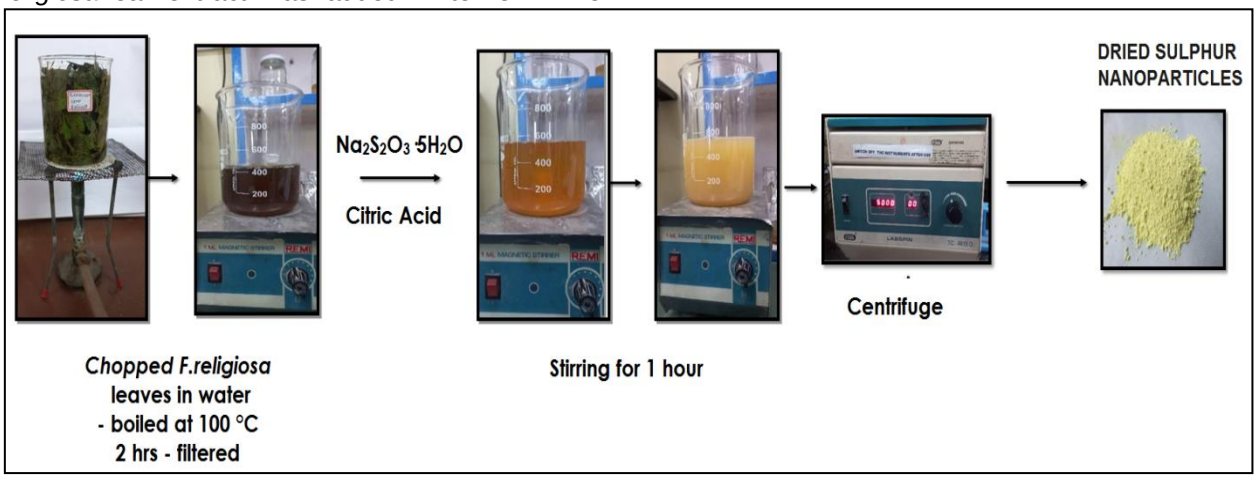

Figure 2. Scheme Diagram - Synthesis of Sulphur Nanoparticles

2.4. Characterization of sulphur nanoparticles (SNPS)

The prepared bio-inspired sulphur nano particles were characterized using various spectral techniques like UV-Visible, FTIR spectroscopy, XRD, SEM and EDAX. The UV-Visible studies were carried out using UV-Visible Spectrophotometer (Model - JAZ; Oceian Optics, USA), and FTIR spectral studies were carried out using Spectrum Two FT-IR / SP10 Software (Perkin Elmer).

The X-ray diffraction and SEM studies were carried out using P-XRD (2θ range5to 130) (Model-Smart Lab SE X-Ray; Rigaku, Japan and Model-Quattro S; Make-Thermo-Fisher Scientific, USA).

2.5. Antibacterial activity of SNPS

The efficiency of the antibacterial property of sulphur nanoparticles was examined by the disc diffusion method on Muller Hinton agar (MHA) medium. Muller Hinton Agar (MHA) medium is poured into the Petri plate. The activities of bio-inspired sulphur nanoparticles were evaluated individually and in combination with the antibiotics by soaking 20µl sulphur nanoparticles solution in the respective antibiotic discs and sulphur nanoparticles alone on a sterile disc. The leaf extract was maintained as a control. On incubation at 37°C for 24 h, the zones of inhibition were measured in millimeter.

3. RESULT AND DISCUSSION

3.1. Testing of sulphur by lassaigne's test

Sulphur present in the resulting product is detected by Lassaigne's test by taking a small piece of Na metal is heated in a fusion tube with the precipitate obtained. To the Lassaigne's filtrate, few drops of sodium nitroprusside have been added and the solution turned purple which confirms the presence of sulphur (Fig. 3).

Figure 3. Testing of Sulphur by Lassaigne's test

3.2. UV analysis of sulphur nanoparticles (SNPS)

Fig. 4 shows the UV-Vis spectrum of sulphur nanoparticles (SNPs), it is well known that α-sulphur exhibits an optical absorption maximum in the range of 260–280 nm.The peak at 274nm in figure 3 indicates the successful formation of SNPs. A secondary peak at ~324nm corresponds to the b2 → e3 transition [24].

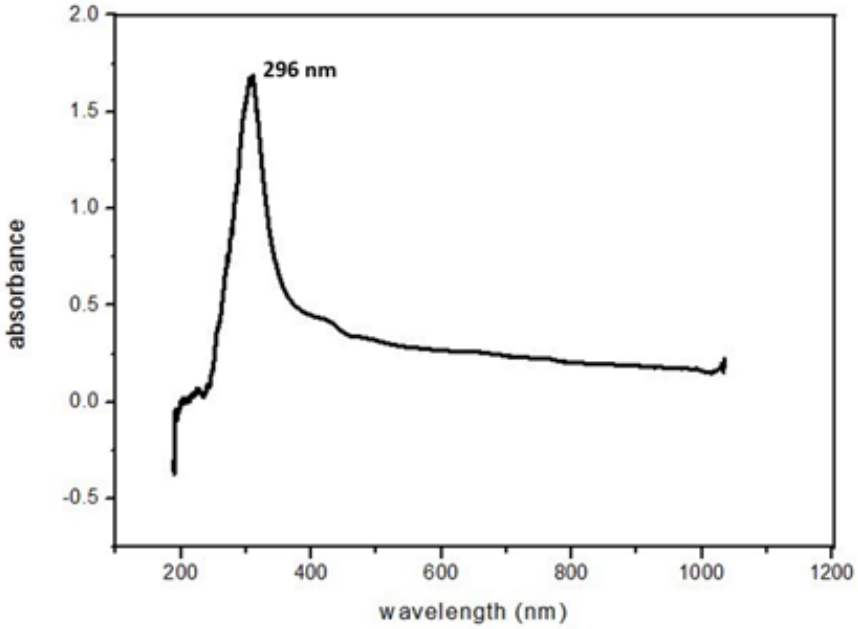

Figure 4. UV-Visible spectrum of sulphur nanoparticles

3.3. FTIR analysis of sulphur nanoparticles (SNPS)

Fig. 5 showsan FTIR spectrum and the corresponding absorbance peaks for SNPs. The prominent peaks at 3334 cm^{-1}, 2915 cm^{-1}, and 1393 cm^{-1} show the presence of –OH groups, –N-H stretching vibration, O=C=O bonds, –COO (sym. Stretching) and these bands revealed the presence of phytoconstituents of *F.religiosa* leaf extract. The peaks at 1584 cm^{-1}, 1082 cm^{-1}, and 880 cm^{-1} are attributed to the presence of –C=O (stretching), –CN bending vibration (secondary amide), O—S, and N—S stretching vibration of sulphur nanoparticles. The nominal changes in peak values, i.e.1052 cm^{-1}, 1513 cm^{-1}, 876 cm^{-1}, 656 cm^{-1}i.e. the peak shift arises due to the interaction of SNPs with amine groups in the biomolecules. The results indicate that the biomolecules from *F.religiosa* leaf extract proteins were bound onto the surface of as-prepared SNPs [25,26].

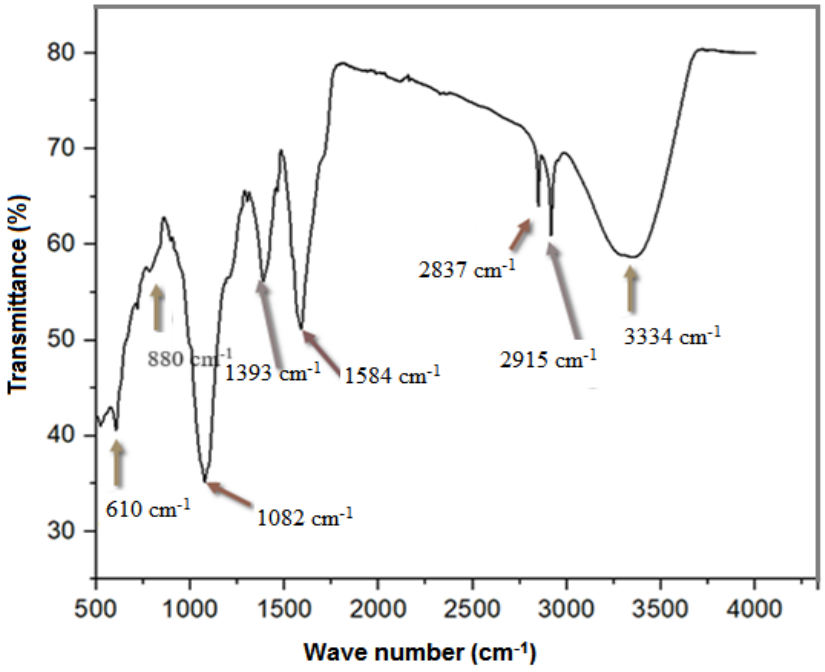

Figure 5. FTIR spectrum of sulphur nanoparticles

3.4.X-Ray diffraction analysis

Fig. 6shows a typical XRD pattern of SNPs. All the diffraction peaks are in good conformity with sulphur and no other impurity phases are observed, indicating the good phase purity of SNPs.

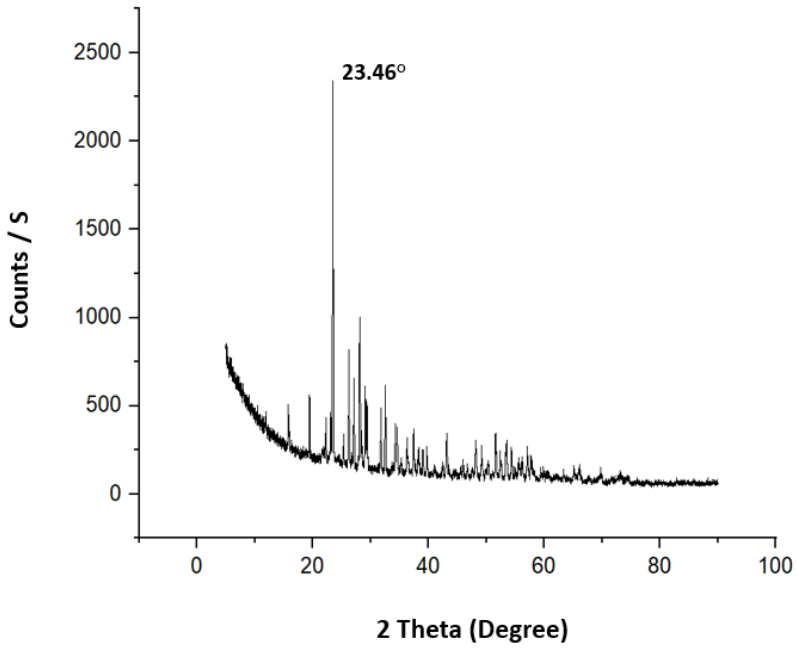

Figure 6. X-RD pattern of sulphur nanoparticles produced from F.religiosa leaf extract

The Debye-Scherrer formula was used to calculate the average crystalline size of the SNPs, which was found to be 23.4nm.

$$D = K\lambda / \beta \cos\theta$$

Where,

K is a dimensionlessshape factor, with a value close to unity.

The shape factor has a typical value of about 0.9, but varies with the actual shape of the crystallite;

λ is the X-ray wavelength;

β is the line broadening at half the maximum intensity (FWHM), after subtracting the instrumental line broadening, in radians. This quantity is also sometimes denoted as θ is the Bragg angle.The 2θ value of 23.46°, 27.07°, 31.78°, 34.53°, 37.40°, 41.03° indicate the crystalline nature of prepared sulphur nanoparticles and the crystalline size was determined to be 23.4nm [27-29].

3.5. SEM with EDS Analysis

The structural characteristics of biosynthesized SNPs were studied by scanning electron microscopy The SEM specimen was prepared by first drop-coating SNFs on a mica film followed by sputter coating of gold, then the mica film was transferred on to a sample holder made of carbon. Fig. 7a & 7b shows SEM images of SNPs. It is obvious that the particles had a low degree of agglomeration.

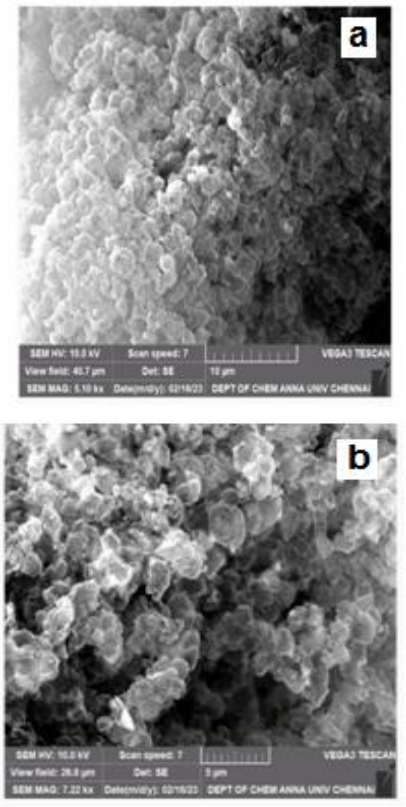

Figure 7. SEM images of SNPs

The SEM micrographs depicted that the particle size ranged from ~25 to ~120 nm. The elemental composition of SNPs was identified by EDS. The energy dispersive X-ray spectroscopy **spectrum (Fig. 8)** showed the presence of sulphur. Other elements such as Na, O and C were also observed due mainly to the presence of the by-product, sodium citrate.

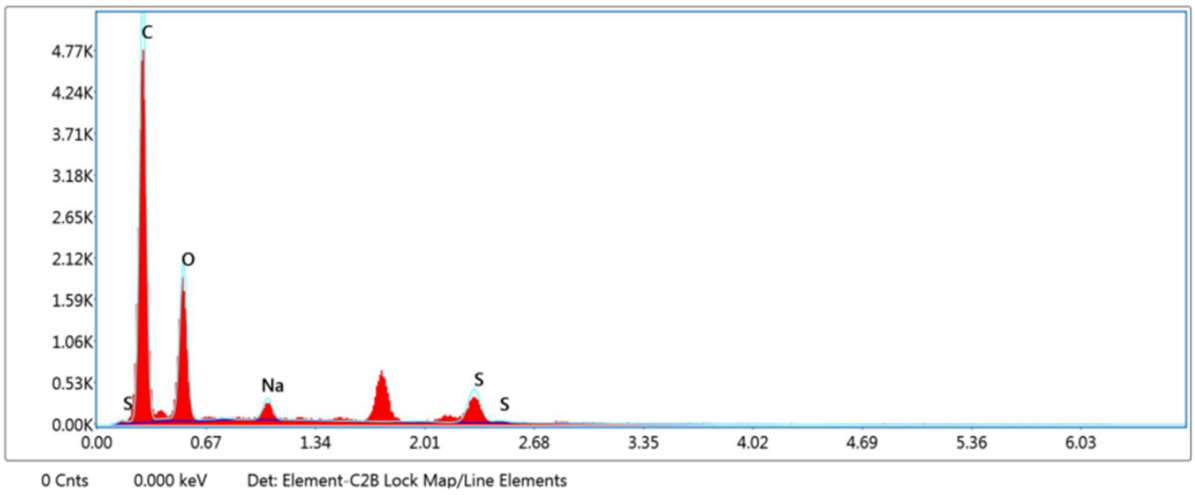

Figure 8. Energy Dispersive X-ray spectroscopy spectrum of Biosynthesized sulphur nanoparticles

3.6.Antibacterial activity of SNPs

The inhibitory effect of prepared sulphur nanoparticles on common pathogenic bacteria, E. coli, and S. aureus, was assessed through disc diffusion and minimum inhibitory concentration methods. The zone of inhibition values obtained isshown in Fig. 9. Once the medium solidified, bacterial inoculums were evenly spread on the plates using a sterile swab moistened with the bacterial suspension. The antibacterial study results revealed significantly heightened bioactivity of sulphur nanoparticles synthesized from F. religiosa leaves against both pathogens, as indicated in Table. 1 [27].

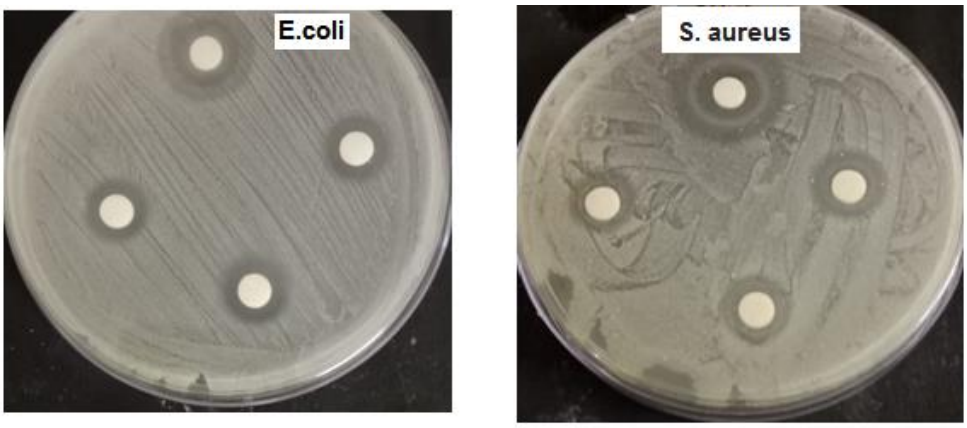

Figure 9. Antibacterial study of sulphur nanoparticles prepared from F.religiosa leaves

Table 1. Antibacterial activity of SNPs

	Zone of inhibition (mm) Sample (µg/ml)				
ORganisms	1000	750	500	Standard	SD
Staphylococcus aureus	18	18	18	20	1
Escherichia coli	14	14	14	20	3

4. CONCLUSIONS

A cost effective, rapid, environmentally friendly method was used for the synthesis of sulphur nano particles using *F.religiosa* leaf extract.The nanoparticles were characterized using UV-Vis, FTIR, XRD, FESEM, the synthesized sulphur nanoparticles were confirmed to be in nano meter scale with the help of X-ray diffraction method.

The SEM analysis have revealed that the synthesized sulphur nano particles have a

spherical size and from XRD the crystalline size of the sulphur nano particles is found to be 23.4 nm

Acknowledgments

The authors are very much thankful to Anna Adarsh College for Women for providing then basic facilities for preparation of sulphur nanoparticles. The authors would extend their heartfelt thanks to the University of Madras for providing UV, FTIR, XRD and SEM facilities.

5. REFERENCES

[1] R.Niranjan, S.Zafar, B.Lochab, R.Privaadarshini (2022) Synthesis and Characterization of Sulfur and Sulfur-Selenium Nanoparticles Loaded on Reduced Graphene Oxide and their Antibacterial Activity against Gram-Positive Pathogens. *Nanomaterials (Basel)*:12(2),191, https://doi.org/10.3390/nano12020191.

[2] Sh.Shankar, L.Jaiswal,R.Jong-Whan (2020) New insight into sulphur nanoparticles:Synthesis and applications. *Critical Reviews in Environmental Sci. Tech., 51 (20) 2329-2356,* https://doi.org/10.1080/10643389.2020.1780880.

[3] A. M. T.Lubis, C.Siagian, E.Wonggokusuma, A.F.Marsetyo, B.Setyohadi (2017) Comparison of Glucosamine-Chondroitin Sulfate with and without Methylsulfonylmethane in Grade I-II Knee Osteoarthritis: A Double Blind Randomized Controlled Trial. *Acta medica Indonesiana*, *49* (2), 105–111,PMID: 28790224.

[4] B.Abuyeva, M.Burkitbayev, G.Mun, B.Uralbekov, N.Vorobyeva, D.Zharlykasimova, F.Urakaev (2018) Preparation of ointment materials based on sulfur nanoparticles in water-soluble polymers. *Materials Today:Proceedings*, 5(11), 22894–22899, https://doi.org/10.1016/j.matpr.2018.07.107.

[5] F.Kh. Urakaev, A.I. Bulavchenko, B.M. Uralbekov, I.A. Massalimov, B.B. Tatykaev, A.K. Bolatov, D.N. Zharlykasimova, M.M. Burkitbayev (2016) Mechanochemical synthesis of colloidal sulfur particles in the $Na_2S_2O_3$–$H_2(C_4H_4O_4)$–Na_2SO_3 system.*Colloid Journal, 78, 210–219,* https://doi.org/10.1134/S1061933X16020150.

[6] S. Shankar, R. Pangeni, J.W. Park, J.-W. Rhim (2018) Preparation of sulfur nanoparticles and their antibacterial activity and cytotoxic effect. *Mater. Sci. Eng. C, Mater. Biol. Appl, 92, pp. 508-517,*https://doi: 10.1016/j.msec.2018.07.015.

[7] R.A.Dop, D.R.Neill, T.Hasell(2023) Sulphur-polymer nanoparticles: Preparation and anti-bacterial activity. ACS *Appl. Mater. Interfaces,* 15(17), 20822–20832,https://doi:10.1021/acsami.3c03826.

[8] P.Paralikar, M.Rai(2018) Bio-inspired synthesis of sulphurnanoparticles using leaf extract of four medicinal plants with special reference to their antibacterial activity*. IET Nanobiotechnol,*12(1),25-31, https://doi.org/10.1049/iet-nbt.2017.0079

[9] S. Roy Choudhury, S. Roy, A. Goswami, S. Basu (2021) Polyethylene glycol-stabilized sulphur nanoparticles: an effective antimicrobial agent against multidrug-resistant bacteria.*J. Antimicrobial Chemotherapy, 67, 1134-1139,* https://doi.org/10.1093/jac/dkr591.

[10] N.Chausali, J.Saxena, R.Prasad (2023) Nanotechnology as a sustainable approach for combating the environmental effects of climate change.*J. Agri. Food Res., 12, 100541*, https://doi.org/10.1016/j.jafr.2023.100541.

[11] S. Bayda, M. Adeel, T. Tuccinardi, M. Cordani, F. Rizzolio (2020) The History of Nanoscience and Nanotechnology:From Chemical-Physical Applications to Nanomedicine.*Molecules,25 (1), 112,* https://doi.org/10.3390/molecules25010112.

[12] J. Singh, T. Dutta, K.H Kim, M.Rawat, P.Samddar, P.Kumar (2018) Green synthesis of metals and their oxide nanoparticles: applications for environmental remediation. *J.Nanobiotech., **16**,84,* https://doi.org/10.1186/s12951-018-0408-4.

[13] S. P. K. Malhotra, M. A. Alghuthaymi (2022b) Biomolecule-assisted biogenic synthesis of metallic nanoparticle. *In Elsevier eBooks,* 139–163*,* https://doi.org/10.1016/B978-0-12-823575-1.00011-1

[14] P.T. Anastas, J.C. Warner(1998) *Green Chemistry: Theory and Practice. Oxford University Press, New York*(online edn)*, 30,* https://doi.org/10.1093/oso/9780198506980.001.0001.

[15] M.Shamsipur,S.M.Pourmortazavi, M.Roushani, I.Kohsari, S.S.Hajimirsadeghi *(2011)* Novel approach for electrochemical preparation of sulphur nanoparticles. *Mikrochimica Acta*, 173(3–4), 445–451, https://doi.org/10.1007/s00604-011-0581-8.

[16] G.Cao(2004) *Nanostructures and nanomaterials, https://doi.org/10.1142/p305.*

[17] J.Wang, W.Liu, G.Luo, C.Zhao, H.Zhang, M.Zhu, Q.Xu, X.Wang, C.Zhao, Y.Qu, Z.Yang, T.Yao, Y.Li, Y.Lin, Y.Wu, Y.Li (2018) Synergistic effect of well-defined dual sites boosting the oxygen reduction reaction. *Energy & Environ. Sci., 11*(12), 3375–3379.,https://doi.org/10.1039/c8ee02656d.

[18] S.Mondal, N.Roy, R.A. Laskar, I.Sk, S.Basu, D.Mandal, N.A.Begum(2011) Biogenic synthesis of Ag, Au and bimetallic Au/Ag alloy nanoparticles using aqueous extract of mahogany (Swietenia mahogani JACQ.) leaves.*Colloids Surf. B Biointerfaces, 82 (2),497-504,* https://doi.org/10.1016/j.colsurfb.2010.10.007.

[19] *D. Acharya, S. Satapathy, P. Somu, U. K. Parida, and G. Mishra (2020) Apoptotic Effect and Anticancer Activity of Biosynthesized Silver Nanoparticles from Marine Algae Chaetomorpha Linum Extract against Human Colon Cancer Cell HCT-116.*Biol.Trace Elem.Res., 199, 1812–1822, https://doi:10.1007/S12011-020-02304-7.

[20] *E. F. Aboelfetoh, R. A. El-Shenody, and M. M. Ghobara (2017)Eco-friendly Synthesis of Silver Nanoparticles Using Green Algae (Caulerpa Serrulata): Reaction Optimization, Catalytic and Antibacterial Activities.* Environ. Monitor Assess., 189, 349. doi:10.1007/s10661-017-6033-0.

[21] H.W.Jung, H.Y.Son, C.V.Minh, Y.H.Kim, Y. Park (2008) *Methanol extract of Ficus leaf inhibits the production of nitric oxide and proinflammatory*

*cytokines in LPS-stimulated microglia via the MAPK pathway.*Phytother.Res.,22(8), 1064-1069. doi: 10.1002/ptr.2442.

[22] P. N. V. K. Pallela, S. Ummey, L. K. Ruddaraju, S. V. N. Pammi, S. G. Yoon (2018) Ultra Small, mono dispersed green synthesized silver nanoparticles using aqueous extract of Sida cordifolia plant and investigation of antibacterial activity. *Microbial Pathogenesis*, 124, 63-69, doi: 10.1016/j.micpath.2018.08.026.

[23] *A.Afreen, R.Ahmed, S.Mehboob, M. Tariq, H.A. Alghamdi, A.A.Zahid, I.Ali, K.Malik,A.Hasan (2020) Phytochemical-assisted biosynthesis of silver nanoparticles from Ajuga bracteosa for biomedical applications.*Mater. Res. Express*, 7, 075404,* https://doi.org/10.1088/2053-1591/aba5d0.

[24] R. G. Chaudhuri, S. Paria (2011) Growth kinetics of sulfur nanoparticles in aqueous surfactant solutions. *J. Colloid. Interface Sci.,*354, 563 –569, https://doi.org/10.1016/j.jcis.2010.11.039

[25] J.Coates (2006) 'Interpretation of infrared spectra, a practical approach'. *Encyclopedia of* Analytical *Chemistry* (eds R.A. Meyers and M.L. McKelvy). 10815–10837, https://doi.org/10.1002/9780470027318.a5606.

[26] P. Paralikar, M. Rai (2017) Bio-inspired synthesis of sulphur nanoparticles using leaf extract of four medicinal plants with special reference to their antibacterial activity. *IET Nanobiotech.*, 23;12(1): 25–31, https://doi: 10.1049/iet-nbt.2017.0079.

[27] M. Suleiman, M. A. Masri, A. A. Ali*(2015)*'Synthesis of nano-sized sulfur nanoparticles and their antibacterial activities'. *J. Mater.Environ.Sci.,*6 (2), 513 –518, ISSN : 2028-2508.

[28] M. Awwad, N. M. Salem, A. O. Abdeen (2015) Novel approach for synthesis sulfur (S-NPs) nanoparticles using *Albizia julibrissin* fruits extract'. *Adv. Mater. Lett*., 6 (5), 432–435, https://doi:10.5185/amlett.2015.5792.

[29] R. M. Tripathi, R. Pragadeeshwara Rao, T. Tsuzuki (2018) Green synthesis of sulfur nanoparticles and evaluation of their catalytic detoxification of hexavalent chromiumin water.*RSC Adv.,* 8, 36345–36352,https://doi.org/10.1039/C8RA07845A.

IZVOD

BIO-INSPIRISANA SINTEZA NANOČESTICA SUMPORAI NJEGOVA PRIMENA

Koriscen je ekonomičan, brz i ekološki prihvatljiv pristup za sintezu nanočestica sumpora, koristeći ekstrakt iz listova Ficus religiosa. Sveobuhvatna karakterizacija ovih nanočestica obavljena je UV-vidljivom spektroskopijom, FTIR, XRD i FESEM tehnikama. Metoda difrakcije rendgenskih zraka nedvosmisleno je potvrdila nanometarske dimenzije sintetizovanih nanočestica sumpora. SEM analiza je razjasnila njihovu sfernu morfologiju, dok XRD podaci ukazuju na veličinu kristala od 23,4 nm za ove pripremljene nanočestice. Pored toga, antibakterijska procena nanočestica sumpora proizvedenih iz listova Ficus religiosa pokazala je superiornu bioaktivnost protiv štetnih vrsta bakterija kao što su Escherichia Coli i Staphilococcus aureus.

Ključne reči: *nanočestice sumpora, Ficus religiosa, bioaktivnost, zelena sinteza*

Naučni rad
Rad primljen: 12.10.2023.
Rad korigovan: 20.06.2024.
Rad prihvaćen: 05.07.2024.

Jeyaprabha Chellappa : https://orcid.org/0000-0001-6729-2157
Sribharathy Vijayagopal: https://orcid.org/0000-0002-0542-3569

VyacheslavGoryany

Düsseldorf, Germany

Scientific paper
ISSN 0351-9465, E-ISSN 2466-2585
https://doi.org/10.62638/ZasMat1199

Zastita Materijala 66 (1)
75 - 89 (2025)

Rings for compound rolls of rolling mills

ABSTRACT

Modern materials for producing rings for compound rolls and their most important application properties are described. The advantages and disadvantages of rings made of cemented carbide, high-speed steel, ceramic materials and their damage mechanisms are analyzed. The structure of composite material rings made of cemented carbide/ iron-based alloys, HSS rings manufactured using powder metallurgy and melt metallurgy, and rings made of silicon nitride are described.
***Keywords**: ring, compound roll, cemented carbide, high-speed steel, silicon nitride, clamping system*

1. INTRODUCTION

The roll rings are the interchangeable components of the composite rolls that are used in the intermediate and finishing stands of wire and bar steel, light section and pipe rolling mills. The roll rings are mostly made of cemented carbide and high-speed steel. The rings made from such materials are usually manufactured using powder metallurgy processes (hot isostatic pressing). Depending on the operating conditions, the roll rings are manufactured with different properties. In order to adapt to the user's requirements, a number of material groups and material qualities have been developed that are used in the production of roll rings.

2. MATERIALS FOR ROLL RINGS

Cemented carbide

The roll rings are mostly made of cemented carbide (WC-Co). The tungsten carbide has absolute wettability with cobalt and the ability to assume a faceted shape in sintered cemented carbidealloys. The cemented carbide rings are used in hot and cold rolling. During hot rolling, the cemented carbide rings are used in:

- Wire rod finishing mills
- Wire rod intermediate mills
- Cantilevered stand mills for rounds and shapes
- Merchant bar mills – rounds, rebar, shapes
- Pinch rolls – guide rolls
- Roller entry guides

During cold rolling, the roll rings are used in:

- Cluster mill work rolls
- 2-Hi narrow strip mills
- Wire flattening and forming mills
- ERW tube mills
- Turks heads[1].

The rings can be made with or without a caliber. The use of cemented carbide rolls leads to [2]:

- Long caliber service life by significantly reducing wear, especially at high rolling speeds
- Higher dimensional accuracy and dimensional accuracy as well as surface quality of the rolling stock, especially in multi-core rolling mills
- Longer service life compared to conventional roll materials, which leads to fewer wear-related roll changes and a significant increase in productivity of the rolling mill
- Possibilities of producing high-quality thin cold strip due to insignificant roll flattening and low coefficient of friction.

The reliability and service life of the rings depend on the operating conditions in a particular rolling stand. Depending on these, the rings are made from alloys that differ in the WC/binding metal ratio. In these materials, the binding metal content can range from 4.5% to 31.5% and will determine the mechanical and thermo-physical

*Corresponding author: Vyacheslav Goryany
E-mail: dr.goryany@o2mail.de
Paper received: 15. 05. 2024.
Paper accepted: 01. 07. 2024.
The website: https://www.zastita-materijala.org/

properties of the cemented carbide, such as hardness, density, fracture toughness, compressive strength, modulus of elasticity, thermal conductivity, coefficient of thermal expansion, etc. strongly influenced. The required operational properties of the cemented carbide will be achieved through a desired compromise between the opposing properties such as hardness and toughness as well as the other important operational properties of the cemented carbide. The rings made from such materials have the following advantages:

- Homogeneous, segregation-free structures with carbides of a defined grain size evenly distributed in the basic structure
- Homogeneous properties
- Near-net-shape raw components.

The cyclical temperature changes and high mechanical roll loads in the slow-running front intermediate stands of the rolling mills can lead to the formation of so-called “orange peel” on the caliber surface as well as quite deep cracks beneath the surface. These often lead to breakage. In order to avoid such damage, the roll rings made of tough cemented carbides types are used in these rolling stands, which contain 25 - 30% binder and have a hardness of 78.0 – 81.0 HRA. The slightly lower hardness and wear resistance of these “soft” cemented carbide rings are offset by increased strength, toughness and thermal fatigue resistance. The roll rings made of slightly harder types of cemented carbides are used in a finishing block of the high-speed wire rolling mills [3, 4]:

- in the front rolling stands, roll rings with a hardness of 83.8 to 84.1 HRA are used (binder content 20 – 15%, respectively)
- in the middle rolling stands, rings with a hardness of 85.7 – 84.1 HRA and a binder content of approx. 15% are used
- the rear rolling stands are equipped with hard roll rings (87.2 – 88.3 HRA, binder content 10 – 8%, respectively).

When rolling ribbed reinforcing steel, cemented carbide alloys with 25 – 30% binder are used in the finishing block, which can withstand the notch effect of the grooves and have better mechanical machinability of the rings.

The rings made of cemented carbide grades (87.7 – 87 HRA) with a binder content of 8 – 10 % are also successfully used in sizing mills.

The cemented carbides roll rings have excellent wear resistance with uniform wear, which is associated with the high hardness of tungsten carbide grains and their uniform distribution in the microstructure. The Knoop hardness of the WC grains can vary between 2500 and 1000 depending on the crystal plane and direction [5]. The cemented carbides still have a sufficiently high hardness even at 1000 °C. The WC grain size influences the properties of the cemented carbide. The grain sizes of cemented carbide rolls are generally between 0.7 and 7.0 µm [1]. Coarse-grained WC powder is most commonly used for the production of roll rings. Although increasing grain size for a given binder content reduces wear resistance, it increases toughness. With regard to thermal fatigue, experience shows that a coarse grain tungsten carbide grain is superior to medium or fine grain grades. Therefore, larger grain sizes are very important in hot rolling. Finer grains, on the other hand, improve wear resistance and compressive strength and are therefore often used in the cold rolling process [1].

Compared to highly wear-resistant iron-based alloys (such as high-alloy hot-work steels, high-chromium steels, high-speed steels), the cemented carbides used in rolling mills have a significantly lower coefficient of thermal expansion of 5,3 – $8.2 \cdot 10^{-6}$ 1/K, which has a major influence on the fatigue strength of cemented carbide. The thermal expansion of the cemented carbide decreases with increasing tungsten carbide content and increases with increasing cobalt content.

The very high values of elastic modulus (420–630 GPa), hardness (78 – 89 HRA, and compressive strength (3000 – 4300 N/mm²), of the cemented carbide ensure high rigidity of the ring and enable its very high resistance to elastic deformation in the deformation zone, which leads to a significant reduction in ring flattening. This also enables higher reductions with the same rolling forces lies in improving the accuracy of the rolled product.

The main types of cemented carbide ring failure arewear,thermal fatigue, mechanical shear due to tangential stress, and corrosion. Ring wear is manifested in the sliding friction of the rolled metal on the surface of the caliber due to the different speed of their movement at the entrance and exit from the deformation zone. Small thermal fatigue cracks may appear on the roll work surface caused by the cyclic temperature changes. The service life of the rings in use is limited by the formation and growth of cracks. A low resistance of the cemented carbide to thermal fatigue is compensated for by the use of efficient cooling systems. Compared to iron-based alloys, the cemented carbide has twice the thermal conductivity (85 – 120 W/m·K) and the heat penetrates deeper into the rolls. The thermal conductivity of cobalt is 100 W/m·K. Rolls withcemented carbide rings must always be cooled during hot rolling and the cooling systems should

have a built-in warning system coupled to a flying shear to allow the workpiece to be sheared in the event of a drop-in water pressure.This requires effective ring cooling to prevent heat transfer from the surface to the deeper areas of the composite roll. Intensive roll cooling is particularly required in the front rolling stands, where the rolling stock has a significantly higher temperature and the contact area of the roll and the rolling stock is larger than in the rear rolling stands. In the front rolling stands, the rolls rotate at a lower speed, which leads to a longer contact time between the roll and the rolling stock and thus promotes heat transfer. The resulting microcracks will slowly propagate from the surface into the depth of the ring. The crack surfaces are attacked by corrosion due to constant contact with the cooling water, which can lead to a decrease in the strength of the cemented carbide and can affect the wear resistance of cemented carbide rings [6-8]. Binder corrosion leads to a decrease in the bond between neighboring carbide grains, which promotes the spalling of individual carbides. The significant differences in the thermal expansion coefficients of WC ($5.4 \cdot 10^{-6}$ 1/K) and cobalt ($12.3 \cdot 10^{-6}$ 1/K) play an important role. The presence of large carbides in the structure or their accumulation can lead to a further accumulation of local stresses, which can lead to a weakening of the boundaries of the carbides and the binders. The individual carbide grains or grain agglomerates can therefore easily be detached or sheared off and can form a crater. The interaction of neighboring cracks can also lead to crater formation. The resulting hills can be sheared off. The detached WC grains that can enter the deformation zone will themselves have an abrasive effect. The effect of abrasive wear can also be enhanced by oxides of the rolled metal, which can enter the deformation zone. The separation of WC grains causes roughening of the caliber surfaces. As the rolls continues to operate, the crack formation in these damaged areas can be increased by diffusion processes and corrosion and can lead to ring breakage.The problem of roll fatigue is therefore purely a problem of crack growth. To reap the benefits of carbide rings, all surface cracks must be eliminated. Before the cracks on the caliber surface reach a depth of 1 – 1.5 mm, it should be regrinded [8]. A ground roll surface must be free of microcracks. The remaining cracks immediately begin to grow when the roll surface comes into contact with the hot rolling stock.

The quality of the cooling water is also very important for the successful use ofcemented carbide rings and the requirements for the cooling water are high. When the pH is high (about 8.5), the Co-binder has good corrosion resistance. A more acidic environment can lead to accelerated erosion of the cobalt binder. At pH below 7.5, cobalt alloys tend to electrochemical corrosion and the corrosion rate is very high. The rate of corrosion varies depending on the type of carbide and is generally inversely related to that of the binder content. The types of cemented carbide that contain nickel in the binder phase have a higher corrosion resistance than the types with a Co-binder [8]. The use of cemented carbide rings with binders containing chromium can minimize the corrosion rate.Multi-component cemented carbide grades such as WC-(Co-Ni) and WC-(Co-Ni-Cr) were developed, which have higher corrosion and temperature resistance [3, 4, 8-11]. Such materials are used at low pH values. Through a controlled pH value and the addition of calcium during the rolling process, the cemented carbide can be coated with a protective film of $CaWO_4$ and thus protected against corrosion [1].

In addition to the water flow, which can be from 10 to 50 m³/h depending on the rolling stand, and the water pressure (from 2.8 to 5.5 baragain depending on the rolling stand) the purity and low ion content of water must be guaranteed, especially with regard to chlorides and sulfates [12]. The recommended water analyzes are (µg/L): chlorides 40 max, sulfates 75 max, nitrites/nitrates 2 max, $CaCO_3$ 200 max; suspended solids 80 max; total basicity 100 max; iron 25 max; pH 7.5 to 8.5 [3] or chlorides 40 max; sulfates 75 max; nitrates 3 max, $CaCO_3$ 400 max; suspended solids 80 max and pH value 8 to 8.5 [8].

Another factor for the successful use of tungsten carbide rings in rolling mills is the temperature of the cooling water. It should not be higher than 32 – 35°C [1] and should not exceed the ambient temperature by more than 6°C [3]. The difference between the temperature of the cooling water and the surface temperature of the ring should not be greater than 10°C [8] or 14°C according to [3]. The water jet should generally be approximately twice as large as the width of the caliber. In addition, attention should be paid to suitable cooling systems for sufficient cooling [1, 3, 8, 10].

A low fracture toughness of the cemented carbide (K_{1C} = 14.2 – 28.5 $MPa \cdot \sqrt{m}$), which limits the shrinkage of the rings on the steel shafts, as well as a 10 – 50% lower impact resistance can limit the transmission of torque via springs and wedges in some cases [13].When rolling with the use of cemented carbide rings, excessive reductions and the increased coefficient of friction must be avoided, especially when rolling alloyed steels that are difficult to form. The optimal cross section of the cemented carbide ring must also be considered.

The calculation of the elastic deformations of roll rings and rolling shafts, especially in the fillet, with the introduction of high loads (rolling forces, torques) in the prestressed compound rolls as well as the stress distribution in their bodies during the rolling process are carried out using mathematical methods based on finite elements occurs [14, 15].The contact conditions are defined for the compound rolls and for the rolling stock and are simulated together with all rolling parameters. The software available makes it possible to determine the mechanical stress on rolls (stresses and deformations) based on the rolling parameters (rolling force, torque, contact surfaces, etc.).

The use of cemented carbide roll rings is characterized by its particular cost-effectiveness. Despite the significantly higher manufacturing and processing costs of the cemented carbide roll rings compared to conventional cast materials, their use in high-performance wire mills makes economic sense due to the significantly increasing campaign length [16-18]. The higher fatigue strength of the cemented carbide and the minimized wear meant that redressing could be reduced. Cemented carbide rings increase groove life by a factor of 10 in rolling special steel bar [19, 20] and have at least 15 times longer life than rings made from AISI D2 tool steel in rolling bar steel [21].

Cemented carbide composite materials

When producing cemented carbide composite materials, the melt of high-quality cast iron is cast around the inner surface of a cemented carbide ring (cast-in carbide or CIC-process) [22]. The cemented carbide binder (cobalt) that comes into contact with the melt is melted and dissolved in the penetrated cast iron. The cobalt is completely replaced by cast iron and only traces of cobalt are observed in the newly formed binder.

The WC particles are well wetted by cast iron melt, which stabilizes the formation process of the composite layer.The penetration depth is proportional to the overheating of the cast melt. The greatest depth of penetration is achieved when using alloys with the widest solidification interval. The alloys with the narrow or not wide enough solidification interval solidify very quickly and the poured melt does not penetrate into the hard metal. As a result – no connection of two materials. The penetration depth depends heavily on the casting temperature of the cast alloy.This must be at around 350°C above the melting point in order for penetration to occur, as the cemented carbide ring will act like a permanent mold and the solidification rate of the melt will be greatly accelerated, which prevents or greatly impairs the penetration of the melt.

The very fine WC particles that come into contact with the melt are partially dissolved. In the areas of the cast iron melt close to the bond, the new tungsten carbides are formed, which have a completely different morphology and sizes.In the area of the tungsten carbides formed, the matrix is depleted of carbon and a pearlite veil forms around tungsten carbide. Practical experience shows that both the tungsten carbides formed and the pearlite veil will not affect the strength of the composite or the overall performance of the rings. The investigations of the mechanical properties of the composite have shown that the composite material formed has a strong metallurgical bond. The graphitization of cast iron is not suppressed by small amounts of dissolved tungsten. The graphite precipitates are observed in the composite zone to a depth of approx. 700 µm.A comprehensive study of the microstructure is presentedin the separate article [23].

The development of cemented carbide composite materials has solved the problem of torque transmission. The tough and easy-to-machine ductile iron transfers the torque to the cemented carbide area of the rolling ring. This manufacturing process makes it possible to save around half of the expensive cemented carbide, which significantly reduces the manufacturing costs of the rings. The unique CIC (Cast-in-Carbide) ringsare successfully used in more than 100 rolling mills worldwide and have a service life up to 20 times longer than conventional cast rolls, which has a significant impact on downtime costs [12, 22]. In pipe rolling mills, the CIC rolls have a service life that is up to 40 times longer than conventional cast iron rolls, with excellent surface quality, tolerances and geometry of the rolled pipe [22].

In order to avoid a negative effect of the brittleness of the cemented carbide, cemented carbide/steel composite rings were developed [24]. The rings are manufactured as a material composite made of cemented carbide and Invar alloy using hot isostatic pressing. The composite materials have a comparable coefficient of thermal expansion, which corresponds to around two thirds of the HSS value, so that only low stresses occur in the composite.

Another material composite developed consists of cemented carbide, Invar alloy and tool steel. The resulting mechanical and thermal stresses are reduced by the Invar alloy, which serves as a buffer in this composite combination [25]. The rings can be shrunk or connected to the shafts using side or bore keys. The torque transmitted from the drive shaft to the steel area is transmitted over a large area to the integrated, wear-resistant cemented carbide ring via an Invar layer. Such rolls are used in cantilever middle mills, in flat rolling and in tube rolling.

High speed steel

Powder metallurgical process (PM process)

The roll rings made of high-speed steel (HSS) produced using powder metallurgy are successfully used in the rolling of steel profiles (wire and round steel, angle and special profiles). The areas of application of HSS roll rings depend on the operating conditions. When rolling wire and bars, the HSS roll rings are used in the intermediate stands and in the pre-finishing stands. When rolling reinforcing bars, the roll rings are used in the intermediate stands.

The HSS roll rings manufactured using powder metallurgy can be designed with or without a caliber [26]. The rings have a homogeneous, pore-free structure. The microstructure contains approximately 20% by volume of carbides with a size of 1 to 5 µm, which ensure exceptionally good wear resistance with the maximum possible toughness of the HSS. The carbide size plays an important role in the propagation of an emerging crack in the basic structure. The small carbides lead to frequent crack deflection or to delaying or stopping the crack. Despite a lower hardness (50 – 64 HRC) compared to carbide rings, HSS rings have a long service life and a uniform wear profile, which is associated with a fine-grained, segregation-free microstructure and evenly distributed, fine, globular-shaped VC carbides is. A high-volume fraction of these carbides leads to high wear resistance and service life of the rings. The HSS rings retain both hardness and wear resistance up to the minimum diameter. The modulus of elasticity of such steels is around 230 – 240GPa, which reduces roll flattening.

Although the powder metallurgy-produced HSS rings have a low thermal conductivity (26 W/m·K), they must be cooled intensively due to a higher thermal expansion coefficient ($11.6 \cdot 10^{-6}$ 1/K), which slows down thermal fatigue cracking.During hot rolling, a firmly adhering oxide layer forms on the ring surface (Figure 1, Table 1).

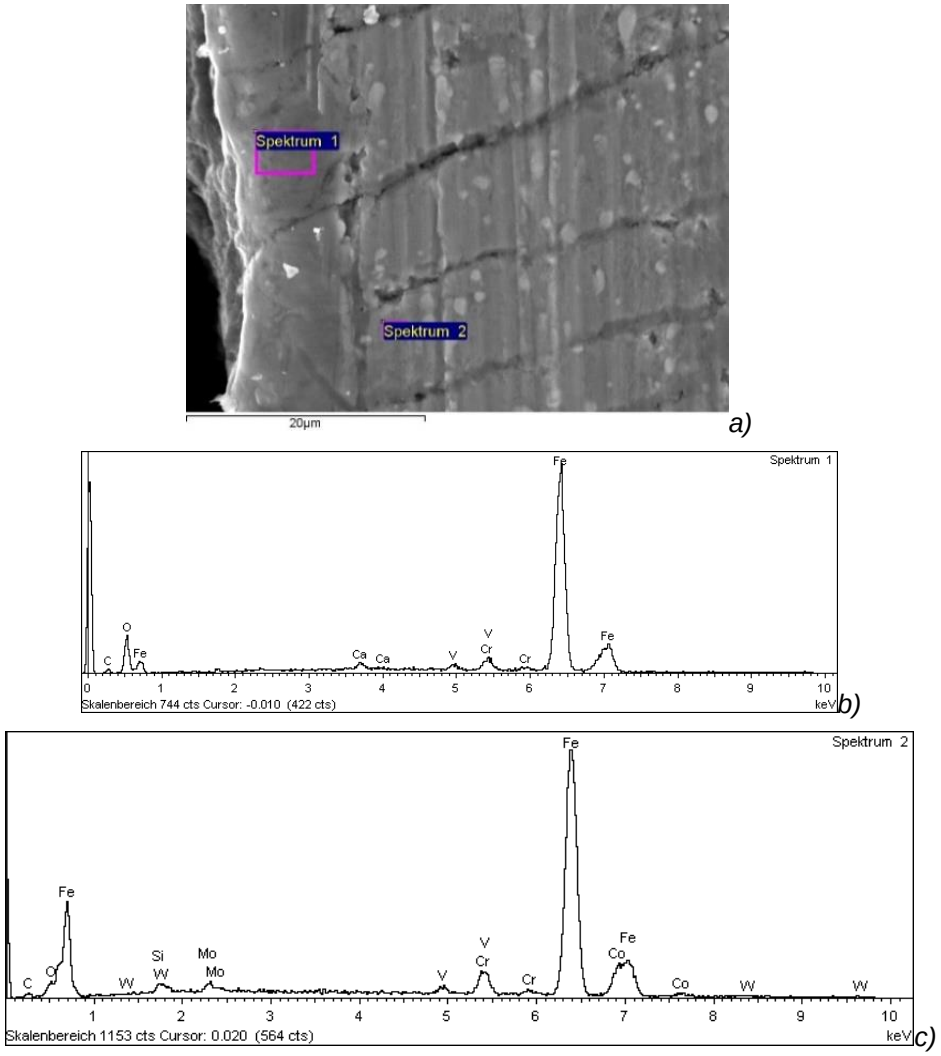

Figure 1. Oxide layer on the caliber surface: a – microstructure (SEM image)with the position of the EDX analysis; b – EDX analysis of the oxide layer; c – EDX analysis of the matrix

Table 1. EDX analysis of the caliber surface (mass%)

Spectrum	O	Si	Ca	V	Cr	Fe	Co	Mo	W	C	Total
1	10,43	-	0,91	1,12	2,52	81,62	-	-	-	3,40	100,00
2	1,97	0,50	-	0,86	3,98	76,20	8,90	2,38	1,79	3,42	100,00

The hard oxide layer protects the ring surface from intensive wear and acts as thermal insulation, which helps to reduce the contact temperature in the tribosystem "rolling stock - work roll" and leads to a reduction in heat transfer from the rolling stock to the rolls, which prevents or slows down the formation of thermal fatigue cracks on their surface. The stability of the oxide layer (formation and growth rate, thickness) depends on the chemical composition of the HSS. The improvement of the corrosion resistance of HSS and the formation of the desired iron oxide layer is achieved by a high chromium content in the steel (approx. 4.5 – 6%). Other elements that are crucial for corrosion resistance (molybdenum and nitrogen) will primarily increase the resistance to pitting corrosion.

Figure 2 shows the surface of a powder metallurgically manufactured HSS rolling ring after use with thermal fatigue cracks and areas of corrosion.

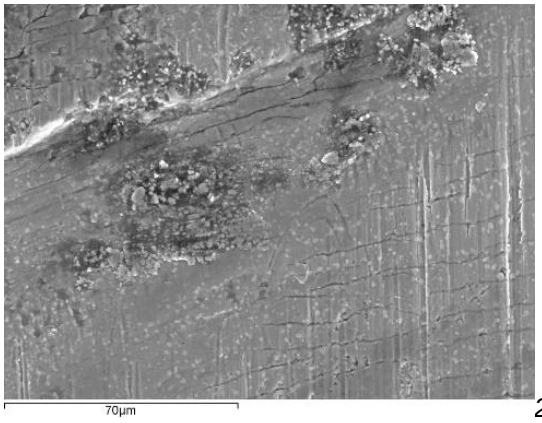

2a)

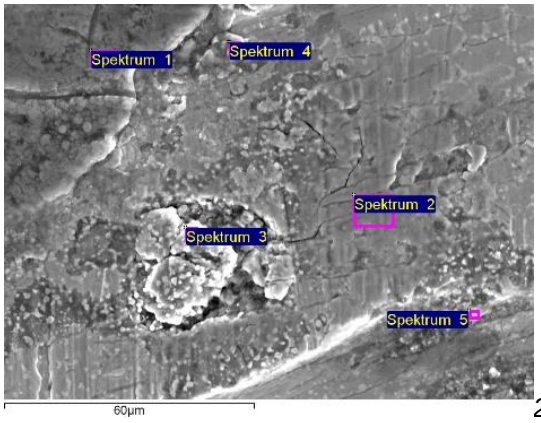

2b)

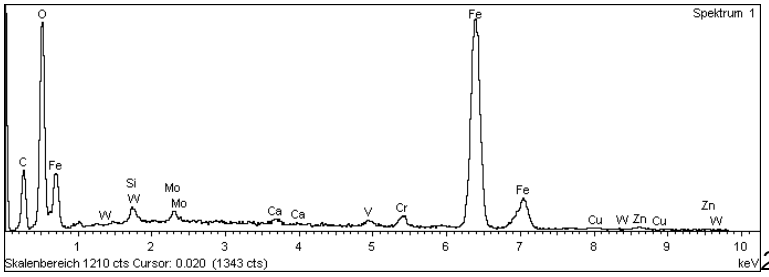

2c)

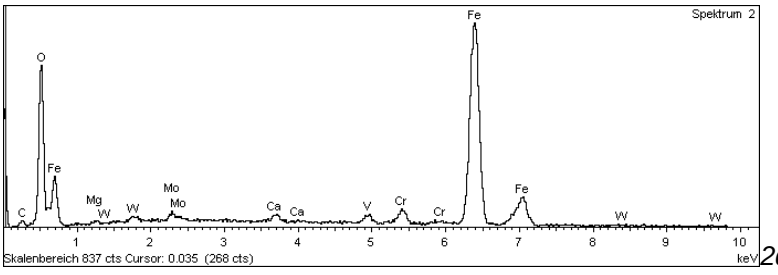

2d)

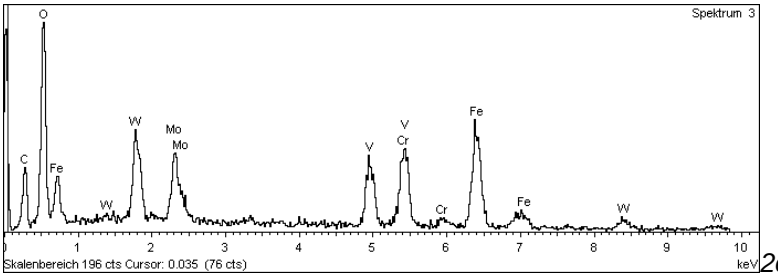

2e)

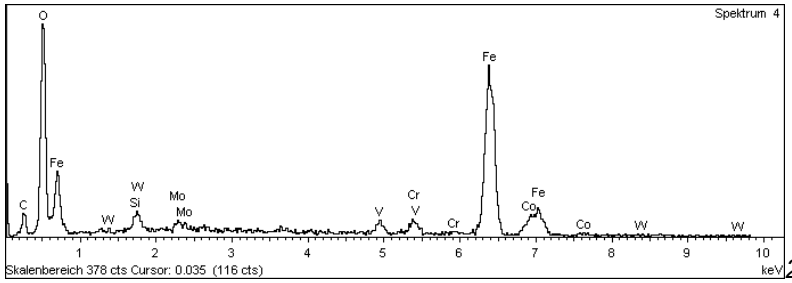

2f)

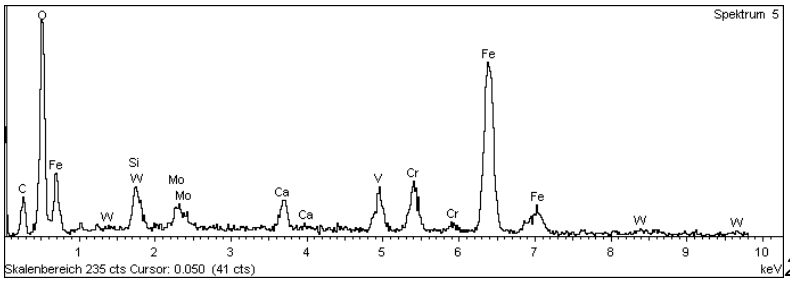

2g)

Figure 2. Thermal fatigue cracks with corrosion areas of an HSS rolling ring: a –surface appearance(SEM image);b – detail with the location of the EDX analysis; c, d, e, f, g – EDX analyzes of the matrix (c, d, f) and MC mixed carbide (e, g)

The corrosion attacks both the matrix and the carbides. The oxidation of carbides under cyclical action of dynamic and thermal loads can lead to the formation of cracks on their surface. This facilitates the carbide decomposition or detachment from the matrix. The calcium identified comes from the water used for ring cooling. Metallographic investigations in the areas of the resulting thermal fatigue cracks showed that their edges are heavily oxidized (Figure 3).

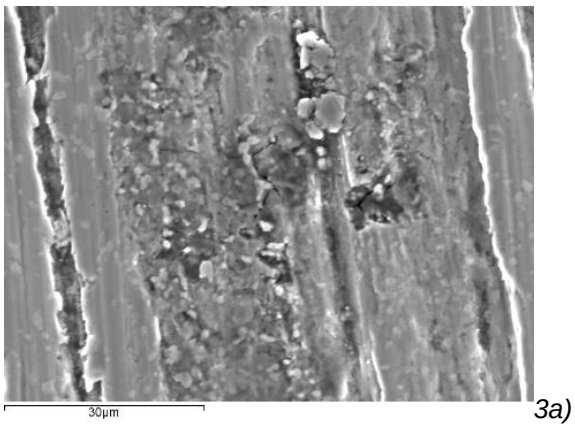

3a)

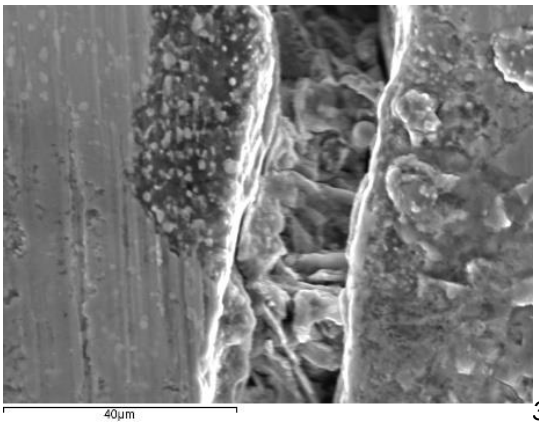

3b)

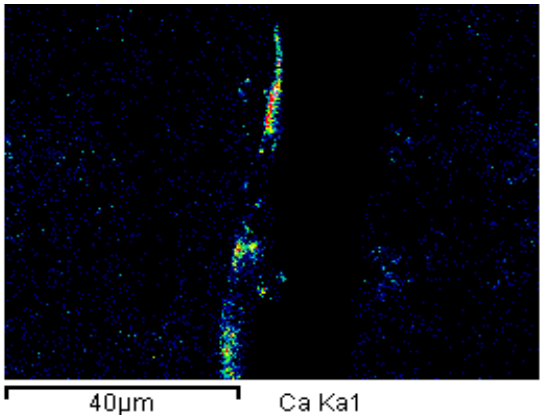

3c)

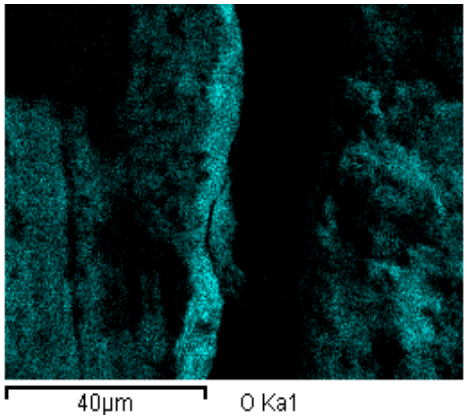

3d)

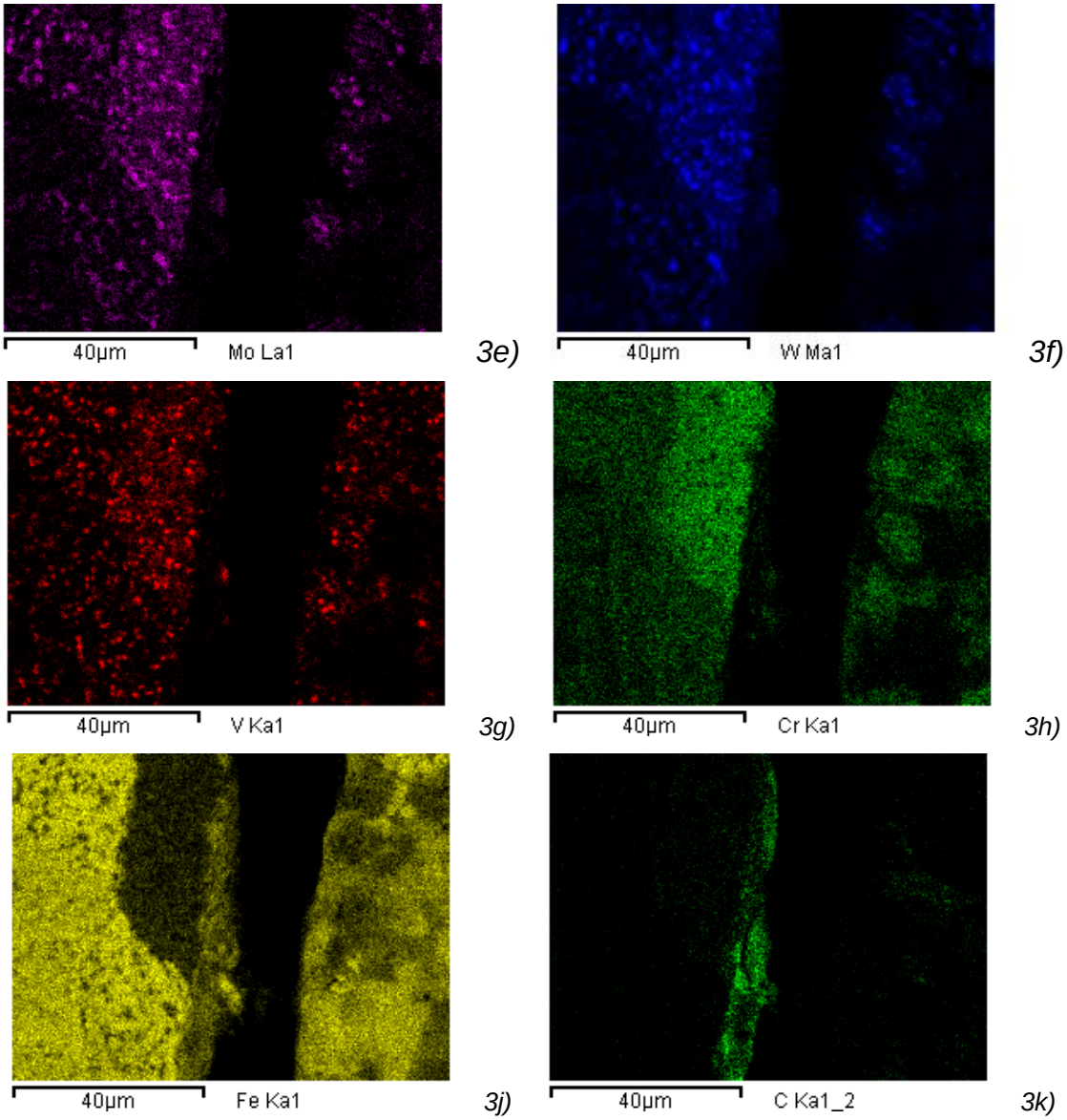

Figure 3. Element distribution in the area of a crack: a – microstructure(SEM image);b – microstructure detail; c, d, e, f, g, h, j, k– mapping

Since the martensitic matrix of HSS is softer than VC carbide, if the ring is used for too long (or depending on the type of steel being rolled), it can be washed out (Figure 4).

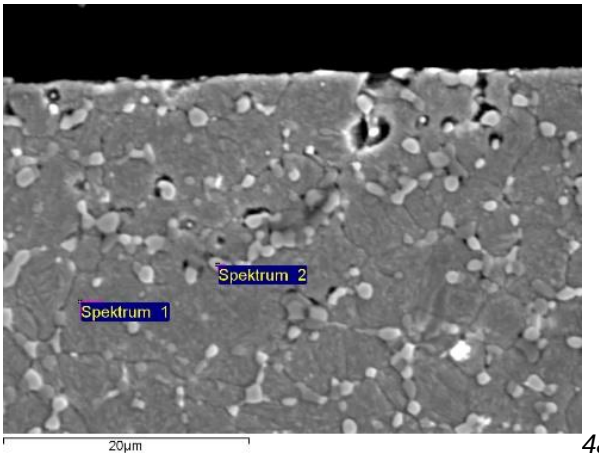

4a)

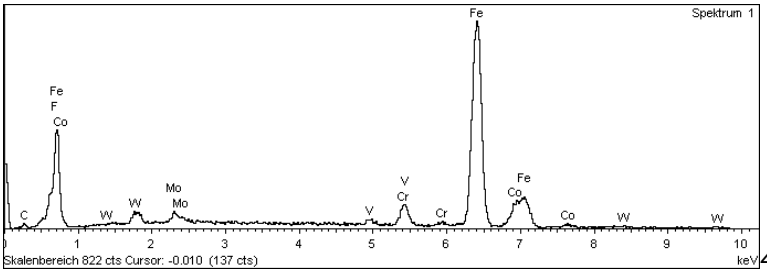

4b)

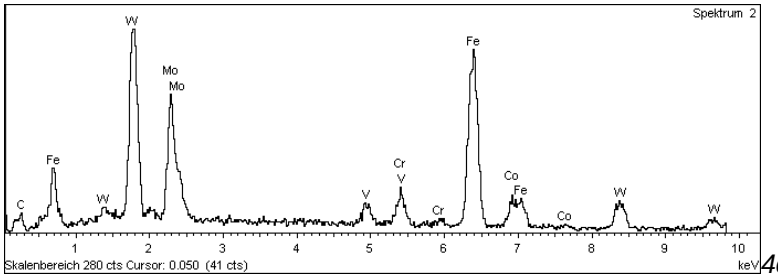

4c)

Figure 4. PM steel ring after use (cross section): a – location of the EDX analysis(SEM image);b –matrix; c – MC mixed carbide

This will compromise the mechanical support of the carbides and facilitate carbide separation from the ring surface. The roughness of the caliber is affected and the formation of cracks in the ring body is promoted.

HSS cast materials

The manufacturing processes described above are energy and cost intensive. Nowadays, cheaper rolled rings that can be manufactured using the casting method are in demand on the market. These are also used effectively with the shorter campaign length. In order to meet the requested requirements of users, ring manufacturers have developed HSS casting grades that are alloyed with different combinations and contents of carbide-forming elements such as Cr, Mo, V, W, Nb and Ti. Depending on the chemical composition and heat treatment parameters, the hardness of the HSS rings varies from 60 to 64 HRC.The microstructure of these materials consists of tempered martensite with a high proportion of embedded primary and secondary carbides and exhibits higher wear resistance even at higher surface temperatures.

Figure 5 shows the structure of a ring made of V-Mo-Cr-W-Nb alloyed HSS casting quality that was developed by us in recent years [27, 28].

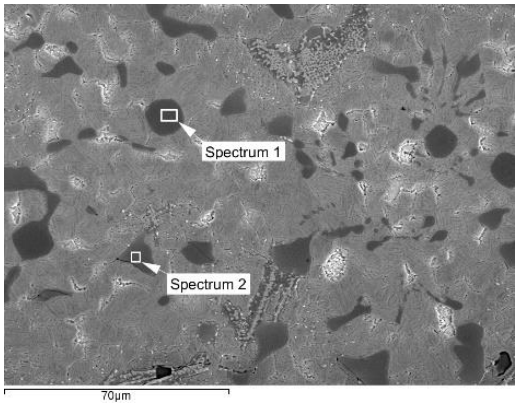

5a)

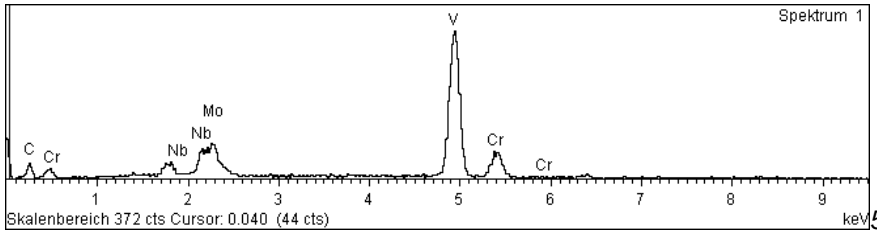

5b)

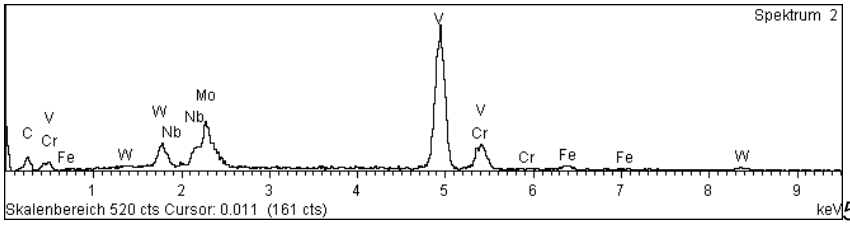

5c)

Figure 5. Microstructure of an HSS ring: a – overview with the location of the EDX analysis (SEM image), b, c – EDX analyzes of MC carbides

The optimal contents of alloying elements and structural components used were determined using ThermoCalc software. In thermodynamic equilibrium, the developed alloy contains approximately 26% by volume of carbides. The majority (approx. 10.4% by volume) is made up of type MC carbides. A high-volume content of VC carbide in the matrix is desirable. The VC carbides have a high hardness (2800 –3000 HV), which is not reduced even at higher temperatures [29], which leads to a high reduction in wear.The morphology of eutectic carbides is influenced by the cooling rate. At high cooling rates, the eutectic does not form a closed network. The very fine MC carbides – mainly VC – are present everywhere in the structure and are homogeneously distributed. A homogeneous arrangement of primary MC carbides was achieved by the fact that the first nucleation sites precipitate out in the melt. The formation and growth of MC carbide is facilitated at these nucleation sites. The primary, face-centered cubic VC carbide contains small amounts of molybdenum, chromium, tungsten and niobium. After the heat treatment (hardening and tempering), the microstructure has a tempered martensite, globular-shaped primary carbides that were not dissolved during the heat treatment and contribute significantly to the good resistance of the material to abrasive wear. When tempering HSS, 10^{16} to 10^{18} 1/cm³ of fine (about 1 x 10 x 10 nm) secondary carbides precipitate from the martensite [30], which is saturated with carbon and alloy elements, which prevent the movement of dislocations according to the Orowan mechanism and thus harden the steel (secondary hardening). The residual austenite remaining as a result of incomplete martensitic transformation acts as a carbon source for secondary carbide formation during tempering. The secondary carbides increase the room temperature and hot hardness, tempering resistance and the thermal stability of the matrix. A secondary hardness maximum corresponds to the maximum crystal lattice strain as a result of the maximum density of the precipitated hardening phases. By increasing the strength of the matrix, the mechanical support of the carbides is increased and prevents them from tearing off from the contact surface.

After heat treatment, such rings have a uniform hardness of 66 to 67 HRC across the cross section and can be re-set several times until the minimum diameter is reached. The tensile strength of the material is 980 MPa. The compressive strength and fatigue strength of the developed HSS are approximately 480 MPa and 3430 MPa, respectively. The manufactured rings were clamped onto roll shafts made of steel [31]. Each roll was equipped with two HSS rings and the manufactured composite rolls were delivered to a rolling mill. The rolls were used in the 10th roll stand of a steel bar rolling mill for rolling high-carbon steel (final diameter 8.5 mm). Figure 6shows the surface of an HSS ring after use.

Figure 6. Surface of an HSS ring after use [27, 28]

After use, the developed HSS rings show uniform surface wear and a dwell time in the roll stand that is desired from user. No fire cracks were registered on the work surfaces.

The developed HSS was also used for the production of rings for the Kocks block.

Compared to cemented carbide rings, the cast HSS roll rings have a lower risk of breakage and therefore a higher safety of the rolling process. The high-speed steels therefore represent a reliable and cost-effective choice of material.

Ceramic materials

As tungsten prices have risen dramatically in recent years, this has led to significant cost increases for users of cemented carbide products, which can contain up to 96% tungsten. This situation stimulates the search for new material science and technological solutions.

Although the high-speed steels have a significantly higher modulus of elasticity (230 – 240 GPa) than conventional iron-based materials (190 – 210 GPa), the HSS rolls cannot avoid flattening. Significantly higher elastic moduli can only be achieved with other materials such as high-performance ceramics. The ceramic materials have some positive properties or combinations of properties that are not achieved by other material groups. The great interest in ceramic materials is based on certain significant advantages compared to metallic materials, such as significantly higher stiffness (elastic modulus), higher strength, a lower coefficient of thermal expansion and very high wear resistance. The further advantages of ceramic materials compared to metallic materials include the significantly higher resistance to temperature changes, which are associated with medium thermal conductivity and low coefficient of thermal expansionof ceramic materials (Figure 7).

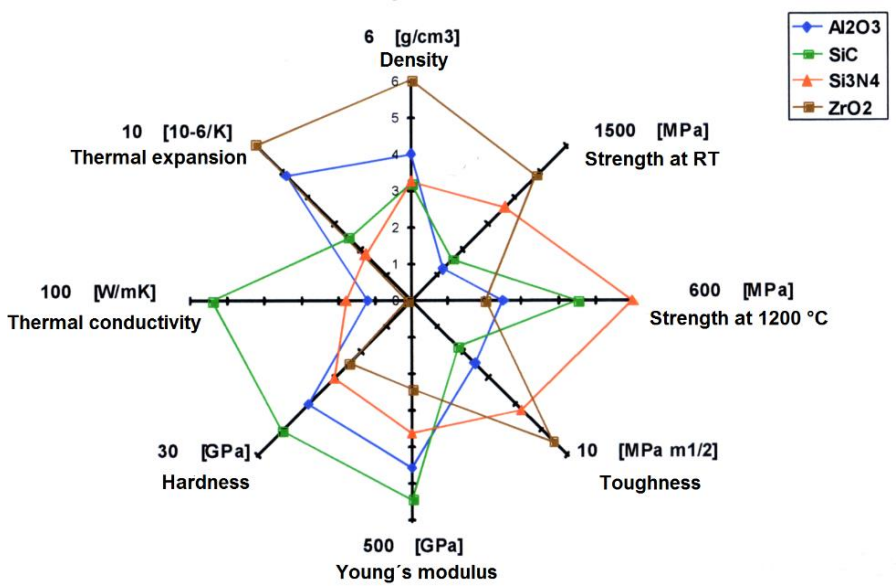

Figure 7. Comparison of the properties of high-performance ceramics [32]

Applications in rolling technology require ceramic materials that, in addition to high hardness and wear resistance, have high strength and crack toughness even at high temperatures. These materials must also have sufficient chemical resistance, in particular sufficiently high oxidation and corrosion resistance. These requirements are well met by many ceramic materials. In recent years, the suitability of technical ceramics as materials for rolls and other components of rolling technology has been intensively investigated. The ceramic rings for wire and bar rolls were made from silicon nitride (Si_3N_4), silicon carbide (SiC) and alumina-toughened zirconia (ATZ) and were used in rolling various types of steel. The last two ceramic types showed no measurable wear, but there were edge fractures, a fracture through the entire ring due to roll clamping, and edge fractures along the entire caliber [33]. The best results were achieved with silicon nitride. The Si_3N_4 composite rolls showed very little wear (max. height difference when comparing new and used calibers approx. 200 µm) and no cracks or breaks.

Silicon nitride occupies a promising position within non-oxide ceramics because it has a combination of many advantageous properties compared to other technical ceramics. Significantly higher strength values at room and higher temperatures as well as crack toughness lead to the long service life of Si_3N_4 composite rolls. This is associated with the unique needle-like or stalk-like structure of the fine-grained and evenly distributed Si_3N_4 grains and their mutual arrangement (Figure 8).

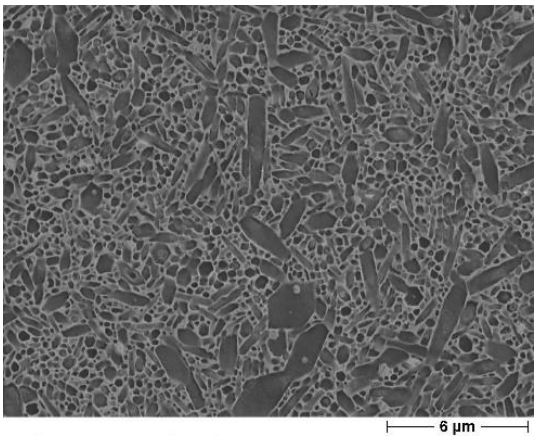

Figure 8. SEM image of a Si_3N_4 material (plasma-etched) [34]

As the Si_3N_4 starting powder is densified, the metastable α-Si_3N_4 modification transforms into the stable β-Si_3N_4 modification. The Si_3N_4 grains grow anisotropically to form needles with a hexagonal cross section. The main growth direction coincides with the c-direction of the Si_3N_4 crystal lattice. Since the starting powders are essentially globular, a texture-free structure of needle-shaped Si_3N_4 grains is formed when green bodies are sintered. The fineness and uniformity of the Si_3N_4 grains are important aspects for strength and high abrasive wear resistance [34]. The excellent high temperature properties of silicon nitride are related to the covalent bond. The excellent wear properties of Si_3N_4 rings lead to a smoothing of the roll surface and a significant improvement in the surface condition of the rolled product. We first observed this effect when rolling thin steel foils

made of austenitic and ferritic steels in a 20-roll Sendzimir mill [35].The average wear rate is $2 \cdot 10^{-10}$ m per ring revolution, which corresponds to a surface loss of about 0.6 µm per rolled ton. Based on the typical service life of conventional cemented carbide rolls of 500 tons of rolled wire, this results in a "noticeable" wear of about 300 µm [36]. Si_3N_4 rolling rings used in Kocks blocks also show no damage after use [37].

Compared to hard metals and steels, the use of silicon nitride results in reduction of frictional forces, lower abrasive wear and no adhesion of rolled metal, which is associated with the non-metallic bonding type in ceramics. The high hardness (15 GPa), elastic modulus (300 – 320 GPa) and compressive strength (3000 MPa) prevent roll flattening in the roll gap and enable the accuracy of the rolled product to be increased.Due to its thermal properties, particularly as a result of its low coefficient of thermal expansion (approx. $3 \cdot 10^{-6}$ 1/K), silicon nitride has excellent resistance to temperature changes.

Good resistance of silicon nitride to oxidation and corrosionis an advantage when used at high temperatures. However, the coolant (water) can penetrate into the pores that can form during ring production and increase their growth through stress corrosion, which can lead to a reduction in the strength of the silicon nitride. Depending on the quality of the starting material and the manufacturing process used, Si_3N_4 products have different surface porosities. As can be clearly seen from Figure 9, the production of Si_3N_4 products with increasing sintering pressure (gas pressure: 100 bar, hot isostatic pressing: 2000 bar) and high quality of the starting material results in material structures with fewer pores and can ensure better resistance to stress corrosion.

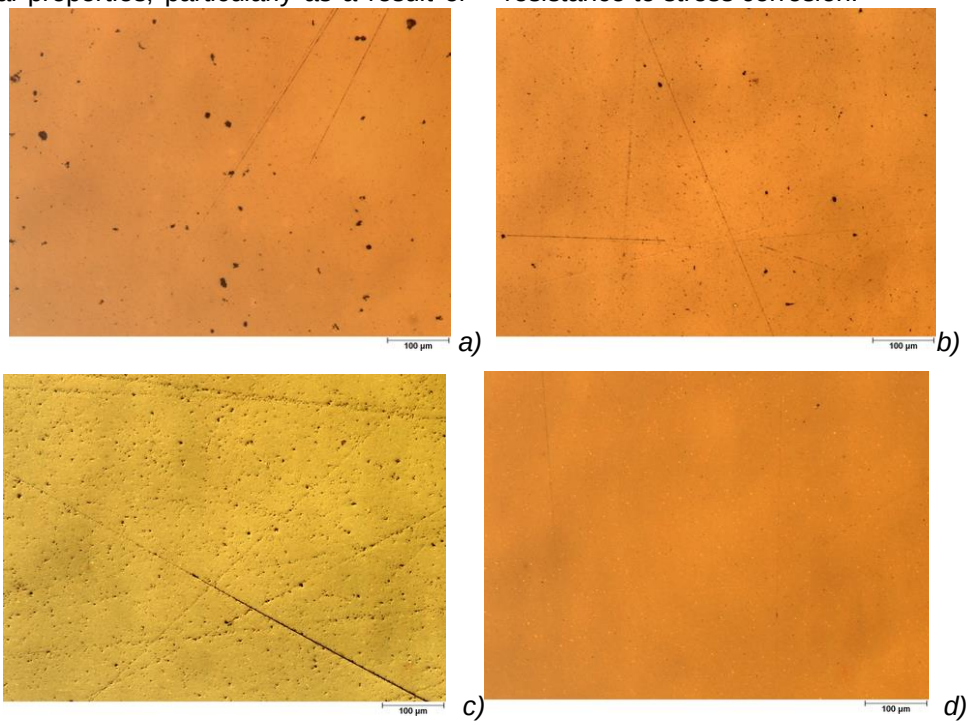

Figure 9. Micrographs of gas pressure sintered (left) and hot isostatically pressed (right) silicon nitride of standard quality (a, b) and high quality (c, d)

Corrosion occurs between Si_3N_4 grains. The grain boundary phase is often less stable than the grains and is triggered by corrosion processes deep into the interior of the structure, while the grains remain stable. Therefore, the grain boundary phase generally determines the corrosion stability of these ceramics. The Si_3N_4 grains can then easily detach from the working surface of the ring, which can lead to the formation of microcavities. Mechanically caused structural damage can intensify the corrosive attack. If a corrosive attack occurs with superimposed abrasive wear, the corrosion rate can increase significantly. As a material for forming tools, silicon nitride has great chemical stability.

Ceramic tools are successfully used as guide rolls in hot rolling. The guide rolls guide the running wire strand exactly into the rolling gap and prevent the oval wire strand from tilting in a round rolling caliber. Significant forces arise which are caused by the high forming strength of the materials being processed. The service life of Si_3N_4 guide rolls is on average 15 times longer [38].The Si_3N_4 pinch rolls, which guide and brake the wire end, have

shown extremely low wear when rolling wire with a final dimension of 5.5 mm [33]. After eight times the service life of the steel rings, the wear depth was in the range of 90 µm, which was the end of the service life [37].

Silicon nitride rings are already routine in individual areas of rolling mills. Compared to standard materials –cemented carbide and steel – ceramic forming tools bring significantly greater efficiency to the production process. Production costs can be reduced without major modifications to production facilities. The economic advantage for the user results from the increased service life, depending on the application, by a factor of 10 to 15 [38].

Silicon nitride is a well-suited material for the production of rings. A comprehensive overview of the studies we have carried out in recent years can be found in [39].

Ring clamping systems

Various types of radial and axial mechanical clamping systems have been developed and used for clamping rolled rings. The load on cemented carbides and silicon nitride rings caused by the radial clamping pressure of a clamping system and by centrifugal force during the rolling process was examined [40]. The calculation results for a rolling ring made of cemented carbide have shown that there are tangential tensile stresses on the outer edge, which become even greater at high speeds and are often the cause of rolling ring fractures when clamped radially. Centrifugal forces that occur at high rolling speeds counteract the effective radial tension and impair the transferable torque. Calculations have shown that this effect is less pronounced when the mass density of the tool is lower [40, 41]. The lower density of the silicon nitride causes significantly smaller centrifugal stresses than with a cemented carbide ring at the same internal clamping pressure. This is of great importance for the transferable torque during rolling, especially for finished wire blocks, where there are very high final rolling speeds of up to 120 m/s.

When using ceramic tools, it must be noted that these materials cannot withstand tensile loads and the smallest tensile stresses lead to the destruction of the tool. Axial hydraulic clamping systems are used to clamp rolled rings. Various types of such tensioning systems have been developed that transmit mechanical tension through hydraulically generated preload. The absence of stress concentrators on the cement carbide ring prevents ring destruction due to the occurrence of critical bending and tensile stresses. This is achieved by using a sliding fit of the rings on the shaft with subsequent fixation using a special clamping device that creates compressive stresses along the roll axis [42]. The roll rings can be clamped with an axial pressure of 2000 bar [31]. To clamp the roll rings on the rolling shaft, this is expanded hydraulically via the ring piston and the resulting gap is closed without play using the patented wedge ring system. After the hydraulic pressure is removed, the high clamping force generated by the expansion of the rolling shaft is safely mechanically maintained via the wedge ring. To change the rings, the user relaxes the composite rolls, the roll rings are changed and tightened again. The hydraulic clamping system with a lower axial pressure of 1500 to 2000 bar can ensure rolling ring tensioning through a shaft expansion of 0.5 mm [43]. Using a hydraulic nut, a high axial contact pressure of up to 4000 bar can be generated, which ensures appropriate torque transmission and prevents the roll rings from slipping [44].

With the clamping systems mentioned above, radial clamping forces, which lead to an increased risk of breakage and reduced service life, are completely avoided. The clamping system is therefore of central importance for operational safety. In addition to secure rolling ring fastening, clamping systems also achieve an increase in production and further cost savings.

CONCLUSIONS

Depending on the operating conditions, the type of steel being rolled and the campaign length, the roll rings made from the available materials (cemented carbide, high-speed steel) can be used successfully to achieve the economic efficiency of the rolling process. The development of composite materials (cemented carbide/cast iron, cemented carbide/steel) has solved the problem of torque transmission and made it possible to save expensive cemented carbide and significantly reduce the production costs of rolled rings.

The ceramic materials offer high potential for use as ring materials for hot and cold rolling mills. This is due to their higher hardness and rigidity, coupled with lower density compared to steel or cemented carbide materials, which makes it easier to solve many rolling problems that are limited by the properties of steel or cemented carbide rings. The application of silicon nitride in the production of rolled rings and their successful use in different operating conditions has shown that there is significant potential for expensive but durable materials that have several advantages. When

producing hot-rolled wire, roll rings made of silicon nitride offer advantages over conventional rings made of cemented carbide or steel and can be used as an alternative to cemented carbide. Substitution of cemented carbide with silicon nitride plays an important role given the likely future resource scarcity of tungsten.

REFERENCES

[1] E.I.Klaphake,W.H.Rackoff (2002) Tungsten Carbide Rolls. In: Rolls for the Metalworking Industries. G.L.Lee (Ed.). Iron and Steel Society, Warrendale, PA, USA, 93-132.

[2] K.-D.Leitzmann, W.Böhlke (1985) For the use of sintered cemented carbide roll rings in high-performance wire mills. Neue Hütte, (30)11, 417-421.

[3] SinterMet LLC: Technical Recommendations to Optimize Roll Performance.Kittanning, PA, USA.

[4] SinterMet LLC: Engineered Product Solutions. Kittanning, PA, USA.

[5] D.N.French, D.A.Thomas (1965) Hardness anisotropy and slip in WC crystals. Transactions of the Metallurgical Society of AIME, (233)5, 950-952.

[6] Y.Kusaba, S.Azuma (1997) Improvement of WC-roll wear in Tube Mill and Wire Rod Mill. Der Kalibreur, (58), 47-56.

[7] O.Sommer (1997) Damage patterns for WC cemented carbides with Co-binders. In:Advances in Metallography. Vol. 28. W.-U.Kopp, M.Kurz (Ed.). Publisher DGM Informationsgesellschaft mbH, p. 295-300.

[8] K.H.Cho, B.U.Cho (2010) Study of Crack Propagation Behavior of Sintered WC-Co-Ni-Cr Alloy under Periodic Loading and Heating. Der Kalibreur, (71), 15-26.

[9] J.-E.Karlsson (2000) Cemented tungsten carbide as a roll material. Steel Times, (228)10, 370- 376.

[10] D.Schuler, T.John (2005) SARACOM – roll rings for flat and angle rolls as well as for intermediate stands in steel bars and wire mills. Der Kalibreur, (66), 31-41.

[11] L.Chen (2003) New Developments in cemented tungsten carbides and powder metal tool steel rolls for long product hot rolling applications. Rolls 2003. Programme and Conference Papers, Birmingham, UK, April 9-11, p. 1-11.

[12] J.E.Karlsson (2008) Cement Carbide as Hot Roll Material – Today and Tomorrow.Der Kalibreur, (69), 19-32.

[13] D.Schuler, T.John (2005) SARACOM – Roll Rings for Flats and Angles and Intermediate-Stands of Bar and Wire Rod Mills. Der Kalibreur, (66), 31-41.

[14] V.Goryany, O.Myronova, E.Schubrikoff, J.Buch, F.Stein (2018) Non-metallic inclusions and fatigue strength of steel 34CrNiMo6. Materials Testing, (60)10, 1004-1012.

[15] V.Goryany, E.Schubrikoff, O.Myronova (2020) Roll optimization via numerical modeling of stress distribution. Materials Testing, (62)1, 35-39.

[16] J.E.Karlsson (2014) The roll choice – a way to increase rolling mill productivity. Der Kalibreur, (75), 8-13.

[17] S.E.Lundberg (2004) Experiences of cemented carbide rolls in bar rolling. Cercetari Metalurgice si de noi Materiale, (12)1, 1-24.

[18] A.B.Muller, S.Ya.Unru, B.I.Voronin, D.V.Nazarov, A.S.Limarev, O.N.Tulupov (2007) On the possibility of replacing cast iron rolls with carbide ones in the finishing group stands of wire mill 170. Bulletin of MSTU,(3), 65-68.

[19] S.E.Lundberg (2011)Cemented Carbide Rolls for Rolling SBQ Bars. AISTech 2011, 2 – 3 May, Proceedings, Vol. 2, p. 297-309. Indianapolis, Indiana, USA.

[20] S.E.Lundberg (2011)Cemented Carbide Rolls for Rolling SBQ Bars. Iron & Steel Technology, (8)9, 47-56.

[21] L.I.Frayman (2017) Cemented Carbide Material for Hot Rolling Applications. General Carbide Corporation. Greensburg, PA, USA, p. 14.

[22] Sandvik (2015) Sandvik Hyperion. Smart Rolling Solutions, p. 16.

[23] V.Goryany (in preparation) Investigations of the composite material cemented carbide/ nodular cast iron.

[24] SAAR-Hartmetall und Werkzeuge GmbH (2012) Roll rings, composite rolls and accessories for hot rolling mills, p. 12.

[25] D.Schuler, W.Altmeyer, F.Kiefer (1997) High speed steel by powder metallurgy „SARAMET“ and WC-steel composite rolls „SARACOM“ for light section-, wire rod- and section mills. Der Kalibreur, (58), 7-20.

[26] D.Schuller (2008) Use of Cemented Carbide Roll Rings in the Stands 8-10 of the Intermediate Mill of BELGO ARCELOR – Juiz de Fora – Brazil.Der Kalibreur, (69), 101-107.

[27] V.Goryany, O.Myronova, J.Buch, A.Buch, F.Stein (2022)High-performance HSS-roll rings. Giesserei, (109)11, 44-51.

[28] V.Goryany, O.Myronova, J.Buch, A.Buch, F.Stein (2023)High-performance HSS-roll rings. Casting Plant & Technology, 1, 24-31.

[29] K.Bungardt, K.Kind, W.Oelsen (1955) The solubility of vanadium carbide in austenit. Archiv für das Eisenhüttenwesen, (27)1, 61-66.

[30] LS.Kremnev (2008) Theory of alloying and development of heat-resistant tool steels and alloys. Metal Science and Heat Treatment of Metals, (11), 18-27.

[31] C.Zybill, V.Goryany, E.Schubrikoff, R.Almeida, K.Fenners (2014) Integral solutions for rolls in section and bar rolling mills. Der Kalibreur, (75), 71–78.

[32] G.Wötting, H.Drachsler (2004) Ceramic rolling tools made of silicon nitride for the production of wire, tube and strip. Symposium Ceramics for rolling technology, 17-18 March, Neuwied, Germany.

[33] M.Schünemann, S.Waengler (2009)Ceramic rolls for wire rods – cost-effectiveness and quality.In:

Rolling with ceramics. Proceedings of the symposium on ceramics for rolling technology.28-29 July, Neuwied, Germany. A.Kailer (Ed.), Fraunhofer Publishing, Stuttgart, Germany, p. 85-94.

[34] V.Goryany, R.Wagner (2011) Ceramic Materials for Rolls and other Components for Hot Rolling.Materials Testing, (53)11, 748-757.

[35] V.Goryany, P.J.Mauk, J.Giersbach (2011) Ceramic work rolls for rolling thin steel foils in the 20-roll Sendzimir mill. Materials Testing, (53)10, 643-648.

[36] R.Danzer, M.Lengauer, W.Harrer (2009) Strength and application limits of ceramic wire rolls. In: Rolling with ceramics. Proceedings of the symposium on ceramics for rolling technology. 28-29 July, Neuwied, Germany. A.Kailer (Ed.), Fraunhofer Publishing, Stuttgart, Germany, p. 95-111.

[37] R.Wagner (2009) Ceramic development and production. Ceramic rolls for wire rods – economy and quality.In: Rolling with ceramics. Proceedings of the symposium on ceramics for rolling technology.28-29 July, Neuwied, Germany. A.Kailer (Ed.), Fraunhofer Publishing, Stuttgart, Germany, p. 33-48.

[38] W.Zleppnig (2009) Wire rolls, driver rolls and guide rolls for high-strength steel alloys, economy and quality. In: Rolling with ceramics. Proceedings of the symposium on ceramics for rolling technology.28-29 July, Neuwied, Germany. A.Kailer (Ed.), Fraunhofer Publishing, Stuttgart, Germany, p. 79-84.

[39] V.Goryany, O.Myronova (2023) Ceramic rolls for rolling of steel foils. Zaštita Materijala, (64)1, 48-57.

[40] P.J.Mauk (2009) Rolling technical aspects and requirements. In: Rolling with ceramics. Proceedings of the symposium on ceramics for rolling technology.28-29 July, Neuwied, Germany. A.Kailer (Ed.), Fraunhofer Publishing, Stuttgart, Germany, p. 113-130.

[41] C.Overhagen, P.J.Mauk (2014) Ceramic materials for rolls and rolling tools in hot and cold rolling. Stahl und Eisen, (134)5, 53-60.

[42] V.V.Pashinsky, D.G.Sidorenko (2013) Use of carbide banded rolling rolls for the production of reinforcing profiles. Metallurgical and Mining Industry, 3, 75-78.

[43] Tungsten Carbide Rolls. ILJIN Diamond, Seoul, South Korea.http://www.diamondsolution.it/assets/Uploads/rulli-laminazione.pdf

[44] D.-W.Bae (2012) Case study on the improvement of clamping mechanism for tungsten carbide composite rolls. 2012 SEAISI Conference and Exhibition, ASEAN Steel Industry: Anticipating, Opportunities, Grows and Chalanges. Nusa Dua, ID, May,p. 28-31.

IZVOD

PRSTENOVI ZA SLOŽENE VALJKE VALJAONICA

Opisani su savremeni materijali za proizvodnju prstenova za kompozitne valjke i njihova najvažnija svojstva. Analizirane su prednosti i nedostaci prstenova izrađenihod tvrdog metala, brzoreznog čelika, keramičkih materijala i mehanizmi njihovog oštećenja. Dalje, predstavljeni su zahtjevi za vodu za hlađenje prstenova. Opisanaje struktura prstenova od kompozitnih materijala izrađenih od tvrdog metala i legura na bazi željeza, brzoreznog čelika, prstenova proizvedenih metalurgijom praha i metalurgijom rastopljenog metala te prstenova izrađenih od silicijum nitrida.
Ključne reči: *prsten, složeni valjak, tvrdi metal, brzorezni čelik, silicijum nitrid, steznisistem*

Naučni rad
Rad primljen: 15.05.2024.
Rad prihvaćen: 01.07.2024.

Auxilia Ruby Sagaya Irudayaraj, Felicita Florence John, Divya Priya Chinnasamy, Kanmani Raman, Amala Infant Joice Joseph*

PG and Research Department of Chemistry, Holy Cross College (Autonomous), Affiliated to Bharathidasan University, Trichy-620002, Tamilnadu, India

Scientific paper
ISSN 0351-9465, E-ISSN 2466-2585
https://doi.org/10.62638/ZasMat1188

Zastita Materijala 66 (1)
90 - 101 (2025)

Synthesis and characterization of *Selenicereus undatus* extract mediated nano-Bi_2O_3 and its application in the adsorption of Rhodamine B dye

ABSTRACT

Betacyanins(BC) arereddish-purple pigment widely found in the peels of white-fleshed dragon fruit (Selenicereus undatus) and peels and pulps ofred-fleshed dragon fruit (Selenicereuscostaricensis). BC pigments are good anti-oxidants that inhibit the formation of reactive oxygen species (ROS) in plants and thereby promote the reduction of metal ions to zero valent metals. It also acts as a good stabilising and capping agent in the synthesis of nanoparticles. Hence, this research aims to extract, and quantize the content of BC from the peels of Selenicereusundatus, to fabricate betacyanin rich-Selenicereusundatus (SU) modified bismuth oxide nanoparticles (Bi_2O_3 NPs) and characterize using UV-Vis, FTIR, XRD, SEM, EDAX and BET. The quantity and stability of the betacyanin are optimized using various parameters like time, temperature, solvent ratio, pH, etc., through UV-Vis spectrophotometer at 538 nm. SynthesizedSU-Bi_2O_3 NPs aims for the alleviation of synthetic dye contaminantsthrough adsorption- an efficient route for water remediation. The nano-adsorbent Bi_2O_3 NPs showed increase in dye adsorption with an increase in reaction time, temperature and Bi_2O_3 NPs dosage, enabling efficient removal of dyes such as Rhodamine B (RhB) dyes.

Keywords:*Betacyanin, selenicereus undatus, bismuth oxide nanoparticles, characterization, Rhodamine B dyes.*

1. INTRODUCTION

The green extract obtained from plant parts, microbes and biomass are used as a non-toxic, eco-friendly reducing and stabilizing agent for the synthesis of metal nanoparticles (M NPs) or metal oxide nanoparticles (M_XO_Y NPs). The bioactive compound present in the green extract reduces the metal ions to the required M NPs or M_XO_Y NPs. One such bioactive compound that attracts the recent research field is the 'Bioactive Natural Colorant'. The food and textile industries seek interest in natural colorants (NC) to promote non-toxic replacement and at the same instant health beneficial products. Major parts of NC are obtained from plant sources like bark (oak dye), roots (madder dye), leaves (indigo), flowers (saffron, hibiscus, butterfly pea and marigold lavender) fruits (dragon fruit, beets, berries and red cabbage) and also from microbes (Streptomyces coelicolor, Actinorhodin)[1,2]. The common bioactive pigments responsible for the color of the dyes are anthocyanin, betalain, carotenoids and chlorophyll.

Among them, betalains are found to show antioxidant, detoxicant and readily get adsorbed and digested in humans. Betalains is a water-soluble nitrogen-containing NC with two types-yellow pigment (betaxanthins) and reddish-violet pigment (betacyanins) found exclusively in the order Caryophyllales which includes, beets, amaranth, pitayas, cactus pear, swiss chard, etc. Besides, replacing synthetic dyes into NC requires overcoming some limitations like high expense, poor stability and poor staining in clothes. The peel of pitayas, both red fleshed(Selenicereus costaricensis) and white fleshed (Selenicereus undatus) contains high content BC which is usually discarded as waste. From the peels of pitayas, BC(Figure 1) can be extracted using water as a solvent and estimate the quantity through spectroscopic techniques [3]. However, these pigments are unstable by their nature and need optimization of a few parameters like temperature, time, solvent nature, dilution and pH.

*Corresponding author: Auxilia Ruby Sagaya Irudayaraj
E-mail: auxiliaruby@gmail.com
Paper received: 05.06. 2024.
Paper accepted: 01.07. 2024.
The website: https://www.zastita-materijala.org/

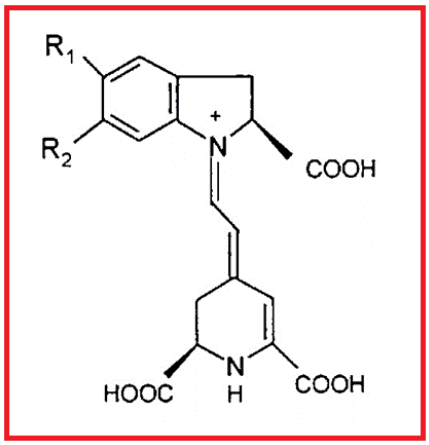

Figure 1. Structure of betacyanins

In the synthesis of nanoparticle, certain features like stability, shape, size and surface area depends on the reduction potential of ions which was governed by the nature of plant extract. Green synthesized MNPs showed vast applications in the field of biomedical, catalysis, adsorption, biosensors, nano-sensors, drug delivery, fertilizer delivery, gene delivery, harmless cosmetics, crop protection and water remediation[4]. Bismuth oxide nanoparticles (Bi_2O_3) (Figure 2) showed considerable advances in many fields of application due to peculiar properties like high surface area, wide band gap, elevated refractive index, high levels of electrical properties and good diamagnetism. Existing polymorphs of Bi_2O_3 are α-Bi_2O_3(monoclinic), β-Bi_2O_3(tetragonal), γ-Bi_2O_3(bcc), δ-Bi_2O_3(fcc cubic), ε-Bi_2O_3(metastable related to α- and β-phase), ω-Bi_2O_3(triclinic). The most stable form at room temperature is monoclinic- α phase $Bi_2O_3$and others are high-temperature phases. Due to the high surface area of Bi_2O_3, it acts as a good nano-adsorbent in the removal of various pollutants like dye, pesticides, fertilizers, heavy metals, industrial effluents, soaps and detergents[5].

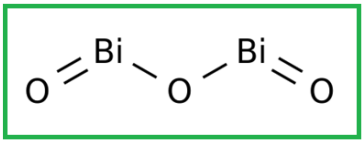

Figure 2. Structure of bismuth oxide

The discharge of dyes into the biosphere, mutilates mankind through dermatitis, carcinogenic, asthmatic disorder, nausea and colon polyps. Stability and resisting power of dyes makes it difficult to degrade by oxidants, photocatalyst, microbes and electrochemical destruction. Adsorption via nanotechnology is a coherent, eminent and advantageous method [6].Hazardous effluents like dyes, heavy metals, Volatile organic compounds (VOCs), pathogens, polymers, radio-active sediments etc., are engulfed all over the water bodies.Synthetic dyes ruin the grandeur features of water via inhibiting photosynthesis, disrupt the biological cycle and promoting skin toxi-city, Septicemia, bone deformities, carcinogenicity and neurological problems. One such menacing dye is Rhodamine B (RhB) which wascategorized as group 3 carcinogenic by International Agency for Research on Cancer (IARC) and also banned its use as artificial food colorant in India[7]. Thus water remediationthrough nano-sorbent is an efficient strategy to demolish ubiquitously available contaminants especially dye abolition.

2. EXPERIMENTAL SECTION:

2.1. Separation of peels from the pulp of Selenicereusundatus (SU):

White dragon fruit *(Selenicereusundatus) was* purchased from the farms of Dharmapuri district, Tamil Nadu, India. The fruit was washed with tap water to remove all the dust and microbes. Further rinsed with DD water for 2 to 3 times and separated the peel part from flesh using a clean knife. The non-red parts like flower end pit, bracts, areole are removed completely. Even though the pulp of the fruit was removed, yet it still contained some white fibers like structure, which was also removed. Finally, the peels were chopped into cubes (1-2 cm) and stored at low temperature for extraction.

2.2. Extraction of BC from the peels of SU:

Quantification of BC was achieved by treatingthe peels with DD water as extraction solvent. Dependence of extraction condition was scrutinized by assorting solvent-peel ratio (5:1, 7.5:1, 10:1, 12.5:1, 15:1, 17.5:1, 20:1, 22.5:1 and 25:1), temperature of extraction (30°C, 40°C, 50°C, 60°C, 70°C, 80°C, 90°C, 100°C, 110°C and 120°C), duration of extraction (0.5 hr, 1 hr, 1.5 hrs, 2 hrs, 2.5 hrs, 3 hrs, 3.5 hrs, 4 hrs, 4.5 hrs, 5 hrs) and pH ranges (1, 2, 3, 4, 5, 6, 7, 8, 9, 10, 11, 12). The above acquired extracts were filtered using Whatman no.1 filter papers and refrigerated until further processing.

2.3. Determination of BC from SU peels extract:

Absorbance of individual peel extract was determined using Visican Spectrophotometer-type 167 at wavelength 538 nm which corresponded to BC pigment [8].

Quantification of BC (mg/100 g) =

$A_{(at\ 538\ nm)}$. м. D. υ. 100/ε. ш. ⌊

where,

$A_{(at\ 538\ nm)}$=Absorbance at 538 nm corresponding to BC

ʍ= Molecular weight of BC ≈ 550g mol^{-1}

D=Dilution factor

ʊ= Volume of extract (in ml)

ε=Molar absorption coefficient $6x10^6$ L mol^{-1} cm^{-1}

ɯ=Gram weight of *SU*peels taken.

ǀ=Path length ≈ 1 cm

2.4. Green synthesis of Bi_2O_3NPs:

Green synthesis of Bi_2O_3NPs was carried out using the optimized*Selenicereusundatus*peels extract. About 10ml of *Selenicereusundatus*extract was added to 0.1M $Bi(NO_3)_3$and stirred continuously for 2hrs at 90℃. Initially, the color of the solution appeared champagne pink and the pH measured 6. Once the pH was increased to 10, the solution start to precipitate and color turnedto pale yellow. After completion of the reaction, the precipitate was centrifuged 3-4 times with ethanol and DD water, dried in hot air oven for 2 hrs and calcinated in muffle furnace for 3hrs at 300℃.

2.5. Characterization of green Bi_2O_3NPs:

Green synthesized Bi_2O_3NPs were characterized by P-XRD (PANalytical X'Pert Pro) to analyze the structural modification with Cu-Kα radiation source ranged from 0°to 90°. XRD helps in determining the crystal structure, nature of crystallinity, lattice parameters, orientation etc., based on the diffraction patterns obtained. Particle size could be identified from the peaks, as the size decreases, the peak gets broadened. Further it was analyzed using FTIR spectrophotometer (Perkin Elmer Spectrum Two) with $LiTaO_3$ detectors. Anhydrous KBr optical transparent salt was used to make pellets with Bi_2O_3 NPs of 13 mm diameter using hydraulic press machine (kimaya-table top). FTIR measured the absorption/ Transmittance of the IR radiation produced by the sample at range 4000cm^{-1} to 400cm^{-1}. Furthermore, UV-Visible spectrophotometer for Bi_2O_3NPswas recorded using Perkin Elmer Lambda 35 with range 190nm-1100nm. Nanoparticles have unique optical characters that affect the size, shape, agglomeration, refractive index etc., which makes UV-Visible spectrophotometer, an efficient tool for characterizing. Additionally, the morphology of the green synthesized Bi_2O_3NPswas studied using SEM (Carel Zeiss-EVO 18). Enhanced topology information was provided by BSD detectors on EVO 18. High resolution of SEM helps to focus and magnify closely packed specimen and provides a visual ideology of shape and size. EDAX helped to identify the elements present in the material and its composition. This technique reassured the presence of required elements with less or no impurities. BET surface area analysis was carried out for Bi_2O_3 NPs using BETSORP Max-Microtrac BEL. Adsorption capacity of Bi_2O_3NPs was tested using N_2 as adsorbate. Known amount of N_2 was passed over the sample till saturation pressure attains and the adsorption layer formed was detached byheating to estimate the desorption process. The obtained data wasexhibited as BET isotherm[9].

2.6. Adsorption studies of Bi_2O_3NPs

Adsorption properties of green Bi_2O_3NPs were investigated using Rhobamine B dye with various concentrations, time of contact, temperature and pH. Based on these factors, the adsorption capacities were measured and the best adsorption behaviours of the nanoparticles were identified minimizing the factors affecting adsorption. Various adsorption processes were carried out at disparate physical conditions are tabulated belowin table 1.

Table 1. List of various adsorption parameters and ranges utilized for adsorption studies

Adsorbent dosage (NPs)	20mg	50mg	100mg	150mg	200mg	250mg
Adsorbate dosage (RhB dye)	10ppm	20ppm	30ppm	40ppm	50ppm	60ppm
Adsorption time	30mins	45mins	1hr	1.5 hrs	2hrs	2.5hrs
Adsorption Temperature	30℃	40℃	50℃	60℃	70℃	80℃
Adsorption pH	1	3	5	7	9	11

3. RESULTS AND DISCUSSION

3.1. Optimization of BC quantity

3.1.1. Optimization of BC based on solvent-peel ratio

The solvent-peel ratio was varied (5:1, 7.5:1, 10:1, 12.5:1, 15:1, 17.5:1, 20:1, 22.5:1, 25:1) and for each extraction process, approximately 1gof peels was added to the required DD water at 40°C for 2 hrs.Based on the absorbance obtained at λ=538 nm for the above solutions, its BC quantity was determined using the equation (1).

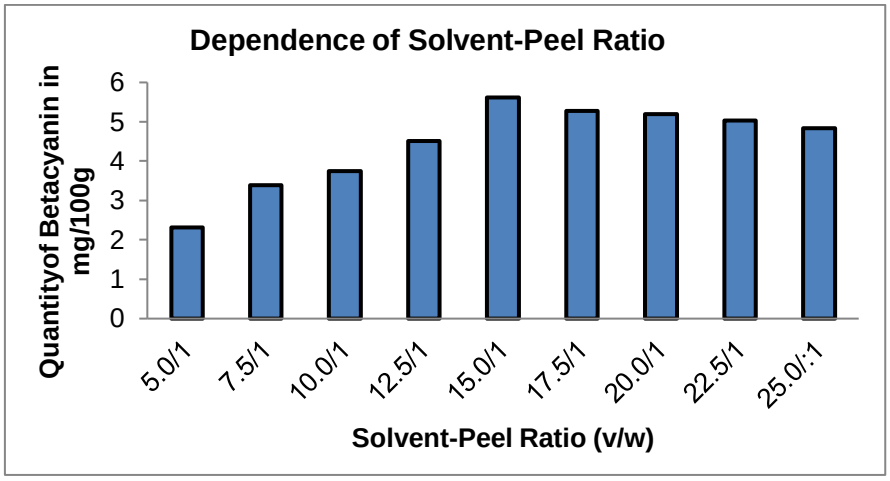

Figure 3. Plot depicting the correlation between Solvent-Peel ratio and BC quantity

Figure 3 represents the quantity of BC modification with respect to the solvent-peel ratio. BC quantity was highest for 15:1 with 5.63 ±0.15 mg of BC content per 100 g of fresh peels of *Selenicereusundatus.*BC being a water-soluble pigment it required an enough quantity of solvent to dissolve it. Hence solvent-peel ratio below 15:1 shows low BC quantity due to insufficient solvent. If the solvent is increased over the optimum condition, no change or slight decrease in BC content, proving that the most suitable solvent-peel ratio is 15:1.

3.1.2. Optimization of BC based on Temperature

BC pigments were highly unstable to thermal condition because it undergoes degradation resulting in decreases in the quantity of BC. Extraction process was carried out with solvent-peel ratio 15:1 and temperature varied from 30°C to 120°C for 2 hrs. Figure 4 represents the quantity of BC with respect to the temperature variation. Optimum temperature for this case was found to be 50°C with BC content 5.87± 0.22 (mg/100g) and further increase leads to a gradual decrease in the quantity of BC. Temperature from 30°C to 50°C showed an increase of BC content because it facilitates diffusion of pigment into solvent. Additional increase of temperature beyond the optimum condition might lead to degradation of pigments resulted in decrease of BC content upto 1.99± 0.11 (mg/100g).

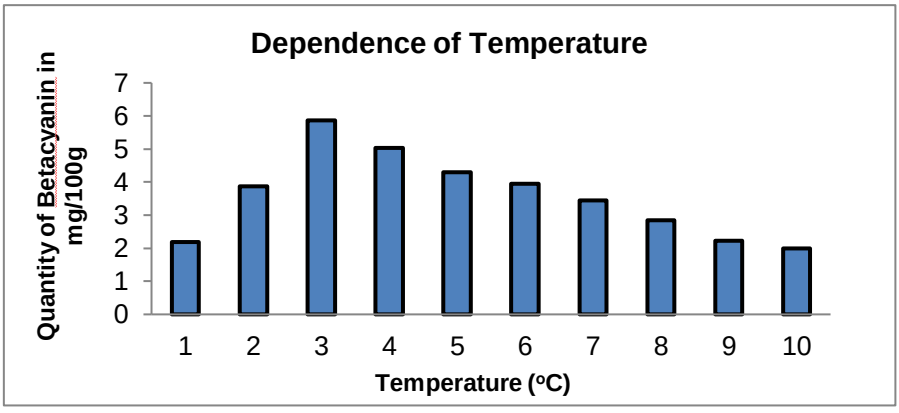

Figure 4. Plot depicting the correlation between Temperature and BC quantity

3.1.3. Optimization of BC based on Time

The dependence of time was illustrated in figure 5. In order to analyse the influence of extraction time, solvent-peel ratio of 15:1 was utilized at temperature 50°C for various time periods (30mins, 1hr, 1hr 30mins, 2hrs, 2hrs 30mins, 3hrs, 3hrs 30mins, 4hrs, 4hrs 30mins and 5hrs). The optimum condition with maximum extraction of BC was found at 3hrs with quantity 4.31± 0.13 (mg/100g). When extraction time increases, naturally the BC content increases and reaches a maximum (at pH-6). Beyond this point, hydrolyzes occurs leading to the formation of betanidine, betalamic acid, aminesand ultimately decreases BC content.

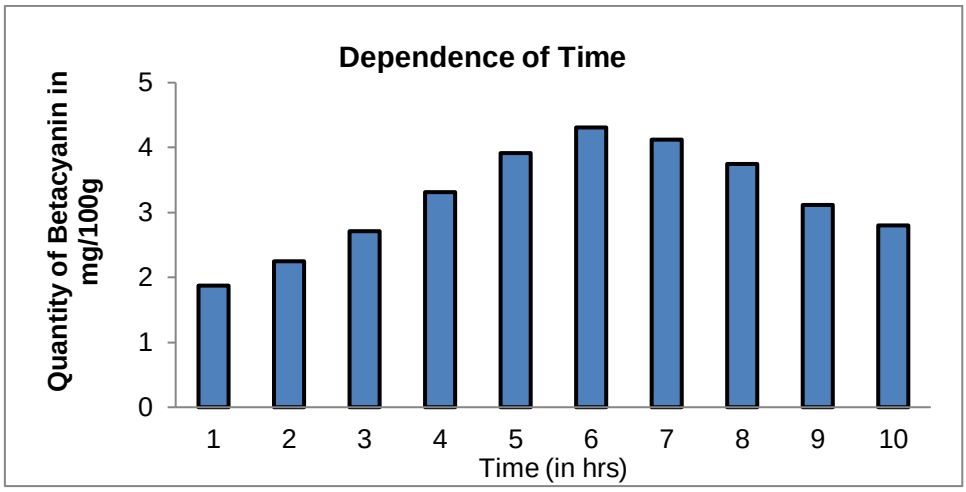

Figure 5. Plot depicting the correlation between Time and BC quantity

3.1.4. Optimization of BC based on pH

To analyse the dependence of pH, extraction processes was carried out with solvent-peel ratio 15:1, at temperature 50°C for 3hrs with pH range from 1.0 to 12.0. Figure 6 represents the correlation between pH and BC quantity. BC pigments show optimal stability at pH 5.0-6.0. This study coincides with the previous theories, and showed maximum BC quantity at pH 6.0 with 3.02 ± 0.19 (mg/100g). Both acidic and basic condition for BC is non-favorable. In acidic medium, the color change to yellow because of re-condensation of betalamic acid with amino acid residues. In basic medium decomposition of betanidin occurs [10].

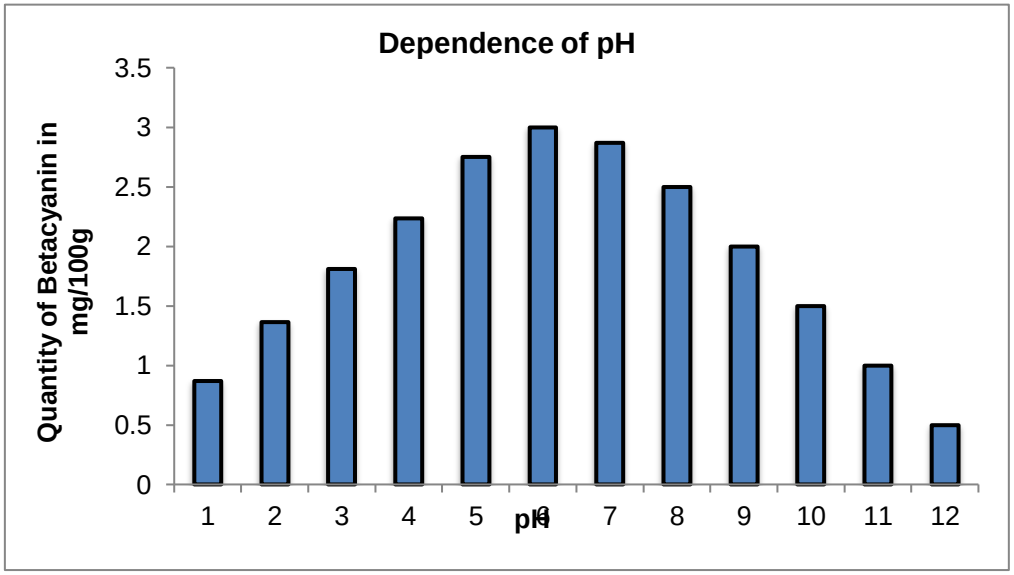

Figure 6. Plot depicting the correlation between pH and BC quantity

3.2. Characterization of Bi_2O_3NPs

3.2.1. UV-Visible Spectroscopy

The UV-Vis spectrum of the green synthesized Bi_2O_3 NPs was given in Figure 7. The sharp absorption peak observed at 290nm confirmed the formation of Bi_2O_3NPs [11] and the band gap of Bi_2O_3 NPs was 3.31 eV calculated using the formula, $Eg = 1240/\lambda_m$, where λ_m represented the maximum absorbance value.

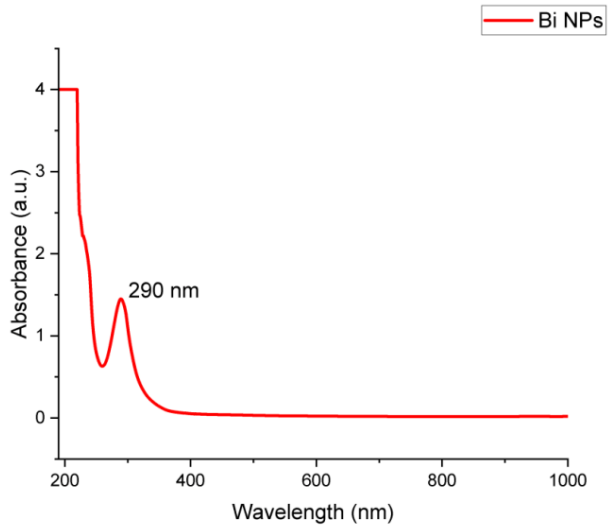

Figure 7. UV-Visible spectrum of Bi_2O_3NPs

3.2.2. FT-IRSpectroscopy

The FTIR spectrum was recorded in the range of 400 – 4000 cm^{-1} to determine chemical bonding and qualitative formation of green synthesized Bi_2O_3 NPs, portrayed in figure 8. The O–Hstretching vibrations appeared at 3436.11 cm^{-1}. The active ingredient in *Selenicereus undatus* is betacyanin pigment (figure1) and the peaks at 2926 cm^{-1}, 1634.47cm^{-1} and 1389.88 cm^{-1} represents C-H stretching, N-H bend (1º amine) and C-C stretching (aromatics) respectively. The characteristic vibrational modes for metal-oxygen bonding are usually found below 1000 cm^{-1}[12]. Bi_2O_3 NPs has two bonding vibration (Bi-O and Bi-O-Bi) and their peaks are found at 845.69 cm^{-1}, 509.99 cm^{-1} and 433.65 cm^{-1}.

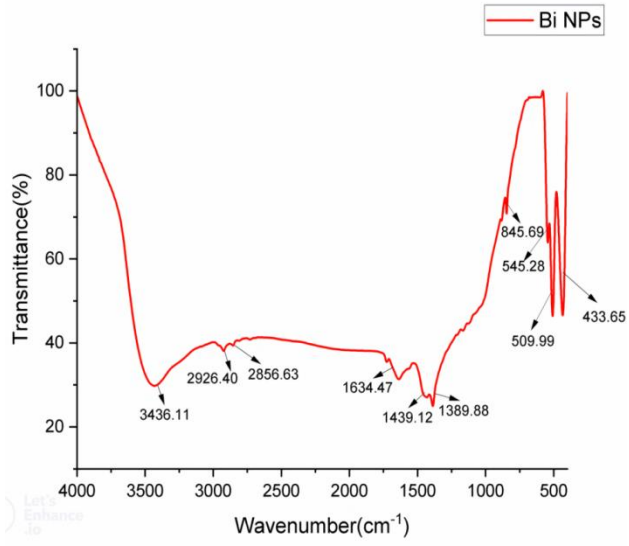

Figure 8. FTIR of Bi_2O_3NPs

3.2.3. X-Ray Diffraction of Bi_2O_3NPs

The crystalline nature and structural composition were illustrated through powder XRD studies of Bi_2O_3NPs measured from diffraction angle 5° to 90°. XRD spectrum of Bi_2O_3 NPs has been shown in figure 9 which showed sharp diffraction angles (2Θ) at 6.55°, 12.33°, 19.65°, 23.31°, 26.28°, 27.87°, 29.45°, 33.01°,37.10°, 39.33°and 42.79° which corresponded to the miller indices of the reflecting angles (110), 020), (102), (111), (120), (012), (212), (121), (112), (131) and (122) respectively [13]. All the peaks could be indexed to the standard Joint Committee on Powder Diffraction Standards (JCPDS) card no.76–1730 and no additional peaks were obtained, proclaims the purity and absence of unstable polymorphs. The XRD pattern manifest the monoclinic structure of Bi_2O_3 which was the most stable allotropes and it was denoted as α-Bi_2O_3. The sharp peaks manifested the high crystalline nature and the crystalline size was ~122.16 nm, calculated using Debye-Scherrer equation, where (120) plane being the maximum intense plane was utilized as Θ value [14].

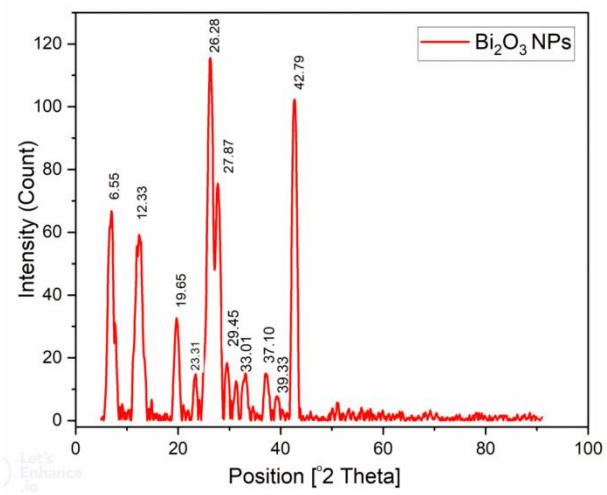

Figure 9. XRD pattern of Bi_2O_3NPs

3.2.4. Scanning Electron Microscope image of Bi_2O_3NPs

The morphology and size of bismuth oxide nanoparticles were analyzed using SEM. Figure 10 represented the SEM image of Bi_2O_3NPs with resolution on the order of 1µm -100nm and magnification range from 10KX to 50KX magnification which showed that the particles are poly-dispersed structures having smooth surface area. The particle size calculated from the SEM micrograph ranged from 120-130 nm.

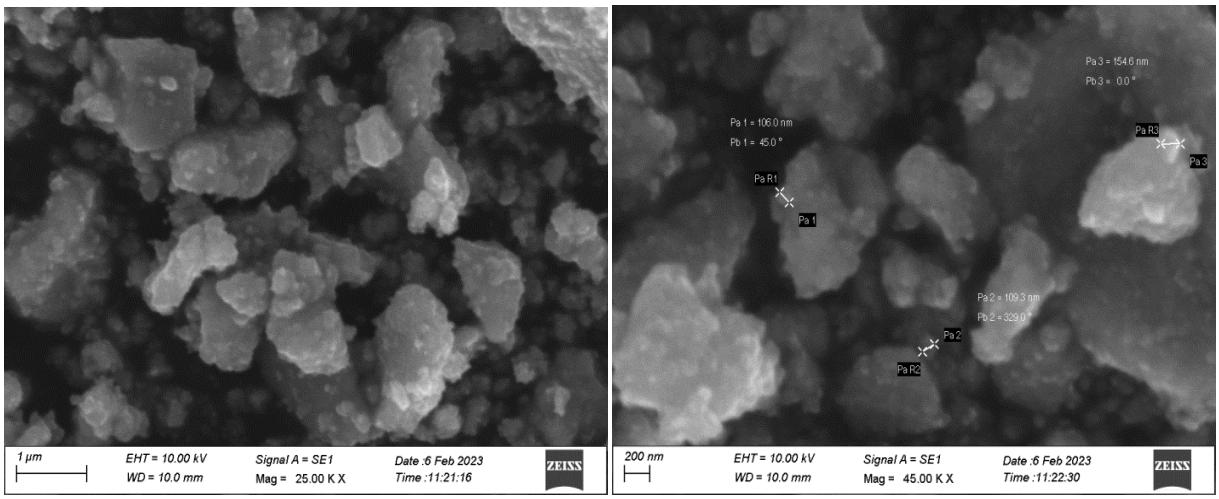

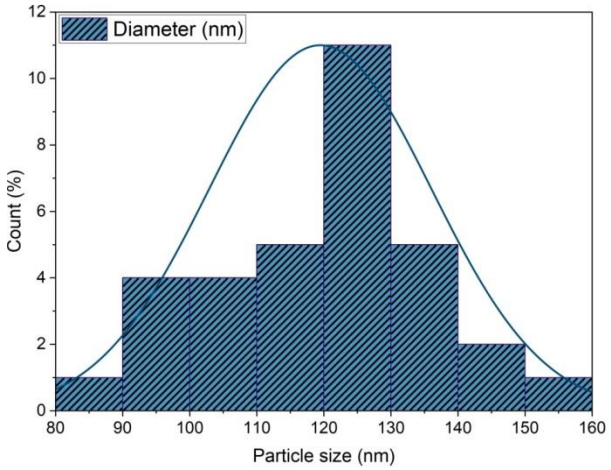

Figure 10.SEM imagesand histogram ofBi_2O_3NPs

3.2.5. EDA Xspectrum of Bi_2O_3NPs

The elemental and compositional properties of Bi_2O_3NPs were investigated by EDAX shown in figure 11. The spectrum showed the presence of Bi and O peaks which indicated the presence of pure Bi_2O_3NPs without any impurities and weight percentages of 72% and 28% for O and Bi respectively.

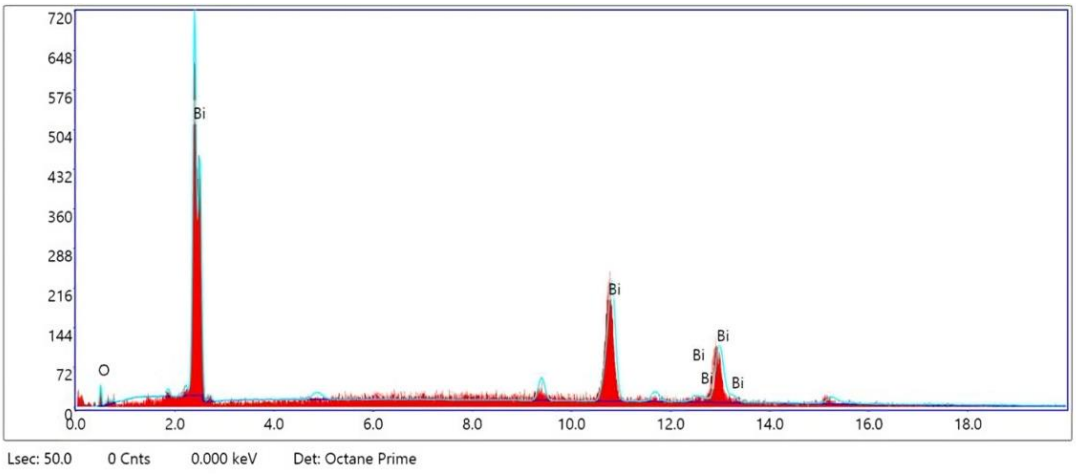

Figure 11. EDAX Spectra of Bi_2O_3NPs

3.2.6. BET Surface area analysis

BET surface area and pore volume of Bi_2O_3NPs was determined using standard N_2 adsorption-desorption method at STP showed in figure 12(A) & (B), which represented the N_2 adsorption-desorption isotherm plot and BET surface area plot. BET surface area of Bi_2O_3NPs was 23.6591 ± 0.4367 m²/g and its total pore volume was less than 1909.324 Å diameter at P/Po=0.989770885 and quantity adsorbed at STP=0.020829 cm³/g. N_2 adsorption and desorption isotherm was plotted which resembled the Type IV isotherm confirming the presence mesoporous structures [15]. Low pressure showed monolayer formation and inflection point occured at the completion of monolayer.

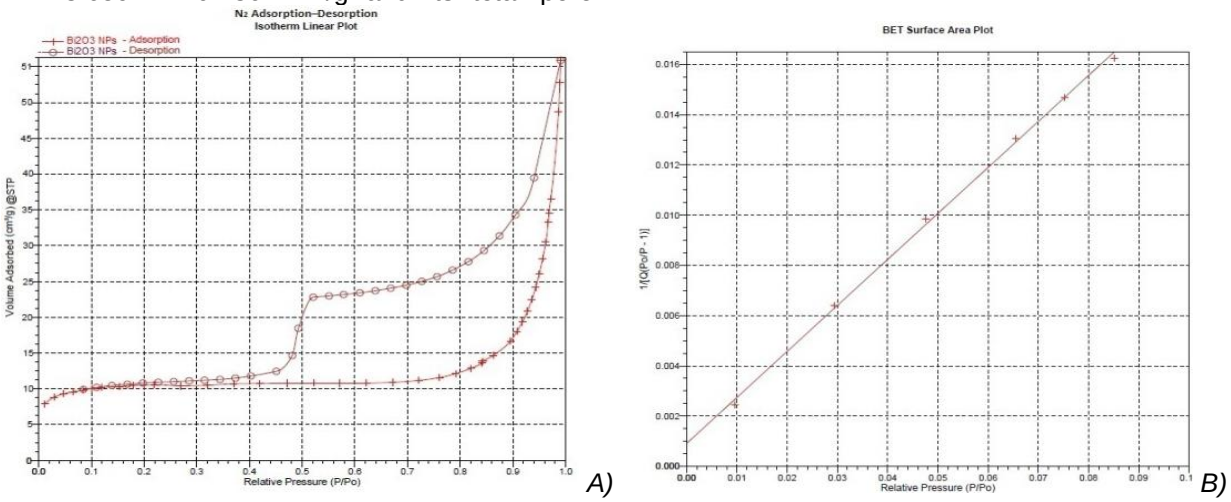

Figure 12. (A) N_2 adsorption–desorption isotherms linear plot. (B) BET surface area plot

3.3. Application-Adsorptionof RhB by Bi_2O_3NPs

Nowadays contagious diseases spread drastically ever before due to many environmental factors and one such prime element responsible is the spread through contaminated water. Currently arising worldwide issue is the poor accessibility to clean and safe drinking water. There is a requirement for sustainable water remediation technique and one such eminent method is adsorption. The dissolved contaminants (adsorbate) in solution when enter into close vicinity of the adsorbent, some of the contaminants gets adsorbed on the surface of the adsorbent through intermolecular force of attraction. One such adsorbent that provides an excellent adsorbing ability is a nanoparticle which has high surface area, more active site, many pores, low intra-species diffusion distance etc. [16]. Commonly known contaminants are textile dyes like RhB which are carcinogenic and creates neurological disorders in humans. In the present work Bi_2O_3NPs, a magnificent nano-adsorbent was utilized to adsorb RhB dye and the extent of adsorption was studied through the intensity of decolouration and the decrease of concentration identified through the decrease of absorbance in the UV-Vis spectra of treated RhB (λ_m=538 nm) [17] contaminated water.

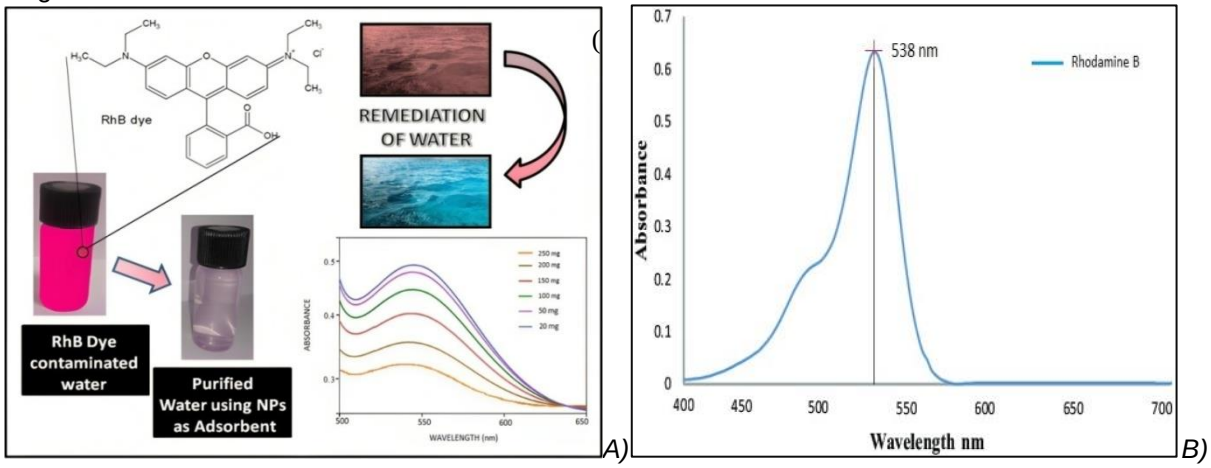

Figure 13. (A) Pictorial representation of RhB adsorption. (B) UV-Vis spectrum of RhB dye

Figure 13(A) illustrates a pictorial representation of RhB dye degradation and figure 13(B) shows the UV-Vis spectrum of RhB dye. The impact of various operational factors on the adsorption of nanoparticles by commercial organic dye was examined. These factors included effect of adsorbent dose, adsorbate dose, time, temperature, and pH of adsorption process.

3.3.1. Effect of adsorbent

The adsorption process was induced through Bi_2O_3NPs, varied from 20mg to 250mg and the RhB dye concentration was maintained as constant (20 ppm) at room temperature for 2 hrs. Table 2 shows the corresponding absorbance (a.u.) for various absorbent dosages in the adsorption process and figure 14 represents the plot between absorbance and adsorbent dosage. The results obtained showed greater adsorption efficiency of Bi_2O_3NPs towards the removal of RhB dye initially and later above 100mg of Bi_2O_3NPs the decrease of absorbance is moderate due to agglomeration of Bi_2O_3NPs after reaching optimum level [18].

Table 2. Absorbance value for various adsorbent dosage (in mg).

Adsorbent Dosage (mg)	Absorbance (a.u.)
20	0.471
50	0.463
100	0.406
150	0.394
200	0.389
250	0.372

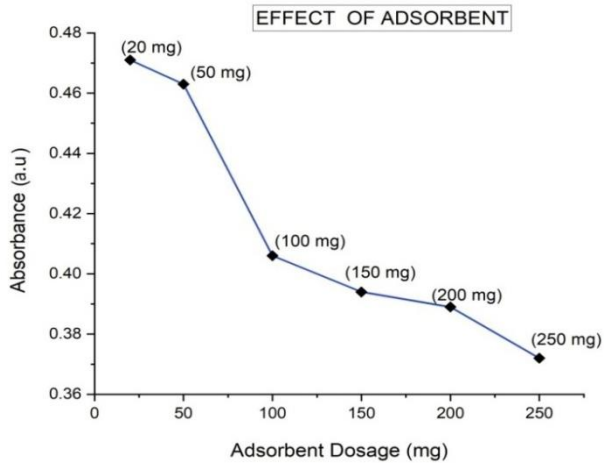

Figure 14. Plot between Absorbance and Adsorbent dosage (in mg).

3.3.2. Effect of adsorbate

RhB dye of different concentrations (10, 20, 30, 40, 50, 60 ppm) were utilized for the study of adsorption behaviors of Bi_2O_3 NPs and agitated at room temperature for 2hrs. The quantity of nanoparticles was maintained as 50 mg for all the adsorbate variation studies. Table 3 shows the corresponding absorbance (a.u.) for various absorbate dosages in the adsorption process and figure 15 represents the plot between absorbance and adsorbate dosage. On increasing the concentration of the dye the activity of adsorbent becomes negligible and inefficient. Initially the increases of concentration were gradual as the possible adsorption ability of Bi_2O_3 NPs played its role to adsorb. Later at high concentrations of dye, the adsorption process becomes incompetent and ultimately the absorbance also increases (gradually and then sharply).

Table 3. Absorbance value for various adsorbate dosages (in ppm)

Adsorbate Dosage (ppm)	Absorbance (a.u.)
10	0.401
20	0.425
30	0.441
40	0.521
50	0.565
60	0.635

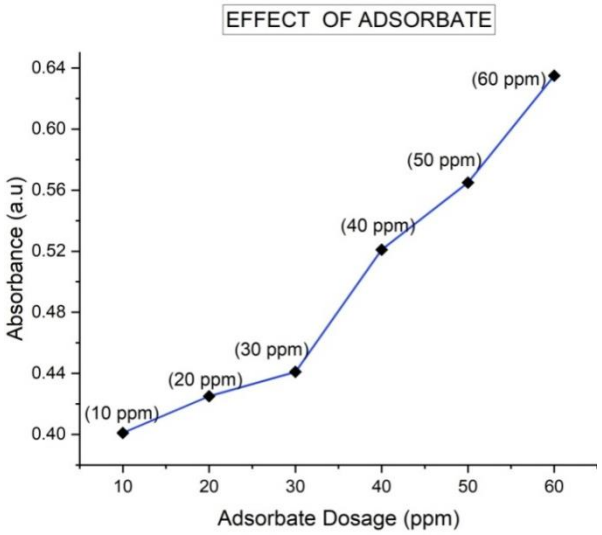

Figure 15. Plot between Absorbance and Adsorbate dosage (in ppm)

3.3.3. Effect of temperature

The temperature had a significant impact on adsorption, which was investigated by varying the temperature range from 30℃ to 80℃ and the concentration of Bi_2O_3 NPs and RhB maintained as constant. Table 4 shows the corresponding absorbance (a.u.) for temperature dependence in the adsorption process and figure 16 represents the plot between absorbance and temperature. It was observed that the adsorption of dye on NPs increased with an increase of temperature. A decrease in the concentration of dye could be

confirmed through the decrease of absorbance value [19]. The optimum temperature was found to be 70℃ and further increase of temperature showed only a gradual decrease.

Table 4. Absorbance value for effect of temperature (in ℃) variation in adsorption process

Temperature of Adsorption reaction (℃)	Absorbance (a.u.)
30	0.571
40	0.508
50	0.462
60	0.391
70	0.349
80	0.335

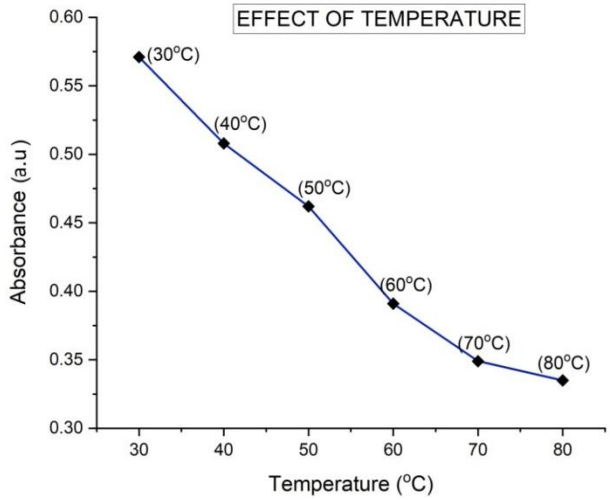

Figure 16. Plot between Absorbance and Temperature variation (in ℃)

3.3.4. Effect of time

Constant dosage of Bi_2O_3 NPs and RhB were agitated at room temperature with different time of reaction starting from 30mins to 150mins. Table 5 shows the corresponding absorbance (a.u.) for various time interval in the adsorption process and figure 17 represents the plot between absorbance and time dependence of adsorption. As the time of reaction increases, the quantity of dye adsorbed by NPs increases abruptly and then gradually which could be confirmed with the decrease of absorbance.

Table 5. Absorbance value for effect of time (in mins) variation in adsorption process

Time of Adsorption reaction (mins)	Absorbance (a.u.)
30	0.558
45	0.542
60	0.482
90	0.435
120	0.4
150	0.394

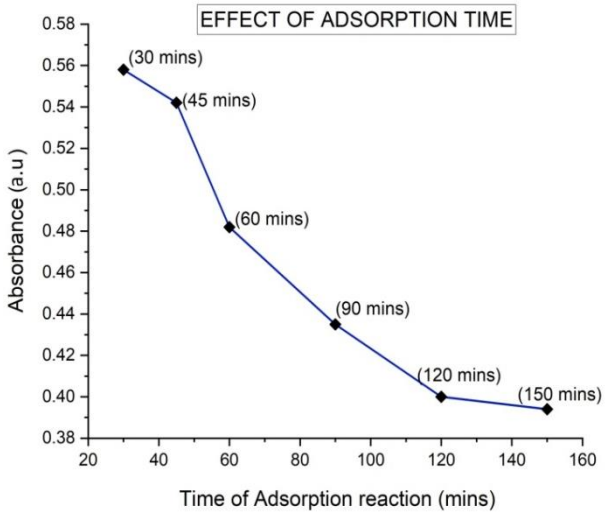

Figure 17. Plot between Absorbance and Time variation (in mins)

Constant dosage of Bi_2O_3 NPs and RhB were agitated at room temperature with different time of reaction starting from 30mins to 150mins. Table 5 shows the corresponding absorbance (a.u.) for various time interval in the adsorption process and figure 17 represents the plot between absorbance and time dependence of adsorption.As the time of reaction increases, the quantity of dye adsorbed by NPs increases abruptly and then gradually which could be confirmed with the decrease of absorbance.

3.3.5. Effect of pH

On varying the pH from 1 to 11, adsorbents demonstrated better adsorption capacity in basic medium than in acidic medium. Table 6 shows the corresponding absorbance (a.u.) for various pH in the adsorption process and figure 18 represents the plot between absorbance and pH dependence of adsorprtion. At basic medium, the accumulation of $-OH^{--}$ ions on the surface of the adsorbent attracts the cationic RhB dye and hence adsorption capacity increases. Since contaminants are wisely adsorbed, concentration of the solution decreases and thereby absorbance decreases [20].

Table 6. Absorbance value for pH change in adsorption process

pH of Adsorption reaction	Absorbance (a.u.)
1	0.428
3	0.403
5	0.384
7	0.376
9	0.359
11	0.347

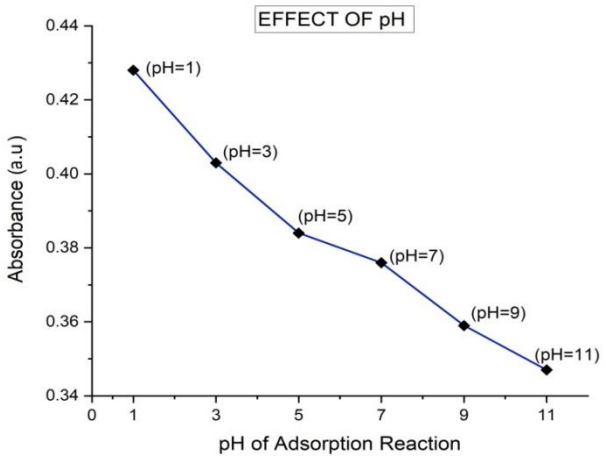

Figure 18. Plot between Absorbance and pH variation

4. CONCLUSION

This study has successfully extracted betacyanin from *Selenicereus undatus* peel extract and achieved in quantizing the maximum content of betacyanin. Further, *Selenicereus undatus* peel modified Bi_2O_3 NPs was synthesized and the formation of Bi_2O_3 NPs was confirmed through UV-Vis, FTIR, SEM, EDAX, XRD and BET surface area. A favorable adsorption method for removal of toxic dyes like RhB dye were investigated via green synthesized Bi_2O_3 NPs as nano-adsorbent and good adsorption behavior were shown. Hence, an incredible adsorption studies were established which could contribute to the sustainable development of the society.

Acknowledgement

The authors sincerely acknowledge the management and the Department of Chemistry, Holy Cross College (Autonomous), Trichy for their constant support and the facilities provided to carry out the research work.

5. REFERENCES

[1] T. Singh, V.K. Pandey, K.K. Dash, S. Zanwar, R.Singh(2023) Natural bio-colorant and pigments: Sources and applications in food processing, J. Agric. Food Res., 12, 100628. https://doi.org/10.1016/j.jafr.2023.100628

[2] P. Shanthy, J.A. Thangakani, S. Karthika, S.C. Joycee, S. Rajendran, J. Jeyasundari (2021) Corrosion inhibition by an aqueous extract of Ervatamia divaricata, Int. J. Corros. Scale Inhib., 10(1), 331–348. https://doi.org/10.17675/2305-6894-2021-10-1-19

[3] M.W. Alam, N. Allag, M. Utami, M. Waheed-Ur-Rehman, M. Al Saleh Al-Othoum, S. Sadaf (2024) Facile Green Synthesis of α-Bismuth Oxide Nanoparticles: Its Photocatalytic and Electrochemical Sensing of Glucose and Uric Acid in an Acidic Medium. Journal of Composites Science, 8(2),47-54. https://doi.org/10.3390/jcs8020047

[4] P. L. Meena, A.K. Surela, K. Poswal, J.K. Saini, L.K. Chhachhia (2024) Biogenic synthesis of Bi_2O_3 nanoparticles using Cassia fistula plant pod extract for the effective degradation of organic dyes in aqueous medium. Biomass Conversion and Biorefinery, 14(3), 3793-3809. https://doi.org/10.1007/s13399-022-02605-y

[5] A.O. Flayyih, W.K. Mahdi, Y.I.M.A. Zaid, F.H. Musa (2022) Biosynthesis, Characterization, and Applications of Bismuth Oxide Nanoparticles Using Aqueous Extract of Beta Vulgaris, Chem. Methodol., 6, 620-628. https://doi.org/10.22034/chemm.2022.342124.1522

[6] A. Pious, S. Muthukumar, D.K. Singaravelu, P. Nantheeswaran, M. Mariappan, A. Sivasubramanian, A. Veerappan (2024) Micelle assisted synthesis of bismuth oxide nanoparticles for improved chemocatalytic degradation of toxic Congo red into non-toxic products. New Journal of Chemistry, 48(1), 96-104. https://doi.org/10.1039/D3NJ04494G

[7] A.P Periyasamy (2024) Recent advances in the remediation of textile-dye-containing wastewater: prioritizing human health and sustainable wastewater treatment. Sustainability, 16(2), 495. https://doi.org/10.3390/su16020495

[8] K.P. Sambasevam, N. Yunos, H.N.M. Rashid, S.N.A. Baharin, N.F. Suhaimi, M. Raaov, S. Shahabuddin (2020) Evaluation of Natural Pigment Extracted from Dragon Fruit(Hylocereus Polyrhizus) Peels, Sci. Res. J., 17(2), 33-44. https://doi.org/10.24191/srj.v17i2.8989

[9] H.A. Alsalmah (2024) Structural, thermal, optical, morphological, electrical, and photocatalytic characteristics of silver-doped bismuth oxide synthesized by the green route. Ceramics International, 50(9), 14675-14685. https://doi.org/10.1016/j.ceramint.2024.01.380

[10] A.S. Ghorband, B. H. Joshi, H. G. Bhatt (2023) Studies on physicochemical and nutritional properties of dragon fruit (Hylocereus polyrhizus). Journal of Pharmacognosy and Phytochemistry, 12(6), 223-226. https://doi.org/10.22271/phyto.2023.v12.i6c.14785

[11] S. Lotfi, M.E. Ouardi, H.A. Ahsaine, A. Assani (2024) Recent progress on the synthesis, morphology and photocatalytic dye degradation of $BiVO_4$ photocatalysts: A review. Catalysis Reviews, 66(1), 214-258. https://doi.org/10.1080/01614940.2022.2057044

[12] C. Mallikarjunaswamy, S. Pramila, G.S. Shivaganga, H.N. Deepakumari, R. Prakruthi, G. Nagaraju, V.L. Ranganatha (2023) Facile synthesis of multifunctional bismuth oxychloride nanoparticles for photocatalysis and antimicrobial test. Materials Science and Engineering: B, 290, 116323. https://doi.org/10.1016/j.mseb.2023.116323

[13] N. Nurmalasari, Y. Yulizar, D.O.B. Apriandanu(2023)Bi_2O_3 nanoparticles: synthesis,

characterizations, and photocatalytic activity, IOP Conf. Ser.: Mater. Sci. Eng., 763, 012036. https://doi.org/10.1088/1757-899X/763/1/012036

[14] M. Alsaiari, M. Ahmad, M. Munir, M. Zafar, S. Sultana, S. Dawood, Z. Ahmad (2023) Efficient application of newly synthesized green Bi_2O_3 nanoparticles for sustainable biodiesel production via membrane reactor. Chemosphere, 310, 136838. https://doi.org/10.1016/j.chemosphere.2022.136838

[15] R. Ranjithkumar, C. Van Nguyen, L.S. Wong, J.G.T. Nandagopal, S. Djearamane, G. Palanisamy, J. Lee (2023) Chitosan functionalized bismuth oxychloride/zinc oxide nanocomposite for enhanced photocatalytic degradation of Congo red. International Journal of Biological Macromolecules, 225, 103-111. https://doi.org/10.1016/j.ijbiomac.2022.11.302

[16] Y. Zhu, L. Ma, L. Wang, X. Li, Z. Yang, M. Yuan, Y. Xiao (2024) Adsorption of Cationic Dyes in Wastewater with Magnetic κ-Carrageenan Nanoparticles. Process Safety and Environmental Protection,189, 177-187. https://doi.org/10.1016/j.psep.2024.06.039

[17] M. Lal, P. Sharma, L. Singh, C. Ram (2023) Photocatalytic degradation of hazardous Rhodamine B dye using sol-gel mediated ultrasonic hydrothermal synthesized of ZnO nanoparticles. Results in Engineering, 17, 100890. https://doi.org/10.1016/j.rineng.2023.100890

[18] A.Q. Malik, T.U.G. Mir, D. Kumar, I.A. Mir, A. Rashid, M. Ayoub, S. Shukla (2023) A review on the green synthesis of nanoparticles, their biological applications, and photocatalytic efficiency against environmental toxins. Environmental Science and Pollution Research, 30(27), 69796-69823. https://doi.org/10.1007/s11356-023-27437-9

[19] M.A Dheyab, N. Oladzadabbasabadi, A.A. Aziz, P.M. Khaniabadi, M.T. Al-ouqaili, M.S. Jameel, M. Ghasemlou (2024) Recent advances of plant-mediated metal nanoparticles: Synthesis, properties, and emerging applications for wastewater treatment. Journal of Environmental Chemical Engineering, 112345. https://doi.org/10.1016/j.jece.2024.112345

[20] A.S. Prabha, N. Vijaya, R. Dorothy, T. Sasilatha, T. Umasankareswari, R. Keerthana, N.R. Devi, S. Rajendran, G.Singh (2022) Use of Nanocomposites as Photocatalysts, Nanocomposites- Jenny Stanford Publishing, 13, 283-327. https://doi.org/10.1201/9781003314479

IZVOD

HIJERARHIJSKI OKVIR, IZRADA I KARAKTERIZACIJA NANO-Bi_2O_3 POSREDSTVOM EKSTRAKTA *SELENICEREUS UNDATUS* I NJEGOVA PRIMENA

Betacijanini (BC) su crvenkasto-ljubičasti pigment koji se široko nalazi u korama zmajevog voća sa belim mesom (Selenicereus undatus) i kore i pulpe crvenog zmajevog voća (Selenicereus costaricensis). BC pigmenti su dobri antioksidansi koji inhibiraju formiranje reaktivnih vrsta kiseonika (ROS) u biljkama i na taj način promovišu redukciju metalnih jona na nula valentnih metala. Takođe, deluje kao dobar stabilizator i agens za zatvaranje u sintezi nanočestica. Dakle, ovo istraživanje ima za cilj da ekstrahuje i kvantizuje sadržaj BC iz kore Selenicereus undatus, kako bi se proizvele nanočestice modifikovanih bizmut oksida (SU) bogate betacijaninom-Selenicereus undatus (Bi_2O_3 NP) i karakterisale korišćenjem UV-Vis, FTIR, XRD, SEM, EDAX i BET. Količina i stabilnost betacijanina se optimizuju korišćenjem različitih parametara kao što su vreme, temperatura, odnos rastvarača, pH, itd., preko UV-Vis spektrofotometra na 538 nm. Sintetizovani SU-Bi_2O_3 NP imaju za cilj ublažavanje zagađivača sintetičkih boja putem adsorpcije – efikasan put za remedijaciju vode. Nano-adsorbenti Bi_2O_3 NP su pokazali povećanje adsorpcije boje sa povećanjem vremena reakcije, temperature i doze Bi_2O_3 NP, što je omogućilo efikasno uklanjanje boja kao što su Rhodamine B (RhB) boje.

Ključne reči: *betacijanin, Selenicereus undatus, nanočestice bizmut oksida, karakterizacija, rodamin B boje.*

Naučni rad
Rad primljen: 05.06.2024
Rad prihvaćen: 01.07.2024.

Auxilia Ruby Sagaya Irudayaraj https://orcid.org/0000-0002-1636-1252
Felicita Florence John https://orcid.org/0000-0002-3255-5997
Divya Priya Chinnasamy -R. Kanmani https://orcid.org/ 0000-0002-9873-1324
Amala Infant Joice Joseph https://orcid.org/0000-0002-8661-2280

Ifeanyichukwu Michael Onyejekwe[1], Nnaemeka Uwaezuoke[1], Ononien Gborienemi George[1] Ubanozie Julian Obibuike[1], Nnanna Onwuegbueha Okoli[1]*

[1]Petroleum Engineering Department, Federal University of Technology, P.M.B 1526, Owerri, Imo State, Nigeria

Scientific paper
ISSN 0351-9465, E-ISSN 2466-2585
https://doi.org/10.62638/ZasMat1088

Zastita Materijala 66 (1)
102 - 108 (2025)

Hydrate formation and its influence on natural gas pipeline: Simulation study

ABSTRACT

This study simultaneously studied the twin problem of hydrate and corrosion that occurs in natural gas pipeline, establishing their interdependent using a simulation approach. CO_2 corrosion was simulated using NORSOK M-506 standard model in matlab. Major factors considered are the relationship between corrosion rate and temperature, corrosion rate and P^H, corrosion-temperature relationship for varying CO_2 mole percent, and P^H values. The result from this study established that both type I and type II hydrates could form at the operating conditions of 5^OC and 60 bar. The obtained result also shows that rate of corrosion decreases and increases with increase in P^H values and temperature respectively to a certain temperature of approximately 78 ^OC, then a dip in rate of corrosion. The result for corrosion-temperature relationship for varying P^H values and CO_2 mole percent shows a decrease in corrosion rate with an in increase in P^H, and an increase with increase in CO_2 mole percent t. Furthermore, the obtained results highlight a rise as high as 5.7 mm/year at a 3 mole percent CO_2. This value and trend portray a bad omen for the affected pipeline. This study recommends that natural gas to be transported by pipeline should be sweetened and processed to remove H_2S, CO_2 and mercaptans if present.

Keywords: *CO_2 corrosion, model, simulation, hydrate, MATLAB*

1. INTRODUCTION

Currently there are global quest ably led by the most advanced economies of the world on the utilization of a more environmentally friendly fuel. The essence which is to cut-down on the volume of emission of dangerous gaseous by-products of combustion of dirty fossil fuel that causes global warming with the propensity of causing environmental pollution and ecological disturbances or destruction. In all these, natural gas boldly stands in the gap as a transition energy source, because it emits relatively lower quantity of pollutants when combusted, compared to the other fossil fuels. The high demand of natural gas has led to large deployment of exploration and exploitation technologies and the building of massive infrastructure for gas processing, treatment and transportation. Among the transportation modes of natural gas is pipeline transportation, and the most popular because its technology is easily understood, and it can be easily adapted to different environment [1]. These appealing features of pipeline transportation has led to a remarkable global rise in its network.

Study by Mokhatab et al. [2] revealed an addition of twelve thousand miles (12,000 miles) of pipeline yearly to the global pipeline infrastructure in the last decade. However, pipeline transportation of natural is faced with the flow assurance problem of hydrate formation and CO_2 corrosion of the internal walls of the pipeline. Proberezhny et al. [3] stated that corrosion of natural gas pipeline can be attributed to H_2S and CO_2 which are constituents of the gas that is transported and by the formed hydrate in the pipeline. Abbas et al. [4] in their study on neural network modeling of high pressure CO_2 corrosion in pipeline steel evaluated the severity of CO_2 pipeline corrosion in economic terms. They stated that CO_2 corrosion is so huge that its cost implications in relation to the production and manufacturing sector of the U.S economy was $34.4 billion in the year 2014. They reported that the gas industry share of this amount was up to 50%. Studies in understanding the interplay between hydrate formation and CO_2 corrosion by researchers have been carried out. Zunzhao et al. [5] deployed a natural gas hydrate loop device to measure the corrosion rate of CO_2 in the presence of hydrate on X80 steel, Obanijesua et al. [6] developed a model to predict CO_2 corrosion rate of natural gas pipeline in the presence of hydrate, their obtained results show that the corrosion rate of CO_2 was higher than the gas liquid equilibrium.

*Corresponding author: Ifeanyichukwu M. Onyejekwe
Email: oronst@yahoo.com
Paper received: 18. 05. 2024.
Paper corrected: 26. 06. 2024.
Paper accepted: 03. 07. 2024.
the website: https://www.zastita-materijala.org/

Studies [7,8] on CO_2 corrosion prediction using model by researchers has shown the availability CO_2 prediction models. Nesic et al. [9] listed the three general groups of models used for CO_2 corrosion prediction as: mechanistic, semi-empirical and empirical while Kahyarian et al. [10] grouped CO_2 corrosion prediction models into empirical/semi-empirical, elementary mechanistic and comprehensive mechanistic with the mechanistic been more complex to handle, though affording user greater insight into major variables moving the entire corrosion process [11]. Recent studies [4,12] have shown the growing interest in the use of Neural Network (NN) modeling for the prediction of CO_2 corrosion. Hatami et al. [13] reported that the use of least square support vector machine (LSSVM) for the prediction of CO_2 corrosion has yielded good result. They further maintained that out of the three kernel functions (linear, polynomial and Gaussian) compared, the Gaussian function was the best in predicting CO_2 corrosion. Different approach is used by CO_2 corrosion prediction models in predicting the effect of protective film on CO_2 corrosion and in predicting the effect of oil wetting on CO_2 corrosion [14].

CO_2 corrosion prediction is also affected by environmental factors, based on this De Ward et al. [15] advocated the use of correction factor for CO_2 corrosion under different environmental settings. Bernandus et al. [16] while making a strong case for the need for a sound knowledge of the governing processes of CO_2 corrosion parameters, asserted that model accuracy is less important than the knowledge of the major corrosive parameters governing the CO_2 corrosion mechanism.

One very reliable model used in CO_2 corrosion prediction is the NORSOK M-506, a standard which is an empirical model used by the Norwegian oil and gas industry capable of matching large volume of laboratory data. The NORSOK M-506 is built to consider the effect that protective film has on CO_2 corrosion mechanism at higher temperature and high P^H more than many other prediction models. This model is well reputed for giving a good representation of the maximum corrosion rate in a CO_2 corrosion controlled system [7,8,17].

2. METHODOLOGY

2.1. Programming used

The programming used in this study includes Matlab software, Excel spreadsheet application and Unisim design software which is an interactive process modeling software that enables engineers to create steady and dynamic state models for plant and process systems

2.2. Method

2.3. Hydrate Formation Simulation

The process simulation for fluid flow with the intent of investigating the hydrate formation potential of the natural gas was done using Unisim R380, a Honeywell's hydrate prediction software. The fluid was modeled as Peng Robinson property package. The operating conditions for the simulation were: temperature of 5^0C and pressure of 60 bar. The composition of the natural gas stream is as represented in Table 1.

Table 1. Mole composition of natural gas

Components	Mole composition (%)
C_1	74.805
C_2	5.633
C_3	4.264
nC_4	2.411
$1C_4$	1.651
nC_5	3.21
$1C_5$	2.104
C_6	1.712
C_7	0.867
C_8	0.652
C_9	0.321
$C0_2$	1.978
N_2	0.294
H_20	0.098
	100.00

2.4. CO_2 Corrosion Simulation

Hydrate prone natural gas from one of the offshore fields in Niger Delta Nigeria was simulated for possible corrosion effect on pipeline using the NORSOK M-506 model. At different temperatures, CO_2 fugacity, P^H and wall shear stress possible state of corrosion was analyzed. The model used for the analysis is derived from research program at the Institute of Energy Technology in Norway. The corrosion rate equation for various temperatures (5^0C - 160^0C) range used for the prediction is given according to Eqs. (1-3).

For T = 5^0C

$$Cr_{CO_2} = K_T \times F_{CO_2}^{0.36} \times f(P^H)_T \quad (1)$$

For T = 15^0C

$$Cr_{CO_2} = K_T \times F_{CO_2}^{0.36} \times \left(\frac{S}{19}\right)^{0.146+0.0324\left(F_{CO_2}\right)} \times f(P^H)_T \quad (2)$$

For: 20^0C T 150^0C

$$Cr_{CO_2} = K_T \times F_{CO_2}^{0.62.} \, x \; x \left(\frac{S}{19}\right)^{0.146+0.0324log\left(F_{CO_2}\right)} f(P^H)_T \quad (3)$$

Where Cr_{CO_2} is CO_2 corrosion rate, mm/year,K_T is constant dependent on operating temperature, S is wall shear stress in Pa, F_{CO_2} is CO_2 fugacity in Mpa and $f(P^H)_T$ is the complex function of P^H and temperature. The fugacity factor is used in

place of partial pressure because, the natural gas does not exist in ideal condition, and is calculated according to Eq. (4).

$$F_{CO_2} = a \times P_{CO_2} \quad (4)$$

Where: a is fugacity co-efficient and P_{CO_2} is the partial pressure of CO_2 which is represented as shown on Eq.(5).

$$P_{CO_2} = \frac{mol\ \%\ of\ corrosion\ in\ the\ gaseous\ phase}{100} \times P \quad (5)$$

The fugacity coefficient 'a' is evaluated according to Eqs. (6-7) respectively.

$$a = 10^{P\left(0.0031-\frac{1.4}{T}\right)} for\ P \leq 250\ bar \quad (6)$$

$$a = 10^{250\left(0.0031-\frac{1.4}{T}\right)} for\ P > 250\ bar \quad (7)$$

The wall shear stress S is evaluated according to Eq. (8).

$$S = 0.5 \times f \times \rho_m \times U_m^2 \quad (8)$$

Where f is the friction factor at the pipe wall, ρ_m is the density of the fluid mixture in $\left({}^{kg}/_{m^3}\right)$ and U_m is the velocity of the fluid mixture in ${}^{m}/_{s}$. The friction factor is evaluated according to Eq.(9).

$$f = 0.001375\left[1 + \left(20000\frac{K}{D}10^6\frac{\mu_m}{\rho_m U_m D}\right)^{0.33}\right] \quad (9)$$

Where *K* is the pipe roughness in inches, *D* is the pipe diameter in mm and μ_m is the viscosity of fluid mixtures in *Ns/m²*.

Matlab 2014b software was used for the prediction of the corrosion rate of the pipeline due to hydrates formation. Scripts were written for solving the corrosion rate equation and performing iterations. With the Matlab software, executable scripts were run on command windows graphical user interface (GUI).

3. RESULTS AND DISCUSSION

The results on the study carried out using Unisim software and NORSOK-506 standard model to investigate hydrate formation and its influence on natural gas pipeline is presented.

3.1. Hydrate Formation

The result of the hydrate formation simulation of the natural gas using Unisim Design R380 software shows that free water was found in the gas sample, and that both type I and type II hydrate will form. This is illustrated in Figure 1; the window showing the highlights under the design menu of the hydrate simulation program. At operating temperatures of 5^{O}C, the performance utility of the software which gives discrete details, as shown in Figure 2 indicates that hydrate will form at 10.92 bar, and that at operating pressure of 60 bar, hydrate will form at 17.03^{O}C. Figure 3 shows the phase envelope utility for the natural gas stream. In line with the presented result from Figure 1 and Figure 2, which suggests that both type I and type II hydrate will be formed at the operating conditions of 5^{O}C and 60 bar.

Figure 3 which represents the phase envelope utility for the analysed natural gas stream affirms the possibilities of hydrate formation in the pipeline. From Figure 3, the red line, blue line, yellow line and green line represents bubble point curve, dew point curve, critical point and hydrate formation line respectively. The phase envelope utility for the analysed natural gas stream shows that hydrate will not form if the natural gas pipeline conveying this gas is operated in the conditions of temperature and pressure to the right-hand side (RHS) of the hydrate formation line. But the result from Figure 3 indicates that hydrate formation line falls within the hydrate formation envelope, hence the prevalence of high threat of hydrate formation in the pipeline. Consequently, the need for hydrate inhibitors for reliable transportation of this gas through pipeline.

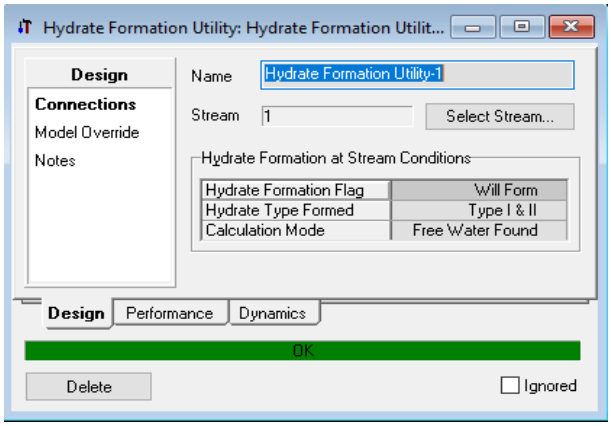

Figure 1. Hydrate formation utility for natural gas stream

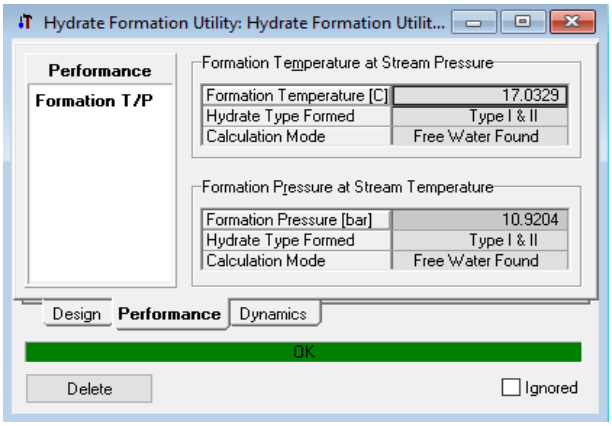

Figure 2. Hydrate formation utility performance for natural gas stream

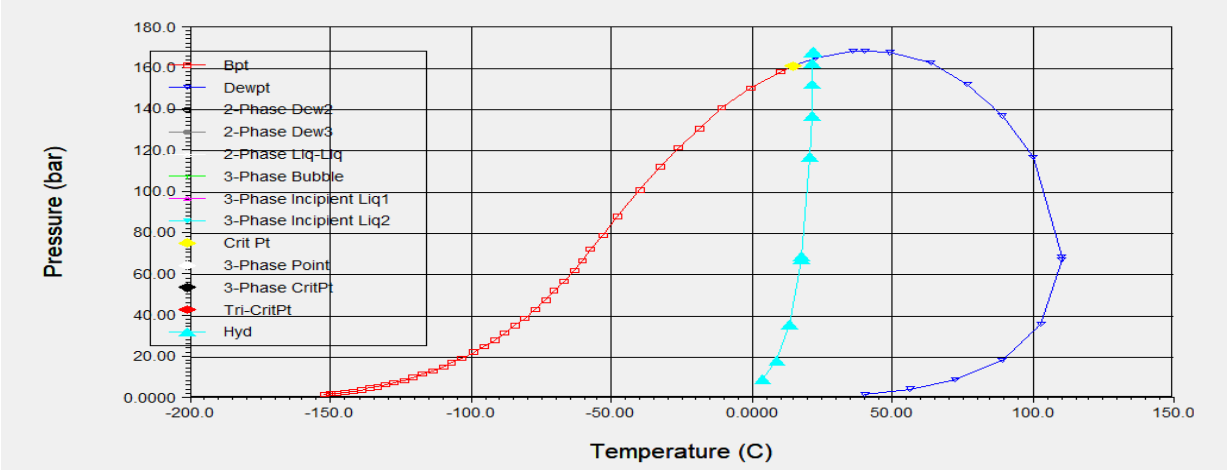

Figure 3. Phase envelope utility for the natural gas stream

3.2. CO_2 Corrosion

The results of the simulation carried out on natural gas well stream to determine the CO_2 corrosion on pipeline and the relationship between corrosion rate and temperature and P^H, corrosion rate-temperature for varying CO_2 mole percent and P^H values are shown in Figures 4 to 7 respectively. The result as obtained from Figure 4 shows that CO_2 corrosion increased with increasing temperature and peaked at 78^{O}C thereafter, a dip in corrosion rate occurred.

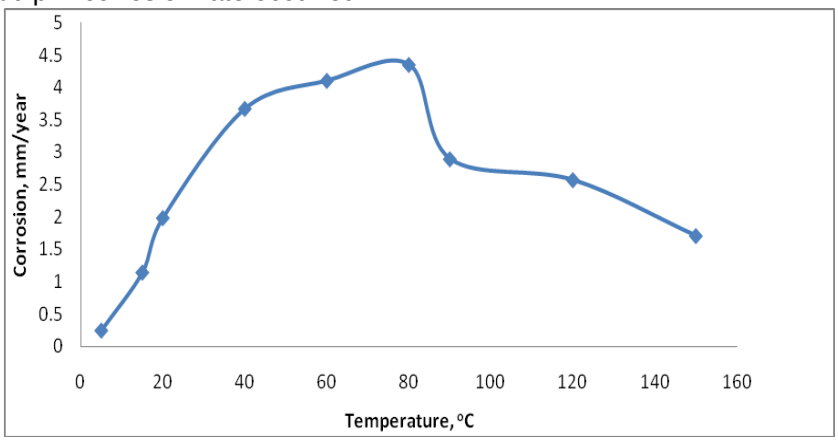

Figure 4. Effect of temperature on CO_2 corrosion rate on natural gas pipeline

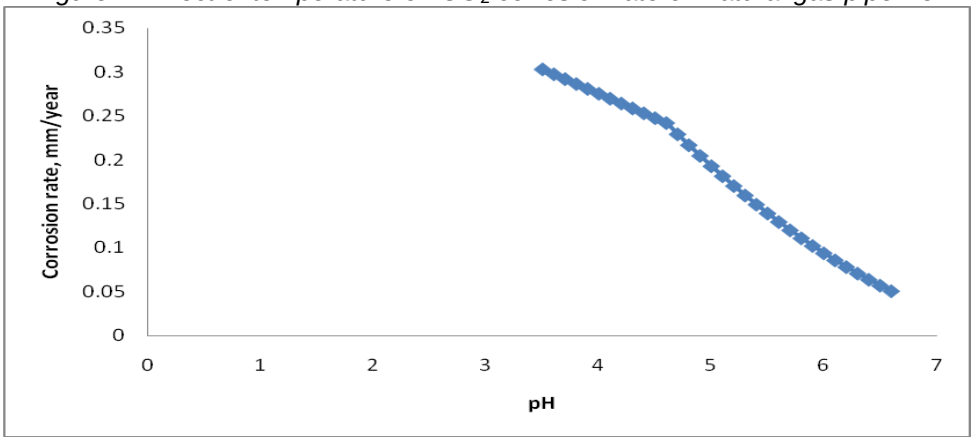

Figure 5. Effect of P^H on CO_2 corrosion rate on natural gas pipeline

The result from Figure 5 clearly indicates that the relationship between corrosion rate and P^H is inverse. The CO_2 corrosion rate decreases with increase in pH value. The corrosion rate-

temperature relationship for varying CO_2 mole percent as obtained from Figure 6 shows that CO_2 corrosion increased in magnitude as the mole percent of CO_2 increases. The obtained result from the corrosion rate-temperature relationship for varying P^H values as represented in Figure 7 shows that the higher the P^H values the lesser the rate of corrosion on the pipeline.

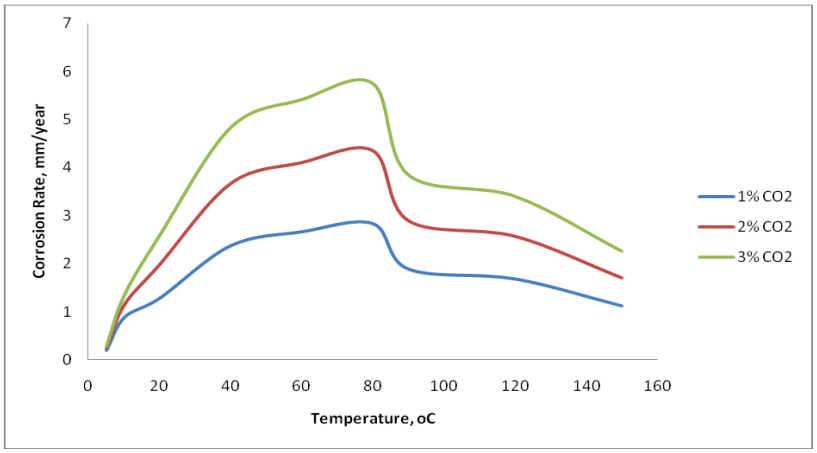

Figure 6. Effect of temperature on CO_2 corrosion rate for varying CO_2 mole percent on natural gas pipeline

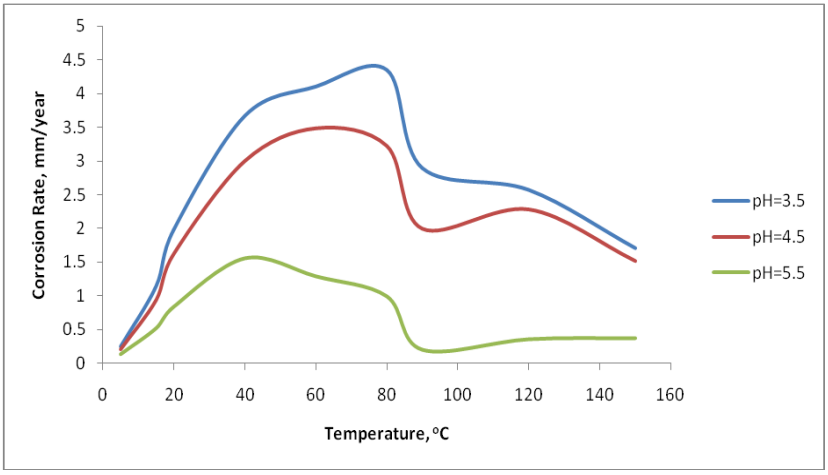

Figure 7. Effect of temperature on CO_2 corrosion rate for varying P^H values on natural gas pipeline

The CO_2 corrosion rate increased with increasing temperature and peaked at 78^{O}C after which follows a dip in rate of corrosion as symbolized in Figure 4. This obtained result compares to that of studies by Niklasson et al. [18] and Krishnan et al. [19]. This can be explained using the concept of the formation of protective film on the pipeline. The film reduces the number of sites open for corrosion attack and also forms a compact ferrous carbonate barrier on the metal surface that is not easily moved. From Figure 5, it is evident that the relationship between corrosion rate and P^H is inverse. The corrosion rate decreases with increase in P^H values. This can be explained by the fact that at lower P^H, the natural gas stream becomes more acidic and the more acidic the natural gas stream, the more its corroding power. On the other hand, the higher the P^H of the natural gas stream, the more alkaline and less corrosive the fluid becomes. It is however worthy of note that the impact of P^H on the CO_2 corrosion rate is dependent on the type of materials used in the construction of the pipe. Some materials are acid soluble (they are easily dissolved in acid solution) hence they are easily affected by corrosion. While others like noble metals are not affected by CO_2 corrosion because they do not dissolve in acid solutions. The result from Figure 6 shows an increase in size in corrosion rate with an increase in mole percent CO_2.

The CO_2 corrosion rate rose as high as 5.7mm/yr at 3mole percent of CO_2. This can simply be explained by the fact that the tendency of carbonic acid which is a corroding species to cause corrosion is higher at higher CO_2 concentrations. It is explicit from Figure 6 that 3mole percent CO_2 of the natural gas stream induced more corrosion on the natural gas pipeline internal wall than the 1mole and 2mole percent CO_2 composition. A 3mole

percent CO_2 induced 49%,53% and 102.5% more corrosion on the natural gas pipeline than the 1mole percent CO_2 for temperature of 5^{O}C, 15^{O}C and 20^{O}C. This values and trend portray a bad omen for the affected natural gas pipeline. From Figure 7 it is crystal clear that the corrosion rate decreases with increase in P^H values. The fluid that has the highest P^H (5.5) value had the least corrosion effect while that with the least P^H (3.5) value has the most corrosion effect. The P^H of natural gas stream affects CO_2 corrosion as P^H controls the rate of dissolution of iron into solution. High P^H equates to high alkalinity which leads to a decreased iron carbonate solubility and scale formation.

4. CONCLUSION

Based on the obtained results and discussions under hydrate formation and its influence on natural gas pipeline using simulation approach, there is higher probability of formation of both type I and type II hydrate at the conditions of 5^{O}C and 60 bar. This above conclusion is in agreement with the principle of hydrate formation where decrease in temperature and increase in pressure favours hydrate formation. This study clearly indicates that the relationship between corrosion rate and P^H is inverse, as CO_2 corrosion rate decreases with increase in P^H. It can therefore be confidently stated from this study that P^H is a parameter that critically affects the CO_2 corrosion rate by influencing the rate of dissolution of iron into solution. The general result obtained shows that rate of corrosion increases with increase in temperature, increase in CO_2 mole percent of the natural gas stream and decreases with increase in P^H values with them all peaking at 78^{O}C before a dip from their respective trend.

From the results obtained in this study, it is concluded that the rise in corrosion rate as much as 5.7 mm/year at 3 mole percent CO_2 is worrisome. This study has successfully established in quantified term from the obtained results the increment in corrosion rate that equates to 49%, 53% and 102.5% for the temperature conditions of 5^{O}C,15^{O}C and 20^{O}C when mole percent increase from 1 to 3. This is a true effects and reflections of the propensity of carbonic acid, a corroding species that remains higher at higher CO_2 concentration. This values and trend as obtained in this study portray a bad omen for the affected natural gas pipeline.

Nomenclature

a - Fugacity coefficient

bar - Unit of pressure measurement

CO_2 - Carbon dioxide (carbon II oxide)

Cr_{CO_2} - CO_2 corrosion rate

D - Internal diameter of pipe (mm)

f - Friction factor

F_{CO_2} - CO_2 Fugacity

$f(P^H)_T$ - Complex function of P^H and temperature

GUI - Graphic user interface

H_2S - Hydrogen sulphide

IFE - Institute for energy technology

K - Kelvin (temperature scale)

K - Pipe roughness

K_T - Operating temperature dependent constant

MATLAB - Matrix laboratory

NORSOK-Norsk sokkels konkurranseposisjon

NORSOK M-506 - CO_2 corrosion prediction model

NN - Neural network

P_{CO_2} - Partial pressure of CO_2

P^H - Hydrogen potential

RHS - Right hand side

S - Wall shear stress

T - Temperature

U_m - Velocity of fluid mixture

Unisim - Equation oriented simulation software package

ρ_m - Mixture density

Acknowledgement

The authors acknowledge the support of the Department of Petroleum Engineering, Federal University of Technology, Owerri Nigeria.

5. REFERENCES

[1] M. Mohitpour (2008) Energy supply and transportation, ASME Press, New York, 79 - 88.

[2] S. Mokhatab, W.A. Poe, J.A Speight (2006) Hand book of natural gas transmission and processing. London: Elsevier Pp. 117 - 132.

[3] L. Proberezhny, A. Hrysanchuk, H. Grytsuliak (2019) Influence of the gas hydrate on the corrosion rate of gas gathering pipeline. Procedia Structural Integrity. 16, 141 - 147. https://doi.org/10.1016/j.prostr.2019.07.033

[4] M.H. Abbas, R. Norman, A. Charles (2018) Neural network modeling of high pressure CO_2 corrosion in pipeline steels. Process safety and environmental protection H.Q.119, 36 – 40, https://doi.org/10.1016/J.Psep.2018.07.006

[5] L. Zunzhao, L. Shihan, W. Xiaolin, X. Qian, D. Kai, L. Mingrui, Z. Wei, M. Fanfei, F.Shuanshi, L. Xuemei (2020) Study on corrosion of CO_2 in pipelines in the presence of hydrate. In: Paper presented at the 30th International Ocean and Polar Engineering Conference, Virtual.

[6] E.O. Obanijesu, V. Pareek, M.O. Tade (2014) Modeling the contribution of gas hydrate to corrosion rate along the subsea pipelines. Petroleum Science and Technology. 32 (21), 2538 - 2548. https://doi.org/10.1080/10916466.2013.842586.

[7] S. Olsen (2003) CO_2 corrosion prediction by use of the NORSOK M-506 model guidelines and

limitations. In: Paper Presented at corrosion 2003, San Diego, California, 2003.
[8] R. Nyborg (2009) Guidelines for prediction of CO_2 corrosion in oil and gas production system. IFE Institute for Energy Technology, Halden Norway, 2 - 13.
[9] S. Nesic, J. Postlethwaite, M. Vrhovic (1997) CO_2 corrosion of carbon steel from mechanistic to empirical modeling. Corrosion Reviews.15 (1-2), 211-270, 1997, https://doi.org/10.1515/CORREV.1997.15.1-2.211.
[10] A. Kahyarian, M. Singer, S. Nesic (2016) Modeling of uniform CO_2 corrosion of mild steel in gas transportation systems: a Review. Journal of Natural Gas Science and Engineering. 29,530-549. https://doi.org/10.1016/J.Jngse.2015.12.052
[11] R.C. Wollam, S.E. Hernandez (2006) Assessment and comparison of CO_2 corrosion prediction models. In: Paper Presented at SPE International Oilfield Corrosion Symposium, Aberdeen, UK. Society of Petroleum Engineers. https://doi.org/10.2118/100673-MS
[12] S. Nesic, M. Nordsveen, N. Maxwell, M. Vrhovac (2001) Probabilistic modelling of CO_2 corrosion laboratory data using neural networks. Corrosion Sci. 43 (9), 1373 - 1392. (https://doi.org/10.1016/S0010-938X(00).00157-8.
[13] S. Hatami, A.A. Ghaderi, K.M. Neknyad, M.F. Karimi, M.R. Rasael, A.H. Mohammadi (2016) On the prediction of CO_2 corrosion in petroleum industry. Journal of Supercritical Fluids, 117, 108-112, https://doi.org/10.1016/J.Supflu.2016.05.047
[14] R. Nyborg (2002) Overview of CO_2 corrosion models for wells and pipelines. In: Paper Presented at the Corrosion 2002, Denver, Colorado, 2002.
[15] C. De Waard, U. Lotz, D.E. Milliams (1991) Predictive model for CO_2 corrosion engineering in wet natural gas pipelines. Corrosion. 47 (12), 976 - 985. https://doi.org/10.5006/1.3585212
[16] B.F.M. Pots, S.D. Kapusta, R.C. John, M.J.J Thomas, I.J. Rippon, T.S Whithan, M. Girgis (2002) Improvement on De-Waard-Milliams corrosion prediction and applications to corrosion management. In: Paper Presented at the Corrosion 2002, Denver, Colorado, 2002.
[17] S. Olsen, A.M. Halversen, P.G. Lunder, R. Nyborg (2005) CO_2 prediction model-basic principles. In: Paper Presented at the Corrosion 2005, Houston, Texas, 2005.
[18] G.A. Niklasson, C.G. Granqvist, A. Hjortsberg (2008) Electrochromic and gasochromic devices. Solar energy materials and solar cells. 92 (4), 384 - 394. https://doi.org/10.1016/j.solmat.2007.06.040.
[19] S. Krishnan, M. Natarajan, V. Balasubramanian, N. Rajendran (2008) Flow-assisted corrosion of 2.25Cr-1Mo steel. Materials chemistry and physics. 107(1), 84-89. https://doi.org/10.1016/J.matchemphys.2007.07.063

IZVOD

FORMIRANJE HIDRATA I NJEGOV UTICAJ NA CEVOVOD PRIRODNOG GASA: SIMULACIONA STUDIJA

Ova studija je istovremeno proučavala dvostruki problem hidrata i korozije koji se javlja u gasovodu prirodnog gasa, utvrđujući njihovu međuzavisnost korišćenjem simulacionog pristupa. CO_2 korozija je simulirana korišćenjem standardnog modela NORSOK M-506 u matlab-u. Glavni faktori koji se razmatraju su odnos između brzine korozije i temperature, brzine korozije i PH, odnos korozije i temperature za različite molske procente CO_2 i PH vrednosti. Rezultat ove studije je pokazao da se i hidrati tipa I i tipa II mogu formirati pri radnim uslovima od 5°C i 60 bara. Dobijeni rezultat, takođe, pokazuje da se brzina korozije smanjuje i povećava sa povećanjem PH vrednosti i temperature do određene temperature od približno 78°C, a zatim pada u stopi korozije. Rezultat za odnos korozije-temperatura za različite vrednosti PH i molskog procenta CO_2 pokazuje smanjenje brzine korozije sa povećanjem PH i povećanje sa povećanjem molskog procenta CO_2 t. Štaviše, dobijeni rezultati ističu porast od čak 5,7 mm/godišnje pri 3 mol procenta CO_2. Ova vrednost i trend predstavljaju loš znak za pogođeni cevovod. Ova studija preporučuje da prirodni gas koji se transportuje cevovodom treba zasladiti i preraditi kako bi se uklonili H2S, CO_2 i merkaptani ako su prisutni.
Ključne reči: *CO_2 korozija, model, simulacija, hidrat, MATLAB*

Naučni rad
Rad primljen: 18.05.2024.
Rad korigovan: 26.06.2024.
Rad prihvaćen: 03.07.2024.

Ifeanyichukwu Michael Onyejekwe ORCID NO: https://orcid.org/0000-0001-6489-6801
Nnaemeka Uwaezuoke ORCID NO: https://orcid.org/0000-0002-4729-4072
Ononien Gborienemi George ORCID NO: https://orcid.org/0009-0006-9519-0864
Ubanozie Julian Obibuike ORCID NO: https://orcid.org/0000-0003-1382-9160
Nnanna Onwuegbueha Okoli ORCID NO: https://orcid.org/0009-0007-9579-7946

*Esmeralda Halo, Bledar Murtaj, Jonida Tahiraj, Sonila Kane, Elda Marku, Alma Shehu, Sonila Duka, Aurel Nuro**

Tirana University, Faculty of Natural Sciences, Department of Chemistry, Tirana, Albania

Scientific paper
ISSN 0351-9465, E-ISSN 2466-2585
https://doi.org/10.62638/ZasMat1132

Zastita Materijala 66 (1)
109 - 118 (2025)

A survey of water quality in areas of Albanian ports

ABSTRACT

Thisstudy reportdata on physical-chemical parameters and on concentrations of organic pollutants in marine water samples of Albanian ports. Nutrients, PH, temperature, conductivity, TSS, DO, BOD, COD, chlorines, sulfates, magnesium and calcium ions were the indicators used for evaluation of water quality. Also, organic pollutants (organochlorine pesticides, PCBs, PAH and benzene) were determined in seawater samples. Albania is facing by Ionian and Adriatic seas in a coastline of more than 300km. Several ports are in function in Albanian coastline. Ship transport and many activities (automobile transport, mechanical activities, deposits, etc.)are the main factors of water pollution in port areas. Water samples from seven ports (the main Albanian ports) starting from Saranda port in the South to Shengjini port in the North, were analyzed in this study. Sampling was realized in May 2023.

Based on physical-chemical indicators the water in the port of Saranda was the cleanest water, while Porto-Romano, Petrolifera and the fishing port in Zvernec was the most polluted one. Organic pollutants were detected in all water samples. Presence of the degradation products of pesticides may be related with previous uses of them. Presence of PCBs can be because of atmospheric deposition (volatile congeners), water currents and mechanical businesses (heavy congeners). PAHs and Benzene were detected on more than 70% of the analyzed samples. Intense ship and automobile transport in the port areas, mechanical businessesdischarge and hydrocarbon processingi(Petrolifera and Porto-Romano) can be main factor for their presence. Water currents and new arrivals from the rivers can influence the levels and profile of pollutants. The found levels of organic pollutants in water samples of Albanian ports were higher than reported levels in previous studies for the Adriatic Sea (Albania coastline).

Keywords: *Albanianports, Physical-chemical parameters, Organic pollutants, Water analyzes*

1. INTRODUCTION

Albania facing byIonian and Adriatic in a coastline of about 316kmof which 260 km belong to the Adriatic Sea [1-3]. Trade and communications through the sea have been used since ancient times, which is confirmed by numerous remains found along the coast. Many small harbors and boat anchorages have been and continue to be used along the coast. They are mainly located in small natural bays such as Saranda, Shengjini or in large natural bayssuch asthe bay of Vlora (Note that, in Vlora Bay areseveral important ports such as Vlora's port, Petrolifera - hydrocarbon port, Marina's port for Delta Force near Radhima, Military Base of Orikum and a fishing harbor near Zverneci). Some other ports are built artificially such as the port of Durres, Porto-Romano, Petrolifera, etc. The construction/function of ports promote the development of these areas, cities, encouragepopulation growth, impact in economic aspect, employment and nowadays the development of tourism and increased communication/ exchange with other countries[1, 2].

In the port areas have anintense activity not only in the marine but also in terrestrial areas near the port. Marine transport of ships/ferries/boats, their anchorages, mechanical/technical services to them, cleaning/sanitization of their interiors, import/export trade (cereals, minerals, hydrocarbons, etc.), the storage of many materials/ food/chemicals near the ports, the movements of cars/cranes and other mechanical equipment in port areas are the main reasons why there is generallyexpected a higher pollution compare to other coastal areas. In many cases, discharges by urban pollution and the various businesses that operate near the port areas can be added. In the

*Corresponding author: Aurel Nuro
E-mail: aurel.nuro@fshn.edu.al
Paper received: 15.06. 2024.
Paper accepted: 06. 07. 2024.
The website:https://www.zastita-materijala.org/

other side, the construction of ports, usually in areas that have depth and protected in the form of a bay, favors the concentration of pollutants inside the port areas. The effects of water currents in/out ports or the new arrivals from the rivers/effluents (even distant from the port) can bring pollution from areas that may be far from the ports[1-3].

The possibility of pollution for the port areas and the lack of information about the quality of marine waters were the main reasons for undertaking this study in which some of the most important indicators (physical-chemical parameters) such as pH, temperature, DO, BOD, COD, TSS, nutrients and some other ions such as chlorides, sulfates, calcium and magnesium have been determined. The values of these parameters are directly related to the quality of marine waters in these areas [2,4-7]. In addition to them, the concentrations of organochlorine pesticides according to EPA 8081B, marker PCBs, Benzene and 13 PAH according to EPA 525 have also been determined. These organic pollutants are classified as priority substances due to their persistence and high toxicity. Although some of them are not common pollutants of ports, they have been reported in various works due to various accidents and/or the influence of water currents. These data will help us and authorities to determine the quality of marine waters in the main Albanian ports according to national and international norms [6, 8] and also identify the possible factors that influence their presence in the analyzed samples.

2. MATERIAL AND METHODS

Water sampling in Albanian ports

To evaluate water quality and water pollution at the ports of Albaniaand their impact in the sea were analyzed a total of 64 water samples(38 samples inside and 26 samples outside port areas) from seven different ports (Figure 1) starting from Saranda's port (South Albania) to Shengjin's port (North Albania). Sampling stations wereas follow:9 stations at Saranda's port (WSP); 12 stations at Vlore's port (WVP); 8 stations at Petrolifera (WPP); 6 stations at fishing port, Zvernec (WZP); 12 stations at Durres's port (WSP);9 stations at Porto-Romano (WPR) and 8 stations at Shengjin's port (WSH). Water samples were collected port areas in May 2023. This sampling period represent a normal period for the activities in these ports. In each sampling station, 2.5 L of sea water were collected in glass bottles equipped withTeflon caps, based in ISO 5667-3: 201 Method [9]. Water samples were stored and transported at 4ºC to the laboratory for further analysis. For each station pH, conductivity, DO(Dissolved oxygen) and temperature were determined in field by using Hanna Multiparameter -portable equipment (HI98194 Model).

Figure 1. Sampling stations in the main ports of Albania

Determination of BOD_5

VELP brand automatic sensors (respirometers) were used to estimate the 5-day biological oxygen demand (BOD_5) in seawater. The measurement was carried out at a level of 250 ppm. The samples were placed at 20ºC for 5 days, and a direct reading of the BOD value was made for each sample [9].

Determination of COD

For the determination of chemical oxygen demand (COD), SPEC COD digestion tubes were used, which use standard 16-mm tubes pre-prepared with mercury sulfate ($HgSO_4$). 2 ml of seawater was taken in the pre-filled COD digestion tube, close the cap and mix vigorously for 1 minute. The tube was placed in the thermo-reactor ECO 16, set at 150ºC. After being heated for 2 hours, the samples were cooled at room temperature, then measured in a PF-3 spectrophotometer at wavelengths suitable for COD analysis [10].

Analyzeof nutrients and sulfates by using SPUV-VIS method

The UV-VIS measurements of nutrients (nitrates, nitrites ammonium, N-Total, Phosphates and P-Total) and sulfate ions were carried out in the UV 31 SCAN ONDA model spectrophotometer as follows:The analysis of NO_3 in water is based on the ISO 7890-3: 1988 method for their determination with the spectrophotometry

technique at a wavelength of 420 nm. The analysis of NO_2 in water is based on the ISO 6777: 1984 method for their determination by the colorimetric method at 540 nm. The analysis of NH_4 in water is based on the ISO 7150/1:1984 method for their determination with the spectrophotometry technique at 655 nm. N-total was determined using complete disaggregation of the sample with $K_2S_2O_8$ and determination of nitrogen at two wavelengths: 220 nm and 275 nm. All forms of nitrogen are oxidized and measured as NO_3(Screening Method). P-total was determined using the disaggregation method, which aims to oxidize all forms of phosphorus into PO_4 ions and further make their determination using the spectro-photometer method at 880 nm. The analysis of sulfates in water is based on method 9038 for the determination of sulfates by the turbidimetry method at a wavelength of 420 nm [2, 6, 9].

Determination of Cl^- (salinity), Ca^{2+} and Mg^{2+} by titration methods

Chloride ions were determined in seawater samples using the argentometric method (4500-Cl^- B, Argentometric Method, known as the Mohr method). The data obtained for chloride ions in seawater were used to calculate the salinity of the samples. The concentration of calcium ions in seawater was realized by using the titration method with EDTA in the presence of the indicator Ericrom black T (3500-Ca B). Magnesium ions have been determined in seawater using the titration with $MgCl_2$ of the complex forming Mg^{2+} with EDTA (3500-Mg B, C) [6, 9].

Determination of TSS (Total Suspended Solids) in seawater

The analysis of total suspend solids (TSS) in water was based on their determination by the gravimetric method. The water is filtered using 32 mm diameter glass filters with 0.45 um pores in a vacuum filtration system. TSS is calculated from the difference of the weights before and after filtration. The conditioning and drying of the filters was done in the thermostat for 8 hours at 105^{o}C [9].

Water treatment for pesticide and PCB analyses

For the determination of OCPs and PCBs in water samples was used liquid-liquid extraction. One liter of water samplewas extracted with n-hexane (2 x 40 ml) in a separatory funnel. After extraction, the organic phase was dried with anhydrous sodium sulphate Na_2SO_4 (5 g) for water removal. A florisil column was used for the sample clean-up. 20 ml n-hexane/dichloromethane (4/1) was used for elution. After concentration to 1 ml hexane, the samples were injected in GC/ECD [3, 4,11,12].

Gas chromatography analysis of pesticides and PCBs

Organochlorine pesticides and PCBs were analyzed simultaneously using capillary column type Rtx-5 (30 m long x 0.25 mm in diameter x 0.25 µm film thicknesses) on a gas chromatograph (Varian 450 GC) with electron capture detection (ECD detector). Helium was used as carrier gas (1 ml/min) while nitrogen as make-up gas (24 ml/min). The manual injection was done in splitlesss mode at 280°C. The 21 individuals of organochlorine pesticides according EPA 8081B were: DDT-related chemicals, HCH isomers, Heptachlor's, Chlordanes, Aldrin's and Endosulfanes. Analysis of PCBs was based on the determination of the seven PCB markers (IUPAC No. 28, 52, 101, 118, 138, 153 and 180). Quantification of OCPs and PCBs was based on external standard method by using five calibration points as follow: 1 ppb, 2 ppb, 5 ppb, 10 ppb and 25 ppb. The R^2 various form 0.9452 (Endrin keton) to 0.9965 (b-HCH) and the LOD for each individual OCP and/or PCB markers was 0.05ppb [3,4,11].

Treatment of water samples for PAH analyses

Two steps liquid-liquid extraction (LLE) was used for extracting PAHs and Benzene from sea water samples. One liter of water with firstly 40 ml dichloromethane (first step LLE) and after that 40 ml hexane (second step LLE) as extracting solvent was added in a separator funnel. After extraction, the organic phase was dried with 5 g of anhydrous Na_2SO_4 for water removing. Extracts were concentrated to 1 ml hexane using Kuderna-Danish and then were injected in GC/FID for qualification/quantification of PAHs [1, 13-16].

Gas chromatography analysis of PAHs in water samples

Gas chromatographic analyses of PAHs and Benzene in water samples were realized with a Varian 450 GC instrument equipped with a flame ionization detector and PTV injector. VF-1 ms capillary column (30 m x 0.33 mm x 0.25 µm) was used for qualification and quantification of 13 PAHs according EPA 525 Method. Helium was used as carrier gas with 1 ml/min. FID temperature was held at 280°C. Nitrogen was used as the make-up gas (25 ml/min). Hydrogen and air were flame detector gases with 30 ml/min and 300 ml/min, respectively. EPA 525 Standard Mixture was used for qualitative and quantitative analyze of aromatic hydrocarbons. Benzene, Acenaphthylene, Fluorene, Phenanthrene, Anthracene, Pyrene, Benzo [a] anthracene, Chrysene, Perilene, Benzo [b] fluoranthene, Benzo [k] fluoranthene, Indeo

[1,2,3-cd] pyrene, Dibenzo [a, b] anthracene and Benzo [g,h,i] perylene were determined in seawater samples. Quantification of PAHs was based on external standard method by using six calibration points as follow: 1ppm, 2.5ppm, 5 ppm, 10 ppm, 25 ppm and 50 ppm. The R^2 various form 0.8912 (Indeo [1,2,2-cd] pyerene) to 0.9964 (Anthracene) and the LOD for each PAH (including Benzene) was 0.05ppm[1,13,15].

3. RESULTS AND DISCUSSION

In this study, water samples from 64 different stations from the main ports of Albania were analyzed. Water samples were taken in May 2023 from the ports of Saranda, Vlore, Petrolifera, fishing port (Zvernec), Durres, Porto-Romano and Shengjin. The physico-chemical parameters were determined in water samples were: temperature, pH, Conductivity, DO, BOD5, COD, TSS, NO3, NO2, NH4, N-total, P-Total, sulfates, chlorides (salinity), ions calcium and magnesium.

The analysis of organic pollutants includes: organochlorine pesticides, their degradation products (21 individuals according to EPA 8081B), PCB markers (7 congeners), Benzene and PAHs (13 individuals according to EPA 525). All methods used for the determinations of physico-chemical indicators and organic pollutants were based on the Albanian and international norms recommended for these analyzes in marine and surface waters.

Physical-chemical parameters

The average data of measurements of physico-chemical parameters for water samples from port stations in Albania was as follows: The average pH of the water samples was in the range from 7.6 for the port of Saranda to 8.2 in Porto-Romano. These slightly basic pH values are suitable for the growth of living organisms in marine waters. The average seawater temperature at the time of sampling was from 17.6^{o}C in the port of Saranda to 22.8^{o}C for the water of Porto-Romano. These temperatures are normal for the seawater in the month of May. Port water conductivity ranged from 38.8 ms/cm for the port of Shengjin to 60.0 ms/cm for Petrolifera. These values indicate relatively high levels of electrolytes in these waters, which is expected both from the salinity of the sea water and from other ions that come from urban/industrial/agricultural pollution [2, 5, 6].

The maximum value for dissolved oxygen in seawater was for the port of Saranda with 10.8 mg/l, while the minimum value for DO was in the fishing port, Zvernec, with 8.3 mg/l. The limit of 5 mg/l is not exceeded for 2 samples in the fishing port, Zvernec, 2 samples in Porto-Romano and 1 sample in Shengjin port. In general, waters are classified as good according to these DO values. BOD5 values ranged from 25.3 mg/l in the port of Saranda to 132.6 mg/l in Porto-Romano. These values classify the marine waters of the ports as moderately good. The minimum COD value was in the port of Saranda with 50.8 mg/l, while the maximum was again for Porto-Romano with 129.7 mg/l. These values are influenced by the presence of chemicals in the water samples. These COD values classify the analyzed water as very good for Saranda port and moderately good for other ports [5-7].The analysis of particles in suspension (TSS) showed that their value was from 31.9 mg/l in the port of Saranda to 141.1 mg/l for the port of Shengjin. These values classify the waters of the analyzed portsfromgood (Saranda port) to moderately good (other ports) [6].Levels of nutrients in Albanian ports were as follows: The minimum concentration of NO3 in the waters of the Albanian ports was for the port of Saranda with 0.5 mg/l. Note that, for more than 60% of NO3 samples were not detected in the water of this port. The maximum was for the samples analyzed from Petrolifera with 8.6 mg/l. The concentration of nitrites in the water samples had an average value from 0.006 mg/l in the waters of the port of Saranda to 0.46 mg/l for the port of Durrës. The average concentration of NH4 was from 0.004 mg/l (Saranda port) to 0.58 mg/l (Vlora port). N-total in analyzed water samples ranged from 0.17 mg/l for the port of Saranda to 4.93 mg/l in Petrolifera.

The average value of PO4 was in the interval between 0.026 mg/l in the port of Saranda to 9.0 mg/l for the port of Vlora. P-total measured in water samples was from 0.018 mg/l (Saranda port) to 4.7 mg/l for the port of Durrës. Nutrient values in the waters of Albanian ports indicate an impact of urban waste discharges and agriculture on seawater. Their levels classify the water of ports as moderately good. The flows for the rivers Vjosa and Semani (for the ports of Vlora Bay), Shkumbini, Erzeni, Ishemi(for the ports of Durres and Porto-Romano) and the rivers Mat and Drin (for the port of Shengjin) have a strong influence on the found values for physical-chemical indicators as well as water quality. Rainfall amount, the direction of the wind and the wave'sgrade (at the time when the samples were taken)are factors that can affect in momentum values [2, 5 – 7].The concentration of sulfates in the water samples ranged from 18.2 mg/l in the port of Shengjin to 521.2 mg/l for the fishing port in Zvrnec. Their presence must be related to urban pollution, natural background, hydrocarbon spills, ship/automobilist transport, etc. The average value of chlorides and/or salinity in the analyzed port water was from 19.93 g/l (36.0 g/l) in the port of

Vlora to 20.38 g/l (36.8 g/l) in the port of Saranda and in the fishing port in Vlora. The Ionian Sea has a higher salinity than the Adriatic Sea and this was expected for Saranda port, while influence of the Narta Lagoon can affect the increase in chloride values for the fishing port in Zvrnec. The concentration of calcium ions was from 1.13 mg/l for the port of Durres to 7.1 mg/l for the port of Saranda, while the concentration of magnesium ions was from 0.44 mg/l for the port of Vlora to 3.76 mg/l for the port of Saranda. These values are related to both the natural background and the geological structure of the sampling stations [6, 7].*i*of organochlorine pesticides was as follows: Total of HCHs (a-, b-, γ- and d-isomers of Hexachlorcyclohexane) ranged from 0.4 ug/l (Saranda port) to 6.9 ug/l (Porto-Romano) ; Heptachlor's (Heptachlor and Heptachlorepoxide) ranged from 0.1 ug/l (Saranda port) to 1.4 ug/l (Porto-Romano); Chlordanes (alpha and gamma-Chlordanes) ranged from 0.2 ug/l (Saranda port) to 1.0 ug/l (Porto-Romano); Aldrin's (Aldrine, Dieldrine, Endrin, Endrin aldehyde and Endrin ketone) ranged from 1.4 ug/l (Saranda port) to 5.3 ug/l (Durres port); DDT-related chemicals (o,p-DDE, p,p-DDE, p,p-DDD, p,p-DDT) ranged from 0.2 ug/l (ports of Saranda, Vlora, Petrolifera and fishing port of Zvernec) to 0.9 ug/l (Porto-Romano) and Endosulfanes (Endosulfan alpha, Endosulfan beta and Endosulfan sulfate) ranged from 0.5 ug/l (Saranda port) to 4.0 ug/l (port of Durres). These data clearly shown that the port of Saranda was lower polluted by pesticides due to the stronger currents of the Ionian Sea and the smaller agricultural areas near this port. The most polluted ports with pesticides were Porto-Romano and the port of Durres. The production and storage of pesticides in Porto-Romano for a period of more than 30 years is the main reason. The new arrivals of pesticides from the rivers Shkumbin, Erzen and Ishem have impact on these values.

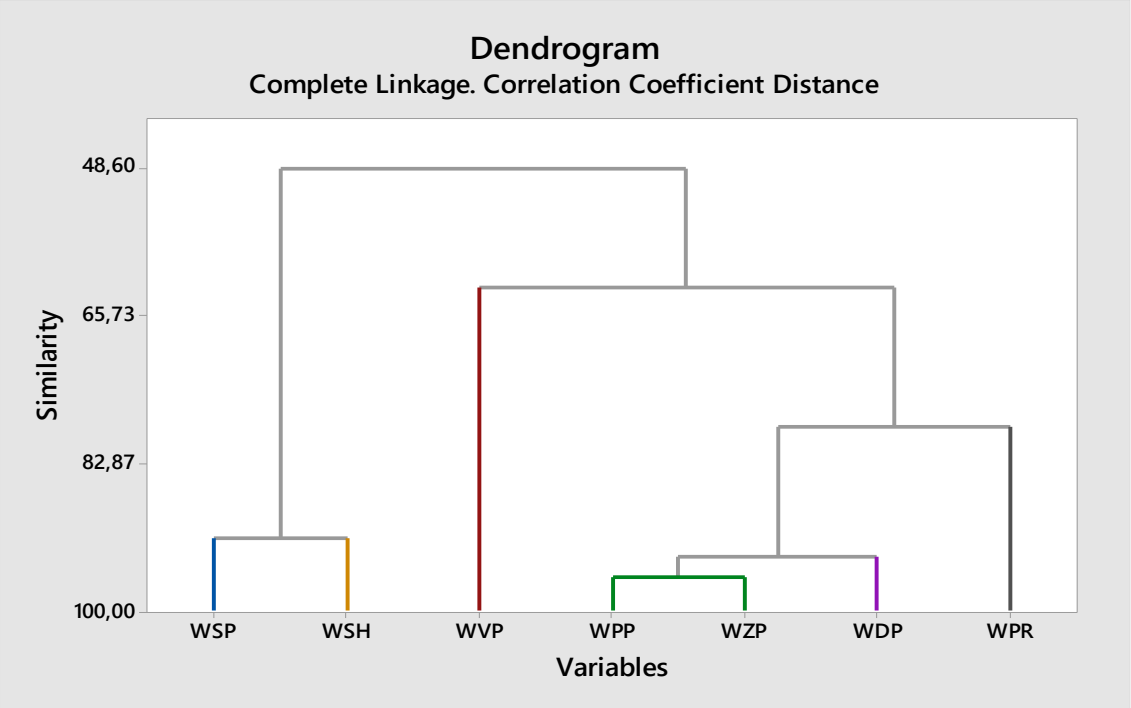

Figure 2. Cluster analyze for distribution of OCPs in Albanian ports

Figure 2 shows cluster analyzes for distribution of OCPs in Albanian ports. The results show that there are two main groups. In the first group were Saranda and Shengjini ports with a similarity level of 92.7%. These groups were built by ports with low level of pesticides. The second group, which is the largest group, includes Petrolifera and the fishing port, Zvernec (similarity level 95.2%). Connected with them was port of Durres (similarity level 91.3%), Porto-Romano (similarity level 75.3%) and port of Vlora (similarity level 73.2%). These ports showed higher levels of contamination for some of the individual pesticides and for their total too. Figure 3 shows the multifactorial cluster analysis data for each individual of the analyzed pesticides. There are five main groups of them as follows: The first group has three subgroups, a-HCH and b-HCH (similarity level of 98.6%), d-HCH and Heptachlor epoxide (similarity level of 96.5%) and Aldrine, Chlordane (similarity level of 97.2%) and Endosulfane I (similarity level of 87.1%). First and second subgroups were connected together

with a similarity level of 86.8% and with the third group with a similarity level of 74.3%. In the second group were two subgroups: Lindane, Methoxychlor (similarity level of 97.3%) and Endrin aldehyde (similarity level of 93.2%) are part of the first subgroup, while in the second DDE and DDT (similarity level of 93.5%). They are connected together with a similarity level of 74.4%. Endrin and DDD built together third group with a similarity level of 72.6%. The fourth group was built by Heptachlor, Dieldrine (98.3%), Endosulfan sulfate (86.6%), Endrin ketone (76.3%) and alpha-Chlordane (70.2%). Endosulfane II and Mirex were part of fifth group with a similarity level of 53.3%. The first and second groups have a similarity level of 51.2%. The connection with the third group was less than 40%, while with the fourth and fifth groups they have a similarity level of less than 10%. These clusters were built by pesticides of the same class and/or the same concentrations. OCP concentrations in the water samples of Albanian ports were in the same range as data reported in previous studies in the Adriatic Sea [3,11,12]. For all analyzed samples levels of individual pesticides were below acceptable levels according to Albanian and EU standards[8].

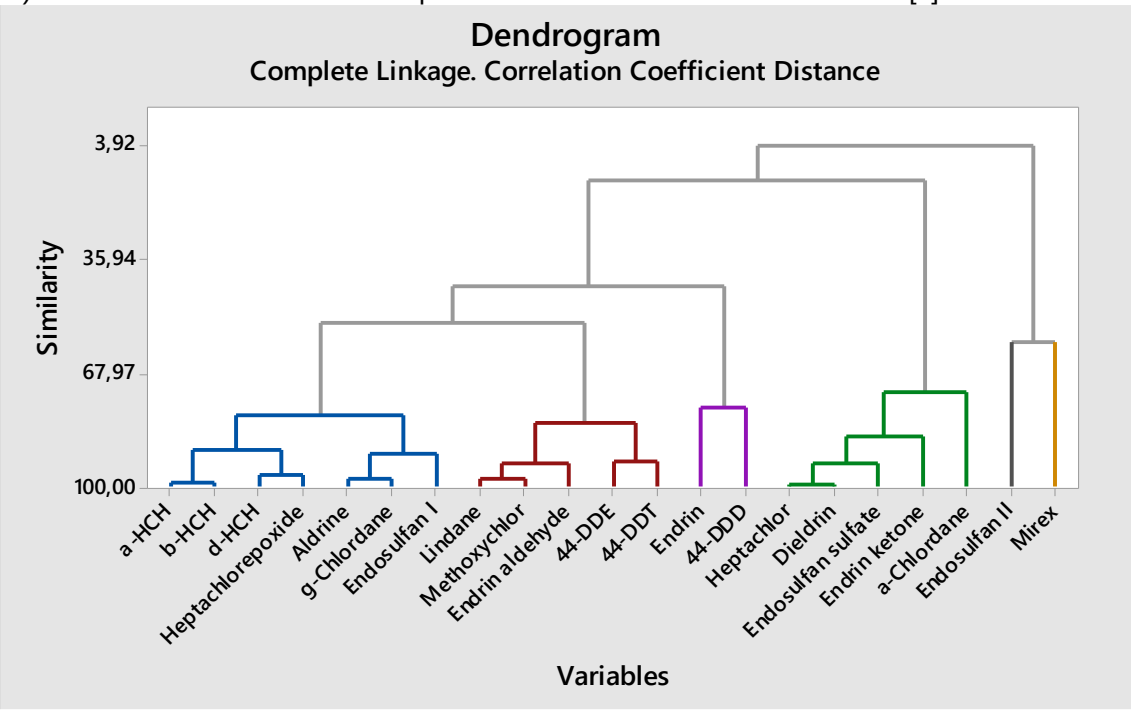

Figure 3. Cluster analyze for organochlorine pesticides (21 individuals) in water samples of Albanian ports

PCB markers were detected in more than 75% of analyzed samples from the Albanian ports. Their total concentrations ranged from 2.9 μg/l (Saranda port) to 15.1 μg/l (Durres port). Their presence in seawater samples can be related to ship transport/anchorage/repair, industrial/mechanical activity near port areas, atmospheric deposition, water currents, and new arrivals from rivers and/or effluents. Oil discharges from some operations/ reparati ofmachineries and activities (in and out of the port) are likely terrestrial sources of PCBs and hydrocarbons in seawater samples. Figure 4 shows cluster analysis data for distribution of PCB markers in Albanian ports. Again, Saranda and Shengjin ports were grouped together with a similarity level of 97.6% because of low levels for PCBs. The higher similarity was for fishing port of Zverneci and Porto-Romano (99.1%) and for Vlora port and Petrolifera (98.2%) which were grouped together in the second group, with a similarity level of 97.5%. Connected with them was Durresi port with a similarity level of 89.6%. This second group was connected with the first one with a similarity level of 65.2%. Note that water pollution with PCBs for all Albanian ports was almost in the same range (high level of similarity) because of the same pollution origin. Figure 5 shows cluster observation of PCB markers in the water samples of Albanian ports. It was noted that clusters were built in three main groups. In the first group were: PCB 52, PCB 118 (96.1%) and PCB 28 (93.6%). These volatile PCBs were detected frequently in all samples. PCB 153 ad PCB 180 (95.2%) were part of the second group which was connected with the first group with a similarity level of 61.1%. The similarity level for PCB 101 and PCB 138 (third group) was 82.2 %. The connection of the third group with the first and the second group was with a similarity level of

10.7%. These clusters were results of levels and profiles of PCB markers in water samples of Albanian ports. PCB levels for analyzed sea water samples were comparable to data reported in previous studies in the Adriatic Sea [3, 11, 12]. The PCB levels were lower than the permitted level by Albanian and EU standards [8].

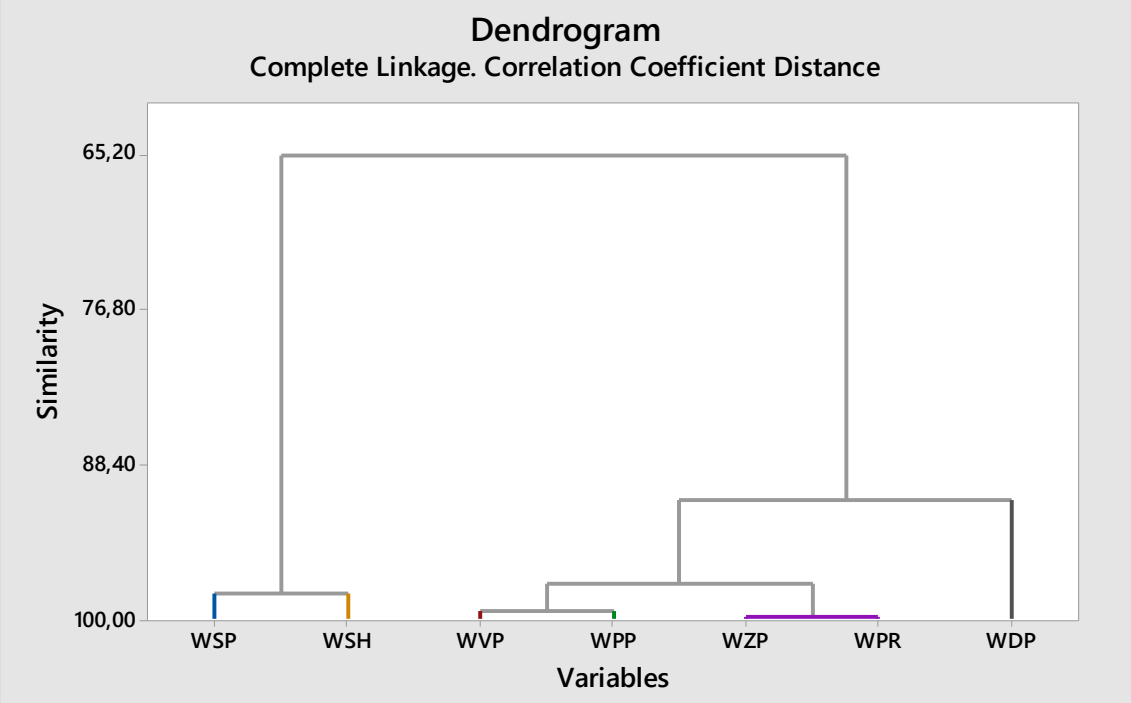

Figure 4. Cluster analyze for distribution of PCBs in ports of Albania

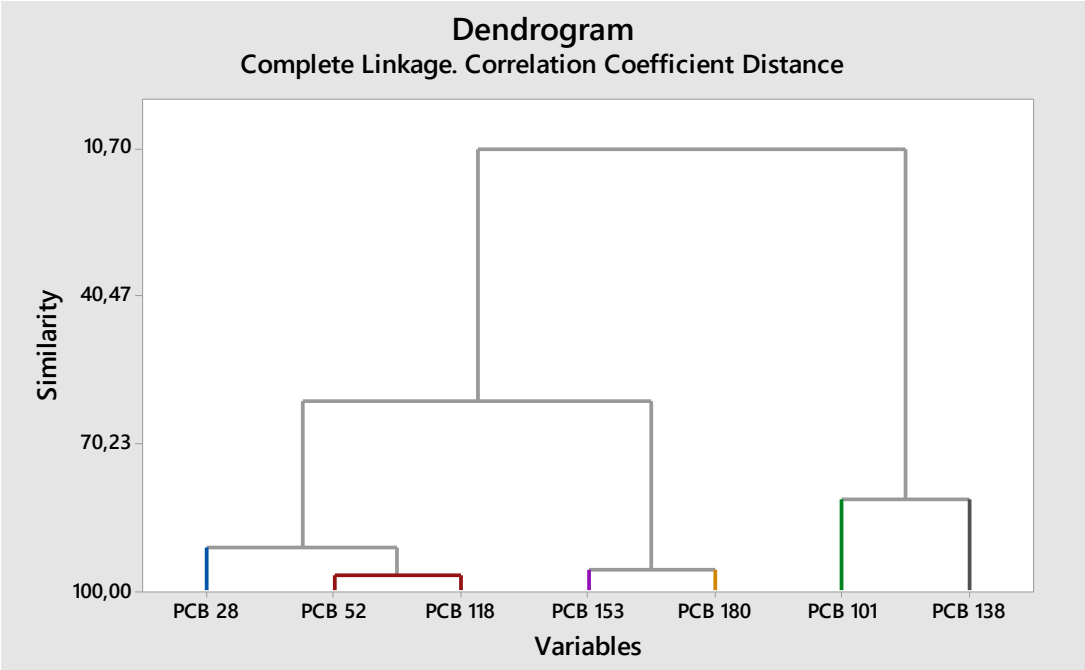

*Figure **5.** Cluster analyze for PCB markers in water samples of Albanian ports*

PAHs and Benzene were detected in more than 60% of water samples analyzed from Albanian ports. The average value for 13 PAHs according EPA 525 standard was between 0.6 mg/l (Saranda port) and 2.9 µg/l (Petrolifera, hydrocarbon port of Vlora) while for Benzene from 0.4 mg/l (Saranda port) to 2.2 mg/l (Porto Romano). The main reasons of hydrocarbon presence could be ship transport and any possible accident of hydrocarbons (in the port areas or near it),

mechanical activities near the port as well as some massive fires near these areas could be sources of hydrocarbons in marine water. Note that, the presence of some individual PAHs were found in higher level for some stations in Petrolifera, Durres and Porto-Romano. PAH presence was a combination of non-pyrogenic PAHs (transport emitting, spillage of hydrocarbons, mechanical activities, etc) and pyrogenic PAHs (forest and urban waste burning, transport emitting, industrial activities, etc).

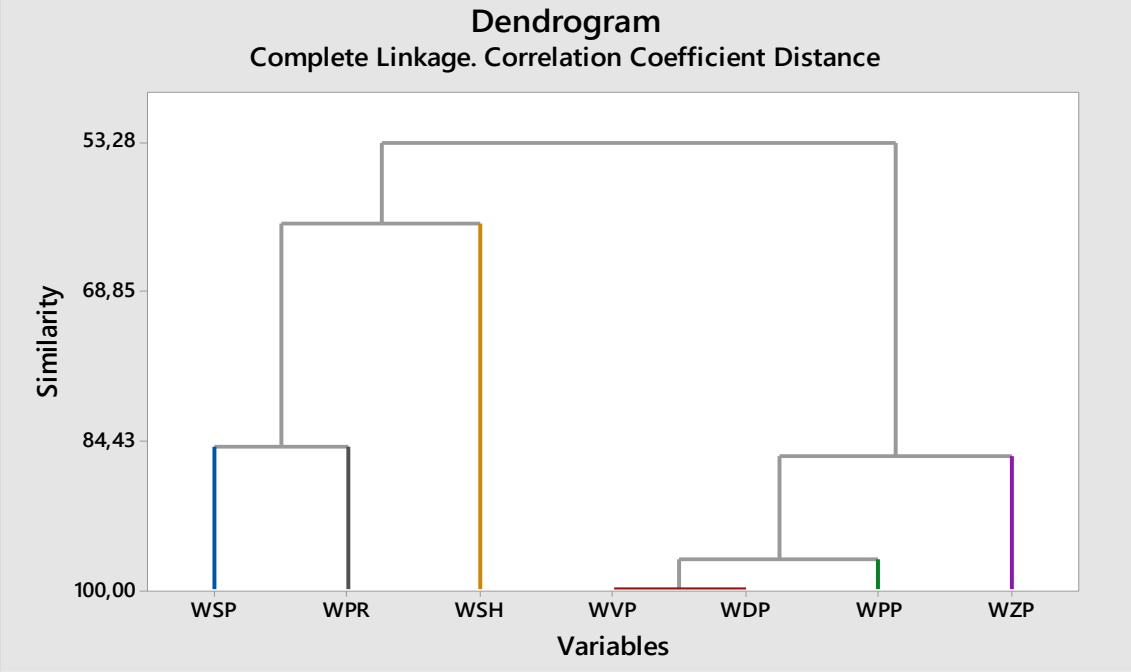

Figure 6. Cluster analyze for distribution of PAHs in water ports

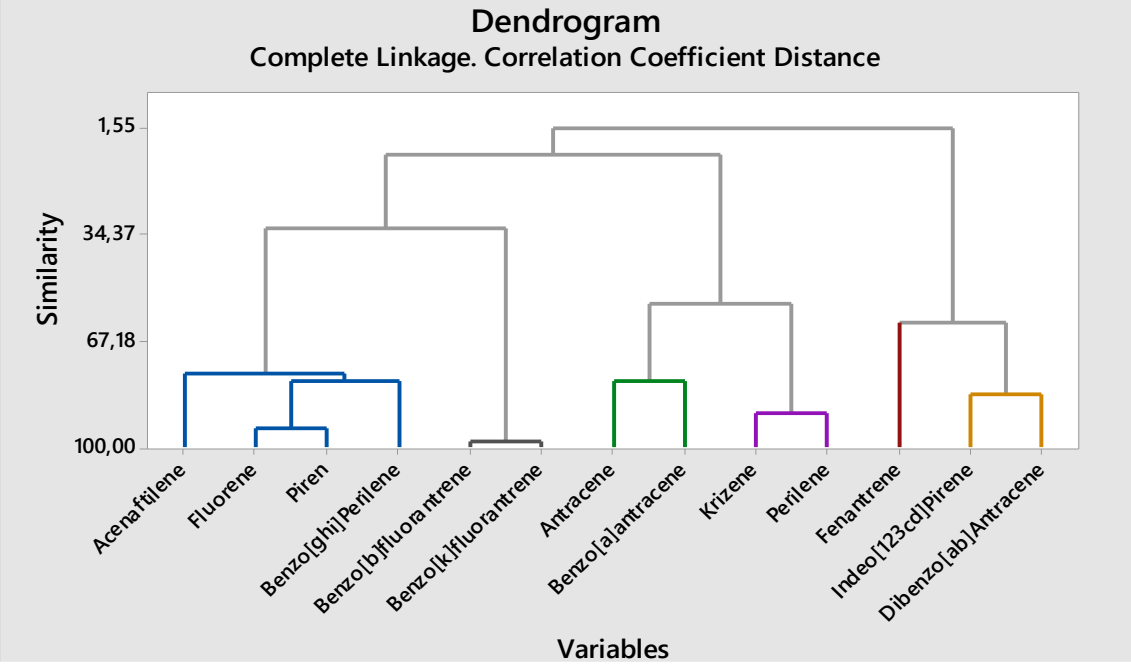

Figure 7. Cluster analyze for 13 individuals of PAHs in water samples of Albanian ports

Figure 6 shows cluster analyze data for distribution of 13 PAH according EPA525 in Albanian ports. In the first group were Saranda, Porto-Romano (84.5 %) and Shengjin ports (60.2 %) while in the second group were ports of Vlora, Durres (99.3%), Petrolifera (95.6%) and fishing port of Zverneci (85.1%). Both groups were linked together with a similarity level of 53.3%.Figure 7

shows clusters for PAHs in Albanian ports. It was noted presence of five main groups (clusters) as follows: In the first group were: Acenaftilene, Fluorene, Pyrene and Benzo [ghi]perilene with a similarity level between 93.2 – 72.1%. In the second group were Benzo[b] fluornathrene and Benzo[k] fluoranthrene (98.3%) which was connected with first group (34.4%). In third group was Anthravene and Benzo[a] Anthracene (73.8%) while in the fourth group were Chrysene and Perilene (79.3%). These groups were connected together (50.2%) and with previous groups (7.3%). The last group was built by Indeo[123cd]Pyrene and Dibenzo[ab[anthracene (74.5%) and Fenantrene (65.7%). These clusters were results of levels and profile of PAHs in water samples. PAH levels in analyzed samples were in the same range/higher than the reported levels for other stations of Adriatic Sea, Albania [1, 13-16]. The presence of Benzene and Anthracene for some stations was higher than permitted level according to Albanian and EU norms [8].

4. CONCLUSIONS

Data of physical-chemical parameters and the determination of organic pollutants in the water of the Albanian ports, shown that the waters of the port of Saranda were cleaner (very good) than other ports. The waters of the other ports were classified as good to moderately good. Anthropogenic activity can influence water quality. This comes mainly from the activities in the port areas, but also from urban pollution and/or agriculture, which are relatively far from the ports but flows from rivers and sea currents can affect them. The values reported in this paper generally do not have significant differences with previous works for the Adriatic Sea [2, 4, 5], however it can be said that these are momentum values and can be change quickly. For this, recommend that the physical-chemical parameters should be kept under continuous monitoring by the relevant institutions.

Pesticides, PCBs and PAHs were detected in water samples of Albanian ports. Their presence could be because of ship/automobilist transport, elevated activity near port areas, new arrivals from rivers, water currents, punctual sources, accidents, etc. Pesticide degradation products were found in high concentrations because of their previous use. The presence of PCBs and PAHs can be related to the transport, industrial/mechanical activity, atmospheric deposition and water currents. Statistical analysis of cluster showed a good connection between the pollutant levels and profile for each class of them. Levels of individual organochlorine pesticides, PCB markers, Benzene and 13 most toxic PAHs according to EPA in water samples were generally lower than permitted levels for surface waters according to EU Directive 2013/39 and Albanian norms. Exception was for some individuals (in some stations) found relatively in higher concentration than others. Monitoring of organic pollutants in Albanian ports should be ongoing, because can be identify many sources of pollution that can affect them. Generally, their concentrations in water samples were similar to the reports made for the Adriatic Sea [3, 4, 11-16]. Continuous analysis of organic pollutants is recommended to realize by using GC/MS/MS and LC/MS/MS techniques.

Acknowledgments

Authors thanks Tirana University about financial support of this study in frame of project entitled "Analyzes of priority substances in water samples of main Albanian ports" as part of program: "UT-Research, Excellence and Innovation" (2021 – 2024).

5. REFERENCES

[1] S. Froehner, J. Rizzi, L.M. Vieira, J. Sanez (2018) PAHS in water, sediment and biota in an area with port activities, Arch. Environ. Contamination Toxicology, 75(2):236-246, doi: 10.1007/s00244-018-0538-6.

[2] S. Kane, P. Lazo, F. Qarri (2015) Environmental situation of Vlora Bay, Albania based on physical-chemical parameters of seawater, Austin Journal of Hydrology, 2, 112-119.

[3] A.Nuro, E.Marku, M.Shehu (2012) Organchlorinated pesticide residues in marine water in the South of Albania". International Journal of Ecosystems and Ecology Sciences, 2, 27-34.

[4] A.Mohammed, P.Peterman, K.Echols, K.Feltz, G. Tegerdine, A. Manoo, D. Maraj, J. Agard, C. Orazio (2011) Polychlorinated Biphenyls (PCBS) and Organochlorine Pesticides (OCPS) in Harbour Sediments from Sea Lots, Port-of-Spain, Trinidad and Tobago, Mar Pollut Bull, 62(6), 1324-32, doi: 10.1016/j.marpolbul

[5] S.Kane, P.Lazo (2012) Assessment of environment situation and water quality of Vlora Bay and Narta Lagoon by nutrients and heavy metals determination. International Interdisciplinary Conference, Vlore, Albania, 26-28 November, ISBN 978-9928-4000-2-4.

[6] S. Poikane, G.M. Kelly, S.F. Herreroa, Jo-A. Pitt, P.H. Jarvie, U. Claussen, W. Leuja, L.A. Solheim, H. Teixeira, G. Phillips (2019) Nutrient criteria for surface waters under the European water framework directive: current state- of-the-art, challenges and future outlook. Science of the Total Environment, 695, 133888. https://doi.org/10.1016/j.scitotenv.2019.133888

[7] A. Campanelli, P. Fornasiero, M. Marini, (2004) Physical and chemical characterization of the water column in the Piceno coastal area (Adriatic Sea). Fresen Environ Bull. 13, 430-435.

[8] [8] Directive 2008/105/EC of The European Parliament and of the Council on environmental quality standards in the field of water policy,

amending and subsequently repealing Council Directives 82/176/EEC, 83/513/EEC, 84/156/EEC, 84/491/EEC, 86/280/EEC and amending Directive 2000/60/EC of the European Parliament and of the Council.
[9] ISO 5667-3:2018, Water quality — Sampling — Part 3: Preservation and handling of water samples.
[10] R. Baird, A. Eaton, E. Rice (2017) Standard Methods for Examination of Water and Wastewater, 23rd Edition, https://doi.org/10.2105/SMWW.2882.216.
[11] A. Nuro, E. Marku, B. Murtaj, S. Mance (2014) Study of Organochlorinated Pesticides, their Residues and PCB Concentrations in Sediment Samples of Patoku Lagoon" International Journal of Ecosystems and Ecology Sciences (IJEES), 2(1), 15-20.
[12] P. B. Lazar, L. Maslov, S.H. Romanić, R. Gračan, B. Krauthacker, D. Holcer, N. Tvrtković (2011) Accumulation of organochlorine contaminants in loggerhead sea turtles, Caretta caretta, from the eastern Adriatic Sea. Chemosphere.82(1), 121-129.
[13] A. Naglaa El-Naggar, I. Hosny Emara, N. Madelyn Moawad, A. Yosry Soliman, A. M. Abeer El-Sayed (2018) Detection of polycyclic aromatic hydrocarbons along Alexandria's coastal water, Egyptian Mediterranean Sea, The Egyptian journal of aquatic research, 44(1), 9-14.
[14] E. Magi, R. Bianco, C. Ianni, M. Di Carro (2002) Distribution of polycyclic aromatic hydrocarbons in the sediments of the Adriatic Sea, Environmental pollution, 119, 91–98.
[15] J. Mandić, M.P. Vrančić (2017) Concentrations and origin of polycyclic aromatic hydrocarbons in sediments of the middle Adriatic Sea, Acta Adriatica: International Journal of Marine Sciences, 58(1), 3 - 24.
[16] M. Marini, E. Frapiccini (2013) Persistence of polycyclic aromatic hydrocarbons in sediments in the deeper area of the Northern Adriatic Sea (Mediterranean Sea), Chemosphere, 90(6), 1839-1846.

IZVOD

ISTRAŽIVANJE KVALITETA VODE NA PODRUČJIMA ALBANSKIH LUKA

Ova studija daje podatke o fizičko-hemijskim parametrima i koncentracijama organskih zagađivača u uzorcima morske vode albanskih luka. Hranljivi sastojci, PH, temperatura, provodljivost, TSS, DO, BPK, COD, hlor, sulfati, joni magnezijuma i kalcijuma bili su indikatori koji su korišćeni za ocenu kvaliteta vode. Takođe, u uzorcima morske vode utvrđeni su organski zagađivači (organohlorni pesticidi, PCB, PAH i benzen). Albanija je suočena sa Jonskim i Jadranskim morem na obali dužoj od 300 km. Nekoliko luka je u funkciji na albanskoj obali. Brodski transport i mnoge delatnosti (automobilski transport, mašinske delatnosti, nanosi i dr.) glavni su faktori zagađenja vode u lučkim područjima. U ovoj studiji analizirani su uzorci vode iz sedam luka (glavnih albanskih luka) počev od luke Saranda na jugu do luke Shengjini na severu. Uzorkovanje je realizovano u maju 2023. godine.
Na osnovu fizičko-hemijskih pokazatelja voda u luci Saranda je bila najčistija voda, dok su Porto-Romano, Petrolifera i ribarska luka u Zvernecu bila najzagađenija. U svim uzorcima vode otkriveni su organski zagađivači. Prisustvo proizvoda razgradnje pesticida može biti povezano sa njihovom prethodnom upotrebom. Prisustvo PCB-a može biti zbog atmosferskog taloženja (isparljivi kongeneri), strujanja vode i mehaničkih poslova (teški kongeneri). PAH i benzen su detektovani na više od 70% analiziranih uzoraka. Intenzivan brodski i automobilski transport u lučkim oblastima, istovar mehaničkih preduzeća i prerada ugljovodonika (Petrolifera i Porto-Romano) mogu biti glavni faktor njihovog prisustva. Vodeni tokovi i novi dolasci iz reka mogu uticati na nivoe i profil zagađivača. Pronađeni nivoi organskih zagađivača u uzorcima vode albanskih luka bili su viši od nivoa prijavljenih u prethodnim studijama za Jadransko more (obala Albanije).
Ključne reči: *albanske luke, fizičko-hemijski parametri, organski zagađivači, analize vode*

Naučni rad
Rad primljen: 15.06.2024.
Rad prihvaćen: 06.07.2024.

Esmeralda Halo https://orcid.org/0009-0003-3569-2553
Bledar Murtaj https://orcid.org/0009-0008-3518-4424
Jonida Tahiraj https://orcid.org/0000-0002-2539-6430
Sonila Kane https://orcid.org/0000-0002-0863-2331
Elda Marku https://orcid.org/0000-0003-1199-8737
Alma Shehu https://orcid.org/0000-0001-8486-6300
Sonila Duka https://orcid.org/0000-0003-1601-5824
Aurel Nuro https://orcid.org/0000-0003-1875-2430

Tamara Tešić[1], Milica Rančič[1], Danica Bajuk Bogdanović[2],Ivana Gavrilović Grmuša[1]*

[1]University of Belgrade, Faculty of Forestry, Belgrade, Serbia,
[2]University of Belgrade, Faculty of Physical Chemistry, Belgrade, Serbia;

Scientific paper
ISSN 0351-9465, E-ISSN 2466-2585
https://doi.org/10.62638/ZasMat1140

Zastita Materijala 66 (1)
119 - 125 (2025)

The influence of tannin on the improvement of adhesive properties of urea-formaldehyde resin

ABSTRACT

The aim of this study was to examine the properties of urea-formaldehyde (UF) adhesive with the addition of tannin, in order to determine whether it is possible to obtain so-called, bio-adhesives for wood with better mechanical properties compared to commercial UF. Tannin-based UF resins, with four different concentrations of tannin (5, 10, 15, and 20%), were prepared, and adhesive properties were tested and compared with properties of pure UF. Testing of tensile shear strength showed that the addition of tannin in UF adhesive formulation significantly increases its performance compared to pure UF adhesive. It was found that tensile shear strength increased with increasing concentration of tannin, while UF-tannin adhesives with tannin concentrations of 15% and 20% showed higher tensile shear strength than the corresponding pure UF adhesive. Therefore, it can be concluded that tannin-based UF adhesive can be a good candidate for application as an environmentally-friendly wood adhesive due to improvement in terms of adhesive and mechanical properties.
Keywords: *wood adhesive,UF resin, tannin, bio-adhesives**,** wood-based composites*

1. INTRODUCTION

Phenolic resins are the first synthetic polymers whose industrial production started at the beginning of the 20th century [1]. Today, these resins have found their widest application in the wood industry. With the increase in the number of inhabitants on earth, the consumption of wood-based products is also increasing every day. Conventional wood adhesives based on formaldehyde (phenol-formaldehyde (PF), urea-formaldehyde (UF) and melamine–formaldehyde (MF)) have a wide use (even though formaldehyde is classified as highly carcinogenic), mostly because of their durability, moisture resistance, low cost, and gap-filling properties. This especially applies to urea-formaldehyde(UF) due to its characteristics such as good binding properties and high reactivity [2], but these resins also have certain disadvantages such as poor water resistance and formaldehyde emission (FE) [3].

Corresponding author: Milica Rančič
E-mail: milica.rancic@sfb.bg.ac.rs
Paper received: 11.06. 2024.
Paper accepted: 02.07. 2024.
The website: https://www.zastita-materijala.org/

These synthetic resins are widely used in the production of wood-based panels thanks to their low cost and good reactivity, but their fossil origin and formaldehyde content have increased the interest in resin synthesis studies with the use of bio-based materials [4]. In recent years, the emphasis has been placed on the so-called "green" approach in the adhesive industry, so many plant sources, like tannins, have been used to make bio-based adhesives, even epoxies [5].

Tannins are polyphenols present in plant species and are widespread in nature [6], with a significantly higher extraction potential than lignin [7]. Tannins have an antibacterial and antifungal effect. Vegetable tannins have been used to tan leather for thousands of years [6]. Tannins are also used in enology (during winemaking) to give color stability, and protection against oxidation, odor, and flavor[8].Due to their natural origin and broad availability, the application field of tannins is spreading from pharmacy and adhesives to solid biofuels. Tannin is one of the most studied raw materials to synthesize bio-based wood adhesives due to its chemical structure and availability [9]. Tannin-formaldehyde resins have been commercially available for several years and are

characterized by very low formaldehyde emission(FE) and fast pressing times.

The term natural plant tannin refers to two broad classes of chemical compounds, condensed or polyflavonoid tannins and hydrolyzable tannins [6].Although tannins have limitations, wood adhesives based on condensed tannins are intensively studied because of theirmoisture resistance[10], unlike hydrolyzable tannins.

Compared to hydrolyzable tannins, condensed tannins show greater reactivity with formaldehyde resulting in reduced formaldehyde emissions (FE), making them one of the most researched wood glue precursors [11].Tannins applied with synthetic adhesives also act as formaldehyde scavengers in phenol-formaldehyde (PF), melamine-formaldehyde (MF), and UF resin [12].

Tannin is considered an additional component that can be mixed with typical UF resins in different ratios [14] to make bio-adhesives with very good adhesion and moisture tolerance [13]. The addition of tannin causes lower formaldehyde emission, even though too much tannin can cause gelation, but also improves the bonding properties and water resistance of conventional UF resin [15].

In this work, new adhesives based on UF resin and tannin were prepared and tested for application as wood adhesives. The influence of different concentrations of tannins on the properties of the commercial UF adhesive was examined by measuring the shear strength of the tested samples.

2.EXPERIMENTAL

2.1 Materials

In this study, we used a commercial UF resin provided by a domestic company (Serbia). Tannin sodium salt was purchased from CHIMAR HELLAS SA (Greece).Ammonium chloride was purchased from Centrohem (Serbia). Beech (*Fagus sylvatica*) logs were selected from a known locality and growth conditions (Goč Mountain, Serbia), and then primary boards (with the desired orientation of growth rings) were cut.

2.2. Tensile shear strength determination

2.2.1. Preparation of wood samples

The sawn timber was dried in a semi-industrial conventional kiln (Nigos MC 3000, capacity 0.8 m^3). The most homogeneous groups of testing samples were selected for further experiments.

2.2.2. Preparation of UF-tannin adhesive

At the beginning of this experiment, we determined the solid content of UF resin as important data for further adhesive formulations and analyses. Every formulation was prepared in concentration calculated using solid weight relative to UF resin solid content. A 20% ammonium chloride salt solution was used as a hardener for all samples (in the concentration of 1% w/w). One group of samples, with pure UF resin, was used as a control group while tannin was added to the others in concentrations of 5, 10, 15, and 20%, respectively, by weight.

2.2.3. Characterization of UF adhesive

Adhesives obtained in this research were performed according to the following standards: determination of pH (SRPS EN 1245:2012); determination of density (SRPS EN 542:2009); determination of conventional solids content and constant mass solids content (SRPS EN 827:2009); determination of tensile shear strength of lap joints for wood adhesives (SRPS EN 205:2017); and adhesives were classified according to the standard fortheclassification of thermosetting wood adhesives (SRPS EN 12765:2017).

The gel time of the resins containing ammonium chloride as hardener was determined by the boiling water test. The time measurement began when a test tube containing approximately 2.0 g of resin together with the hardener ammonium chloride (1 % based on the adhesive dry matter) was immersed in boiling water. The resin in the test tube was gently stirred throughout the test. The gel time was taken as the time elapsed from immersion of the test tube until hardening of the resin, when stirring was no longer possible.

The FTIR-ATR spectra were obtained with an FTIR spectrometer (iS20, Thermo Nicolet) with a resolution of 4 cm^{-1} in the wavelength region 4000–525cm^{-1}, using a diamond single reflection attenuated total reflectance (ATR). All spectra were obtained with 32 scans and the background measurement was made using air.

2.2.4. Determination and optimization of glue-line quality

The adhesive mixes were applied by a rubber roller onto one surface of the two wood specimens to be bonded (200 g/m^2). Assembling was always performed in a parallel grain direction. The ply without direct application of the adhesive mix was always in the bottom position to improve the penetration into its structure. Again, a special effort was made to have the taper as low as possible, guaranteeing equal penetration conditions for all samples. Ten joint samples were pressed in a hydraulic press at 120°C and 1.5 MPa for 15 minutes. Before testing, the single lap shear test specimens (150 mm × 20 mm × 5 mm) were

conditioned at 20 ± 2°C and 65 ± 5% relative humidity for one week. The lap shear test was conducted according to SRPS EN 205 standard test on a hydraulic test machine (Wood tester WT4) with a measuring scale of 50 kN at a testing speed of 6 mm/min loading rate in tensile mode with the load direction always parallel to the grain in all tested specimens. The failure zone (shear area 20 mm × 10 mm) was examined using a light microscope to determine the proportion of wood failure and the thickness of the wood layer in the wood failure. Ten replications were performed for each set of parameters. An analysis of variance was applied to obtain centralized values and standard errors.

3. RESULTS AND DISCUSSION

For any type of bio-based wood adhesives, it is important to effectively evaluate their prospects for wood composite application and understand the adhesive/wood interaction to gain scientific insights to guide the adhesive development in terms of the mechanical strength, water resistance, thermal and rheological properties of the adhesives, as well as the adhesive penetration. To interpret the measured bonding strength of wood adhesives, it is also essential to take into consideration the type of failure or separation that occurred in the mechanical tests. There are four main types of failure modes for the adhesive bonded wood composites: (a) cohesive failure of the adhesive; (b) adhesive failure (c) mixed failure - a combination of (a) and (b), and (d) wood cohesive failure or wood failure.

UF adhesive is the most important adhesive in the wood industry, especially in the production of wood-based panels, primarily because of its relatively good characteristics and low price. However, considering that it has poor water resistance and high formaldehyde emission, it is necessary to make some modifications to the chemistry of the glue itself in order to make it more environmentally friendly.Herein, we prepared modified adhesive formulations based on commercial UF resins (UF), cured alone (cUF) and with tannin (labels UFT5, UFT10, UFT15, and UFT20 correspond to samples with 5, 10, 15 and 20% of tannin added to UF). The maximum tannin concentration of 20% was chosen because in the case of higher tannin concentration, it was hard to achieve homogeneity of the adhesive system due to its high viscosity, and consequently, the application on the wood surface was difficult. Their adhesive properties wereevaluated following the change in shear strength of samples with different tannin content.

Commercial UF resin was characterized and its technical specifications are given in Table 1. Properties, such as solid content, density, pH, viscosity, free formaldehyde content, and gel time were determined (Table 1).

Table 1. The technical properties of UF resin

Sample	Property					
	Solid content (wt%)	Density (g/cm^3)	Gel time (s)	pH	Free-F (wt%)	Viscosity, F^4_{20} (s)
UF	68	1.290	71	8.0	0.14	84

3.1. FTIR analysis

Fourier transform infrared (FTIR) spectroscopy was used to characterize the chemical structures of the resins. The obtained FTIR spectra of commercial UF adhesive emulsions examined in this work are given in Figure 1for UF adhesive emulsion and for cured cUF resin. The following four spectra given in Figure 2are for cured resin with tannin addition of different concentrations, respectively: a) 5%, b) 10%, c) 15%, and d) 20%.

The wide bands at 3321 cm^{-1} are related to the stretching vibration of O–H and N–H and originate from the presence of by-products such as water and excess formaldehyde that can hydrogen bond to the CH_2OH, NH_2, and NH functional groups present in the UF resins and their intensities decreased in cured samples, as it was expected. A sharp but small peak occurring at 2959 cm^{-1} arising from the stretching C–H vibrations originated from dimethylene ether bonds (CH_2–O–CH_2), hydroxymethyl (CH_2OH) and methylene bonds (N–CH_2). The characteristic bands that appear at 1629, 1531, and 1243 cm^{-1} represent amide I (C=O stretching vibration in –CONH), amide II (stretching vibration of C-N and deformation of vibration of N-H in NH-CO), and amide III and all amide bands become broader after curing. The peak at 1457 cm^{-1} of methylene bonds (–CH_2–) which appear only as a shoulder in UF emulsion broadens and becomes stronger after curing leading to the conclusion that the resulting resin contains more methylene bridges liberating formaldehyde for further crosslinking. The methylene ether bridge (–CH_2–O–CH_2–) characteristic absorption peak at 1129 cm^{-1} ascribed to the C–O stretching vibration of hydroxymethyl decreases after curing compared with UF resin, as well as the peak at 1011 cm^{-1},

assigned to ν(C–O–C) of ether linkage indicated additional crosslinking probably due to the transformation of unstable ether bridges (–CH_2–O–CH_2–), initially formed, to methylene ones (–CH_2–). On the contrary, the weak band at 1361 cm^{-1} in UF emulsion, broaden after curing. This area of UF polymer spectra is usually assigned to C–H vibrations in CH_2 and CH_3 structures. A small peak at 767 cm^{-1} which appears in cured samples is the characteristic absorption peak of the uronic structure that is formed.

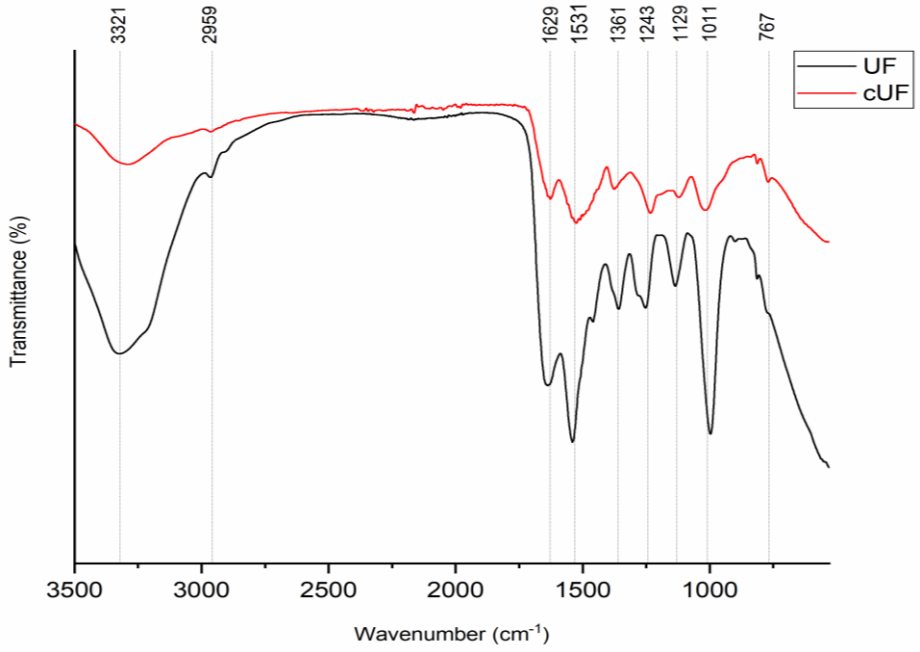

Figure 1. FTIR spectra of pure commercial UF resin and cured adhesive (cUF)

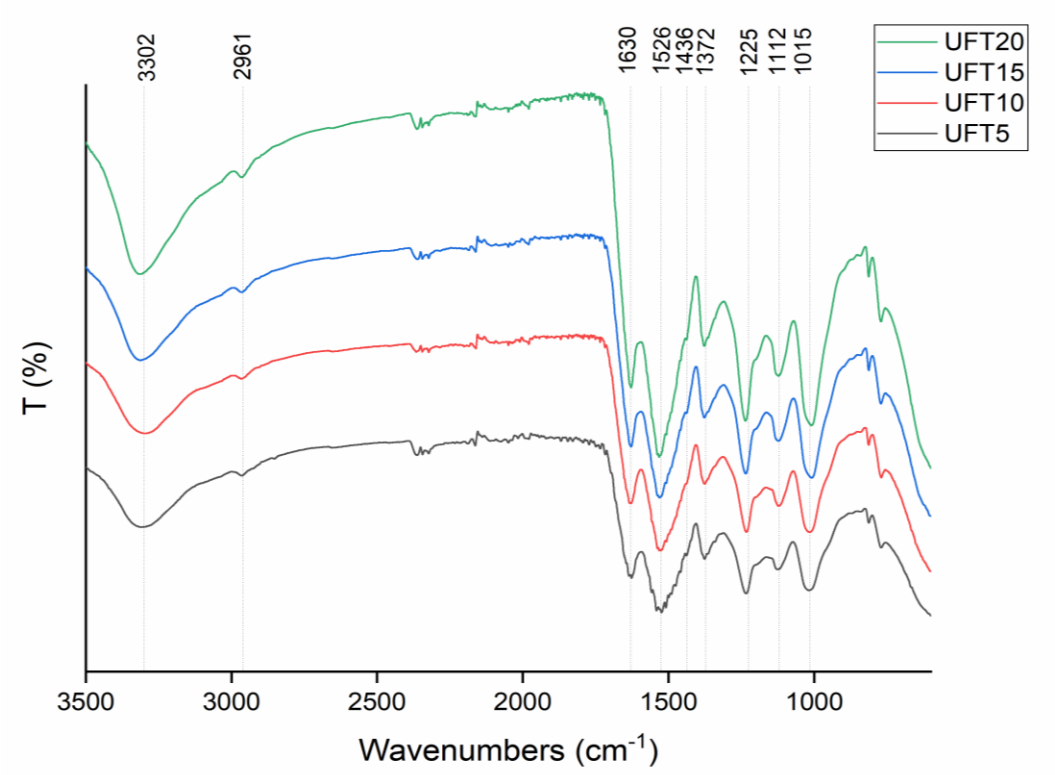

Figure 2. FTIR spectra of cured UF adhesive with different tannin concentrations: 5%, 10%, 15%, and 20%

According to FTIR analysis of UF resin cured after tannin addition, all amid bands did not show significant change. The peak at 1436 cm^{-1} indicates the presence of methylene linkages and increases with tannin percentage. However, characteristic absorption peaks at 1112 cm^{-1} (–C–O stretching vibrations) and 1015 cm^{-1} originated from the methylene ether bridge (–CH_2–O–CH_2) that belong to the C–O stretching vibration of hydroxymethyl increased with increasing tannin concentration indicating the reaction of UF resin and tannin and formation of new ether linkages. Similarly, the weak band at 1361 cm^{-1} (–C–H vibrations in CH_2 and CH_3 structures), broadens with increased tannin concentration. This area of UF polymer spectra is usually assigned to C–H vibrations in CH_2 and CH_3 structures. The spectra of all UFT samples indicated a greater amount of ether and methylene linkages compared to pure UF resin which increased with the addition of tannin.

3.2. Tensile shear strength determination

The tensile shear strengths of examined adhesives are shown in Figure 3.The tensile test results of the samples demonstrated that the resin mixed with tannin (10,15, and 20% by weight) had better performance than the corresponding pure UF resin. Compared to pure UF resin, shear strength was slightly lower in the case with 5% tannin addition but increased with every higher content of tannin. Some authors showed that the addition of tannin to UF resins in particleboards appears to decrease formaldehyde emission over some time proportional to the amount of tannin added but the improvement of the strength performance caused by the denser cross-linking was offset by the decrease of the amount of UF resin [16]. In that case, the formaldehyde emission of tannin-UF resin decreased but the bonding strength was also decreased compared with pure UF resin.Additionally, Zanetti et al. [17] used condensed tannins to improve the heat resistance of UF resins and the result showed that a high percentage of tannin in a UF-tannin blend improves the overall UF thermal resistance to a great extent. However, in this study, tannin was used to substitute some of the UF resin, to reduce formaldehyde emission and to produce an environmentally friendly wood adhesive along with enhanced adhesive properties. The higher shear strength ofUFT compared to UF might be the result of better water resistance of the product arising from the reaction between tannin and UF resin.

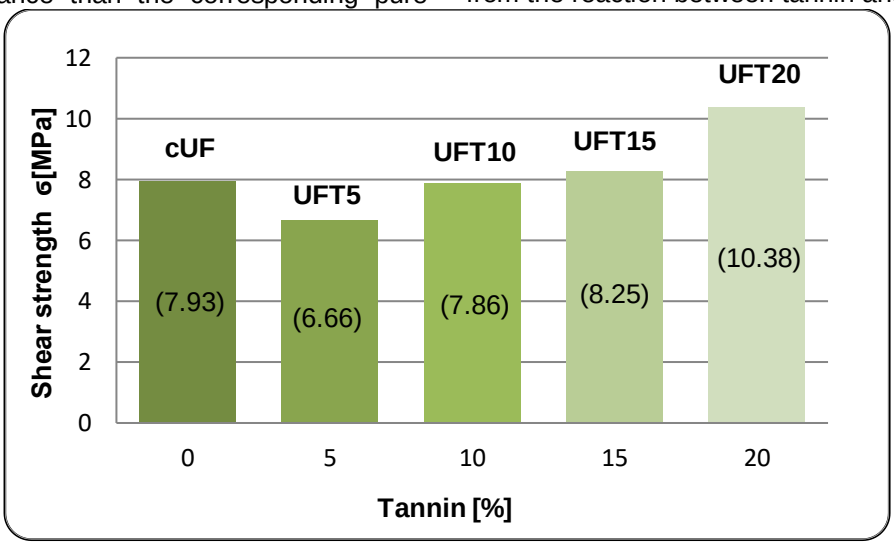

Figure 3. Tensile shear strength of beech wood samples with cured pure UF adhesive (cUF) and samples with added tannin in different concentrations (UFT)

The diverse types of failure after completion of the adhesion tests i.e., cohesive, adhesive, and substrate failure, were considered by analysing the surface of both specimens through high-resolution imaging. Cohesive failure was considered when both samples presented adhesive on the overlapping surfaces; adhesive failure means that only one of the overlapping surfaces had adhesive, whereas substrate failure indicates breakage of the substrate itself so that the bonding surface was not altered.Examination of the failure showed that all samples had a 100% fracture through the wood (Figure 4).The mode of failure is important to take into consideration when discussing the strength of wood adhesives. If the adhesive is stronger than the wood itself, the wood fibers in contact with the adhesive are ripped off. Thus, regarding wood adhesives, wood failure is preferred to obtain well-bonded and high-performance wood composites.

Figure 4. The failure zone of all sample groups: (a) cured pure UF, (b) UF cured with 5% tannin, (c) UF cured with 10% tannin, (d) UF cured with 15% tannin and (e) UF cured with 20% tannin

4. CONCLUSION

Wood adhesives based on UF resin and tannin were prepared (using different concentrations of tannin – 5, 10, 15, and 20%) and characterized and their adhesion properties were investigated to determine their potential as wood adhesives.The main goal of this study was to determine if natural adhesive materials, presented above, can significantly reduce the negative environmental impact of formaldehyde emissions and provide better performance of the adhesive. FTIR results confirmed the reaction between UF resins and tannin due to increased content of ether and methylene linkages. The addition of tannin improved crosslinking in UF resins.Based on characterization results, it was found that tensile shear strength increased with increasing concentration of tannin, while UF-tannin adhesives with tannin concentrations of 15% and 20% showed higher tensile shear strength than the corresponding pure UF adhesive. It was shown that a tannin content of 20% in UF adhesive formulation gave the best performance compared to the one with 5, 10, and 15%, even compared to pure UF adhesive. Therefore, the general conclusion after the experiment is that UF adhesives with the addition of tannin could be used as "green", environmentally-friendly wood adhesives that can show much better characteristics than pure UF in terms of adhesion and mechanical properties.

Acknowledgements

This research was funded by the Ministry of Science, Technological Development and Innovation of the Republic of Serbia, grant number 451-03-65/2024-03/200169.

5. REFERENCES

[1] K.Hirano, M.Asami (2013) Phenolic resins-100 years of progress and their future, React Funct Polym**,** 73(2), 256-269. https://doi.org/10.1016/j.reactfunctpolym.2012.07.003

[2] R.N.Kumar, A.Pizzi (2019) Adhesives for wood and lignocellulosic materials, Beverly, MA: Scrivener Publishing LLC.

[3] M.A.R.Lubis, M.K.Hong, B.D.Park (2018) Hydrolytic removal of cured urea-formaldehyde resins in medium-density fiberboard for recycling, J Wood Chem Technol**,**38(1), 1-14. https://doi.org/10.1080/02773813.2017.1316741

[4] S.Oktay, A.PIzzi, N.Koken, B.Bengu (2024) Tannin-based wood panel adhesives, International, Journal of Adhesion and Adhesives,130, 103621. https://doi.org/10.1016/j.ijadhadh.2024.103621

[5] G.Mashouf Roudsari, A.K.Mohanty, M.Misra (2017) Green approaches to engineer tough biobased epoxies: a review,ACS Sustain Chem Eng *5,* 9528–9541.https://doi.org/10.1021/acssuschemeng.7b01422

[6] A.Pizzi, H.Pasch, K.Rode, S.Giovando (2009) Polymer structure of commercial hydrolyzable tannins by matrix-assisted laser desorption/ionization-time-of-flight mass spectrometry, J Appl PolymSci,113, 3847–3859. https://doi.org/10.1002/app.30377

[7] S.Laurichesse, L.Avérous, L (2014) Chemical modification of lignins: Towards biobased polymers, Prog PolymSci,39, 1266–1290. https://doi.org/10.1016/j.progpolymsci.2013.11.004

[8] M.Parker, P.A.Smith, M.Birse, I.L.Francis, M. J. Kwiatkowski,K.A.Lattey, B.Liebich, M.J.Herderich (2007) The effect of pre-and post-ferment additions of grape derived tannin on Shiraz wine sensory properties and phenolic composition, Aust JGrape Wine Res,13, 30–37. https://doi.org/10.1111/j.1755-0238.2007.tb00069.x

[9] S.Ghahri, X.Chen, A.Pizzi, R.Hajihassani, A.N. Papadopoulos (2021) Natural tannins as new cross-linking materials for soybased adhesives, Polymers, 13(4), 595-610. https://doi.org/10.3390/polym13040595

[10] M.Zanetti, E.Cesprini, M.Marangon, A.Szczurek and G.Tondi (2021) Thermal valorization and elemental composition of industrial tannin extracts, Fuel, 289, 119907.https://doi.org/10.1016/j.fuel.2020.119907

[11] X.Zhou, G.Du (2020) Tannins - Structural Properties, Biological Properties and Current Knowledge, IntechOpen.

[12] M.H.Hussin, N.Latif, T.S.Hamidon, N.N.Idris, R. Hashim, J.N.Appaturi,N.Brosse, I.Ziegler-Devin, L. Chrusiel,W.Fatriasari, F.A.Syamani, A.H.Iswanto, L.S.Hua, S.S.A.O.A.Edrus, W.C. Lum, P.Antov, V.Savov, M.A.R.Lubis, L.Kristak, R.Reh, J.Sedliacik (2022) Latest advancements in high-performance bio-based wood adhesives: A critical review, J Mater Res Technol, 21, 3909-3946. https://doi.org/10.1016/j.jmrt.2022.10.156

[13] X.Chen, A.Pizzi, E.Fredon, C.Gerardin, J.Li, X. Zhou, G.Du (2020) Preparation and properties of a novel type of tannin-based wood adhesive, J Adhes,98(7), 871-888. https://doi.org/10.1080/00218464.2020.1863215
[14] D.Danielli, M.R.Pires, E.da SilvaAraujo, M.S. Lorenço, F.A.Mori (2021) Application of Myrcia Splendens Tannins in the Composition of Urea-Formaldehyde Adhesive for Sustainable Wood Bonding, Res Soc Dev,10(12), e370101220543. https://doi.org/10.33448/rsd-v10i12.20543
[15] J.Peng, X.Chen, J.Zhang, H.Essawy, G.Du, X.Zhou (2022) Characterization on the Copolymerization Resin between Bayberry (Myrica rubra) Tannin and Pre-Polymers of Conventional Urea–Formaldehyde Resin, Forests, 13(4), 624-641. https://doi.org/10.3390/f13040624
[16] G.Xu, H.Tian, X.Xi, J.Song, H.Lei, G.Du (2022) Preparation and characterization of ureafor-maldehyde adhesives modified with glyoxalated tannin, EurJ of Wood Wood Prod, 80, 1215–1223.https://doi.org/10.1007/s00107-022-01819-1
[17] M.Zanetti, V.Causin, R.Saini, A.Cardin, R.Cavalli (2014) Effect of tannin on increasing UF adhesive performance at high temperature investigated by TMA and TGA analysis, EurJ of Wood Wood Prod, 72, 385–392.https://doi.org/10.1007/s00107-014-0795-7

IZVOD

UTICAJ TANINA NA POBOLJŠANJE ADHEZIVNIH SVOJSTAVA UREA-FORMALDEHIDNIH ADHEZIVA

Cilj ovog rada je bio da se ispitaju svojstva urea-formaldehidnog (UF) adheziva sa dodatkom tanina, kako bi se utvrdilo da li je moguće dobiti bioadheziv sa poboljšanim mehaničkim svojstvima u poređenju sa komercijalnim UF. Pripremljene su UF smole na bazi tanina, sa četiri različite koncentracije tanina (5, 10, 15 i 20%), a adhezivna svojstva su ispitana i upoređena sa svojstvima čistog UF. Ispitivanje zatezne čvrstoće na smicanje pokazalo je da dodavanje tanina u formulaciju UF adheziva značajno povećava njegove performanse u poređenju sa čistim UF lepkom. Utvrđeno je da se zatezna čvrstoća na smicanje povećava sa povećanjem koncentracije tanina, dok su UF-taninski lepkoviadhezivi sa koncentracijom tanina od 15% i 20% pokazali veću zateznu čvrstoću na smicanje od odgovarajućeg čistog UF adheziva. Stoga se može zaključiti da UF adheziv na bazi tanina može biti dobar kandidat za primenu kao ekološki prihvatljiv adheziv za drvo sapoboljšanimadhezivnim i mehaničkim svojstvima.
Ključne reči:*adheziv za drvo, UF smola, tanin, bioadhezivi, kompoziti na bazi drveta*

Naučni rad
Rad primljen: 11.06.2024.
Rad prihvaćen:02.07.2024.

Milica Rančić, https://orcid.org/0000-0002-3135-654X
Danica Bajuk Bogdanović, https://orcid.org/0000-0003-2443-376X
Ivana Gavrilović Grmuša, https://orcid.org/0000-0002-6278-4002

Rachana Gaur[1], Ruby Jindal[1], Archana Tripathi[2]

[1]Department of Physics, School of Basic and Applied Sciences, K.R. Mangalam University, Gurugram, Haryana, 122103, India
[2]Department of Physics, Deshbandhu College (University of Delhi), New Delhi, 110019, India

Scientific paper
ISSN 0351-9465, E-ISSN 2466-2585
https://doi.org/10..62638/ZasMat1214

Zastita Materijala 66 (1)
126 -132 (2025)

Identification of optically active vibrational modes of columbite AB_2O_6 using correlation method

ABSTRACT

In the modern era, the examination of molecular structure heavily relies on the application of infrared and Raman spectra within crystalline structures. These methodologies are essential in understanding the arrangement of atoms within molecules and the internal forces governing them. An essential aspect of this analysis involves identifying vibrational modes that can be detected optically. The correlation method is employed to establish rules for selecting these vibrational modes, both in crystals and molecules, through a systematic calculation process that aids in predicting their activity in Infrared (IR) and Raman spectra. The correlation method utilizes group theory to determine which vibrational modes are spectroscopically active in crystals. In our research, our aim is to employ this method to identify the irreducible representations and determine the IR and Raman active vibrational modes of orthorhombic AB_2O_6 compounds within the Pbcn space group. By conducting comprehensive group theory calculations, our objective is to elucidate the spectroscopic properties using the correlation method.

Keywords: *Correlation method, spectroscopy, group theory, columbite-type structure*

1. INTRODUCTION

Due to the large application of IR and Raman modes of crystals, it is useful to know the active spectroscopic modes. The correlation method is employed to establish the selection criteria for both crystals and molecules. The correlation method is preferred over the conventional selection rules due to their time-consuming and laborious procedure. For the molecular structures, it is easy to derive the vibrational modes using selection rules but for the crystals it becomes cumbersome. Lately, there has been an increasing fascination with the investigation of AB_2O_6 oxides, mainly due to their wide-ranging applications and their prevalence in the natural environment.

As a result, there is a pressing demand for comprehensive investigations into their structural characteristics[1], properties, and lattice arrangements. The AB_2O_6 structure represents a class of semiconductor metal oxides that have demonstrated potential for photocatalysis. Columbite-structure AB_2O_6 Oxides are attractive for various applications due to its excellent dielectric properties, as well as its photocatalytic and organic catalytic activities. Typically, the columbite-type structure crystallizes in the orthorhombic space group Pbcn[2].

AB_2O_6 Oxides ($A=Mn^{2+}$, $B=V^{5+}$, here) crystallize in the columbite structure. The cations of A and B are located in the center of the octahedra are surrounded by six oxygen atoms while the AO_6 and BO_6 octahedra share the edges, forming independent zigzag chains. This sequential situation repeats as ABBABB octahedral layers as the chains are connected by sharing corners in order to the AO_6 chain-BO_6 chain-BO_6 chain [3].

In this ongoing dialogue, we have explored AB_2O_6 oxides in their orthorhombic phase with the Pbcn space group, employing the correlation method [4,5].

Through meticulous calculations, we have successfully anticipated the Raman and infrared activities, as well as their associated vibrational modes. Prior to delving into specifics, it is essential to grasp the following terms:

1.t^{γ} = the quantity of movements within the specific site species γ, which can vary between 0 and 3. This data is accessible through the character table.

*Corresponding author: Ruby Jindal
E-mail: ruby.jindal@krmangalam.edu.in
Paper received: 05. 03. 2024.
Paper accepted: 18. 07. 2024.
The website: https://www.zastita-materijala.org/

2.R^{γ} = no. of rotations in site species, it may also have values 0,1,2, or 3 and represented as R_x, R_y, R_z.

3.f^{γ} = the degree of freedom for vibrational and is obtained from $f^{\gamma} = nt^{\gamma}$; n represent no. of equivalent atoms, ions, or molecules in site species.

4.$F_R{}^{\gamma}$ = the degree of freedom for rotational modes inherent in each species γ within an equivalent set of ions or molecules, determined by $F_R{}^{\gamma} = n.R^{\gamma}$

5. a_{γ} = the degrees of freedom provided by each site species γ to a factor group ξ, with a_{γ} derived from $a_{\gamma} = f^{\gamma}/\sum_{\xi} C_{\xi}$

6.C_{ξ} = the multiplicity of species γ within the factor group, as detailed in Table 1. At times, it demonstrates its relationship to the species within the site group.

Table 1: Types of Species and their Corresponding C_{ξ} Values [4]

Species	Value of C_{ξ}
A	1
B	1
E	2
F	3
G	4
H	5

Within the realm of factor group species, irreducible equation provides a clear insight into the tally of lattice vibrations within a corresponding group of similar atoms. Additionally irreducible-representation symbolized as' Γ,' to emphasize that, for the crystal precisely indicates the quantity of lattice vibrations existing within each category of the factor group. It's noteworthy that the irreducible-representation 'Γcrystal' encompasses both acoustical and optical vibrations.

Entire irreducible-representation is obtained by adding irreducible-representations of each equivalent set of atoms [6]

To specifically isolate the optical vibrations, this process entails subtracting the irreducible-representation of acoustical vibrations, resulting in the representation denoted as 'Γoptical':

$$\Gamma optical = \Gamma crystal - \Gamma acoustical$$

A step-by-step discussion of correlation using MnV_2O_6 in orthorhombic structure with space group Pbcn [7] as an example is done here.

Factor group analysis of orthorhombic MnV_2O_6 in Pbcn structure

2. CRYSTALLOGRAPHIC INFORMATION AND SPACE GROUP IDENTIFICATION

The first step of the correlation method is to find the space group and Bravais lattice. The space group and Bravais lattice must be known to get the crystallography of the compound. Here we have the Pbcn space group and orthorhombic crystal structure for the present compound MnV_2O_6.

Z(No of molecules in unit cell)/ L P (lattice points)= Z^B

MnV_2O_6 is four formula unit crystal belonging to space group Pbcn. MnV_2O_6 has 4 equivalent Mn atoms, 8 atoms of Vanadium, and 24 Oxygen atoms in the Bravais unit cell.

Site symmetry

The site symmetry for MnV_2O_6 is as follows:

$$D_{2h}^{14} : 2C_i\,(4);\ C_2(4);\ C_1(8)$$

The number enclosed within the parentheses of site symmetry [9] signifies the count of equivalent atoms that possess that specific site symmetry. For instance, there are four equivalent atoms on sites labeled as C_2, and eight equivalent atoms on sites denoted as C_1. The site C_i can accommodate up to four equivalent atoms, and the coefficient '2' indicates the existence of two distinct types of C_i sites within the unit cell, given in Table 2. It's possible to have atoms on either, both, or neither site within the crystal. It's crucial to verify that the quantity of equivalent atoms corresponds to the capacity stipulated by the site symmetry.

Table 2. Site symmetry and Wycoff position of atoms [8,9]

Atom	Wycoff position	Site symmetry
Mn	4c	$C_2(4)$
V	8d	$C_1(8)$
O_1	8d	$C_1(8)$
O_2	8d	$C_1(8$
O_3	8d	$C_1(8)$

Site $C_2(4)$ is filled with Manganese, while site $C_1(8)$ accommodates both Vanadium and Oxygen. Site $2C_i$ (4) remains unoccupied. The Wyckoff positions are specified as follows: 4c for Manganese, 8d for Vanadium, and 8d each for Oxygen sites labelled as O_1, O_2, and O_3.

Correlation

The subsequent stage involves aligning the site group with the factor group through correlation. Utilizing the correlation table [4], each species within the site group is matched with its counterpart in the factor group. This correlation aids in identifying the species responsible for lattice

vibrations in the crystal, facilitating the prediction of infrared and Raman activity [10,11]. This correlation process establishes the connection between each species in the site group and its corresponding species in the factor group [12].

3. APPLICATION OF CORRELATION METHOD TO MANGANESE ATOMS IS AS FOLLOWS

Manganese is situated at site $C_2(4)$, which accommodates four atoms. According to the character table of site C_2, displacements along the x, y, and z axes are associated with site species A and B. The proper correlation method for relating the C_2 site symmetry to the D_{2h} factor group, as indicated by the Wyckoff description, is based on the presence of Manganese Mn atoms located at the Wyckoff site 4c, where 'c' is associated with the site correlation column C_2 (y) within D_{2h}^{14}. Referring to the correlation table, we can establish that A corresponds to A_g, B_{2g}, A_u, B_{2u}, while B corresponds to B_{1g}, B_{3g}, B_{1u}, and B_{3u}. Therefore, following table 3 & 4 utilizes the correlation method for this purpose.

Table 3. Character Table for C_2 Point Group [4]

C_2	E	C_2		
A	1	1	T_z; R_z	α_{xx}, α_{yy}, α_{zz}, α_{xy}
B	1	-1	T_x, T_y; R_x R_y	α_{xz},, α_{yz}

Table 4: Correlation for the Lattice Vibrations of Manganese in the MnV_2O_6 Crystal in the Pbcn Phase between the Site Group C_2 and Factor Group D_{2h}

n	$f^\gamma = nt^\gamma$	t^γ	Site species $\gamma(C_2)$	correlation	Factor group $\xi(D_{2h})$	C_ξ	a_ξ	species
4	4	T_z (1)	A	→	A_g	1	1	
				→	B_{2g}	1	1	
				→	A_u	1	1	
				→	B_{2u}	1	1	
8	T_x, T_y (2)		B	→	B_{1g}	1	2	
				→	B_{3g}	1	2	
				→	B1u	1	2	
				→	B_{3u}	1	2	

Using the relation, $f^\gamma = a_\gamma \sum_\xi C_\xi$,we can determine the value of the degrees of freedom provided by each site species γ to a factor group a_γ

There are two possible values of f^γ,$f^\gamma = 4$, $f^\gamma = 8$

By employing the equation $f^\gamma = a_\gamma \sum_\xi C_\xi$,

For $f^\gamma = 4$, we find that $4 = 4a_\gamma$, which leads to $a_\gamma = 1$

For $f^\gamma = 8$, the equation $8 = 4a_\gamma$ yields $a_\gamma = 2$.

Utilizing the equation $\Gamma = \sum a_\xi C_{\xi:}$, for the irreducible-representation for the Manganese atom, $\Gamma_{Mn} = A_g + B_{2g} + A_u + B_{2u} + 2B_{1g} + 2B_{3g} + 2B_{1u} + 2B_{3u}$. However, this irreducible-representation encompasses both acoustical and vibrational modes. To isolate the vibrational modes, the acoustic modes must be subtracted.

The correlation method is applied to Vanadium atoms as follows:

The vanadium atom lies on site $C_1(8)$ as shown in Table 5.

Table 5. Character table for the Symmetry Group C_1[4]

C_1	E	
A	1	T_x,T_y,T_z

From the character table of site C_1, translations along x, y, and z corresponds to site A, and from the correlation table A corresponds to A_g, B_{1g}, B_{2g}, B_{3g}, A_u, B_{2u}, B_{1u}, B_{2u}, B_{3u} According to the character table of site C_1, Displacements along the x, y, and z axes are attributed to the site species A. According to the Wyckoff description, the appropriate correlation method to link the C_1 site symmetry to the D_{2h} factor group relies on the existence of Vanadium atoms situated at the Wyckoff site 8d,

where 'd' is associated with the site correlation column C_2 (y) within D_{2h}^{14} . Referring to the correlation table, we can establish that A corresponds to A_g, B_{1g}, B_{2g}, B_{3g}, A_u, B_{2u}, B_{1u}, B_{2u}, B_{3u} Therefore, following Table 6 utilizes the correlation method for this purpose.

Table 6. Correlation for the Lattice Vibrations of Vanadium in the MnV_2O6 Crystal in the Pbcn Phase between the Site Group C_1 and Factor Group D_{2h}

n	$f^\gamma = nt^\gamma$	t^γ	Site species $\gamma(C_1)$	Correlation	Factor group species $\xi(D_{2h})$	C_ξ	a_ξ
8	24	Tx, Ty, Tz	A	→	Ag	1	3
					B1g	1	3
					B2g	1	3
					B3g	1	3
					Au	1	3
					B1u	1	3
					B2u	1	3
					B3u	1	3

Using the relation, $f^\gamma = a_\gamma \sum_\xi C_\xi$,we can determine the value of the degrees of freedom provided by each site species γ to a factor group a_γ

For f^γ =24, 24=8a_γ, we get a_γ =3

Using $\Gamma=\sum a_\xi C_\xi$, irreducible-representation for Vanadium atom

$$\Gamma_V = 3A_g + 3B_{1g} + 3B_{2g} + 3B_{3g} + 3A_u +$$
$$+ 3B_{2u} + 3B_{1u} + 3B_{2u} + 3B_{3u}$$

The correlation method is applied to all three types of Oxygen atom is O_1, O_2 & O_3 atoms as follows:

From the character table of site C_1, translations along x,y, and z corresponds to site A, and from the correlation table A corresponds to A_g, B_{1g}, B_{2g}, B_{3g}, A_u, B_{2u}, B_{1u}, B_{2u}, B_{3u} According to the character table of site C_1, displacements along the x, y, and z axes are associated with site species A.

Table 7. Correlation concerning the lattice vibrations of oxygen atoms O_1, O_2, and O_3 within the MnV_2O_6 crystal in the Pbcn phase, comparing Site Group C_1 with Factor Group D_{2h}

n	$f^\gamma = nt^\gamma$	t^γ	Site species $\gamma(C_1)$	Correlation	Factor group species $\xi(D_{2h})$	C_ξ	a_ξ
8	24	T_x, T_y, T_z	A	→	Ag	1	3
					B1g	1	3
					B_{2g}	1	3
					B3g	1	3
					Au	1	3
					B1u	1	3
					B2u	1	3
					B3u	1	3

The proper correlation method for relating the C_1 site symmetry to the D_{2h} factor group, as indicated by the Wyckoff description, is based on the presence of Oxygen atoms located at the Wyckoff site 8d, where 'd' is associated with the site correlation column C_2 (y) within D_{2h}^{14} . Referring to the correlation table, we can establish that A corresponds to A_g, B_{1g}, B_{2g}, B_{3g}, A_u, B_{2u}, B_{1u}, B_{2u}, B_{3u} Therefore, table 7 gives the correlation method for this purpose**.**

Using the relation, $f^{\gamma} = a_{\gamma} \sum_{\xi} C_{\xi}$,we can determine the value of the degrees of freedom provided by each site species γ to a factor group a_{γ}

For f^{γ} =24,24=8a_{γ}, we get a_{γ} =3.

Using $\Gamma=\sum a_{\xi} C_{\xi}$,we can determine the irreducible representations .Since O_1,O_2,O_3 lies on same Wycoff site 8d , irreducible representations for each Oxygen atom will be same .Therefore, Irreducible-representation for Oxygen O_1, O_2 & O_3

$$\Gamma_{O1,\,O2,\,O3} = 3A_g + 3B_{1g} + 3B_{2g} + 3B_{3g} + 3A_u + 3B_{2u} + 3B_{1u} + 3B_{2u} + 3B_{3u}$$

The overall representation of the crystal, denoted as Γcrystal, can be determined by summing the irreducible representations for each group of equivalent atoms i.e. Mangnese Mn, Vanadium V, three types of Oxygen O_1, O_2, O_3

$$\Gamma_{crystal} = \Gamma_{Mn} + \Gamma_{V} + \Gamma_{O1} + \Gamma_{O2} + \Gamma_{O3}$$

$$\Gamma_{crystal} = 13A_g + 13B_{2g} + 14B_{1g} + 14B_{3g} + 13A_u + 13B_{2u} + 14B_{1u} + 14B_{3u}$$

Acoustic modes are recognized within the factor group due to their similarity in character to translational motion. The acoustical mode representation is denoted as $\Gamma_{acoustical}$ and comprises B_{1u}, B_{2u}, and B_{3u} as indicated in the character table for D_{2h}, which assigns translations to these modes.

The representation $\Gamma_{acoustical}$ consists of B_{1u}, B_{2u}, and B_{3u} as these modes are associated with translations according to the character table of D_{2h} (Table 8).

$$\Gamma_{acoustical} = B_{1u} + B_{2u} + B_{3u}$$

In the realm of vibrational spectroscopy, crystals exhibit vibrational modes that can be categorized into irreducible representations of their respective point groups. Acoustical modes represent the translational motions of the crystal and typically have zero frequency. They are included in the irreducible representations [14] but are not physically meaningful for vibrational spectroscopy. To analyze the relevant vibrational modes, you need to remove these acoustical modes from the irreducible representations.

$$\Gamma_{optic} = \Gamma_{crystal} - \Gamma_{acoustical} = 13A_g + 13B_{2g} + 14B_{1g} + 14B_{3g} + 13A_u + 12B_{2u} + 13B_{1u} + 13B_{3u}$$

Table 8. Character Table for D_{2h} Point Group [4]

D_{2h}	E	$C_2(z)$	$C_2(y)$	$C_2(x)$	i	σ(xy)	σ(zx)	σy(z)	Rot./trans.	Polarization
A_g	1	1	1	1	1	1	1	1		$\alpha_{xx}, \alpha_{yy}, \alpha_{zz}$
B_{1g}	1	1	-1	-1	1	1	-1	-1	R_z	α_{xy}
B_{2g}	1	-1	1	-1	1	-1	1	-1	R_y	α_{xz}
B_{3g}	1	-1	-1	1	1	-1	-1	1	R_x	α_{yz}
A_u	1	1	1	1	-1	-1	-1	-1		
B_{1u}	1	1	-1	-1	-1	-1	1	1	T_z	
B_{2u}	1	-1	1	-1	-1	1	-1	1	T_y	
B_{3u}	1	-1	-1	1	-1	1	1	-1	T_x	

By using character table & correlation table used for D_{2h} space group, infrared and Raman activity can be anticipated. In addition to characters, the character table contains two columns. the vibrational modes represented by symbols Tx, Ty, and Tz belong to irreducible representations that exhibit the same transformation properties as x, y, and z, and they are also active in the infrared spectrum. Another additional column contains various binary combinations of coordinates from which the Raman activity of vibrations can be obtained.

Therefore, we find that Raman active modes are - A_g, B_{1g}, B_{2g}, and B_{3g} and Infrared active modes are A_u, B_{1u}, B_{2u}, and B_{3u}. with A_u representing an inactive mode. These results are presented in tabular form in Table 9. These findings are also reported in the works of Dapeng Xu et al. [15] and Tyagi et al. [16], thereby validating our results.

Table 9. D_{2h} Character Species, Raman and Infrared Active, Acoustical and Silent Modes in the MnV_2O_6 Crystal in phase Pbcn obtained by Correlation Method

Factor Group Species	Translational species	Acoustical mode species	Γcryst	Γvib	Infrared activity	Raman polarization tensor	Raman activity
A_g			13	13		α_{xx}, α_{yy}, α_{zz}	√
B_{1g}			14	14		α_{xy}	√
B_{2g}			13	13		α_{xz}	√
B_{3g}			14	14		α_{yz}	√
A_u			13	13			
B_{1u}	T_x	1	14	13	√		
B_{2u}	T_y	1	13	12	√		
B_{3u}	T_z	1	14	13	√		

4. CONCLUSION

The application of group theory calculations to orthorhombic MnV_2O_6 has facilitated the identification of spectroscopically active vibrational modes within the crystal This calculation involves correlating the site symmetry of each atom within the crystal with the factor group of the crystal. This correlation is crucial in deriving an irreducible-representation for the vibrational modes of the crystal, enabling the separate examination of each mode. The results obtained can be reinforced by accounting for both the atomic degrees of freedom within the crystal and the vibrational degrees of freedom. This comprehensive analysis ensures the accuracy and reliability of the calculated vibrational mode. These results hold significant value, as they can be applied to the study of the microstructure of both the molecules and crystals, shedding light on their dynamic behavior and structural properties. Such insights are essential for understanding the fundamental characteristics of materials and their potential applications.

5. REFERENCES

[1] M. L. Hneda, J.B.Da Cunha, M. A. Gusmão, S.R.Neto, J.Rodríguez-Carvajal O.Isnard (2017) Low-dimensional magnetic properties of orthorho-mbic MnV2O6 : A nonstandard structure stabilized at high pressure.Phys. Rev. B, 95, 024419.

[2] A. Nagarajan, S. Naraginti (2021) Facile solid solution of trirutile and columbite structured oxides Zn1-xLixNb2-xMoxO6 and Zn1-xLixNb2-xWxO6 (x = 0.0-1.0): synthesis and photocatalytic studies. International Journal of Environmental Analytical Chemistry, 103(10), 2240-2253.

[3] L. F. Guleryuz (2023) Effect of Nd3+ Doping on Structural, Near-Infrared, and Cathodoluminescent Properties for Cadmium Tantalate Phosphors. JOTCSA, 10(1), 77–88. doi: https://doi.org/10.18596/jotcsa. 1202284

[4] W.G.Fateley (1972) Infrared and Raman selection rules for molecular and lattice vibrations: the correlation method (No title).

[5] W.Haase , G.William, R.F.Dollish, N. T. McDevitt und F Freeman Bentley (1974) Infrared and Raman Selection Rules for Molecular and Lattice Vibrations: The Correlation Method.Wiley-Interscience, New York 1972. 222 Seiten. Preis:£ 5.45. (Wiley Online Library)

[6] D.Tuschel (2015) The correlation method for the determination of spectroscopically active vibrational modes in crystals. Spectroscopy, 30, 17–22

[7] H.P.Beck (2012) A study on AB2O6 compounds, part II: the branches of the hcp family .Z Für Krist.-Cryst. Mater. 227, 843–58.

[8] E. Tetsi (2017) AB2O6 oxides: potential thermoelectric and magnetic materials. The University of Liverpool (United Kingdom).

[9] T.Hahn, U.Shmueli, J.W.Arthur (1983) International tables for crystallography. (Vol. 1, p.182). Dordrecht: Reidel.

[10] J.R. Ferraro (1975) Factor group analysis for some common minerals. Applied Spectroscopy, 29(5), 418-421. Appl. Spec. 29, 418–421.

[11] D.Rousseau, R.Bauman, S.P.Porto (1981) Normal mode determination in crystals. Journal of Raman Spectroscopy, 10(1), 253-290.

[12] H.Winston, R. S. Halford (1949) Motions of molecules in condensed systems: V. Classification of motions and selection rules for spectra according to space symmetry. The Journal of Chemical Physics, 17(7), 607-616.

[13] J.Peña, P.Bouvier, M.Hneda, C.Goujon, O.Isnard (2021) Raman spectra of Vanadates MV_2O_6 (M= Mn, Co, Ni, Zn) crystallized in the non-usual columbite-type structure. Journal of Physics and Chemistry of Solids, 154, 110034.

[14] A.Tyagi, P.Botella, A.B.Garg, J.Sanchez-Martín, D.Díaz-Anichtchenko, R. Turnbull, S.Anzellini, C.Popescu, D.Errandonea (2024) Temperature and high-pressure study on columbite structured $ZnNb_2O_6$. Results in Physics, 60, 107681.

[15] D.Xu, Y.Liu, Q.Zhou, T.Cui, H.Yuan, W.Wang, Z.Shi, L.Li (2015) Optical phonon behaviors of columbite $ZnNb_2O_6$ single crystal. Journal of Alloys and Compounds, 618 , 694-699.

IZVOD

IDENTIFIKACIJA OPTIČKI AKTIVNIH VIBRACIJSKIH REŽIMA KOLUMBITA AB_2O_6 KORIŠĆENJEM METODE KORELACIJE

U modernoj eri, ispitivanje molekularne strukture se u velikoj meri oslanja na primenu infracrvenog i Ramanovog spektra unutar kristalnih struktura. Ove metodologije su neophodne za razumevanje rasporeda atoma unutar molekula i unutrašnjih sila koje njima upravljaju. Suštinski aspekt ove analize uključuje identifikaciju vibracionih modova koji se mogu optički detektovati. Korelacioni metod se koristi za uspostavljanje pravila za odabir ovih vibracionih modova, kako u kristalima tako i u molekulima, kroz sistematski proces proračuna koji pomaže u predviđanju njihove aktivnosti u infracrvenom (IR) i Raman spektru. Korelacioni metod koristi teoriju grupa da odredi koji su vibracioni modovi spektroskopski aktivni u kristalima. U našem istraživanju, naš cilj je da upotrebimo ovu metodu za identifikaciju nereducibilnih reprezentacija i određivanje IR i Raman aktivnih vibracionih modova ortorombskih AB2O6 jedinjenja unutar Pbcn prostorne grupe. Sprovođenjem sveobuhvatnih proračuna teorije grupa, naš cilj je da razjasnimo spektroskopska svojstva korišćenjem metode korelacije.

Ključne reči: *Korelacioni metod, spektroskopija, teorija grupa, struktura tipa kolumbita*

Naučni rad
Rad primljen: 05. 03. 2024.
Rad prihvaćen: 18. 07. 2024.

Dr. Ruby Jindal: https://orcid.org/0000-0002-8589-5549
Ms. Rachna Gaur: https://orcid.org/0009-0007-8862-6903

*Indu Bhushan[1], Malvika Mehta[1], Mahima Sharma[1], Chitrakshi Chopra[1], Ratna Chandra[1], Ikhwan Syafiq Mohd Noor[2], Muhd Zu AzhanYahya[3], Ashutosh Tripathi[4], Arvind Kumar Yadav[1]**

[1]School of Biotechnology, Shri Mata Vaishno Devi University, Katra, India, [2]Physics Division, Centre of Foundation Studies for Agricultural Sciences, Universiti Putra Malaysia, UPM Serdang, Selangor Darul Ehsan, Malaysia, [3]DefenceScience and Technology, University Pertahanan, Nasional Malaysia(UPNM), Malaysia, [4]Department of Environmental Science, Nagaland University, Hqrs Lumami, Nagaland, India

Review paper
ISSN 0351-9465, E-ISSN 2466-2585
https://doi.org/10.62638/ZasMat 1098

Zastita Materijala 66 (1)
133 - 147 (2025)

Role of nanomaterials in modern agriculture

ABSTRACT

Agriculture is a foundation of several emerging countries, and it is one of the most economically significant drivers. Farmers, consumers, and the environment are all at risk as a result of the increased usage of mineral fertilizers and harmful pesticides. Over the last few years, substantial research into the application of Nanotechnology to boost agricultural productivity has been undertaken. Nanoparticles (NPs) have been discovered to be beneficial as nanopesticides, nanobiosensor, nanofertilizers, and nanoremediation in agrifood production. Nutrients, pesticides, fungicides, and herbicides are compacted with a variety of NPs to facilitate the progressive release of fertilisers and pesticides, resulting in exact dose accessibility to plants. Nanofertilizers improve nutrient utilization, reduce nutrient deficiencies, reduce soil toxicity, and lessen the negative consequences of overdosing, all while reducing treatment frequency. Nanoformulations are used in agriculture to boost germination of seed, reduce nutrient losses in fertilization, reduce the amount of pesticides dispersed, aid water and nutrient management, and. This review also discusses various challenges and concerns about pesticide product development, formulation, and toxicity for ecologically friendly and sustainable agriculture.

Keywords:*Agriculture, nanofertilizers, nanobiosensors, nanopesticides, nanoformulations, nanomaterials*

1. INTRODUCTION

Nanotechnology has gained prominence in recent decades as a technological breakthrough in the food industry. It is a nanometer-scale platform that enables the creation and usage of novel materials by macromolecules, molecules, or atoms with a size of 1–100 nm- [1].Nanoscience has revolutionized the concept of industrialization, and both the developing and developed nations are keen to invest more in this innovation due to the plethora of opportunities for the creation and application of novel structures, materials, and systems in fields such as agriculture, food, and medicine, among others [2]. Consumers' growing knowledge of the health advantages of food and agricultural goods is pressuring research communities, industry leaders, and farmers to discover a solution to increase food quality without compromising nutritional values.

Currently, nanoscience and its associated technologies are widely regarded as having enormous promise for a wide range of research and applications, including the food and agriculture industries [2]. Agriculture is also optimistic about the long-term viability of this fast-growing technology. Nanotechnology aids agriculture in the production of pesticides and chemical fertilizers by utilizing nanocapsules and nanoparticles (NPs) that have the potential to increase effectiveness, control or delay delivery, absorption, and the production of eco-friendly nanocrystals to enhance the capacity of pesticides for their implementation at lower doses, thereby reducing pollution [3].Nanotechnology can be used as a broad prospect and covers all major application areas, including, agriculture wastewater treatment, bioremediation of pesticide resistance, nano-biosensors, and nanomaterial production for agriculture, due to its unique features[4, 5].Less use of chemical fertilizers and pesticides will help in maintaining the natural ecological balance of geo-biological cycles, which has been mess up or disrupted by synthetic chemicals. Researchers are developing agricultural input nano-formulations and encapsulation, which they have tested in vitro and in vivo on a number of

*Corresponding author: Arvind Kumar Yadav
E-mail: arvind.smvdu@gmail.com
Paper received: 22.05. 2024.
Paper corrected: 24.07. 2024.
Paper accepted: 15.08. 2024.
The website: https://www.zastita-materijala.org/

crops. According to Kuzma et al., 2006 food packaging, animal decontamination and nano-medication, plant defense and fertilizer implementation, genetic manipulation of plants, pollution and restoration of water in the ecosystem, and nano-sensing are all examples of how nanotechnology can be employed in the agri-food business [6]. Insufficiencies in amount of macronutrient and micronutrient, population growth, industrial development, shrinking of water sources, alteration in soil conditions, and erosion of top most soil layer are all factors that affect agriculture, according to this. The fundamental basis for using fertilizer in crop production is to deliver complete micro and macro nutrients that are mostly lacking in soil. Although some fertilizers have a direct impact on plant development, thus accounts for 35-40% of agricultural productivity. To solve all of these shortcomings in a quicker and summary way, nanotechnology can be one of the applications. Given the importance of fertilizers, producing nano-based fertilizers would be a groundbreaking invention in this field [7].

Nanofertilizers boost nutrient usage efficiency (NUE) by three times and help plants deal with stress. Nanotechnology increases biological source utilisation and is environmentally friendly in nature, boosts carbon absorption, and enhances soil aggregation, regardless of the type of crop. Nanotechnology is the study of atoms at the nanoscale level, with an emphasis on their optical, catalytic, magnetic, and physical characteristics [8]. On the other hand, much as biotechnology has a detrimental influence on acquired resistance or gene modification, nanotechnology has a negative imprint on the biological and chemical atmosphere[9]. As a result, before integrating nanotechnology in agricultural techniques, an environmental impact analysis is required. As NUE (nano-fertilizers) increase the nutrient use efficiency three times as well as it also enables plant to tolerate various biotic and abiotic stresses. Nanotechnology can be used on all crop types, it increase the biosource use and also is ecofriendly in nature. It also helps plant in carbon uptake and improves aggregation of soil. As nanotechnology is the science based on nanoscale range, it collects information of atomic particles, with respect to physical, magnetic, optical and catalytic properties [8].On the other hand, we also know that there are some negative impact of biotechnology like resistance development, manipulation of gene pool, same case is with nanotechnology. It also have some side effects on chemical and biological environment [9]. Thus, it also becomes important to access the environmental impact of nanotechnology before approving it for agricultural practices.

2. FACETS OF NANOTECHNOLOGY IN AGRICULTURE AND FOOD SCIENCE

Nanotechnology is an illustration of a commonly utilised technology with the potential to revolutionise civilisation. Packaging, irrigation, and water filtration, animal feed aquaculture, and other related industries may practically cover every aspect of the agriculture and food sector [10]. Nanotechnology has the potential to transform the agriculture and food industries by offering new techniques and instrumentsfor diagnosis of diseases, targeted treatment, and enhancing plants' capability of nutrient absorbance, fight infections, and withstand environmental stresses, as well as improving plant processing, storage, and packaging [11]. Nanotechnology has given rise to novel customized solutions to problems in plants and food science (post-harvest commodities), as well as novel approaches for rational raw material procurement and processing to enhance crop product quality [12]. Oxygen can cause food to decay and discolour, which is a problem in food packaging and hence was resolved with the development of new nonmaterial for the food packaging. In order to develop these polymers, nanoparticles are used in a zigzag pattern which displayed novel characteristics by acting as a barrier that stops oxygen from entering. Fruit has recently been coated with nano-coatings that completely cover it and prevent it from losing weight or shrinking in size [13]. With the usage of different novel mediators such as nano-sensors, nanoparticles, nano-pesticides, nano-fertilizers, and antimicrobial agentsthe fast spread of nanotechnology has accelerated the changes of traditional food and agriculture systems.The food industry has taken an interest in nanomaterial-based components since many of them include critical nutrients while being non-toxic. Furthermore, the nanoparticles are found to withstand pressure and temperature extremes [2].Nanotechnology has been suggested as having a positive impact on food science and nutrition by increasing the shelf-life of eatables, assisting in the tracking and tracing of contaminants, developing improved food storage strategies, and developing value-added health supplements or antimicrobial agents into food. Nanotechnology could make a significant contribution to food science and agriculture by employing a variety of unique processes and materials such as nanofibers nanomaterials, nanoencapsulation, nanoemulsions, and carbon nanotubes [14].

3. NANOMATERIALS

Nanoparticles are one to one hundred nanometers in size (10^{-9} m). Each particle throughout this scale exhibits different mechanical,

optical, and electrical properties as compared to substantial matter, which makes sense given the increased surface area per unit weight or volume in the nano form. Nanoparticles have a privilege over bulk counterparts because of their Surface Plasma Resonance (SPR), Surface Enhanced Raman Scattering (SERS), and Enhanced Rayleigh Scattering (ERS) attributes, which contributes to their development as the foundation for optoelectronics, next-gen electronics, biochemical, and chemical sensors[15, 16]. As a result, nanomaterials have successfully established themselves as among the most intriguing microscopic materialswith enormous implications in engineering, medicine, food, and agriculture. A variety of nanomaterials have been suggested for application in agriculture to greatly lower pesticide usage through smart delivery systems, eliminate nutrient deficiencies, and boost productivity through better water and nutrient management [17]. Nonmaterial which can be amorphous or crystalline can function as transporters for gases or liquid droplets. These nanoparticles should be considered a different state of matter from solid, gaseous, liquid, and plasma states due to their quantum size outcomes and large surface area[18]. Several types of nonmaterial are now in use, including crystalline nonmaterial (fullerenes and carbon nanotubes)[19].

4. NANOEMULSION

Nanoemulsions are heterogeneous particulate complexes with oil-in-water emulsion properties that contain solid spheres with amorphous and lipophilic surfaces and droplet sizes ranging from 10 to 1000 nm[20]. Nanoemulsions provide superior optical clarity, physical stability, and bioavailability as compared to conventional emulsions[21]. Nanotechnology applications have been investigated in the food and agriculture sector to enhance food security around the world, such as providing edible coatings for dairy products, cheese, vegetables, fruits, meat, and fish, or smart packaging of foods, which helps to improve the standard of the food [22].Nanoemulsions are a new food bioactive delivery technology made up of emulsified water in oil or oil in water droplets ranging in size from 50 to 1000 nanometres. The molecule's centre is made up of either oil or water. Even dispersion and active component diffusion through the surfaces are benefits of tiny droplet size in nanoemulsions. Nanoemulsions further improve bioactive component penetration due to the low surface tension and large surface area of the whole emulsion. Furthermore, the manufacturing of both water in oil or oil in water emulsions necessitates a surfactant concentration of 3–10% [23]. Food-grade nanoemulsions are being used more and more to improve encapsulation, absorbability, digestibility, targeted delivery, and bioavailability of active ingredients. Because of the earlier advantages of nanoemulsions over normal emulsions, their use in the food industry has increased. Stabilizers including emulsifiers, weighing agents, ripening retarders and texture modifiers can improve the kinetic stability of nanoemulsions. To improve and enhance pharmacological effects, food-grade derived nanoemulsions are progressively getting employed to incorporate diverse bioactive constituents such as polyunsaturated fatty acids (PUFAs) and Omega-3 fatty acids [24].

5. NANOENCAPSULATION

With the passage of time and advancements in nanotechnology, food bioactive constituents have been explored in systems ranging from simple food systems to very sophisticated systems dubbed innovative bioactive delivery systems. Several of nanotechnology's fundamental achievements in food science include altering the texture of food products, discovering new flavours and fragrances, controlling the discharge of flavours, enhancing the bioavailability of nutritive value, and encapsulating additives and bioactive food components. Encapsulation was first used in biotechnology to enhance the quality of production processes and to promote the degradation of generating cells and their by-product [25]. Later, encapsulation was used to nanotechnology and was shown to be substantially more effective than conventional encapsulating. Encapsulation is a novel method of entrapping active elements or bioactive components/substances in matrix that allow for the controlled release of their payload under regulated settings and rates. Nutrients are protected from uncontrolled conditions using encapsulation methods until they are released in a controlled way. As a result, nanoencapsulation, also known as nanocapsules, is defined as the encapsulation of active components (solids, liquids, and gases) in nanometre-sized capsules[26]. The distribution of any bioactive material to different bodily regions is influenced by particle size [27].When compared to microencapsulation, nanoencapsulation has the potential to improve the controlled release, precise targeting and bioavailability of bioactive substances[28]. Particle size, surface area, shape, size distribution, encapsulation efficiency, solubility, andas well as release mechanisms, have all been documented to be affected by the encapsulation technique and delivery system. As a result, selecting the appropriate encapsulation method based on the required size, physicochemical properties, core material type, and wall material is becoming increasingly crucial. Nanoencapsulation

techniques are also more difficult to master than microencapsulation techniques. The major reasons for this include the difficulties in establishing a complex morphology of the capsule and core material, as well as the needs of nanoencapsulate release rates[29].

6. NANOPARTICLES AS A SMART DELIVERY AGENT

The use of nanoparticles as 'smart' delivery systems is an intriguing use of nanoparticles in the field of life sciences. They have already been proposed as 'magic bullets' in 1906 by Nobel laureate P. Ehrlich [30].Delivery systems are critical in agriculture for pesticide and fertiliser administration, as well as plant improvement via genetic material. Pesticide application techniques must focus on efficacy improvement and spray drift management, whereas fertiliser bioavailability is hindered by soil chelation, over-application, and run-offs. Controlled delivery systems for pesticide and fertiliser application offer a feasible solution to these issues. Figure 1 depicts various applications of nanomaterials in the form of nanosensores, nanofertilizers, nanopesticides, nanoherbicides, etc in agriculture for assessing the risk factors and preventing them. The goal of the controlled delivery strategy is to release essential and sufficient amounts of agrochemicals over time in order to achieve maximum biological efficacy while minimising negative consequences [31].In a species-independent method, gene transfer via bombardment of DNA-absorbed gold particles has proved successful in producing transgenic plants [32]. Torney et al. (2007) discovered that silica nanoparticles internalised in plant cells may efficiently transfer DNA and chemicals without the use of specialised equipment[33]. To do this efficiently, it is necessary to conduct research on how transport andpenetration operate within the entire plant, its tissues, and cells. The purpose of this study is to develop and apply microscopy tools and techniques with a range of resolutions that are readily available in most research institutes in order to visualise and track the transport and deposition of magnetic nanoparticles inside plants, as well as to explore the potential of concentrating magnetic nanoparticles into specific areas of plants using small magnets. For this reason, sub-micronic and micronic particles were studied as pesticide delivery vehicles. Due to its larger surface area, easy adhesion, and rapid mass transfer, nanoparticles (1000 nm) have the advantage of effective loading over micronic particles (1000 nm). The slow release features of the nanomaterial, the bonding of the chemicals to the material, and the ambient circumstances all contribute to controlled release of the active ingredient. When it comes to genetic material, delivery mechanisms confront obstacles such as restricted cell membrane transit, host range, and nucleus trafficking. Nonetheless, the use of NPs to assist in the transmission of genetic information in order to generate insect-resistant crops is being researched. For example, DNA-coated gold nanoparticles are used as bullets in a device called a 'gene gun' to assault plant tissues and cells in order to induce gene transfer[34].

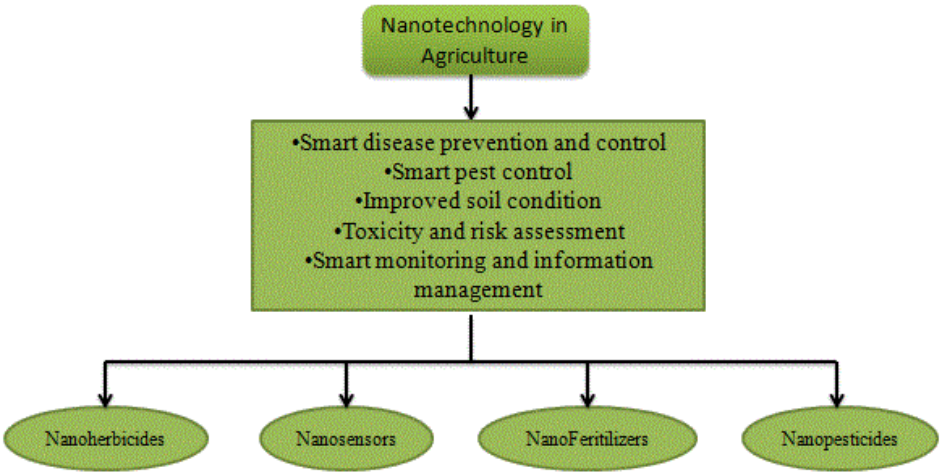

Figure 1. Applications of nanomaterials in the form of nanosensores, nanofertilizers, nanopesticides, nanoherbicides, etc in agriculture for assessing the risk factors and preventing them

7. NANOSENSORS

Nanotechnology-based sensing has exploded in popularity, with a wide range of applications in the food and agriculture industries. Nano-technology enables real-time monitoring of crop progress and farm status, including soil fertility, moisture content, crop nutrition capacity, temperature, plant diseases and pathogens [35]. Nanosensors are emerging as feasible agricultural and food production technology. They significantly

outperform conventional chemical and biological approaches in terms of selectivity, speed, and sensitivity. Nanosensors may be used to assess the presence of pollutants, microbes, and the freshness of food. Nanosensors are made up of tiny particles such as carbon nanotubes (high surface area), nanoscale wires (high detection sensitivity), nanoparticles, polymer nanomaterials and thin films.These sensors determine a swap in conductance when a semiconducting carbon nanotube is revealed to specific chemicals. In this current study, we are exploring the applicability and significance of nanosensors in agricultural production and crop management. [35]. Nanosensors, with their chemical and electrooptical capabilities, can help to mitigate the drawbacks of food packaging. Gases, smells, chemical pollutants, viruses, and even changes in ambient conditions can all be detected by nanosensors. Food safety is enhanced by the use of nanosensors, which guarantee that customers receive fresh and appealing foods and help prevent the spread of food-borne diseases. Nanosensors provide a number of benefits over conventional sensors, notably near real-time detection and high sensitivity and selectivity, low cost and mobility, and other significant characteristics that are enhanced when nanoparticles are incorporated into their design. [36].Smart nanosensors have been constructed that can be connected to a GPS system, enabling real-time surveillance of crop husbandry feasible through the use of separate biosensors [37]. Numerous nanosensors are being designed for a variety of agricultural and food industry purposes, including rapidly identifying hazards in the event of potential food illness and putting nanotracers into packaging to demonstrate the food product's history and standard at any given moment. For occasion, nanosensors embedded in food packaging that ascertain microbe growth and alter colour when a preset threshold is met, and nanosensors used during on-line management system to track storage conditions, can assist avoid food poisoning. [38]. It should be noted that nanosensors are important for sensing as well as reporting real-time information about products from production through distribution to consumers. Nanosensors are distant from being merely a passive information-gathering gadget. Nanosensors dispersed throughout the field can detect the presence of plant viruses as well as the quantity of soil nutrients. They also reduce fertilizer use and pollutants in the environment [39]. They are capable of collecting and evaluating data both from remote and local areas, as well as recording, recording, and reporting on it. Nanosensors may be used to handle critical control points along the distribution chain, from the stage of manufacturing or packaging to the point of consumption. Recent improvements have enabled nanosensors to give superior assurance by detecting germs, toxins, and pollutants across the food production chain and capturing data for automated control functions and documentation[36].

8. NANOFERTILIZERS

Fertilizers have been utilised in agriculture for many years forthe advantage of farmers. Traditional fertilisers are not only costly, but they are also damaging to humans and the environment. Nanotechnology is emerging as a possible option in the form of nanofertilizers for the development of environmentally friendly fertilisers with high nutritional value and soil and environment friendliness[40]. A nanofertilizer is made up of nanoformulations of nutrients that are delivered to plants in a way that allows for prolonged and uniform absorption. Nanofertilizers are divided into three types based on the kind of formulation:1) nanoscale fertiliser, which is traditional fertiliser that has been decreased in size and is usually in the form of nanoparticles; 2) standard fertiliser including a supplement nanomaterial is known as nanoscale additive fertiliser, and 3) Nutrients enclosed by nanofilms or intercalated into nanoscale pores of a host material are referred to as nanoscale coating fertiliser [40]. The classification of nanofertilizers is based on nutritional categorization in this case. As a result, micronutrient (Fe, Mn, Zn, Cu, Mo, and Ni) and macronutrient (N, P, K) nanofertilizers are the two most common forms of nanofertilizers.Chemical (bottom-up), physical (top-down), and biological (biosynthetic) techniques can all be used to make nanomaterials for nanofertilizers. The top-down method focuses on lowering the density of bulk counterparts to well-organized nanoscale assemblies. Top-down is a physical method based on material milling. Two disadvantages of this method are the limited control over the size of nanoparticle and a larger quantity of impurities. The bottom-up method begins with molecular level chemical reactions to make nanoparticles. Due to the fact that this is a scientifically controlled synthetic process, it improves particle size control and removes impurities [41, 42]. In addition to physical and chemical methods, nanoparticles may be made biologically utilising the so-called biosynthetic methodology. There are a variety of natural sources for this function, including plants, fungus, and bacteria. The advantage of this method is that it allows for more precise control of particle toxicity and size [43, 44].

Nanofertilizers should be developed to have all of the required features, such as high solubility, stability, time-controlled release, efficiency,

increased targeted action with effective concentration, lower eco-toxicity with a safe, and simple means of administration. The following is the procedure for loading nutrients onto these nanoparticles: (a) Assimilation of nanoparticles, (b) Ligand mediated adherence on nanoparticles, (c) Encapsulation of nanoparticles in polymeric jacket, (d) Nanoparticles entrapment, and (e) Nanoparticles synthesis formed of the nutrient itself [45].

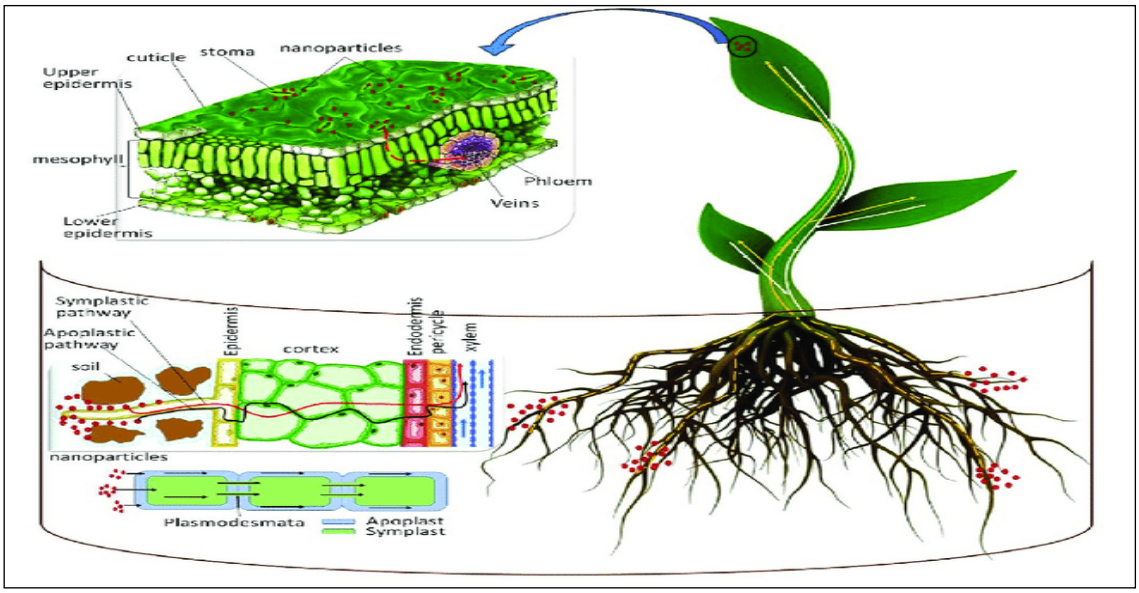

Figure 2. Mechanism of action ofnano-fertilizer

Crops can be fertilised with nanoparticles via leaves and roots. NPs have the ability to penetrate endodermis and epidermis of the root, penetrating the xylem vessels and delivering them to aerial portion of the plant. Additionally, NPs can be captured by the stomata of the leaf and transported throughout the plant via the phloem. [46]. NPs must pass through pores in the cell wall that typically range from 3 to 8 nanometers in both cases. As a result, only NPs with a diameter smaller than 8 nm may flow via holes and penetrate the plasma membrane. Absorption and translocation of nanoparticles may vary amongst plants, dependent on the plant's physiology and numerous routes of uptake, transportation, and dispersion[47]. Plants respond to NPs in a number of ways. This emerges to be especially relevant for metal oxide-based nanofertilizers, in which the plant must battle with both the parent nanomaterials and the metal ions produced during the dissolution of customised nanofertilizers[48, 49]. A carrot experiment contrasting the absorbance of metallic oxide nanoparticles (ZnO, CeO_2, or CuO) to that of metal ions indicated because both non-metal oxides and metal ions were absorbed. Such absorption and accumulation in edible portions may not only affect the physiology of plants, but also offer serious health risks to humans [50]. Metallicoxide nanoparticles accumulated on the carrot's outermost surface and did not penetrate the fleshy edible portion, although metallic ions did. Cucumber plants have demonstrated biotransformation in the presence of CeO_2nanoparticles. The biotransformation reduced Ce (IV) to Ce (III) by 15% and 20% in roots and shoots, respectively[51].

The aggregation of nanoparticles is determined by a variety of parameters, but mostly by the plant species, the tissue/organ utilised straightforwardly as food or for food preparation, and the kind and size of the nanoparticles. Due to the variety in the interactions between NPs and plants, nanoparticles employed in nanofertilizers can aggregate in plants and, in certain situations, create toxicity hazards to both plants and humans. For instance, multi-walled carbon nanotubes cause phytotoxicity in red spinach (*Amaranthus tricolour L.),* inhibiting growth, producing reactive oxygen species, and resulting in cell death [52]. CeO_2 nanoparticles can aggregate and inhibit soybean's ability to fix nitrogen[53]. In chick pea, nanoparticles of zinc oxide boosted germination, root growth, and indole acetic acid production. In Maize, nano-silicon dioxide conferred drought tolerance, increased the number of lateral roots, and increased shoot length. In spinach, nano-TiO_2 boosted vigour indicators and chlorophyll content[54]. In maize, nano-iron slag powder decreased insect pest incidence. In cotton, nano-iron and organic organic fertilizers regulate nutrient release, operate as an effective pesticide, and promote soil fertility. Grapes contain gold

nanoparticles and sulphur, which works as an antioxidant. Polyethylene and indium oxide were discovered to promote vegetable photosynthesis. Apart from these, there are a variety of nanofertilizers that offer good characteristics to agriculture from a human welfare standpoint [54].

Nanofertilizers increase the efficiency with which nutrients are used. They improve yield by enhancing plant growth and metabolic processes such as photosynthesis. More nutrient availability aids in the improvement of crop quality parameters such as protein, sugar content,the prevention of biotic and abiotic stress and oil content. Nanofertilizers regulate the rate and dose of encapsulated nutrients and fertilisers to increase crop plant uptake and also reduce fertiliser waste and demand. They increase microbial activity and improve water-holding capacity and soil quality [55].Due to their sensitivity, nanomaterials can combine with many components of their surroundings, resulting in transformation and modification of their physicochemical characteristics. Nanofertilizers can collect in plant sections, inhibiting development, generating reactive oxygen species, and ultimately causing cell death. Due to the reactivity and unpredictability of nanomaterials, safety concerns have been raised for employees who may come into contact with them during their manufacture and use in the field [55].

Table 1. Impact of nanofertilizers on various crop growths

Nanofertilizers					
Nanoparticles	Plant source	Size	Concentration	Impact	Ref.
Aluminium	Ryegrass, Corn, lettuce	1–100 nm	2,000 mg L^{-1}	Decreased root length	[56]
Copper	Lettuce	1–100 nm	0.013% (*w*/*w*)	improved shoot/root ratio	[57]
Copper	Mung bean	1–100 nm	<200 mg L^{-1}	Reduced seedling growth	[58]
Copper	Zucchini	50 nm	1,000 mg L^{-1}	Reduced biomass	[59]
Gold	Cucumber, lettuce	10 nm	62, 100 and 116 mg L^{-1}	Positive effect on germination index	[60]
Iron	Barley, flax, ryegrass	1-100 nm	2,000 and 5,000 mg L^{-1}	Completely inhibited germination	[61]
Silver	Wheat	10 nm	0.5, 1.5, 2.5, 3.5 and 5.0 mg kg^{-1}	Reduced shoot and root length	[62]
Zinc	Corn, cucumber, lettuce, radish, rapeseed, ryegrass		2,000 mg L^{-1}	Reduced root growth and elongation	[56]

9. ROLE OF NANOPARTICLES IN CROP PROTECTION AND PEST MANAGEMENT

Pesticides are valuable for crop protection, disease prevention, food safety, and material safety. However, it is lethal to humans, animals, and non-target organisms. Nanopesticide compositions can improve water solubility, bioavailability, and preserve agrochemicals from deterioration in the environment, revolutionising disease, weed, and pest management in crops [74]. By manipulating the outer layer of the nanocapsules, which releases a small dose over a long period of time and eliminates undesirable pesticide run-off, nanoencapsulation of pesticides is advantageous in controlled and gradual release of active component[37].The size range of nanocapsules and nanoparticles between 0.1 and 1000 nm is critical for plant defence. The nanocapsule's shell contains medicinal substances in its centre. This nanocapsule assists in the entry of agrochemicals into plant tissue, stabilises active ingredients, and releases steadily, gently, or completely once the shell is opened. Shell rupture is reliant on physiological pH changes or enzymatic breakdown and is also dependent on the external environment of nanocapsules[75]. Pesticides embedded in nanoparticles are now being designed with the objective of delivering them on a scheduled basis or in response to an environmental trigger[37].

The use of Ag nanoparticles (AgNPs) as a pesticide-free alternative to suppress sclerotium-forming phytopathogenic fungus was examined. When fungal hyphae were exposed to AgNPs, the sections of the hyphal wall disintegrated and the hyphae collapsed. AgNPs were also tested for their effect on undiscovered fungal species of the genus Raffaelea that cause oak tree mortality, and it was discovered that AgNPs had a detrimental influence on conidial germination [76].

Table 2. Impact of various nanopesticides

Nanoparticles	Size	Concentration	Effective against	Impact	Ref.
Silicon	20–60 nm	1, 1.5, 2, and 2.5 g/kg	*Callosobruchus maculates*	Insects and larvae are killed in a dose-dependent manner. It's good for keeping grain safe while it's being kept.	[63]
Silicon		200, 300, and 400 ppm	*Spodopteralittoralis*	Induces the death of larvae in a dose-dependent manner. After 15 days, the plant's lifetime and number of leaves per plant had increased.	[64]
Silicon	20–30 nm	50, 100, 200, and 300 ppm	*Rhyzoperthadominica, Triboliumconfusum*	Insects are killed in a dose and size-dependent manner. The effect of NPs was found to be stronger on wheat grains than on barley grains. It's good for keeping grains safe while they're being stored.	[65]
Silver		0.1 µg/mL	*Xanthomonascampestris pv. Campestris*	Substantial cabbage decrease, black rot in the growth chamber	[66]
Validamycin loadednano sized calciumcarbonate	50–200 nm		*Rhizoctoniasolani*	Validamycinnano formulation has a higher germicidal efficacy	[67]
Thiamine di-lauryl sulfate (TDS) nano	(258.6 nm)	100 ppm	*C. gloeosporioides*	The Halfa was destroyed by 80 percent growth suppression of C. gloeosporioides and TDS nano particles	[68]
Chitosan nano particles	20-100 nm		*Rhizopus sp. Colletotrichum capsici, C. gloeosporioides,*	In comparison to the control, mycelia growth is delayed.	[69]
Nano copper		0.2 ppm	*Xanthomonasaxonopodis pv. punicae*	Nano copper suppressed development 10,000 times more effectively than the commonly prescribed amount of Cu-oxychloride	[70]
Titanium		≈500 to 800 ppm	*Xanthomonasperforans*	Photocatalytic activity that is significantly higher than that of the control and decreasedbacterial spotwithout causing any negative consequencesimpact on yield.	[71]
Copper nano particles	11–55 nm		*Phytophthorainfestans*	At lower doses, it was more effective than commercial agrochemicals	[72]
Silvernano particles	1-100 nm		*Xanthomonas performance*	When compared to untreated tomato transplants, the bacterial spot disease was reduced.	[73]
Titanium with zinc	1-100 nm		Bacteria	When compared to the untreated control and other commercial bactericides, there was a signify-cant reduction in bacterial spot.	[71]

10. NANOPARTICLES MECHANISM OF ACTION

Here we discuss the major mechanisms underlying nanomaterial toxicity, including (1) NPs' effects on ATP production, DNA replication, and gene expression; (2) NPs' generation of reactive oxygen species (ROS); (3) NPs' disruption of the integrity of cell membranes; (4) NPs' disruption of energy transduction; (5) NPs' release of toxic components; and (6) NPs' destabilisation and oxidation of proteins.

11. IMPACT ON ATP PRODUCTION, DNA REPLICATION AND GENE EXPRESSION

At low concentrations, nano ions may interact with enzymes in the respiratory chain, including NADH dehydrogenase, leading to the uncoupling of ATP generation from respiration. Furthermore, the binding of ionic nanoparticles to the transport protein results in proton leakage and the breakdown of the proton motive force[77]. Additional proteomic tests on *Bacillus thuringiensis*-exposed silver nanoparticles demonstrated an influence on the aggregation of envelope protein precursors, suggesting a function for the proton motive force[78]. DNA marking and DNA cleavage are two applications of nanomaterial interactions with nucleic acids. In contrast to the beneficial uses of DNA-nanomaterial conjugation, fullerenes have been discovered to bind DNA and produce strand deformation, thereby impacting the molecule's function and stability. Cross-linking, DNA strand breakage, and sugar or base adducts are all secondary effects of ROS released by certain nanoparticles[79]. Gene polymerization in vivo utilising polymerase chain reaction (PCR) revealed frequent DNA alterations in cells that had taken up nano ions .Sunscreens containing titanium dioxide nanoparticles may cause supercoiled DNA to become nicked due to the presence of oxygen radicals. Cleavage of double-stranded DNA by photosensitive fullerenes is very context-dependent and requires a specific fullerene derivative. Despite these findings, few investigations on nanoparticle genotoxicity using Ames tests or other protocols have been undertaken, and little is known about their mutagenic effect [80]. Nanoparticles and ions may impact DNA replication and gene expression. Silver ions impede DNA replication [79]. Silver nanoparticles attach to E. coli DNA, impairing DNA replication [81].

12. REACTIVE OXYGEN SPECIES (ROS) GENERATION

Distinct kinds of nanoparticles create different forms of ROS by reducing oxygen molecules. Mitochondria produce most ROS from oxidative cellular metabolism. ROS are hydroxyl (OH^{-}), superoxide (O^{2-}), hydrogen peroxide (H_2O_2), and singlet oxygen ($^1O_2$) [82, 83]. Chemical constitution of designed nanoparticles determines ROS production [84]. ROS are created by nanoparticle absorption and cause cellular oxidative stress, nanotoxicity, DNA damage, cell signalling manipulation, cell motility changes, apoptosis, cytotoxicity, and cancer promotion and initiation [85]. ROS targets DNA. Oxidative DNA damage includes base and sugar lesions, DNA-protein crosslinks, double- and single-strand breaks, and basic sites [86]. ROS play a significant role in some biological processes and in governing cell physiology and function by influencing signal transduction pathways [87]. Normal circumstances balance ROS generation in microbial cells. Cell redox balance promotes oxidation with high ROS production. Unbalanced conditions generate oxidative stress, which destroys microbial cells. Xia et al. (2008) and Yin et al. (2012) found that oxidative stress alters cell membrane permeability and damages microbial cell membranes [82, 88].

13. NANOTECHNOLOGY IN SUSTAINABLE FARMING

The most challenging global issue is ensuring food security for the world's rapidly growing population. According to projections, the world's food demand would climb from 59 to 98 percent by 2050, when the global population will reach 9 billion people [89]. Agriculture supports the majority of the world's population, either directly or indirectly. Chemicals such as insecticides and fertilizers are commonly used to increase food production. Pesticides are employed in agriculture to combat biotic stressors, but they have a detrimental impact on crop quality and soil health. Excessive fertiliser application, such as ammonium salts, nitrate, phosphate compounds, or urea results in a deterioration in soil quality [90]. Nanotechnology is being widely used in modern agriculture to make precision agriculture a reality. Nanoparticles with one or more dimensions of 100 nm or less are included in nanotechnology [90]. It's an exciting new field of science with plentiful applications in both basic and applied sciences [91]. As a future instrument, nanotechnology may be utilised to repair agricultural divisions; it aids in the discovery of crops' biochemical pathways by displacing conventional methods for studying environmental problems and their implementation to production upgrades [92]. Nanotechnology has led to the development of a wide range of nanomaterials, including nanopesticides, nanoinsecticides, nanoparticles and nano emulsions. The material used for production of nanomaterials are plant extracts, metal oxides, silicates, ceramics, lipids, emulsions and polymers[93].The potential use of nanoscale agro - chemicals such as nanoformu-lations, nanopesticides, nanosensors and nano-fertilizershas revolutionised traditional agricultural approaches. Nanotechnology in agriculture can play a vital role to remediate wastewater, improve soil quality and increase crop output using sensors that detect diseases [2, 94]. It is critical to develop cost-effective, high-performing insecticides, pesti-cides that are environmentally friendly too. Pesticides that are made using concepts like nanotechnology, which could reduce toxicity, improve shelf life, and enhance the solubility of pesticides that are poorly water soluble, all of which could have a good environmental impact [95,96]. There are about 400 companies which are commencing research and development in

nanotechnology sector throughout the world, and the number is predicted to rise to more than 1000 in this decade. In the imminent era of agricultural mechanization, new nanotechnology tools and methods can enhance the way agriculture is seen and has a significant future. Precision delivery of fertilizers and nutrients, as well as disease diagnosis at an early stage, have a bright future thanks to biotechnological advancements and the use of nanomaterials to create faster and more precise diagnosis instruments [97].

Nanoparticles possess distinctive interactions within the human body, owing to their diminutive size and heightened responsiveness, which give rise to a range of health issues. Nanoparticles have the ability to trigger oxidative stress by producing reactive oxygen species (ROS), which can result in cellular damage and inflammation [98]. These can have an impact on many organs and systems, potentially leading to the development of diseases such as cancer, cardiovascular ailments, and neurodegenerative disorders. Exposure to specific nanoparticles can induce both acute and chronic inflammation, which can result in tissue damage and contribute to the development of illnesses such as asthma and other respiratory disorders [99]. Nanoparticles have the ability to engage with DNA, resulting in genetic alterations and abnormalities in the structure of chromosomes. The genotoxic effect has the potential to elevate the susceptibility to cancer and other genetic problems. Nanoparticles have the ability to disturb cell membranes, resulting in either cell demise or impairment [100]. This can undermine the structural soundness of different tissues and organs. Nanoparticles can elicit an immunological response as they are perceived as alien entities by the immune system, which can have either beneficial or detrimental effects on the body. This can lead to either hypersensitivity or immunological suppression, which can impact the body's capacity to combat infections and diseases[101]. Certain nanoparticles have the ability to traverse the blood-brain barrier, which could result in neurological consequences and harm to the brain[102]. This gives rise to worries regarding their utilization in medical applications and the possibility of neurotoxicity.

14. CONCLUSION

Innovative tools are now being created that will incorporate nanodevices that will be capable of successfully replacing a variety of various forms of biological equipment. Nanotechnology may enable quick improvements in agricultural research, including reproduction science and technology capable of producing vast amounts of seeds and fruits regardless of the season or period. Nanofertilizers are critical in agriculture for increasing output and resilience to abiotic stressors. Thus, the potential uses of nanofertilizers, nanosensors, and other nanomaterials in agriculture, biotechnology, and horticulture cannot be underestimated. Additionally, nanomaterials were evaluated for their ability to enhance plant height, germination rate, root growth and number of roots, leaf chlorophyll, and antioxidant content of fruits. To attain sustainable crop yields, smart nanofertilizers with the ability to release nutrients according to the plants' temporal and geographical requirements must be developed. In plants, early diagnosis of stress and alleviation of stress effects, as well as disease prevention and treatment are all important.

The entire potential of nanotechnology in the agriculture and food sectors has not yet been realised, although it is rapidly progressing from theoretical knowledge to implementation. To combat viruses, spores, and other crop diseases, agriculture will benefit from smart sensors and smart delivery systems. Before items are commercialised, we must assess the influence of nanotechnology on agriculture. Nanomaterial accumulation and its negative impact on the environment are also key concerns and crucial in the application of nanotechnology. More research is needed to examine the environmental effect of nanomaterials and estimate the non-toxic concentration for each crop.

Acknowledgements

We are really grateful to the School of Biotechnology, Shri Mata Vaishno Devi University, and also to our students who were involved in this work for their unremitting efforts.

Author contribution For research and conceptualization, M.M., M.S.,A.K.Y, A.S.and I.B.; methodology, M.M., M.S.,A.K.Y; validation, M.M., M.S., and I.B.; formal analysis, M.M., M.S., A.K.Yand I.B.; investigation,M.M. and M.S.; resources, A.K.Y., M.M., and M.S.; data curation, M.M. and M.S., C.C.,A.K.Y. ; writing—original draft preparation, M.M., M.S.,R.C.; writing—review and editing, M.Z.A.Y.,A.S.,I.M.N., M.M., M.S., R.C., C.C.; visualization, M.M., M.S.,,A.S. and I.B.; supervision, AKY; all authors have read and agreed to the published version of the manuscript.

Data availability All data generated or analysed during this study are included in this published article and its supplementary information file.

Declarations

Ethics approval and consent to participateNot applicable.

Consent for publication: Not applicable.

Conflict of interest: The authors declare no competing interests.

15. REFERENCES

[1] V.Mohanraj, Y.Chen (2006) Nanoparticles-a review. Tropical Journal of Pharmaceutical Research, 5(1), 561-573. https://doi.org/10.4314/tjpr.v5i1.14634.

[2] T.Singh, S.Shukla, P.Kumar, V.Wahla, V.K. Bajpai, I.A. Rather (2017) Application of nanotechnology in food science: perception and overview. Frontiers in Microbiology, 8, 1501-1512. https://doi.org/10.3389/fmicb.2017.01501.

[3] R.L. Manjunatha, D. Naik, K. V. Usharani (2019) Nanotechnology application in agriculture: A review. Journal of Pharmacognosy and Phytochemistry, 8(3), 1073-1083.

[4] N. Dasgupta, S. Ranjan, A.R. Chakraborty, C. Ramalingam, R. Shanker, A. Kumar (2016) Nano agriculture and water quality management. Nanoscience in Food and Agriculture, Springer, 1, 1-42, https://doi.org/10.1007/978-3-319-39303-2_1.

[5] A.Haleem, M.Javaid, R.P.Singh, S.Rab, R.Suman (2023) Applications of nanotechnology in medical field: a brief review. Global Health Journal, 7(2), 70-77. https://doi.org/10.1016/j.glohj.2023.02.008.

[6] J. Kuzma, P. VerHage (2006) Nanotechnology in agriculture and food production: anticipated applications. Project on emerging nanotechnologies

[7] E. Corradini, M. De Moura, L. Mattos (2010) A preliminary study of the incorporation of NPK fertilizer into chitosan nanoparticles. Express Polymer Letters, 4(8), 324-329. https/doi.org/ 10.3144/expresspolymlett.2010.64.

[8] O. Sadik, A. Zhou, S. Kikandi, N. Du, Q. Wang, K. Varner (2009) Sensors as tools for quantitation, nanotoxicity and nanomonitoring assessment of engineered nanomaterials. Journal of Environmental Monitoring, 11(10), 1782-1800, https://doi.org/10.1039/B912860C.

[9] H.C. Sharma, K.K. Sharma, N. Seetharama, J.H. Crouch (2003). The utility and management of transgenic plants with Bacillus thuringiensis genes for protection from pests. Journal of New Seeds, 5(1), 53-76,https://doi.org/10.1300/J153v05n01_04.

[10] X. He, H. Deng, H..M.. Hwang (2019). The current application of nanotechnology in food and agriculture. Journal Of Food And Drug Analysis, 27(1), 1-21, https://doi.org/10.1016/j.jfda.2018.12.002

[11] G.N.G. Saritha, T. Anju, A. Kumar (2022) Nanotechnology-Big impact: How nanotechnology is changing the future of ag-riculture? Journal of Agriculture and Food Research, 10, 100457, https://doi.org/10.1016/j.jafr.2022.100457.

[12] M. Sharon, A.K. Choudhary, R. Kumar (2010) Nanotechnology in agricultural diseases and food safety. Journal of Phytology, 2(4).

[13] B. Predicala (2009) Nanotechnology: potential for agriculture. Prairie Swine Centre Inc, University of Saskatchewan, Saskatoon, SK, 123-134.

[14] C.D. Ferreira, I.L. Nunes (2019) Oil nanoencapsulation: development, application, and incorporation into the food market. Nanoscale Research Letters, 14, 1-13, https://doi.org/10.1186/s11671-018-2829-2.

[15] M.A. Hahn, A.K. Singh, P. Sharma, S.C. Brown, B.M. Moudgil (2011) Nanoparticles as contrast agents for in-vivo bioimaging: current status and future perspectives. Analytical and Bioanalytical Chemistry, 399, 3-27, https://doi.org/10.1007/s00216-010-4207-5.

[16] A. Gloskovskii, D. Valdaitsev, L. Viduta, S. Nepijko, G. Schönhense (2010) Investigation of the local electron emission from current-carrying silver nanoparticle films by an emission electron microscope. Thin Solid Films, 518(14), 4030-4034, https://doi.org/10.1016/j.tsf.2010.01.021.

[17] S. Dwivedi, Q. Saquib, A.A. Al-Khedhairy, J. Musarrat. (2016) Understanding the role of nanomaterials in agriculture. Microbial Inoculants in Sustainable Agricultural Productivity: Vol. 2: Functional Applications, 271-288, https://doi.org/10.1007/978-81-322-2644-4_17.

[18] E. Gaffet (2011) Nanomatériaux: Une revue des définitions, des applications et des effets sur la santé. Comment implémenter un développement sûr. Comptes Rendus Physique, 12(7), 648-658, https://doi.org/10.1016/j.crhy.2011.06.002.

[19] D. Vollath. (2013). Nanomaterials: an introduction to synthesis, properties and applications. John Wiley & Sons,978-3-527-67186-1

[20] M. Jaiswal, R. Dudhe, P. Sharma (2014) Nanoemulsion: an advanced mode of drug delivery system. 3 Biotech ,5(2),123-127. https://doi: 10.1007/s13205-014-0214-0.

[21] D.J. McClements, J. Rao (2011) Food-grade nanoemulsions: formulation, fabrication, properties, performance, biological fate, and potential toxicity. Critical Reviews in Food Science and Nutrition, 51(4), 285-330, https://doi.org/10.1080/10408398.2011.559558.

[22] J. Jampilek, J. Kos, K. Kralova (2019) Potential of nanomaterial applications in dietary supplements and foods for special medical purposes. Nanomaterials, 9(2), 296-304. https://doi.org/10.3390/nano9020296.

[23] N.H. Che Marzuki, R.A. Wahab, M. Abdul Hamid (2019) An overview of nanoemulsion: concepts of development and cosmeceutical applications. Biotechnology & Biotechnological Equipment, 33(1), 779-797. https://doi.org/10.1080/13102818.2019.1620124

[24] M.A. Salem, S.M. Ezzat (2019) Nanoemulsions in food industry. Some New Aspects Of Colloidal Systems in Foods, 2, 238-267, http://dx.doi.org/10.5772/intechopen.79447.

[25] S.M. Jafari (2017) Nanoencapsulation technologies for the food and nutraceutical industries. Academic Press.

[26] V. Suganya, V. Anuradha. (2017) Microencapsulation and nanoencapsulation: a review. Int. J. Pharm. Clin. Res., 9(3), 233-239 https://doi.org/10.25258/ijpcr.v9i3.8324

[27] Y. Kawashima (2001). Nanoparticulate systems for improved drug delivery. Adv. Drug Del. Rev., 47, 39-54.

[28] M.R. Mozafari, J. Flanagan, L. Matia-Merino, A. Awati, A. Omri, Z.E. Suntres, H. Singh (2006) Recent trends in the lipid-based nanoencapsulation of antioxidants and their role in foods. Journal of the Science of Food and Agriculture, 86(13), 2038-2045, https://doi.org/10.1002/jsfa.2576.

[29] C.F. Chau, S. H. Wu, G. C. Yen (2007) The development of regulations for food nanotechnology. Trends in Food Science & Technology, 18(5), 269-280, https://doi.org/10.1016/j.tifs.2007.01.007.

[30] F. Himmelweit (2017) The collected papers of paul ehrlich: In four volumes including a complete bibliography. Elsevier. 9780080090542.

[31] K. Tsuji. (2001) Microencapsulation of pesticides and their improved handling safety. Journal of Mcroencapsulation, 18(2), 137-147, https://doi.org/10.1080/026520401750063856.

[32] P. Christou, D.E. McCabe, W.F. Swain (1988) Stable transformation of soybean callus by DNA-coated gold particles. Plant Physiology, 87(3), 671-674, https://doi.org/10.1104/pp.87.3.671.

[33] F. Torney, B.G. Trewyn, V.S.-Y. Lin, K. Wang (2007). Mesoporous silica nanoparticles deliver DNA and chemicals into plants. Nature nanotechnology, 2(5), 295-300, https://doi.org/10.1038/nnano.2007.108.

[34] P.S. Vijayakumar, O.U. Abhilash, B.M. Khan, B.L. Prasad (2010) Nanogold-loaded sharp-edged carbon bullets as plant-gene carriers. Advanced Functional Materials, 20(15), 2416-2423, https://doi.org/10.1002/adfm.200901883.

[35] M.S. Johnson, S. Sajeev, R.S. Nair (2021) Role of Nanosensors in agriculture. In 2021 International Conference on Computational Intelligence and Knowledge Economy (ICCIKE) (pp. 58-63). IEEE https://doi.org/10.1109/ICCIKE51210.2021.9410709

[36] J. Lu, M. Bowles (2013) How will nanotechnology affect agricultural supply chains? International Food and Agribusiness Management Review, 16(2), 21-42 http://dx.doi.org/10.22004/ag.econ.148580.

[37] S. Agrawal, P. Rathore (2014) Nanotechnology pros and cons to agriculture: a review. Int J Curr Microbiol App Sci,. 3(3), 43-55.

[38] M.A. Augustin, P. Sanguansri. (2009) Nanostructured materials in the food industry. Advances in Food and Nutrition Research, 58, 183-213 https://doi.org/10.1016/S1043-4526(09)58005-9.

[39] R. Prasad, V. Kumar, K.S. Prasad (2014) Nanotechnology in sustainable agriculture: present concerns and future aspects. African Journal of Biotechnology, 13(6), 705-713, https://doi.org/10.5897/AJBX2013.13554.

[40] E. Mastronardi, P. Tsae, X. Zhang, C. Monreal, M.C. DeRosa (2015) Strategic role of nanotechnology in fertilizers: potential and limitations. Nanotechnologies in Food and Agriculture, 25-67, https://doi.org/10.1007/978-3-319-14024-7_2

[41] G. Singh, H. Rattanpal (2014) Use of nanotechnology in horticulture: a review. Int. J. Agric. Sci. Vet. Med, 2(1): p. 34-42.

[42] S. Pradhan, D.R. Mailapalli (2017) Interaction of engineered nanoparticles with the agri-environment, Journal of Agricultural and Food Chemistry.65(38) (2017) 8279-8294, https://doi.org/10.1021/acs.jafc.7b02528.

[43] H. El-Ramady, N. Abdalla, T. Alshaal, A. El-Henawy, M. Elmahrouk, Y. Bayoumi, T. Shalaby, M. Amer, S. Shehata, M. Fári (2018) Plant nano-nutrition: perspectives and challenges, Nanotechnology, food security and water treatment, Springer, 129-161 https://doi.org/10.1007/978-3-319-70166-0_4.

[44] T.P. Yadav, R.M. Yadav, D.P. Singh (2012) Mechanical milling: a top down approach for the synthesis of nanomaterials and nanocomposites. Nanoscience and Nanotechnology, 2(3), 22-48, https//doi.org/10.5923/j.nn.20120203.01.

[45] T. Kalra, P.C. Tomar, K. Arora (2020) Micronutrient encapsulation using nanotechnology: nanofertilizers. Plant Arch, 20(2), 1748-1753.

[46] S.D. Ebbs, S.J. Bradfield, P. Kumar, J.C. White, C. Musante, X. Ma. (2016) Accumulation of zinc, copper, or cerium in carrot (Daucus carota) exposed to metal oxide nanoparticles and metal ions. Environmental Science: Nano, 3(1), 114-126, https://doi.org/10.1039/C5EN00161G.

[47] N. Odzak, D. Kistler, R. Behra, L. Sigg (2014) Dissolution of metal and metal oxide nanoparticles under natural freshwater conditions. Environmental Chemistry, 12(2), 138-148 https://doi.org/10.1071/EN14049..

[48] G.V. Lowry, K.B. Gregory, S.C. Apte, J.R. Lead (2012) Transformations of nanomaterials in the environment. ACS Publications https://doi.org/10.1021/es300839e.

[49] J.C. White, J. Gardea-Torresdey (2018) Achieving food security through the very small. Nature Nanotechnology, 13(8), 627-629 https://doi.org/10.1038/s41565-018-0223-y.

[50] M.L. López-Moreno, C. Cassé, S.N. Correa-Torres (2018) Engineered NanoMaterials interactions with living plants: Benefits, hazards and reg-ulatory policies. Current Opinion in Environmental Science & Health, 6, 36-41 https://doi.org/10.1016/j.coesh.2018.07.013.

[51] Y.K. Mohanta, D. Nayak, K. Biswas, S.K. Singdevsachan, E.F. Abd_Allah, A. Hashem, A.A. Alqarawi, D. Yadav, T.K. Mohanta (2018) Silver nanoparticles synthesized using wild mushroom show potential antimicrobial activities against food borne pathogens. Molecules, 23(3), 655, https://doi.org/10.3390/molecules23030655.

[52] V.L.R. Pullagurala, I.O. Adisa, S. Rawat, S. Kalagara, J.A. Hernandez-Viezcas, J.R. Peralta-Videa, J.L. Gardea-Torresdey. (2018) ZnO nanoparticles increase photosynthetic pigments and decrease lipid peroxidation in soil grown cilantro (Coriandrum sativum). Plant Physiology and Biochemistry, 132, 120-127 https://doi.org/10.1016/j.plaphy.2018.08.037.

[53] J.H. Priester, Y. Ge, R.E. Mielke, A.M. Horst, S.C. Moritz, K. Espinosa, J. Gelb, S.L. Walker, R.M. Nisbet, Y.-J. An (2012) Soybean susceptibility to manufactured nanomaterials with evidence for food quality and soil fertility interruption. Proceedings of the National Academy of Sciences, 109(37) , E2451-E2456, https://doi.org/10.1073/pnas.1205431109.

[54] M.A. Iqbal (2029) Nano-fertilizers for sustainable crop production under changing climate: a global perspective. Sustainable crop production, 8 ,1-13, http://dx.doi.org/10.5772/intechopen.89089

[55] M. Bernela, R. Rani, P. Malik, T.K. Mukherjee. (2021) Nanofertilizers: Applications and Future Prospects, Nanotechnology: Principles and Applications. Routledge, 289-332

[56] D. Lin, B. Xing (2007) Phytotoxicity of nanoparticles: inhibition of seed germination and root growth, Environmental pollution,150, 243-250, https://doi.org/10.1016/j.envpol.2007.01.016.

[57] V. Shah, I. Belozerova (2009) Influence of metal nanoparticles on the soil microbial community and germination of lettuce seeds. Water, Air, and Soil Pollution, 197(1), 143-148 https://doi.org/10.1007/s11270-008-9797-6.

[58] W.M. Lee, Y.J. An, H. Yoon, H.S. Kweon, Toxicity and bioavailability of copper nanoparticles to the terrestrial plants mung bean (Phaseolus radiatus) and wheat (Triticum aestivum): plant agar test for water-insoluble nanoparticles. Environmental Toxicology and Chemistry: An International Journal, 27(9), 1915-1921 https://doi.org/10.1897/07-481.1.

[59] D. Stampoulis, S.K. Sinha, J.C. White. (2009) Assay-dependent phytotoxicity of nanoparticles to plants. Environmental Science & Technology, 43(24) ,9473-9479, https://doi.org/10.1021/es901695c.

[60] R. Barrena, E. Casals, J. Colón, X. Font, A. Sánchez, V. Puntes (2009) Evaluation of the ecotoxicity of model nanoparticles. Chemosphere, 75(7) , 850-857, https://doi.org/10.1016/j.chemosphere.2009.01.078

[61] Y.S. El-Temsah, E.J. Joner. (2012) Impact of Fe and Ag nanoparticles on seed germination and differences in bioavailability during exposure in aqueous suspension and soil. Environmental Toxicology, 27(1), 42-49.

[62] C.O. Dimkpa, J.E. McLean, N. Martineau, D.W. Britt, R. Haverkamp, A.J. Anderson. (2013) Silver nanoparticles disrupt wheat (Triticum aestivum L.) growth in a sand matrix. Environmental Science & Technology , 47(2), 1082-1090.

[63] M. Rouhani, M. Samih, S. Kalantari (2013) Insecticidal effect of silica and silver nanoparticles on the cowpea seed beetle, Callosobruchus maculatus F.(Col.: Bruchidae).

[64] A. El-Helaly, H. El-Bendary, A. Abdel-Wahab, M. El-Sheikh, S. Elnagar (2016) The silica-nano particles treatment of squash foliage and survival and development of Spodopteralittoralis (Bosid.) larvae, Pest Control, 5,6.

[65] M. Ziaee, Z. Ganji (2016) Insecticidal efficacy of silica nanoparticles against Rhyzopertha dominica F. and Tribolium confusum Jacquelin du Val. Journal of Plant Protection Research ,56(3).

[66] L. Gan, W. Xu, M. Jiang, B. He, M. Su. (2010) A study on the inhibitory activities of nano-silver to Xanthomonas campestris pv. campestris. Acta Agriculturae Universitatis Jiangxiensis, 32(3) ,493-497.

[67] K. Qian, T. Shi, T. Tang, S. Zhang, X. Liu, Y. Cao (2011) Preparation and characterization of nano-sized calcium carbonate as controlled release pesticide carrier for validamycin against Rhizoctonia solani. Microchimica Acta, 173(1), 51-57. https://doi.org/10.1007/s00604-010-0523-x.

[68] Y.-C. Seo, J.-S. Cho, H.-Y. Jeong, T.-B. Yim, K.-S. Cho, T.-W. Lee, M.-H. Jeong, G.-H. Lee, S.-I. Kim, W.-B. Yoon (2011) Enhancement of antifungal activity of anthracnose in pepper by nanopaticles of thiamine di-lauryl sulfate. Korean Journal of Medicinal Crop Science, 19(3), 198-204, https://doi.org/10.7783/KJMCS.2011.19.3.198.

[69] N. Chookhongkha, T. Sopondilok, S. Photchanachai (2012) Effect of chitosan and chitosan nanoparticles on fungal growth and chilli seed quality, International Conference on Postharvest Pest and Disease Management in Exporting Horticultural Crops, 973, 231-237 https://doi.org/10.17660/ActaHortic.2013.973.32.

[70] K.K. Mondal, C. Mani (2012) Investigation of the antibacterial properties of nanocopper against Xanthomonas axonopodis pv. punicae, the incitant of pomegranate bacterial blight. Annals of Microbiology, 62(2) ,889-893. https://doi.org/10.1007/s13213-011-0382-7.

[71] M.L. Paret, G.E. Vallad, D.R. Averett, J.B. Jones, S.M. Olson (2013) Photocatalysis: effect of light-activated nanoscale formulations of TiO2 on Xanthomonas perforans and control of bacterial spot of tomato. Phytopathology, 103(3) , 228-236, https://doi.org/10.1094/PHYTO-08-12-0183-R..

[72] K. Giannousi, G. Sarafidis, S. Mourdikoudis, A. Pantazaki, C. Dendrinou-Samara (2014) Selective synthesis of Cu2O and Cu/Cu_2O NPs: antifungal activity to yeast Saccharomyces cerevisiae and DNA interaction. Inorganic Chemistry, 53(18), 9657-9666, https://doi.org/10.1021/ic501143z.

[73] I. Ocsoy, M.L. Paret, M.A. Ocsoy, S. Kunwar, T. Chen, M. You, W. Tan (2013) Nanotechnology in plant disease management: DNA-directed silver nanoparticles on graphene oxide as an antibacterial against Xanthomonas perforans,.Acs Nan , 7(10), 8972-8980, https://doi.org/10.1021/nn4034794.

[74] M. Chaud, E.B. Souto, A. Zielinska, P. Severino, F. Batain, J. Oliveira-Junior, T. Alves (2021) Nanopesticides in agriculture: Benefits and challenge in agricultural productivity, toxicological risks to human health and environment. Toxics, 9(6), 131, https://doi.org/10.3390/toxics9060131.

[75] H. Chhipa, P. Joshi (2016) Nanofertilisers, nanopesticides and nanosensors in agriculture. Nanoscience in Food and Agriculture, Springer, 247-282 https://doi.org/10.1007/978-3-319-39303-2_9.

[76] R. Nair, S.H. Varghese, B.G. Nair, T. Maekawa, Y. Yoshida, D.S. Kumar (2010) Nanoparticulate material delivery to plants. Plant science, 179(3), 154-163

[77] K.B. Holt, A.J. Bard, Interaction of silver (I) ions with the respiratory chain of Escherichia coli: an electrochemical and scanning electrochemical microscopy study of the antimicrobial mechanism of micromolar Ag+. Biochemistry, 44(39), 13214-13223,https://doi.org/10.1021/bi0508542.

[78] C.N. Lok, C.M. Ho, R. Chen, Q. Y. He, W. Y. Yu, H. Sun, P.K.H. Tam, J. F. Chiu, C.M. Che (2006) Proteomic analysis of the mode of antibacterial action of silver nanoparticles. Journal of Proteome Research, 5(4) , 916-924. https://doi.org/10.1021/pr0504079.

[79] S.J. Klaine, P.J. Alvarez, G.E. Batley, T.F. Fernandes, R.D. Handy, D.Y. Lyon, S. Mahendra, M.J. McLaughlin, J.R. Lead (2008) Nanomaterials in the environment: behavior, fate, bioavailability, and effects. Environmental Toxicology and Chemistry: An International Journal, 27(9) ,1825-1851,https://doi.org/10.1897/08-090.1.

[80] E. Karimi, E. Mohseni Fard (2017) Nanomaterial effects on soil microorganisms. Nanoscience and plant–soil systems,Springer, 137-200 https://doi.org/10.1007/978-3-319-46835-8_5

[81] W. Yang, C. Shen, Q. Ji, H. An, J. Wang, Q. Liu, Z. Zhang (2009) Food storage material silver nanoparticles interfere with DNA replication fidelity and bind with DNA. Nanotechnology, 20(8), 085102, https://doi.org/10.1088/0957-4484/20/8/085102

[82] J. J. Yin, J. Liu, M. Ehrenshaft, J.E. Roberts, P.P. Fu, R.P. Mason, B. Zhao (2012) Phototoxicity of nano titanium dioxides in HaCaT keratinocytes—generation of reactive oxygen species and cell damage. Toxicology and applied pharmacology, 263(1), 81-88. https://doi.org/10.1016/j.taap.2012.06.001.

[83] P.P. Fu, Q. Xia, H.-M. Hwang, P.C. Ray, H. Yu (2014) Mechanisms of nanotoxicity: generation of reactive oxygen species. Journal of Food and Drug Analysis, 22(1) , 64-75. https://doi.org/10.1016/j.jfda.2014.01.005

[84] L. Gonzalez, D. Lison, M. Kirsch-Volders. (2008) Genotoxicity of engineered nanomaterials: a critical review. Nanotoxicology, 2(4), 252-273 https://doi.org/10.1080/17435390802464986.

[85] C. Blaise, F. Gagné, J. Ferard, P. Eullaffroy (2008) Ecotoxicity of selected nano-materials to aquatic organisms. Environmental Toxicology: An International Journal, 23(5), 591-598. https://doi.org/10.1002/tox.20402.

[86] M. Valko, C. Rhodes, J. Moncol, M. Izakovic, M. Mazur (2006) Free radicals, metals and antioxidants in oxidative stress-induced cancer. Chemico-biological interactions, 160(1), 1-40. https://doi.org/10.1016/j.cbi.2005.12.009.

[87] D. Vara, G. Pula (2014) Reactive oxygen species: physiological roles in the regulation of vascular cells. Current Molecular Medicine, 14(9), 1103-1125

[88] T. Xia, M. Kovochich, M. Liong, L. Madler, B. Gilbert, H. Shi, J.I. Yeh, J.I. Zink, A.E. Nel (2008) Comparison of the mechanism of toxicity of zinc oxide and cerium oxide nanoparticles based on dissolution and oxidative stress properties. ACS Nano., 2(10), 2121-2134. https://doi.org/10.1021/nn800511k.

[89] J.A. Duro, C. Lauk, T. Kastner, K.H. Erb, H. Haberl (2020) Global inequalities in food consumption, cropland demand and land-use efficiency: A decomposition analysis, Global Environmental Change, 64, 102124.

https://doi.org/10.1016/j.gloenvcha.2020.102124.

[90] A.F. McCalla (2001) Challenges to world agriculture in the 21st century, UPDATE. Agriculture and Resource Economics, 4(3),1-2.

[91] M.W. Aktar, D. Sengupta, A. Chowdhury (2009) Impact of pesticides use in agriculture: their benefits and hazards. Interdisciplinary Toxicology, 2(1), 1. https://doi.org/10.2478/v10102-009-0001-7.

[92] R. Prasad, M. Kumar, V. Kumar (2017) Nanotechnology: an agricultural paradigm, Springer.

https://doi.org/10.1007/978-981-10-4573-8.

[93] B. Ruttkay-Nedecky, O. Krystofova, L. Nejdl, V. Adam (2017) Nanoparticles based on essential metals and their phytotoxicity. Journal of Nanobiotechnology, 15(1), 1-19.

https://doi.org/10.1186/s12951-017-0268-3.

[94] M.A. Axelos, M. Van de Voorde (2017) Nanotechnology in agriculture and food science, John Wiley & Sons.

[95] S.C. Mali, S. Raj, R.Trivedi (2020) Nanotechnology a novel approach to enhance crop productivity. Biochemistry and Biophysics Reports, 24 (2020) 100821, https://doi.org/10.1016/j.bbrep.2020.100821.

[96] E.A. Worrall, A. Hamid, K.T. Mody, N. Mitter, H.R. Pappu (2018) Nanotechnology for plant disease management. Agronomy, 8(12), 285. https://doi.org/10.3390/agronomy8120285.

[97] S. Tripathi, S. Sarkar (2015) Influence of water soluble carbon dots on the growth of wheat plant. Applied Nanoscience, 5(5), 609-616. https://doi.org/10.1007/s13204-014-0355-9.

[98] M.M. Sufian, J.Z.K. Khattak, S. Yousaf, M.S. Rana (2017) Safety issues associated with the use of nanoparticles in human body. Photodiagnosis and Photodynamic Therapy, 19,67-72. https://doi.org/10.1016/j.pdpdt.2017.05.012.

[99] S. Sonwani, S. Madaan, J. Arora, S. Suryanarayan, D. Rangra, N. Mongia, T. Vats, P. Saxena (2021) Inhalation exposure to atmospheric nanoparticles and its associated impacts on human health: A review. Frontiers in Sustainable Cities 3, 690444.https://doi.org/10.3389/frsc.2021.690444.

[100] L. Xuan, Z. Ju, M. Skonieczna, P.K. Zhou, R. Huang (2023) Nanoparticles-induced potential toxicity on human health: applications, toxicity mechanisms, and evaluation models. MedComm, 4(4) e327, https://doi.org/10.1002/mco2.327.

[101] A.A. Aljabali, M.A. Obeid, R.M. Bashatwah, Á. Serrano-Aroca, V. Mishra, Y. Mishra, M. El-Tanani, A. Hromić-Jahjefendić, D.N. Kapoor, R. Goyal, G.A. Naikoo, M.M. Tambuwala. (2023) Nanomaterials and Their Impact on the Immune System. International Journal of Molecular Sciences, 24(3) https://doi.org/10.3390/ijms24032008.

[102] S. Zha, H. Liu, H. Li, H. Li, K.L. Wong, A.H. All (2024) Functionalized nanomaterials capable of crossing the blood–brain barrier. ACS Nano, 18(3),1820-1845, https://doi.org/10.1021/acsnano.3c10674

IZVOD

ULOGA NANOMATERIJALA U SAVREMENOJ POLJOPRIVREDI

Poljoprivreda je temelj nekoliko zemalja u usponu i jedan je od ekonomski najznačajnijih pokretača. Poljoprivrednici, potrošači i životna sredina su u opasnosti kao rezultat povećane upotrebe mineralnih đubriva i štetnih pesticida. Tokom poslednjih nekoliko godina, preduzeta su značajna istraživanja o primeni nanotehnologije za povećanje poljoprivredne produktivnosti. Otkriveno je da su nanočestice (NP) korisne kao nanopesticidi, nanobiosenzor, nanođubriva i nanoremedijacija u proizvodnji poljoprivredne hrane. Hranjive materije, pesticidi, fungicidi i herbicidi su sabijeni sa raznim NP-ima kako bi se olakšalo progresivno oslobađanje đubriva i pesticida, što rezultira tačnom dozom dostupnosti biljkama. Nanođubriva poboljšavaju iskorišćenje hranljivih materija, smanjuju nedostatak hranljivih materija, smanjuju toksičnost zemljišta i smanjuju negativne posledice predoziranja, a sve to istovremeno smanjujući učestalost tretmana. Nanoformulacije se koriste u poljoprivredi za povećanje klijanja semena, smanjenje gubitaka hranljivih materija u đubrenju, smanjenje količine raspršenih pesticida, pomoć u upravljanju vodom i hranljivim materijama i. Ovaj pregled takođe razmatra različite izazove i zabrinutosti u vezi sa razvojem proizvoda pesticida, formulacijom i toksičnošću za ekološki prihvatljivu i održivu poljoprivredu.

Ključne reči: *poljoprivreda, nanođubriva, nanobiosenzori, nanopesticidi, nanoformulacije, nanomaterijali.*

Pregledni rad
Rad primljen: 22.05.2024.
Rad korigovan: 24.07.2024.
Rad prihvaćen: 15.08.2024

Indu Bhushan	https://orchid.org/0009-0001-5169-0142
Malvika Mehta	https://orchid.org/0009-0009-1543-0453
Mahima Sharma	https://orchid.org/0009-0000-5220-1961
Chitrakshi Chopra	https://orchid.org/0009-0008-9812-2300
Ratna Chandra	https://orchid.org/0000-0002-9575-0802
Ikhwan Syafiq Mohd Noor	https://orchid.org/0000-0003-0983-782X
Muhd Zu Azhan Yahya	https://orchid.org/0000-0003-1129-0552
Ashutosh Tripathi	https://orchid.org/0000-0003-4469-7017
Arvind Kumar Yadav	https://orchid.org/0009-0001-5573-2546

Bendaoud Mebarek[1], Abdelkader Maatoug[1], Sid Ahmed Mokhtar Mostefaoui[1],Halim Benali[3], Yassine El Guerri[2]*

[1]Laboratoire de Recherche en Intelligence Artificielle et Systèmes (LRIAS), University of Tiaret, Algeria,[2]Research Laboratory of Industrial Technologies, University of Tiaret, Algeria, [3]Mathematics Departement, University of Tiaret, Algeria

Scientific paper
ISSN 0351-9465, E-ISSN 2466-2585
https://doi.org/10.62638/ZasMat1090

Zastita Materijala 66 (1)
148 – 157 (2025)

Adomian decompositionmethod for modelling the growth of FeB/Fe_2B layer in boronizing process

ABSTRACT

The main objective of this paper is to explore the practical implementation of the Adomian decomposition method (ADM) in effectively solving the system of equationsgoverning boron diffusion during the boronizing process. This study uses ADM to investigate the kinetics of the boronizing process, assess the influence of various parameters on the growth of the layer thickness, and determine the boron concentration in FeB and Fe_2B phases. To validate the simulation results, data obtained from the literature were utilized. Overall, this research contributes to understanding the boronizing process and demonstrates the effectiveness of ADM as a mathematical tool for solving complex diffusion equations.

Keywords:*Adomian decomposition method, Model, Diffusion, Boronizing, kinetic,simulation*

1. INTRODUCTION

Different treatments are used to improve steel surfaces' physical, chemical, and mechanical properties [1]. Iron-based coatings have recently attracted attention for their mechanical properties [1,2], resistance to friction, and corrosion resistance. Compared to ceramics or traditional ceramic and cermet materials [3], iron-based materials offer affordability, reduced strategic importance, and can be economically manufactured using various thermal methods, making fabrication and processing simpler [1,4].

In boronizing, the modification of the surface's chemical composition is based on diffusing the boron atoms into the material. The reaction leads to the formation of a single or bilayer boride [5], which depends on the material's chemical composition and treatment process [6]. The single boride layer is preferable in industrial applications. Boronizing is frequently employed to enhance resistance against abrasion, corrosion, wear, and oxidation [1,2].It finds applications across diverse industries, including petroleum and gas refining, chemical mining, automotive, agriculture, casting, textile extrusion, and injection molding [7].

*Corresponding author: Bendaoud Mebarek
E-mail: mebarekbendaoud@yahoo.fr
Paper received: 14.07.2024.
Paper accepted: 22.08.2024.
The website: https://www.zastita-materijala.org/

Iron boride encompasses a range of inorganic compounds denoted by the formula Fe_xB_y, with FeB and Fe_2B being the stable and primary forms [8]. Certain iron borides exhibit advantageous traits like magnetism, electrical conductivity, corrosion resistance, and remarkable hardness. Combining ceramic attributes such as high hardness with metallic properties like thermal and electrical conductivity, iron borides offer a versatile range of properties [9].FeB exhibits greater hardness compared to Fe_2B, yet it is more prone to brittleness and fractures upon impact. Boronizing is a versatile technique applicable to numerous metals, including all ferrous alloys [6,10], as well as titanium, nickel, cobalt alloys, and refractory metals such as chromium, molybdenum, vanadium, niobium, tantalum, tungsten, and zirconium. Certain non-metals like cemented carbides can also undergo boronizing [11]. However, copper is an exception, as its atoms act as a barrier hindering the diffusion of boron atoms [12]. The speed of boronizing increases with higher substrate purity, i.e., fewer alloying elements present in the substrate [1,5], with alloying elements also influencing the thickness and structure of the resulting boride layer.

During the boronizing process, the surface layer of the material becomes saturated with boron, conducted in either a solid, liquid, or gaseous medium [13]. For steel, this process typically occurs within temperatures ranging from 1113 to 1323 K for durations of up to 10 hours, yielding FeB and Fe_2B borides with a needle-shaped

structure and hardness levels reaching up to 2000 HV [14,15].

The modeling and simulation of the growth kinetics of boride layers produced by this process allow for the optimization of the operating conditions of this treatment [16]. Kinetic models are developed to predict the thickness of the boride layer formed as a function of two critical parameters: temperature and treatment time [17].The main goal of applying these models is to predict the thicknesses of borided layers [18]. Most of these models are based on the resolution of Fick's equations. They are applied either to the study of the kinetic growth of the Fe_2B monolayer or to the bilayer (FeB+Fe_2B)[17]. Indeed, these diffusion models assume that the formation of boride layers obeys a parabolic-type law.

Brakman et al. [19] tookinto account the difference in specific volumes between FeB and Fe_2B layers, with boron concentration profiles that are linear through the FeB and Fe_2B layers. Another kinetic model was proposed by Campos et al. [20] for the growth kinetics of Fe_2B layers obtained on the surface of high-alloy steel. This kinetic approach is based on the conservation of mass equation at the interface (Fe_2B/substrate), where a linear-type distribution gives the boron diffusion profile. Keddam et al. [17] suggested a diffusion model for the bilayer (FeB+Fe_2B) formed on Armco iron by the powder method. In this model, they adopted a nonlinear boron concentration profile in each layer, taking into account the diffusion of boron in the substrate.

Experimental and artificial intelligence approaches [21] also allow measurements of the wear behavior.Bindal etal.[22] used empirical techniques to calculate the boron diffusion coefficient, Keddam et al. [23] simulated the kinetics of the boronizingprocess using the integral approach, Dybkov et al. [8,24] modeled the bilayer configuration in different processes, Mebarek et al.[25,26] developed an artificial intelligence model based on RNN and in another work proposed an FNN approach to simulate the growth of the boride layer. The Ls-SVM model for predicting the layer thickness was used by Mebarek et al.[27], and to evaluate and estimate the effect of different parameters, [28] used the fuzzy system.

Numerical computation has become a powerful tool for scientific research and is essential for engineering development. The development of approximate solution methods for mathematical and physical problems, along with powerful computers, has made it possible to simulate physical phenomena. This type of development relies on integrating traditional disciplines: applied mathematics, computer science, and engineering sciences.

Numerous methods are available to solve the diffusion model of boron in steel. In this paper, we focus on applying the Adomian Decomposition Method (ADM) to solve the Dybkov equations within the context of the boronizing process. The main objective of this research is to develop a robust and efficient computational model that accurately simulates the boron diffusion phenomenon through the surface of ferrous alloys. This study enhances the predictive capabilities of diffusion models in the boronizing treatment of steel by employing the Dybkov equations and solutions derived from the ADM method

2. DYBKOV MODEL

The diffusion model is based on Dybkov's equations [8]. It is used to study the kinetics of biphasic layer formation (FeB, Fe_2B) on steel subjected to boronizing via powder technique. Fig.1 illustrates a schematic representation of the boron concentration profiles within the FeB and Fe_2B layers.

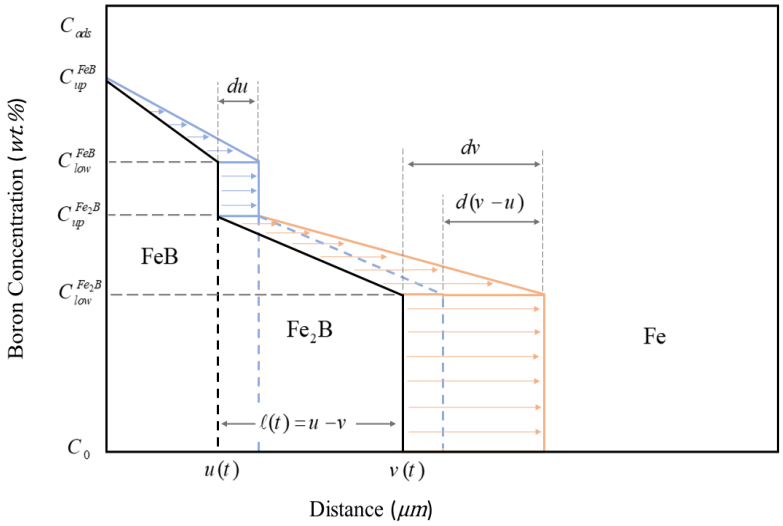

Figure 1.Schematic profile of boron concentration along the FeB and Fe_2B layers [29]

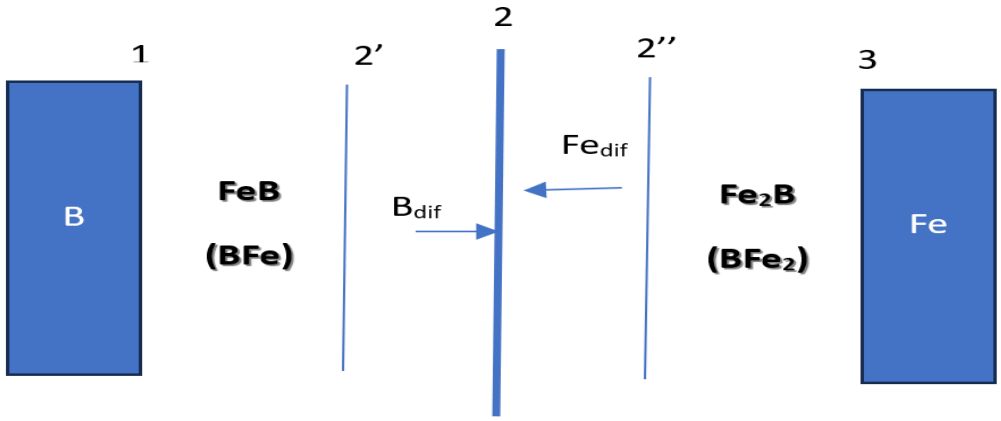

Figure 2.Schematic diagram illustrating the growth process of FeB and Fe₂B layers under diffusion-controlled conditions

The Dybkov model [8] is extensively employed to depict the growth kinetics of boronized layers on steel, accounting for the influence of boride incubation periods. According to this model, the progression of boride layers is governed by the diffusion process. Entailing the diffusion of boron atoms into the FeB layer, followed by their reaction with the Fe₂B compound. Likewise, the expansion of the Fe₂B layer is governed by the diffusion of iron atoms into its structure, followed by their reaction with the FeB compound.

The growth kinetics of layers of chemical compounds is commonly modeled using a parabolic equation of the form:

$$u = \sqrt{2k_1 t} \qquad (1)$$

Where

u - represents the thickness of the layer

k_1 - is the growth rate constant of the layer

t - is the time

This equation (1) is derived from Fick's laws of diffusion. The parabolic equations have been shown to provide a satisfactory fit to the experimental data for sufficiently thick layers in the order of micrometers, particularly for iron borides. However, for a more accurate description of the growth kinetics of FeB and Fe₂B layers, equations (2) and (3) are given.

$$\frac{dx}{dt} = \frac{a}{1+\frac{a.x}{b}} + \frac{a'}{1+\frac{a'}{b'}x} - \frac{rg}{p}\frac{c}{1+\frac{c.y}{d}} \qquad (2)$$

$$\frac{dy}{dt} = \frac{c}{1+\frac{c.y}{d}} + \frac{c'}{1+\frac{c'}{b'}} - \frac{q}{sg}\frac{a'}{1+\frac{a'x}{b'}} \qquad (3)$$

Where

x: is the thickness of the outer layer of FeB

x: is the thickness of the inner layer of Fe₂B

$a = k_0 Fe_1$ and $a' = k_0 B_1$ are the chemical growth rate constants of the FeB layer at the expense of the diffusion of iron and boron atoms, respectively

$b = k_1 Fe_1$ and $b' = k_1 B_1$ are the diffusional (physical) growth rate constants of the FeB layer at the expense of the diffusion of iron and boron atoms, respectively

$c = k_0 Fe_2$ and $c' = k_0 B_2$ the chemical growth rate constants of the Fe₂B layer at the expense of the diffusion of iron and boron atoms, respectively;

$d = k_1 Fe_2$ and $d' = k_1 B_2$ are the diffusional (physical) growth rate constants of the Fe₂B layer at the expense of the diffusion of iron and boron atoms, respectively

g is the ratio of the molar volumes of the compounds FeB and Fe₂B

$p = q = r = 1$ and $s = 2$ factors of the chemical formulas of FeB (written as BFe) and Fe₂B(BFe₂)

The value of g is determined from the density of the compounds *FeB* $\rho_1 = 6{,}70x10^3$ kgm^{-3} and *Fe₂B* $\rho_2 = 7.34x10^3$ kgm^{-3}[30] $M_1 = 66{,}65$ $gmol^{-1}$ and $M_2 = 122.49$ $g\,mol^{-1}$; $g = M_1\rho_2/M_2\rho_1 = 0.60$.

The set of equations (2) and (3) characterizes the stage of reaction-controlled growth in boride layers, wherein the rapid diffusion rates of iron and boron atoms through the layer render their influence on overall layer formation rates negligible compared to the subsequent chemical transformations occurring at phase interfaces. As a result, the rate is mainly governed by chemical processes alone (referred to as chemical control) due to the plentiful scattering of atoms of both types facilitating layer growth. However, it is essential to

note that the occurrence and growth of FeB and Fe_2B layers at the interface are not necessarily simultaneous. The Dybkov model provides a means to study the kinetics involved in the formation of FeB and Fe_2B layers. The changes over time in the thickness of these layers can be described using the following system of ordinary differential equations:

$$\frac{du(t)}{dt} = \frac{D_{FeB}}{u(t)} - \frac{rg}{p}\frac{D_{Fe_2B}}{\left(v(t)-u(t)\right)} \quad (4)$$

$$\frac{d[v(t)-u(t)]}{dt} = \frac{D_{Fe_2B}}{v(t)-u(t)} + \frac{q}{sg}\frac{D_{FeB}}{u(t)} \quad (5)$$

With *u(t)* and *v(t),* the thicknesses of FeB and Fe_2B layers. The constant g depends on the molar volume of FeB and Fe_2B phases, as obtained from the stoichiometric coefficients for phases FeB and Fe_2B.

The two growth parameters k_{FeB} and k_{Fe_2B}, which are provided by equations (6, 7) [8], can be obtained from the fitting of experimental data [19]. From the preceding system, the expressions of the diffusion coefficients are given as follows:

$$D_{FeB} = \frac{0.5\,k_{FeB}}{\left(p-\frac{rq}{s}\right)}\left[(p-rg)k_{FeB} + rgk_{Fe_2B}\right] \quad (6)$$

$$D_{Fe_2B} = \frac{0.5\left(K_{Fe_2B}-k_{FeB}\right)}{\left(1-\frac{rq}{sp}\right)\left[k+\left(\frac{q}{sg}-1\right)D_{FeB}\right]} \quad (7)$$

3. ADOMIAN DECOMPOSITION METHOD

The Adomian decomposition method has been applied to solve various types of differential and integral equations in mathematics, physics, biology, and chemistry, and many research papers have been published to demonstrate its effectiveness.

The Adomian decomposition method provides a solution expressed as an infinite series of terms, offering flexibility for reevaluation. This approach demonstrates effectiveness across various types of equations, including linear and nonlinear differential equations, integral equations, and Integro-differential equations. George Adomian introduced this method in his publications [31], characterizing it essentially as a power series technique. Widely recognized as a semi-analytical approach for solving differential equations, its convergence has been validated through prior research [32].

Previous research has shown that the Adomian decomposition method is helpful in solving inverse problems of differential equations [33]. In the current section, we extend this approach to tackle various nonlinear functional equations, including but not limited to differential, integral, integro-differential, and algebraic equations.

The Adomian decomposition method consists of decomposing the unknown function $y(x)$ of any equation into a sum of an infinite number of components defined by the decomposition series.

$$y(x) = \sum_{n=0}^{n} y_n(x) \quad (8)$$

Generally, the nonlinear differential equation is given as follows:

$$Ly + Ny + Ry = Q \quad (9)$$

Where

L : invertible linear operator

Ly : a linear term with a higher-order derivative

N : the nonlinear operator

Ny :represents the nonlinear terms

R : a linear differential operator of order less than L

Ry :remaining parts of the equation under consideration

Q: the specified bounded function

Once the inverse operator L^{-1} is applied to Eq. 9, we obtained the following equation:

$$y = c - L^{-1}Q - L^{-1}Ny - L^{-1}Ry \quad (10)$$

Where

c is the parameter resulting from the integrations such that $Lc = 0$, for the case of a first-order ODE, c is the constant of integration.

For initial value problems, we conveniently

defined L^{-1} for$L = \frac{d^n}{dx^n}$as the n-fold definite integration from 0 to x.

By employing the ADM method, wherein the solution ofEq. 9 is represented by Eq. 14 as an infinite series, and by selecting the initial solution component as:

$$Ly + Ny + Ry = Q \quad (11)$$

The solution is given by the recursive relationship given by the following system:

$$y = c\text{-}L^{-1}Q\text{-}L^{-1}Ny\text{-}L^{-1}Ry \quad (12)$$

The nonlinear terms as $Ny = \sum_{n=0}^{+\infty} A_n$ is decomposed by the ADM

where:

$A_n$represent the Adomian polynomials given by the following expression:

$$A_n(y_0, y_1, \dots y_n)\frac{1}{n!}\left[\frac{d^n}{d\lambda^n}N\left(\sum_{i=0}^{+\infty}\lambda^i y_i\right)\right]_{\lambda=0} \quad (13)$$

Using the recursive relationship given by the precedent system (12), we can construct the solution y as:

$$y(x) = \lim_{i\to+\infty}\sum_{i=0}^{i=n} y_n(x) \quad (14)$$

Many researchers have guaranteed the convergence of the ADM and the series of the Adomian polynomials [32,34].We not thatADM can converge to the exact solution more efficiently under certain conditions, especially for linear and non-linear differential equations. Generally ADM provides a series solution that can offer analytical insight into the problem, which is often not directly available with numerical methods.

4. SOLUTION OF THE DYBKOV SYSTEM BY ADM

In this study, we adapted the model calculation of Fatoorehchi et al. [35], which was applied to describe the growth dynamics of Al_3Mg_2 and $Al_{12}Mg_{17}$ layers. However, in this case, we applied the ADM to modeling the boronizing process.

From Eq. 4 and Eq. 5, we replace u in the equation system by x and $(v-u)$ by y. We get the growth kinetics of boride layers at the diffusional stage of their formation described by a system of two differential equations:

$$\frac{dx}{dt} = \frac{D_{FeB}}{x} - \frac{rg}{p}\frac{D_{Fe_2B}}{y} \quad (15)$$

$$\frac{dy}{dt} = \frac{D_{Fe_2B}}{y} - \frac{q}{sg}\frac{D_{FeB}}{x} \quad (16)$$

where the solution components are calculated as

$$\begin{cases} y_0 = \alpha + \beta t \\ y_{i+1} = -\boldsymbol{D_{Fe_2B}}\int_0^t dt\int_0^t A_i\,dt' + \frac{s^2g^2}{q^2\boldsymbol{D_{FeB}}}\int_0^t dt\int_0^t B_i dt' - \frac{sg^2r\boldsymbol{D_{Fe_2B}}}{qp\boldsymbol{D_{FeB}}}\int_0^t dt\int_0^t C_i dt' \end{cases} \quad (21)$$

For$i \geq 0$. Two parameters, α,andβ, have to be determined by the initial conditions of theproblem, i.e.

$$\alpha = y(0) \qquad \beta = \frac{dy}{dt}(0) \quad (22)$$

We apply the ADM method to solve the system (15) and (16) given by Dybkovmodel. This system describes the diffusion of boron in the treated steel.

With the use of the precedent system, the expression of x is as follows:

$$x = \frac{qD_{FeB}}{sg}\left(\frac{D_{Fe_2B}}{y} - \frac{dy}{dt}\right)^{-1} \quad (17)$$

Withthe derivative of x, we obtained the equation given by:

$$\frac{dx}{dt} = \frac{qD_{FeB}}{sg}\frac{\left(\frac{D_{Fe_2B}dy}{y^2\ dt} + \frac{d^2y}{dt^2}\right)}{\left(\frac{D_{Fe_2B}}{y} - \frac{dy}{dt}\right)^2} \quad (18)$$

We replace Equations (17) and (18) into Equation (15) to obtain the second-order ODE given by Equation (19):

$$\frac{d^2y}{dt^2} = -\frac{D_{Fe_2B}}{y^2}\frac{dy}{dt} + \frac{s^2g^2}{q^2D_{FeB}}\left(\frac{D_{Fe_2B}}{y} - \frac{dy}{dt}\right)^3 - \frac{sg^2rD_{Fe_2B}}{qpD_{FeB}}\frac{1}{y}\left(\frac{D_{Fe_2B}}{y} - \frac{dy}{dt}\right)^2 \quad (19)$$

The ODE given in Eq. 19 can be solved by the ADM, and its solution is given as:

$$y = \sum_{i=0}^{\infty} y_i \quad (20)$$

In (19) we use the following operator

$$L(.) = \frac{d^2}{(dt^2)(.)}$$

and we note that

$$L^{-1}(.) = \int_0^t dt\int_0^t dt'(.)$$

In turn, A_i , B_i and C_i are the Adomian polynomials such that

$$\sum_{i=0}^{+\infty} A_i = \frac{1}{y^2}\frac{dy}{dt} \ , \ \sum_{i=0}^{+\infty} B_i = \left(\frac{D_{Fe_2B}}{y} - \frac{dy}{dt}\right)^3 , \sum_{i=0}^{+\infty} C_i = \left(\frac{D_{Fe_2B}}{y} - \frac{dy}{dt}\right)^2 \quad (23)$$

After evaluating the function y, calculating the function x using Eq. (15) is simple.

5. EXPERIMENTAL PROCEDURE

In order to validate the simulation, experimental data carried out by Brakman et al. [19] using the boronizing technique on pure iron powders were used, and the chemical composition of pure iron is presented in Table 1.

Table 1. Chemical composition of used pure iron (mass%) [19].

Elements	C	Mn	Ni
%(wt)	0.005	0.0013	0.004

Boronizingwith solid substances has numerous industrial applications due to its cleanliness and simplicity. The technique involves packing the parts in steel boxes filled with boronizingpowder (amorphous boron or ferroboron) and introducing them into muffle furnaces. It is the most widely used technique in the industry.

FeB and Fe_2B borides have an acicular shape and are oriented perpendicularly to the sample's surface. In practice, it is not easy to experimentally measure the thickness of the boride layer due to the nature and structure of the boride/substrate interface. The thickness determined experimentally for biphasic borided layers is the average of 10 measurements made at different locations on the sample [19]. Consequently, experimental data regarding the thickness of the FeB and Fe_2B layers are illustrated in Table 2.From the experimental data presented in Table 2 of layerthickness,we calculated the values of the growth rate constants, given in Table 3.

Table 2.Experimental data of FeB and Fe_2B layer thickness [19]

Time (h) / Temperature (K)	1	1.25	2.5	4	4.25	6	8	8.5
	FeB (µm)							
1023				6.96		8.52	9.842	
1073	6.84				14.1			19.94
1123		13.15	16.59	21.52				
	Fe_2B (µm)							
1023				37.08		45.41	52.44	
1073	25.5				52.56			75.34
1123		42.13	59.58	75.34				

6RESULTS AND DISCUSSIONS

The ADM is applied to describe the growth dynamics of FeB and Fe_2Blayers, denoted by xand y, respectively. The five numerical values of the Adomian coefficients A_i, B_i, and C_i used in the calculations are taken from Fatoorehchia et al. [35].

Theresults are compared with the experimental data from [19]. $D_B^{Fe_2B}$ and D_B^{FeB} are the growth rate constantsfor Fe_2B and FeBgiven by the following expressions [17]:

$$D_B^{FeB} = 1.28\times10^{-5}\exp(-\frac{175\times10^3}{RT})$$

$$D_B^{Fe_2B} = 6.3\times10^{-6}\exp(-\frac{157\times10^3}{RT})$$

Where, *R=8.32 j/mol k*

To simulate the boronizing kinetics using a simple model, we set the boron concentration at the surface to 27.26 wt%.Additionally, we assumed that the concentration of boron at the interface (FeB/Fe_2B) is 16.23 wt%. Specifically, for the Fe_2B/Fe interface,the boron concentration is 8.83wt%. The initial concentration of boron in the substrate is $35x10^{-4}$ wt%.

Using a biphasic boride layer kinetic model and the boron diffusivity data, a simulation code was developed to calculate the thickness of the Fe_2B and FeB layers and predict the boron concentration.

The ADM approach is used to simulate the Dybkov model, utilizing the parameters illustrated

in this simulation. The input data for the simulation calculations comprises a ratio of molar volumes of Fe_2B and FeB denoted as g = 0.6. Additionally, α = $0.1012x10^{-13}$m represents the initial layer thickness y, and the initial slope of y is denoted asβ, which is equal to$5.5x10^{-15}$ m/s.

The stoichiometric coefficients used in this study are specified as (p, q, r, s) = (1, 1, 1, 2).

Table 3 depicts the comparison between the simulation and experimental data.Comparing the calculated growth rate constants with the experimental values reveals a strong agreement between the experimental data and the simulation results.

Table 3. Comparing the calculated growth rate constants with the experimental ones

Temperature (K)	Growth rate constant (μm/s)					
	FeB			Fe_2B		
	Exp [19]	Simulation		Exp [19]	Simulation	
		Simple Model [17]	ADM-Dybkov Model		Simple Model [17]	ADM-Dybkov Model
1023	0.058	0.0607	0.0635	0.3090	0.2818	0.2988
1073	0.144	0.1012	0.1123	0.4250	0.4356	0.4527
1123	0.196	0.1611	0.1722	0.6280	0.6479	0.6650

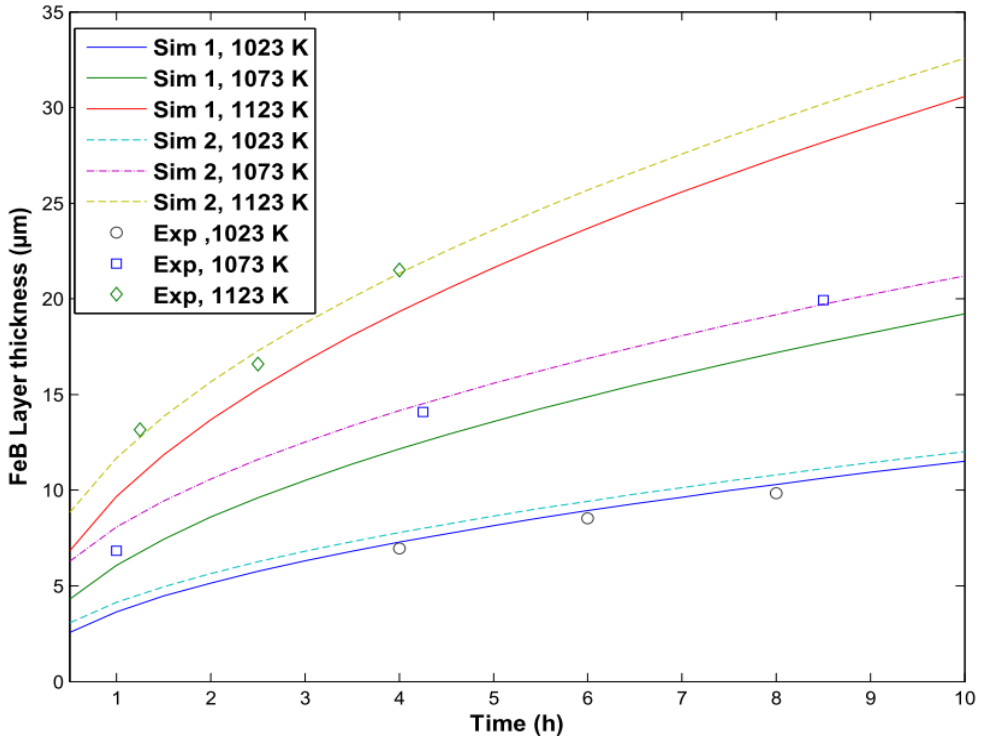

Figure 3. Comparison between Sim1 (simple model) [17], Sim2 (ADM-Dybkov model) and Experimental thicknessesof FeB layer

Fig.3 illustrates a comparative analysis between Sim1 (simple model), Sim2 (ADM-Dybkov model), and experimental thicknessesof the FeB layer. This comparison aims to evaluate the performance and accuracy of these models.

Fig.4 presents a comparative assessment involving Sim1 (simple model), Sim2 (ADM-Dybkov model), and experimental data related to the Fe_2B layer. The objective of this comparison is to assess the effectiveness and precision of these models.

This comparison between Sim1 (simple model), Sim2 (ADM-Dybkov model), and experimental data of the Fe_2B layer provides a comprehensive evaluation of the model's predictive capabilities in simulating the growth kinetics of the boronized layers on steel. The ADM-Dybkov model gives good results when compared with experimental data. The error of the ADM-Dybkov model compared to the experimental data is estimated to be 2.9 μm for the Fe_2B layer and 1.4 μm for the FeB layer.

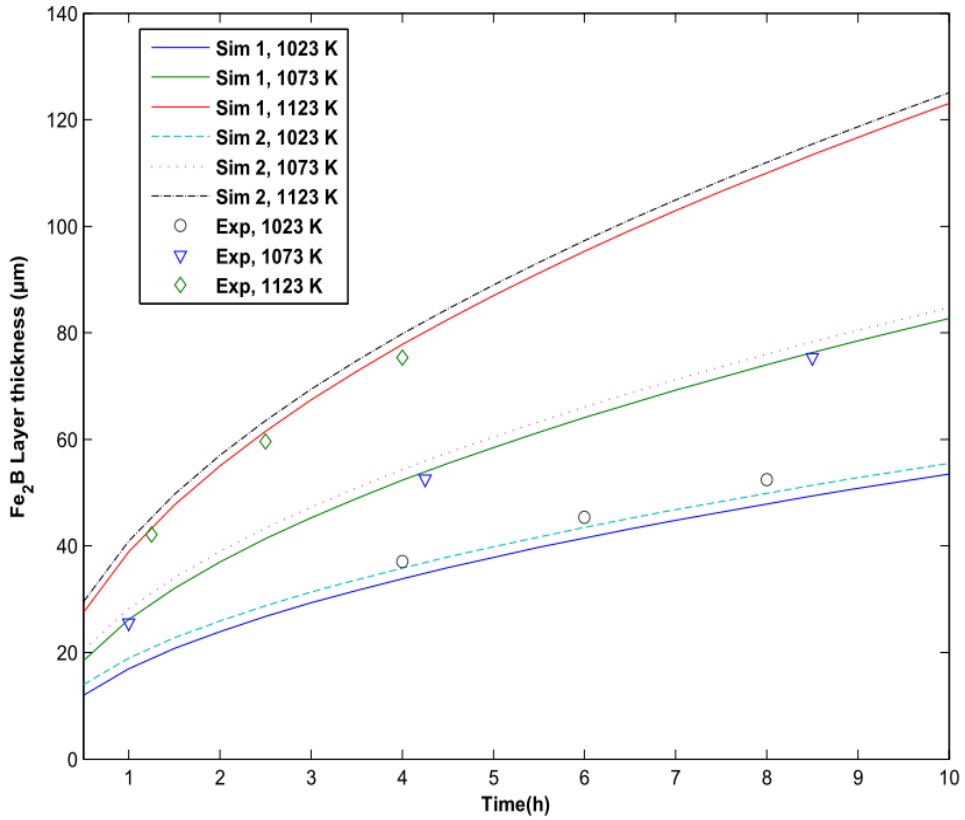

Figure 4.Comparison between Sim1 (simple model) [17], Sim 2 (ADM-Dybkov model) and Experimental data of Fe_2B layer

7. CONCLUSION

This study introduces the Adomian decomposition method (ADM) as a robust strategy for approximating solutions to nonlinear equations through an infinite series, typically converging to the precise solution. Applied to first-order differential equations, ADM exhibits convergence of series solutions to exact solutions for each problem. Utilizing ADM, the study effectively models boron diffusion in the boronizing process, demonstrating its capability to closely match experimental data, which are the thicknesses of FeB and Fe_2B layers. The investigation delves into the kinetics of boronizing, exploring how various parameters influence layer thickness growth and boron concentration across phases. Simulation results are validated using data from literature sources, underscoring ADM's effectiveness in tackling intricate diffusion equations and advancing understanding of the boronizing process.

As prospects for future work, we aim to combine ADM with other computational techniques, such as machine learning and optimization algorithms, to create hybrid models. These models could enhance predictive accuracy and provide more robust solutions for complex problems.

APPENDIX

We assume a standard form of an integro-differential equation defined by the standard form:

$$\begin{cases} y^{(n)}(x) = f(x) + \int_0^x M(x,t)y(t)dt \\ y^{(n)}(0) = b_k\,, \qquad 0 \le k \le n-1 \end{cases} \qquad (A)$$

It is natural to seek an expression for *y(x)* that will be derived from equation (A). This can be done by integrating both sides of equation (A) from 0 to *x* as many times as the order of derivative involved. Therefore, we obtain:

$$y(x) = \left[\sum_{k=0}^{n-1} \frac{1}{k!} b_k x^k\right] + L^{-1}\left(f(x)\right) + L^{-1}\left(\int_0^x M(x,t)y(t)dt\right) \qquad (B)$$

With

$$\sum_{k=0}^{n-1} \frac{1}{k!} b_k x^k$$

the solution is obtained using the initial conditions, and L^{-1} is an integration operator. Now, we can

apply the decomposition method by defining the solution y(x) of equation (B) as a series.

$$y(x) = \sum_{n=0}^{\infty} y_n(x) \qquad (C)$$

By substituting equation *(C)* into *(B),* we obtain

$$\sum_{n=0}^{\infty} y_n(x) = \left[\sum_{k=0}^{n-1} \frac{1}{k!} b_k x^k\right] + L^{-1}\left(f(x)\right) + \cdot$$
$$+ L^{-1}\left(\int_a^x M(x,t)\left[\sum_{n=0}^{\infty} y_n(t)\right]dt\right) \qquad (D)$$

This equation can be explicitly written as:

$$\sum_{n=0}^{\infty} y_n(x) = \sum_{k=0}^{n-1} \frac{1}{k!} b_k x^k + L^{-1}\left(f(x)\right) +$$
$$+ L^{-1}\left(\int_a^x M(x,t)\left[\sum_{n=0}^{\infty} y_n(t)\right]dt\right) \qquad (E)$$

We have the solution in the form:

$$y_0(x) = \sum_{k=0}^{n-1} \frac{1}{k!} b_k x^k + L^{-1}(f(x)) \qquad (F)$$

$$y_{n+1}(x) = L^{-1}\left(\int_a^x M(x,t) y_n(t) dt\right) n \geq 0 \qquad (G)$$

8. REFERENCES

[1] A. G. Von Matuschka (1980) Boronizing,Carl Hansen Verlag, Germany. ISBN: 9783446131767

[2] A.K.Sinha (1991)Boronizing, ASM Handbook, OH, USA, Journal of Heat Treating, 4, 437-447.

[3] G.Wahl (1975) Boronizing, A Method for the Production of Hard Surfaces for Extreme Wear, Durferrit-Technical Information, Germany: Reprint from VDI-Z117, 785-789.

[4] W.Fichtl (1980) Boronizing and its practical applications,Materials & Design,2(6), 276-286.doi.org/10.1016/0261-3069(81)90034-0

[5] M. Kulka (2019) Current Trends in Boriding, Switzerland, Springer. doi.org/10.1007/978-3-030-06782-3

[6] O. Allaoui, N. Bouaouadja, G. Saindernan (2006) Characterization of Boronized layers on a XC38 steel,Surface and Coatings Technology,201(6) 3475-3482.doi.org/10.1016/j.surfcoat.2006.07.238

[7] B.Mebarek (2012) Etude numérique de la cinétique de boruration de l'acier inoxydable, Doctorat Science Physique, ENP d'Oran, Algeria.

[8] V. I.Dybkov (2016) Basics of Formation of Iron Boride Coatings, Journal of Mineral, Metal and Material Engineering, 2, 30-46. ISSN: 2414-2115

[9] A.S. Dehlinger, J.F. Pierson, A. Roman, P.Bauer (2003) Properties of iron boride films prepared by magnetron sputtering, Surface and Coatings Technology, 174-175,331-337, doi.org/10.1016/S0257-8972(03)00399-2

[10] B.Mebarek, S.A.Bouaziz, A.Zanoun (2012) Simulation model to study the thermochemical boriding of stainless steel «AISI 316» (X5CrNiMo17-12-2),Matériaux& Techniques, 100(2), 167-175. doi.org/10.1051/mattech/2012009

[11] L.Casteletti, A.N.Lombardi,G.E.Totten(2013) Boriding. In:Q.J. Wang, Y. W. Chung (Eds.) Encyclopedia of Tribology, Springer, Boston. doi.org/10.1007/978-0-387-92897-5_727

[12] C. Zimmerman (2013) Boriding (boronizing) of metals, in: J.L. Dossett, G.E. Totten (Eds.) Steel Heat Treating Fundamentals and Processes, ASM International, Ohio, 709–724. doi.org/10.31399/asm.hb.v04a.a0005772

[13] A.Calik, N.Ucar, M.S.Karakas, and H.Tanis (2019) Pack-Boriding of Pure Iron with Powder Mixtures Containing ZrB_2, High Temperature Materials and Processes, 38(2019), 342-346. doi.org/10.1515/htmp-2017-0081

[14] V.Jain, G.Sundararajan (2002) Influence of the pack thickness of the boronizing mixture on the boriding of steel, Surface and Coatings Technology, 149(1), 21-26,doi.org/10.1016/S0257-8972(01)01385-8

[15] J. Subrahmanyam and K. Gopinath (1984), Wear studies on boronized mild steel, Wear, 95(3), 287-292.doi.org/10.1016/0043-1648(84)90143-1

[16] B. Mebarek, D. Madouri, A.Zanoun, A.Belaidi (2015) Simulation model of monolayer growth kinetics of Fe_2B phase, Matériaux& Techniques, 103(7), 703. doi.org/10.1051/mattech/2015058

[17] M.Keddam, S. M.Chentouf (2005)A diffusion model for describing the bilayer growth (FeB/Fe_2B) during the iron powder-pack boriding, Applied Surface Science, 252 (2), 393-399. doi.org/10.1016/j.apsusc.2005.01.016

[18] B. Mebarek, A. Benguelloula, A. Zanoun (2018) Efect of Boride Incubation Time During the Formation of Fe_2B Phase, Materials Research, 21(1), 1-7. doi.org/10.1590/1980-5373-MR-2017-0647

[19] C. M. Brakman, A.W. J. Gommers and E. J. Mittemeijer (1989)Boriding of Fe and Fe–C, Fe–Cr, and Fe–Ni alloys; Boride-layer growth kinetics, Journal of Materials Research, 4(6),1354–1370. doi.org/10.1557/JMR.1989.1354

[20] I.Campos-silva, M.Ortiz-Domínguez, C.Tapia-Quintero, G.Rodriguez-Castro, M.Y. Jiménez-Reye, E.Chavez-Gutiérrez(2012) Kinetics and boron diffusion in the FeB/Fe_2B layers formed at the surface of borided high-alloy steel. Journal of Materials Engineering and Performance, 21(8), 1714-1723.doi.org/10.1007/s11665-011-0088-9

[21] M.G.Albayrak, E.Evin, O.Yiğit, M.Toğaçar, B.Ergen (2023) Experimental and artificial intelligence approaches to measuring the wear behavior of DIN St28 steel boronized by the box boronizing method using a mechanically alloyed powder source, Engineering Applications of Artificial Intelligence, 120,105-910. doi.org/10.1016/j.engappai.2023.105910

[22] C. Bindal, A. Erdemir (1996) Ultralow friction behavior of borided steel surfaces after flash annealing, App. Phys. Lett, 68(7), 923-925.doi.org/10.1063/1.116232

[23] M. Keddam, M. Kulka (2018) Analysis of the growth kinetics of Fe_2B layers by the integral method, Journal of Mining and Metallurgy, 54(3), 361–367.doi.org/10.2298/JMMB180405026K

[24] V.I.Dybkov, L.V.Goncharuk, V.G.Khoruzha, K.A. Meleshevich, A.V.Samelyuk, V.R.Sidorko (2008) Diffusional growth kinetics of boride layers on iron-chromium alloys,Solid State Phenomena, 138, 181–188, doi.org/10.4028/www.scientific.net/SSP.138.181

[25] B. Mebarek, M. Keddam (2019) Prediction model for studying the growth kinetics of Fe_2B boride layers during boronizing, Ingénierie des Systèmesd'Information, 24(2),201-205. doi.org/10.18280/isi.240212

[26] B.Mebarek and M.Keddam (2018), A fuzzy neural network approach for modeling the growth kinetics of FeB and Fe_2B layers during the boronizing process, Matériaux& Techniques, 106(6),603. doi.org/10.1051/mattech/2019002

[27] B.Mebarek, M.Keddam, H.Aboshighiba (2018) LS-SVM approach for modeling the growth kinetics of FeB and Fe_2B layers formed on Armco iron, Ingénierie des Systèmes d'Information,23(5),29-41.doi.org/10.3166/ISI.23.5.29-41

[28] B.Mebarek, M.Keddam (2020) Fuzzy logic approach for modelling the formation kinetics of Fe2B layer, International Journal of Computational Materials Science and SurfaceEngineering,9(2),147-156. doi.org/10.1504/IJCMSSE.2020.109563

[29] O.Belguendouz, B.Mebarek, Y.El Guerri, M. Keddam, N.Hadjadj, Y.Djafri (2023) Simple model and integral method for simulating the growth of the borided layer FeB/Fe_2B on the AISI H13 steel, Zaštita materijala (Material Protection),64(4), 491-502.doi.org/10.5937/zasmat2304491B

[30] V.I.Dybkov, W.Lengauer, K.Barmak(2005) Formation of boride layers at the Fe–10% Cr alloy–boron interface, Journal of Alloys and Compounds, 398(1-2),113-122.doi.org/10.1016/j.jallcom.2005.02.033

[31] G.Adomian (1998) A review of the decomposition method in applied mathematics, Journal of Mathematical Analysis and Applications 135(2), 501-544, doi.org/10.1016/0022-247X(88)90170-9

[32] Y. Cherruault (1989) Convergence of Adomian's Method, Kybenetes, 18(2), 31-38. doi.org/10.1108/eb005812

[33] G. Adomian (1990) A review of decomposition method and some recent results for nonlinear equations, Mathematical and Computer Modelling, 13(7) 17-43. doi.org/10.1016/0895-7177(90)90125-7

[34] K. Abbaoui and Y. Cherruault (1994) Convergence of Adomian's Method Applied to Differential Equations, Computers & Mathematics with Applications,28(5),103-109.doi.org/10.1016/0898-1221(94)00144-8

[35] H. Fatoorehchia and R. Rach(2021) Decomposition Solution for Nonlinear Model Describing Diffusional Growth of Intermetallic Layers, Acta Physica Polonica A, 1(140),91-96. doi.org/10.12693/APhysPolA.140.91

IZVOD

ADOMIJANSKA DEKOMPOZICIONA METODA ZA MODELIRANJE RASTA FeB/Fe_2B SLOJA U BORONIZIRANJE PROCESA

Glavni cilj ovog rada je da se ispita praktična implementacija Adomianove metode dekompozicije (ADM) u efikasnom rješavanju sistemske jednadžbe koja upravlja difuzijom bora tokom procesa boriranja. Ovaj rad koristi gore pomenutu metodu za istraživanje kinetike boroniziranje procesa, procjenu utjecaja različitih parametara na rast debljine sloja i određivanje koncentracije bora u FeB i Fe_2B fazama. Za validaciju rezultata simulacije koristili smo podatke dobijene iz literature.

Ključne riječi: *Adomian metoda dekompozicije, Model, Difuzija, Boroniziranje, kinetička, simulacija*

Naučni rad
Rad primljen: 14.07.2024.
Rad prihvaćen: 22.08.2024.

Bendaoud Mebarek: https://orcid.org/0000-0002-6838-3867
Yassine El Guerri : https://orcid.org/0009-0008-9664-2361
Sid Ahmed Mokhtar Mostefaoui : https://orcid.org/0000-0002-3426-6881

OleksandrKrotiuk, Leonid Dvorkin*

National University of Water and Environmental Engineering, Rivne, Ukraine

Scientific paper
ISSN 0351-9465, E-ISSN 2466-2585
https://doi.org/10.62638/ZasMat1134

Zastita Materijala 66 (1)
158 - 166 (2025)

Effect of Hemihydrate gypsum on the basic properties of oil-well cement

ABSTRACT

During this research has been used laboratory mill and production cement mill for comparing results. The purpose of the research was to determine the influence of the gypsum with different phase state (dihydrate or hemihydrate), active additive of blast granulated slag and the total SO_3 content to the free water separation, spreading of the well cement slurry and flexural and compressive strength of the cement mortar. The conducted cycle of research made it possible to obtain quantitative dependences of that parameters. At the researches was used gypsum preheated at the furnace with 200°C for 60 minutes. During this research was discovered that presence of hemihydrate gypsumin the cement don't have big impact on the free water separation, but it has some impact on the spreading of the well cement slurry. Also, at this research has been discover influence of hemihydrate gypsum to compressive strength at the age of 28 days and flexural strength at the age of 1 day. During this research was discovered that presence of hemihydrate gypsum at the cementreduce the thickening time for 60 minutes. Presence of blast granulated slag at the cement reduce free water separation of the well cement slurry. During research at the production cement mill was ensured that presence of hemihydrate gypsum at the cement reduce spreading for 25 mm and reduce free water separation for 1 ml. The results of the tests from the production cement mill and laboratory mill are comparable and representative.
Keywords.*oil-well cement, free water separation, spreading of the well cement slurry*

1. INTRODUCTION

The properties of the well cement slurries intended for cementing oil and gas wells are produced both by the composition of determined mixtures and by the composition of cement, as well as by the finesses of grinding [1]. The requirements for the composition of well cements are regulated by an international standards ISO-10426-1 and API Specification 10A which establish requirements for the chemical, mineralogical and material composition of cement [2,3]. An important component of the cement is dihydrate gypsum. The main task of gypsum is to regulate the setting time due to formation on the C_3A surface - the most rapidly hardening cement phase of hydrosulfoaluminate protective shells [4,5].

Recent studies have shown that the mechanism of gypsum influence is also associated with a change in the concentration of active centers on cement particles and, accordingly, the speed of the coagulation process [5]. Gypsum also effects on the most other properties of cement [6]. Optimizing the addition of gypsum leads to a certain increase in early strength, a decrease in shrinkage deformation, and an increasing in the plasticity of cement mortars [6]. Gypsum content in well cements, in terms of total SO_3, normalized within 1,5-3,5%, for cements with high sulfate resistance – up to 3%, taking into account the low C_3A content.

One of the important properties of well cement slurries is a high water-holding capacity, which can be ensured both by adding various additives and by the composition of well cement, including hemihydrate gypsum [7,8]. During grinding cement, the temperature can reach to 150°C and more, which leads to dehydration of gypsum and the formation of hemihydrate $CaSO_4 \cdot 0,5H_2O$. At a high content of hemihydrate, so-called "false set" is possible, which causes to the rapid loss of plasticity of the mortar mixture, the need for a significant

*Corresponding author: Oleksandr Krotiuk
E-mail: o.i.krotyuk@nuwm.edu.ua
Paper received: 12. 06. 2024.
Paper accepted: 28. 08. 2024.
The website: https://www.zastita-materijala.org/

increase in water consumption and, as a result, the deterioration of the main properties of mortar [1]. However, when the hemihydrate gypsum content is below the critical level, his effect on the properties of well mortars is ambiguous. There is no simple rule to determine the optimal SO_3 content, as it depends on a range of different parameters including particle size[6].

It was established [9] that with presence of hemuihydrate gypsum in the cement, associated with a lack of SO_3 ions in the initial period of cement hydration, ettringite is not formed on the C_3A surface, but formed in the intergranular space. This increases the degree of hydration and increases the strength of the cement in the early stages [9].

Experimental results [9] showed that cements containing hemihydrate gypsum have reduced free water separation due to the difference in the mechanism of formation of hydrated phases [9]. However, in this research were studied Ordinary PortlandCements (OPC) and a technique was used to determine free water separation in percentage and with W/C=1,0 [10], while at this article attention is focused specifically on the well cements with a different method of determining free water separation, which is measured in milliliters with W/C=0,5 [11].

The available experimental data will not allow to quantitatively assess the influence of the ratio of dihydrate and hemihydrate gypsum on the main properties of oil-well mortars, considering the content of active mineral additives in the cement. The influence of this ratio allows to select the appropriate mode of cement grinding to ensure the necessary parameters of its properties. Solving this task is the goal of the research, the results are given in this article.

2. MATERIALS AND METHODS

The clinker used for research of oil-well cement class I-Ghad the following chemical and mineralogical composition: SiO_2 – 22,1%, Al_2O_3 – 4,06%, Fe_2O_3 – 5,31%, CaO – 64,63%, MgO – 0,61%, SO_3 – 0,71%, K_2O – 0,53%, Na_2O -–0,14%, CaO_{Free} – 0,65%, LSF – 0,914; C_3S – 57,75%; C_2S – 21,59%; C_3A – 1,57%; C_4AF – 15,81%.Gypsum stone, which was added to the cement, had a $CaSO_4 \cdot 2H_2O$ content - 93,1%.The blast granulated slag had the following chemical and mineralogical composition:SiO_2 – 36,44%, Al_2O_3 – 5,87%, CaO – 43,48%, MgO – 4,63%, Cao+MgO+SiO_2 – 84,55%, Glass – 97,89%, Merwinite – 1,41%, Melilite – 0,38%, Hedenbergite – 0,32%.

For the purpose to generate experimental-statistical models and establishing the relationship between the presence of hemihydrate gypsum and blast granulated slag (as the active additive in quantity of 15%) in cement and total SO_3 content, was applied full factors experiment for the three factors [12]: clinker content (x_1), hemihydrate gypsum content (x_2) and total SO_3 content of cement (x_3). The terms for planning experiments are given in table 1.The interval of the amount of gypsum hemihydrate from 1 to 3 % was chosen from the state of limited content in oil-well cement class I-G. The researches were conducted using the mathematical planning of experiments [12]. The phase state of gypsum (dihydrate and hemihydrate) was determined by X-ray Difraction(XRD diffractometer) (Fig. 1, a), total SO_3 content by analyzer LECO CS744 (Fig. 1, b), free water separation and spreading were determined according to the methods by Ukrainian standard “DSTUBV.2.7-86-99” for oil-well cements, testing methods (Ukraine) [11].This techniques are similar to the requirement of international standards [2, 3,11].

a)

b)

Figure 1. Common view of the XRD diffractometer (a) and LECO CS744 analyzer (b)

Table 1. Terms for planning experiments

Factors		The levels of variation	
Natural view	Coded names	-1	+1
Clinker content at the cement, %	x_1	80	95
Hemihydrate gypsum content at the cement, %	x_2	1	3
SO_3 content, %	x_3	1,8	3,5

3. RESULTS AND DISCUSSION

Research was conducted in laboratory conditions on a laboratory mill with mixed (balls and cilpebs) loading.To study the influence of hemihydrate gypsum, which used in a laboratory mill, gypsum was preheated to a temperature of 200°C in a muffle furnace for 60 minutes.After heat treatment, the XRD diffractometer confirmed the complete transition of dihydrate gypsum to hemihydrate gypsum. At the same time, the received cements were also checked for compliance with other requirements according to Ukrainian standard “DSTUBV.2.7-86-99 Portland oil-well cements. Technical terms” (Ukraine) [5], that is: flexural strength in 1 day (should be not less than 3,5 MPa)and thickening time to the consistency 30 Bc(not less than 90 min).

The XRD diffractograms of cements are presented in Fig. 2 and 3.The experimental results, that were obtained during the implementation of the experiments, are given in the table. 2.

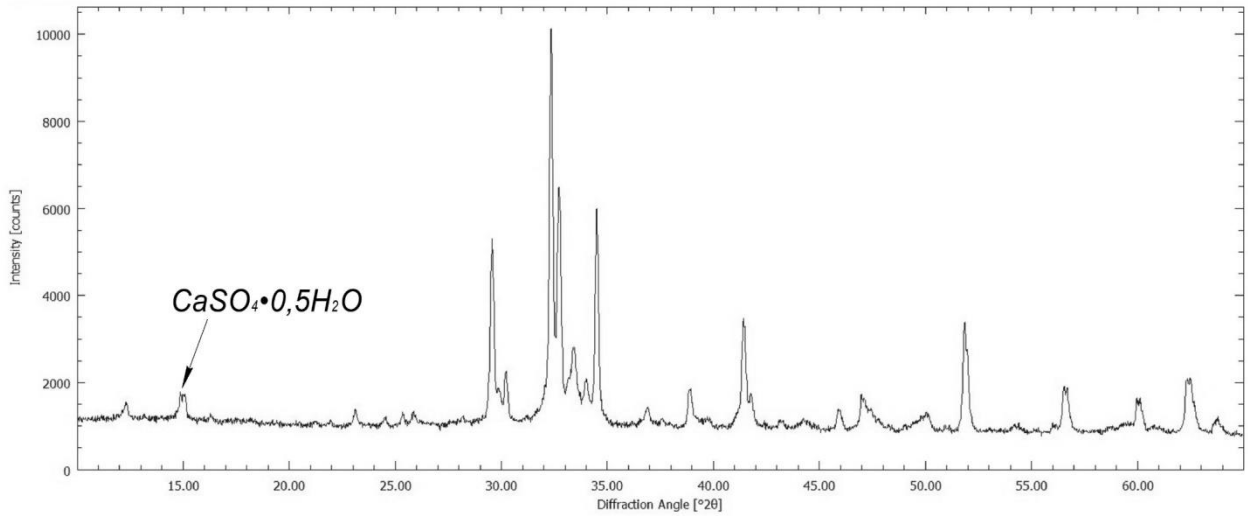

Figure 2. XRD diffractogram of cement with hemihydrate gypsum in the amount of 3%

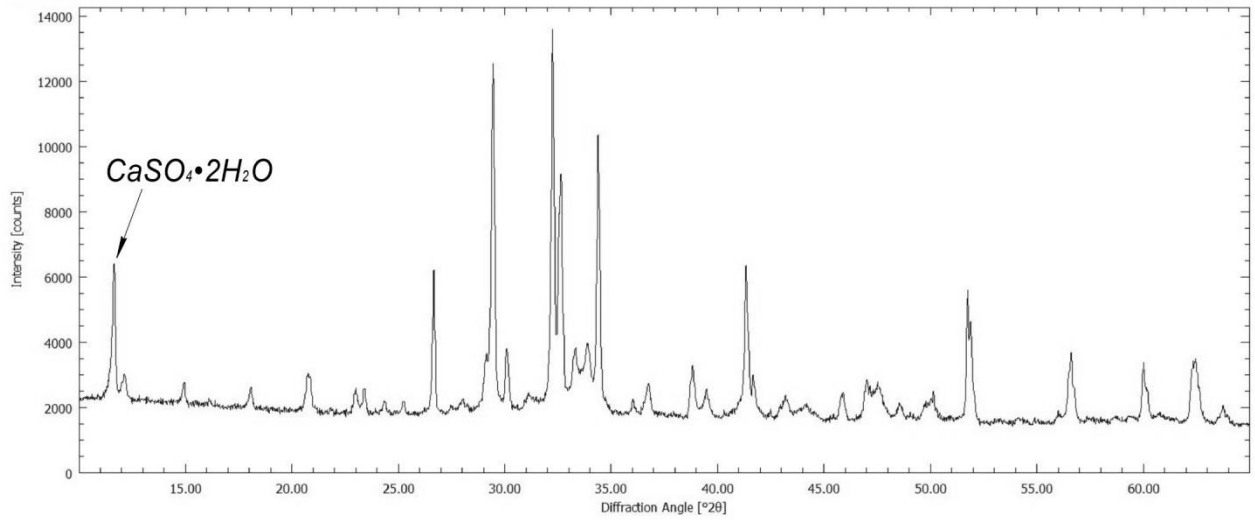

Figure 3. XRD diffractogram of cement with dihydrate gypsum in the amount of 5%

Statistical processing of the results made it possible to obtain experimental-statistical models of free water separation (Eq. 1), spreading (Eq. 2), flexural strength at the age of 1 day (Eq. 3) and thickening time to a consistency of 30 Bc (Eq. 4):

$$y_1=4,56+1,0625x_1-0,1875x_2-0,3125x_3-0,4372x_1x_2- 0,0625x_1x_3 +0,1875x_2x_3 \quad (1)$$

$$y_2=240,63+15,625x_1-9,375x_2-6,875x_3-9,375x_1x_2- 1,875x_1x_3 -1,875x_2x_3 \quad (2)$$

$$y_3=6,09+0,085x_1-0,1975x_2-0,0225x_3-0,6275x_1x_2+0,0975x_1x_3 -0,135x_2x_3 \quad (3)$$

$$y_4=150,13+5,875x_1-9,625x_2+2,875x_3+22,125x_1x_2+4,625x_1x_3 +7,625x_2x_3 \quad (4)$$

Table 2. Experimental results

Points of the plan	Factors			Experimental results					
	X_1	X_2	X_3	Free watersep ara-tion, ml	Spre-ading, mm	Flexu-ralstre-ngth, 1 day, MPa	Thicke-ning time to the consis-tency 30 Bc, min	Compres-sive strength 2 days, MPa	Compres-sive strength 28days, MPa
1	95	3	3,5	5	225	5,4	192	20,95	44,04
2	95	3	1,8	5	250	5,3	145	19,17	41,6
3	95	1	3,5	5,5	270	7,1	135	17,5	42,6
4	95	1	1,8	7	280	6,9	152	19,71	41,79
5	80	3	3,5	3,5	220	6,07	110	17,89	43,43
6	80	3	1,8	4	230	6,8	115	19,54	41,12
7	80	1	3,5	3	220	5,7	175	11,83	38,96
8	80	1	1,8	3,5	230	5,45	177	15,93	41,03

Analyzing the mathematical model of free waterseparation (Eq. 1), can see that an increase of the clinker content (absence of slag), during grinding cement, significantly increases the indicator of free water separation, and the combination of factors of slag content and the presence of dihydrategypsum -reduces free water separation.The presence of hemihydrate gypsum slightly affects to the indicator of free water separation (Fig. 4, a).

During analyzing the mathematical model of spreading (Eq. 2), it can be stated that the content of blast granulated slag in cement significantly reduces the indicator of spreading, the presence of hemihydrate in cement, and combination of slag content and dihydrate gypsum also reduces spreading. The presence of hemihydrate gypsum in cement reduces spreading by 15-20 mm compared to dihydrate gypsum (Fig. 4, b).

Analysis of the mathematical model of flexural strength at the age of 1 day (Eq. 3) shows that the combination of factors of slag content and the presence of dihydrate gypsum reduces the strength index.

A mathematical model of the thickening time to a consistency of 30 Bc (Eq. 4) shows that the combination of the factors of slag content and the presence of dihydrate gypsum adds 22 minutes to the thickening time, while the presence of hemihydrate gypsum - reduces the thickening time.

According to the results of the experiments and the processing of that results, was found that in the presence of hemihydrate gypsum in additive-free cement, the free water separation decreases by 1 ml, compared to the presence of dihydrate gypsum, which can be seen in fig. 4, a.In percentage terms, this figure will be 0.24%, which is not a significant decrease.

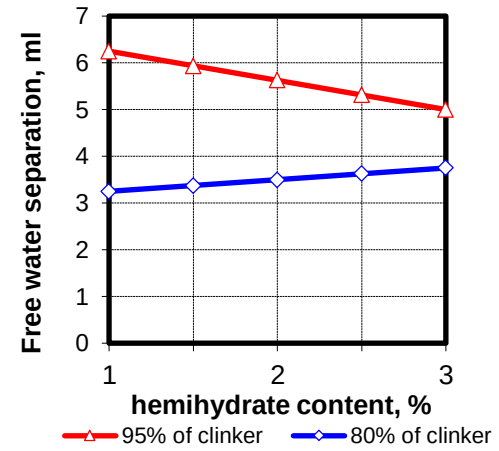

a)

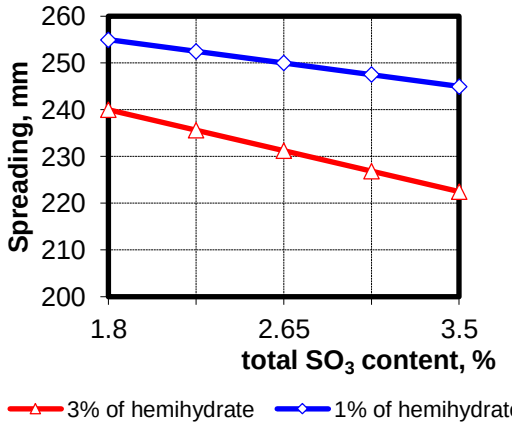

b)

Figure 4. Dependencies of free water separation fromhemihydrate gypsum content and % of additive (slag) in cement (a), and spreading

fromhemihydrate gypsum content and % of total SO_3content in the cement (b)

Analyzing the results, it can be seen that the flexural strength (3) decreases in the presence of hemihydrate and without the blast granulated slagcontent (Fig. 5, a), as well as with the simultaneous presence of hemihydrate in the cement and the total SO_3content of 3,5%.

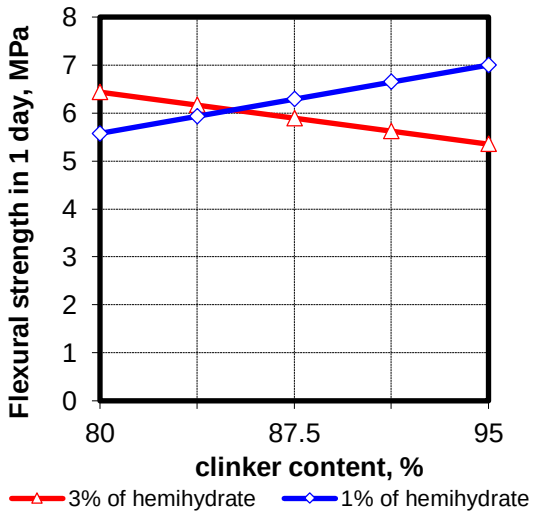

a)

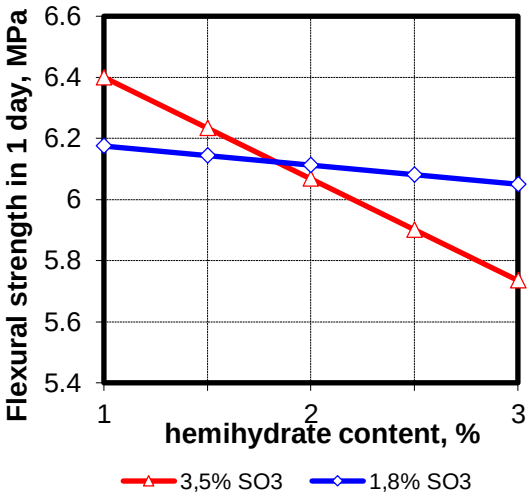

b)

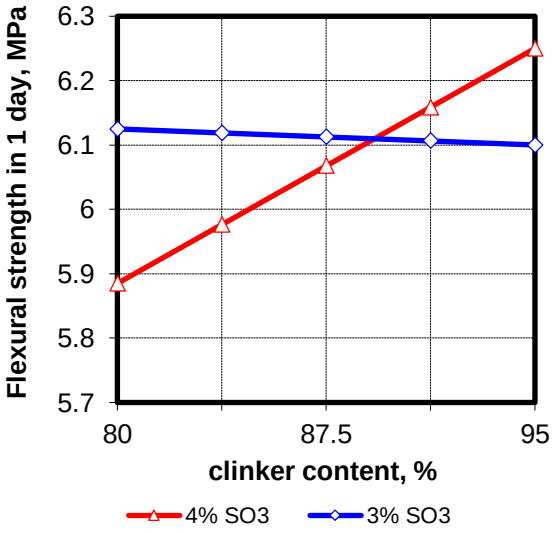

c)

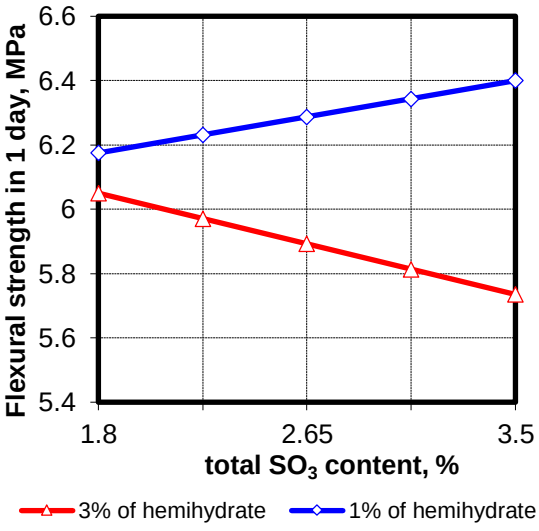

d)

Figure 5. Dependencies of flexural strength at the age of 1 day fromhemihydrare gypsum content and clinker content (%) in cement (a), to the total SO_3content in cement and hemihydrate gypsum content (b), to the total SO_3content in cement and clinker content (c), tohemihydrate gypsum content and the total SO_3content in the cement (d)

It should be especially noted that with an SO_3 content of 1,8%, the presence of hemihydrate gypsum in cement does not affect to the flexural strength at the age of 1 day, which can be seen in Fig. 5, c. In fig. 5, d shows that when the total SO_3 content in the cement is 3,5% and the presence of 3% hemihydrate gypsum - the strength decreases.

Considering the results of the thickening time to a consistency of 30 Bc, it can be concluded that the time decreases by 60 min with the presence of hemihydrate gypsum in the cement at the same time with slag, which can be seen in fig. 6, a.The thickening time increases to 170 min in the cement without additives and with the presence of hemi-hydrate gypsum, which can be seen in fig. 6, b.

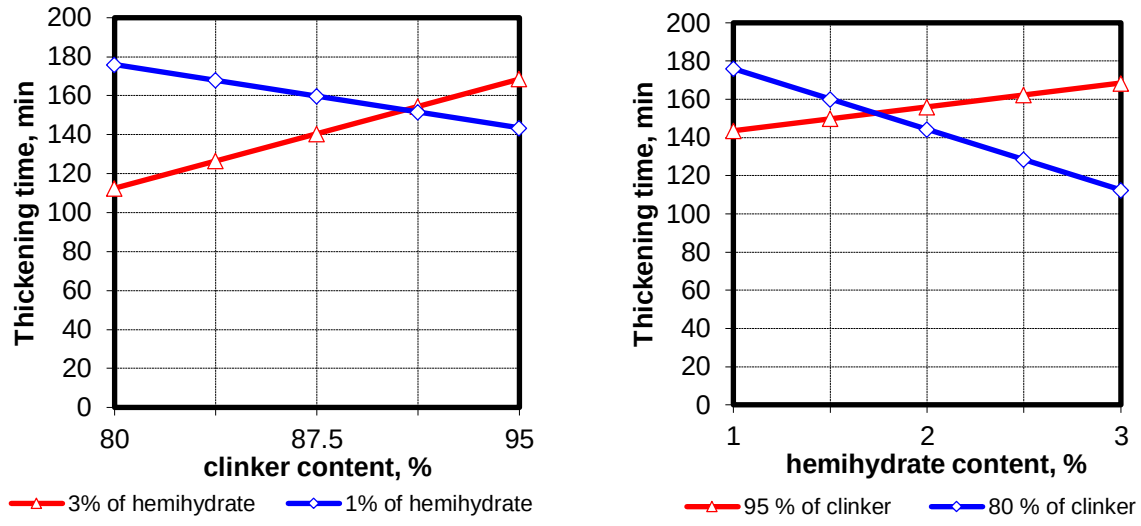

a) *b)*

Figure 6. Dependencies of the thickening time to a consistency of 30 Bcfrom the hemihydrate gypsum content and clinker content (%) in cement (a), from the clinker content (%) in cement and the hemihydrate gypsum content (b)

In addition, during the experiments, was noted that the free water separation decreases with the slag content in the cement, which can be seen in fig. 1, a.Also spreading increases with additive-free cement compared to slag including cement, which can be seen in fig. 1, b. According that information we can conclude that the presence of an additive (in the form of slag) in cement has a positive effect on the indicator of free water separation and a negative effect on the indicator of spreading.

During laboratory tests, were performed also the compressive strength analyzes of the received cements at the age of 2 and 28 days, according to the methods for OPC [7].The data are presented in table 2. Statistical processing of the results made it possible to obtain mathematical models of compressive strength at the age of 2 days (Eq. 5) and 28 days (Eq. 6).

$$y_5=17,82+1,5175x_1+1,5725x_2-0,7725x_3-0,845x_1x_2+0,665x_1x_3+0,805x_2x_3 \quad (5)$$

$$y_6=41,82+0,68625x_1+0,72625x_2+0,43625x_3-0,41375x_1x_2+0,37625x_1x_3+0,75125x_2x_3 \quad (6)$$

Analyzing the mathematical model of the compressive strength at the age of 2 days (Eq. 5), can see that cement without additives and presence of hemihydrate gypsum has increased early strength. The minimum level of total SO_3 content reduce the compressive strength at the age of 2 days. The combination of factors of additive content (slag) and hemihydrate gypsum also reduces compressive strength. The combination of factors of additive-free cement content together with the presence of hemihydrate gypsum - increases early compressive strength.

The mathematical model of compressive strength at the age of 28 days (Eq. 6) shows that the presence in additive-free cement hemihydrate gypsum and an increased total SO_3 content increased the compressive strength. The combination of factors of slag content cement with dihydrate gypsum reduces compressive strength. Combination factors of hemihydrate gypsum and the increased total SO_3 content has increased the compressive strength at the age of 28 days. Compressive strength (2 and 28 days) graphs are shown in fig. 7 and 8.

Along with this, was carried out a production test on a cement mill with two-chambersof standard size of 3.2x15 m with ball loading of the 1st and 2nd chambers.During the production process, the required contents of hemihydrate and dihydrate gypsum were achieved.The data are shown in table 3.

Analyzing the data obtained during the production experiment, it can confirm the results obtained during the laboratory study, namely: the presence of hemihydrate gypsum in the cement reduces free water separation and reduces spreading.

Table 3. Results of production experiments

№ of sample	Free water separation, ml	Spreading, mm	Flexural strength at 1 day, Mpa	Thickening time to the consistency 30 Bc, min	Total SO_3 content, %	Dihydrate gypsum ($CaSO_4$* $2H_2O$),%	Hemihydrate gypsum($CaSO_4$* $0,5H_2O$), %	Anhydrite ($CaSO_4$), %
1	3,0	220	7,6	110	3,49	5,47	0,53	0,00
2	2,0	195	6	140	3,40	0,58	3,06	0,15

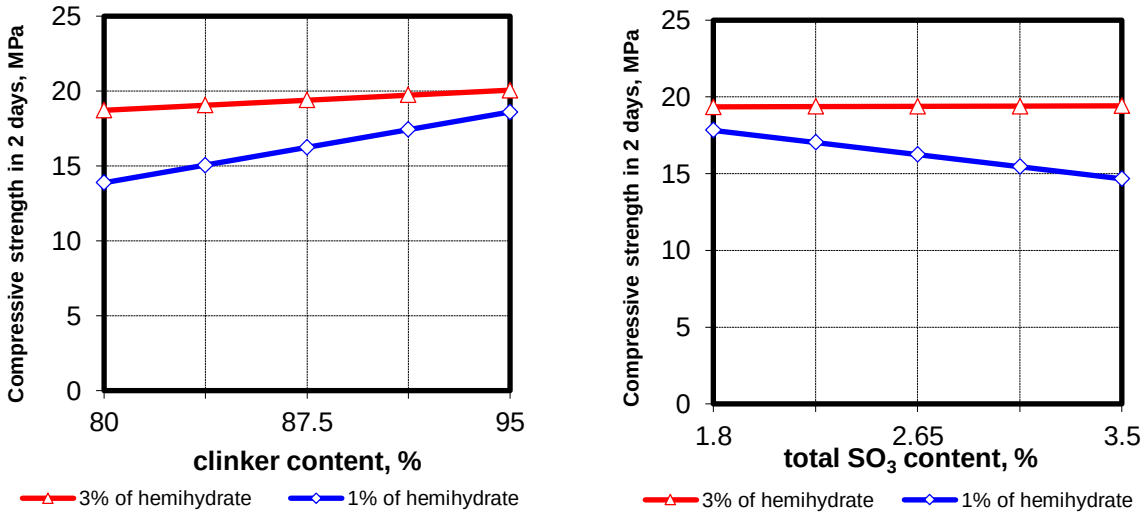

a) *b)*

Figure 7. Dependencies of compressive strength at the age of 2 days from thehemihydrates gypsum content and clinker content (%) in the cement (a), from the hemihydrate gypsum content and total SO_3 content (b)

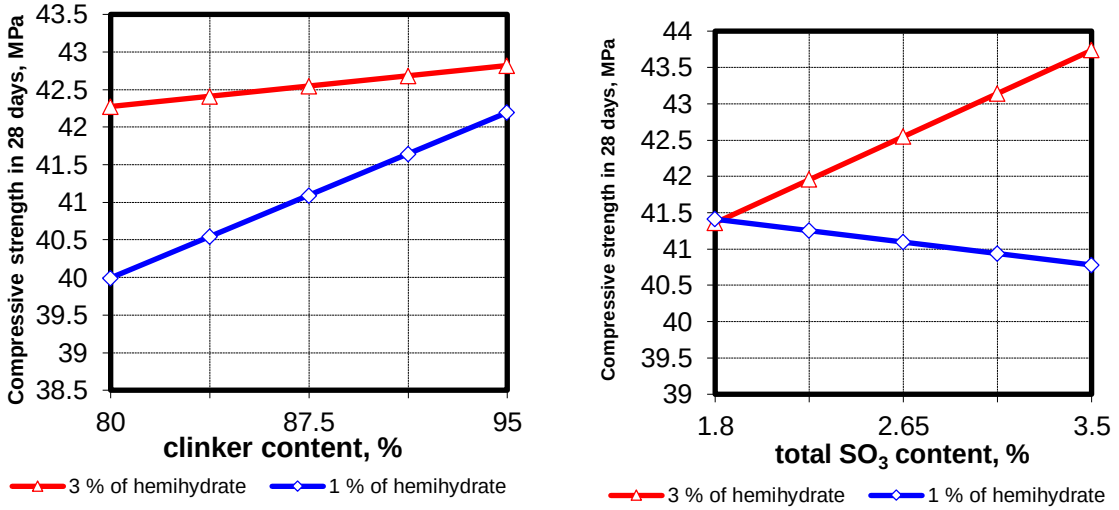

a) *b)*

Figure 8. Dependencies of compressive strength at the age of 28 days from the hemihydrates gypsum content and clinker content (%) in the cement (a), from the hemihydrate gypsum content and SO_3 content (b)

Analyzing the intensity of influence researched factors on the studied properties (Eqs. 7-12)in the direction of reduction it can be ranked in the following sequence (the most significant coefficients are selected):

free water separation (y_1)

$$x1x2>x3>x2 \quad (7)$$

spreading (y_2)

$$x1>x2>x1x2>x3 \quad (8)$$

flexural strength at the age of 1 day (y_3)

$$x_1x_2> x_2> x_2x_3 \quad (9)$$

thickening time to a consistency of 30 Bc (y_4)

$$x1x2>x2>x2\ x3>x1>x1x3 \quad (10)$$

compressive strength at the age of 2 days (y_5)

$$x2>x1>x1x2>x2x3>x3 \quad (11)$$

compressive strength at the age of 28 days (y_6)

$$x2x3> x2>x1>x3 \quad (12)$$

4. CONCLUSION

The conducted cycle of research made it possible to obtain quantitative dependences of the influence of the additive content in cement (slag), the hemihydrate gypsum content and the total SO_3content in cement.

The analysis of the obtained models allows that the presence of hemihydrate gypsum has an ambiguous effect on the properties of oil-well cement, reducing the spreading of the well cement slurry, but at the same time increasing the flexural strength at the age of 1 day.

The presence of hemihydrate in the cement in the amount of 3% - reduces free water separation and the thickening time to the consistency of 30 Bc.The presence of hemihydrate gypsum in the cement with a total SO_3 content of 1,8% practically does not affect the flexural strength.Also, in the presence of hemihydrate gypsum, the thickening time level is not less than the requred 90 minutes.

Numerical analysis of the coefficients of the models allows to rank the factors according to growth or decline and their influence on the corresponding initial parameters.

5. REFERENCES

[1] L.Dvorkin (2019) Construction building materials. – K.: «Kondor». – p. 628

[2] ISO 10426-1:2009 Petroleum and natural gas industries — Cements and materials for well cementing, Part 1: Specification

[3] API SPEC 10A:2019+ADD1:2019 Specification for Cements and Materials for Well Cementing.

[4] H.F.W. Taylor (1997) Cement chemistry, 2-nd edition.– London, England, Thomas Telford Publishing. – p. 560

[5] A.A.Pashchenko, F.A.Myasnikova, V.S.Gumen (1991) The theory of cement.– K.: Builder–p. 168

[6] E. B. Nelson, D. Guillot (2006) Well cementing, 2-nd edition., Texas; Schlumberger, - p. 774

[7] DS. Smirnov, S. V. Stepanov, G. R. Hilaviea (2015) The analysis of the state of the question about possible ways to improve the quality of oil-well mixtures. – Bulletin of the Technological University., T.18, №20.

[8] S. Igbani, K. Kotingo, B.J. Igolima, V.W. Osakwe (2022) Mix-Water as a Chemical Additive for Oil Well Cement Compressive Strength Development, International Journal of Chemistry, Ontario.

[9] A.S.Normantovich(2005) Regulation of the process of free water separation of cement-water dispersed systems. Abstract for the dissertation. – Bilgorod.

[10] National standard of Ukraine. building materials. cements. method of determining free water separation. DSTUBV.2.7-186:2009. Ministry of Regional Development and Construction of Ukraine. – Kyiv, 2010.

[11] State standard of Ukraine. Building materials. oil-well portland cements. testing methods. DSTUBV.2.7-86-99.

[12] L. Dvorkin, O. Dvorkin, Y. Ribakov (2012) Mathematical experiments planning in concrete technology.– Nova Science Publishers, Inc. + New York. – p.173

[13] National standard of Ukraine. building materials. cements. methods of determining flexural and compressive strength. dstu BV.2.7-187:2009. Ministry of Regional Development and Construction of Ukraine. – Kyiv, 2010.

IZVOD

UTICAJ HEMIHIDRATNOG GIPSA NA OSNOVNA SVOJSTVA ULJNOG CEMENTA

Tokom ovog istraživanja korišćeni su laboratorijski mlin i mlin za proizvodnju cementa za poređenje rezultata. Svrha istraživanja je bila da se utvrdi uticaj gipsa različitog faznog stanja (dihidrat ili hemihidrat), aktivnog aditiva granulisane šljake i ukupnog sadržaja SO_3 na separaciju slobodne vode, rasprostranjenost cementne suspenzije bunara i savijanje i pritisak. čvrstoća cementnog maltera. Sproveden ciklus istraživanja omogućio je dobijanje kvantitativne zavisnosti tih parametara. Za istraživanja je korišćen gips prethodno zagrejan u peći na 200°C u trajanju od 60 minuta. Tokom ovog istraživanja otkriveno je da prisustvo hemihidrata gipsa u cementu nema veliki uticaj na separaciju slobodne vode, ali ima izvestan uticaj na širenje cementne suspenzije bunara. Takođe, ovim istraživanjem je otkriven uticaj hemihidratnog gipsa na čvrstoću na pritisak u dobi od 28 dana i čvrstoću na savijanje u dobi od 1 dana. Tokom ovog istraživanja otkriveno je da prisustvo hemihidrata gipsa na cementu smanjuje vreme zgušnjavanja za 60 minuta. Prisustvo granulirane šljake na cementu smanjuje slobodnu separaciju vode u cementnoj suspenziji bunara. Tokom istraživanja u proizvodnom mlinu cementa obezbeđeno je da prisustvo hemihidrata gipsa na cementu smanji širenje za 25 mm i smanji slobodnu separaciju vode za 1 ml. Rezultati ispitivanja iz proizvodnog mlina za cement i laboratorijskog mlina su uporedivi i reprezentativni.
Ključne reči: *cement iz bunara, slobodna separacija vode, nanošenje bušotine cementne suspenzije.*

Naučni rad
Rad primljen: 12.06.2024.
Rad prihvaćen: 28.08.2024.

Krotiuk Oleksandr: https://orcid.org/0009-0007-2712-8644
Dvorkin Leonid : https://orcid.org/0000-0001-8759-6318

Nikita Singh[1], Satish Kumar Yadav[2], Aradhana Shukla[1], Amit Misra[3], Jyotsna Singh[1], Rajendra Bahadur Singh[1]*

[1]Department of Physics, University of Lucknow, Lucknow, India, [2]Instituteof New and Renewable Energy, University of Lucknow, Lucknow, India, [3]Manipal Academy of Higher Education, Dubai Campus, UAE

Scientific paper
ISSN 0351-94, E-ISSN 2466-2585
https://doi.org/10.62638/ZasMat1186

Zastita Materijala 66 (1)
167 - 178 (2025)

Study of green microalgae as a feedstock for biodiesel production

ABSTRACT

Biodiesel as an energy source has marked an edge to a growing energy crisis issue. There are multiple ways by which biodiesel can be produced, and aggressive researchisgoing on in the field of biodiesel. In this work, we have focused on biodiesel production from microalgae. Green microalgae, a third-generation feedstock, are promising candidates for biodiesel production because of their high lipid content and rapid growth. In this study, for the cultivation of microalgae, an environment of varying temperatures that was between 27°C to 32°C was created. Also, three different concentrations (2:2, 2.5:1.5, and 3:1) of aquarium and freshwater were considered in this work for algae growth, and the lipid extraction method like mechanical cell destruction was investigated to determine its efficiency. Once the lipid extraction process was optimized, the extracted lipids were subjected to a transesterification process, converting them into biodiesel. The results of this study show that the greater concentration of aquarium water resulted in better algae production, i.e., dried weights of algae extracted from the above-considered concentrations were 2.69 grams, 2.79 grams, and 2.92 grams respectively. Biodiesel produced from the dried algae was 3.15 ml, 3.96 ml, and 4.95 ml, respectively. These results suggest that green microalgae can be considered an enticing raw material for biodiesel production. Optimizing cultivation and lipid extraction methods can improve biomass and lipid productivity, boosting overall biomass yield. This study concludes that algal biodiesel can be an alternative source to petroleum-based diesel fuel.

Keywords: *Biodiesel; microalgae; lipid extraction; biomass; temperature*

1. INTRODUCTION

The global energy consumption through energy sources like petroleum, coal, and diesel in the last thirty years has increased very drastically with an average annual increase of 3.4 %, which is almost 1.2 % points higher than the average growth of energy consumption (1). Humans fulfill their energy demand by burning fossil fuels, as they are easy to use, provide high energy density, and have a low cost compared to any other alternative energy source or non-conventional energy source. However, prolonged use of petroleum-based fuels has led to the emission of greenhouse gases like carbon dioxide at a high rate, causing acid rain and global warming—the earth's mean temperature increased by an average of 0.14 °F per decade since 1880, or about 2 °F in total (2).

Also, because of the continuous use of fossil fuels, their reserves are depleting fast, so they may not last more than a hundred years from now. According to the Millennium Alliance for Humanity and the Biosphere (MAHB) report, the world's oil reserves will run out by 2052, natural gas by 2060, and coal by 2090(3). Therefore, several research projects and experiments are being carried out to find different alternative sources for the fulfillment of energy demand that can be renewable, economical, and environmentally friendly. It includes solar energy, wind energy, geothermal energy, and biofuels. A lot of innovative work is going on in these fields (4–7), and in the future, they will change the pattern of energy production.

The transport sector uses approximately 25% of the total energy consumption and islargely dependent on petroleum (8). Fortunately, biofuels can be used as an alternative to diesel engines. Biofuels are combustible fuels produced from renewable biomass resources, i.e., agricultural or forest products, animal waste, and biodegradable portions of industrial waste. Biofuels are classified into two categories: primary and secondary

*Corresponding author: Jyotsna Singh
E-mail: singh.jyotsnalu@gmail.com
Paper received: 27.03. 2024.
Paper corrected: 20.07. 2024.
Paper accepted: 23.08. 2024.
The website: https://www.zastita-materijala.org/

biofuels, based on whether biomass undergoes processing or remains unprocessed to be used as biofuel. Primary biofuel (solid biofuel) is an unprocessed form of biofuel generally used for cooking, heating, and electricity generation. Wood pallets, charcoal, sugarcane, corn, maze, etc. are a few examples of primary biofuels. On the other hand, secondary biofuel is produced by processing biomass through fermentation or transesterification processes(9).It includes liquid and gaseous forms of biofuel, such as biodiesel and bioethanol in the liquid phase, while biogas and biomethane in gaseous form can be used as an alternative source for petroleum-based fuels in the transport and industrial sectors. Assuming that in the future there will be high demand and extensive use of biofuel, which will require a much greater supply of feedstock on a sustainable basis. To fulfill that demand, there is considerable enthusiasm that is being taken to include many potential biomass sources other than edible crops to increase the production of biofuel at a large scale while avoiding the conflict of fuel versus food security. In this context, biofuel feedstock is classified into four generations depending on the characteristics of biomass feedstock and the technology involved in biomass processing. First-generation feedstocks like corn, hay crops, etc. undergo distillation, hydrolysis, transesterification, and fermentation technology, but they pose a threat to the food crisis. While second-generation feedstock contains all the non-edible crops such as rice husk, jatropha, agricultural residue, etc. They produce biofuels from expensive technologies like thermochemical and complex biochemical. Third- and fourth-generation biofuel feedstocks are microorganisms or microalgae and modification of microorganisms genetically, respectively.

This study focuses on third-generation biofuel feedstock microalgae. Biodiesel produced from microorganisms through the transesterification process is a better alternative to conventional diesel fuels. It is renewable and biodegradable and is considered a ‘carbon neutral fuel’ because its net emission of greenhouse gases is almost nil. Biodiesels have the property of high lubricity, which, when used in diesel engines, increases the vehicle's life span. Biodiesel can be used in its pure form as well as in blended form, where it is blended with petroleum diesel. According to the Mubarak et al.(10), the pure (unblended) biodiesel that is used is termed B100 and when it is blended with fossildiesel fuel,in different ratios, it is termedB2, B5, and B20 where the numberindicates the percentage of biodiesel blended with the fossil diesel fuel withshares2%, 5%,20% and100% in agallonofdiesel fuel.

Microalgae is a unicellular or eukaryotic photosynthetic microorganism that has a simple cell structure that uses sunlight, water, carbon dioxide, and materials like phosphorus and nitrogen as their main nutrient for its growth. They can easily be found in seawater as well as fresh water. Microalgae particularly have high oil content and grow rapidly, so they can double their mass in 24 hours(11).Microalgae have great flexibility and adaptability to grow even in diverse environments. In other words, it uses less arable land than any of the other terrestrial plants; therefore, the conflict with food production is not the issue here. The growth rate of microalgae is about 5–10 times faster than any conventional food crop. Moreover, microalgae have high lipid productivity which is the major reason for using it as analternative to biodiesel feed stock (11).According to a study, microalgae can have 15-300 times more lipid or fat productivity than any common oil crop (12).

In recent years, microalgae have attracted much more attention for producingbiodiesel.

At present, several studies are being carried out with different compositions of biodiesel from different species of microalgae. A California company, Salarymen, has already generated tens of thousands of gallons of algae-based fuels as part of their research and development agreement (13). In a study conducted by Lim et al., they successfully converted microalgal oil into bio-jet fuel using a hydroprocessing technique(14). Previous studies performed by Maria et al., Yanan et al., Sushant et al., and Jassinnee et al.have proven that different species of microalgae have a great potential to produce biodiesel(15–18). According to the literature review(19–22) marine and freshwater species of microalgae should be considered to produce biodiesel because of their high lipid content.However, in recent yearsstudies conducted by Tahir et al., Gang et al., and Alejandra et al.revealed that algae cultivated in wastewater also have the potential to produce a significant amount of biodiesel, and algae can also effectively remove the toxic elements from the wastewater, playing an important role in wastewater treatment (23–25). Their capability of wastewater treatment and being a rich source for biodiesel production makes them suitable sources to be grown on a large scale (26).

However, this study focuses on microalgae cultivation in different compositions of aquarium and freshwater and its impact on lipids. It also gives a picture of the filtration methodused for microalgae harvesting,and a brief description of thebead-beating oil extraction technique, where a household blender RPM 18000 is used for cell

disruption. Furthermore, this study also discusses the production of the catalyst potassium hydroxide (KOH)through rainwater. So far, this is the first-time aquarium and freshwater composition have been discussed for algal cultivation. Though this study was performed on a small scale, it can be implemented on a large-scale project because it is economical and achievable.

2. MATERIAL AND METHOD USED

The material and methods used in this study are mentioned below:

2.1.Algae production process

Algae can be cultivated in open ponds, conventional bioreactors, and photobioreactors through phototropic, heterotropic, mixotrophic, and photo-heterotropiccultivation processes. Abrief presentation of the different stages of biodiesel production is shown in Figure 1. In this study, microalgae were cultivated for biodiesel production. The cultivation required sunlight, water, carbon dioxide, and nutrients in a 19:19:19 ratio of nitrogen, phosphorus, and potassium (19:19:19 NPK). This water-soluble fertilizer mixture is a product of the Indian Farmers Fertilizer Co-operative Limited (IFFCO).

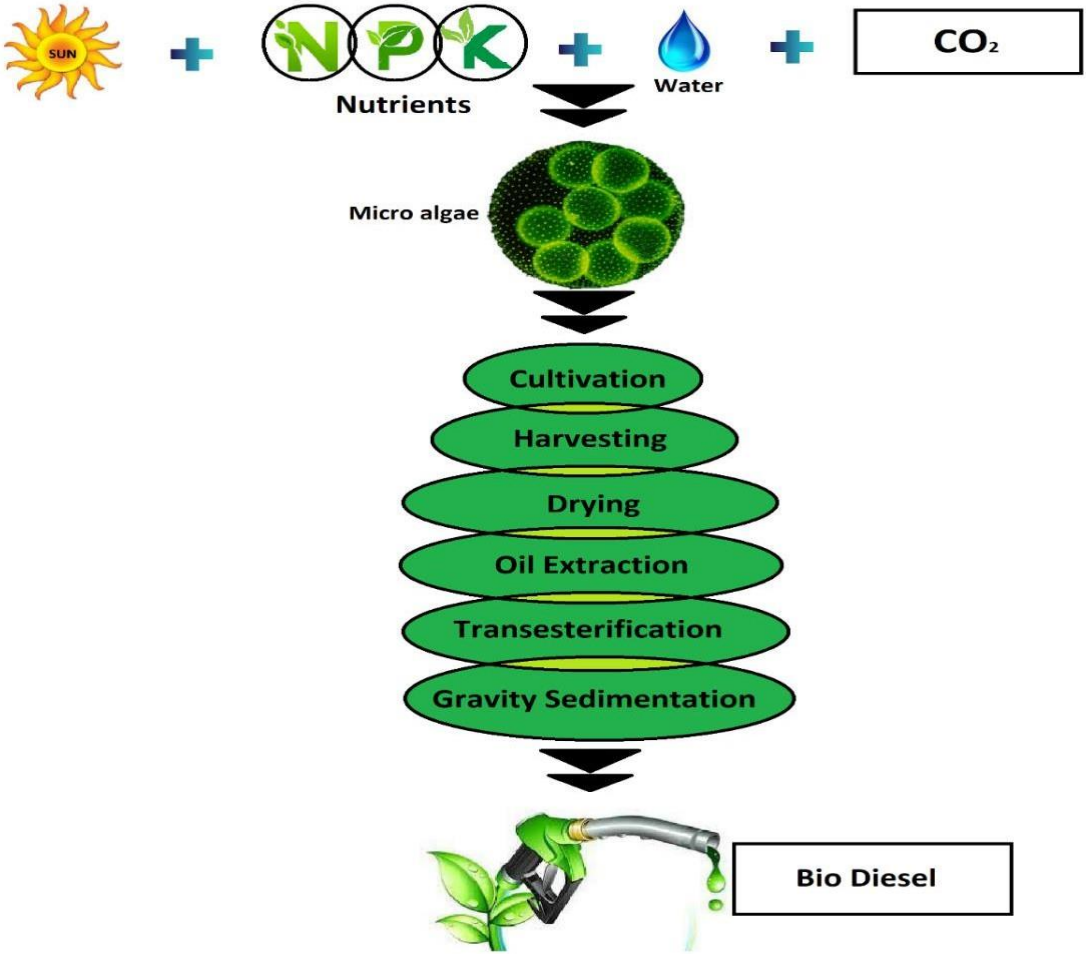

Figure 1. Different steps of biodiesel production

2.1.1.Preparation of culture media

There are two most common microalgal cultivation systems:(i) openmicroalgalcultivation systems and (ii) closed microalgal cultivation systems (27). The proper light and temperature are required for algal growth with the other specific components in both culture systems. In the closed cultivation system, different types of enclosed photo-bioreactors areused for the growth of phototrophs like microalgae under controlled conditions. In this work, for the production of microalgae, fish aquarium water that was stored for28 days was mixed with fresh water (213 TDS) in differentratiosi.e. 2:2,2.5:1.5, and 3:1 in three different glass jars (Figure2) and 5 ml of micro-algal sample were added in each concentration. Continuousshaking was administered,so it didnotproduce excessive CO_2.

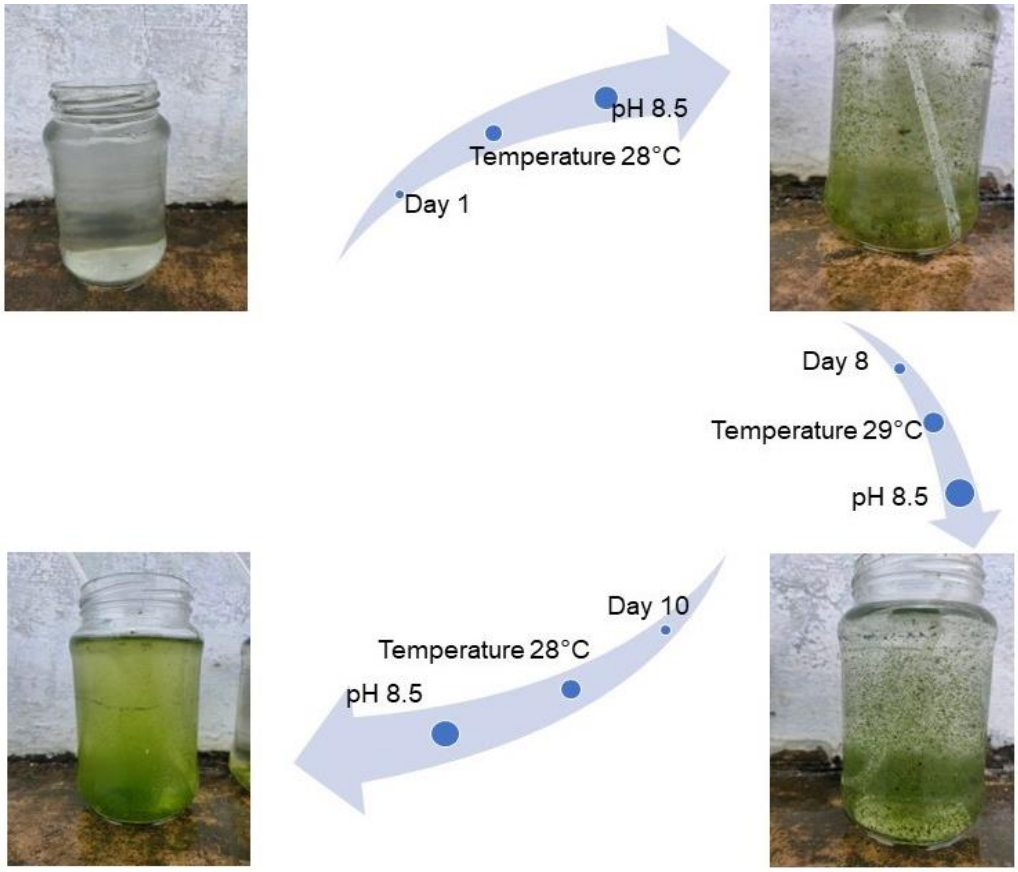

Figure 2.Stages of Microalgae Cultivation

2.1.2. Culturing Conditions

Microalgal growth depends on light, carbon dioxide, pH value, temperature,andthe presence of materials like phosphorus and nitrogen. The basic condition for algae cultivation is, the presence oflight wavelengthbetween 600nm to 700nm, a temperature range between 10°C–35°C, a pHvalue between 7-9, and a water salinity range between 12–40 g/l issuitable.During the experiment, to maintain the temperature and avoid the production of excess CO_2 in culturing media, the Orbital Shaking Incubator (tabletop VSLI-144 model) was used. In this work, microscopic green algae were used,the selection of this algae is based on itsrelatively high lipid accumulation in comparison to red algae and brownalgae. However, red algae can be used as a key for accelerating biodiesel production.

2.1.3. Monitoring culture growth

During the experiment, temperature and pH valueswere monitoredand maintained between 27°C-32°C and 8.5 respectively. This cultural growth was monitored for 16 days.

2.1.4. Microalgae Harvesting

Algal harvesting has many different harvesting techniques such as gravitysedimentation, filtration, floatation, and centrifugation (28). In this experiment, the filtration technique was used as it does not require any kind of installation, has quite high recovery efficiency, and produces much more clear material than the sedimentation process. The micro-algal culture of the jar was poured on the filter paper (Weightoffilterpaper=0.23 g) placedover the other jar and we waited till the complete draining. The green slime found on the filterpaper (Figure3)wasalgalbiomassthatwasfurther used foroil extraction. The total dry weight of algae is calculated using the given formula:

Total dry weight of algae = Weight of filter paper without filtrate - Weight of filter paper without filtrate (1)

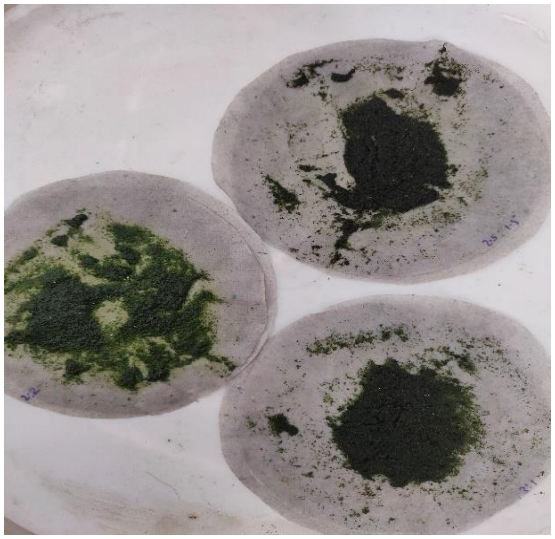

Figure 3: Algae Sample for Different Concentrations

2.1.5. Oilextraction from microalgae

There are several oil extraction methods to extractlipids from microalgae, but all those methods areclassified into two broad categories: (i) the Mechanical OilExtraction Method and (ii) the Chemical Oil ExtractionMethod.However, in recent years, some scientists classifiedthe oil extraction method for microalgae into threemore different groups that are based on Enzymes i.e. (i) Enzyme-Assisted Method, (ii) Accelerated Solvent Extraction (ASE),and (iii) Microwave-Assisted Extraction (MAE) (29)In this work, bead beating a mechanical method was used for lipid extraction during the experiment. This method refers to the disruption of microalgae cells, where damage isdirectly caused to the cell by high-speed spinning. There are two very common types of bead millmethods, the Shaking VesselMethod (SVM) and the Agitated Beads Method (ABM) (30). In shaking vessels, the cells aredamaged by continuous shaking of the entire vessel on a vibrating platform whereas a rotating agitator is fixed inside the culture ves sel which damages the cells of microalgae in ABM.

A complete ABM technique is shown in Figure 4.Duringtheexperiment,due to the unavailability of oil extraction equipment, a household blender (RPM 18000) was used for breakingcells of microalgae usinga mechanical technique and water was addedto form a solution. Then it was left to be settled. Oil was separated as itformed a layer at the top of the jar (Figure5). The volume of the algal oil was initially measured**,** and the volume yield per liter was determined using the formula given below:

$$Concentration\ of\ algae\ per\ litre = \frac{Dry\ weight\ of\ algae}{Algal\ water\ collected} \times 1000 \qquad (2)$$

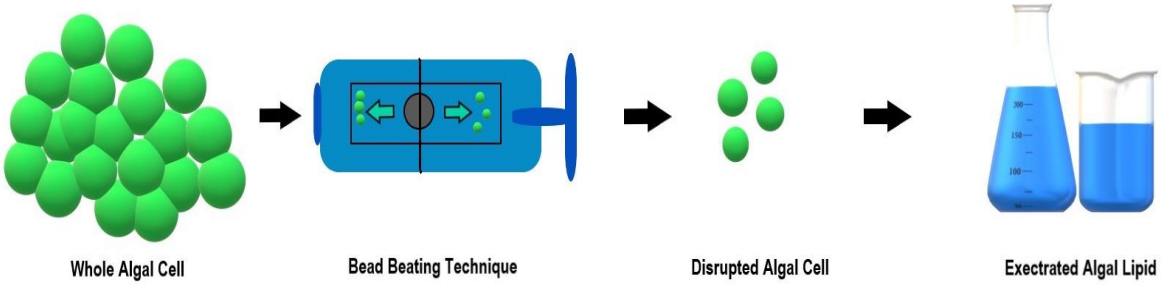

Figure 4.Bead Beating Oil Extraction Technique

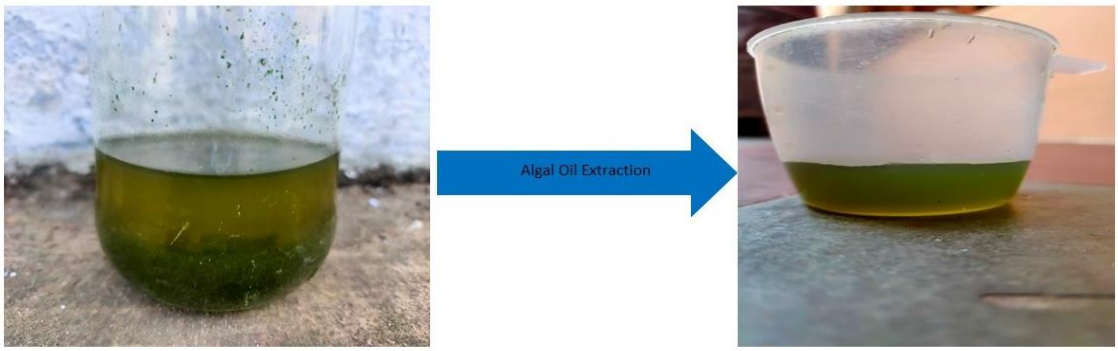

Figure 5. Oil Extraction

2.1.6. Preparation of catalyst KOH for thetransesterification process

For this study potassium hydroxide solution was made from white ashes of hardwood. When hardwood trees like sugar maple, buckeye, and beech grow they extract potassium from the ground(31) In this experiment, Indian Horse Chestnut tree ashes were used as the potassium present in the wood does not burn with fire and is in the ashes.

Figure 6: Preparation of Potassium Hydroxide Solution

The second thing we need is soft water, in this work, rainwater is taken as soft water because it is ideal for preparing KOH solution as it has a lower concentration of other components and is available in large quantities. After this layers of pebbles, dried straw, hardwood ashes, and rainwater are filled in a disposable glass from bottom to top (31) as shown in Figure 6. The glass has holes at the bottom, for the drainage of water. This drained water is collected, and the pH value is testified. If the pH value is 13, it is a strong KOH solution but if its value is less, then the entire water is again poured into the barrel. In this work, 15 ml of rainwater with 10 g of hardwood ashes was taken to prepare the catalyst that produced 12.5 ml of potassium hydroxide (KOH) solution with a pH of 13.48.

2.1.7.ConversionofMicro-AlgalLipidtoBiodiesel

Following the oil extraction process, the resultant micro-algal lipidor oilcan be converted into biodiesel by any of the mechanical or chemical methods.However, in this study lipid is converted into biodiesel by theprocess of transesterification which is a chemicalprocess where triglyceride (TAG) i.e. algal oilwas reactedwith ethanolin the presence of catalyst i.e. KOH resulting in the formation of biodiesel andgly cerolasaby-product (Figure7).

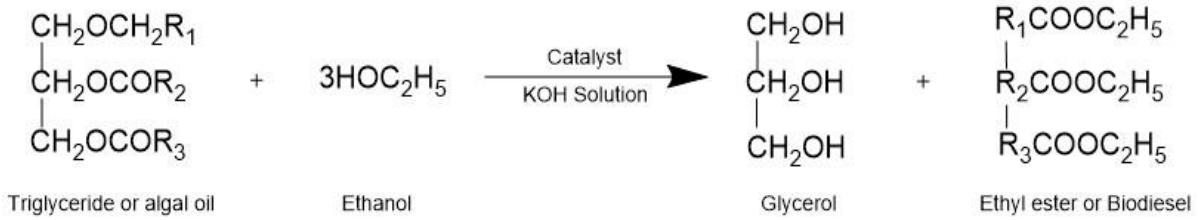

R1, R2& R3 represent the chain of fatty acids in TAG and ethylester.

2.1.8. SeparationofBiodieselandGlycerinbyGravitySettlementMethod

After the transesterification process, the mixture of glycerol and ethylesteriskeptforapproximately 24 hourstoseparate biodieselandglycerin. Figure7shows the separation of biodiesel from glycerin.

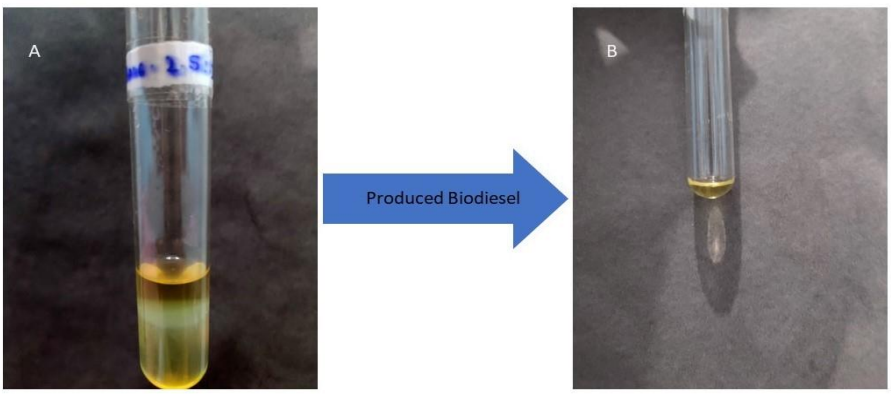

Figure 7.(a) Transesterification process, (b) Produced Biodiesel

3. RESULT AND DISCUSSION

The amount of cultivated algae, algal oil extraction, andbiodiesel produced for 2:2, 2.5:1.5, and 3:1 concentrations are shown in Figures.

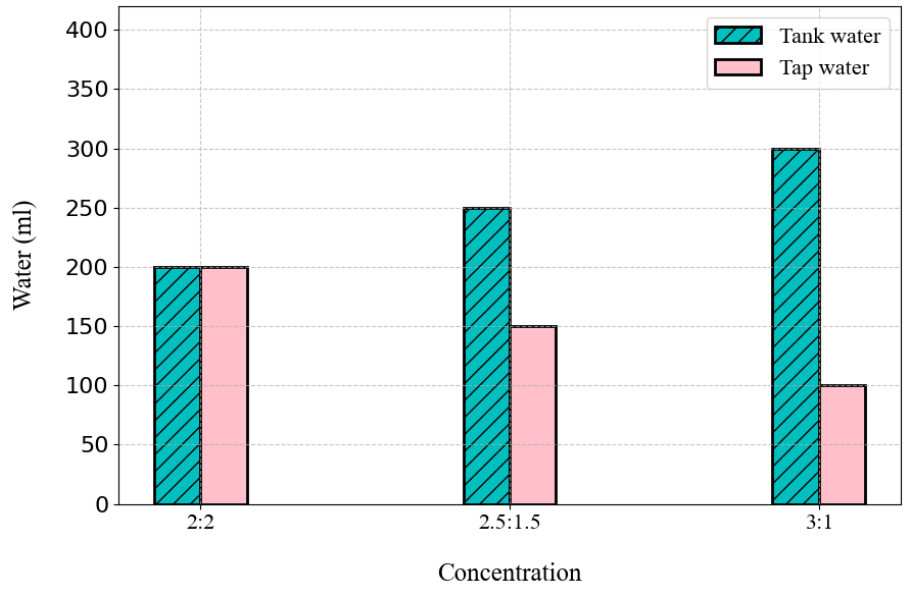

Figure 8. Proportion of aquarium and freshwater for different concentrations utilized for the experiment

The previous studies conducted by Sanchez-Bayo et al. and Osundeko et al. (19–22), they had cultivated algae in seawater, freshwater, and wastewater.However,this study cultivated algaeusingaquarium water and freshwater composition.Figure8 shows the composition of aquarium water (tank water) and freshwater (tap water) used at three different concentrations for algae production.The x-axis represents the different concentrations (2:2, 2.5:1.5, and 3:1), while the y-axis represents the volume of water in milliliters (ml).For 2:2 concentration 200 ml of aquarium and 200 ml of fresh water were taken while for 2.5:1.5 concentration, 250 ml of aquarium and 150 ml of fresh waterwere used. And for 3:1, 300 ml of aquarium water and 100 ml of fresh water wereemployed.The blue hatched bars indicate the volume of aquarium water, and the pink bars show the volume of freshwater used in each concentration.

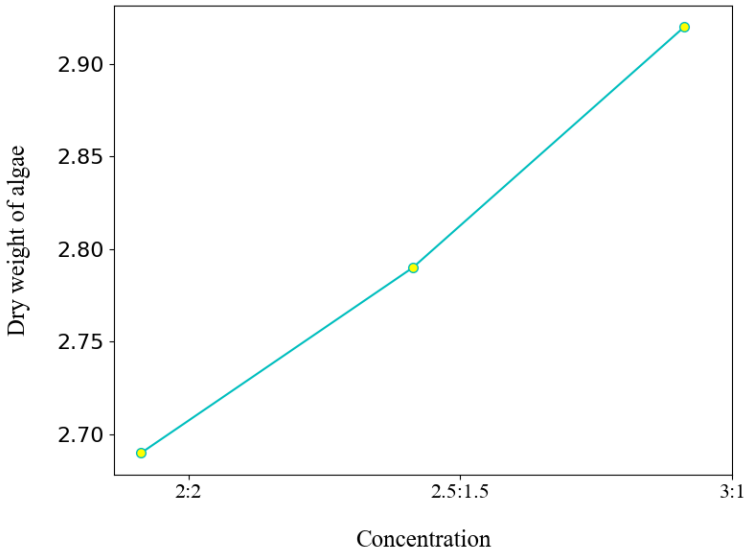

Figure 9.Dry weight of Algae Produced from different Concentrations.

The dry weight of microalgae produced from different concentrations is represented in Figure 9. The graph indicates a positive linear relationship between the concentration ratio of aquarium water to fresh water and the dry weight of algae. We can see that a higher amount of 2.92 g microalgae is produced in concentration 3:1 while in concentration 2:2 lower amount of 2.69 g microalgae was cultivated.As the proportion of aquarium water increases relative to fresh water, the dry weight of algae also increases. This suggests that higher concentrations of aquarium water led to greater algae cultivation.

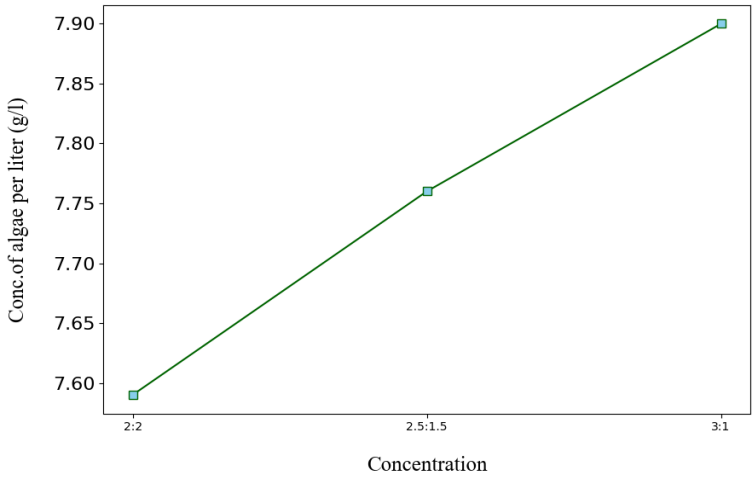

Figure 10. Concentration of Algae PerLiter (g/l) for Different Concentrations

In the experiment performed by Amit et al.(32) they took four algal strains and produced biomass yield per liter- 0.65 g/l, 0.37 g/l, 0.35 g/l, and 0.32 g/l in STS (secondary-treated sewage), PTS (primary-treated sewage), CWW (IIT Roorkee Saharanpur campus wastewater), and PWW (paper mill wastewater)respectively. In their experiment, STS had the highest algal biomass yield. Anotherexperiment performed byVíctor et al. produced 1.69 g/l and 2.25 g/l from two algae strains *Chlorella* and *Nannochloris* respectively and had the highest biomass yield in the Nannochloris algae strain(33). Whereas, in this study, algal biomass found was 7.59 g/l, 7.76 g/l, and 7.90 g/l for three different concentrations of aquarium and freshwater. Thisamount of algae per liter is calculated for the different concentrations using equation (2) and is shown in Figure 10. However, the concentration of algae per liter depends on the produced algal biomass. The concentration of algae per liter was higher for concentration 3:1 while it was lower for 2:2 concentration.

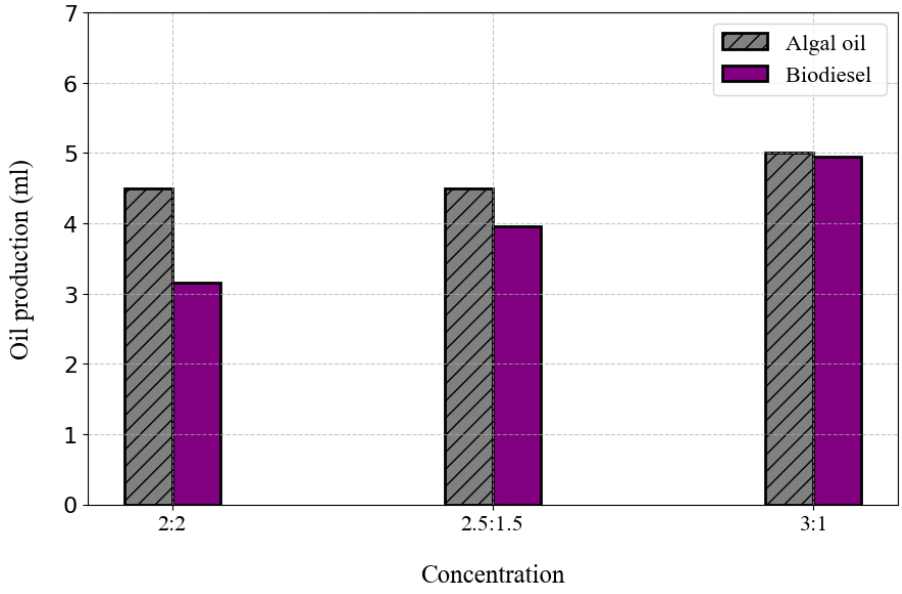

Figure 11. Algal Oil and Biodiesel Produced from Different Concentrations

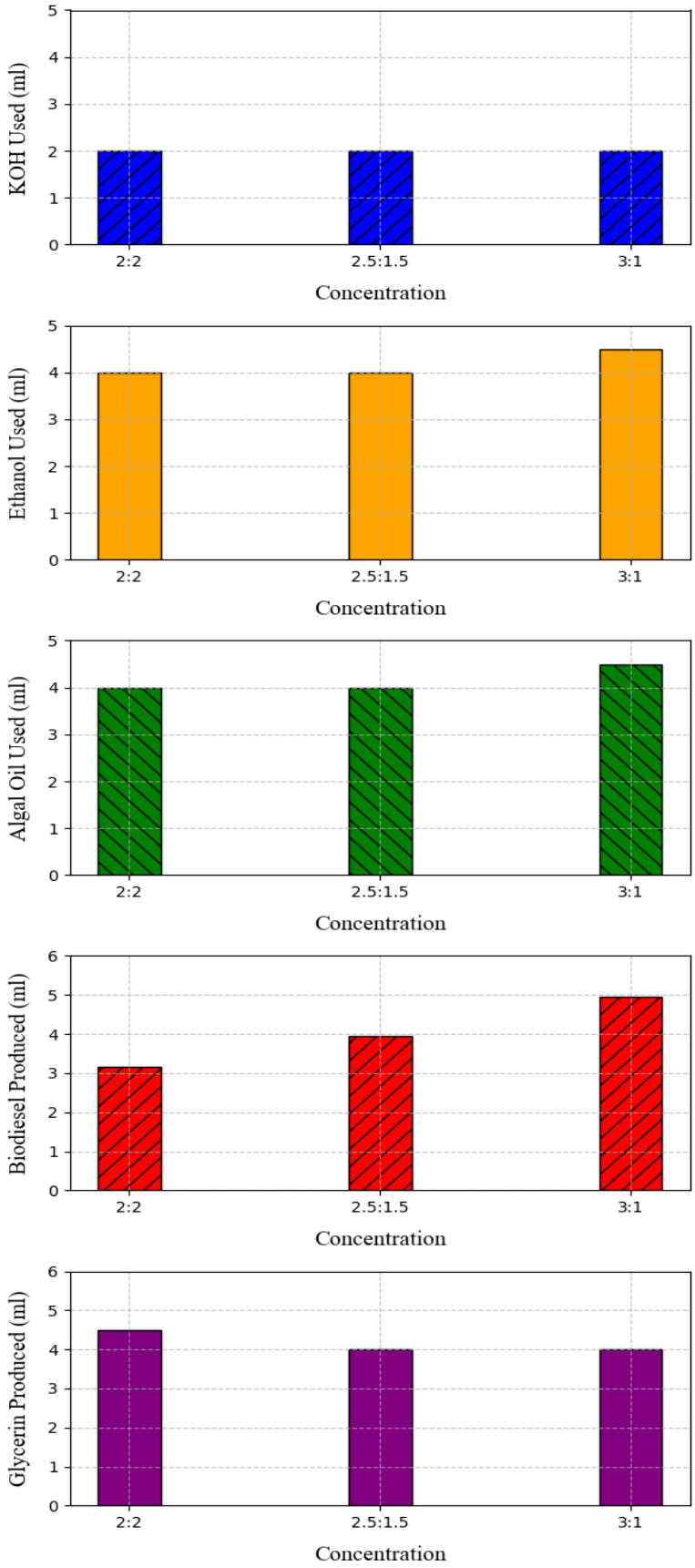

Figure 12.Chemicals Used for Biodiesel Production

The algal oil extracted from algal biomass and biodiesel produced from algal oil are shown in Figure 11. As we can see, algal oil extracted from different compositions of aquarium and freshwater is high in 3:1 concentration i.e. 5 ml, the biodiesel produced from algal oil is also high in this concentration i.e. 4.95 ml produced by bead beating oil extraction technique. Algal oil produced in 2:2 and 2.5:1.5 was in equal amounts i.e. 4.5 ml, while biodiesel produced in 2:2 was the least 3.15 ml. Also, the produced biodiesel from 2.5:1.5 concentration was 3.96 ml. On comparing our study's results with experiment results performed by Reem et al., the total algal oil content was found to be 5.8+- 0.16% through the Folch oil extraction method, and the produced biodiesel yield was 19.3% (34).

Figure 12 shows the usage of KOH, ethanol, and algal oil and the resultant production of biodiesel and glycerin across three different concentrations 2:2, 2.5:1.5, and 3:1. For each concentration 2ml of KOH was used. The algal oil and ethanol were in equal amounts for 2:2 and 2.5:1.5 concentration i.e. 4 ml each while for concentration 3:1 their amount was increased to 4.5 ml each so that we can observe the changes in the biodiesel production reaction. The production of biodiesel increased with higher concentrations, yielding 3.15 ml for 2:2, 3.96 ml for 2.5:1.5, and 4.95 ml for 3:1 concentration. The production of by-product i.e. glycerin was relatively constant for 2.5:1.5 and 3:1 concentration, both producing 4.0 ml of glycerin, whereas it was slightly higher for 2:2 concentration. We have analyzed, that as we increased the concentration of algal oil and ethanol the production of biodiesel increased while the by-product production remained constant.

4. CONCLUSION

This study concludes that microscopic green algae can be effectively cultivated in glass jars under controlled conditions. The findings suggest that algal biodiesel can be an alternative source to petroleum-baseddiesel fuel as it is environment-friendly, does not affect human health, and issustainable.

In this study, three different ratios of aquarium water to freshwater (2:2, 2.5:1.5, and 3:1) were used for microalgae cultivation. The bead-beatingoil extraction technique was used because of its high efficiency in cell disruption and shorter processing time compared to other methods. It was observed that a higher concentration of aquarium water in the considered mixture resulted in greater microalgae growth.

The results of this study showed that the highest concentration of algal oil and ethanol resulted in a higher quantity of biodiesel. However, comparing the two concentrations i.e. 2:2 and 2.5:1.5, and adding equal amounts of algal oil and ethanol to both, yields different biodiesel outcomes. In the 2:2 concentration, less biodiesel was produced, and a higher amount of by-product i.e. glycerin was generated. On the other hand, in the 2.5:1.5 concentration, more biodiesel was produced, and less glycerin was generated. The third concentration that was considered was in the ratio 3:1 and in this mixture amount of algal oil and ethanol was also increased by 0.5 ml resulting in a higher quantity of biodiesel, while the glycerin production remained the same as it was present in the 2.5:1.5 concentration.

A limitation of this study was that the processes of cultivation, harvesting, oil extraction, and transesterification process of microalgae were time-consuming. However, refiningtheseprocesses could potentiallymaximize the yield and will lead the transport sector towards a green fuel.

5. REFERENCES

[1] Z. Liu (2015) Chapter 1 - Global energy development: the reality and challenges.*Glo. Energ. Int.,* 1–64, https://doi.org/10.1016/B978-0-12-804405-6.00001-4

[2] L. Qian, J. M. McInerney, S. S. Solomon, H. Liu, A. G. Burns (2021) Climate changes in the upper atmosphere: contributions by the changing greenhouse gas concentrations and earth's magnetic field from the1960s to 2010s. *J. of Geo. Res.: Space Phy.*,126, https://doi.org/10.1029/2020JA029067.

[3] G. Kuo (2019) When Fossil Fuels Run Out, What Then?https://mahb.stanford.edu/library-item/fossil-fuels-run/

[4] S. Khatoon, S. K. Yadav, V. Chakravorty, J. Singh, R. B. Singh, M. S. Hasnain, S.M.M. Hasnain (2023) Perovskite solar cell’s efficiency, stability and scalability: a review. *Mate. Sci. for Energ. Tech.*, 6, 437–59 https://doi.org/10.1016/j.mset.2023.04.007.

[5] A. Shukla, S. K. Yadav, A. Yaqub, J. Singh, R. B. Singh (2024) Performance assessment of a 1 MW grid-connected rooftop solar photovoltaic (GCRPV) plant on an institutional building in composite climate of Northern India, *Int. J. Amb. Energ*. (2024). https://doi.org/https://doi.org/10.1080/01430750.2024.2392167.

[6] S. Khatoon, V. Chakraborty, S.K. Yadav, S. Diwakar, J. Singh, R.B. Singh (2023) Simulation study of $CsPbI_xBr_{1-x}$ and $MAPbI_3$ heterojunction solar cell using SCAPS-1D. *Solar Energy*, 254, 137–57, https://doi.org/10.1016/j.solener.2023.02.059.

[7] S.K. Yadav, N. M. Kumar, U. Bajpai (2023) Quantitative impact assessment of temperature on the economics of a rooftop solar photovoltaic system. *Environ. Sci. Pollut. Res*., 30, 21900–21913,https://doi.org/10.1007/s11356-022-23592-7.

[8] P.Moriarty, & D.Honnery, (2016) Chapter 61 Global transport energy consumption. *Alt.energ. and sha. gas encyc.*, 651-656. https://doi.org/10.1002/9781119066354.ch61.

[9] O. Awogbemi, D. V. V.Kallon, E. I.Onuh, & V. S. Aigbodion, (2021) An overview of the classification, production and utilization of biofuels for internal combustion engine applications. *Energies*, *14*(18), 5687. https://doi.org/10.3390/en14185687.

[10] M. Mubarak, A. Shaija, T. V. Suchithra (2021) Experimental evaluation of salvinia molesta oil biodiesel/diesel blends fuel on combustion, performance and emission analysis of diesel engine. *Fuel.* 287, 119526, https://doi.org/10.1016/j.fuel.2020.119526.

[11] Z. Shao, D. Wu, J. Liang, W. Cong, K. Liang (2023) The effect of porous media on the thermal storage performance of salinity-gradient solar pond. *J. of Phy.: Conf. Ser*., 2584, https://doi.org/10.1088/1742-6596/2584/1/012015.

[12] K. Venkiteshwaran, T. Xie, M. Seib, V. P. Tale, D. Zitomer (2022) (Chapter 8) Anaerobic digester biogas upgrading using microalgae. *Int. Was. Manag. and Valo. using Algal Cult.*, 183–214, https://doi.org/10.1016/B978-0-323-85859-5.00004-X

[13] A. Kose, S. S. Oncel(2016) Algae as a promising resource for biofuel industry: facts and challenges. *Int.J. of Energ. Res*., 41 (7), 924-951. https://doi.org/10.1002/er.3699.

[14] J.H.K. Lim, Y.Y. Gan, H.C. Ong, B.F. Lau, W.H. Chen, C.T. Chong, T.C. Ling, J.J. Klemeš (2021) Utilization of microalgae for bio-jet fuel production in the aviation sector: challenges and perspective. *Ren. and Sus. Energ. Rev.*, 149, p.111396, https://doi.org/10.1016/j.rser.2021.111396.

[15] M. L. N. Carneiro, F. Pradelle, S. L. Braga, M. S. P. Gomes, A. R. F. Martins, F. Turkovics, R. N. Pradelle (2017) Potential of biofuels from algae: comparison with fossil fuels, ethanol and biodiesel in Europe and Brazil through life cycle assessment (LCA). *Ren. and Sus. Energ. Rev.*, 73, 632-653, https://doi.org/10.1016/j.rser.2017.01.152.

[16] Y. Xu, P. Hellier, S. Purton, F. Baganz, N. Ladommatos (2016) Algal biomass and diesel emulsions: an alternative approach for utilizing the energy content of microalgal biomass in diesel engines. *Applied Energy*, 172, 80-95, https://doi.org/10.1016/j.apenergy.2016.03.019.

[17] S. S. Satputaley, D.B. Zodpe, N.V. Deshpande (2017) Performance, combustion and emission study on CI engine using microalgae oil and microalgae oil methyl esters. *J. of the Energ. Ins.*, 90(4), 513-521, https://doi.org/10.1016/j.joei.2016.05.011.

[18] J. Milano, H. C. Ong, H.H. Masjuki, W.T. Chong, M.K. Lam, P. K. Loh, V. Vellayan (2016) Microalgae biofuels as an alternative to fossil fuel for power generation. *Ren. and Sus. Energ. Rev.*, 58, 180-197, https://doi.org/10.1016/j.rser.2015.12.150.

[19] A.S. Bayo, D. L. Chicharro, V. Morales, J. J. Espada, D. Puyol, F. Martínez, S. Astals, G. Vicente, L. F. Bautista, R. Rodríguez (2020) Biodiesel and biogas production from isochrysis galbana using dry and wet lipid extraction: a biorefinery approach. *Renewable Energy*, 146, 188-195, https://doi.org/10.1016/j.renene.2019.06.148.

[20] R. Halim, M.K. Danquah, P.A. Webley (2012) Extraction of oil from microalgae for biodiesel production: a review. *Biotechnology Advances*, 30(3), 709-732, https://doi.org/10.1016/j.biotechadv.2012.01.001.

[21] A. Demirbas (2010) Use of algae as biofuel sources. *Energ. Con. and Man.*, 51(12), 2738–2749, https://doi.org/10.1016/j.enconman.2010.06.010.

[22] O. Osundeko, H. Davies, J. K. Pittman (2013) Oxidative stress-tolerant microalgae strains are highly efficient for biofuel feedstock production on wastewater. *Biomass and Bioenergy* 56, 284–94, https://doi.org/10.1016/j.biombioe.2013.05.027.

[23] T. Fazal, M. S. U. Rehman, F. Javed, M. Akhtar, A. Mushtaq, A. Hafeez, A. A. Din, J. Iqbal, N. Rashid, F. Rehman (2021) Integrating bioremediation of textile wastewater with biodiesel production using microalgae(chlorella vulgaris). *Chemosphere*, 281, 130758, https://doi.org/10.1016/j.chemosphere.2021.130758

[24] G. Li, J. Zhang, H. Li, R. Hu, X. Yao, Y. Liu, Y. Zhou, T. Lyu (2021) Towards high-quality biodiesel production from microalgae using original and anaerobically-digested livestock wastewater. *Chemosphere*, 273, 128578, https://doi.org/10.1016/j.chemosphere.2020.128578

[25] A.S. Bayo, D.L. Chicharro, V. Morales, J. J. Espada, D. Puyol, F. Martínez, S. Astals, G. Vicente, L. F. Bautista, R. Rodriguez (2020) Biodiesel and biogas production from isochrysis galbana using dry and wet lipid extraction: a biorefinery approach. *Renewable Energy*, 146, 188–95, https://doi.org/10.1016/j.renene.2019.06.148.

[26] S. Khan, R. Siddique, W. Sajjad, G. Nabi, K. M. Hayat, P. Duan, L. Yao (2017) Biodiesel production from algae to overcome the energy crisis. *Hay. J. of Bio*., 24(4), 163–167, https://doi.org/10.1016/j.hjb.2017.10.003.

[27] G. Zuccaro, A. Yousuf, A. Pollio, J. P. Steyer (2020) (Chapter 2) Microalgae Cultivation Systems. *Micro. Cul. for Bio. Prod.*, 11–29, https://doi.org/10.1016/B978-0-12-817536-1.00002-3

[28] G. Singh, S. K. Patidar (2018) Microalgae harvesting techniques: A review. *J. of Env. Man.*, 217, 499–508, https://doi.org/10.1016/j.jenvman.2018.04.010.

[29] Y. S. Pradana, B. R. Sadewo, S. A. Haryanto, H. Sudibyo (2021) Selection of oil extraction from chlorella species of microalgae by using multi-criteria decision analysis technique for biodiesel production. *Open Chemistry*, 19(1), 1029–42, https://doi.org/10.1515/chem-2021-0092.

[30] R. R. Kumar, P. H. Rao, M. Arumugam (2015) Lipid extraction methods from microalgae: a comprehen-sive review. *Front. in Energ. Res.*, 2, 125610, https://doi.org/10.3389/fenrg.2014.00061.

[31] J. Zhai, I. T. Burke, & D. I. Stewart, (2021) Beneficial management of biomass combustion ashes. *Ren. and Sus. Energ. Rev.*, *151*, 111555

[32] Amit, U. K. Ghosh (2018) An approach for phycoremediation of different wastewaters and biodiesel production using microalgae. *Env. Sci. and Pol. Res.,* 25(19), 18673–81, https://doi.org/10.1007/s11356-018-1967-5.

[33] V.M. Ortiz-Martínez, P. Andreo-Martinez, N. Garcia-Martinez, A.P. de los Ríos, F.J. Hernández-Fernández, J. Quesada-Medina (2019) Approach to biodiesel production from microalgae under supercritical conditions by the PRISMA method. *FuelPro. Tech.*, 191, 211-222, https://doi.org/10.1016/j.fuproc.2019.03.031.

[34] R. Shomal, H. Hisham, A. Mlhem, R. Hassan, S. Al-Zuhair (2019) Simultaneous extraction–reaction process for biodiesel production from microalgae. *Energy Reports*, 5, 37–40, https://doi.org/10.1016/j.egyr.2018.11.003

IZVOD

STUDIJA ZELENIH MIKROALGI KAO SIROVINE ZA PROIZVODNJU BIODIZELA

Biodizel kao izvor energije označio je ivicu rastuće energetske krize. Postoji više načina na koje se biodizel može proizvesti, a u toku su agresivna istraživanja u oblasti biodizela. U ovom radu smo se fokusirali na proizvodnju biodizela iz mikroalgi. Zelene mikroalge, sirovina treće generacije, su obećavajući kandidati za proizvodnju biodizela zbog visokog sadržaja lipida i brzog rasta. U ovoj studiji, za uzgoj mikroalgi, stvoreno je okruženje različitih temperatura koje su bile između 27°C i 32°C. Takođe, tri različite koncentracije (2:2, 2,5:1,5 i 3:1) akvarijumske i slatke vode razmatrane su u ovom radu za rast algi, a istražen je metod ekstrakcije lipida kao što je mehaničko uništavanje ćelija da bi se utvrdila njegova efikasnost. Kada je proces ekstrakcije lipida optimizovan, ekstrahovani lipidi su podvrgnuti procesu transesterifikacije, pretvarajući ih u biodizel. Rezultati ovog istraživanja pokazuju da je veća koncentracija akvarijumske vode rezultirala boljom proizvodnjom algi, odnosno, osušene mase algi ekstrahovanih iz gore navedenih koncentracija bile su 2,69 grama, 2,79 grama, odnosno 2,92 grama. Biodizel proizveden od sušenih algi bio je 3,15 ml, 3,96 ml i 4,95 ml, respektivno. Ovi rezultati sugerišu da se zelene mikroalge mogu smatrati primamljivom sirovinom za proizvodnju biodizela. Optimizacija metoda uzgoja i ekstrakcije lipida može poboljšati biomasu i produktivnost lipida, povećavajući ukupan prinos biomase. Ova studija zaključuje da biodizel iz algi može biti alternativni izvor za dizel gorivo na bazi nafte.

Ključne reči: *Biodizel; microalgae; ekstrakcija lipida; biomasa; temperatura.*

Naučni rad
Rad primljen: 27.03.2024.
Rad korigovan: 20.07.2024.
Rad prihvaćen: 23.08.2024.

Nikita Singh: https://orchid.org/0009-0004-4039-2552
Satish Kumar Yadav: https://orchid.org/0000-0003-0795-9452
Aradhana Shukla: https://orchid.org/0009-0004-9441-1480
Amit Misra: https://orchid.org/0009-0002-6293-7782
Jyotsna Singh: https://orchid.org/0000-0003-3250-3326
Rajendra Bahadur Singh: https://orchid.org/0000-0001-9025-1900

*Nishant Kumar[1], Ashutosh Sahu[2], Ikhwan Mohd Noor[3], Pramod K. Singh[4], Lavish Kumar Singh[5,]**

[1]Department of Civil Engineering, Sharda University, Greater Noida, India, [2]Department of Mechanical Engineering, Chaitanya Bharathi Institute of Technology, Hyderabad, India, [3]Physics Division, Centre of Foundation Studies for Agricultural Sciences, Universiti Putra Malaysia, UPM Serdang, Selangor Darul Ehsan, Malaysia, [4]Center for Solar Cells and Renewable Energy (CSRE), Department of Physics, Sharda School of Basic Sciences and Research, Sharda University, India, [5]School of Engineering, Jawaharlal Nehru University, New Delhi, India

Scientific paper
ISSN 0351-9465, E-ISSN 2466-2585
https://doi.org/10.62638/ZasMat1240

Zastita Materijala 66 (1)
179 - 186 (2025)

Investigating the effect of polypropylene fibres and curing parameters on the workability and mechanical properties of concrete

ABSTRACT

Polypropylene fibres possess certain characteristics that make them an ideal counterpart to attain explicit advantages when used for building works, more specifically, when added to concrete. In this investigation, polypropylene fibres were added by weight of cement (0.25%, 0.5% and 0.75%) in M20 grade of concrete and their impact on workability, compressive strength and flexural strength was assessed and analyzed. The slump test revealed that as the polypropylene fiber loading in the concrete mix was increased, the workability of the mixture continued to decrease; the workability decreased by 11.11%, 19.44% and 45.83% upon addition of 0.25 %, 0.5%, and 0.75% fibres respectively in the concrete. The compressive strength as well as the flexural strength of the concrete increased monotonously with increase in the curing time and fibre loading. For instance, in case of acidic water curing, the compressive strength enhanced from 19.08 MPa to 22.85 MPa upon increasing the fibre content from 0.25% to 0.75%. Adding 0.25% polypropylene fibre resulted in an increase in the flexural strength of conventional concrete mix by 15.78% and 10.29% when cured in normal water for 28 days and 56 days, respectively. Both compressive and flexural strength of the samples cured in normal water was found to be higher than the samples cured in acidic water and it was observed that the fibre reinforced concretes were more resistant to acids than the normal unreinforced concrete.

Keywords:*Cement,curing time, slump behavior, compressive strength, flexural strength*

1. INTRODUCTION

In the construction sector, concrete is the most popular building material.It consists of a carefully selected mixture of binders such as cement, well-classified fine and coarse aggregates, water and additives.To improve the qualities of conventional concrete, short, discrete fine fibers are randomly dispersed throughout the material [1-3]. The strength properties, aspect ratio, orientation, volume, shape, spacing and dispersion of the fibers affect how well a structure performs. A variety of fibers, including asbestos, steel, glass, carbon, nylon, and others, have been employed to enhance the characteristics of typicalconcrete [4-6].Off late, a noveldevelopment in concrete related research has been the reinforcement of variousfibers, which has displayedexcellentoutcomes in the form of enhanced compressive and flexural strength of the concrete. Polypropylene (PP), also known as polypropene, is a fiber that is used for strengthen concrete and for protection of concrete against micro cracks [7-10]. The durability of concrete has been found to improve by adding polypropylene fibers. Zhang et al. [1] noted that the compressive strength of concrete increased with increase in fiber dosage up to 0.3%. However, additional upsurge in the fibre content caused a reduction in the compressive strength. The incorporation of chopped basalt fibers to concrete mixtures exerted a positive impact on both compressive and flexural strength without compromising on the workability. Addition of 1% basalt fibersled to an upsurge in the flexural and tensile strength by 64% and 46%, respectively [2]. Toutanji [10] investigated the consequence of adding polypropylene fibers and silica fume on the mechanical properties of cement concrete. The silicon fume contents used were 5

Corresponding author: Lavish Kumar Singh
Email: lavish.singh2011@gmail.com
Paper received: 28. 05. 2024.
Paper corrected: 27. 08. 2024.
Paper accepted: 29. 08. 2024.
The website: https://www.zastita-materijala.org/

and 10%, and the fiber volume fractions were 0.10, 0.30, and 0.50%. The findings showed that 5% fumed silica in combination with 0.30% fiber volume fraction provided the best mix design for repair applications in terms of processability, bonding, strength, elongation, and permeability. However, it is noteworthy that adding silica fume alone ensued a substantialreduction in permeability. Curing is essential to the development of the dense microstructure and pore structure, which in turn controls the concrete's moisture loss during cement hydration and leads to the achievement of desired properties. Yan and Cui [11] discovered that grinding fine slag powder with cement, fly ash, silicon ash composite, and gelled material at curing temperatures over 50°C greatly increases the reactivity of cement. However, a high curing temperature exerts a detrimental impact on adhesion and mechanical properties [12].

In this investigation, polypropylene fibres were added by weight of cement (0.25%, 0.5% and 0.75%) in M20 grade of concrete to assess their impact on the various properties of the concrete.Concrete specimens reinforced with and without polypropylene fibres were casted and subsequently cured in normal and acidic water for 7, 28 and 56 days. The impact of polypropylene content, curing medium and curing time on workability, compressive and flexural properties were determined, analyzed and discussed during the investigation.

2. MATERIALS AND METHODOLOGY

2.1. Materials Used

Materials utilized in the production of concrete mixtures include cement, aggregates (coarse and fine),polypropylene fibers, and sodium sulfate. Each material has been tested and its physical properties are described below. Digital photograph of polypropylene fibre used in this work.

Cement:Grade 43 ordinary Portland cement (OPC) was used as recommended by IS-8112 [13]. A cement plant was used throughout the JK OPC experimental work. Table 1 shows the characteristics of OPC.

Table 1. Properties of cement

Properties of Cement	Experimental value
Normal consistency (% by weight of cement)	35
Setting time (minutes) Initial Final	 45 350
Specific gravity	3.14

Fine Aggregate:Sand present in the nearby locality was utilized as the fine aggregate. The physical properties of these aggregates enumerated in Table 2 were determined according to the test procedure described in IS-383 [13].

Table 2. Properties of fine sand aggregates

Physical properties	Values
Grading zone	III
Specific gravity	2.7
Moisture content (%)	2.5

Coarse Aggregate: Natural crushed stone with a maximum size of 20 mm were used as coarse aggregate. The aggregates were tested in accordance with IS-2386[13] and the findings are illustrated in Table 3.

Table 3.Properties of coarse natural stone aggregates.

Physical properties	Values
Specific gravity	2.63
Water absorption	1.11%
Free surface moisture	1.976
Water content	1.4%

Polypropylene fibre: Polypropylene fibre was taken from Indiamart. The length of the fibres was 2-12mm; diameter was 0.01-0.1mm and was having an aspect ratio of 200. Other specifications of these fibres are presented as under. The digital photograph of polypropylene fibre used in this work and its properties are recorded in Table 4.

Table 4. Properties of polypropylene fibre

Properties	Value
Unit weight	0.91 g/cc
Length	2-12 mm
Diameter	0.01-0.1 mm
Colour	White
Moisture absorption	Nil
Modulus of elasticity	3500 MPa
Tensile strength	40,000 psi
Dispensability	Excellent

Sodium sulfate:The sodium sulfate which was used in the work was procured from ROYAL CHEM in Delhi. The properties are shown in Table 5.

Table 5. Properties of sodium sulfate.

Properties	Value
Chemical formula	Na_2SO_4
Appearance	White crystalline solid
Odor	Odorless
Density	2.664 g/cm^3
Melting point	884 ℃
Boiling point	1429 ℃

Figure 1. Digital photo graph of polypropylene fibre used in this work

2.2. Mix Proportioning

The mix proportion followed in this study was1:1.479:3.19 according to IS-10262[13] with water-cement ratio of 0.5 for M20 grade of concrete. The calculated proportion for 1m^3 is illustrated in Table 6.

Table 6. Mix proportions per cubic meter

Material	Quantity
Cement	383.33
Fine aggregate	567.102
Coarse aggregate	1224.9
Water	191.61
Water/cement ratio	0.5

Figure 2. Digital photograph of (a) cast samples, (b) curing process, (c) compressive test and (d) flexural test being carried out on the samples

2.3. Mixing of Concrete

Mixing was carried out manually. First, the dry mix components, cement and both types of aggregates, were mixed for 2 minutes, then water was added and mixing was carried out for additional 2 minutes. The cumulative time of mixing was maintained at 4 min in all experiments until a homogeneous mixture was produced. Compaction was first done manually using a standard tamping rod, with appropriate blows to ensure layered filling of the mold, and finally compaction was performed using a vibrator.All samples were taken out from the mold after 24 h and placed in water until the testing was performed.

2.4. Casting and Curing of Test Specimens

For compressive strength, total 72 cubes of size 150x150x150mm were casted using M20 mix of concrete. Demoulding of the casted cubes was done after 24 hours from the time of casting of cubes. Water curing of the respective cubes was done for 7, 28 and 56 days in normal water and acidic water. These cubes were removed from the curing tank and tested while still wet, immediately after removal from the water. The support surface of the cube was wiped clean to remove all the loose particles adhered on to the surface. For permeability, 3 cubes were casted which includes one cube of normal concrete, one cube by adding 0.25% of fibre by weight of cement in concrete and one cube by adding 0.75% of fibres to the concrete.

For flexural strength, total 72 beams were prepared using M20 mix of concrete having size of 100x100x500mm. Demoulding of the casted beams was done after 24 hours from the time of casting of beams. Water curing of the respective beams of normal concrete and fibre reinforced concrete was done for 7, 28 and 56 days in normal and acidic water. These beams were removed from the curing tank and tested while still wet, immediately after removal from the water.

2.5. Testing of Specimens

Test methods include workability testing of fresh concrete mixtures and compressive and flexural strength testing of hardened concrete samples. To estimate the workability, slump test was conducted as per IS-1199 [13]. Compressive strength tests were conducted as per IS-516 [13].72 cubes of size 150x150x150mm were prepared for each mix which includes 36 cubes for normal water curing and 36 cubes for acidic water curing. After 24 hours, the samples were taken out from the molds and allowed to cure in water for 7, 28, and 56 days. Flexural strength was measured according to IS-516. Tests were conducted on beam samples with dimensions of 100 x 100 x 500 mm after 7, 28 and 56 days of curing. The reported values of both types of strengths is the average of the results obtained from three identical test samples for each configuration. Digital photograph of cast samples, curing process, compressive test and flexural test being carried out on the samples is shown in Fig. 2.

3. RESULTS AND DISCUSSION

3.1. Slump values

The slump values obtained for the fabricated specimens is shown in Fig. 3. Results reveal that concrete without fibre exhibitedthe highest slump value (72 mm). Continuous increase in the quantity of fibres resulted in a decline in the slump value from 64 mm for concrete containing 0.25% fibres to 39 mm for concrete containing 0.75% fibres. The slump decreased with the incorporation of polypropylene fibre due to the high absorption characteristics of the fibers. The results of the slump test conclude that as the fiber content in the concrete mixture increases, the workability of the mixture continues to decrease. The workability of the concrete mix decreased by 11.11%, 19.44% and 45.83% upon addition of 0.25 %, 0.5%, and 0.75% of fibres respectively to the concrete.

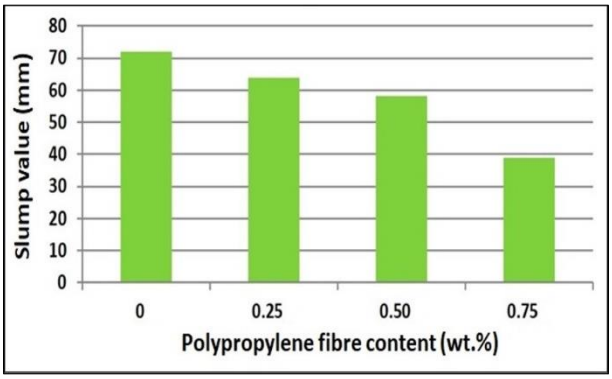

Figure 3. Slump values of concrete mixtures containing different proportions of polypropylene fibers

3.2. Compressive Strength

The results of compressive strength test performed over the fabricated samples is displayed in Table 7 (normal water curing) and Table 8 (acid water curing). It is evident that the compressive strength of the concrete increases monotonously with increase in the fibre loading irrespective of the curing medium.In case of water curing, with increase in concentration of polypropylene fibre from 0.25% to 0.75%, the average compressive strength got enhanced from 28.11 MPa to 30.76 MPa showing an increase of 8.7%. Similarly, for acid curing the compressive strength enhanced by 19.8% upon increasing the fibre content from 0.25% to 0.75%. This behavior may be attributed to

the fact that the polypropylene fibres hold the micro-cracks and delay their propagation when the concrete is subjected to compressive load [14]. Furthermore, the table indicates that increasing the curing time led to an upsurge in the compressive strength for both type of curing medium. In case of normal water curing, for the sample containing 0.75% fibre, the compressive strength increased from 22.96 MPa to 29 MPa upon increasing the curing time from 7 days to 28 days. Further increasing the curing time to 56 days led to a further increase in compressive strength to 40.35 MPa. In case of acidic water curing, the compressive strength of 0.75% fibre reinforced concrete was found to be 15.23 MPa, 20.32 MPa and 32.99 MPa for 7, 28 and 56 days of curing, respectively. Among all tested configurations, highest compressive strength of 40.35 MPa was reported for the specimenhaving 0.75% polypropylene fibers cured for 56 days in normal water. The compressive strength of the specimens cured in normal water was found to be greater than the samples cured in acidic water. Consequently, the loss in compressive strength for the considered concrete mixes as a result of change in the curing medium from normal water to acidic water post 28 and 56 days of curing.is displayed in Fig. 4.

Table 7. Influence of polypropylene fibres on the compressive strength of concrete mix post normal water curing

S.No.	Polypropylene fibre(%)	Compressive strength (MPa)			Avg. compressive strength (MPa)
		7 days	28 days	56 days	
1	0	18.40	24.93	35.86	26.394
2	0.25	19.87	26.88	37.58	28.11
3	0.5	20.32	28.06	38.57	28.98
4	0.75	22.96	29.00	40.35	30.76

Table 8. Influence of polypropylene fibres on the compressive strength of concrete mix post acidic water curing

S. No.	Polypropylene fibre(%)	Compressive strength (MPa)			Avg. compressive strength (MPa)
		7 days	28 days	56 days	
1	0	11.06	16.94	22.94	16.98
2	0.25	13.74	18.33	25.19	19.08
3	0.5	14.70	19.61	28.05	20.78
4	0.75	15.23	20.32	32.99	22.85

It is apparent that the loss in compressive strength is much more substantial in case of unreinforced concrete than the reinforced concrete specimens. Additionally, the loss in compressive strength diminished with upsurge in the fibre loading. For instance, the loss in compressive strength for 0.25% fibre reinforced concrete post 56 days of curing is 32.9%, which reduces significantly to 18.2% upon 0.75% fibre reinforcement.

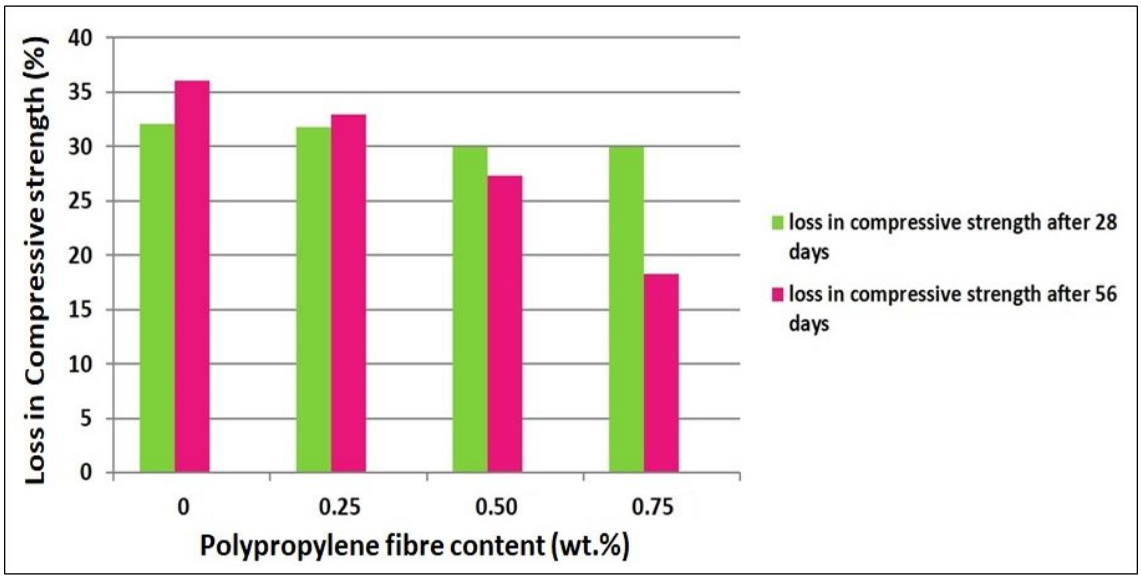

Figure 4. Loss in compressive strength for the considered concrete mixes as a result of change in the curing medium from normal water to acidic water post 28 and 56 days of curing

3.3. Flexural Strength

Flexural strength of concrete mix comprisingof varied loadings of polypropylene fibre after 7, 28 and 56 days of curing in normal water and acidic water is illustrated in Fig. 5a and 5b, respectively. Remarkable improvement in the flexural strength was obtained on addition of polypropylene fibres into the concrete. Adding 0.25% polypropylene fibres caused an increase in the flexural strength of conventional concrete mix by 15.78% and 10.29% when cured in normal water for 28 days and 56 days, respectively.

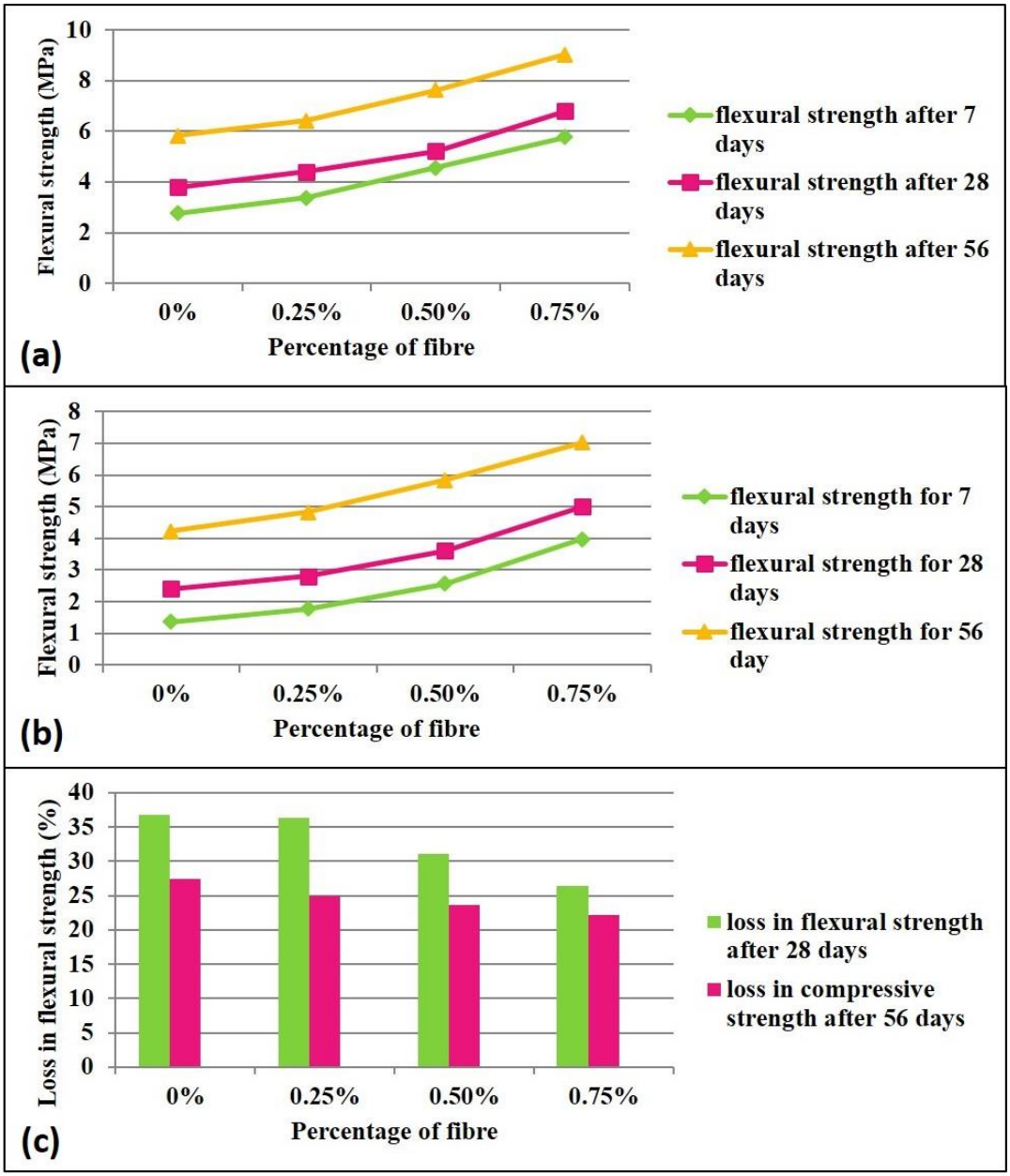

Figure 5.Influence of polypropylene fibres on the flexural strength of concrete mix post (a) normal water curing and (b) acidic water curing; and (c) loss in flexural strength for the considered concrete mixes as a result of change in the curing medium post 28 and 56 days of curing

Increase in the loading of polypropylene fibre to 0.75% led to a further improvement in the flexural strength of the concrete mix by 78.94% for 28 days and 54.88% for 56 days of normal water curing. Similar behavior was found for the samples cured in acidic water. The flexural strength of the specimens cured in normal water was found to be greater than the samples cured in acidic water. Fig.

5c depicts the reduction in the flexural strength for the considered concrete mixes as a result of change in the curing medium from normal water to acidic water post 28 and 56 days of curing. It is clear that the fibre reinforced concretes are more resistant to acids than the normal concrete. The loss in flexural strength in case of normal unreinforced concrete was found to be 27.61% for 28 days and 22.06% for 56 days of curing. However, the addition of 0.75% of fibre in concrete reduced the loss in strength to 16.13% for 28 days and 11.97% for 56 days of curing. The loss in flexural strength decreased upon increasing the percentage of polypropylene fibres in the concrete. It is worth mentioning that the findings of the flexural test were in line with the observations found in case of compressive test.

4. CONCLUSION

In this investigation, polypropylene fibres were added by weight of cement (0.25%, 0.5% and 0.75%) in M20 grade of concrete and their effect on workability, compressive strength and flexural strength was assessed and analyzed. Additionally, the specimens were cured in normal and acidic water for 7, 28 and 56 days to understand the effect of curing medium and curing time. The findings of the study are summarized in the following observations and conclusions.

- The slump test revealed that as the polypropylene fiber loading in the concrete mix was increased, the workability of the mixture continued to decrease. The workability decreased by 11.11%, 19.44% and 45.83% upon addition of 0.25 %, 0.5%, and 0.75% of fibres respectively to the concrete.
- The compressive strength as well as the flexural strength of the concrete increased monotonously with increase in the curing time and fibre loading. For instance, in case of acidic water curing, the compressive strength enhanced from 19.08 MPa to 22.85 MPa upon increasing the fibre content from 0.25% to 0.75%. Adding 0.25% polypropylene fibre resulted in an increase in the flexural strength of conventional concrete mix by 15.78% and 10.29% when cured in normal water for 28 days and 56 days, respectively.
- Both compressive and flexural strength of the samples cured in normal water was found to be higher than the samples cured in acidic water and it was observed that the fibre reinforced concretes were more resistant to acids than the normal unreinforced concrete.

5. REFERENCES

[1] K. Zhang, Q. Zhang, J. Xiao (2022) Durability of FRP bars and FRP bar reinforced seawater sea sand concrete structures in marine environments. *Construction and Building Materials*, 350, 128898.

[2] C. Jiang, K. Fan, F. Wu, D. Chen (2014) Experimental study on the mechanical properties and microstructure of chopped basalt fibre reinforced concrete. *Materials & Design*, 58, 187-193.

[3] R. Kurda (2023) Effect of Silica Fume on Engineering Performance and Life Cycle Impact of Jute-Fibre-Reinforced Concrete. *Sustainability*, 15, 8465.

[4] Z.A. Mohammed, L.A. Al-Jaberi, A.N. Shubber (2021) Effect of Polypropylene Fiber on Properties of Geopolymer Concrete Based Metakolin.*Journal of Engineering and Sustainable Development*, 25, 58-67.

[5] N.S. Al-Saffar,J.R. Al-Feel (2009)Properties of Self Compacting Concrete at Different Curing Condition and their Comparison with properties of Normal Concrete. *Al-Rafidian Engineering Journal*, 17, 30-38.

[6] M. Vafaei, A. Allahverdi, P. Dong, N. Bassim (2018) Acid attack on geopolymer cement mortar based on waste-glass powder and calcium aluminate cement at mild concentration. *Construction and Building Materials*, 193, 363-372.

[7] S. Kanmani, P.K. Umesha, P. Asha (2021) Behaviour of steel fibre reinforced concrete with wood ash as partial replacement. *IOP Conf. Series: Earth and Environmental Science*,822, 012053.

[8] R.K. Gupta, A.K. Hindoriya (2016) Effects of Acidic Curing on the Properties of Treated and Untreated Polyester Fiber Reinforced Concrete. *International Journal for Scientific Research & Development*, 4, 57-59.

[9] P. Jangra, A. Sharma (2013) Structural Behaviour of Fibrous Concrete Using PolypropyleneFibres. *International Journal of Modern Engineering Research*, 3, 1279-1282.

[10] H.A. Toutanji (1999) Properties of polypropylene fiber reinforced silica fume expansive-cement concrete. *Construction and Building Materials*, 13, 171-177.

[11] P.Y. Yan and Q. Cui (2015) Effects of curing regimes on strength development of high-strength concrete.*Journal of the Chinese Ceramic Society*,43, 133–138.

[12] P. Shen, L. Lu, Y. He, F. Wang, S. Hu (2019) The effect of curing regimes on the mechanical properties, nano-mechanical properties and micro-structure of ultra-high performance concrete, *Cement and Concrete Research*,118, 1-13.

[13] Handbook on Building Construction Practices (1997), Publisher: Bureau of Indian Standards, New Delhi 110002, India, ISBN 81-7061-048-6.

[14] S. Alsadey, M. Salem (2016) Influence of Polypropylene Fiber on Strength of Concrete. *American Journal of Engineering Research*, 5, 223-226.

IZVOD

ISPITIVANJE UTICAJA POLIPROPILENSKIH VLAKANA I PARAMETARA OČVRŠĆAVANJA NA OBRADIVOST I MEHANIČKA SVOJSTVA BETONA

Polipropilenska vlakna poseduju određene karakteristike koje ih čine idealnim parom za postizanje eksplicitnih prednosti kada se koriste za građevinske radove, tačnije kada se dodaju betonu. U ovom istraživanju dodata su polipropilenska vlakna po masi cementa (0,25%, 0,5% i 0,75%) u betonu marke M20 i procenjen je i analiziran njihov uticaj na obradivost, čvrstoću na pritisak i čvrstoću na savijanje. Test sleganja je otkrio da kako je opterećenje polipropilenskim vlaknima u betonskoj mešavini bilo povećano, obradivost smeše je nastavila da opada; obradivost je smanjena za 11,11%, 19,44% i 45,83% nakon dodavanja 0,25%, 0,5% i 0,75% vlakana u beton respektivno. Čvrstoća na pritisak kao i čvrstoća betona na savijanje monotono su se povećavala sa povećanjem vremena očvršćavanja i opterećenja vlaknima. Na primer, u slučaju kiselog očvršćavanja u vodi, čvrstoća na pritisak se povećava sa 19,08 MPa na 22,85 MPa povećanjem sadržaja vlakana sa 0,25% na 0,75%. Dodavanje 0,25% polipropilenskih vlakana rezultiralo je povećanjem čvrstoće na savijanje konvencionalne betonske mešavine za 15,78% i 10,29% kada se osuši u normalnoj vodi tokom 28 dana i 56 dana, respektivno. Utvrđeno je da su i tlačna i savojna čvrstoća uzoraka očvršćanih u normalnoj vodi veća od uzoraka očvrsnutih u kiseloj vodi i uočeno je da su betoni ojačani vlaknima otporniji na kiseline od normalnog nearmiranog betona.
Ključne reči: *Cement, vreme očvršćavanja, ponašanje pri slijeganju, čvrstoća na pritisak, čvrstoća na savijanje*

Naučni rad
Rad primljen: 28.05.2024.
Rad korigovan: 27.08.2024.
Rad prihvaćen: 29.08.2024.

Nishant Kumar: https://orcid.org/0000-0001-5477-3293
Ashutosh Sahu: https://orcid.org/0000-0002-9289-2848
Ikhwan Syafiq Bin Mohd Noor: https://orcid.org/0000-0003-0983-782X
Pramod K. Singh: https://orcid.org/0000-0002-3155-6621
Lavish Kumar Singh: https://orcid.org/0000-0001-6319-9318

Vesna Obradović, Marija Perović, Predrag Pajić*

Jaroslav Černi Water Institute, Belgrade, Serbia

Scientific paper
ISSN 0351-9465, E-ISSN 2466-2585
https://doi.org/10.62638/ZasMat1082

Zastita Materijala 66 (1)
187 - 195 (2025)

Evaluation of biocorrosion, biofouling, and health risks in the two study locations in danube alluvium

ABSTRACT

Within conducted research the results of microbiological investigations on specific metabolic (phenotypic) groups of bacteria that play crucial roles in the biogeochemical cycling of iron, manganese, nitrogen, sulfur, and carbon are presented. These bacteria are also involved in the development of biocorrosion and biofouling processes, with some posing risks to public health. Utilizing results from applied biological activity reaction tests (BART tests), processed using specialized software, potential risks for the development of microbiologically mediated corrosion, biofouling, and health risks were calculated for seven wells within two oxic sites in the Danube alluvium – Vinci and Veliko Gradište, Serbia.Moderate to high corrosion risk was determined for all seven wells at both sites (CR=5.4). Microbiological fouling risk was very high in three out of the seven investigated wells (PR=8.10). Among the seven sites studied, one site stood out based on the calculated high value of health risk coefficient (HR=8.10).The research results provide new insights into the microbiological role in aging wells in oxic groundwater of the Danube alluvium. It is demonstrated that the physicochemical composition and chemical species such as minerals, organic matter, and the specific composition of microbial communities in the studied groundwater have the potential to stimulate biocorrosion and the formation of deposits and biofilms within well structures.In addition to biochemical analyses, hydrogeological characteristics of the analyzed area are presented to define the geological stratigraphy, for which specific microbiological transformations would be expected based on the obtained results.

Key words:*biocorrosion, biofouling, groundwater, health risk, Serbia*

1. INTRODUCTION

Well corrosion and biological clogging affect water quality, the operational lifespan of pumps, pipelines, and the quality of hydraulic structure operation in general.The occurrence of 'aging' wells and reduced yields, attributed to heightened resistance in the pre-filter zone, primarily stems from “unfavorable” groundwater chemistry that promotes chemical and biological incrustation (clogging) of the pre-filtering zone and the well filter structures. Specific water composition and increase of hydraulic resistance in the pre-filtering zone intensify these processes. The impact of well 'aging' is evident in wells operational limitations, particularly in their inability to maintain the required (adopted) protection criteria and achieve the permissible groundwater level relative to the terrain surface. Due to the expenses related to labor, equipment, and production caused by biofouling, this issue poses a notable economic concern [1].Biofouling is the term used to describe the unwanted accumulation of microbial organisms and their extracellular substances [1,2]. The micro-organisms (bacteria, archaea, and fungi) naturally present in groundwater can significantly impact the surface processes and expedite corrosion in environments where corrosion would not typically occur favorably [3, 4]. The biofilm forming community is diverse and contains species that have often been linked with corrosion, such as sulphate reducing bacteria (SRB) and methanogenic archaea (MA) [3]. Alongside the conventional assessment of well aging processes primarily centered around calculated risks (Langelier Saturation Index, Riznar stability index) associated with chemical corrosion and incrustation - chemical fouling [5], contemporary research is

*Corresponding author:Marija Perović
E-mail: marija.perovic@jcerni.rs
Paper received: 28. 04. 2024.
Paper accepted: 02. 09. 2024.
The website: https://www.zastita-materijala.org/

placing a growing emphasis on investigating the impact of microorganisms on well aging and the formation of biofouling [6]. The type of clogging and biofouling associated with the growth and activity of specific bacterial groups can vary and depends on the chemistry of groundwater, particularly on the availability of electron donors (mostly available reactive organic carbon), electron acceptors (oxygen, trivalent iron, manganese, nitrates, sulfates, carbon dioxide), and parameters such as temperature and pH of groundwater.

Bacterial activity oxidizing reduced iron can result in various consequences for water chemistry. These include scaling due to high carbonates, encrustation caused by elevated iron levels, nodules forming cores rich in iron and organic matter, and the production of slime. These alterations can impact the color, odor, and taste of groundwater, as well as induce turbidity.According to [7] bacteria most commonly associated with microbiologically influenced clogging (MIC) area) Iron-reducing bacteria (IRB), which tend to dominate where iron accumulates (nodules, encrustations), and heterotrophic aerobic bacteria (HAB), particularly dominant when biomass resembles slime.Microbially mediated biofouling can occur through activity of aerobic and facultative anaerobic corrosive bacteria from groundwater reaching pipelines that have organic and inorganic film on the surface [7].Heterotrophic bacteria producing extracellular polymeric saccharides initially attach to the walls of the pipeline/metal surfaces, creating a favorable environment for the adhesion of other microorganisms. The action of microaerophilic bacteria oxidizing iron in the biofilm results in the accumulation of iron oxide hydroxide deposits, leading to pipe volume reduction (clogging), generation of sulfuric acid released by sulfur-oxidizing bacteria, which accelerates environmental acidification, lowering Ph [7]. Conditions with low oxygen concentration and organic acids released by acid-producing bacteria (e.g., fermentation) favor the attachment and development of sulfate-reducing bacteria, producing hydrogen sulfide (H_2S), accelerating the corrosion process and lowering pH, causing localized corrosion.In groundwater a certain chemical equilibrium is established under natural conditions. It can be disrupted by groundwater exploitation, resulting in the appearance or acceleration of sedimentation processes affecting the clogging of well filters and the pre-filter zone, as well as processes leading to corrosion of filter structures.

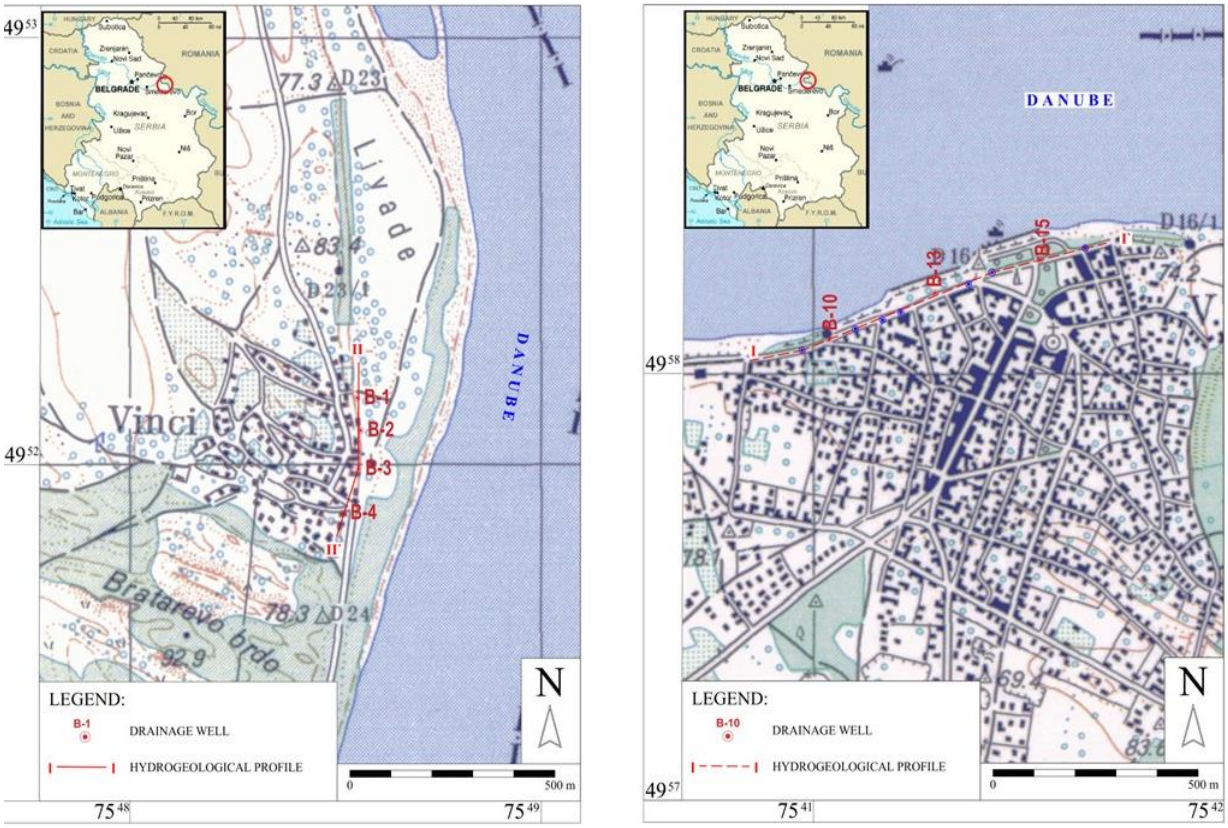

Figure 1. The position of examined areas with marked well's location (left Vinci, right VelikoGradište)

This paper seeks to clarify the roles of sulfate-reducing, iron-related, heterotrophic-aerobic bacteria, denitrification and slyme forming microorganisms (SRB, IRB, HAB, DN, and SLYME, respectively) in the investigated biofouling and related health risk, that could substantially influence the maintenance of groundwater extraction facilities and associated costs. By employing a system of five types of Biological Activity Reaction Tests (BART tests), the risks for the development of biological processes leading to the formation of various types of deposits, encrustations, and clogging (biofouling), as well as the development of biocorrosion processes, primarily by indigenous bacterial groups, were assessed. The ubiquitous nature of biofouling and the substantial challenges associated with material protection for its prevention across various applications are well-documented in numerous studies [8-13].

Investigations were carried out at two groundwater sampling sites near the settlements of Vinci and Veliko Gradište, Serbia, where a yield decrease of installed drainage wells was observed. At the Vinci site, samples were collected from four drainage wells (B-1, B-2, B-3, B-4), whereas at the Veliko Gradište location, three drainage wells were analyzed (B-10, B-13, and B-15) (Figure 1). The observed decrease in yield led to an increase in the groundwater level, posing a threat to both the settlement and existing structures because of the shallow depth of the groundwater.

2. MATERIALS AND METHODS

IRB BART tests were utilized to identify iron-related bacteria and specific enteric species with the ability to precipitate iron. SLYME BART biotests are employed to identify various bacteria capable of generating extracellular polymeric substances, particularly those that form biofilms, which encompass enteric and opportunistic pathogenic fluorescent *Pseudomonas* species. SRB BART biotests are utilized to detect sulfate-reducing bacteria responsible for producing biogenic H_2S and inducing pitting corrosion. HAB BART biotests are used to identify a diverse array of heterotrophic aerobic and facultatively anaerobic bacteria crucial for biofilm development, playing a role in biocorrosion and biofouling processes. Applied DN BART biotests, besides the detection of denitrifying bacteria can indirectly indicate organic pollution as well as potential presence of pesticides and pathogens. Based on the timing of occurrence and type of reliably identified signature reactions in each applied BART biotest, entered into the dedicated software in the order they are observed, risks were calculated, ranging from 0 to 9, depending on community structure and estimated bacterial population size. Lower numerical values suggest lower potential risks for the development of biofouling processes, biocorrosion, as well as potential risks to public health.

The examined area - Vinci

The settlement of Vinci is located on the right bank of the Danube River (Figure 1). A section of the settlement, located at lower elevations ranging from 71 to 72 meters asl, is situated next to the Danube River. This area extends partially inland to the north and northwest, reaching towards the lower terrains of the Vinci-Požežena reclamation system, and towards the west, close to the "Vinci" water supply source for the Golubac municipality. Increase of groundwater levels, observed in the coastal part of the settlement, has posed a threat to existing structures. These levels have been recorded at depths of less than 2.0 meters from the ground surface. The necessary protection was obtained by constructed drainage system consisting of 4 wells (B-1, B-2, B-3, and B-4) with their own submerged pumping units and separate discharge outlets into the Danube. Within the hydrogeological investigations in the wider area of the Vinci settlement, aquifer is formed within the aquiferous sandy-gravelly complex of Quaternary age (Figure 2). Surficial aquifer layer, consisting of transposed fine-grained sands, mainly 2-3 meters thick, while it is absent in the coastal part of the settlement. Aquitard layer, poorly permeable, composed of clayey-silty sediments, mainly 1-3 meters thick. Semi-permeable layer in the upper part of the aquifer complex, composed of fine-grained sands, silts, mainly 1-4 meters thick. Main aquifer layer consists of medium to coarse-grained, highly gravelly sands, and in the lower part, gravelly sandy, even gravelly. The thickness of these sediments in the settlement area is up to 6 meters [14].

The examined area – VelikoGradište

The settlement of Veliko Gradište is located on the right bank of the Danube upstream from the confluence of the Pek River, at station km 1059 (Figure 1). The lowest parts of the settlement are situated to the north along the Danube and in the central-eastern part of the town towards the lowlands of the reclaimed area of the Pek - Veliko Gradište. The southern and southwestern parts of the settlement are built on a high river terrace. Veliko Gradište settlement protection was obtained by constructed drainage system consisting of wells (B-9 to B-16) with their own submerged pumping units. The rise in groundwater levels, indicating the development of aging processes in the wells was observed. The alluvial complex in Veliko Gradište settlement consists of surface humus and sandy sediments overlaying a basic aquifer gravelly-sandy layer. The humus layer is located at the surface of the terrain and ranges in thickness from

0.5 to 2 meters. Beneath the humus, there are yellow clays, silts, and sandy loams, generally with a thickness of 3 to 5 meters, increasing slightly towards the hinterland. The aquifer complex consists of very gravelly sandy gravel and sand, with layers of medium-grained sand. The thickness of this aquifer complex varies but is typically within the range of 15 to 18 meters. Hydrogeological profile of examined area Veliko Gradište is presented in Figure 3.

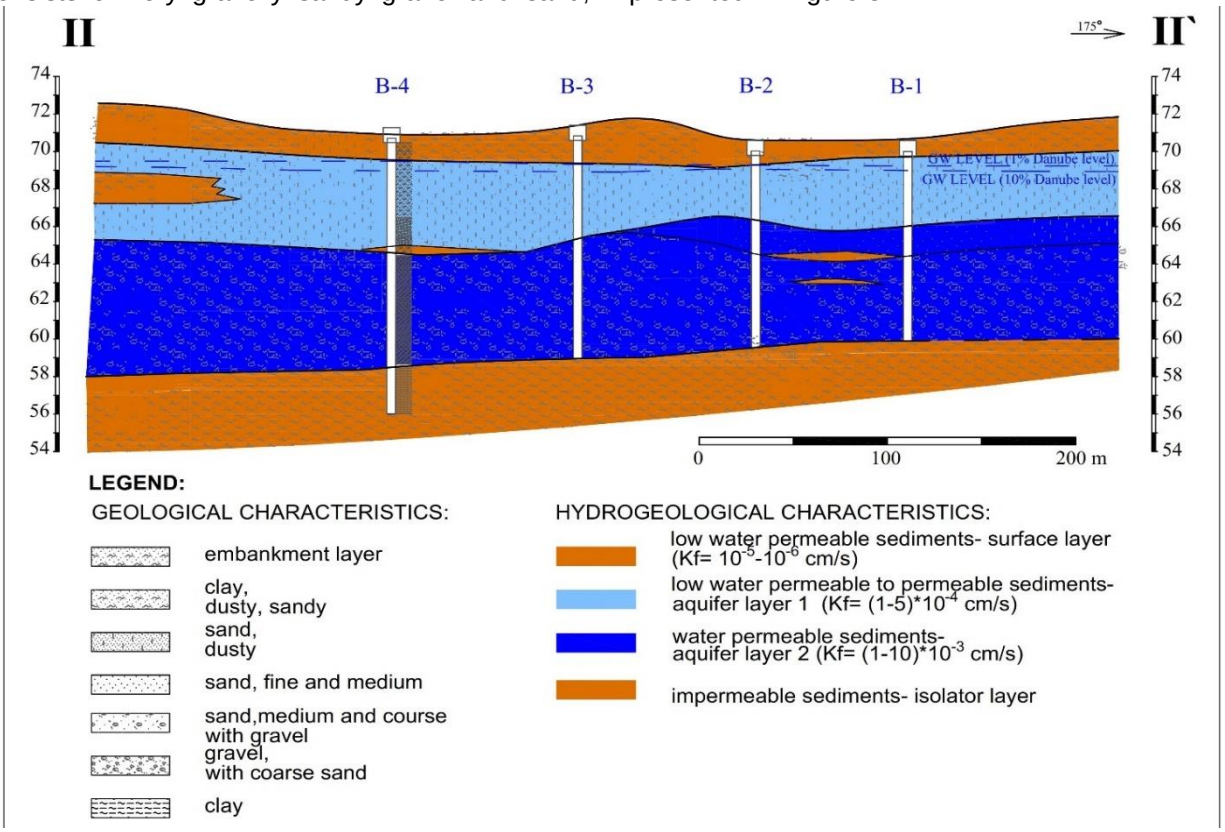

Figure 2. The characteristic hydrogeological profile of examined area - Vinci

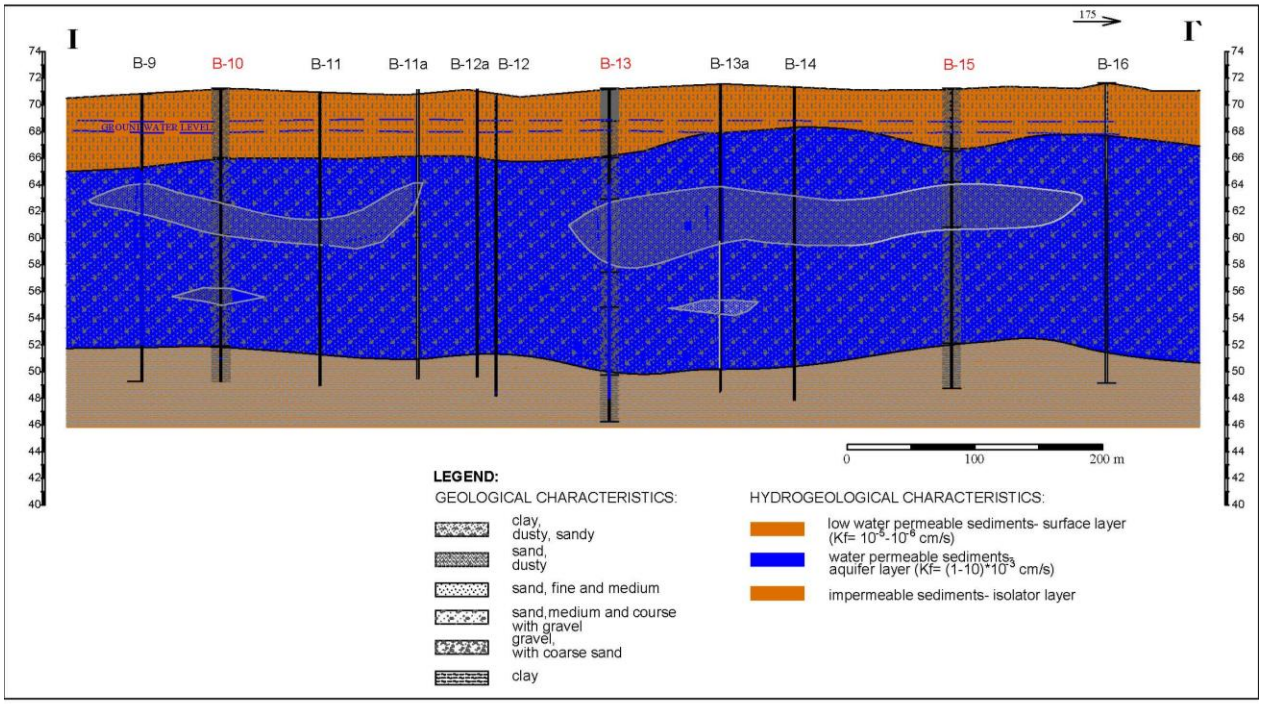

Figure 3. The characteristic hydrogeological profile of examined area - VelikoGradište

Observation dataof groundwater levels over time, from both locations, have indicated a weakening of the effects of well operation during the previous exploitation period, potentially due to the occurrence of "aging" of the wells because of long-term operation [14,15]. This has led to an increase in groundwater levels in the coastal area, with levels recorded in the lowest parts of the terrain behind the well array during the spring period at depths of less than 2.0 meters.

In 2021, the groundwater quality from the wells B-1, B-2, B-3, and B-4 in the Vinci area and B-10, B-13, and B-15 from Veliko Gradište area was analyzed in a one-time campaign (Figure 4 and Figure 5). The sampling was carried out in accordance with *SRPS EN ISO 19458:2009, Water Quality - Sampling for Microbiological Analysis standard. Quality control and quality assurance were guaranteed by ISO/IEC 17025:2017 General requirements for the competence of testing and calibration laboratories*.Details of applied physico-chemical analysis are stated in Standard Methods for the Examination of Water and Wastewater, 21st Edition (2005) [16]. The BART test results were processed using specialized software known as BART-SOFT V.6 [17, 18].

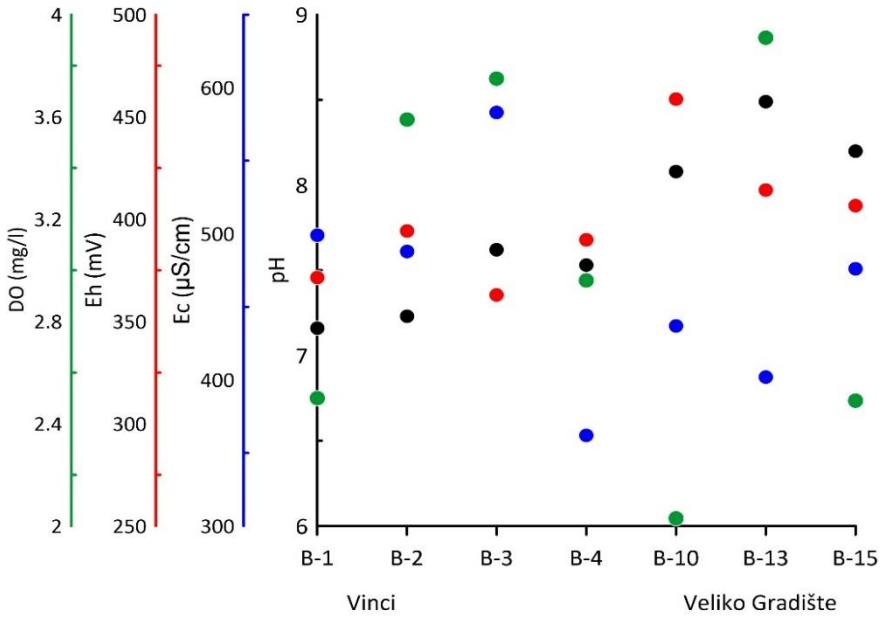

Figure 4. The values of groundwater state parameters in examined wells at two locations

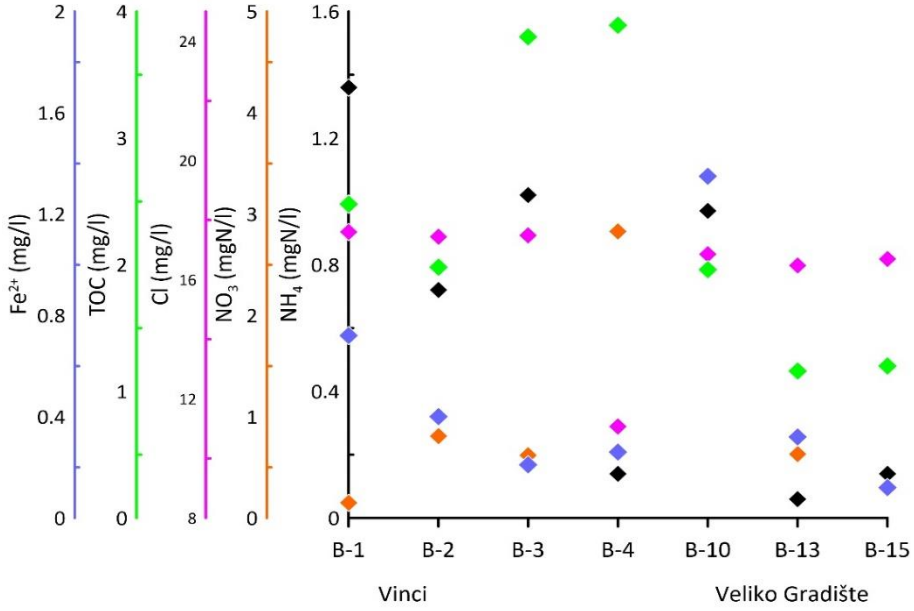

Figure 5. The values of groundwater quality parameters in examined wells at two locations

Based on the type and time of signature reaction appearance the description of consortia and estimation of the abundance and aggressiveness of detected bacterial groups and the corrosion risk, clogging risk, and potential health risks were calculated. The corrosion risk (CR) and biofouling risk (BF) scale is represented by a numerical value ranging from 0 (indicating no risk) to 9 (denoting maximum risk) for the progression of these phenomena. During the Lag period (10-15 days) of sample incubation, the appearance of reactions in biodetectors was observed, photographed, and archived daily.

3. RESULTS AND DISCUSSION

Analysis of Groundwater Quality - Vinci

The oxygen content in groundwater in the Vinci wells B-1, B-2, B-3, and B-4 ranged from 2.5 mg/l to 3.75 mg/l. The standard redox potential ranged from 363 mV to 394 mV, confirming that oxidation processes of reduced chemical species likely dominate in investigated area. Electrolytic conductivity in the range of 362 µS/cm to 583 µS/cm proved oligosalinity. The pH value was within a narrow range from 7.16 to 7.62. The concentrations of ammonium ions were from 0.14 mgN/l to 1.36 mgN/L. The concentration of nitrite and nitrate were not significant, while iron and especially manganese were increased. The moderately increased concentrations of organic carbon in B-4, B-3, and B-1 (3.9 mg/l, 3.8 mg/l, 2.5 mg/l, respectively), could indicate the presence of organic pollution, thus possible high numbers of aerobic heterotrophic bacteria and a health risk due to possible presence of pathogens. The determined content of divalent iron and oxygen at the same time of measurement indicates imbalance and disequilibrium of redox-sensitive species (redox state) due to artificially intruded oxygen, likely because of lowering the static level and depression cone due to excessive pumping or infiltration through the unsaturated zone [6,14]. The mixing of different hydrochemical zones, reductive and slightly oxidative, due to significant content of reduced iron, suggests potential for chemical and microbiological oxidation and the formation of iron oxides-hydroxides precipitates, resulting in biofouling in the pre-filter zone and on well screens, as well as corrosion on hydro-technical elements and well construction. A wide range of sulfate concentrations from 3.33 mg/l to 25.47 mg/l suggests intensive microbiological processes of sulfate reduction, oxidation of ferrous sulfide with nitrate reduction (B-4). Dissolved sulfides were not detected in any groundwater sample, but their value may be underestimated due to precipitation by rapid reaction with dissolved divalent iron (insoluble ferrous sulfides-black precipitates) [19]. Groundwater in the B1, B2, B3 exhibits similar biochemical diversity and a very high number of aerobic heterotrophic bacteria and bacteria producing extracellular polymers, i.e., biofilm-forming groups, with values ranging from very high values of 6.84-6.95 log pac/ml (Figure 6). The population of iron-manganese oxidizing bacteria was present in the range of 3.95-5.15log pac/ml. A uniform population of sulfate-reducing bacteria, with their aggressiveness assessed as high (3.78 log pac/ml), was observed in all four samples in Vinci. Groundwater in the B-4 stood out from the examined group due to the positive finding of fluorescent Pseudomonas species (*Pseudomonas aeruginosa*), biofilm-forming, motile, opportunistic pathogenic species. The population counts of the tested bacterial groups are given in the form of a logarithm for ease of representation due to the population size, with the tested groups indicated by color (Figure 6 and Figure 7).

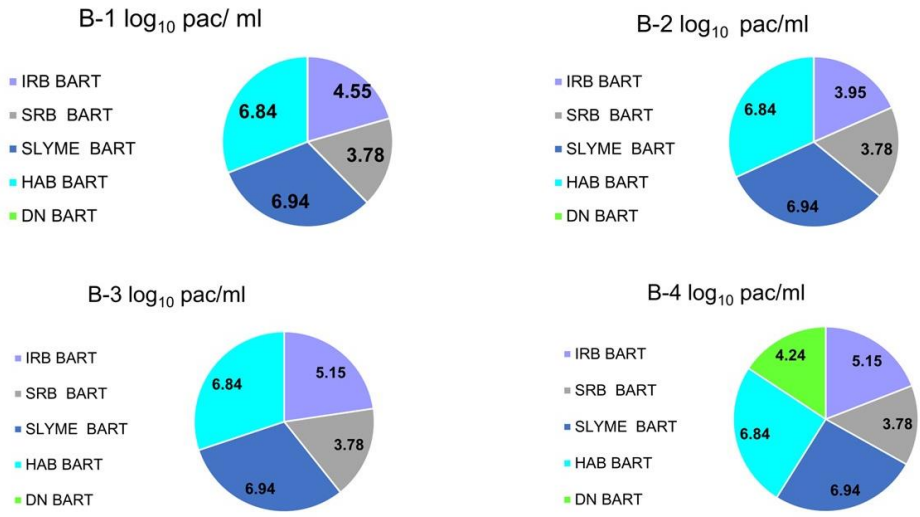

Figure 6. Abundance and Biochemical Diversity of Tested Samples - Vinci

Analysis of Groundwater Quality - VelikoGradište

In the groundwater sampled from selected, tested drainage wells B-10, B-13, B-15, i*n situ* measurements indicated oxic environment, with the dissolved oxygen (DO) concentration in the range of 2.0 mg/l -3.9 mg/l. The values of the standard redox potential in groundwater varied in the range of 406 mV - 459 mV. The electrolytic conductivity ranged from 402 to 476 µS/cm. The pH was within a narrow range of basic values of 8.1-8.5. Concentrations of iron and manganese in all wells were increased. Dissolved sulfides were detected in one groundwater sample (B-10). Sodium, chloride, and sulfate concentrations were not significant. Groundwater from B-10, B-13, B-15 exhibits similar biochemical diversity and very high number of aerobic heterotrophic bacteria and bacteria producing extracellular polymers, (i.e., biofilm-forming groups, ranging from 6.84 to 6.94 log pac/ml) (Figure 7). The population of iron-manganese oxidizing bacteria ranged from 3.95 log pac/ml in B-15 to 5.15 log pac/ml in B-10 and B-13. Sulfate reducing bacteria, whose aggressiveness (biochemical activity) was assessed as high (3.78 log pac/ml), were detected in the groundwater of all three examined wells.

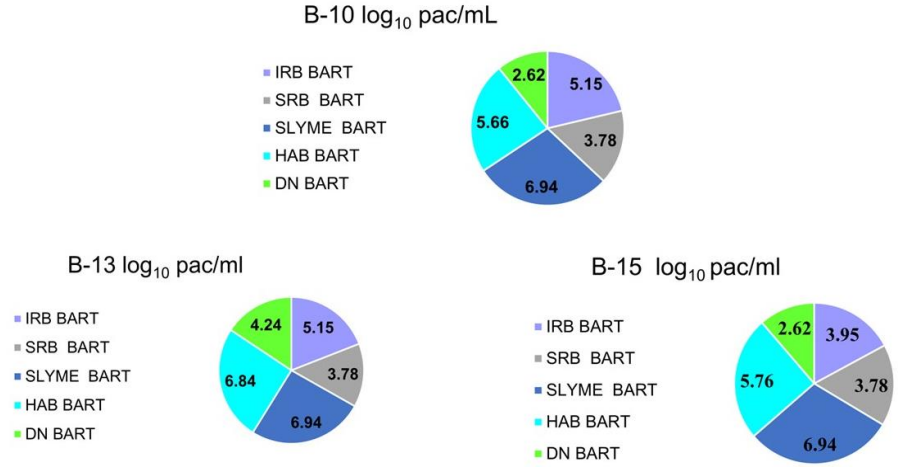

Figure 7. Abundance and Biochemical Diversity of Tested Samples – VelikoGradište

Calculated risks for bio-corrosion, bio-clogging and health risk

Based on the timing of all recognized reactions in the system of five types of BART, the structure of consortia, and the estimated numbers and aggressiveness of detected bacterial groups, software-predicted risks for the development of biocorrosion and biofouling processes, as well as risks to public health, are calculated. The calculated risk for the development of corrosion processes beneath deposits and biologically generated pitting corrosion in the groundwater was uniform within moderately high-risk ranges (Table 1).Very high risks for the development of biologically induced clogging were determined for groundwater in B-4 (Vinci) B-10 (Veliko Gradište) and B-13 (Veliko Gradište).In B-4, denitrification activity has been detected, indicating a sanitary risk as well. Within the same wellthe positive finding of fluorescent pseudomonas species (*Pseudomonas aeruginosa*), which is biofilm-forming, motile, opportunistic pathogenic species was observed. Additionally, identified signature reactions within the IRB BART testing indicated that in the groundwater within zones B-1, B-3, and B-4, some enteric species were likely present as well.High risks to public health and the probable presence of pathogens have been identified for groundwater in B-13. In B-13 and B-15, the presence of biofilm-forming, motile, opportunely pathogenic species (Pseudomonas aeruginosa) was indicated. Also, signature reactions within IRB BART testing indicated that some enteric species were present in groundwater in B-10. Denitrifying bacteria were also detected in groundwater B-13 with significant numbers.

Table 1. Software-predicted risks for the development of biocorrosion, biofouling, and health risks in groundwater in the drainage wells zone (CR – biocorrosion risk; PR – biofouling risk; HR – health risk)

Software-predicted risks	B-1	B-2	B-3	B-4	B-10	B-13	B-15
	Vinci	Vinci	Vinci	Vinci	VelikoGradište	VelikoGradište	VelikoGradište
CR	5.40	5.40	5.40	5.40	5.40	5.40	5.40
PR	7.20	7.00	7.20	8.10	8.10	8.10	6.30
HR	5.40	2.10	4.50	5.40	6.30	8.10	1.80

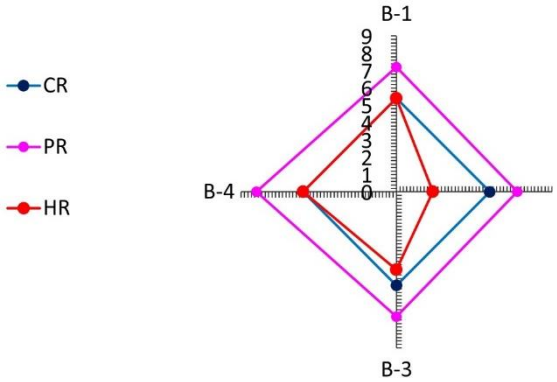

Figure 8.Graphical presentation of software-predicted risks for biocorrosion, biofouling, and health risk in groundwater– Vinci

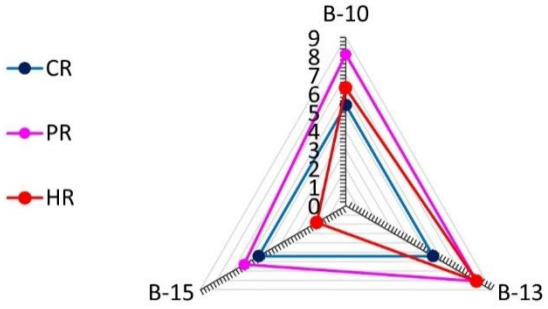

Figure 9. Graphical presentation of software-predicted risks for biocorrosion, biofouling, and health risk in groundwater – VelikoGradište

4. CONCLUSION

The potential impact of the analyzed chemical and microbiological parameters on the aging process of the wells was thoroughly analyzed on twoalluvial groundwater sites. The results of the conducted physico-chemical analyses of groundwater in the drainage well zone indicated an oxic environment (elevated values of oxygen and redox potential) along with the increased concentrations of iron and manganese; thus, a potential for aerobic oxidation of reduced chemical species, which could be mediated both chemically and microbiologically. The rapid "aging" and decline in specific yield of examined wells are influenced by a combination of chemical instability (oxidation) of the environment conducive to this process and suboptimal well operation (over-pumping by high-capacity pumps, low engagement, with short intervals of operation).A moderately high risk was observed for corrosion of all examined wells, while a very high risk was calculated for biofouling for three of total seven wells. In one out of seven examined wells, the high risk for human health was determined. Special attention needs to be paid to the design of newly planned drainage wells to optimize their operation, ensuring a functional dependency on the installed capacities of the units, their engagement, and maintenance of required groundwater levels.This study highlights the significance of comprehensive understanding of physico-chemical and microbiological composition of water,as well as their interconnections and mutual dependencies. This interconnection not only signals potential health risks but also explicitly defines the probability of bio-induced corrosion and biofouling occurrences through coefficient calculations.Based on these results the engineers and technicians can implement preventive measures and treatments to mitigate clogging issues, ensuring the sustained functionality and efficiency of the well system.

5. REFERENCES

[1] R. Brigmon, H. Martin, H. Aldrich (1997) Biofouling of Groundwater Systems by Thiothrix spp., Curr Microbiol 35, 169 –174 https://doi.org/10.1007/s002849900233.

[2] W. G. Characklis (1990) Biofilm Processes.In: WG Characklis, KC Marshall (eds) Biofilms. New York: JohnWiley, p. 195–233.

[3] P. Rajala, E. Huttunen-Saarivirta, M. Bomberg, L. Carpén (2019) Corrosion and biofouling tendency of carbon steel in anoxic groundwater containing sulphate reducing bacteria and methanogenic archaea, CorrosionScience,159,108148, https://doi.org/10.1016/j.corsci.2019.108148.

[4] I.E.Okorie, N.R.Chukwudi (2021) A review of fungal influenced corrosion of metals, Zaštita materijala, 62 (4), 333-339, ISSN 0351-9465, E-ISSN 2466-2585 UDC: 620.193.472/.479:582.28 https://doi.org/10.5937/zasmat2104333O

[5] V. Obradović, M. Perović, J. Lekić (2024) Evaluation of corrosion potential using physicochemical water quality assessment. 31th Ecological Truth & Environmental Research 2024, 18-21 June 2024,Sokobanja, Serbia, in press.

[6] V.Šaraba, J.Nikodinovic-Runic, V.Obradović, I. Dimkić, T.Janakiev, V.Dragišić, M.Ciric (2023) Biocorrosion, biofouling and health risk: biological activity reaction tests of selected brackish groundwater occurrences in Serbia. 2nd International Conference on Chemo and Bioinformatics ICCBIKG_2023, 28-29 September 2023, Kragujevac, Serbia. doi: 10.46793/ICCBI23.086S.

[7] M.C. Moura, E.V. Pontual, P.M Paiva, L.C. Coelho,M. Rêgo(2013) An Outline to Corrosive Bacteria.

[8] J.D.Gu (2005) Chapter 9-Biofouling and prevention: Corrosion, biodeterioration and biodegradation of materials, Handbook of Environmental Degradation of Materials, William Andrew Publishing,p. 179-206. https://doi.org/10.1016/B978-081551500-5.50011-2.

[9] V.B. Damodaran, N.S. Murthy (2016) Bio-inspired strategies for designing antifouling biomaterials. *Biomater* ***Res,*** **20,** 18-26.

https://doi.org/10.1186/s40824-016-0064-4.
[10] S. Liu, W. Guo (2018) Anti-Biofouling and Healable Materials: Preparation, Mechanisms, and Biomedical Applications, Advanced Functional Materials, https://doi.org/10.1002/adfm.201800596.
[11] L.M.Prasad, R.Saravanathamizhan, V.T.Perarasu (2023) Corrosion protection of mild steel using nanomaterials coating, Zastita Materijala 64 (4), 365 –371. https://doi.org/10.5937/zasmat2304365P.
[12] B. Stojanović, B. Đukić, N. Stojanović, S. Smiljanić (2012) Korozija i zaštita rashladnog Sistema, Zaštita materijala 53 (1),51-57.
[13] P. Vuong, A. McKinley,P. Kaur (2023) Understanding biofouling and contaminant accretion on submerged marine structures. npjMater Degrad. **7**, 50. https://doi.org/10.1038/s41529-023-00370-5.
[14] Jaroslav Černi Water Institute (2021), Naselje Vinci Utvrđivanje stanja I efekata rada drenažnih bunara sa predlogom rešenja, Idejno rešenje, In Serbian.
[15] Jaroslav Černi Water Institute, 2022, Naselje Veliko Gradište, Obezbeđenje predviđenih efekata rada drenažnih bunara sa predlogom rešenja, Idejno rešenje, in Serbian.
[16] APHA (2005) Standard Methods for the Examination of Water and Wastewater. 21st Edition, American Public Health Association/American Water Works Association/Water Environment Federation, Washington DC.
[17] D. R. Cullimore (2007) Practical Manual of Groundwater Microbiology, 2nd ed.; CRC Press.
[18] D. R. Cullimore(2010) Standard Methods for the Application of BART Testers in Environmental Investigations of Microbiological Activities; DBI: Canada.
[19] M.Perović, V.Obradović, S.Kovačević, D. Mitrinović, N. Živančev, T.Nenin (2017) Indicators of groundwater potential for nitrate transformation in a reductive environment. Water Environ. Res., 89, (1), 4–16.

IZVOD

PROCENA BIOKOROZIJE, BIOOBRASTANJA I ZDRAVSTVENIH RIZIKA NA DVE ISTRAŽIVANE LOKACIJE U DUNAVSKIM ALUVIJUMIMA

U radu su prezentovani rezultati mikrobioloških istraživanja posebnih metaboličkih (fenotipskih) grupa bakterija koje igraju važnu ekološku ulogu u biogeohemijskom kruženju gvožđa , mangana, azota, sumpora i ugljenika, a koje učestvuju i u razvoji procesa biokorozije, biofulinga a neke od njih predstavljaju i rizik za javno zdravlje. Na osnovu dobijenih rezultata primenjenih reakcionih testova biološke aktivnosti (BART testovi), koji su obrađeni u namenskom softveru, izračunati su potencijalni rizici za razvoj mikrobiološki posredovanih procesa korozije, mikrobiološkog kolmiranja i zdravstveni rizici za podzemne vode u zoni sedam hidrotehničkih objekata dva oksična lokaliteta u aluvijonu Dunava - Vinci i Veliko Gradište, u Srbiji. Umereno visok rizik za biokoroziju određen je za svih sedam bunara na oba lokaliteta (CR=5.4). Rizik od mikrobiološkog kolmiranja bio je vrlo visok u tri od sedam ispitivanih bunara (PR=8.10). Među sedam ispitivanih lokaliteta, jedan se posebno izdvojio na osnovu izračunate visoke vrednosti koeficijenta zdravstvenog rizika (HR=8.10). Rezultati istraživanja su pružili nove uvide u mikrobiološku ulogu u starenju bunara u oksičnim podzemnim vodama dunavskog aluvijona. Pokazano je da fizičko-hemijski sastav i hemijske vrste poput minerala, organske materije i specifičan sastav zajednica mikroorganizama u ispitivanim podzemnim vodama imaju potencijal da podstaknu biokoroziju I formiranje naslaga i biofilmova unutar strukture bunara. Osim biohemijskih analiza, prikazane su i hidrogeološke karakteristike analiziranog područja, kako bi se definisala geološka stratigrafija za koju bi, na osnovu dobijenih rezultata, bilo očekivano odvijanje specifičnih mikrobioloških transformacija.

Ključne reči: *biokorozija, biozačepljavanje, podzemna voda, zdravstveni rizik, Srbija*

Naučni rad
Rad primljen: 28.04.2024.
Rad prihvaćen: 02.09.2024.

Vesna Obradović: https://orcid.org/0009-0008-2157-0615
Marija Perović: https://orcid.org/0000-0003-2045-001X
Predrag Pajić: https://orcid.org/0000-0002-3148-3231

Canute Sherwin[1], Kandavalli Raju[2]*

[1]Atria University, Bengaluru, India – 560 024, [2]St Joseph Engineering College, Mangaluru, India – 575 028

Review paper
ISSN 0351-9465, E-ISSN 2466-2585
https://doi.org/10.62638/ZasMat1066

Zastita Materijala 66 (1)
196 - 205 (2025)

Advancements in thermal barrier coatings for internal combustion (IC) engines

ABSTRACT

Pistons of diesel engines are made of aluminum alloys. There has always been a need to increase the thermal efficiency of engines which use these pistons. Aluminum Alloy pistons find their application because they are lightweight and have a comparatively good heat transfer ability and strength to weight ratio. However, aluminum alloys exhibit increased coefficient of thermal expansion, low durability at high temperatures, increased wear rates and formation of aluminum oxide due to interaction with oxygen in air at high temperatures. These challenges are solved by coating a ceramic material onto the piston, known as the thermal barrier coatings (TBCs), due to its low specific heat and heat transfer properties. TBCs play an important role in improving the effectiveness of elevated temperatures in industrial applications like gas turbines, automobiles and aeronautical systems. TBCs tend to quickly reduce the upper surface temperature of the piston crown. This paper highlights the prominent methods of producing thermal barrier coatings including Diffusion coating, thermal spray technique, Electric Arc Wire Spray Technique, PVD, CVD, Electrodeposition and Additive Manufacturing Method. The crucial discussion is on the materials and emerging trends in developing an efficient thermal protection system. Additionally, the review throws light on employing novel materials like advanced ceramics, alloys and nanocomposites for their impact as TBCs. The paper also focuses on future prospects and current challenges in research and development of TBCs. Factors such as thermal conductivity, environmental stability and manufacturing processes are evaluated to meet the demands of high temperature internal combustion (IC) engine application. Finally, this brief review combines the existing information on TBCs for engineers, practitioners and scientists to understand the present practices and contribute to the improvement in thermal protection technologies in IC engines.

Keywords: *Thermal Barrier Coatings (TBCs), Internal Combustion (IC), Air Plasma Sprays (APS), Vacuum Plasma Spray (VPS), Physical Vapor Deposition (PVD), High-Velocity Oxy-Fuel (HVOF), Suspension Plasma Spray (SPS), Sol-Gel, Ceramics.*

1. INTRODUCTION

IC engines fall under the category of high temperature applications and there is a standing need to improve the thermomechanical behavior and service life of pistons [1]. Thermal barrier coatings (TBCs) are protective coatings applied onto metallic surfaces, exposed to high temperatures, corrosive and harsh conditions. TBCs are usually ceramics or composite systems consisting of metallic and ceramic materials to enhance the thermal insulation and thermal expansion of components [2].

The demand for electric cars globally has doubled over the past decade. However, the vehicle sales aspect of electric vehicles is still small in number pertaining to issues on charging infrastructure, customer satisfaction on cost and batteries [3]. Further, the electrification of transportation is primarily focused on passenger cars and two-wheeler segments [4]. IC engines are set to remain for heavy duty diesel vehicles beyond 2040 as well. Therefore, attempts to create an environmentally friendly and energy-efficient IC engine are set to continue [5]. Some innovations in this direction includes; innovative combustion systems, piezo fuel injection system (FIS) and additive manufacturing to create pistons [6].Engine thermal management remains one of the prime innovation areas to improve engine efficiency. Reducing the losses involved in conversion of fuels chemical energy to useful work is the practice applied to enhance the efficiency of IC engines.

Corresponding author: Canute Sherwin
E-mail: canute.sherwin@atriauniversity.edu.in
Paper received: 15. 04. 2024.
Paper corrected: 24. 08. 2024.
Paper accepted: 05. 09. 2024.
The website: https://www.zastita-materijala.org/

Automobile diesel engines expel about 50-60% of energy as heat [7]. The heat transferred from within the combustion chamber to the walls, leads to reduction of work per cycle being transferred to the piston. This leads to incomplete oxidation [8].

To overcome this TBCs were infused to various components of IC engines in the 1980s. They are usually ceramic based coatings having poor heat conductivity, such as valves, liners, cylinder heads, and piston crowns, applied to the combustion chamber's surface [9]. The aim is to reduce the heat transfer from the fuel (working gas) to the cylinder walls during the combustion process by reducing thermal conductivity; thereby reducing heat lost to the coolant. This improves engine performance [10].

The most popular TBC material which is widely used today is Yttria Stabilized Zirconia (YSZ). It delivers best performance at high temperatures [11]. Using YSZ decreases engine volumetric efficiency, increases working temperature of gas leading to lower work output and poor emission characteristics. This is observed as the wall temperature remains high even during intake and compression strokes [12].

A lot of developments have taken place in recent years, especially low-temperature-conductivity thin ceramic coatings for compression, and spark ignition engines [13, 14]. A major breakthrough in TBC technology was development of Silica Reinforced Porous Anodized Aluminum (Si RPA) coating by Toyota, also known as Thermo-swing Wall Insulation Technology (TSWIN). This coating has the ability to change wall temperatures rapidly following the transient gas temperature. The TSWIN coating's low heat-capacity and low thermal conductivity lead to fast surface temperature changes, even in short cycle durations. The surface temperatures increase during combustion and decrease during intake and exhaust stroke with gas temperature. This reduces heat loss compared to traditional TBC coatings [15, 16].

Many drawbacks were observed by researchers for anodized TBCs [17-20]. High surface roughness of TBCs was observed to increase the heat transfer rate, THC emissions and reduce combustion. Along with surface roughness, imperfections, porosity and non uniformity in coating thickness, limited the benefits of TSWIN. The problem was countered by the application of a sealant of silica.

Plasma Electrolytic Oxidation (PEO) is an innovative surface coating method that overcomes many of these problems with benefits of high hardness, wear resistance, adhesion, corrosion resistance, ultra-low thermal conductivity, heat capacity and improved homogeneity in porosity, surface finish and coating thickness [21, 22].

2. THERMAL BARRIER COATINGS DESIGN

TBCs provide solutions to various problems related to thermal insulation of IC engines by lowering the thermal conductivity and improving the system's overall effectiveness. TBCs also reduce the degradation of the substrate material. The substrate, bond coat, thermally grown oxide (TGO) layer, and topcoat are the components of the TBC design. The schematic representation of the structure of TBCs is displayed in figure 1 [23].

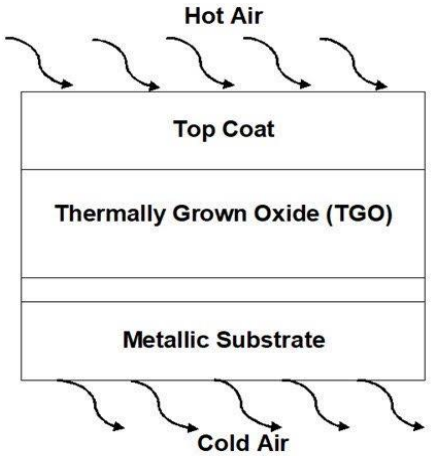

Figure 1. Schematic of TBC Design [23]

The bond coat forms an adhesive layer between the substrate and the other layers by imparting the coating's structural stability. The TGO layer is formed by diffusion of oxygen during the manufacturing stage. The top coat is a ceramic layer which protects the substrate thermally [23].

2.1. Top Coat Materials

Ideal materials for top coat should possess the following properties; phase stability, low thermal diffusivity, thermal shock resistance, strong adhesion, and corrosion resistance [24]. Some of the materials that can be considered as top coat materials include; zirconia, titania (titanium oxide), porcelain, alumina, pyrochlores, porcelanite, garnets, monazite, perovskites, lanthanum magnesium hexa-aluminate and diamond [25].

Yttria partially stabilized zirconia (YTZP) exhibiting properties like low thermal diffusivity, high dielectric constant, excellent fracture toughness and chemically inert at high temperatures is widely used [26]. Yttria-stabilized zirconia (YSZ) is observed to display higher resistance to thermal shocks compared to other ceramics viz Magnesia stabilized zirconia (MSZ), Magnesium oxide partially stabilized zirconia (Mg-PSZ), Glass-infiltrated zirconia-toughened alumina (ZTA), Zirconia-containing lithium silicate ceramics (Zls). Under applied external stress, it maintains the zirconia tetragonal phase at room temperature through a monoclinic phase transition [27]. This phase change builds up compressive stress in the

vicinity of cracks, building transformational toughness. The disadvantage associated with YSZ is that its application is limited to temperatures below 1200℃ [28, 29]. This happens predominantly because of the metastable tetragonal phase transition and sinterability leading to increase in heat transfer and spallation in TBCs [30, 31].

Among the other top coat materials, Zirconates are introduced. One such alternative to YSZ is Pyrochlore $La_2Zr_2O_7$ due to low young's modulus (160–125 GPa at temperatures between 200°C and 1000°C) and thermal conductivity (1.8–3.0 W/mK at temperatures between 200°C and 1000°C) [32]. Monazite or $LaPO_4$, a topcoat material, is stable at high temperatures (around 1300°c) with high coefficient of thermal expansion and low conductivity.

The $LaTi_2Al_9O_{19}$ (LTA) system is tested for stability at high temperatures around 1300℃ and it exhibits excellent stability of phase [33]. LTA has a thermal expansion coefficient similar to YSZ. However, LTA displayed lower fracture toughness compared to YSZ. This can be solved by having a double layer of YSZ/LTA [34, 35]. Introducing dopants like Yb_2O_3, Gd_2O_3, CeO_2 etc. decreases heat conductivity and Young's modulus while preserving YSZ-like fracture toughness. The phase instability problems associated with conventional YSZ are resolved by this technique [36]. Use of few garnets like $Y_3Al_5O_{12}$ are gaining importance among researchers because of its ideal mechanical and thermal properties with phase stability and low diffusivity of oxygen [37, 38].

2.2. Bond Coat Materials

Diffusion and overlay coatings are two forms of bond coats used in TBC applications. In diffusion coatings, an intermetallic layer is diffused to form a boundary for oxygen diffusion. Aluminum coated superalloy like NiAl with silicon and chromium inclusions is one such example of diffusion bond coats [39]. Platinum-modified NiAl bond coats are presently used for many applications [40]. It is observed that for longer thermal cycles Pt-modified NiAl bond coatings work effectively, yet for smaller thermal cycles overlay coatings are proved to be better. One such prominent overlay coating is MCrAlX bond coat where X stands for Y or Zr and M for base material such as Co, Ni or Fe. M is intended to improve the substrate material's compatibility. and X helps in thermal resistivity with grown aluminum oxide and ceramic coating [41].

2.3. Thermally Grown Oxide (TGO) Layer

The TGO layer develops and grows at high temperatures between bond and ceramic top coats. Growth stresses are introduced because of differences in thermal expansion coefficients of TBC layers and continuous formation of TGO material [42].

2.4. Multi Ceramic Layer Coatings

The commonly used YSZ single layered coating exhibits short Thermal cyclic fatigue (TCF) life time. To enhance the lifetime of coatings, researchers have started working on double layered and triple layered TBCs. Using double-ceramic layer (DCL) coatings is a novel method of improving TBC performance. It is achieved by introducing Zirconate layers into YSZ top coat [43].

Zirconates like La_2Zr2O7 (LZ), $Gd_2Zr_2O_7$ (GZ) and $Nd_2Zr_2O_7$ (NZ) exhibit low thermal conductivity, high temperature for phase transformations and corrosion resistance properties but have low coefficients of thermal expansion and fracture toughness [44]. By using multiple layers of Zirconates the mismatch in thermal expansions are reduced and fracture toughness is improved [45, 46].

Mahade and Dolekar et al. [47] compared GZ / YSZ (double layered), GZ dense / GZ / YSZ (three layered) and single-layered YSZ coatings. Single-layered YSZ coating exhibits low thermal life cycle, while the three-layered TBC exhibited the highest [47]. Also, multi layered coatings are more resistant to corrosion as tested for different molten salts [48,49]. The schematic representation is provided in figure 2.

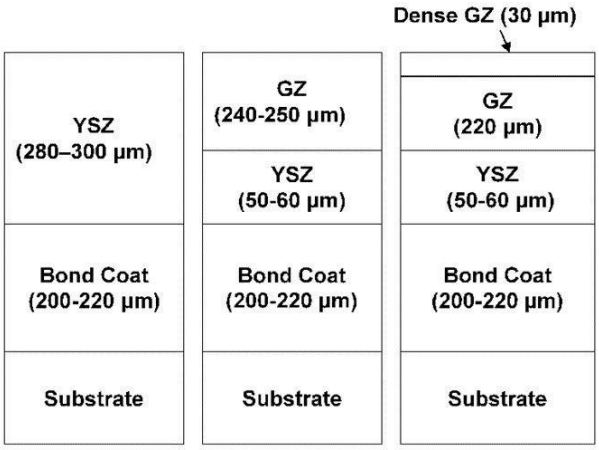

Figure 2. Coating architectures of single layered, double layered and triple layered coatings [47]

3. FABRICATION TECHNIQUES

Among the prominent TBC fabrication techniques; electric arc wire spray coating, thermal spray techniques, diffusion coating, Ni-dispersion coating, magnetron sputtering and physical vapor deposition (PVD) dominate the most. Figure 3 represents the broad classification of fabrication techniques.

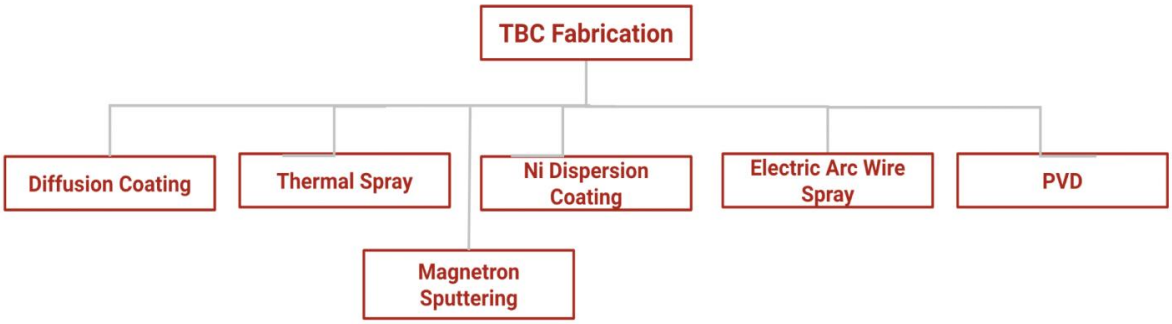

Figure 3. Broad Classification of TBC Fabrication Techniques

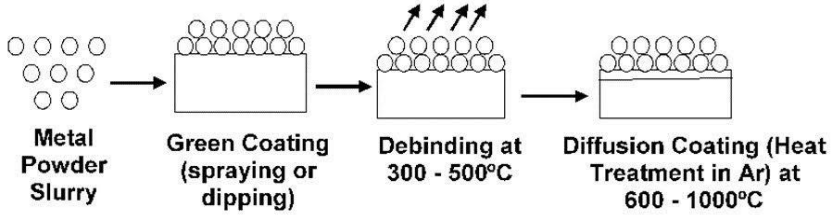

Figure 4. Diffusion Coating Process

During diffusion coating, protective materials like aluminum + silicon or aluminum + chromium are evaporated on the hot component at approximately 900℃. In this process a slurry of metal powder is initially sprayed on the base material followed by debinding and oxidation at high temperatures [50]. Figure 4 displays the diffusion coating process.

In thermal spray technique, the material of high melting point is deposited onto the substrate material using a plasma jet or HVOF method. The energy carrying media (plasma) heats and melts the feed, followed by injection in the form of rod, wire or powder. The peak velocity and pressure causes the particle droplets to flatten and deposit as layers [51]. Figure 5 displays the schematic representation of thermal spray technique.

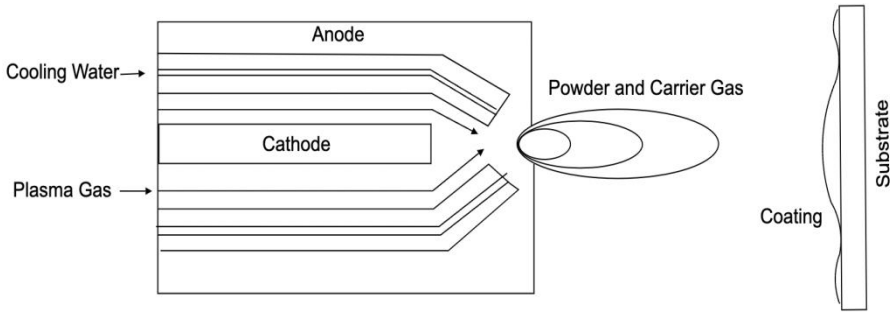

Figure 5. Schematic representation of coating process by thermal spray technique

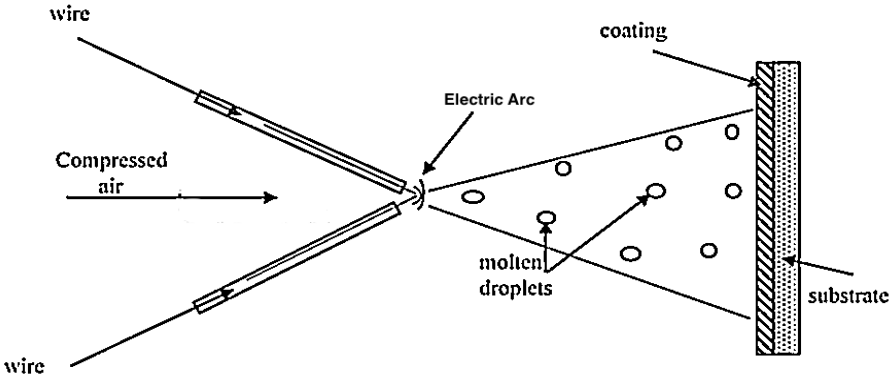

Figure 6. Schematic representation of electric arc wire spray technique

Electric arc wire spray technique uses an electric arc which is struck between two feedstock wires. The heat generated is sufficient to melt the material. The molten metal is then transported by gas stream onto the target surface where it solidifies [52]. The schematic representation of electric arc wire spray technique is represented in figure 6.

Physical Vapour Deposition (PVD) is a thermal barrier coating technique in which the material to be deposited is sublimated and evaporated into atoms or molecules and is transported towards the substrate where it is condensed. It is very much crucial to maintain the chamber under low pressure like plasma or vacuum [53]. Among the different PVD deposition techniques EB-PVD (Electron Beam-PVD) is most commonly used in industries, in which the electron beam is used to melt the target material followed by vaporizing and depositing on the surface with unique columnar microstructure [54]. Aluminium Titanium Nitride, ceramic, titanium, and zirconium are the coating materials utilized in EB-PVD [55]. The PVD process is represented in figure 7.

Chemical Vapour Deposition (CVD) is used to deposit thin films. The material gets deposited in vapor phase onto the heated substrate. One or more precursors are kept in a chamber throughout this process for reaction and decompose on the substrate surface as thin film [56]. Figure 8 represents a simple CVD process.

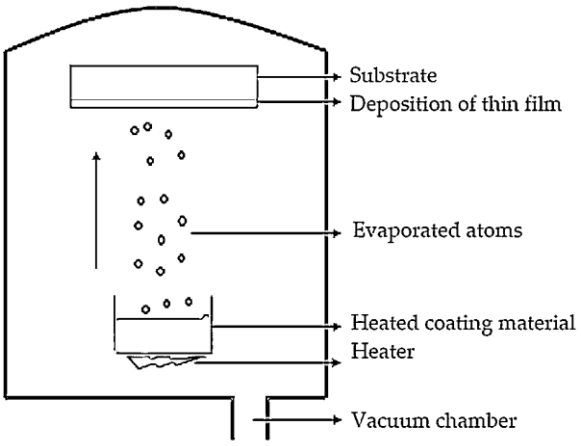

Figure 7. PVD arrangement and process

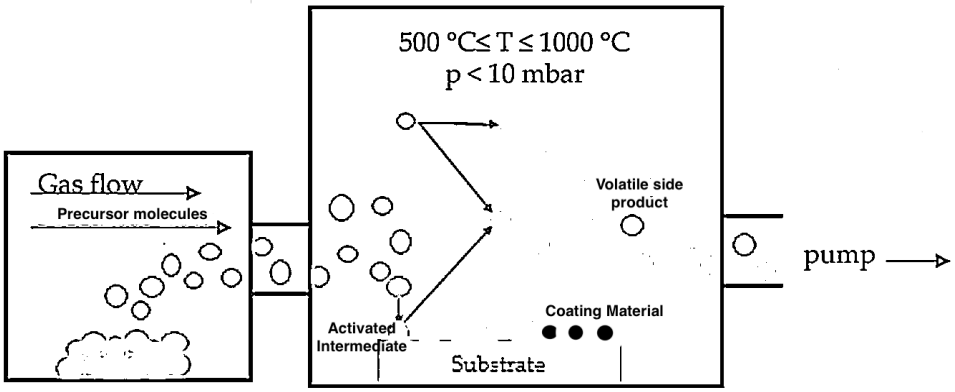

Figure 8: CVD process

Electrochemical processes are being tried recently to fabricate metal and ceramic thermal barrier coatings. The electrochemical processes are categorized as; electrophoretic and electro-deposition. In electrophoretic deposition, charged particles are deposited onto oppositely charged electrodes from a suspension source [57]. Electrolytic deposition uses soluble salt solution of the metal to be coated and deposits the oxide layer [58].

One of the latest advancements in fabricating Functionally Graded Materials (FGM) is through additive manufacturing process. Among the AM methods, material jetting, powder bed fusion, stereolithography, directed energy deposition (DED), and fused deposition modelling are presently used for thermal barrier coatings. These processes exhibit better control of process parameters [59].

4. CORROSION RESISTANCE AND MECHANICAL PROPERTIES OF THERMAL BARRIER COATINGS

Thermal barrier coatings in IC engines are aimed to operate at very high temperature and pressure. A lot of tests are being conducted to determine oxidation and mechanical properties. The properties are greatly affected because of the microstructure of coating, usually columnar and lamellar depending on coating technique. Also the parameters selected for the process like powder size, spray distance, spray rate, current etc., will have an impact [60].

Failure in TBCs occurs due to growth of TGO due to oxidation. The growth causes additional stresses leading to nucleation and propagation of microcracks between layers. Therefore, controlling the formation and thickness of TGO is critical in determining the life of TBCs. Applying ceramic layers was observed to provide higher oxidation resistance as compared to nickel based alloy material, typically used for IC engines. The coated components were tested by exposing for 100 h at 1000℃. Microstructural changes due to oxidation were observed up to the depth of 35 μm in coated samples as compared to 80 μm in as received alloy material [61].

TBCs also fail due to mismatch in thermal expansion coefficients between metals / alloys and ceramics on cooling. Crack formation can be avoided by selecting materials with almost similar thermal expansion coefficients [62]. The coatings after deposition are usually marked by a significant quantity of smooth craters. Exposure to high temperature forms needle-like features and with the exposure to corrosive environments leads to the growth of certain crystals [63].

The microstructures of coatings produced by SPS, EB-PVD methods are made of columns in the top coat (third layer of coating). The columns are thinner in comparison to other coatings. This is due to lower surface roughness and diffusion layers. This provides higher adhesion of layer particles during deposition creating more peaks. However, there is an issue of spallation due to poor bonding between SPS top coat and bond coat surface [64-66]. HVAF and diffusion coats form a dense, thin and uniform TGO layer after certain exposures to high temperatures [63]. A gradually grown TGO layer is ideal to prevent oxidation. Comparing HVAF and VPS, HVAF bond coats exhibit a 20% higher lifetime for corrosion. Comparing APS, SPS and PS-PVD TC in porous, standard and dense configurations, dense PS-PVD coating is more durable for thermal cycle fatigue and corrosion lifecycles. High column density due to much narrower column width, small intercolumnar gaps for enhanced strain tolerance, and medium intra-columnar porosity for reduced thermal conductivity are characteristics of the ideal columnar microstructure [67].

The fracture toughness is the critical factor which determines the durability of TBCs [68]. The fracture in brittle materials is initiated by thermo mechanical loading or processing defects like pores, cavities, and cracks [69]. Besides thermomechanical loading or manufacturing defects, the complex mechanical loading also leads to accelerated total failure [70].

The durability of coating is measured by the bending test, by which modulus of elasticity and fracture toughness is determined [71]. The results show that the TC elastic modulus gradually decreases for increasing temperatures. Three-point bending and micro cantilever bending are two prominent methods to analyze the strength of thermal barrier coatings [72]. Regardless of the length of heating, it is intended that ceramic coating enhance yield strength and ultimate tensile strength [73]. Higher the heating duration, higher the difference between yield strength and ultimate tensile strength [74].

5. CONCLUSIONS

The following conclusions may be drawn from the present study on Thermal Barrier coatings (TBC) for Internal Combustion (IC) engines:

- TBCs provide better solutions to various problems on thermal insulation of IC engines for improving the overall efficiency.
- The TBC design consists of a topcoat, a bond coat and a thermally grown oxide (TGO) layer
- Use of two and / or three layer coatings is a novel method of improving TBC performance.
- Besides traditional methods, Electrochemical Processes and Additive Manufacturing techniques are being explored to develop thermal barrier coatings.
- Corrosion resistance and Mechanical properties are the crucial parameters in estimating the life of thermal barrier coating.
- The finer the coating's microstructure is, the better are the corrosion resistance and mechanical properties

6. REFERENCES

[1] É. Lima, K. Costa, A. Medeiros, J. Medeiros (2006) Life Cycle Analysis of an Internal Combustion Engine Through Thermal History of the Cylinder Head and Scanning Electron Microscopy. SAE Technical Paper 2006-01-2802 https://doi.org/10.4271/2006-01-2802.

[2] N. P. Padture (2022) Thermal barrier coatings for gas-turbine engine applications. Science, 296, 280–284, https://doi.org/10.1126/science.1068609.

[3] REUTERS. Electric dream: Britain to ban new petrol and hybrid cars from 2035. Available on: https://uk.reuters.com/article/us-climate-change-accord-idUKKBN1ZX2RY. (accessed 15 Nov 2023).

[4] International Energy Agency (IEA). Global EV outlook 2019 - Scaling-up the transition to electric mobility. May 2019.

[5] International Energy Agency (IEA). The Future of trucks – Implications for energy and the environment. 2017.

[6] A. Hegab, A. La Rocca, P. Shayler (2017) Towards keeping diesel fuel supply and demand in balance: Dual-fuelling of diesel engines with natural gas. Renewable Sustainable Energy Revs, 70, 666–697, https://doi.org/10.1016/j.rser.2016.11.249.

[7] J. B. Heywood (2018) Internal combustion engine fundamentals. McGraw-Hill, New York, USA, 2nd Edition, ISBN: 9781260116106.

[8] G. Borman, K. Nishiwaki (1987) Internal-combustion engine heat transfer. Prog Energy Combust Sci, 13 (1), 1–46 https://doi.org/10.1016/0360-1285(87)90005-0.

[9] R. Kamo (1987) The adiabatic engine for advanced automotive applications, in: R. L. Evans (Ed.). Automotive Engine Alternatives, Plenum Press, New York, USA, 143–165, https://doi.org/10.1007/978-1-4757-9348-2_6.

[10] G. Woschni, W. Spindler, K. Kolesa (1987) Heat Insulation of Combustion Chamber Walls– A Measure to Decrease the Fuel Consumption of I.C, Engines?. SAE Tech Pap, 8703397, https://doi.org/10.4271/870339.

[11] S. Dhomne, A. M. Mahalle (2019) Thermal barrier coating materials for SI engine. Mater Res Technol, 8 (1), 1532–1537, https://doi.org/10.1016/j.jmrt.2018.08.002.

[12] M. Andrie, S. Kokjohn, S. Paliwal, L. S. Kamo, A. Kamo, D. Procknow (2019) Low heat capacitance thermal barrier coatings for internal combustion engines. SAE Tech Pap, 2019–01-0228, https://doi.org/10.4271/2019-01-0228.

[13] A. Kikusato, K. Terahata, K. Jin, Y. Daisho (2014) A numerical simulation study on improving the thermal efficiency of a spark ignited engine –- Part 2: predicting instantaneous combustion chamber wall temperatures, heat losses and knock. SAE Tech Pap, 2014–01-1066, https://doi.org/10.4271/2014-01-1066

[14] S. Caputo, F. Millo, G. Cifali, F. C. Pesce (2017) Numerical investigation on the effects of different thermal insulation strategies for a passenger car diesel engine. SAE Tech Pap, 2017–24-0021, https://doi.org/10.4271/2017-24-0021.

[15] H. Kosaka, Y. Wakisaka, Y. Nomura, Y. Hotta, M. Koike K. Nakakita (2013) Concept of "temperature swing heat insulation" in combustion chamber walls, and appropriate thermo-physical properties for heat insulation coat. SAE Tech Pap, 2013–01-0274, https://doi.org/10.4271/2013-01-0274.

[16] K. Fukui, Y. Wakisaka, K. Nishikawa, Y. Hattori, H. Kosaka, A. Kawaguchi (2016) Development of instantaneous temperature measurement technique for combustion chamber surface and verification of temperature swing concept. SAE Tech Pap 2016–01-0675, https://doi.org/10.4271/2016-01-0675.

[17] J. Somhorst, M. Oevermann, M. Bovo, I. Denbratt (2019) Evaluation of thermal barrier coatings and surface roughness in a single-cylinder light-duty diesel engine. Int J Engine Res, 22 (3), 1–21, https://doi.org/10.1177/1468087419875837.

[18] A. Kawaguchi, Y. Wakisaka, N. Nishikawa (2019) Thermo-swing insulation to reduce heat loss from the combustion chamber wall of a diesel engine. Int J Engine Res, 20 (7), 805–816, https://doi.org/10.1177/1468087419852013.

[19] S. Memme, J. S. Wallace (2012) The influence of thermal barrier coating surface roughness on spark-ignition engine performance and emissions. Proceedings of the ASME 2012 internal combustion engine division fall technical conference, Vancouver, BC, Canada, 23–26 September 2012, 893–905. New York: ASME. DOI: 10.1115/ICEF2012-92002.

[20] H. Osada, H. Watanabe, Y. Onozawa, K. Enya, N. Uchida (2017). Experimental analysis of heat-loss with different piston wall surface conditions in a heavy-duty diesel engine. Proceedings of the Comodia 9th international conference, Okayama, Japan, 25–28 July 2017. Tokyo, Japan: JSME.

[21] G. B. Darband, M. Aliofkhazraei, P. Hamghalam, N. Valizade (2017) Plasma electrolytic oxidation of magnesium and its alloys: Mechanism, properties and applications. Magnesium Alloys, 5 (1), 74–132, https://doi.org/10.1016/j.jma.2017.02.004.

[22] F. C. Walsh, C. T. J. Low, R. J. K. Wood, K. T. Stevens, J. Archer, A. R. Poeton, et al., (2013) Plasma electrolytic oxidation (PEO) for production of anodised coatings on lightweight metal (Al, Mg, Ti) alloys. Trans IMF, 87(3), 122–135, https://doi.org/10.1179/174591908X372482.

[23] M. Kunal, N. Luis, M. Downey Calvin, J. Van Rooyen Isabella (2021) Thermal barrier coatings overview: Design, manufacturing, and applications in high-temperature industries. Industrial and Engineering Chemistry Research, 60 (17), 6061-6077. https://doi.org/10.1021/acs.iecr.1c00788.

[24] E. J. Young, E. Mateeva, J. J. Moore, B. Mishra, M. Loch (2000) Low Pressure Plasma Spray Coatings. Thin Solid Films, 377−378, 788−792. https://doi.org/10.1016/S0040-6090(00)01452-8.

[25] A. K. Saini, D. Das, M. K. Pathak (2012) Thermal Barrier Coatings - Applications, Stability and Longevity Aspects. Procedia Eng. 38, 3173−3179. https://doi.org/10.1016/j.proeng.2012.06.368.

[26] X. Song, M. Xie. F. Zhou, G. Jia, X. Hao, S. An (2011) High- Temperature Thermal Properties of Yttria Fully Stabilized Zirconia Ceramics. Rare Earths, 29 (2), 155−159. https://doi.org/10.1016/S1002-0721(10)60422-X.

[27] X. Ren, W. Pan (2014), Mechanical Properties of High-Temperature- Degraded Yttria-Stabilized Zirconia. Acta Mater, 69, 397−406. https://doi.org/10.1016/j.actamat.2014.01.017.

[28] M. F. Smith, A. C. Hall, J. D. Fleetwood, P. Meyer (2011) Very Low Pressure Plasma Spray- A Review of an Emerging Technology in the Thermal Spray

Community. Coatings, 1 (2), 117−132. https://doi.org/10.3390/coatings1020117.

[29] R. Hashaikeh, J. A. Szpunar (2009) Electrolytic Processing of MgO Coatings. Phys. Conf. Ser., 165, 012008. DOI: 10.1088/1742-6596/165/1/012008.

[30] I. Zhitomirsky (2002) Cathodic Electrodeposition of Ceramic and Organoceramic Materials Fundamental Aspects. Adv. Colloid Interface Sci., 97 (1−3), 279−317,https://doi.org/10.1016/S0001-8686(01)00068-9

[31] A. R. Boccaccini, I. Zhitomirsky (2002) Application of Electrophoretic and Electrolytic Deposition Techniques in Ceramics Processing Curr. Opin. Solid State Mater. Sci., 6 (3), 251−260. https://doi.org/10.1016/S1359-0286(02)00080-3.

[32] J. Zhang, X. Guo, Y. G. Jung, L. Li, J. Knapp (2017) Lanthanum Zirconate Based Thermal Barrier Coatings: A Review. Surf. Coat. Technol., 323, 18−29. https://doi.org/10.1016/j.surfcoat.2016.10.019.

[33] O. Sudre, J. Cheung, D. Marshall, P. Morgan, C. G. Levi (2001) Thermal Insulation Coatings of LaPO4. Ceramic Engineering and Science Proceedings; Singh, M., Jessen, T., Eds.; John Wiley & Sons, Inc.: Hoboken, NJ, USA, 22, 367−374. https://doi.org/10.1002/9780470294703.ch44.

[34] X. Xie, H. Guo, S. Gong, H. Xu (2011) Thermal Cycling Behavior and Failure Mechanism of LaTi2Al9O19/YSZ Thermal Barrier Coatings Exposed to Gas Flame. Surf. Coat. Technol., 205 (17−18), 4291−4298. https://doi.org/10.1016/j.surfcoat.2011.03.047.

[35] S. Ghosh (2015), Thermal Barrier Ceramic Coatings A Review. Advanced Ceramic Processing; Mohamed, A. M. A., Ed.; InTech, DOI: 10.5772/61346. DOI: 10.5772/61346.

[36] W. Ma, D. Mack, J. Malzbender, R. Vaßen, D. Stöver (2008) Yb2O3 and Gd2O3 Doped Strontium Zirconate for Thermal Barrier Coatings. Eur. Ceram. Soc. 28 (16), 3071−3081. https://doi.org/10.1016/j.jeurceramsoc.2008.05.013.

[37] K. Jiang, S. Liu, X. Wang (2018) Low-Thermal-Conductivity and High-Toughness CeO2-Gd2O3 Co-Stabilized Zirconia Ceramic for Potential Thermal Barrier Coating Applications. Eur. Ceram. Soc., 38 (11), 3986−3993. https://doi.org/10.1016/j.jeurceramsoc.2018.04.065.

[38] N. P. Padture, P. G. Klemens (1997) Low Thermal Conductivity in Garnets. Am. Ceram. Soc., 80 (4), 1018−1020. https://doi.org/10.1111/j.1151-2916.1997.tb02937.x.

[39] X. Fan, B. Zou, L. Gu, C. Wang, Y. Wang, W. Huang, L. Zhu, X. Cao (2013) Investigation of the Bond Coats for Thermal Barrier Coatings on Mg Alloy. Appl. Surf. Sci., 265, 264−273, https://doi.org/10.1016/j.apsusc.2012.10.192.

[40] G. M. Kim, N. M. Yanar, E. N. Hewitt, F. S. Pettit, G. H. Meier (2002) The Effect of the Type of Thermal Exposure on the Durability of Thermal Barrier Coatings. Scr. Mater., 46 (7), 489−495, https://doi.org/10.4028/www.scientific.net/KEM.197.145

[41] M. Bai, B. Song, L. Reddy, T. Hussain (2019) Preparation of MCrAlY-Al_2O_3 Composite Coatings with Enhanced Oxidation Resistance through a Novel Powder Manufacturing Process. Therm. Spray Technol., 28 (3), 433−443. http://dx.doi.org/10.1007/s11666-019-00830-y.

[42] P. Rahul, Zh. Sulin, K. Hsia Jimmy (2003) Bond coat surface rumpling in thermal barrier coatings. Acta Materialia, 51 (1), 239-249. DOI: 10.1016/S1359-6454(02)00456-8.

[43] Z. H Xu, L. M. He, R. D. Mu, S. M. He, G. H Huang, X. Q. Cao (2010) Double-Ceramic-Layer Thermal Barrier Coatings Based on La2(Zr0.7Ce0.3)2O7/La2Ce2O7 Deposited by Electron Beam- Physical Vapor Deposition. Appl. Surf. Sci., 256 (11), 3661−3668. https://doi.org/10.1016/j.apsusc.2010.01.004.

[44] R. Vassen, X. Cao, F. Tietz, D. Basu, D. Stöver (2000) Zirconates as New Materials for Thermal Barrier Coatings. Am. Ceram. Soc., 83 (8), 2023−2028. https://doi.org/10.1111/j.1151-2916.2000.tb01506.x

[45] X. Guo, Z. Lu, H-Y Park, L. Li, J. Knapp, Y-G Jung, J. Zhang (2019) Thermal Properties of $La_2Zr_2O_7$ Double-Layer Thermal Barrier Coatings. Adv. Appl. Ceram. 118 (3), 91−97, DOI: 10.1080/17436753.2018.1542997.

[46] E. Jordan, M. Gell (2015) Low Thermal Conductivity, High Durability Thermal Barrier Coatings for IGCC Environments. Technical Report: 1182555. https://doi.org/10.2172/1182555.

[47] S. Mahade, N. Curry, S. Bjo¨rklund, N. Markocsan, P. Nyle´n (2015) Thermal conductivity and thermal cyclic fatigue of multilayered $Gd_2Zr_2O_7$/YSZ thermal barrier coatings processed by suspension plasma spray. Surf Coat Technol., 283, 329-336, https://doi.org/10.1016/j.surfcoat.2015.11.009.

[48] S. Mahade, N. Curry, S. Bjo¨rklund, N, Markocsan, P. Nyle´n, R. Vaßen (2017) Functional performance of $Gd_2Zr_2O_7$/YSZ multi-layered thermal barrier coatings deposited by suspension plasma spray. Surf Coat Technol., 318, 208-216, https://doi.org/10.1016/j.surfcoat.2016.12.062.

[49] K. M. Doleker, H. Ahlatci, A. C. Karaoglanli (2017) Investigation of isothermal oxidation behavior of thermal barrier coatings (TBCs) consisting of YSZ and multilayered YSZ/$Gd_2Zr_2O_7$ ceramic layers. Oxid Met. 88(1–2) 109-119, https://doi.org/10.1007/s11085-016-9690-4.

[50] J. Th. Bauer, X. Montero, M. Ch. Galetz (2020) Fast heat treatment methods for al slurry diffusion coatings on alloy 800 prepared in air. Surface and Coatings Technology, 381, 125140, https://doi.org/10.1016/j.surfcoat.2019.125140.

[51] A. J. Ruys, B. A. Sutton (2021) Metal-ceramic functionally graded materials (FGMs). Metal-Reinforced Ceramics; Ruys, A.J., Ed.; Woodhead Publishing: Cambridge, UK, 327–359, https://doi.org/10.1016/B978-0-08-102869-8.00009-4

[52] E. Bakan, D. E. Mack, G. Mauer, R. Vaßen, J. Lamon, N. P. Padture (2020) High-temperature

materials for power generation in gas turbines. Advanced Ceramics for Energy Conversion and Storage; Guillon, O., Ed.; Elsevier: Amsterdam, The Netherlands, 3–62, https://doi.org/10.1016/B978-0-08-102726-4.00001-6

[53] S. Mbam, S. E. Nwonu, O. A. Orelaja, U. S. Nwigwe, X. F. Gou (2019) Thin-film coating; historical evolution, conventional deposition technologies, stress-state micro/nano-level measurement/models and prospects projection: A critical review. Mater. Res. Express, 6, 122001. DOI: 10.1088/2053-1591/ab5647.

[54] S-Y Qiu, C-W Wu, C-G Huang, Y. Ma, H-B Guo (2021) Microstructure Dependence of Effective Thermal Conductivity of EB-PVD TBCs. Materials, 14 (8), 1838. https://doi.org/10.3390/ma14081838.

[55] V. Miguel-Pérez, A. Martínez-Amesti, M. L. Nó, J. Calvo- Angós, M. I. Arriortua (2014) EB-PVD Deposition of Spinel Coatings on Metallic Materials and Silicon Wafers. Int. J. Hydrogen Energy, 39 (28), 15735−15745. https://doi.org/10.1016/j.ijhydene.2014.07.115.

[56] G. L. Doll, B. A. Mensah, H. Mohseni, T. W. Scharf (2009) Chemical Vapor Deposition and Atomic Layer Deposition of Coatings for Mechanical Applications. Therm. Spray Technol., 19, 510–516. DOI: 10.1007/s11666-009-9335-8.

[57] V. B. Mišković-Stanković (2014) Electrophoretic Deposition of Ceramic Coatings on Metal Surfaces. Electrodeposition and Surface Finishing: Fundamentals and Applications; Djokić, S. S., Ed.; Springer New York: New York, 133−216. https://doi.org/10.1007/978-1-4939-0289-7_3.

[58] E. I. Meletis, X. Nie, F. L. Wang, J. C. Jiang (2002) Electrolytic Plasma Processing for Cleaning and Metal-Coating of Steel Surfaces. Surf. Coat. Technol., 150 (2), 246−256. https://doi.org/10.1016/S0257-8972(01)01521-3.

[59] B. E. Carroll, R. A. Otis, J. P. Borgonia, J. Suh, R. P. Dillon, A. A. Shapiro, D. C. Hofmann, Z-K Liu, A. M. Beese (2016) Functionally Graded Material of 304L Stainless Steel and Inconel 625 Fabricated by Directed Energy Deposition: Characterization and Thermodynamic Modeling. Acta Mater., 108, 46−54. https://doi.org/10.1016/j.actamat.2016.02.019.

[60] D. Kukla, M. Kopec, K. Wang, C. Senderowski, Z. L. Kowalewski (2021) Nondestructive Methodology for Identification of Local Discontinuities in Aluminide Layer-Coated MAR 247 during Its Fatigue Performance. Materials, 14, 3824. https://doi.org/10.3390/ma14143824.

[61] J. He (2022) Advanced MCrAlY alloys with doubled TBC lifetime. Surf. Coat. Technol., 448, 128931. https://doi.org/10.1016/j.surfcoat.2022.128931.

[62] T. A. Taylor, P. N. Walsh (2004) Thermal expansion of MCrAlY alloys. Surf. Coat. Technol., 177–178, 24–31. https://doi.org/10.1016/j.surfcoat.2003.05.001.

[63] M. Gupta, N. Markocsan, X. H. Li, L. Östergren (2018) Influence of Bond Coat Spray Process on Lifetime of Suspension Plasma-Sprayed Thermal Barrier Coatings. Therm. Spray Technol., 27, 84–97, https://doi.org/10.1007/s11666-017-0672-0.
N. Curry, Z. Tang, N. Markocsan, P. Nylén (2015) Influence of Bond Coat Surface Roughness on the Structure of Axial Suspension Plasma Spray Thermal Barrier Coatings—Thermal and Lifetime Performance. Surf. Coat. Technol., 268, 15–23. https://doi.org/10.1016/j.surfcoat.2014.08.067.

[64] B. Bernard, A. Quet, L. Bianchi, V. Schick, A. Joulia, A. Malié, B. Rémy (2017) Effect of Suspension Plasma-Sprayed YSZ Columnar Microstructure and Bond Coat Surface Preparation on Thermal Barrier Coating Properties. Therm. Spray Technol., 26, 1025–1037 https://doi.org/10.1007/s11666-017-0584-z.

[65] P. Sokołowski, L. Pawłowski, D. Dietrich, T. Lampke, D. Jech (2016) Advanced Microscopic Study of Suspension Plasma-Sprayed Zirconia Coatings with Different Microstructures. Therm. Spray Technol., 25, 94–104. https://doi.org/10.1007/s11666-015-0310-7.

[66] D. Seo, K. Ogawa, T. Shoji, S. Murata (2007) Effect of Particle Size Distribution on Isothermal Oxidation Characteristics of Plasma Sprayed CoNi- and CoCrAlY Coatings. Therm. Spray Technol., 16, 954–966, DOI: 10.1007/s11666-007-9125-x.

[67] N. P. Padture, M. Gell, E. H. Jorda (2002) Thermal Barrier Coatings for Gas-Turbine Engine Application. Science 296, 280–284, doi: 10.1126/science.1068609.

[68] M. Parchovianský, I. Parchovianská, O. Hanzel, Z. Netriová, A. Pakseresht (2022) Phase Evaluation, Mechanical Properties and Thermal Behavior of Hot-Pressed LC-YSZ Composites for TBC Applications. Materials, 15, 2839. https://doi.org/10.3390/ma15082839.

[69] A. K. Ray, E. S. Dwarakadasa, D. K. Das, V. R. Ranganath, B. Goswami, J. K. Sahu, J. D. Whittenberger (2007) Fatigue behavior of a thermal barrier coated superalloy at 800℃. Mater. Sci. Eng., A 448, 294–298. https://doi.org/10.1016/j.msea.2006.10.035.

[70] W. Zhu, Q. Wu, L. Yang, Y. C. Zho (2020) In situ characterization of high temperature elastic modulus and fracture toughness in air plasma sprayed thermal barrier coatings under bending by using digital image correlation. Ceram., Int. 46, 18526–18533, https://doi.org/10.1016/j.ceramint.2020.04.158.

[71] A. G. Evans, D. R. Mumm, J. W. Hutchinson, G. H. Meier, F. S. Pettit (2001) Mechanisms controlling the durability of thermal barrier coatings. Prog. Mater. Sci., 46, 505–553, https://doi.org/10.1016/S0079-6425(00)00020-7.

[72] Q. Wei, J. Zhu, W. Chen (2016) Anisotropic Mechanical Properties of Plasma-Sprayed Thermal Barrier Coatings at High Temperature Determined by Ultrasonic Method. Therm. Spray Technol., 25, 605–612. https://doi.org/10.1007/s11666-016-0378-8

[73] Y. Tan, A. Shyam, W. B. Choi, E. Lara-Curzio, S. Sampath (2010) Anisotropic elastic properties of thermal spray coatings determined via resonant ultrasound spectroscopy. Acta Mater., 58, 5305–5315. https://doi.org/10.1016/j.actamat.2010.06.003.

IZVOD

NAPREDOVANJE U PREMAZIMA TERMIČKE BARIJERE ZA MOTORE SA UNUTRAŠNJIM SAGOREVANJEM (IC)

Klipovi dizel motora su napravljeni od legura aluminijuma. Uvek je postojala potreba za povećanjem toplotne efikasnosti motora koji koriste ove klipove. Klipovi od aluminijumske legure nalaze svoju primenu jer su lagani i imaju relativno dobru sposobnost prenosa toplote i odnos snage i težine. Međutim, legure aluminijuma pokazuju povećan koeficijent toplotnog širenja, nisku izdržljivost na visokim temperaturama, povećanu stopu habanja i formiranje aluminijum oksida usled interakcije sa kiseonikom u vazduhu na visokim temperaturama. Ovi izazovi se rešavaju nanošenjem keramičkog materijala na klip, poznatih kao prevlake termalne barijere (TBC), zbog svojih niskih specifičnih svojstava prenosa toplote. TBC igraju važnu ulogu u poboljšanju efikasnosti povišenih temperatura u industrijskim primenama kao što su gasne turbine, automobili i vazduhoplovni sistemi. TBC imaju tendenciju da brzo smanje temperaturu gornje površine krune klipa. Ovaj rad naglašava istaknute metode proizvodnje termičkih barijernih premaza uključujući difuzioni premaz, tehniku termičkog spreja, tehniku prskanja električnim lukom, PVD, CVD, elektrodepoziciju i metodu proizvodnje aditiva. Ključna diskusija je o materijalima i trendovima koji se pojavljuju u razvoju efikasnog sistema toplotne zaštite. Pored toga, pregled baca svetlo na korišćenje novih materijala kao što su napredna keramika, legure i nanokompoziti za njihov uticaj kao TBC. Rad se, takođe, fokusira na buduće izglede i trenutne izazove u istraživanju i razvoju TBC-a. Faktori kao što su toplotna provodljivost, stabilnost životne sredine i proizvodni procesi se procenjuju kako bi se ispunili zahtevi primene motora sa unutrašnjim sagorevanjem na visokim temperaturama (IC). Konačno, ovaj kratak pregled kombinuje postojeće informacije o TBC za inženjere, praktičare i naučnike kako bi razumeli sadašnju praksu i doprineli poboljšanju tehnologija toplotne zaštite u IC motorima.

Ključne reči: *prevlake za termičku barijeru (TBC), unutrašnje sagorevanje (IC), sprejevi vazdušne plazme (APS), vakuum plazma sprej (VPS), fizičko taloženje pare (PVD), oksi-gorivo velike brzine (HVOF), suspenzija plazma sprej (SPS), Sol-Gel, Keramika.*

Pregledni rad
Rad primljen: 15.04.2024.
Rad korigovan: 24.08.2024.
Rad prihvaćen: 05.09.2024.

Canute Sherwin: 0000-0002-9807-3966
Raju Kandavalli: 0000-0002-6328-5758

Pavel Anatolyevich Nikolaychuk[1,2]*

[1]*Kurganskij gosudarstvennyj universitet, Kurgan, Russian Federation*
[2]*Novosibirskij gosudarstvennyj universitet, Novosibirsk, Russian Federation*

Scientific paper
ISSN 0351-9465, E-ISSN 2466-2585
https://doi.org/10.62638/ZasMat999

Zastita Materijala 66 (1)
206 - 214 (2025)

The inhibitory properties of the boiling extracts from *Fagus sylvatica purpurea* fallen leaves on the corrosion of mild steel in acidic environments

ABSTRACT

The inhibitory ability of the boiling extracts from the fallen leaves ofFagus sylvatica purpurea on the corrosion of mild steel EN Fe37-3FN in 0.5 M hydrochloric acid and 0.5 M sulphuric acid media was investigated using gravimetric, electrochemical, and EIS methods. It was shown that the addition of 100 mg/l of the Fagus sylvatica purpureafallen leaves extract reduces the corrosion rate by 20–25%, and that of of 1 g/l and more – by 65–70%. The adsorption of the extract components on a steel surface follows the Langmuir adsorption model, and the nature of adsorption is physical. The Fagus sylvatica purpureafallen leaves extractshowsitself as prospective and environmentally friendly substance for reducing the steel corrosion rate in acidic environments.

Keywords*: Fagus sylvatica purpurea, purple beech, boiling extracts, acid medium corrosion inhibition, mild steel, gravimetric study, electrochemical study, electrochemical impedance spectroscopy, Langmuir adsorption isotherm.*

1. INTRODUCTION

The usage of industrial side products and wastes [1], expired drugs [2], food and biomass waste [3,4] and compounds extracted from natural products [4]attracts a growing interest of the corrosion engineers around the globe. By employing environmentally degradable natural compounds one could drastically reduce the costs and the ecological impactof both production of inhibitors, and their subsequent utilisation. A plant's roots, leaves, aerial parts, fruits, and seeds are frequently used as the source of extracted compounds [4].

The purple beech (*Fagus sylvatica purpurea*) is a cultivar of the European beech, which is widely distributed in several parts of Europe, Middle Asia and North America [5]. Due to its unusual purple colour or leaves, it is commonlyused as the ornamental tree. The bark and the leaf of the European beech are well-known strong antioxidants [6,7], and contain several polyphenolic compounds including phenolic acids and flavonoids [7–9]. However, both flavonoids [10, 11] and phenols exhibit inhibitory properties on metal oxidation. Moreover, there is a clear dependency between the antioxidant and inhibition properties of natural compounds [12], and therefore, the compounds extracted from *Fagus sylvatica* leaves might be useful and environmentally friendly corrosion inhibitors.

Acidic environments are often employed for the study of the effectiveness of inhibitors, because acids give the most demonstrative results [11]. In addition, the study of the acidic corrosion of metals is important for oil and gas industry, the galvanic electroplating of metals, the development of the solutions for the metal pickling, and for the rust removal [11]. Only a single study concerning the usage of extract of the common beech leaves as the inhibitor of the corrosion of carbon steel in sulphuric acid was already published [13]. However, in that paper a commercial ethanolic extract was used, and its concentration was not specified, therefore, it is impossible to understand the dependency on the inhibitory properties on the concentration of the extracted compounds. Moreover, the employment of toxic organic extractant undermines the sustainability of the obtained extract. The usage of boiling water extract seems a more environmentally friendly solution.

At the end of September, the beech tree exhibits the leaf fall producing the considerable amount of fallen leaves. It was previously found [8]

Corresponding author:Pavel Anatolyevich Nikolaychuk
E-mail: pavel.nikolaychuk@kgsu.ru
Paper received: 29. 02. 2024.
Paper corrected: 24. 09. 2024.
Paper accepted: 01. 10. 2024.
The website:https://www.zastita-materijala.org/

that the concentration of the bioactive compounds in the beech leaves remain stable till the leaf fall. Therefore, collecting the freshly fallen leaves and extracting phenolic compounds from them is a sustainable way to produce extract without jeopardising the growing tree.

Therefore, in the present study, the inhibitory properties of the boiling extracts of the *Fagus sylvatica purpurea*freshly fallen leaves on the corrosion of mild steel EN Fe37-3FN in 0.5 M hydrochloric acid and 0.5 M sulphuric acid media are aimed to be investigated.

2. METHODS

2.1. Reagents and Equipment

Ethanol (analytical grade) and hydrochloric and sulphuric acids (pure grade)were purchased from LLC “Sigma Tek”. Steel electrodes were manufactured from cylindrical ingots made of mild steel EN Fe37-3FN (containing no more than 0.14% C, 0.3% Ni, Cu, and Cr, 0.05% Si, 0.4% Mn, 0.05% P and 0.04% S).The unused flat end surface of the ingots was sealed by the epoxy resin, and the cylindrical working surface immersed in the solution was equal to 0.04 cm^2.

Weighting of the samples was performed using the analytical balanceEX224/AD (Ohaus Corp.).Electrochemical and EIS measurements were conducted using the potentiostat-galvanostat PS-50 (LLC “SmartStat”).The mercury-mercurous sulphate reference electrode by Schott Intstruments GmbH was used. A water for solution preparation was first distilled using the aquadistiller AE-15 (LLC “Livam”) and then deionised using the water purification system AkvaLab S18 (LLC “Akvalab”). The magnetic stirrer MS-200 LT (LLC “Labtex”) was used for stirring and heating the solutions. The single-channel laboratory pipettes manufactured by Thermo Fisher Scientific were used for pipetting the solutions. A laboratory glassware of 2nd grade was used.

2.2. Preparation of the Extracts

The freshly fallen leaves of the purple beeches (*Fagus sylvatica purpurea*)were collected in early October from the trees located in the woods in the outskirts ofNovosibirsk, Russia. The leaves were air-dried in the absence of the direct sunlight during three months and subsequently ground.

A total of 100 g of dried and ground*Fagus sylvatica purpurea*leaves were weighted, immersed into a litre of the deionised water,heated and boiled under the reflux condenser during 3 h. The boiling extracts were cooled, the plant materialwas removed, and the solid residues were filtered off through the filter paper with the pore diameter of 12 μm.

A total of 10 ml of the extract was taken, placed in a beaker and heated to dryness in order to determine the mass of the dissolved substances and the initial concentrations of the extract solutions. Then the working solutions of the *Fagus sylvatica purpurea* leaf extract with the concentrations ranging from 0.2 to 20 g/l were prepared by the appropriate dilutions. The solutions were then equally diluted by 1 M hydrochloric acid or by 1 M sulphuric acid to finally produce a series of acidic solutions of *Fagus sylvatica purpurea* leaf extractin 0.5 M HCl or 0.5 M $H_2SO_4$with concentrations ranging from 0.1 to 10 g/l.

2.3. Gravimetric studies

For gravimetric tests, rectangular flat plates made of EN Fe37-3FN mild steel with thickness 3 mm, width 20 ± 2 mm, and height 30 ± 2 mm were polished using the P2500 emery paper and degreased by ethanol. The weighted plates (m_0) were immersed into corrosive media for 2 h, then washed with distilled water, dried, and reweighted (m). Each experiment was performed in triplicate. From the measured weight losses ($\Delta m = m_0 - m$), sample surfaces (S), and immersion times (t) the average corrosion rates (ω) were estimated [11]:

$$\omega = \Delta m / (S \cdot t). \quad (1)$$

An inhibitory ability (IE) of the compound was estimated from the ratio of the corrosion rates in the absence (ω_0) and in the presence (ω) of the inhibitor [11]:

$$IE = (\omega_0 - \omega) / \omega_0 \cdot 100\%. \quad (2)$$

2.4. Polarisation studies

For polarisation tests,electrodes made of EN Fe37-3FN mild steeland sealed with the epoxy resin with the working surface of 0.04cm^2were polished using theP2500 emery paperand degreased by ethanol.The measurements were conducted in a standard three-electrode electro-chemical cell, consisting from the working electrode (steel sample), auxiliary electrode from the porous graphite, and the mercury-mercurous sulphate reference electrode. An open circuit potential (E_{corr}) was recorded during 30 min.

For the measurement of the linear polarisation resistance the polarisation curves were recorded in the current range from –10 μA and to +10 μAin galvanodynamic mode with the current sweep rate of 2μA/s. Each experiment was performed in triplicate. The obtained polarisation curves were presented in the coordinates $E(I)$, and the polarisation resistances were evaluated as the slopes of these curves using the least squares technique:

$$R_p = dE / dI. \quad (3)$$

The inhibitory ability of the compound was estimated from the ratio of the polarisation resistances in the presence (*R*) and in the absence (R_0) of the inhibitor [11]:

$$IE = (R - R_0) / R \cdot 100\%. \quad (4)$$

For the measurement of the Tafel slopes [14] and the corrosion current density the polarisation curves were recorded in both directions in the potential ranges from the measured open circuit potential to –500 mVand to +500 mV relatively to it with the potential sweep rate of 10 mV/s. Each experiment was performed in triplicate. The obtained polarisation curves were presented in the coordinates*E*(lg *i*), and the Tafel slopes (*b*) and the corrosion current density (i_{corr}) were evaluated from them [15]. Subsequently, the polarisation resistances (R_p) were estimated from the Tafel slopes and the corrosion current densities using the Stern – Geary equation [16,17]:

$$R_p = \frac{1}{ln\,10} \cdot \frac{1}{i_{corr}} \cdot \frac{b_a \cdot |b_c|}{b_a + |b_c|}, \quad (5)$$

where b_a and b_c are the slopes of the anodic and cathodic branches of the polarisation curve. The inhibitory ability of the compound was estimated from the ratio of the corrosion current densities in the absence (i_0) and in the presence (*i*)of the inhibitor [11]:

$$IE = (i_0 - i) / i_0 \cdot 100\%, \quad (6)$$

and also from the ratio of the polarisation resistances in the presence (*R*) and in the absence (R_0) of the inhibitor using equation (4).

2.5. EIS studies

For EIS tests, electrodes were prepared similarly to that described in the previous section.An open circuit potential was recorded during 30 min.Impedance values were recorded at the open circuit potential value in the alternating current frequency interval from 100mHzto10kHzwith the potential amplitude of 10 mV. Each experiment was performed in triplicate.The obtained results were presented in the form of Bode and Nyquist plots [18].

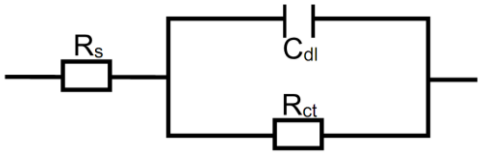

Figure 1. The Randles equivalent electrical circuit used to fit the EIS data

For the estimation of the impedance parameters, a simplified Randles equivalent electrical circuit (Figure 1) [19], containing the solution resistance R_s, the consecutive charge transfer resistance R_{ct} of the passivation layer, and the parallel constant-phase element representing the double electric layer, was employed.

The impedance (*Z*) of the Randles equivalent circuit is expressed by the equation [17]:

$$Z = R_s + \frac{1}{\frac{1}{R_{ct}} + P \cdot (i \cdot \omega)^n} = R_s + \frac{1}{\frac{1}{R_{ct}} + P \cdot \omega^n \cdot \left(cos\left(\frac{\pi \cdot n}{2}\right) + i \cdot sin\left(\frac{\pi \cdot n}{2}\right)\right)}, \quad (7)$$

where *ω*is the frequency of the alternating current, *P* and *n* are the parameters of the constant phase element.

The fitting of the equivalent circuit parameters to the experimental impedance values was performed using the free software EIS Spectrum Analyser [20]. In addition, the capacitance (C_{dl}) and the thickness (*d*) of the double electric layer were estimated [21]:

$$C_{dl} = P^{\frac{1}{n}} \cdot \left(\frac{R_s \cdot R_{ct}}{R_s + R_{ct}}\right)^{\frac{1-n}{n}}, \quad (8)$$

$$d = (S \cdot \varepsilon_0 \cdot \varepsilon) / C_{dl}. \quad (9)$$

where *S*is the electrode surface, *ε* is the dielectric constant of water, and ε_0 = 8.85 10^{-12} F/m is the dielectric constant of vacuum.

The inhibitory ability of the compound was estimated from the ratio of the charge transfer resistances in the presence (*R*) and in the absence (R_0)of the inhibitor using equation (4) [11].

3. RESULTS AND DISCUSSION

3.1. Gravimetric studies

The dependence of the measured inhibition efficiencies at the different inhibitor concentrations (c_{inh}) is presented in Table 1.

Table 1.Variation of corrosion rates and inhibition efficiencies for mild steel in 0.5 M HCl and 0.5 M H_2SO_4 acid solutions with different concentrations of Fagussylvaticapurpureafallen leaves extracts obtained in the gravimetric measurements

Medium	0.5 M HCl		0.5 M H_2SO_4	
c_{inh}, g/l	ω, mg/(cm^2 · h)	IE, %	ω, mg/(cm^2 · h)	IE, %
0	0.89 ± 0.08	–	1.1 ± 0.1	–
0.1	0.67 ± 0.07	24.9	0.81 ± 0.09	25.9
0.3	0.51 ± 0.06	43.1	0.72 ± 0.08	34.7
1	0.30 ± 0.04	66.3	0.54 ± 0.06	51.3
3	0.28 ± 0.04	67.9	0.40 ± 0.05	63.8
10	0.26 ± 0.04	70.8	0.26 ± 0.05	76.2

3.2. Polarisation studies

The graphs of the open circuit potential measurements are presented in Figure 2.

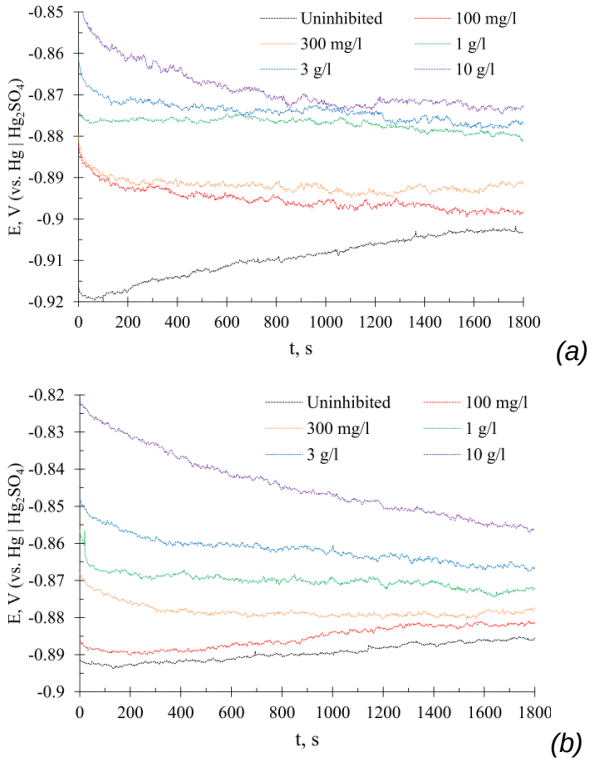

Figure 2. The open circuit potential of steel in (a) 0.5 M HCl, and (b) 0.5 M H_2SO_4 with the different additions of the Fagussylvaticapurpurea leaf extract after 30 min of exposure

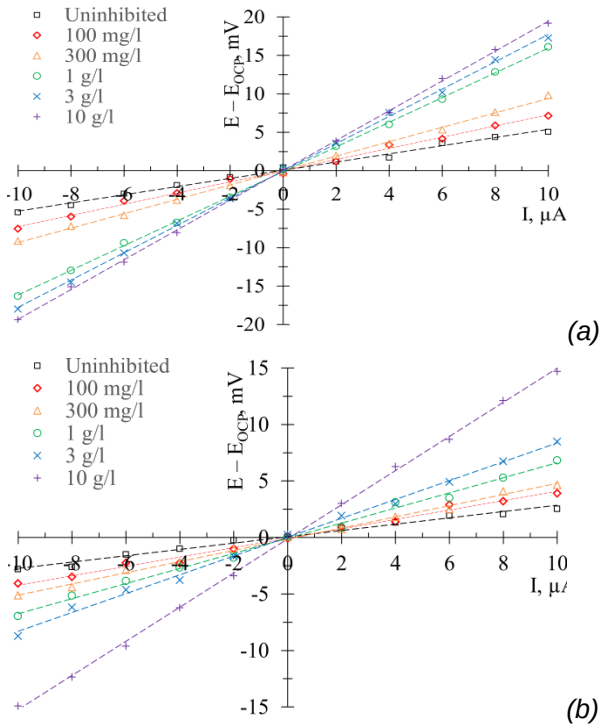

Figure 3. The linear polarisation resistance curves of steel in (a) 0.5 M HCl, and (b) 0.5 M H_2SO_4 with the different additions of the Fagussylvaticapurpurea leaf extract

The results of the linear polarisation resistance measurements are presented in Figure 3 and in Table 2.

Table 2. Variation of the measured polarisation resistance and estimated inhibition efficiencies of mild steel in 0.5 M HCl and 0.5 M H_2SO_4 acid solutions with different concentrations of Fagussylvaticapurpurea fallen leaves extracts

Medium	0.5 M HCl		0.5 M H_2SO_4	
c_{inh}, g/l	R_p, Ohm ·cm^2	IE, %	R_p, Ohm ·cm^2	IE, %
0	520±10	–	300±10	–
0.1	700±20	25.2	450±10	32.2
0.3	950 ± 20	45.0	510 ± 20	40.0
1	1460 ± 30	64.1	660 ± 20	53.3
3	1640 ± 30	68.0	860 ± 20	64.4
10	1790 ± 30	70.7	1540 ± 30	80.1

The results of the potentiodynamic polarisation measurements are presented in Figure 4 and in Table 3.

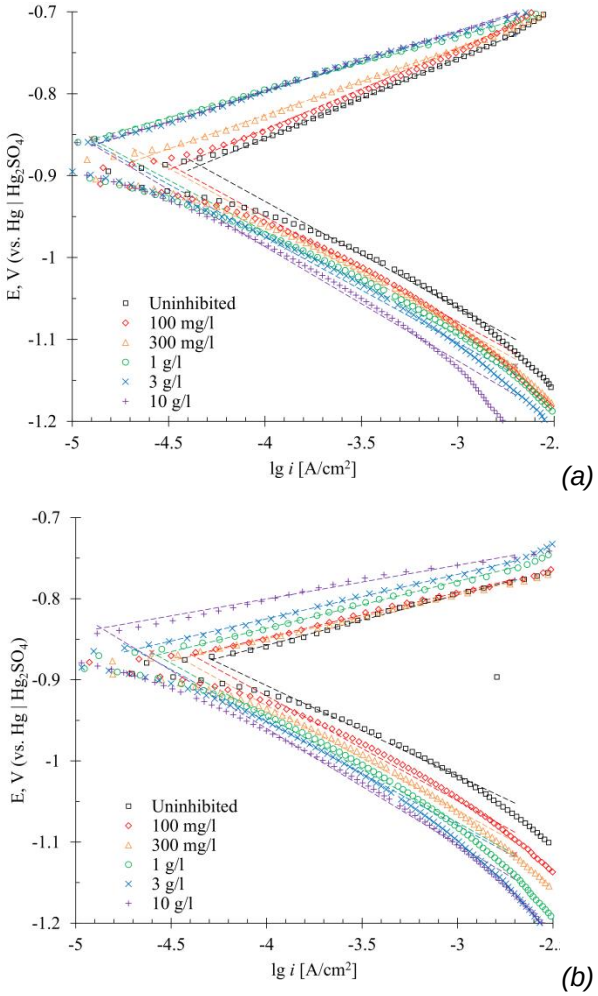

Figure 4. The polarisation curves of steel in (a) 0.5 M HCl, and (b) 0.5 M H_2SO_4 with the different additions of the Fagussylvaticapurpurea leaf extract after 30 min of exposure

Table 3.Variation of the measured open circuit potentials, Tafel slopes of polarisation curves,and estimated corrosion current densities, polarisation resistance and inhibition efficiencies of mild steel in 0.5 MHCl and 0.5 M H_2SO_4 acid solutions with different concentrations of Fagussylvaticapurpureafallen leaves extracts

c_{inh}, g/l	E_{cor}, mV	b_a, mV/dec	b_c, mV/dec	i_{cor}, µA/cm^2	IE, %	R_p, Ohm·cm^2	IE, %
0.5 M HCl with additions of *Fagussylvaticapurpurea*leaf extract							
0	–903	98.8	–129.8	45.9	–	527	–
0.1	–898	92.7	–128.3	33.9	26.1	715	26.3
0.3	–892	82.2	–129.6	24.5	46.7	891	40.9
1	–881	66.1	–126.1	12.7	71.2	1482	64.5
3	–877	74.0	–129.1	12.9	71.8	1529	65.5
10	–873	72.7	–129.4	13.2	72.4	1622	67.6
0.5 M H_2SO_4 with additions of *Fagussylvaticapurpurea*leaf extract							
0	–886	65.2	–131.4	51.7	–	335	–
0.1	–881	55.5	–129.2	40.8	21.2	414	19.1
0.3	–877	52.3	–129.3	35.6	31.1	466	28.2
1	–872	47.8	–130.0	26.6	48.5	655	48.9
3	–865	44.2	–128.2	20.3	60.7	821	59.2
10	–857	41.6	–133.0	13.6	73.6	1026	67.4

3.3. EIS studies

The results of electrochemical impedance measurements are presented in Figure 5 and in Table 4.

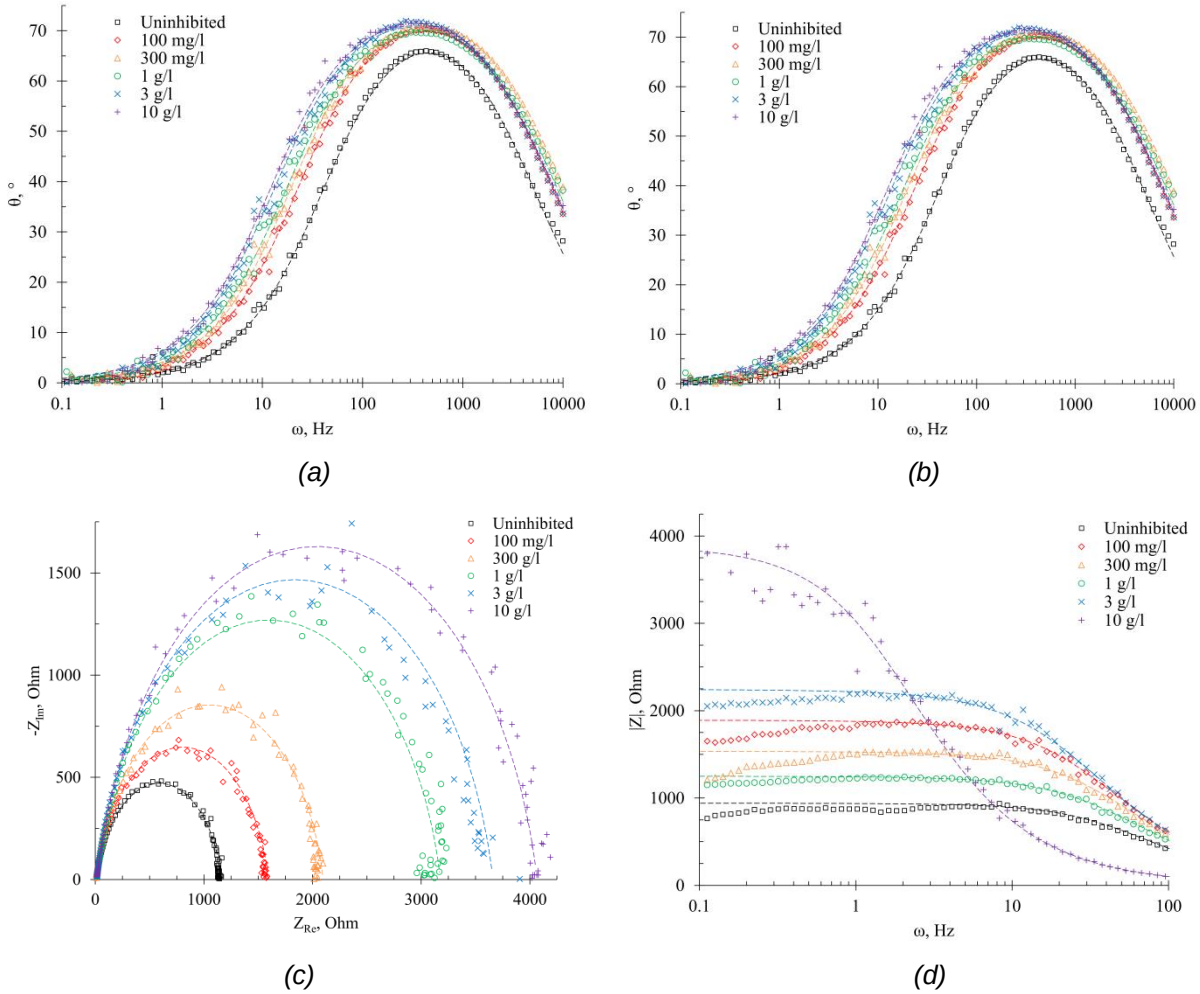

(a) *(b)*

(c) *(d)*

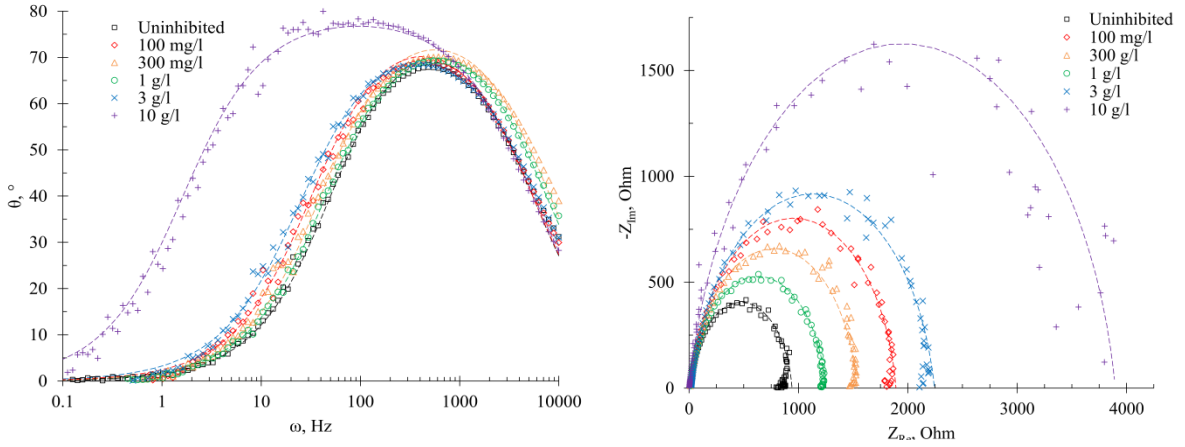

(e) *(f)*

Figure 5. The Bode plots of steel in (a), (b) 0.5 M HCl, and (d), (e) 0.5 M H_2SO_4, and the Nyquist plots of steel in (c) 0.5 M HCl, and (f) 0.5 M $H_2SO_4$with the different additions of the Fagussylvaticapurpurea leaf extract after 30 min of exposure

Table 4.Variation of theestimatedelectrochemical parameters obtained in the electrochemical impedance measurements and of inhibition efficiencies of mild steel in 0.5 MHCl and 0.5 M H_2SO_4 acid solutions with different concentrations of Fagussylvaticapurpureafallen leaves extracts

c_{inh}, g/l	R_s, Ohm	P, μOhm^{-1}·s^n	n	C_{dl}, μF	d, nm	R_{ct}, Ohm	IE, %
0.5 M HCl with additions of *Fagussylvaticapurpurea*leaf extract							
0	17.0	67.6	0.88	26.8	1.04	1144.7	–
0.1	9.9	82.4	0.87	28.4	0.98	1583.5	27.7
0.3	9.8	71.3	0.87	24.1	1.15	2087.0	45.1
1	14.8	55.7	0.86	17.5	1.58	3163.2	63.8
3	14.4	60.7	0.86	19.3	1.44	3645.5	68.6
10	14.7	59.1	0.86	18.8	1.48	4052.8	71.7
0.5 M H_2SO_4 with additions of *Fagussylvaticapurpurea*leaf extract							
0	13.3	55.6	0.91	342	0.08	927.4	–
0.1	12.5	50.9	0.90	290	0.10	1237.1	25.0
0.3	12.5	43.0	0.91	256	0.11	1521.8	39.1
1	18.5	44.5	0.90	261	0.11	1873.1	50.4
3	18.1	52.7	0.88	279	0.10	2225.4	59.3
10	2.8	32.9	0.89	138	0.20	3894.1	76.2

3.4. Langmuir adsorption model

The description of the adsorption of the leaf extract components on the steel surface was performed in terms of the Langmuir adsorption model, because this model is simple and used in most corrosion inhibition studies [22]. The Langmuir adsorption isotherm equation was linearised in the form:

$$c_{inh}/\theta = 1/K_{ads} + c_{inh}, \quad (10)$$

where $c_{inh}$is the concentration of the *Fagus sylvatica purpurea* leaf extract solution, $K_{ads}$is the adsorption-desorption equilibrium constant, and $\theta$is the degree of surface coverage which represents the fraction of the surface of the metal covered by the inhibitor molecules adsorbed on to the metal surface. It is connected to the inhibition efficiency, IE of the inhibitor through the relation:

$$IE = \theta \cdot 100\% \quad (11)$$

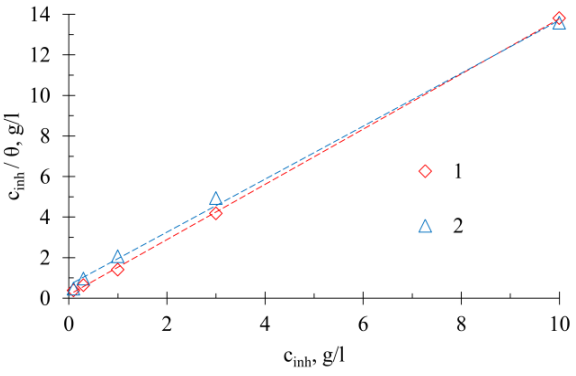

Figure 6. The plots of c_{inh} / θ vs. c_{inh} for the adsorption of the Fagussylvaticapurpurea leaf extract on the steel surface

The dependencies of c_{inh}/θ on c_{inh} are presented in Figure 6 and in Table 5.

The data were processed using the least squares technique [23], and the equilibrium constants K_{ads} were estimated as the intercepts of the regression equations. The Gibbs energy changes of the sorption ($\Delta_{ads}G$) were estimated from the equation:

$$\Delta_{ads}G = -RT \ln (K_{ads} \cdot c_{water}), \quad (12)$$

where $c_{water} = 10^3$ g/l is the water concentration in the extracts. The results are presented in Table 5.

Table 5. The estimated parameters of the Langmuir adsorption model, sorption-desorption equilibrium constants and the Gibbs energies of adsorption for the sorption of Fagussylvaticapurpureafallen leaves extracts on the steel surface

C_{inh}, g/l	θ	C_{inh} / θ, g/l	Regression equation	K_{ads}, l/g	$\Delta_{ads}G$, kJ/mol
0.5 M HCl with additions of *Fagussylvaticapurpurea*leaf extract					
0.1	0.261	0.383	$c_{inh}/\theta = (1.36 \pm 0.01) \cdot c_{inh} + (0.16 \pm 0.06)$; $R^2 = 0.999$	7 ± 3	–21 ± 2
0.3	0.467	0.642			
1	0.712	1.404			
3	0.718	4.178			
10	0.724	13.812			
0.5 M H_2SO_4 with additions of *Fagussylvaticapurpurea*leaf extract					
0.1	0.212	0.472	$c_{inh}/\theta = (1.31 \pm 0.04) \cdot c_{inh} + (0.6 \pm 0.2)$; $R^2 = 0.997$	1.8 ± 0.6	–18 ± 2
0.3	0.311	0.965			
1	0.485	2.062			
3	0.607	4.942			
10	0.736	13.587			

3.5. Discussion

The results of the open circuit potential measurements show that with the addition of a *Fagus sylvatica purpurea* leaf extract the potential of the mild steel both in the solution of 0.5 M HCl and 0.5 M H_2SO_4 shifts to the more positive values. In addition, the Tafel slopes of the anodic branches of the polarisation curves decrease with alteration of the extract concentration, whereas the slopes of the cathodic branches remain nearly the same. This implies that in the solutions of both acids the purple beech leaf extract acts as the anodic-type inhibitor [24,25].

The values of the inhibition efficiencies estimated from the data of gravimetric, electrochemical and EIS experiments coincide well and show the similar trend (see Table 6). The values of the polarisation resistance of the absorbed inhibitor estimated from the data of linear polarisation and from the Tafel slopes also coincide well.

Table 6. The comparison of the inhibition efficiencies of Fagussylvaticapurpureafallen leaves extractsobtained by the various methods

C_{inh}, g/l	Inhibition efficiency, %				
	Gravimetric experiment	Linear polarisation resistance	Corrosion current density	Calculated polarisation resistance	Charge transfer resistance
0.5 M HCl with additions of *Fagussylvaticapurpurea*leaf extract					
0.1	24.9	25.2	26.1	26.3	27.7
0.3	43.1	45.0	46.7	40.9	45.1
1	66.3	64.1	71.2	64.5	63.8
3	67.9	68.0	71.8	65.5	68.6
10	70.8	70.7	72.4	67.6	71.7
0.5 M H_2SO_4 with additions of *Fagussylvaticapurpurea*leaf extract					
0.1	25.9	32.2	21.2	19.1	25.0
0.3	34.7	40.0	31.1	28.2	39.1
1	51.3	53.3	48.5	48.9	50.4
3	63.8	64.4	60.7	59.2	59.3
10	76.2	80.1	73.6	67.4	76.2

With the increase of the extract concentration from 0.1 to 1 g/l its inhibition efficiency on the corrosion of mild steel EN Fe37-3FN in a 0.5 M hydrochloric acid medium rises from ~25–30% to ~65–70%, but the further concentration increase gives no significant improvement of the inhibition efficiency. In contrast, the inhibition efficiency of the extract on the corrosion of the same steel in a 0.5 M sulphuric aicd medium continues to increase with the rise of extract concentration, and approaches ~70–75% when the concentration of 10 g/l is achieved.

The adsorption of the extracted components on the steel surface fairly obeys the Langmuir adsorption model. The values of the sorption–desorption equilibrium constants and the Gibbs energies of sorption estimated using the degrees of surface coverage obtained from the different methods coincide within their ranges of uncertainty. The calculated Gibbs energies of sorption are in the range ~ –20 kJ/mol for both hydrochloric and sulphuric acids, which means that the nature of the adsorption is physical due to the electrostatic interactions [26].

Despite the experimental values of the inhibition efficiencies may vary significantly with alteration of both the solution composition and temperature [27], the leaf extracts of *Fagus sylvatica purpurea*revealed the prospective inhibition potential against the corrosionofmild steel in acidic environments. The addition of common beech leaf extracts to a corrosive environment can be used to protect equipment from corrosion in pickling areas of metal processing industries, and in electroplating baths.The extracts may also be used as the part of products for removing corrosion products from steel surfaces [28,29]. Moreover, using the freshly fallen leaves for extract preparation does not put the trees into danger, and could contribute to the biomass waste usage.

4. CONCLUSION

The inhibitory ability of the *Fagus sylvatica purpurea*leaf boiling extracts on the corrosion of mild steel EN Fe37-3FN in 0.5 M hydrochloric acid and 0.5 M sulphuric acid media was investigated using the gravimetric, electrochemical, and EIS methods. It was shown that the addition of 100 mg/l of the extract reduces the corrosion rate in HCl by 25% and in H_2SO_4 by 20–25%, and that of of 1 g/l – by 65–70% and 45–50%, respectively, whereas the addition of 10 g/l of the extract further reduces the corrosion rate in $H_2SO_4$by 70–75%.The inhibition efficiency values obtained by the various methods show the similar trends. The adsorption of the extract components on a steel surface follows the Langmuir adsorption model, and the nature of adsorption is physical. The *Fagus sylvatica purpurea* leaf extract showsitself as prospective and environmentally friendly substance for reducing the steel corrosion rate in acidic environments.

5. REFERENCES

[1] R.Haldhar, S.C.Kim, E.Berdimurodov, D.K.Verma, C.M.Hussain (2021) Corrosion inhibitors: industrial applications and commercialization, book Sustainable corrosion inhibitors II: Synthesis, design, and practical applications, ACS Symposium Series, Vol. 1404, American Chemical Society, p. 219-235. doi: 10.1021/bk-2021-1404.ch010.

[2] N.Vaszilcsin, A.Kellenberger, M.L.Dan, D.A.Duca, V.L.Ordodi (2023) Efficiency of Expired Drugs Used as Corrosion Inhibitors: A Review, Materials, 16(16), 5555. doi: 10.3390/ma16165555.

[3] A.Thakur, S.Sharma, R.Ganjoo, H.Assad, A.Kumar (2022) Anti-corrosive potential of the sustainable corrosion inhibitors based on biomass waste: a review on preceding and perspective research, book Journal of Physics: Conference Series, Vol. 2267, No. 1, IOP Publishing, p. 012079. doi: 10.1088/1742-6596/2267/1/012079.

[4] S.Marzorati, L.Verotta, S.P.Trasatti (2018) Green corrosion inhibitors from natural sources and biomass wastes, Molecules, 24(1), 48. doi: 10.3390/molecules24010048.

[5] M.Ž.Nonić, D.M.Skočajić, M.N.Grbić, M.T.Šijačić-Nikolić (2017) Variability of Quantitative and Qualitative Characteristics of *Fagus sylvatica 'Purpurea'* Clones Produced by Grafting, Notulae Botanicae Horti Agrobotanici Cluj-Napoca, 45(2), 400-407. doi: 10.15835/nbha45210896.

[6] T.Hofmann, E.Nebehaj, É.Stefanovits-Bányai, L.Albert (2015) Antioxidant capacity and total phenol content of beech (*Fagus sylvatica L.*) bark extracts, Industrial Crops and Products, 77, 375-381. doi: 10.1016/j.indcrop.2015.09.008.

[7] L.Pirvu, A.Grigore, C.Bubueanu, E.Draghici (2013) Comparative analytical and antioxidant activity studies on a series of *Fagus sylvatica L.* leaves extracts, JPC-Journal of Planar Chromatography-Modern TLC, 26(3), 237-242. doi: 10.1556/jpc.26.2013.3.6.

[8] M.Formato, F.Scharenberg, S.Pacifico, C.Zidorn (2022) Seasonal variations in phenolic natural products in *Fagus sylvatica* (European beech) leaves, Phytochemistry, 203, 113385. doi: 10.1016/j.phytochem.2022.113385.

[9] E.Cadahía, B.Fernández de Simón, I.Aranda, M.Sanz, D.Sánchez-Gómez, E.Pinto (2015) Non-targeted metabolomic profile of *Fagus sylvatica L.* leaves using liquid chromatography with mass spectrometry and gas chromatography with mass spectrometry. Phytochemical Analysis, 26(2), 171-182. doi: 10.1002/pca.2549.

[10] N.Bhardwaj,P.SharmaV.Kumar(2021)Phytochemicals as steel corrosion inhibitor: an insight into mechanism, Corrosion Reviews, 39(1), 27-41. doi: 10.1515/corrrev-2020-0046.

[11] A.Kadhim A.A.Al-Amiery R.Alazawi M.K.S.Al-Ghezi R.H.Abass (2021) Corrosion inhibitors. A review,International Journal of Corrosion and Scale Inhibition, 10(1), 54-67. doi: 10.17675/2305-6894-2021-10-1-3.

[12] V.I.Vorobyova, M.I.Skiba, A.S.Shakun, S.V. Nahirniak (2019) Relationship between the inhibition and antioxidant properties of the plant and biomass wastes extracts-A Review, International Journal of Corrosion and Scale Inhibition, 8(2), 150-178. doi: 10.17675/2305-6894-2019-8-2-1.
[13] A.Cojocaru, I.Maior, D.I.Vaireanu, C.Lingvay, I. Lingvay, S.Caprarescu, G.E.Badea (2010) Ethanol extract of Fagus Sylvatica leaves as an eco-friendly inhibitor for carbon steel corrosion in acidic solutions, Journal of Sustainable Energy, 1(3), 64-71.
[14] J.Tafel (1905) Über die Polarisation bei kathodischer Wasserstoffentwicklung, Zeitschrift für Physikaliche Chemie, 50(1), 641-712. doi: 10.1515/zpch-1905-5043.
[15] F.Mansfeld (1973) Tafel slopes and corrosion rates from polarization resistance measurements, Corrosion, 29(10), 397-402. doi: 10.5006/0010-9312-29. 10.397.
[16] M.Stern (1958) A method for determining corrosion rates from linear polarization data, Corrosion, 14(9), 60-64. doi: 10.5006/0010-9312-14.9.60.
[17] M.Stern, A.L.Geary (1957) Electrochemical polarization: I. A theoretical analysis of the shape of polarization curves, Journal of Electrochemical Society, 104(1), 56-63. doi: 10.1149/1.2428496.
[18] X.Z.Yuan, C.Song, H.Wang, J.Zhang (2010)EIS equivalent circuits,bookElectrochemical Impedance Spectroscopy in PEM Fuel Cells: Fundamentals and Applications,Berlin, Springer, p. 139-192. doi: 10.1007/978-1-84882-846-9_4.
[19] J.E.B.Randles (1947) Kinetics of rapid electrode reactions, Discussions of the Faraday Society, 1, 11-19. doi: 10.1039/DF9470100011.
[20] A.S.Bondarenko, G.A.Ragoisha(2005) Inverse problem in potentiodynamic electrochemical impedance spectroscopy, book A.L.Pomerantsev. Progress in Chemometrics Research,New York, Nova Science Publishers, p.89–102, http://www.abc.chemistry.bsu.by/vi/analyser.
[21] A.Lasia (2014) Electrochemical Impedance Spectroscopy and its Applications, Springer, New York. doi: 10.1007/978-1-4614-8933-7.
[22] I.Langmuir (1918) The adsorption of gases on plane surfaces of glass, mica and platinum, Journal of the American Chemical Society, 40(9), 1361-1403. doi: 10.1021/ja02242a004.
[23] R.Adrain (1808) Research concerning the probabilities of the errors which happen in making observations, &c, The Analyst; Or Mathematical Museum, 1(4), 93-109.
[24] S.-I.Pyun (2021) Strategies of metal corrosion protection, ChemTexts, 7(1), 2. doi: 10.1007/s40828-020-00121-y.
[25] X.Xie, R.Holze (2018) Experimental methods in corrosion research, ChemTexts, 4(1), 5-13. doi: 10.1007/s40828-018-0057-0.
[26] A.Kokalj (2022) Corrosion inhibitors: physisorbed or chemisorbed? Corrosion Science, 196, 109939. doi: 10.1016/j.corsci.2021.109939.
[27] A.B.Kičenko, V.M.Kušnarenko (2005) O nekorektnosti točnyh značenij ocenki zašitnogo dejstviâ ingibitorov korrozii, Praktika protivokorrozionnoj zašity, 4(38), 17-22.
[28] T.J.Harvey, F.C.Walsh, A.H.Nahlé (2018) A review of inhibitors for the corrosion of transition metals in aqueous acids, Journal of Molecular Liquids, 266, 160-175. doi: 10.1016/j.molliq.2018.06.014.
[29] M.Goyal et al (2018) Organic corrosion inhibitors for industrial cleaning of ferrous and non-ferrous metals in acidic solutions: A review, J. of Molecular Liquids, 256, 565-573. doi: https://doi.org/10.1016/j.molliq.2018.02.045.

IZVOD

INHIBITORNA SVOJSTVA EKSTRAKATA IZ OPALOG LIŠĆA *FAGUS SILVATICA PURPUREA* NA KOROZIJU BLAGOG ČELIKA U KISELIM SREDINAMA

Inhibiciona sposobnost ekstrakata iz opalog lišća Fagus silvatica purpurea na koroziju mekog čelika EN Fe37-3FN u 0,5 M medijumu hlorovodonične kiseline i 0,5 M sumporne kiseline ispitivana je gravimetrijskim, elektrohemijskim i EIS metodama. Pokazalo se da dodatak 100 mg/l ekstrakta opalog lišća Fagus silvatica purpurea smanjuje stopu korozije za 20–25%, a od 1 g/l i više – za 65–70%. Adsorpcija komponenti ekstrakta na čeličnoj površini prati Langmuir model adsorpcije, a priroda adsorpcije je fizička. Ekstrakt opalog lišća Fagus silvatica purpurea pokazuje se kao perspektivna i ekološki prihvatljiva supstanca za smanjenje stope korozije čelika u kiselim sredinama.

Ključne reči: *Fagus silvatica purpurea, ljubičasta bukva, ključajući ekstrakti, inhibicija korozije u kiseloj sredini, blagi čelik, gravimetrijska studija, elektrohemijska studija, spektroskopija elektrohemijske impedanse, Langmuir adsorpciona izoterma*

Naučni rad
Rad primljen: 29.02.2024.
Rad korigovan: 24.09.2024.
Rad prihvaćen: 01.10.2024.

Pavel Anatolyevich Nikolaychuk https://orcid.org/0000-0003-0335-3955